Université Catholique de Louvain

Secteur des Sciences de la Santé, Faculté de Médecine

Institut de Recherche Expérimentale et Clinique (IREC)

Pôle de Recherche en Gynécologie

From in-depth human ovary characterization toward a biomimetic artificial ovary

Emna OUNI

Promoter: Prof. Christiani Andrade Amorim

Co-promoter: Dr. Didier Vertommen

Thesis submitted with a view to obtaining a doctoral degree (PhD) in Medical Science

JURY MEMBERS

President	Prof. Etienne Marbaix, *MD, PhD* Université Catholique de Louvain, Belgium
Promotor	Prof. Christiani Andrade Amorim, *DVM, PhD* Université Catholique de Louvain, Belgium
Co-promotor	Dr. Didier Vertommen, *PhD, research associate* Université Catholique de Louvain, Belgium
Members	Prof. Marie-madeleine Dolmans, *MD, PhD* Université Catholique de Louvain, Belgium
	Prof. Sophie Demoustier, *PhD* Université Catholique de Louvain, Belgium
	Prof. Bernard Gallez, *PhD* Université Catholique de Louvain, Belgium
Invited member	Prof. Jean-Christophe Jonas, *MD, PhD* Université Catholique de Louvain, Belgium
External members	Prof. Vincent Fleury, *PhD* Université Paris Diderot, France
	Dr. Gabriel Mazzucchelli, *PhD* Université de Liège, Belgium

To my mom,

To my dad,

To all the female patients
who contributed to this project,

ACKNOWLEDGMENT

A project work does not complete without the support and heartfelt wishes of numerous people. As the present project has acquired this final structure, memories unreel in my mind, reminding me the ups and downs confronted during this tenure. I learned that the only way we are going to get anywhere in life is to work hard and smart. Problems can become opportunities, when the right people come together. This is the correct time to say thanks for the timely help of people, who showed me direction and guidance to achieve my aim. This is not just a formal thank; it is rather a deep gratitude, which comes from my heart.

I would like to first thank my promotor Prof. Christiani Amorim, who warmly welcomed me to the artificial ovary team and challenged me to build the most complete description, to date, of the extracellular matrix of the human ovarian cortex, while putting all her trust in my skills as a bioengineer. Faced with such a challenge and such an ambitious mission, I can only express my immense gratitude and also my pride in having accomplished my mission. I would like to thank you for giving me so much freedom to think and act in order to carry out my project. A freedom that allowed me to remain so enthusiastic and creative even after five years of pure hard work, as if it was the first day of my thesis. Now as we said in 2016, "the sky is the limit". I will always admire your dreamy set of mind and determination.

I am deeply grateful to Prof. Marie Madeleine Dolmans, head of the laboratory, an admirable gynecologist and surgeon. You are the driving

force of this laboratory, thanks to your attention to detail and pursuit of excellence. I had the honour during these years to meet you and to discover the world of clinical research in gynecology. You are without a doubt the vital link of this project with the clinic.

My mission would hardly have been accomplished without the immense help, listening, training and caring of my promoter Dr. Didier Vertommen. Thanks to whom we have succeeded in deciphering the proteomics of the ovarian matrisome, which are rather capricious proteins. I am very grateful to you for all the information I have learned on proteomics today. I admire your modesty and expertise, as well as your way of telling me "try" as soon as I propose an idea, even if you already know the result, thus leaving room for my autonomy and personal initiatives. I hope I have been a good ambassador for proteomics in the GYNE lab.

A deep thank you to Professors Etienne Marbaix, Bernard Gallez and Sophie Demoustier for their advice and support during this training. Presenting the progress of my work each year to a panel of scientists of your quality was a stimulating and pricking challenge. All your advice were considered and allowed me to optimize my project. You were right, the aims of this project were impossible to achieve in four years. But I could not defend my project in front of you, before reaching all its objectives, which cost me a few unpaid months, but allowed me to keep my promise.

I also thank the external members who honored me by judging this

work. Thanks to Pr. Jean-Christophe Jonas, for his scientific precision and his constructive criticism during my mid-term evaluation. Special thanks to Pr. Vincent Fleury and Dr. Gabriel Mazzucchelli, both experts in their respective fields, biophysics and mass spectrometry, for reviewing the manuscript and for attending my private defense. I was very honoured by your encouraging comments.

At the interface between gynecology, proteomics and biomechanics, this project required working side by side with several collaborators. First of all, I would like to thank the professionalism of the MASSPROT platform team, mainly Gaëtan Herincks, with whom I had the pleasure to work and shape the methods deployed in this project. Other platforms of the Université Catholique de Louvain opened their doors to me and put at my disposal their devices and materials, in particular the imaging platforms directed by Dr. Caroline Bouzin at the IREC and Dr. Nicolas van Baren at the Institut de Duve. I am grateful to you.

I am delighted to have worked with Dr. Alexis Peaucelle and Dr. Kalina Haas, from INRAE in Versailles, exceptional creative researchers, thanks to whom I was able to carry out the biomechanical study of human ovarian tissue and conduct the data sonification. I remember working with you in a cheerful atmosphere and sharing our mutual fascination of the extracellular matrix. I look forward to meeting you in Paris for the next breakthrough.

The architectural studies of the ovarian tissue under electron microscopy were carried out thanks to the precious help and training

of Dr Corry Charlier, from the University of Namur. A big thank you for having accepted to do the topography study, an acquisition that takes a lot of time and requires a lot of rigor and patience.

Certainly, the collaboration with Clinique Saint-Luc, the anapath service and the department of obstetrics and gynecology at the University Hospital of Helsinki was essential in this project to build the biopsy bank necessary to characterize the human ovary. I am deeply grateful to all the people who contributed.

Many collaborators from the private sector offered their technical support by giving me access to their software licenses, while encouraging me to pursue my project. In this context, I would like to thank Valérie Nedbal and Paolo Chiappa from SAS institute GmbH; Marta Da Pian and Hongbao Cao from Elsevier; François Petiteau from Digital Surf; and Sergei Saveliev and Marylene Focant from Promega, who offered me the privilege of becoming an alpha tester for the upcoming MS-friendly surfactants.

These past years have given me exceptional professional relationships but also amazing international human relationships from different backgrounds that I am unlikely to forget. I sincerely thank the girls of the TAO office with whom I could share article celebrations, smiles and cakes and keep a healthy competition. Maria-Costanza the bubbly Italian and hard worker, Parinaz the smiling and ultimately optimistic Iranian, Emy the spicy Japanese who went for a short period of time to explore the synthesis of the in vitro matrix and Janice the charming Brazilian who is eagerly awaited to ensure the

formulation of the ovarian tissue-tailored transportation solution.

The TAO team has been growing steadily in the last few years, where we have recently welcomed the PhD students: Hanne from Belgium, and Saïd and Arezo, from Iran. A trio that brings so much freshness and new ideas to the team. I am sure that you will make good use of the data collected during my project especially under the supervision of Professor Amorim.

I am delighted to have met before my departure Thu a very helpful and sweet PhD student from Vietnam. I wish you success and best results as soon as possible.

It is inevitable to say that the cheerful ambiance has never left GYNE, especially thanks to the presence of the exceptional doctors who have decided to venture into research: Alessandra, Luciana, Alice, Rossella, Camille and Diego. I salute your audacity and I thank you for having brought so much solidarity and spunk within the GYNE group. However, I am still not the fastest student in learning Italian or Spanish. Specially, when I remember mixing the words, 'Prego' with 'Promega'.

With former members of the endometriosis team, I shared memorable coffee breaks and dialectical debates with Javier, Renan and Guillaume. And recently Christina joined the group to conduct her project on adenomyosis. I wish you courage and perseverance.

During my thesis I also had the pleasure to supervise two brilliant students, Thuy and Soulaima, who allowed me to play the role of professor for a short time and to transmit to them all that I would have

liked to receive when I was a student at their age. They have significantly contributed to my work on elastic proteins of the matrisome and I am grateful to them. In the last days of my training, two new exceptional and brilliant students came to my office and brightened my days with their quirky humour, Francesca and Sarah. Thank you for your good vibes and I hope to have helped you to apprehend your master projects with more serenity.

I cannot thank enough the pillars of the laboratory, our technicians: Dolores, Sarah and Olivier. Although my experiments are outside of GYNE's scope, I would like to express my gratitude to Olivier who showed great interest in the project and explored and designed new techniques with me, always with a smile, good humor and lots of chocolate. I have discovered a wonderful and a warm-hearted person who deserves all my respect.

I would also like to thank our administrative team members who do a tremendous amount of work to ensure that our orders are delivered on time and that our administrative records are in order, Dora, Deborah and Patricia. I would also like to thank Mira, our English proofreading fairy, who makes sure that our publications are flawless.

I could say today that I have been working on the extracellular matrix for a little more than 6 years. A world that I first discovered, within the Centre Européen d'Etude du Diabète (CEED) where I did my end of study project. Thanks to the supervision of Dr Elisa Maillard and Dr Anaïs Schaschkow, I received an intensive training that taught me the technical and scientific rigor necessary to persevere in research. I am

very grateful to you and I am delighted to finally show you the outcome of some ideas that started to blossom during my internship.

It's time to confess that I have not only been a member of the GYNE lab since 2016, but I have also been a member of the OMFI lab (One Moment of Free improvisation). It's a free musical improvisation group based in Brussels, which allowed me to combine science with art and thanks to which I played at the fête de la musique in 2019, on my electric guitar. This is one of the most remarkable acquaintances during my stay in Brussels. I will always remember the philosophy of improvisation: stepping back and forth between the past and the present to edit the future, while keeping a deep consciousness of the moment. An exercise that I have adopted even during my PhD. I thank the whole team for welcoming me and I hope to merge music and science even more, in the coming years.

Without science, art and love, one could not evolve in life. I was lucky to have all three. I am especially grateful to Omar who encouraged me to go further and persist at every step of this project by giving me all the support he could offer.

I dedicate my thesis to my parents who have always believed in me and who have forged my personality, while letting me trace my path and follow my passion. They are the only ones who know the backstage of the completion of my thesis…

To my mother who has enrobed me every day with love and positive energy, making me indestructible in the face of the most tenacious

challenges. You are still my role model, a beautiful, intelligent woman with a sharp critical and scientific mind, an inexhaustible source of inspiration with a big heart (despite the many inspiring ladies I have met over the years).

To my father, who has taught me a lot about the art of listening, patience, perseverance and who has carefully read all my articles with an ongoing constructive feedback. I hope that I have succeeded in making you proud of me and I look forward to catching up on these years spent far away from you. A few words will never sum up my overwhelming gratitude for your unconditional love and caring. I also thank my big sister Tima, an architect and the artistic soul of the house, who helped me to forge my personality and my identity. I look forward to see your opinion on the bioarchitecture of the human ovary.

In the end, I owe a debt of gratitude to my country, which has offered me a free and high quality education throughout my academic training, which has allowed me to compete with prestigious international institutions. And without the support, hospitality and training of Université Catholique de Louvain and its rector Mr. Vincent Blondel, this project would never have achieved all its objectives. I would like to express my heartfelt gratefulness to this noble institution.



“Nature is the source of all true knowledge. She has her own logic, her own laws, she has no effect without cause nor invention without necessity.”

Leonardo da Vinci

TABLE OF CONTENTS

LIST OF ABBREVIATIONS 1

LIST OF FIGURES 5

LIST OF TABLES 8

CHAPTER 1. Female fertility from the ovarian perspective 9

I. The human ovary from genesis to menopause 10

I.1. Prenatal period 10

I.2. Neonatal and prepubertal period 14

I.3. Reproductive age period 16

I.3.1 Hormonal orchestration 16

I.3.2. Folliculogenesis 20

I.4. Menopause 27

II. Cryopreservation and transplantation of ovarian tissue as a strategy to preserve fertility in cancer patients 31

II.1. A brief history of ovarian tissue cryopreservation 31

II.3. Transplantation of cryopreserved ovarian tissue 35

III. The transplantable artificial ovary (TAO) 37

CHAPTER 2. Learning from mother nature:a roadmap to construct a biomimetic TAO 41

I. TAO strategy 42

I.1. Cellular population 42

I.1.1. Stromal cells 42

I.1.2. Endothelial cells 43

I.1.3. Other ovarian cell populations 43

I.2. Physical support 44

II. Developing TAO three-dimensional matrix 47

II.1. Scaffolds tested to replace the native ovarian ECM 47

II.1.1. Synthetic scaffolds 47

II.1.2. Natural scaffolds 48

II.1.3. Hybrid scaffolds 56

II.2. Limitations of used strategies 57
II.3.What we know from the native ovarian ECM 61
II.3.1. Mesoscale organization 61
II.3.2. Ovarian ECM biochemical composition andturnover 62
II.3.3. The role of mechanical signaling in follicle activation and maturation 67
II.4. Lessons learned from other organs on the role of the different ECM facets 78
II.4.1. ECM proteomic identity 78
II.4.2. ECM nano and microarchitectural features:more than pretty fibrils 92
II.4.3. ECM topography and its role in cell signaling 97
II.5. How to build a road map to construct a functional biomimetic TAO. 100
II.5.1. ECM proteomic characterization 102
II.5.2. Characterization of ovarian biomechanics 104
II.5.3. Elucidation of the architectural and topographical features of the ovary 105
CHAPTER 3. Personal contribution 107
A draft map of the human ovarian proteome for tissue engineering and clinical applications 111
Divide-and-Conquer Matrisome Protein (DC-MaP) Strategy: An MS-Friendly Approach to Proteomic Matrisome Characterization 135
Spatiotemporal changes in mechanical matrisome components of the human ovary from prepuberty to menopause 163
Proteome-wide and matrisome-specific atlas of the human ovaryfrom prepuberty to menopause 191
Multi-scale study of the architecture, topography and mechanicsof the human ovary from prepuberty to menopause: a blueprint for next-generation bioengineering and diagnosis 267
CHAPTER 4. Discussion, perspectives and emerging opportunities. 326
I. Discussion 327
I.1. Proteomic characteristics of the human ovaryand reproductive-age biomarkers at the ECM level 329
I.1.1. Discovery proteomics 329
I.1.2. An ECM-tailored proteomic method 334

I.1.3. Potential fertility biomarkers at the ECM level 337
I.2. Multi-scale architecture and topography ofthe human ovary 338
I.3. Elasticity and viscoelasticity of the ovarian ECM..... 343
II. Perspectives and emerging opportunities..... 348
II.1. How to build a TAO..... 348
II.1.1. Cell derived ECM 349
II.1.2. Bioprinting 351
II.1.3. FluidFM 353
II.1.4. Shape morphing polymers..... 354
II.2. The virtual ovary 356
II.3. In vivo mass-spectrometry for personalized therapy..... 357
II.4. Ovarian rejuvenation..... 358
CHAPTER 5. Other contributions to the field..... 361
CHAPTER 6. References 456

LIST OF ABBREVIATIONS

Abbreviation	Full designation
ADAM	A disintegrin and metalloproteinase
ADAMTS	A disintegrin and metalloproteinase with thrombospondin motif
AFM	Atomic force microscopy
AGE	Advanced glycation end product
AKAP13	A kinase anchor protein 13
Akt	Serine/threonine-specific protein kinase
AMH	Anti-Mullerian hormone
AMPK	5’ adenosine monophosphate-activated protein kinase
bFGF	Basic fibroblast growth factor
BIRC	Baculoviral inhibitor of apoptosis repeat
BMP2	Bone morphogenetic protein 2
BMP4	Bone morphogenetic protein 4
BMP7	Bone morphogenetic protein 7
C1QTNF3	C1q/tumor necrosis factor-related protein 3
CDC25B	M-phase inducer phosphatase 2
CTGF/CCN2	Connective-tissue growth factor
CYR61/CCN1	Cysteine-rich protein 61
DC-MaP	Divide and conquer matrisome protein
DDM	Dodecyl-β-D-maltoside
ECM	Extracellular matrix
EDN2	Endothelin 2
EDNRA	Endothelin receptor, subtype A
EGFR	Epidermal growth factor receptor
ERK 1/2	Extracellular signal-regulated kinase 1/2

FAK	Focal adhesion-associated kinase
FMOD	Fibromodulin
FOXO3	Transcription factor forkhead box O3
FSH	Follicle-stimulating hormone
GAG	Glycosaminoglycan
GDF9	Growth differentiation factor 9
GLYT1	Glycine transporter 1
GnRH	Gonadotropin releasing hormone
HILIC	Hydrophilic interaction liquid chromatograpgy
HPLC	High-performance liquid chromatography
HRT	Hormonal replacement therapy
HSPG2	Heparan sulfate proteoglycan 2
ICSI	Intracytoplasmic sperm injection
IGF	Insulin-like growth factor
IGFALS	Insulin-like growth factor-binding protein complex acid labile subunit
IGFIR	Insulin-like growth factor 1 receptor
iTRAQ	Isobaric tags for relative and absolute quantitation
KL	Kit Ligand
LAB	Laser-assisted bioprinting
LATS1/2	Tumor suppressor homolog 1/2
LH	Luteinizing hormone
Lhx8	LIM homeobox 8
LIF	Leukemia inhibitory factor
LIFT	Laser-induced forward transfer
LKb1	Liver kinase b1
LOX	Lysyl oxidase

LRP1	Low density lipoprotein-receptor related protein 1
LTBP1	Latent transforming growth-factor β-binding protein 1
MAPK 3/1	Mitogen-activated protein kinase 3/1
MAPK1	Mitogen-activated protein kinase 1
MAPK3	Mitogen-activated protein kinase 3
MMP	Metalloproteinase
MSC	Mesenchymal stem cell
MST1/2	Macrophage stimulating 1/2
mTORC	Mammalian target of rapamycin complex
NFAT15	Nucleor factor of activated T-cell 5
NOV/CCN3	Nephroblastoma overexpressed gene
OGN	Osteoglycin
PA	Plasminogen activator
PAI-1	Plasminogen activator-inhibitor type 1
PAI-2	Plasminogen activator-inhibitor type 2
PDGF	Platelet-derived growth factor
PEG	Polyethylene glycol
PEG-VS	Polyethylene glycol-vinyl sulfone
PI3K	Phospholinositide 3-kinase
PIP2	Phosphatidylinositol-4,5-biphosphate
PIP3	Phosphatidylinositol-3,4,5-triphosphate
PM	ProteaseMax
POI	Primary ovarian insufficiency
PRP	Platelet-rich plasma
PTEN	Phosphatase and tensin homolog
RAS	Renin angiotensin system
RGD	Arginine-Glycine-Aspartate

ROCK	Rho-associated protein kinase
RP	Rapigest
RUNX2	Runt-related transcription factor 2
SAV1	Salvador 1
SCP	Shape-changing polymer
SDS	Sodium dodecyl sulfate
SEM	Scanning electron microscopy
Slc6a9	Solute carrier family 6, member 9
SLM alginate	Lyophilized high mannuronate alginate
SLRP	Small leucine-rich proteoglycan
SMP	Shape-memory polymer
TAO	Transplantable artificial ovary
TAZ	Transcriptional coactivator with PDZ-binding motif
TDF	Testis-determining factor
TGFβ	Transforming growth factor β
TIMP	Tissue-inihibitor of metalloproteinase
TMT	Tandem-mass tag
TNF-α	Tumor necrosis factor-alpha
t-PA	Tissue-type plasminogen-activator
TSC	Tuberous sclerosis complex
u-PA	Urokinase activator-inhibitor type 1
YAP	Yes-associated protein

LIST OF FIGURES

Figure 1. Gonads prenatal development.

Figure 2. Schematic illustrations showing differentiation of the indifferent gonads in a 5-week embryo into ovaries or testes.

Figure 3. Ovarian endocrine control of reproductive cyclicity.

Figure 4. Folliculogenesis stages.

Figure 5. From follicle activation toward secondary follicle formation.

Figure 6. Hypothalamic and ovarian function at menopause.

Figure 7. Major milestones in cryopreservation in the context of fertility restoration.

Figure 8. Transplantation techniques of frozen – thawed ovarian tissue.

Figure 9. Design of fertility restoration using the transplantable artificial ovary (TAO).

Figure 10. Structure of PEG-vinyl sulfone (PEG-VS).

Figure 11. Alginate crosslinking.

Figure 12. Fibrin clotting and cleavage.

Figure 13. An example of preclinical evaluation of cytotoxicity, immunogenicity and biodegradation of decellularized matrices.

Figure 14. The components of the follicular basal lamina and the call-exner bodies at different stages of follicular development.

Figure 15. Potential interactions between the plasminogen activator (PA-) and metalloproteinase (MMP-) systems during ECM remodeling in the ovary.

Figure 16. Follicle activation through Hippo and Akt signaling.

Figure 17. The matrisome divisions and categories.

Figure 18. Collagen crosslinking and impact on ECM topography and mechanics in human ovarian tissue.

Figure 19. Glycosaminoglycans (GAGs) interaction with collagen network.

Figure 20. Bioprocesses where fibrillin-1 (FBN1) is implicated.

Figure 21. Examples of physical ECM properties affecting cell signalling.

Figure 22. 2D-LC/MS illustration.

Figure 23. Graphical summary of the divide and conquer matrisome protein (DC-MaP) technique.

Figure 24. Graphical illustration of essential procedures used for the characterization of ECM topology and biomechanics.

Figure 25. Preliminary steps for reverse engineering the human ovarian matrisome.

Figure 26. Bioprocesses where elastin (ELN) has been implicated.

Figure 27. Possible strategies to build a TAO.

LIST OF TABLES

Table 1. Commercial decellularized scaffolds.

Table 2. Biomaterials tested for the encapsulation of ovarian cells and follicles.

CHAPTER 1

Female fertility from the ovarian perspective

I. The human ovary from genesis to menopause

The word 'ovary' is derived from the Latin word 'ovum', meaning egg. The human ovary has two biological roles: it contains the supply of germ cells to produce decedents; and is the female reproductive gland, controlling many aspects of female development and physiology. The ovarian follicle is the functional unit of the ovary that carries out both functions (Adhikari and Liu 2009).

I.1. Prenatal period

After the union of an oocyte and a spermatozoon become a zygote, all cells up to the eight-cell stage of embryogenesis appear to have similar totipotency (potential to become any lineage). However, with the formation of a 16-cell morula, the cells begin differentiation, with cells being allocated either inside or outside of the embryo. This process is exaggerated further at the blastocyst stage in which three lineages are defined: trophectoderm (future placenta), epiblast (future embryo), and primitive endoderm (future yolk sac). After implantation and further differentiation, cells within the epiblast eventually form the precursors of the primordial germ cells, the first cells of the future ovary to be defined (Edson et al. 2009).

These primordial germ cells proliferate and migrate from the yolk sac into the mesoderm colonizing the genital ridge at five weeks of gestation (Grive and Freiman 2015) (Figure 1). Between 6 and 7 weeks of pregnancy, sexual differentiation ensues due to the absence of the Y chromosome with its sex-determining region and female sex-determining genes, leading to distinction of primordial germ cells in oogonia and creation of the ovaries (Grive and Freiman 2015; Sarraj and Drummond 2012) (Figure 2).

During this process, oogonia undergo mitotic divisions with incomplete cytokinesis resulting in nests where germ cells remain connected by cytoplasmic bridges up to 18 - 19 weeks (Cordeiro et al. 2015).

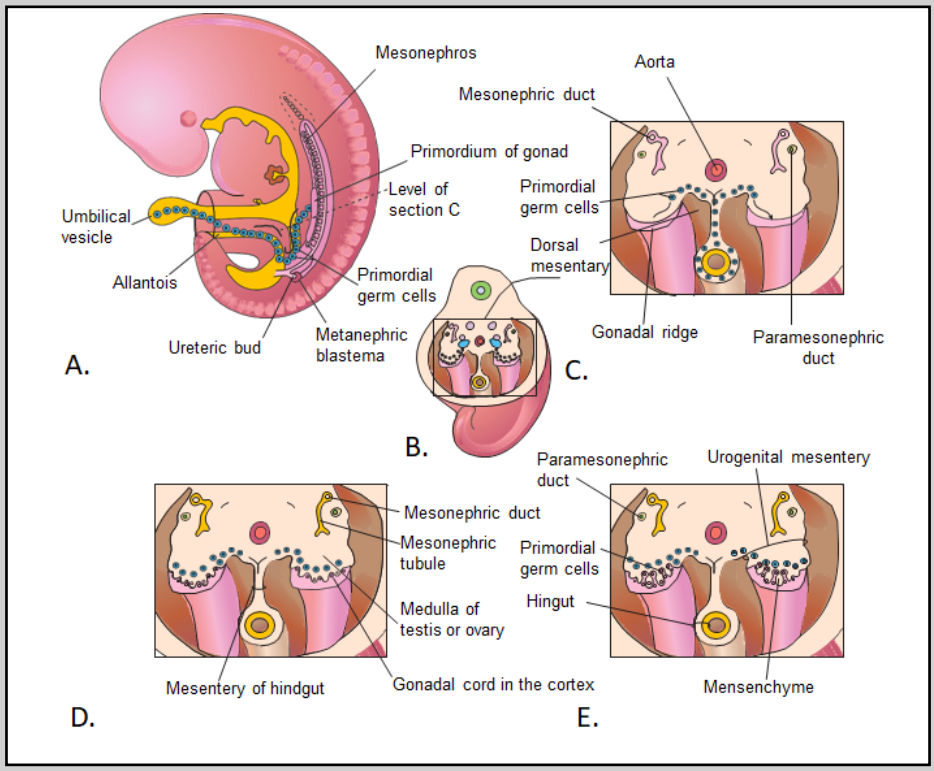


Figure 1 | Gonads prenatal development. A. Graphical representation of a 5-week embryo illustrating the migration of primordial germ cells from the umbilical vesicle into the embryo. **B.** The caudal region of the 5-week embryo, showing the location and extent of the gonadal ridges. **C.** Transverse section showing the gonadal ridges and the migration of primordial germ cells into the developing gonads. **D.** Transverse section of a 6-week embryo showing the gonadal cords. **E.** Similar section at a later stage showing the indifferent gonads and paramesonephric ducts (Moore 2015).

Once the maximum number of oogonia per ovary (5-7 million) is reached, the mitotic process is halted. Some of these oogonia enter in meiosis, generating oocytes arrested at the diplotene stage (prophase I), while others undergo extensive elimination through apoptosis. The early ovary develops distinct structural features, including the formation of ovigerous cords by the interaction of the germ cell clusters with surrounding flattened-pregranulosa cells (Konishi et al. 1986) (Hummitzsch et al. 2019) (Figure 2).

Around ten weeks of gestation, germ cells enter meiosis in an anterior-to-posterior gradient believed to be driven by retinoic acid (Koubova et al. 2006). This process begins in the medulla and spreads radially into the cortex. Around the fifth month of gestation, the germ cell nest begins to breakdown because the pregranulosa cells invade and degrade the cytoplasmic bridges within the cysts while some germ cells are systematically eliminated (Pepling and Spradling 2001). During this period, the earliest follicles are formed, namely primordial follicles, with a central oocyte surrounded by flattened pre-granulosa cells (Ford et al. 2020).

Then, as was the case with oogonia, some of these earliest follicles are eliminated by apoptosis and/or other not conclusively proved processes (Hartshorne et al. 2009; Kerr et al. 2013), yielding 1-2 million follicles at birth. From the sixth month of gestation, the first wave of primordial follicle activation (differentiation into primary follicle) commences, as the oocyte grows and granulosa cells divide and differentiate from their flattened, squamous shape to a cuboidal structure. At around the time of birth, a small proportion of preantral and antral follicles are present. However, until puberty occurs at around 13 years of age, activated follicles can only grow until the early antral stage (Ford et al. 2020).

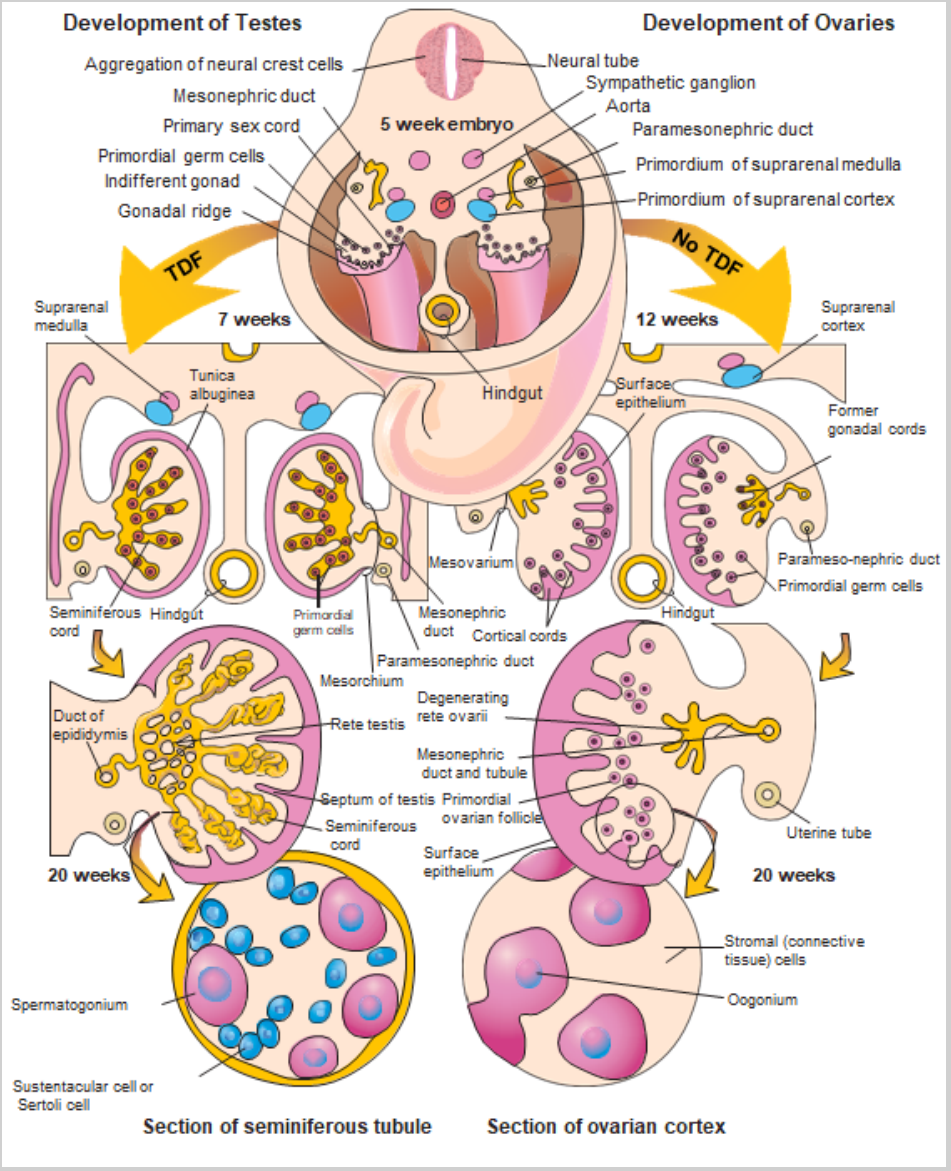


Figure 2 | Schematic illustrations showing differentiation of the indifferent gonads in a 5-week embryo into ovaries or testes.

The left side of the drawing shows the development of testes resulting from the effects of the testis-determining factor (TDF) located on the Y chromosome. Gonadal cords become seminiferous cords, the primordia of the seminiferous tubules. The parts of the gonadal cords that enter the medulla of the testis form the rete testis. In the section of the testis at the bottom left, there are two kinds of cells: spermatogonia, derived from the primordial germ cells; and sustentacular or Sertoli cells, derived from mesenchyme. **The right side** shows the development of ovaries in the absence of TDF. Cortical cords have extended from the surface epithelium of the gonad, and primordial germ cells have entered them. They are the primordia of the oogonia. Follicular cells (pre-granulosa) are derived from the surface epithelium of the gonad and primordial germ cells have entered them (Moore 2015).

I.2. Neonatal and prepubertal period

At birth, high placental estrogen and progesterone levels decrease drastically, releasing the neonatal hypothalamic-pituitary axis from the negative feedback specific occurring during the late second and third trimester of pregnancy. This release of negative feedback inhibition results in a rise in the pituitary gonadotropins, follicle-stimulating hormone (FSH) and luteinizing hormone (LH), under the influence of pulsatile gonadotropin-releasing hormone (GnRH) secretion from the hypothalamus. Pituitary gonadotropin stimulation of the newborn ovarian follicular apparatus results in follicle growth and significant gonadal steroid production (Winter et al. 1976). Sufficient estrogen production by the neonatal ovary may be present to stimulate the mother's reproductive tract following childbirth.

Although gonadotropin secretion increases shortly after birth due to the loss of placental steroid negative feedback on the neonatal pituitary gland,

gonadotropin secretion returns to low levels within the first few years of life (Racowsky and Gelety 1998). This fall is due in part to an increased sensitivity of the hypothalamic-pituitary axis (estimated to be 6-15 times more sensitive than in the adult) to the negative feedback from low levels of gonadal steroids (estrogens) characteristic of the prepubertal ovary (Winter and Faiman 1973). However, such a decline in gonadotropin secretion is also observed in children without gonadal steroid production, as in the case of gonadal dysgenesis, or in children whose ovaries have been removed surgically during the neonatal period. Therefore, a steroid-independent mechanism may be operative at the central nervous system's level to inhibit pulsatile secretion of GnRH from the hypothalamus, which results in inhibition of pituitary gonadotropin secretion before the onset of puberty.

Morphological maturation of the ovary is described by increases in ovarian weight and size, flattening of the surface epithelium, development of the tunica albugínea ovarii, changes in the orientation and quantity of connective tissue in the stroma, and increased vascularization (Forabosco and Sforza 2007).

The most striking characteristic of the infant ovary is the presence of follicles in all stages of development other than the preovulatory stage (Lintern-Moore et al. 1974; Peters et al. 1978). The ovarian reserve remains relatively constant for the first two years of life, followed by a steady increase in follicle loss that reaches a peak around 14 years of age (Kelsey et al. 2012), leaving around 300,000-400,000 follicles per ovary at menarche (Hansen et al. 2008). This is further reflected in rising anti-Mullerian hormone (AMH) concentrations through childhood. Still, there is a transient plateau or decline in AMH in adolescence (Hagen et al. 2012; Kelsey et al. 2011, suggesting non-linear changes in follicle development rate and extent. Studies monitoring early follicle activity through serum AMH measurement have

shown that there is a steady increase in follicle growth in the prepubertal years, with a poorly understood plateau after the onset of puberty (Hagen et al. 2012; Kelsey et al. 2011. These findings indicate that the post-natal ovary may not merely be a gonadotrophin-deficient version of the adult organ but show intrinsic maturational changes in childhood. The presence of a large population of abnormal primordial follicles was clearly identified (Anderson et al. 2014). These follicles were characterized by an indistinct germinal vesicle membrane and absent nucleolus and were larger than those with normal morphology. Their number decreases in pubertal girls and none were observed in adults indicating that these follicles are preferentially lost, perhaps through unknown 'quality control' mechanisms (Anderson et al. 2014).

I.3. Reproductive age period

I.3.1 Hormonal orchestration

The follicles within an adult ovary produce steroid and protein hormones in cyclical patterns in response to trophic factors from the hypothalamus and pituitary axis. These hormones then act locally to support follicle and oocyte development; and systemically to support reproductive health, bone health, and cardiovascular function (Nejat and Chervenak 2010).

Ovarian follicle development is a carefully orchestrated event directed by both endocrine signaling within the hypothalamic-pituitary ovarian axis and paracrine signaling occurring within and between follicles in the ovary (Eppig 2001).

Hormone-regulated follicular development involves the integration of feedback loops between estrogen, progesterone, inhibin A and inhibin B from the ovary, FSH and LH, from the pituitary, and hypothalamic GnRH to direct

follicle and oocyte development (Edson et al. 2009). On the other hand, early follicle growth is driven by intrinsic ovarian factors that regulate oocyte and follicle development before the follicles acquire FSH responsiveness (Edwards et al. 1977). These locally acting factors and their roles in maintaining the dormant follicle pool, activating selected primordial follicles, and supporting the earliest stages of follicle development are less well understood and of intense interest in the reproductive field. Understanding the early signaling events associated with maintaining a healthy quiescent follicle pool may provide insights into fertility preservation and restoration.

Hypothalamic GnRH pulses control pituitary gonadotropin (LH and FSH) release, which regulates follicle growth and production of steroid and peptide hormones (oestrogen, inhibins and progesterone) (Figure 3). These gonadal hormones then exert negative feedback on the pituitary and hypothalamus. The frequency of GnRH pulses determines FSH and LH release, stimulating follicle development. During follicular growth, oestrogen and inhibin are produced, causing negative feedback in the hypothalamus and pituitary (Figure 3). Increased GnRH pulses frequency induces LH release, triggering ovulation during which a mature oocyte is released from the surface of the ovary into the fallopian tube, where it can be fertilized.

The residual follicle unit (the remaining theca and mural granulosa cells) transforms into the corpus luteum that will produce progesterone, responsible for preparing the endometrium (uterine wall) for implantation and pregnancy.

If pregnancy is not achieved, the uterine wall disintegrates, causing the menses, at a time when a new group of gonadotropin-responsive follicles will start to grow, initiating a new cycle (M. H. Cordeiro et al. 2015) (Figure 4). Although multiple follicles are selected to begin growing and eventually reach

the antral stage, many are lost due to atresia, and only one will reach the preovulatory stage. This growth process requires an accurate regulation of both the hypothalamus-pituitary-ovary axis and intraovarian regulators, such as growth factors, cytokines and gonadal steroids (Yang et al. 2013).

Fertility is determined by the number of primordial follicles available in the ovary. A delicate balance between primordial follicle activation and loss is required to prevent premature depletion of the ovarian reserve under the accurate regulation of both hypothalamus-pituitary-ovary axis and intraovarian regulators (Yang et al. 2013).

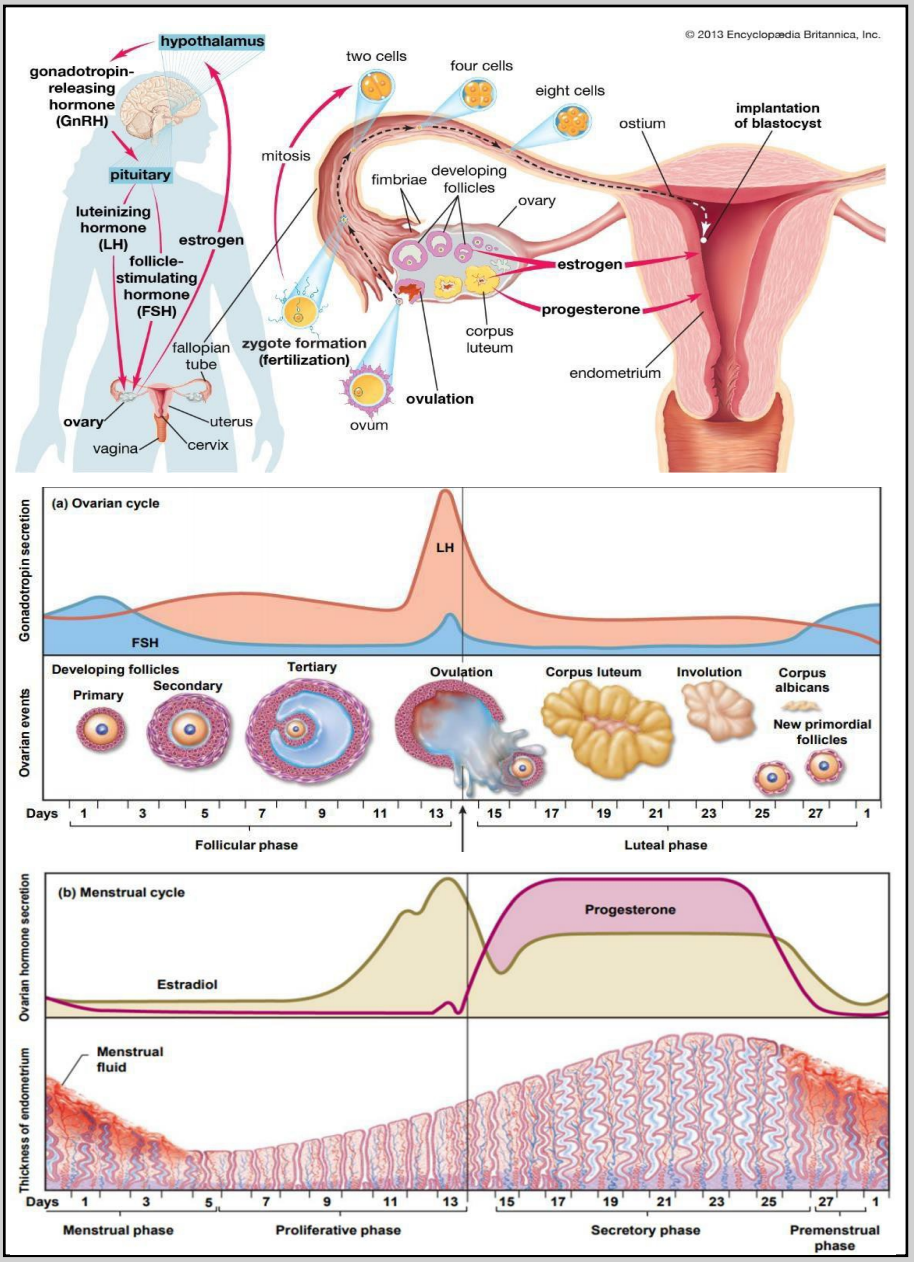


Figure 3 | Ovarian endocrine control of reproductive cyclicity.

Normal ovarian function and cyclicity are regulated by a complex hormonal feedback loop between the organs of the hypothalamus pituitary ovary axis. Hypothalamic gonadotropin-releasing hormone (GnRH) pulses control pituitary gonadotropin (luteinizing hormone [LH] and follicle-stimulating hormone [FSH]) release, which regulates follicle growth and production of steroid and peptide hormones (oestrogen and progesterone). These gonadal hormones then exert a negative feedback on the pituitary and hypothalamus. The frequency of GnRH pulses determines FSH and LH release, stimulating follicle development. During follicular growth the produced estrogen causes a negative feedback in the hypothalamus and pituitary. Increased frequency of GnRH pulses induces LH release, triggering ovulation. The residual follicle structure forms the corpus luteum and produces progesterone, which is responsible for preparing the endometrium (uterine wall) for implantation and pregnancy. If pregnancy is not achieved, the uterine wall disintegrates causing the menses, at a time when a new group of gonadotropin-responsive follicles will start to grow, initiating a new cycle. (*Adapted from Encyclopædia Britannica 2013, Inc).*

I.3.2. Folliculogenesis

Upon puberty, throughout a woman's reproductive years, nongrowing follicles will be recruited to ovulate through a physiological process called folliculogenesis (Wallace and Kelsey 2010). From the primordial stage until ovulation, it is required approximately 355 days. In humans, waves of follicles are recruited to grow throughout reproductive life, even during early pregnancy and the use of contraceptive pills (Li et al. 2011; Masse et al. 2011).

Follicle recruitment varies substantially with age, from more than 1400 per month in the early twenties to fewer than 30 in the late forties (Faddy and Gosden 1995). For the sake of simplicity, this process can be divided into 3 main stages:

I.3.2.1. Primordial follicle activation and recruitment

Morphologically, primordial follicles (~30 µm in diameter) consist of a central oocyte arrested in the prophase I of meiosis, surrounded by a single layer of flattened or squamous pre-granulosa cells. They are externally delimited by a basal membrane, representing a barrier between the follicle and its surrounding ovarian environment. Primordial follicles are metabolically quiescent and known to be the most abundant follicle population in the ovary (Gougeon 2010) (Figure 4).

Primordial-to-primary follicle transition, known as follicle activation, remains one of the least understood stages of follicular development. A balance between stimulatory and inhibitory signals has been shown to regulate follicle dormancy and activation. Nevertheless, the exact dynamic of events has not yet been fully elucidated. Indeed, extensive bidirectional signaling occurs between the follicle units, mainly oocytes and granulosa cells, from the primordial stage onwards (Reddy et al. 2010). The phosphatidylinositide 3-kinase (PI3K) pathway is critical for regulating the initiation of primordial follicle growth. When this intracellular signaling pathway is activated by growth factors, like kit ligand (KL), which is a cytokine produced by granulosa cells in primordial follicles, an increase in PI3K results in more significant phosphorylation of serine/threonine-specific protein kinase b (Akt), leading to cell proliferation, inhibition of apoptosis and increased survival (Hsueh et al. 2015) (Figure 5).

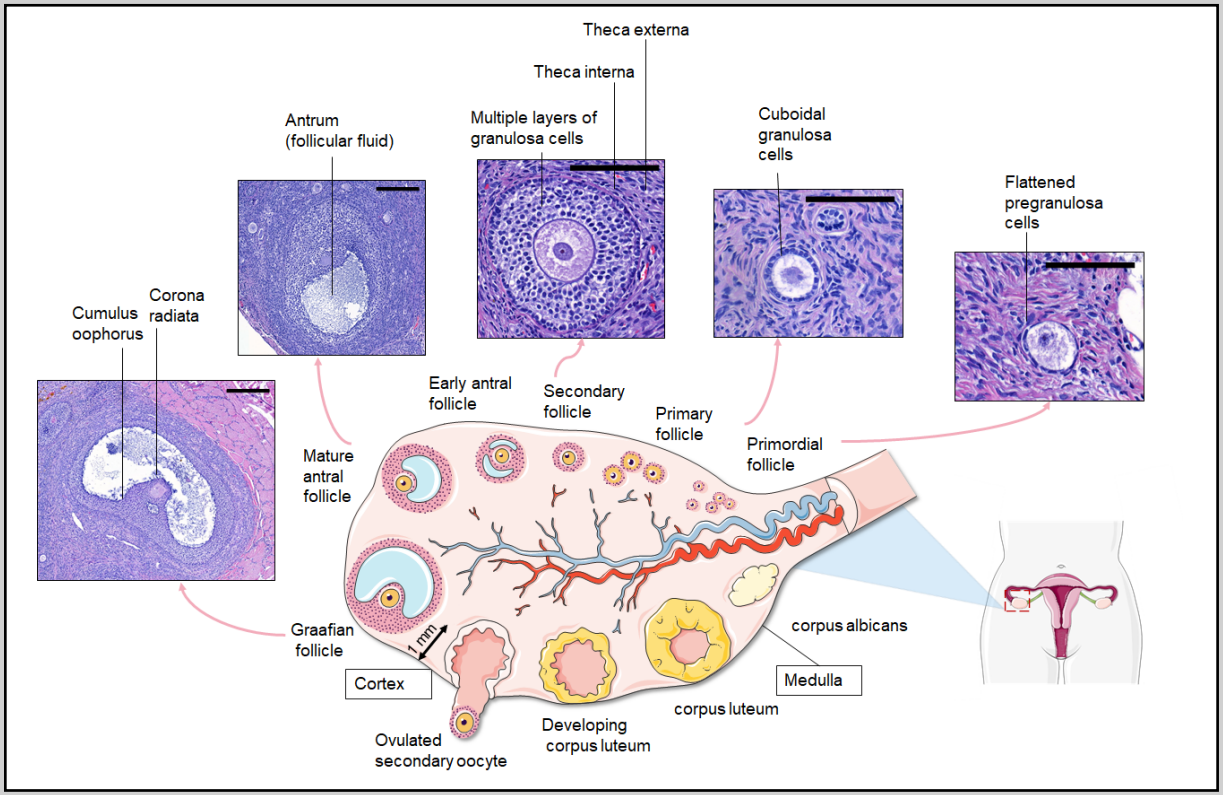


Figure 4 | Folliculogenesis stages. *(Ouni, Unpublished)*

Follicular activation can also be stimulated via the mammalian target of rapamycin complex (mTORC) (McLaughlin et al. 2011). Recent studies have pointed to the possible initiation of follicle activation in pre-granulosa cells of primordial follicles through phosphorylated mitogen-activated protein kinase 3/1 (MAPK3/1), which participates in activating the mTORC pathway and, in return, triggers the KL and c-kit (KL receptor) pathway in oocytes (Zhang and Liu 2015; Zhao et al. 2018). The PI3K pathway is regulated by inhibitory factors, including phosphatase and tensin homolog (PTEN) (Adhikari and Liu 2009; Reddy et al. 2008) and the transcription factor forkhead box O3a (FOXO3a) (Castrillon et al. 2003) (Figure 5). Another intracellular signaling pathway, the Hippo signaling pathway, has been lately implicated in follicle activation (Kawamura et al. 2013; Kawashima and Kawamura 2018). Lessons learned from developmental studies of *Drosophilia* introduce the compression-induced growth suppression principle (Mammoto et al. 2013). Like the follicles in the prepubertal ovarian cortex, densely packed cells undergo fiber actin remodeling, which activates the Hippo pathway and thereby induces the phosphorylation of Yki (the *Drosophila* ortholog of YAP) and arrests the development of these cells. This mechanical feedback of growth is a homeostatic mechanism aiming to suppress local overgrowth and reduces tissue distortion during developmental stages. This mechanism has been found to act on ovarian follicle activation. It may also explain why fragmentation of the ovarian cortex before transplantation or in vitro culture leads to an increased follicle activation by facilitating the conversion of globular actin into filamentous actin thus mechanically disrupting the Hippo signaling pathway (Hsueh and Kawamura 2020; Zhao et al. 2018).

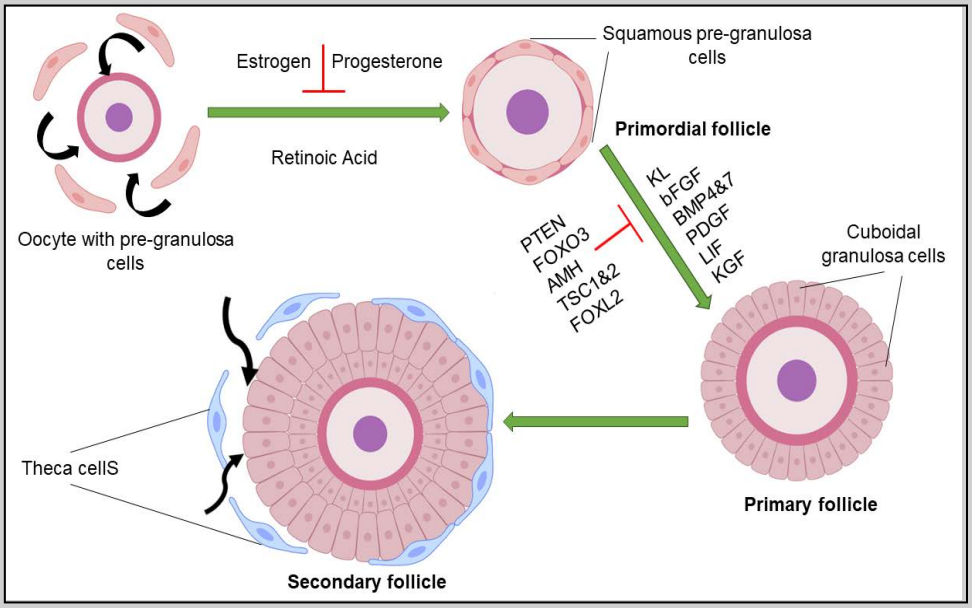


Figure 5 | From follicle activation toward secondary follicle formation. The oocyte under the stimulatory effects of retinoic acid recruits squamous type granulosa cells to form the primordial follicle Steroid hormones (estrogen and progesterone) inhibit the formation of primordial follicles. Under the activating effects of kit ligand, basic fibroblast growth factor (bFGF), bone morphogenetic proteins 4 and 7 (BMP-4 and -7), platelet derived growth factor (PDGF), leukemia inhibitory factor (LIF) and keratinocyte growth factor (KGF), the primordial follicle further develops into the primary follicle with accompanying morphological changes of the supportive cells, from a monolayer of squamous type granulosa cells to cuboidal type. Theca cells then surround the now multiple layers of granulosa cells which encloses the developing oocyte to form the secondary follicle. Repressive signals like phosphatase and tensin homolog (PTEN), FOXO3 and anti-Mullerian hormone (AMH), tuberous sclerosis complexes (TSC) 1 and 2 and FOXL2 inhibits the development of primordial follicles to secondary follicles. *(Ouni, Unpublished).*

Several other factors have been shown to activate primordial follicles. Bone morphogenetic proteins 4 and 7 (BMP4 and BMP7), members of the transforming growth factor β (TGFβ) family, have been linked to early follicular development. Leukemia inhibitory factor (LIF) and fibroblast growth factor (bFGF or FGF2) also appear to stimulate the primordial to primary transition in various species (Skinner 2005). Conversely, there are essential inhibitory factors present in the ovary that control the primordial activation rate. One of them is the AMH. Like BMPs, AMH is a member of the TGFβ superfamily, but one of its key roles appears to be the suppression of primordial follicle recruitment (Carlsson et al. 2006; Durlinger et al. 2002; Yang et al. 2017). AMH is produced by granulosa cells in preantral and small antral follicles, with a sharp decline in larger antral ones (Jeppesen et al. 2013). Indeed, AMH produced by the cohort of growing preantral and early antral follicles may inhibit the growth of neighboring primordial follicles, restricting the number of activated ones at any given time. Moreover, AMH can also suppress activation indirectly by reducing the expression of KL and FGF2 (Skinner 2005).

I.3.2.2. Initial growth

This stage of folliculogenesis takes several months and represents a slow growth phase during which development from primary (50-100 µm in diameter) to secondary (120 -200 µm in diameter) and then tertiary (2-5 mm in diameter) follicles occurs. It is characterized by the expression of FSH-receptor (FSHR) in granulosa cells and LH-receptor (LHR) in theca cells. Although early preantral follicles are independent of FSH for their initial growth, FSH receptors are present on the granulosa cells of these follicles (Adriaens et al. 2004; Gougeon 1996).

Following activation and progression to the primary stage, the development into the secondary or preantral follicle, requires further oocyte growth, the proliferation of granulosa cells, and the formation of theca cells. At this point, the dimeric protein activin (a member of the TGFβ superfamily) promotes granulosa cell responsiveness to FSH, resulting in further follicular growth dependant on gonadotrophins (Knight et al. 2012). Growth differentiation factor 9 (GDF9) and BMP15 are expressed by oocytes and essential to developing growing follicles (Wijayarathna and de Kretser 2016). They work synergistically to regulate cell proliferation within follicles and govern KL expression. Downregulation of AMH expression as follicles grow coincides with equivalent upregulation of aromatase expression, and hence, their capacity to produce estradiol (Jeppesen et al. 2013). Thus, AMH actions may be stage-dependent, directly promoting preantral follicle growth while inhibiting antral follicle maturation and dominant follicle selection (Xu et al. 2016). Therefore, serum AMH levels are used as a biomarker to determine the size of the ovarian reserve and a predictor of the reproductive lifespan. Its serum levels reach a peak around 24-25 years of age and then progressively decline (Kelsey et al. 2012).

Other promoters of follicular development have been continuously discovered, such as C1q/tumor necrosis factor-related protein 3 (C1QTNF3), which have been recently shown to induce proliferation of granulosa cells in human follicles, from primary to antral stage, and protect them from apoptosis (Gershon and Dekel 2020).

I.3.2.3. Selection, maturation of the dominant follicle and ovulation

During the growth process, follicles become progressively more dependent on gonadotropins for continued development and survival. When the antrum is created out of follicular fluid secreted by granulosa cells, further follicle

development becomes entirely FSH-dependent, promoting granulosa cell proliferation and differentiation, allowing the follicle to increase its volume. At this stage, granulosa cells can be classified into two groups: cumulus cells surrounding the oocyte and promoting its maturation; and mural granulosa cells around the outer portions of the follicle producing sex steroids. An antral follicle will only become preovulatory if both its granulosa cells and theca cells express LH receptors at the time of LH surge that leads to ovulation. The effect of the LH surge is mediated through epidermal growth factor family members, including epiregulin and amphiregulin produced by mural granulosa cells and acting on the cumulus (Hsieh et al. 2007). The oocyte plays a leading role in regulating the dominant follicle selection process and subsequent ovulation (Matzuk and Li 2013). The ovulatory follicle is approximately 10-12 mm in diameter and can be accurately monitored by ultrasound.

I.4. Menopause

Continuous follicular development, arrest, and germ cell loss are ongoing processes that occur during a period spanning over 50 years. The ovarian germ cell population is inevitably lost through the process of atresia during reproductive life and exhausted upon menopause. Calculations of the expected rate of loss of germ cells during regular cyclic menses have suggested that this is dramatically accelerated during the decade prior to menopause (Hertig 1944). It has been suggested that follicles remaining until the end of reproductive life may be less responsive to gonadotropin stimulation. The age of menopause onset is related to the size of the primordial follicle population at its peak during embryo development at 18- 22 weeks of gestation (Wallace and Kelsey 2010). A lower prenatal peak number of primordial follicles correlates with an early menopause onset and *vice versa.*

Menopause is defined by amenorrhea for at least one year. On a physiological level, menopause reveals itself in the loss of the ability to conceive, disturbed thermoregulation (hot flushes), high risk of cardiovascular diseases and osteoporosis, among others (Davis et al. 2015) (Figure 6). On an endocrine level, changes in the hormonal profile are observed, such as elevated FSH levels and reduced serum estrogen and AMH concentrations. With the exhaustion of the follicular pool following menopause, ovarian estrogen and progesterone production ends, which results in the cessation of cyclic uterine endometrial bleeding (Figure 6). Pituitary FSH secretion rises prior to menopause due to deficient estrogen and inhibin secretion by the granulosa cells. FSH levels continue to rise withfollicular depletion and reach a peak around 130 mIU/ml, 1-3 years after LH levels also rise, but not to the same degree, reaching an average serum concentration of 90 mIU/ml.

With the loss of the follicular pool, the postmenopausal ovarian cortex becomes markedly reduced in size. In contrast, the ovarian stroma becomes dominant, with prominent interstitial cells. In the absence of ovarian follicles, elevated gonadotropin levels maintain stimulation to the remaining stromal tissue.

Following menopause, serum testosterone levels do not decline, and ovarian testosterone secretion may be increased relative to the premenopausal ovary. However, androstenedione levels, derived equally from the ovary and the adrenal gland before the menopause, decrease by 50% following menopause (Judd 1976).

On a molecular level, changes in the ovary following menopause onset are less known. However, a recent study on ovary aging in non-human primates suggested oxidative stress as a key player (Wang et al. 2020). The subsequent analysis of human granulosa cells suggested similar

mechanisms at play during the process of human ovarian aging: granulosa cells isolated from follicular fluid showed aging-associated decrease in antioxidant activity and an increase in oxidative stress induced damage (Wang et al. 2020).

Although the existence of ovarian stem cells in the aging ovary as well as their possible valorisation for menopause reversal and fertility restoration had been disputed for many years, recently single-cell analysis of cellular populations in the human ovary gave more insights into the topic (Wagner et al. 2020). Indeed, there are no germline stem cells in adult human ovaries, reinforcing the dogma of a limited ovarian reserve.

Age is a natural cause of menopause. However, the early onset of menopause can be caused by premature ovarian insufficiency. The origins of premature ovarian insufficiency are manifold, including diabetes mellitus, autoimmune disorders, polycystic ovarian syndrome and chemical insults like smoking and anti-cancer treatment.

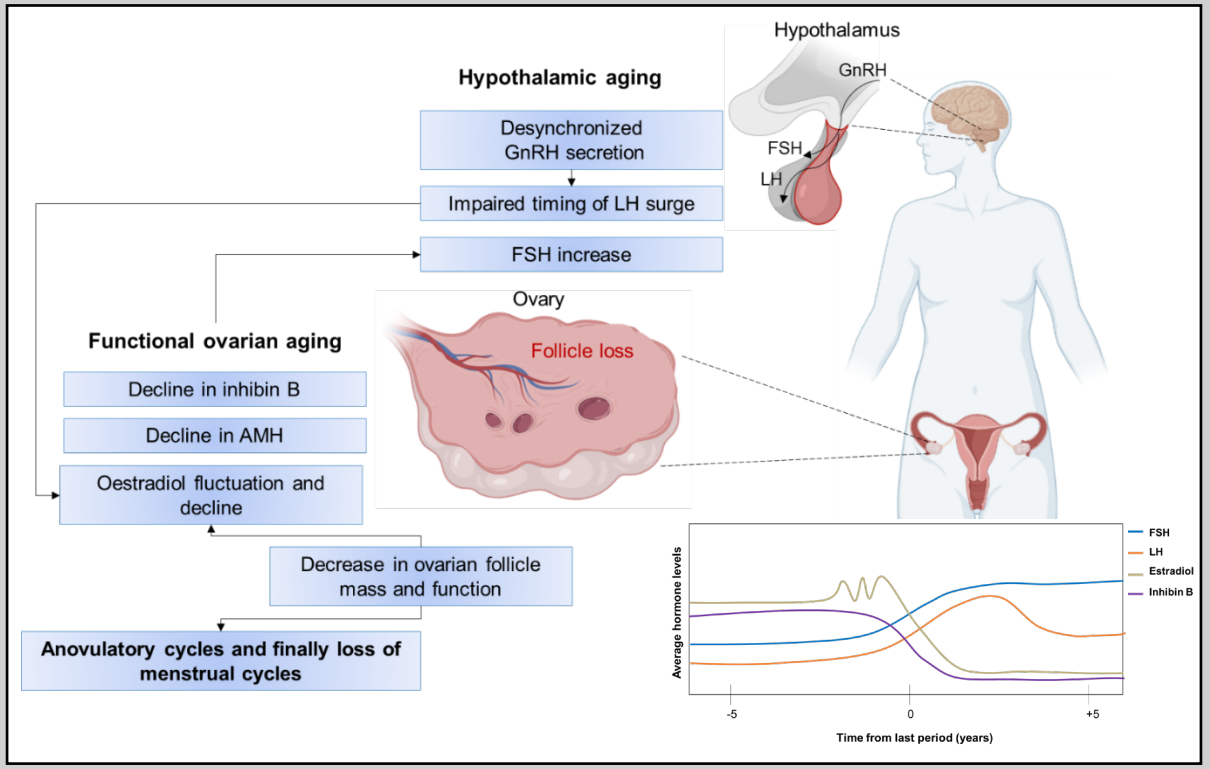


Figure 6 | Hypothalamic and ovarian function at menopause. *(Ouni, Unpublished).*

II. Cryopreservation and transplantation of ovarian tissue as a strategy to preserve fertility in cancer patients

The loss of fertility and early menopause are common after gonadotoxic therapies and radical pelvic surgery. This loss of ovarian function, in addition to primary infertility and amenorrhoea, can have far-reaching clinical and psychological effects such as failure to develop secondary sexual characteristics in young girls, loss of self-confidence, depression, and an increased risk of osteoporosis and heart disease (Campbell et al. 2014). The strategy of ovarian tissue cryopreservation and auto-transplantation was introduced to prevent this significant health quality burden. Ovarian transplantation with cryopreserved ovarian tissue has gone through a remarkable evolution in the last 20 years.

Ovarian tissue cryopreservation emerged as an experimental option to safeguard ovarian tissue and its follicle reserve. It is currently the only pre-treatment fertility preservation option for prepubertal children and patients who cannot delay life-saving therapy (Wallace et al. 2005). Invasiveness of procedures, inability to delay treatment, and high costs are often barriers to standard fertility preservation, particularly for adolescents (Wallace et al. 2005).

II.1. A brief history of ovarian tissue cryopreservation

During the 1950s, cryopreservation studies started mainly using ovaries from laboratory animals. The efforts were largely abandoned until the 1990s because of poor results deriving from the lack of effective cryoprotectants and freezing protocols. In fact, until the 1970s, the only available cryoprotectant was glycerol, which was initially used for sperm freezing in the field of reproduction (Marin et al. 2020). When utilized for ovarian tissue freezing, glycerol proved to be ineffective because only about 10% of the

primordial follicles survived thawing (Parrott 1960). In the 1970s, more effective cryoprotectants, including propanediol, ethylene glycol, and dimethyl sulfoxide (DMSO) were discovered, opening the door for advancements in ovarian tissue cryopreservation (Newton et al. 1996; Oktay 2001). The first transplantation procedures of frozen-thawed sheep ovaries during 1970s were unsuccessful due to the complexity of the surgical act and subsequent post-surgery complications. In the 1990s, ovarian tissue cryopreservation and transplantation studies were repeated in rodents using small pieces of the ovarian cortex (~1mm) and modern cryoprotectants, resulting in restoration of ovarian endocrine function and fertility (Cox et al. 1996; Harp et al. 1994; Sztein et al. 1998) (Figure 7).

Despite the promising results in rodent ovaries, human counterparts are very different, as they are much larger and more fibrous. A closer model is the ovary of mono-ovulatory large animal species, such as sheep, cow and goat. Using ovine ovaries and DMSO as the cryoprotectant, the first pregnancies from large animal models after ovarian transplantation were reported in 1994, one from a fresh transplant and another from a frozen-thawed graft (Gosden et al. 1994). These studies also showed significant revascularisation of the frozen-thawed graft and follicle growth.

After these successful results, several groups described promising findings with human ovarian tissue freezing using up-to-date cryoprotectants. Hovatta et al. (1996) reported that human primordial follicles could survive reasonably well using DMSO and propanediol-sucrose as cryoprotectants (Hovatta et al. 1996). Oktay et al. (1997) also demonstrated that human primordial follicles could survive and remain viable after freezing and thawing of ovarian tissue using ethylene glycol. In 2004, Donnez et al. reported the first live birth after cryopreservation and transplantation of human ovarian tissue (Figure 7).

From then on, pregnancy and live birth rates have continued to climb steadily,

showing an exponential increase in the last years (Dolmans and Donnez 2021).

Currently, more than 200 live births have been reported (Dolmans et al. 2020). Based on these successful results, ovarian tissue cryopreservation and transplantation is no longer considered to be an experimental procedure in a growing number of countries (Nahata et al. 2020). Based on cumulative evidence, the most recent guideline published by the American Society for Reproductive Medicine (ASRM) states that this approach is an "acceptable fertility preservation technique and is no longer considered experimental". This label change will certainly have implications on the clinical practice.

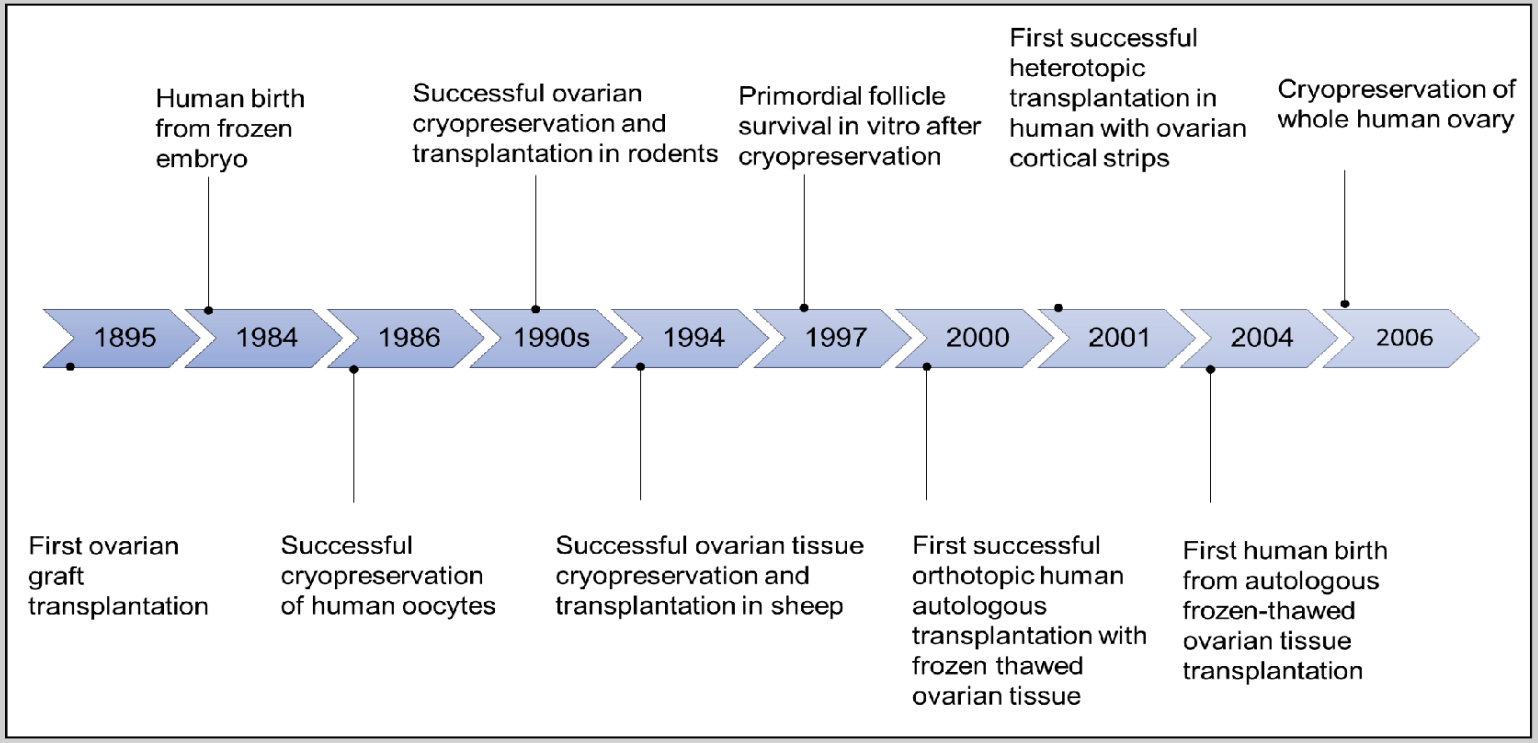


Figure 7 | Major milestones in cryopreservation in the context of fertility restoration. *(Ouni, Unpublished).*

II.3. Transplantation of cryopreserved ovarian tissue

Orthotopic transplantation of ovarian tissue is defined as the surgical procedure in which the ovarian graft is transplanted back to the pelvic cavity where ovaries naturally reside. It involves the grafting of the ovarian cortex near the ovary primary blood supply, to the exposed ovarian medulla(if at least one ovary is still present) or reimplanted inside a specially created peritoneal window (Donnez et al. 2006). This approach exploits the existing ovarian vascular system to restore perfusion and function to the grafted tissue. It has the great advantage of allowing natural pregnancy if the fallopian tubes are intact. Transplantation can be performed using laparoscopy or mini-laparotomy approaches.

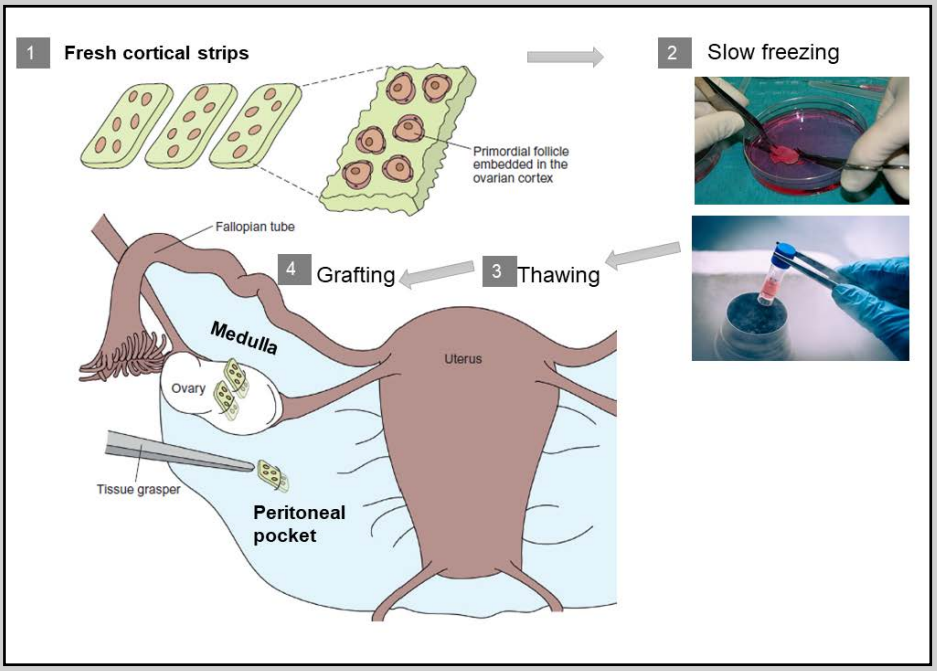


Figure 8 | Transplantation techniques of frozen – thawed ovarian tissue. *(Ouni, Unpublished).*

As recently reviewed by Donnez and Dolmans, the gonadotoxicity of cancer treatments depends on multiple factors, such as the ovarian reserve, patient age at the time of treatment, administered therapies (chemo- and/or radiotherapy) and their doses and duration (Dolmans and Donnez 2021). Given the limited lifespan of ovarian tissue grafts, transplantation should be postponed until the patient is ready to conceive or begins to experience symptoms of ovarian insufficiency. The patient should be in remission from the disease, have support from oncology to proceed with the transplantation and pregnancy, and may benefit from a consultation with a perinatologist or high-risk obstetrics specialist to discuss the potential perinatal complications unique to cancer survivors. Depending on the amount of tissue that has been cryopreserved, it may be possible to reserve a portion of the tissue for future transplants if the primary graft fails.

It is crucial to bear in mind that a fundamental variable that influences the success of the transplantation and strongly determines the graft lifespan is the number of viable primordial follicles after ovarian tissue freezing and thawing. While ovarian tissue transplantation has yielded the recovery of ovarian function and fertility, it has also been reported to significantly decrease follicle population due to early post-transplantation hypoxia which remains an issue because of its negative impact on follicle survival (Van Eyck et al. 2009; Van Eyck et al. 2010), with follicle loss of >50% often observed during the first few days post-grafting (Baird et al. 1999; Kim 2006). Our laboratory is currently developing new strategies to counter or at least limit these caveats (Cacciottola et al. 2020; Dolmans et al. 2019a).

III. The transplantable artificial ovary (TAO)

Fertility preservation remains a challenge, particularly in hematologic cancers (Hodgkin's lymphoma, non-Hodgkin's lymphoma, and leukemia), neuroblastoma, and breast cancer with high metastatic spread to the ovary. For the concerned patients, there is a risk of reimplanting malignant cells together with the frozen-thawed autologous tissue, so this strategy is not recommended. A safer approach involves grafting isolated preantral follicles, mainly primordial and primary ones, obtained from frozen-thawed tissue and their subsequent embedding inside a 3D scaffold that mimic their native environment, along with fresh stromal cells and endothelial cells retrieved from the patient after cancer remission. The ensemble can be transplanted to restore the patient's fertility. In this artificial organ, isolated human follicles are intended to survive and resume their growth in vivo, as it would occur if they would have been enclosed in a fragment of ovarian tissue (Figure 9).

Primordial and primary follicles were chosen because they represent more than 90% of the total follicle population in the ovary and are the most cryoresistant class of follicles (Shaw et al. 2000). As they are surrounded by a basement membrane that protects them from contact with capillaries, white blood cells, and nerve processes, by isolating follicles, the transplantable artificial ovary ensures that no malignant cells are returned to the patient. After mechano-enzymatic isolation, both follicles and cells can be found in the isolate suspension, so during pick-up of isolated follicles to embed inside the artificial ovary, malignant cells may also be present.

As the artificial ovary goal is to avoid the reintroduction of malignant cells that could potentially reside in transplanted ovarian tissue, it is essential to prevent any possible contamination during follicle pick-up and embedding.

Soares et al. (2015) therefore devised a washing step whereby isolated follicles were transferred three times from one medium droplet to another to separate them from surrounding isolated cells. Such a small modification to the original protocol was enough to wash away leukemic cells (Soares et al. 2017). All suspensions containing washed isolated follicles were tested negative for leukemic cells with PCR, giving leukemia patients genuine hope of fertility restoration. This provides further reassurance about the safety of the bioengineered TAO.

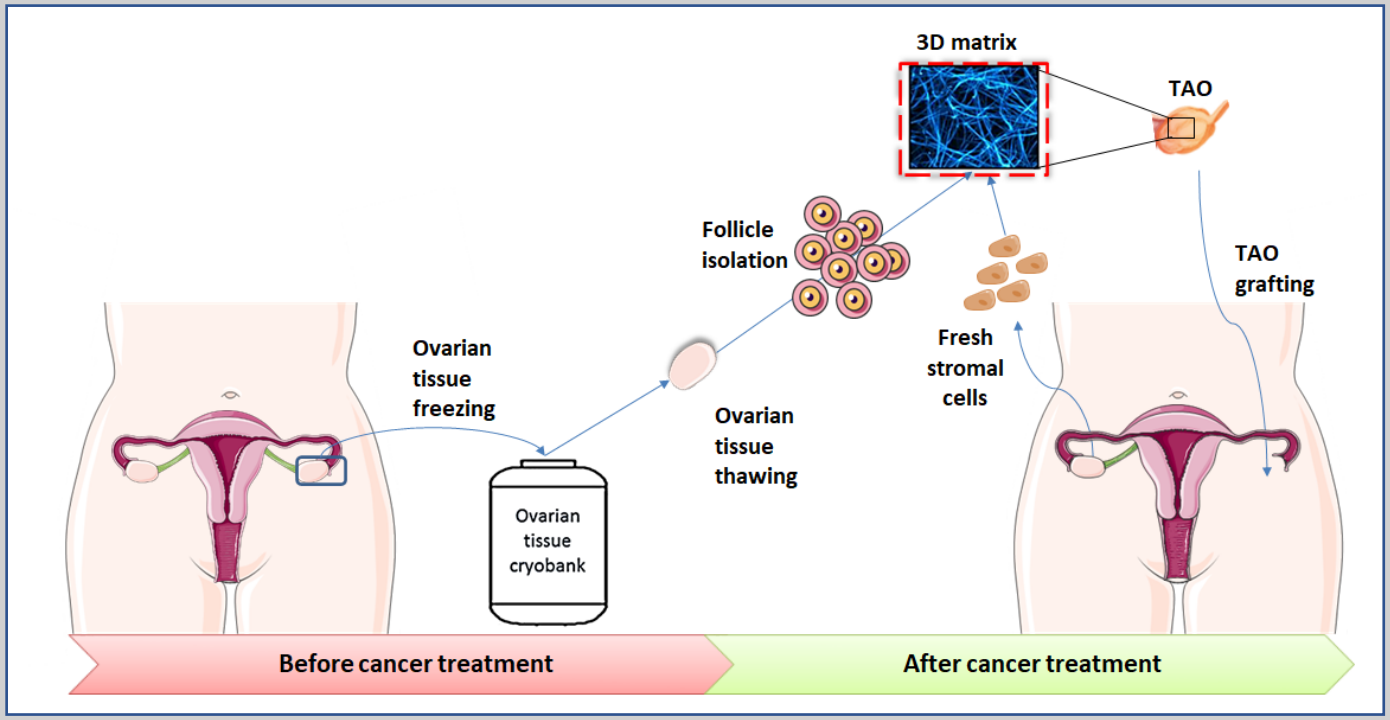


Figure 9 | Design of fertility restoration using the transplantable artificial ovary (TAO).
(Drawing by Ouni).

CHAPTER 2

Learning from mother nature:

a roadmap to construct a biomimetic TAO

I. TAO strategy

I.1. Cellular population

While the main players in creating a TAO are isolated preantral follicles, integration of cells in the construct may be fundamental to achieving complete folliculogenesis and improving ovarian regeneration. Indeed, several studies have highlighted the impact of ovarian cell number and spatial distribution in an engineered ovary and how they play a key role in follicle development (Da Silva-Buttkus et al. 2009; Gaytan et al. 2015; Hornick et al. 2013).

I.1.1. Stromal cells

Prof. Gosden's studies have provided the first evidence of the role of ovarian stromal cells in an engineered TAO (Gosden 1990; Telfer et al. 1990). Indeed, stromal cells can synthesize numerous factors that regulate primordial follicle activation. In turn, granulosa cells and oocytes from growing primary follicles will secrete growth factors to recruit and differentiate cells from the ovarian stromal compartment into theca cells (Honda et al. 2007; Orisaka et al. 2006), which is essential for further follicle development. Stromal cells synthesize extracellular matrix (ECM) and can also contribute to matrix degradation, forming an ovary-like structure (Dath et al. 2011).

In practice, autologous stromal cells can be easily isolated from fresh or frozen-thawed ovarian tissue biopsies (Soares et al. 2015). The safest option is to harvest them from ovarian samples when the patient is disease-free, i.e., after cancer treatment, so there is no risk of malignant cell contamination in the engineered ovary. However, it is possible that some patients may not have any remaining ovarian tissue to collect these cells. In such cases, stromal cells can be retrieved from tissue samples cryopreserved before

chemo- or radiotherapy and isolated after follicle pick-up (Chiti et al. 2017b; Paulini et al. 2016). Still, a purging step is paramount to avoid any possible malignant cell contamination (Mouloungui et al. 2018; Schroder et al. 2004).

I.1.2. Endothelial cells

Vascularization is the cornerstone essential for the survival of a fully functional tissue-engineered organ after transplantation. Vascularization in the TAO can initially be induced by isolated endothelial cells encapsulated in the matrix. Our first evidence that endothelial cells isolated from ovarian tissue play a significant role in the engineered ovary came from Dath et al. (Dath et al. 2011). After comparing grafts containing isolated stromal cells with or without endothelial cells, they observed a larger grafted area showing an impressive number of vessels as early as one week after transplantation in the presence of endothelial cells (Dath et al. 2011). Our team subsequently assessed the influence of endothelial cell concentrations on vessel area and demonstrated a positive correlation between the number of grafted isolated cells and vascularization after 7 days of xenografting to immunodeficient mice (Soares et al. 2015). In practice, as endothelial cell concentrations are relatively low in the ovarian cortex, we could consider isolating these cells from the medullary layer, as suggested by Soares et al. (2015).

I.1.3. Other ovarian cell populations

While it is known that human ovaries contain a vast majority of stromal cells, followed by endothelial cells (Kinnear et al. 2020), it was only recently that in-depth characterization of cell populations was undertaken in human ovarian tissue (Wagner et al. 2020). Wagner et al. (2020) identified and calculated the proportions of different subpopulations of cells in the cortical layer of human ovaries. Stromal, endothelial, and perivascular cells correspond to around 83%, 5%, and 10% of cells in the ovarian cortex, respectively, while macrophages and T-cells account for approximately 0.5%.

These findings are essential for the development of an engineered TAO. For instance, macrophages play a role in matrix remodeling and synthesize growth factors and cytokines (Wu et al. 2004). Moreover, M1 macrophages appear to be implicated in folliculogenesis in mouse ovaries (Ono et al. 2018), while M2 macrophages are involved in tissue repair through the synthesis of anti-inflammatory cytokines, such as VEGF and TGFβ (Sica et al. 2015). Interestingly, these authors did not find a population of germline stem cells, a somewhat contentious finding by Tilly's group (Martin et al. 2019; Woods and Tilly 2013). Analysis of the inner cortical layer of human ovaries revealed clusters of stromal, endothelial, theca, immune, smooth muscle and granulosa cells (Fan et al. 2019).

In summary, ovarian cells represent an integral unit of a functional TAO promoting angiogenesis, follicular survival and development, and structural support.

Nevertheless, at present, no consensus has been reached describing the most appropriate amount of ovarian cells that need to be embedded in the TAO and their spatial distribution and localization to ensure proper follicular development and fast neovascularization. Indeed, if only a few ovarian cells are introduced, they risk being far apart from each other and follicles, without correct cell-cell interactions. In contrast, if a large number of cells are added, there is a risk of starving the follicles of oxygen and nutrients, leading to apoptosis (Amorim 2016; Tagler et al. 2011). Moreover, cell signaling appears to be influenced by follicle communication and organization (Faire et al. 2015; Quan et al. 2020).

I.2. Physical support

A myriad of biomaterials for supporting the different ovarian cell populations has been tested in vitro and in vivo during the last five years.

Since the TAO will be grafted in the human body, the choice of the biomaterial should take into consideration several requirements. For instance, it should provide protection and support for the isolated follicles during transplantation, be biocompatible and biodegradable to allow follicle development and vessel formation to provide oxygen and nutrients to cells for successful grafting (Amorim and Shikanov 2016; Laronda et al. 2017; Vanacker et al. 2012).

One of the critical steps in developing a TAO is finding the right biomaterial to encapsulate isolated ovarian preantral follicles. Different hydrogels have been used for the transplantation of isolated follicles in an effort to enhance efficacy (Kniazeva et al. 2015; Luyckx et al. 2014; Paulini et al. 2016; Vanacker et al. 2014). Despite significant advances, we still have not identified the best matrix to support complete human folliculogenesis. Indeed, our knowledge of human ovarian tissue remains incomplete, and considerable differences emerged when murine and human follicles were transplanted inside a TAO prototype (Pors et al. 2019). Therefore, in this section, we will first briefly mention the general features of a 3D matrix for isolated preantral follicles and then discuss the main findings obtained from murine and human ovarian follicles in various *in vivo* studies.

Irrespective of the nature of the matrix (biological, synthetic, or hybrid), there are crucial points to consider before selecting one material over another. First of all, we must look at biocompatibility and biodegradability. These features are usually closely interconnected. Greater biocompatibility and biodegradability have been demonstrated with natural polymers (ie., collagen, gelatin, alginate, fibrin, decellularized ECM) because cell metalloproteinases cleave them without producing toxic compounds that may affect cell survival (Caliari and Burdick 2016; Yoon and Fisher 2009). Indeed,

broader application of biological matrices rather than synthetic scaffolds is documented in the literature (Amorim and Shikanov 2016). Besides, natural hydrogels like collagen or fibrin provide better cell adhesion than their synthetic counterparts thanks to the presence of peptides containing arginine-glycine-aspartate (RGD) sequences involved in integrin binding on cell surfaces. The architecture of the hydrogel's structure, as well as its viscoelastic properties and biochemical constitution, are also key elements. The composition and porosity of the network will determine the rate at which nutrients, gas and metabolic waste move through the hydrogel and how follicle survival and development are affected. Indeed, it has already been demonstrated that scaffold controlled microporous geometry can impact mouse follicle survival, growth, and maturation (Laronda et al. 2017).

The ovarian environment is highly dynamic. Once activated, human ovarian follicles increase in size up to 600X during growth and release various proteases essential to modifying their surrounding ovarian ECM and generating a more acquiescent milieu for their complete development. A hydrogel's viscoelastic properties are, therefore, essential parameters to consider in the matrix choice. In this context, the ideal matrix should be rigid enough to mimic the stiffness of the collagen-rich ovarian cortex in the first few days post-transplantation but then provide enough elasticity to allow complete follicle growth and protease degradation.

A more challenging goal is mimicking the native biochemical ovarian environment. Since our knowledge of the biochemical composition of ovarian tissue is still in its infancy, a complete characterization of the ovarian follicle microenvironment is a primordial step to design a TAO resembling the native tissue.

II. Developing TAO three-dimensional matrix

II.1. Scaffolds tested to replace the native ovarian ECM

II.1.1. Synthetic scaffolds

II.1.1.1. Poly (ethylene) glycol

Among synthetic scaffold materials, polyethylene glycol (PEG) is currently the only one being investigated. It is a linear-chained polymer consisting of a simple oxygen-carbon-carbon repeating unit. One of its most significant advantages is its ability to be crosslinked with other polymers in order to create complex matrices with specific and controlled properties, such as degradation rate or adhesion capacity (Amorim and Shikanov 2016).

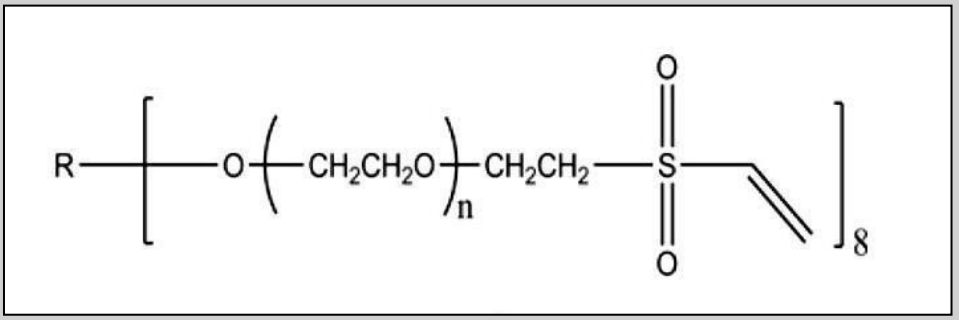


Figure 10 | Structure of PEG-vinyl sulfone (PEG-VS).

In the only study testing PEG, partially isolated mouse preantral follicles were encapsulated in a PEG-vinyl sulfone (PEG-VS) matrix combined with integrin-binding peptides like Arg-Gly-Asp (RGD), essential to driving cell-matrix interaction (Kim et al. 2016) (Figure 10). PEG-VS was then crosslinked with protease-sensitive peptides to enable cell-driven degradation and matrix remodeling after grafting to immunocompromised mice. After 30 days of transplantation, multiple antral follicles, corpora lutea, and reduced FSH levels were recorded, proving that an artificial ovary prototype based on

PEG was able to support folliculogenesis and steroidogenesis. Moreover, on day 60, around 60% of primordial and primary follicles were still detected in the graft, proving selective follicle recruitment over time (Kim et al. 2016). Despite these promising results, one can argue that these findings were due to the remaining attached stromal cells surrounding primordial follicles before their transplantation, which have been previously shown to play an important role in follicle survival during in vitro culture (Telfer et al. 2008).

II.1.2. Natural scaffolds

II.1.2.1. Plasma clots

Plasma clots have been successfully used as a biomaterial to transplant cells because they are an autologous material with no allogeneic and xenogeneic factors. Thanks to their excellent biocompatibility and rich composition of growth factors, plasma clots promote cell adhesion, proliferation, and differentiation (Seybold et al. 2010). Autologous plasma clots are usually derived from centrifuged venous blood, followed by polymerization initiation by touching the liquid's surface with a sterile needle or in the presence of calcium chloride (Gosden 1990). Complete polymerization of the clot then occurs at 37°C for around 30 minutes. Gosden et al. (1990) were the first group to use plasma clots as natural scaffolds to assemble and transplant an artificial ovary prototype in sterile mice. They have enzymatically digested fresh mouse ovaries, which were then encapsulated inside mouse plasma drops. After plasma polymerization and grafting beneath the ovarian bursa of sterile mice. This procedure proved that digested ovaries are able to reassemble themselves into an ovary-like structure, with a full restoration of endocrine and reproductive functions in mice. Later on, Dolmans et al. used autologous plasma clot to encapsulate human preantral follicles, which were then xenografted to the ovarian bursa of immunodeficient mice. These

authors observed that after one week of transplantation, follicles were able to survive and develop up to the secondary stage (Dolmans et al. 2007), while after five months, antral follicles could also be found in the grafts (Dolmans et al. 2008).

II.1.2.2. Collagen

Since collagen is the most abundant protein type in the human body, it has been applied in several tissue engineering applications (Parenteau-Bareil et al. 2010). In addition, thanks to its biocompatibility and low immunogenicity, it would be logical to assume that collagen is a promising candidate for constructing an artificial ovary. One of the first studies on the grafting of isolated follicles was performed by Telfer et al. (1990), who used collagen as a matrix to encapsulate murine follicles. The authors isolated preantral follicles from murine ovaries, encapsulated them in collagen gel, and in vitro-cultured them for seven days before allotransplantation to the kidney capsule of female hosts. Embryos were obtained following in vitro fertilization of oocytes recovered from large antral follicles, after 10 days of grafting.Despite these promising results, no other studies investigated collagen for isolated follicle transplantation.

II.1.2.3. Gelatin

Collagen-derived gelatin contains cell adhesion sites and soft, yet durable, mechanical properties that would be favorable to use as a matrix of an artificial ovary (Young et al. 2005). Due to its biocompatibility, degradability and applicability in 3D bioprinting, a gelatin ink was developed by Laronda group (Laronda et al. 2017). Gelatin print was obtained by manipulating the ink temperature to one in-between the liquid (>33 °C) and fully crosslinked gel (<25 °C) state.

As the amount of scaffold interaction with follicles increased, follicle

spreading was limited, and survival increased. Follicle-seeded scaffolds became highly vascularized, and ovarian function was fully restored when implanted in surgically sterilized mice, resulting in alive pups through natural mating (Laronda et al. 2017). Nevertheless, this was the only experiment using gelatin with ovarian follicles.

II.1.2.4. Alginate

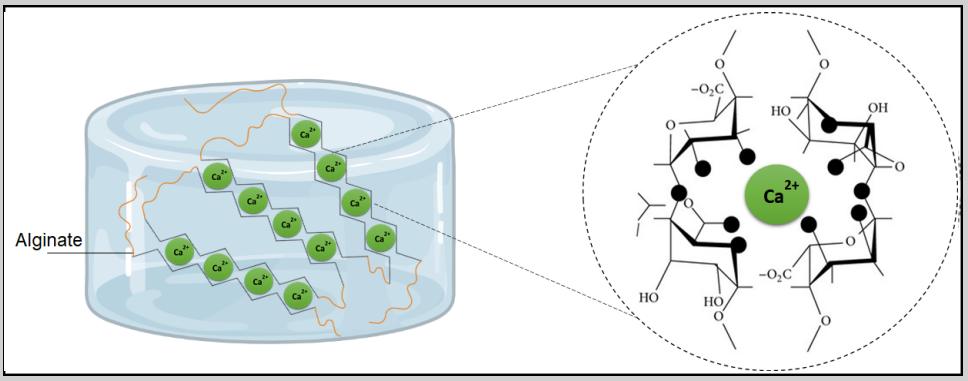


Figure 11 | Alginate crosslinking. Alginate polymers are composed of G (Guluronic acid) and M (Mannuronic acid) blocks. Ionic crosslinking of alginate is formed by the binding of multivalent cations (ie. Calcium) between (G-blocks) on different alginate chains forming and egg-like shape. *(Ouni, Unpublished)*

Alginate is a general term for a polysaccharide family derived from brown seaweed or bacteria. As a water-soluble linear polysaccharide, alginate comprises linear blocks of (1 → 4)-linked β-d-mannuronic acid (M) and α-l-guluronic acid (G) monomers assembled in an egg-like shape (Zhu et al. 2019) (Figure 11).

While alginate was highly applied for in vitro culture of isolated preantral follicles, it was more modestly tested for transplantation purposes (Vanacker and Amorim 2017). Vanacker et al. (2012) first tested this polymer combined with Matrigel to transplant isolated murine ovarian cells.

In order to control matrix degradation, the authors chose alginate lyase-encapsulated poly (lactic-co-glycolic acid) microspheres. After one week of grafting, cell proliferation and formation of tissue-like structures were observed. This matrix was able to degrade, allow vascularization, and elicit a low inflammatory response. In their second study, the same authors replaced their matrix with good manufacturing practice (GMP)-produced sterile lyophilized high mannuronate (SLM)-alginate, since alginate lyase cannot be used in human subjects (Luyckx et al. 2014). After isolation and encapsulation in 1% alginate beads, murine preantral follicles and ovarian cells were autotransplanted for one week. After this period, the authors recovered 20% of grafted follicles at different stages of development, including antral follicles. Despite these positive results, the degradation rate in the alginate matrix was very slow and, consequently, vascularization was observed mainly at the periphery of the graft.

II.1.2.5. Fibrin

Fibrin is a blood component involved in the clotting process. Polymerization of fibrin is initiated with thrombin, and the fibrin gel can be naturally degraded in vivo (Figure 12). This hydrogel is applied in a broad range of procedures due to its valuable properties, such as minimal inflammation, high compatibility and degradation, and angiogenesis promotion (Dietrich and Lelkes 2006; Li et al. 2015). Fibrin degradation rate, rigidity, morphology, and fiber network can be easily modulated by varying fibrinogen and thrombin concentrations (Li et al. 2015). Fibrin was tested to graft isolated mouse and human preantral follicles (Chiti et al. 2017a).

Luyckx et al. first tested numerous fibrinogen-thrombin formulations to achieve an optimal fibrin concentration for human ovarian cells (Luyckx et al. 2013). Then, based on their results, they chose two best formulations that

they used to autograft isolated murine preantral follicles. After one week of transplantation, they recovered 31% of grafted follicles, which were growing up to the antral stage (Luyckx et al. 2014). Moreover, they observed high rates of vascularization, cell proliferation and matrix degradation (Luyckx et al. 2014). These findings were further investigated by Chiti et al., who applied the same experimental design but separated the population of isolated follicles into two different fibrin matrices, one containing primordial and primary follicles, and the other, mainly secondary follicles (Chiti et al. 2016). Interestingly, after one week of grafting, the recovery rate was significantly different between the two groups, demonstrating that smaller preantral follicles are somehow negatively affected by the isolation and/or transplantation procedure (Chiti et al. 2017c). Although softer fibrin formulations have been successfully used to transplant isolated mouse follicles (Chiti et al. 2016; Luyckx et al. 2014), our team experience has shown that isolated human follicles require a stiffer fibrin matrix (higher fibrinogen and thrombin concentrations). After xenografting them inside a fibrin matrix containing increased fibrinogen and thrombin concentrations, follicle recovery rates were 20-35% (Paulini et al. 2016), which is comparable to the results of xenografting of human ovarian tissue (Amorim et al. 2012).

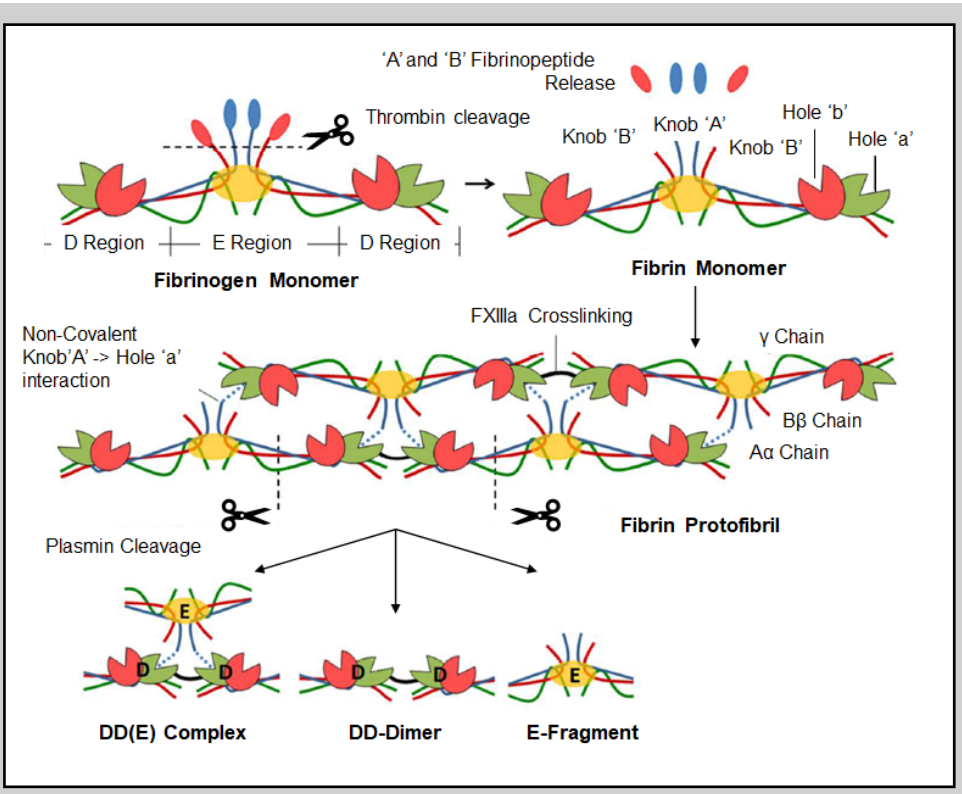


Figure 12 | Fibrin clotting and cleavage. Illustration of the conversion of fibrinogen to fibrin, subsequent assembly of fibrin monomers into a protofibril, and finally, plasmin mediated fibrin degradation and resultant products. Alpha, beta, and gamma chains are depicted in blue, red, and green, respectively. *(Stefanelli and Barker 2015).*

Smith et al. also used a fibrin matrix to graft isolated mouse preantral follicles, but at higher fibrinogen and thrombin concentrations (Smith et al. 2014). They reported a significant increase in the population of secondary and antral follicles after three weeks of transplantation to the ovarian bursa. Moreover, the presence of corpora lutea and decrease in follicle-stimulating hormone levels proved that the grafts were able to restore hormone cyclicity.

In a second study, this group tested their fibrin formulation loaded with VEGF to transplant isolated mouse follicles. This matrix successfully yielded pups (Kniazeva et al. 2015).

II.1.2.6. Decellularized ovary

Decellularization is the process of removing the allogeneic or xenogeneic cellular antigens from a tissue that would initiate an immune response while ideally leaving behind an intact ECM comprising a mixture of structural and functional molecules (Table 1, Figure 13). A few studies have reported decellularization of murine (Alshaikh et al. 2019), porcine (Liu et al. 2017), bovine (Laronda and Woodruff 2017) and human (Hassanpour et al. 2018; Pors et al. 2019) ovarian tissue.

It is important to stress that decellularization protocols have been shown to differently affect matrix architecture and composition, changing concentrations of collagen, GAGs, and elastic fibers (Alshaikh et al. 2019) and leaving behind cytotoxic traces of chemicals used during the decellularization process.

When rodent ovarian cells were seeded in such a matrix, they survived, proliferated, synthesized estradiol (Laronda et al. 2015; Liu et al. 2017), and even induced puberty in mice after grafting (Laronda et al. 2015). This matrix was also successfully tested in the context of isolated mouse follicle transplantation (Pors et al. 2019). When decellularized bovine and human ovarian tissue were used as scaffolds to graft primary murine ovarian cells, the hosts showed higher levels of estradiol and inhibin A, after2–4 weeks of grafting (Laronda et al. 2015).

Table 1| Commercial decellularized scaffolds. *(Ouni, Unpublished).*

Product	Company	Material	Use
AlloDerm	LifeCell	Human skin	Abdominal wall, breast, ENT/head. and neck reconstruction, grafting
CollaMend	Bard	Porcine dermis	Soft tissue repair
MatriStem	ACell, Inc	Porcine urinary bladder	Soft tissue repair and reinforcement, burns, gynecologic
CuffPatch	Arthrotek	Porcine SIS	Reinforcement of soft tissues
Dura-Guard	Synovis Surgical	Bovine pericardium	Spinal and cranial repair
PriMatrix	TEI Biosciences	Fetal bovine skin	Wound management
OrthADAPT	Pegasus Biologicals	Horse pericardium	Reinforcement, repair and reconstruction of soft tissue in orthopedics

Another strategy to take advantage of the biochemical cues of ovarian ECM is its application in the form of decellularized hydrogels. Studies have revealed that these hydrogels can promote de novo formation of functional tissue (Badylak et al. 2011), as they retain their biological regenerative cues (Hoganson et al. 2010). After the decellularization process, numerous ECM proteins from native tissue can be found in the hydrogel. Recently, our team developed a decellularized bovine ovarian ECM hydrogel (Chiti et al. 2020), in which ovarian follicles and cells could easily be seeded. Our preliminary results showed that after 10 days of in vitro culture, preantral follicles remained viable in the hydrogels (Chiti et al. 2020).

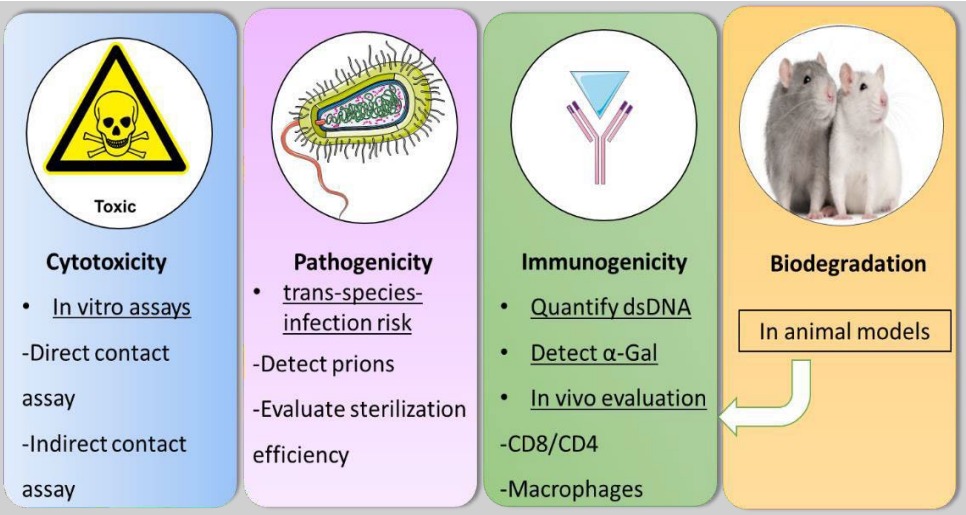


Figure 13 | An exemple of preclinical evaluation of cytotoxicity, immunogenicity and biodegradation of decellularized matrices. *(Ouni, unpublished)*

II.1.2.7. Matrigel

Matrigel is a commercial reconstituted basement membrane derived from extracts of Engelbreth-Holm-Swarm mouse tumors (Kleinman et al. 1986). Although the use of matrigel is not allowed in clinical applications, it is still used in research. Recently, Pors et al. (2019) created scalpel-made pockets in decellularized human ovarian ECM to insert isolated human follicles. However, they did not find any follicles after transplantation to mice. Positive results were achieved only when isolated follicles were embedded in Matrigel before being poured onto the constructs, which demonstrates the positive effect of this hydrogel.

II.1.3. Hybrid scaffolds

In order to improve follicle viability and development, hybrid scaffolds have

been tested, using a combination of different hydrogels.

To increase follicle survival rate after grafting, hyaluronic acid was incorporated into fibrin matrix to encapsulate isolated human preantral follicles (Paulini et al. 2016). However, after one week of xenografting to immunodeficient mice, it did not affect follicle survival or growth. Rajabzadeh et al. enriched their fibrin matrix with platelet lysate since it is known to be a source of growth factors, including angiogenic cytokines (VEGF, platelet-derived growth factor [PDGF], and FGF) (Rajabzadeh et al. 2015). Isolated mouse preantral follicles were encapsulated in fibrin clots with or without different concentrations of platelet lysate and grafted for 14 days. This study revealed that the fibrin matrix with 15% platelet lysate significantly increased the recovery rate of follicles.

II.2. Limitations of used strategies

All the scaffolds mentioned above led to some encouraging outcomes. Although holding tremendous potential, these technologies are primarily proof of concept and remain at the preclinical phase (Figure 13). One possible explanation for why these methods have not advanced further is a reliance on reductionist approaches. In contrast, an effective TAO must authentically recapitulate the complexity of the in vivo ovarian environment. Moreover, each of the used scaffolds presented some limitations hampering its use as a faithful model of ovarian ECM (Table.2).

Ideally, the TAO should offer an appropriate initial environment for follicles that will be gradually replaced by a new 'ovary-like' structure after grafting. While past attempts by our team have demonstrated the feasibility of this concept (Dolmans and Amorim 2019a), they also revealed that the development of an artificial ovary requires more than the utilization of biomaterials and the application of tissue engineering strategies. Indeed, an

essential requirement for reproducing the complex, heterogeneous architecture of a functional ovary is a comprehensive understanding of the composition, architecture, biomechanical properties, and organization of its biological, structural, and functional components, which have not been sufficiently elucidated yet. Thus, to ensure fertility restoration, we need to develop a matrix tailored explicitly to support human ovarian follicles. To do so, it is crucial to first acquire sufficient knowledge of the human ovarian ECM and its interaction with preantral follicles to reproduce them within the TAO.

Table 2 | Biomaterials tested for the encapsulation of ovarian cells and follicles. *(Ouni, Unpublished).*

Scaffold	Limitations	Ref
PEG	Cytotoxicity of photocrosslinkers Neutral composition Poor cell adhesion Poor cell-ECM interaction	(Malmstenet al. 1998; J. Wu et al. 2014)
Plasma clots	Variable composition Variable outcomes Fast degradation rate Follicle loss Weak mechanical properties Delicate structure, difficult to manipulate in the surgery room	(Amorim and Shikanov 2016; Dolmans and Amorim2019b)
Collagen	Limited follicle growth Limited diversity in commercial collagen types (mainly collagen I use) Structural unstability upon hydratation	(Abir et al. 1999; Abir et al. 2001)
Gelatin	Weak mechanical properties	(Lee and Mooney 2001)
Hyaluronic acid	Folliculogenesis disturbance	(Desai et al. 2012)

Alginate	Slow degradation rate Poor cell adhesion Poor cell-ECM interaction Low developmental competence in oocytes derived from follicles encapsulated in alginate	(Huebsch etal. 2010; Laronda et al. 2014; Yin et al. 2016)
Fibrin	Variable batch to batch composition	(Noori et al. 2017)
Decellulari-zed ovary	High pore size leading to follicle loss in non-hydrogel decellularized scaffolds Cytotoxicity of used detergents ECM key molecule degradation during decellularization process Possible graft rejection for some xenograft sources No consensus on optimal decellularization criteria Zoonose risks	(Bilodeau etal. 2020; White et al.2017)

Matrigel	High batch to batch variability Undefined composition Not compliant with clinical use Tumorigenic source	(Caliari and Burdick 2016)
Hybrid scaffolds	Limited control over scaffold topology, rigidity and degradability	(Pina et al. 2019)

II.3.What we know from the native ovarian ECM

II.3.1. Mesoscale organization

The ovary is one of the most dynamic organs in the human body, with a continuously changing organization during women's reproductive life. Preantral follicles are broadly known to be situated in the ovarian cortex and migrate toward the medulla as they grow. There, they encounter a softer, more pliant ECM, allowing their expansion and development. In the last years, an increasing number of researchers has been demonstrating that follicle organization is not random but instead it plays a key role in follicle interactions, development, and regulation (Telfer and Zelinski 2013).

Recently, Quan et al. (2020) analysed growth trajectories of human ovarian follicles and mapped their spatial distribution relative to each others, to articulate the growing follicle landscape in the context of age and previous treatment history, using an existing biospecimen repository of fixed human ovarian tissue. The team reported that in a healthy ovary, a primary follicle is surrounded by around 15 primordial follicles, spaced as close as ~ 100 μm, but within ~ 300 μm radius. They also observed that secondary follicles are separated from other follicles by ~ 200–300 μm. By comparing ovarian tissue from patients who have received cancer treatments with patients who have not, the team found dysregulated follicle growth trajectories in treated patients, similar to the altered follicle growth trajectories observed in a mouse model of physiologic reproductive aging where there is disrupted bidirectional communication between the oocyte and its surrounding granulosa cells (Duncan et al. 2017; El-Hayek et al. 2018).

In a comparable analytical way, Schenck et al. (2021) have found that primordial and transitory follicles (which contain one layer of cuboidal and flattened granulosa cells) lay in a clustered manner in the human ovarian

cortex, with an average cluster radius of ~ 270 μm in the ovarian cortex of 20-35-year-old subjects. Within the same patient cohort, follicle density decreased significantly with age, but the degree of clustering tended to increase as well as the distance of follicles to the nearest neighboring one. This study demonstrated that primordial and transitory follicles lie in different clusters in the human ovarian cortex. With the help of a spatiotemporal computer simulation, the team suggests that interfollicular signals may hinder follicle loss and therefore may drive clustered follicle distribution.

Although these studies have provided a significant insight into the organization of growing follicles within the human ovary, the use of two-dimensional images of histological sections to describe the follicle-spatial distribution, as well as the menstrual cycle stage, may present significant limitations.

II.3.2. Ovarian ECM biochemical composition and turnover

As described in the first chapter, a developing follicle undergoes extensive morphological and biochemical changes during folliculogenesis. At the same time, the composition of the ECM is dynamically remodeled throughout follicle growth, ovulation and atresia. The ovarian ECM has been characterized in several mammalian species, including bovine (Irving-Rodgers et al. 2004; Matti et al. 2010; McArthur et al. 2000; Nguyen et al. 2012; Zhao and Luck 1995), murine (Berkholtz et al. 2006), ovine (Huet et al. 2001; Bellego et al. 2002), and human (Adam et al. 2012; Iwahashi et al. 2000; Nagyova 2015). For the sake of clinical translation of these findings, we will highlight in this section studies reporting human ECM characteristics. Particularly in this specie, perifollicular ECM studies have focused on follicular basement proteins (Rodgers et al. 1999) (Figure 14).

It is now recognized that the unique composition of each basal lamina contributes to its specific functional properties. Basal laminae are composed of a lattice-type network of collagen type IV intertwined with a network of laminin. The follicle is encapsulated by a basal lamina separating it from the surrounding stromal elements in primordial and primary follicles or the theca interna in secondary and antral follicles. In healthy follicles, it excludes capillaries, white blood cells, and nerve processes from the granulosa compartment until ovulation. At this time, the basal lamina is degraded as the follicles develop into corpora lutea. During the process of ovulation, a new hyaluronan-rich matrix critical for fertility forms within the cumulus–oocyte complex tissue, either providing osmotic forces that could be important for follicular fluid formation or filtering soluble materials, which could occur across the follicular basal lamina (Figure 14). Indeed, nutrients, hormones, and other extracellular signals are often required to traverse the matrix in order to reach target cells. The matrix can bind growth factors, including those found in follicles, and regulate their release and activity. For instance, the follicular basal lamina may trap large molecules (e.g. heparan sulfate, perlecan) synthesized by granulosa cells and oocytes in the follicular fluid.

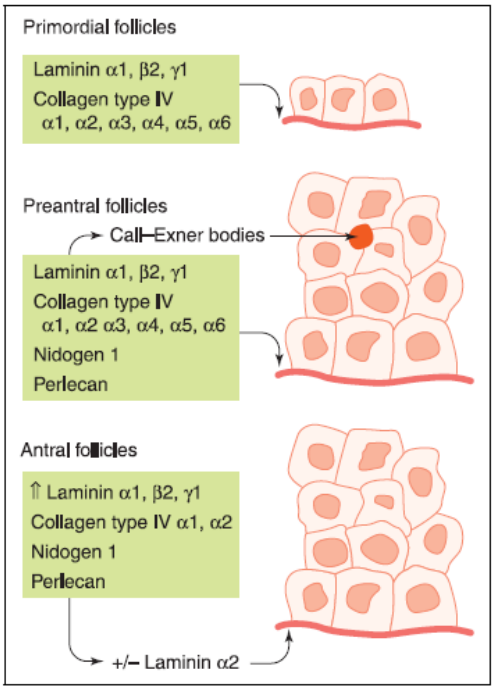


Figure 14 | The components of the follicular basal lamina and the call-exner bodies at different stages of follicular development.

The illustration highlights components produced by granulosa cells (shown on top of the basal lamina). Laminin α2 is probably derived from the theca cells. +/- indicates that Laminin α2 expression is sometimes present and sometimes absent from antral follicles. Call-exner bodies are entities similar in ultrastructure to basal lamina and have been observed within the membrana granulosa of follicles. *(Rodgers et al. 2003).*

The molecular mass cut-off is calculated to be 100–500 kDa based upon comparisons of the composition of follicular fluid with that of plasma (Shalgi et al. 1973). Moreover, the follicular basal lamina is important for maintaining the polarity and the extent of specialization of granulosa cells that align the follicular basal lamina (Luck etal. 1995).

During folliculogenesis, the follicular basal lamina becomes less collagenous and more laminin rich as the follicle extends its surface area. Such basal laminae, by the nature of the different bonds between laminins and collagens, are more expandable, which is required for follicle enlargement (Rodgers et al. 2000; Rodgers et al. 2003). In primordial follicles, nidogen 1 and perlecan

are absent, being expressed later in follicular development (McArthur et al. 2000). Laminin 2 is very unusual; it is expressed only in a few healthy antral follicles (Irving-Rodgers et al. 2002).

Although the composition of the interstitial ECM remained under-investigated, many researchers studied the functional role of the plasminogen activator and matrix metalloproteinase (MMP) systems (Ny et al. 2002). Follicular development, ovulation, formation, regression of corpus luteum and follicular atresia, are processes characterized by dramatic tissue remodeling and angiogenesis that require controlled and targeted proteolysis. Although a definitive functional role for individual matrix degrading proteases in the ovary has yet to be demonstrated, correlative data implicate that members of the plasminogen activator- and MMP- systems may be involved in several of the proteolytic events that take place in the ovary during the reproductive cycle (Curry and Osteen 2001; LeMaire1989) (Figure 15).

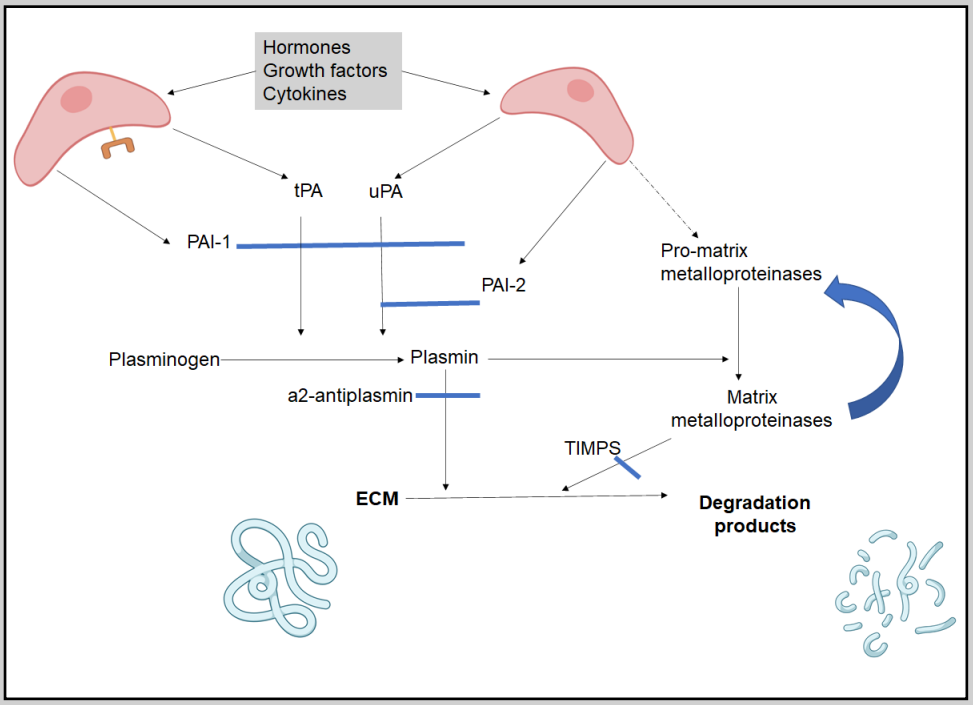


Figure 15 | Potential interactions between the plasminogen activator (PA-) and metalloproteinase (MMP-) systems during ECM remodeling in the ovary. The synthesis of PAs, MMPs and their inhibitors, by specific cells is regulated by hormones, growth factors, and cytokines. The PA-system is a versatile temporally controlled enzymatic system that comprises plasminogen, which is activated to the proteolytic enzyme plasmin by either of the two physiological PAs, tissue-type PA (tPA) or urokinase-type PA (uPA). In the ECM, PA and plasmin activities are controlled by specific inhibitors, PA- inhibitor type 1 (PAI-1), PA- inhibitor type 2 (PAI-2) and α2-antiplasmin, whereas MMP activities are controlled by tissue inhibitors of MMPs (TIMPS).

Binding of uPA and plasmin to cellular binding sites can result in localized proteolytic activity on the cell surface. Activation of proMMPs is also regulated by a positive feedback mechanism in which some active MMPS can activate other proMMPs. Plasmin can degrade some components of the ECM and convert some proMMPs into the active forms which in turn degrade ECM. *(Adapted from Ny et al. 2002).*

II.3.3. The role of mechanical signaling in follicle activation and maturation

Mechanical signaling or mechanotransduction is the process through which mechanical stimuli are translated into biochemical signals affecting gene expression or cellular signaling. The role of mechanical signaling in the ovary has attracted a lot of attention in the last few years. However, most studies have focused on animal models, mainly murine, as described below. Thus, our knowledge of the human ovarian mechanics is still very limited despite the clear involvement of ovarian tissue rigidity in follicle activation and development.

II.3.3.1. Mechanotransduction and follicle activation

In the murine model, the Hippo and Akt signaling pathways have been recognized as two major regulators of primordial follicle activation in response to mechanical stimuli.

The Hippo signaling pathway is known for conserving optimal organ size via growth inhibition (Kawamura et al. 2013; Zhai et al. 2016). Through a complex kinase cascade, which is mechanoresponsive, mediators of the Hippo pathway phosphorylate and inhibit yes-associated protein (YAP) and transcriptional coactivator with PDZ-binding motif (TAZ) to arrest organ

growth (Kawamura et al. 2013; Xiang et al. 2015) (Figure 16). An increase in internal mechanical stress likely results in the expression of negative growth factors (i.e., macrophage stimulating [MST1/2], salvador 1 [SAV1], and the large tumor suppressor homolog [LATS1/2]) through phosphorylation and consequent inhibition of YAP/TAZ translocation from the cytoplasm to the nucleus by Rho GTPase and Rho-associated protein kinase (ROCK), in humans and mice (Abbassi et al. 2016; Y. Cheng et al. 2015b; Kawashima and Kawamura 2018). Nuclear localization of YAP is necessary for the transcription of growth factors (i.e., cysteine-rich protein 61 [CYR61/CCN1], connective tissue growth factor [CTGF/CCN2], and nephroblastoma overexpressed [NOV/ CCN3]) (Brigstock 1999), and baculoviral inhibitors of apoptosis repeat-containing (BIRC) proteins (Kawashima and Kawamura 2018). Thus, inhibition of follicle growth and maintenance of its quiescence through the Hippo signaling pathway can be achieved through high internal mechanical stress as a cellular response to a rigid external environment in mice and humans (Figure 16).

Conversely, the application of ovarian tissue fragmentation-altering ovarian mechanical forces has been demonstrated to disrupt the Hippo signaling pathway leading to primordial follicle activation (Kawashima and Kawamura 2018). Kawamura et al. demonstrated that ovarian fragmentation leads to increased actin polymerization, decreased phosphorylated YAP levels with consequent increased nuclear localization of YAP, and enhanced expression of CCN growth factors and BIRC proteins (Kawamura et al. 2013). In this study, disruption of Hippo signaling was characterized by measuring the polymerization rate calculated as the ratio of filamentous polymerized actin (F-actin) to globular actin (G-actin) (Wada et al. 2011). The tissue fragmentation and consequent increase of actin polymerization resulted in increased CCN2 levels, higher ovarian graft weights, and an increased

number of late secondary follicles in mice and humans (Cheng et al. 2015b). Notably, fewer primordial and more secondary/antral follicles were found in the fragmented ovaries when compared to intact counterparts (Kawamura et al. 2013).

These data show that manipulating the mechanical release of the force applied on the follicle through ovarian fragmentation and disruption of the Hippo pathway can result in follicular activation and reinforces the notion that mechanical signaling plays a key role in the initiation and progression of folliculogenesis. Kawamura et al. (2013) work led to the development of their innovative follicle activation approach, called IVA (in vitro activation), a fertility restoration strategy for patients with primary ovarian insufficiency (POI).

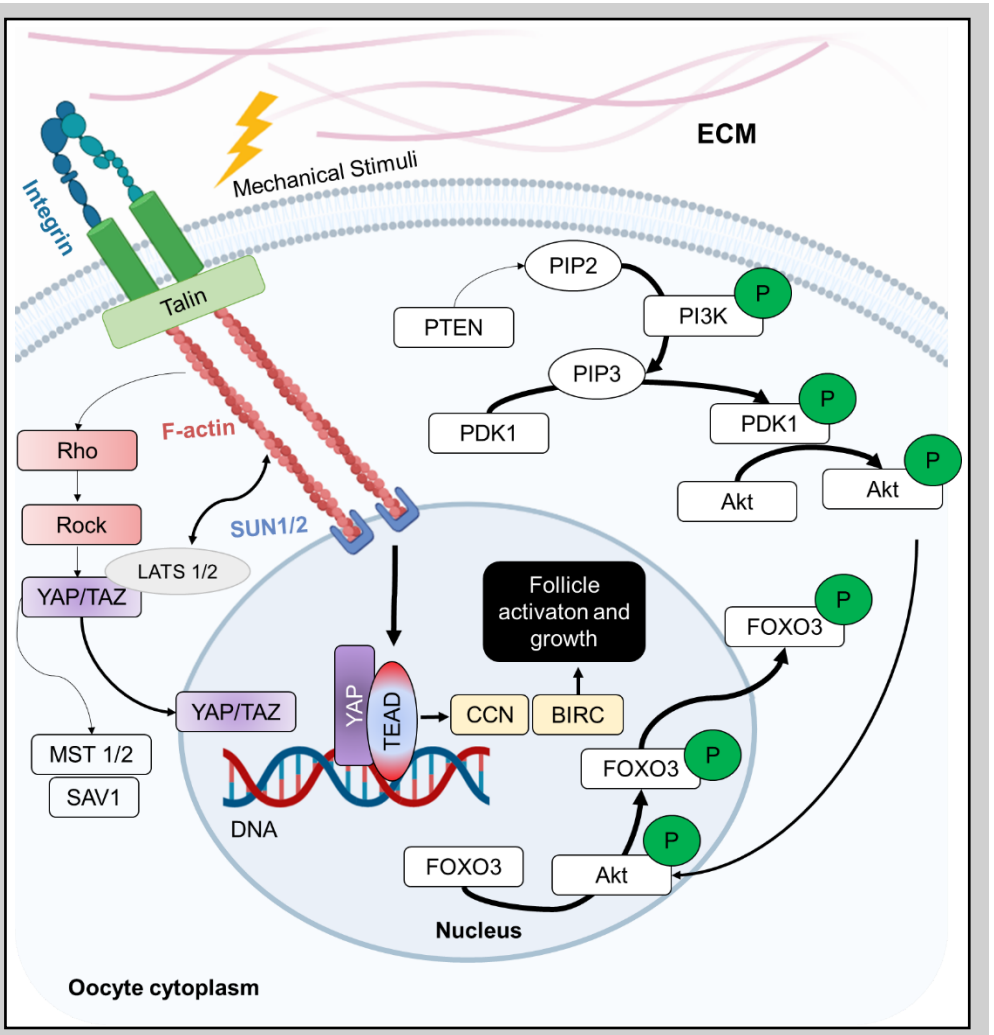


Figure 16 | Follicle activation through Hippo and Akt signaling. Mechanical stimulus (eg. fragmentation force) is likely transmitted through actin to activate the Hippo signaling pathway via Rho GTPase and Rho-associated protein kinase (ROCK).

This leads to a dephosphorylated yes-associated protein (YAP) and transcriptional coactivator with PDZ-binding motif (TAZ) which enables translocation to the nucleus. At the same moment, the Akt (protein kinase B) pathway is also activated by the phosphorylation of phosphatidylinositol-4, 5-bisphosphate (PIP2) to phosphatidylinositol-3,4,5-triphosphate (PIP3), which leads to Akt phosphorylation allowing it to enter the nucleus. Upon entry, the forkhead box O3 (FOXO3) transcription factor, an essential mediator of follicle dormancy, is phosphorylated at the Akt site causing nuclear export into the cytoplasm. The nuclear YAP/TAZ binds the transcriptional enhancer associate domain (TEAD) permitting the expression of growth factors (i.e., cysteine- rich protein 61(CYR61/CCN1), connective tissue growth factor (CTGF/CCN2), and nephroblastoma overexpressed (NOV/CCN3)) and baculoviral inhibitors of apoptosis repeat containing (BIRC) proteins. CCN and BIRC are growth factors implicated in follicular activation and cell growth. PI3K, phosphatidylinositol 3-kinase; PDK1, 3 phosphoinositide- dependent protein kinase-1; LATS1/2, large tumor-suppressor homolog; MST1/2, macrophage stimulating; SAV1, salvador 1. *(Ouni. Unpublished).*

In this procedure, primordial follicles within the ovarian cortical tissue are activated via mechanical disruption of the tissue in vitro using a culture media composed mainly of Akt stimulators (PI3K stimulator and PTEN inhibitor). After autotransplantation of these little cortical fragments, the follicles are stimulated to develop. Nevertheless, due to the irreproducibility of this procedure, Lunding et al. (2020), among others (Dolmans et al. 2019b), have raised a new debate doubting the implication of Hippo pathway, the relevance of tissue fragmentation, and the safety of IVA culture medium (Dolmans et al. 2019b).

The second major signaling pathway known to be involved in follicular

activation is Akt. The Akt pathway mediates primordial follicle activation via two main targets: PI3K and PTEN genes. The PI3K pathway upregulates cellular survival, growth, and proliferation, in the human ovary, while the PTEN protein downregulates PI3K (Cantley 2002; Cecconi et al. 2012). It is possible that ligands in oocytes bind to tyrosine kinase receptors to activate PI3K downstream (Li et al. 2010). Once PI3K is activated, it can phosphorylate and activate phosphatidylinositol-4,5-bisphosphate (PIP2) into phosphatidylinositol-3,4,5-triphosphate (PIP3), which activates Akt (Cordeiro et al. 2016) (Figure 16). The activated Akt suppresses FOXO3 transcription factor, an essential regulator of follicular quiescence (Ernst et al. 2017). A phospho-specific antibody that detects FOXO3 phosphorylated (Thr32) at its Akt phosphorylation site was found exclusively in the cytoplasm in a murine model (John et al. 2008). This suggests that the Akt pathway in humans and mice has an important role in regulating the location of FOXO3 and activating the primordial follicle (Ernst et al. 2017; John et al. 2008). Similarly, when the stem cell factor Kit receptor binding occurs in murine models, it is suggested that there is an increased proportion of cytoplasmic as compared to active nuclear FOXO3 causing primordial follicle activation (Ezzati et al. 2015; Saatcioglu et al. 2016). This was further supported by knock-out FOXO3-mouse model, which resulted in global follicular activation, leading to premature oocyte depletion and secondary infertility (Castrillon et al. 2003).

While the follicle activation is governed by Akt pathway, negative regulation of this pathway by PTEN is believed to be crucial to the maintenance of follicular dormancy in humans (Goto et al. 2007). PTEN dephosphorylates activated PIP3 to PIP2, preventing follicular activation by suppressing the FOXO3 gene in mice (Cordeiro et al. 2016). The initial recruitment of primordial follicles is tightly regulated by PI3K/PTEN signaling in mice (Kim

et al. 2015). If PTEN gene is absent or deleted, the entire pool of primordial follicles will become activated in ovaries of this animal species (Reddy et al. 2008; Reddy et al. 2009).

Another known mediator of primordial follicle activation is mTOR signaling, which works upstream of Akt pathway in mice (Cheng et al. 2015b; Cordeiro et al. 2016; Tong et al. 2013) and, once activated, promotes Akt phosphorylation leading to suppression of FOXO3 nuclear transcription and follicle activation. However, tuberous sclerosis complex 1 or 2 (TSC) negatively regulates mTOR complex 1 (mTORC1). With oocyte-specific deletion of TSC1 or TSC2, this will promote activation of all primordial follicles, leading to premature ovarian failure in mice (Adhikari et al. 2010). In addition, when 5'adenosine monophosphate-activated protein kinase (AMPK) is inhibited, it inactivates TSC2 and promotes phosphorylation of mTOR in mice (Lu et al. 2017). This impacts the Akt pathway by causing YAP localization to the nucleus, which promotes follicular activation (Lu et al. 2017). Also, the mitogen-activated protein kinase 3 and 1 (MAPK3/1) signaling in mice has an important role in follicle activation by prompting mTOR (Zhao et al. 2018).

Treating mice ovaries simultaneously with both Akt and mTOR signaling activators showed a significant increase in the number of antral follicles compared to just Akt activators (Cheng et al. 2015a). In contrast, the mTOR inhibitor, rapamycin, can suppress the Akt activation to aid in follicular latency (Cheng et al. 2015a). It was also demonstrated that rapamycin treatment in a rat model caused a two-fold increase in the number of primordial follicles, which can be attributed to the suppression of follicular atresia with no significant difference in the primary or secondary follicular count (Zhang et al. 2013). Of note, rapamycin-treated rats had irregular estrous cycles and were

unable to be impregnated, likely due to decreased estrogen levels from having fewer antral follicles (Zhang et al. 2013). Another mouse study showed liver kinase b1 (Lkb1) was critical in maintaining a primordial follicle pool (Jiang et al. 2016). If this gene is absent, the entire primordial follicular pool will be depleted because the mTOR signaling pathway is enhanced without a change in Akt activity and reduced AMPK activity (Jiang et al. 2016). Another gene, LIM Homeobox 8 (Lhx8), has been shown in a knock-out mouse model to indirectly interact with the Akt/PI3K/mTOR pathway to suppress primordial follicular activation partially (Ren et al. 2015). The resultant interactions of mechanical signaling with mTOR, TSC1/2, rapamycin, AMPK, MAPK3/1, Lkb1, Lhx8, and the Akt pathway provide evidence of influence on follicle activation or quiescence.

II.3.3.2. Mechanical implication in follicle maturation

If activation takes place, the developing follicle grow and acquires gonadotropin receptors while being progressively displaced toward the less rigid ovarian medullary layer. Different ovarian rigidity zones may modulate the follicle's response to hormones leading to a cascade of cellular processes (Woodruff and Shea 2011). For instance, follicles growing in vitro in stiffer and denser scaffolds secrete higher levels of androgen and progesterone and relatively lower levels of estrogen (West et al. 2007). The differential response to steroids may be mediated through mechanically responsive signaling by A kinase anchor protein 13 (AKAP13) in humans (Kino et al. 2010). AKAP13 can modulate sex steroid receptor activity and has been shown to impact intracellular osmolarity through stress stimulated expression of nuclear factor of activated T-cells 5 (NFAT5) in lymphocytes (Kino et al. 2010). These data reinforce the interplay between the ovarian environment stiffness, cellular osmolarity, and hormonal secretion through mechanical signaling.

By the end of folliculogenesis, only one competent follicle reaches the ovulation stage following ECM continuous remodeling, a decrease in tensile strength in the apical follicle wall, and an increase in intrafollicular pressure (Matousek et al. 2001). These changes in tensile strength and intrafollicular pressure are generated by the action of smooth muscle cells and by osmotic fluid shifts. Regulation of the intracellular osmotic pressure is accomplished by a glycine transporter (GLYT1) encoded by the solute carrier family 6, member 9 (Slc6a9) gene in mice (Richard et al. 2017). The oocytes are able to regulate their cell volume by releasing adhesions between the oocyte and the zona pellucida and by a sharp raise in GLYT1 activity (Richard et al. 2017). The LH surge that precedes ovulation impacts ECM turnover by inducing follicular cells to synthesize and secrete multiple proteolytic enzymes, including plasmin and MMPs that degrade the surrounding ECM (Thorne et al. 2015) (Figure 15). The fragmented ECM releases ECM-bound ligands, including tumor necrosis factor-alpha (TNFα), which promotes collagenases and apoptosis of apical superficial epithelial cells from the pre-ovulatory follicle, as seen in many mammalian species (Murdoch 2000; Murdoch and Gottsch 2003). TNFα, an obligate intermediate of the ovulatory ovarian rupture process, is controlled by increased granulosa cell expression of tissue inhibitor of MMPs (TIMP1) and α2-macroglobulins (Murdoch 2000). Proteolytic activity at the apical region of the follicle results in structural weakening due to less apical smooth cells and ECM degradation. The resulting structural defect at the ovarian cortex and apical follicle becomes later the site of oocyte expulsion (Ko et al. 2006).

Endothelin 2 (EDN2) is a mechanotransduction gene proposed to be the driving force of follicular rupture and ovulation by transiently being expressed by granulosa cells in mice (Ko et al. 2006). EDN2 production is confined to

the granulosa cells while the critical smooth muscle layer is physically separated in the theca externa. With the assistance of proteolytic enzymes to weaken the ECM and follicle wall, EDN2 can diffuse into the theca externa and bind to smooth muscle cells, leading to the contractile activity necessary for follicular rupture (Ko et al. 2006). Contraction of smooth muscle cells causes an increase in intrafollicular force, leading to a rupture at the weakest point of the follicle (i.e., the apex) (Ko et al. 2006). EDN2 acts upon the smooth muscle cells in rats by binding endothelin receptor subtype A (EDNRA), which causes a contractile response expulsing the oocyte from the dominant follicle during ovulation and enables transportation of the cumulus-oocyte complex within the oviduct (Al-Alem et al. 2007; Bridges etal. 2010).

II.3.3.3. Oocyte and embryo mechanical homeostasis

Upon ovulation, the primary oocytes resume meiosis and complete meiosis I, entering meiosis II which is not completed until oocyte fertilization. Oocyte's internal state may also be reflected in its mechanical properties. In mouse and human embryos, cortical granule release during fertilization causes a physical change in stiffness, called 'zona-hardening' (Khalilian et al. 2010; Yanez et al. 2016), a process previously described only biochemically. The response of the oocyte membrane to needle puncture during intracytoplasmic sperm injection (ICSI) was found to be predictive of embryo morphology and survival in culture (Ebner et al. 2003; Palermo et al. 1996). Embryo and oocyte stiffnesses have also been correlated to pregnancy in humans and maternal age in mice, indicating that there may be a link between mechanics and viability (Liu et al. 2010; Murayama et al. 2006; Murayama et al. 2008).

In this context, Yanez et al. (2016) report that zygote viscoelastic properties can predict blastocyst formation in humans and mice within hours after fertilization, with >90% precision, 95% specificity, and 75% sensitivity. This is achieved by using an automated micropipette aspiration system attached

to a light microscope to record each oocyte aspiration and measure accordingly the deformation and the viscoelastic properties characterizing viable oocytes. Moreover, a support-vector machine classifier was trained to determine the optimal decision boundary between viable and non-viable embryos based on those mechanical parameters. The results showed that some oocytes fail to achieve optimal maturation because of external stress during maturation or inherent poor quality. At the time of fertilization, these oocytes may be overly stiff and still immature, or they could fail to release cortical granules properly and be too soft after fertilization. Conversely, optimally matured oocytes release cortical granules into the perivitelline space, undergo the appropriate changes in mechanical properties, and succeed to develop (Yanez et al. 2016).

Recently, another striking finding on the oocyte mechanics was reported by Nagamatsu et al. (2019), who provided more insights into the mechanisms by which oocytes are kept dormant to sustain female reproductive life. The authors demonstrated that mechanical stress created by the compression of the oocyte by the surrounding granulosa and ECM plays a crucial role in maintaining the dormant state of the oocytes in primordial follicles in mice. This environmental state is functionally crucial, as oocytes became activated upon loosening the structure. Intriguingly, whilst the oocyte nucleus in primordial follicles rotated in response to the mechanical stress, stopping the rotation triggered activation of oocytes through nuclear export of FOXO3. The authors considered that nuclear rotation could arise from the fulfillment of particular conditions. One of them would be the transmission of sufficient mechanical force to the nucleus. Another would be an adequate distance between the nucleus and the centrosome based on a previous report proposing that the distance is one of the requirements for rotation (Wu et al. 2011).

By demonstrating that mechanical stress accompanied by nuclear rotation is one of the critical factors required for the follicle dormancy, this study demonstrates why age-related ovarian fibrosis (Briley et al. 2016; Umehara et al. 2018) (high mechanical stress) may have a negative impact on the production of mature oocytes.

Clinical applications of research studies on ovarian mechanics are slowly integrated, such as ovarian drilling for polycystic ovarian syndrome (PCOS) patients, which has been shown to promote actin polymerization and disrupt Hippo signaling, resulting in follicle growth (Kawamura et al. 2013). As previously mentioned, IVA has also been applied in POI patients, leading to a few cases of successful pregnancies (Suzuki et al. 2015). Nevertheless, our lack of knowledge of the intricate follicle environment and limited tools to modify it and modulate its related signaling pathways hamper the translation of recent findings from bench to bed.

II.4. Lessons learned from other organs on the role of the different ECM facets

II.4.1. ECM proteomic identity

II.4.1.1. An overview of the matrisome composition

The availability of complete genome sequences coupled with accumulated knowledge about ECM proteins have enabled the deduction of a complete list of ECM proteins. Indeed, ECM proteins typically contain repeats of a characteristic set of domains (Hynes and Naba 2012), many of which are not unique to ECM proteins, but their arrangements are highly distinct.

The architecture of ECM proteins is unique; they are built from assemblies of many old, and a few more recent protein domains, each of which is typically

encoded by one or a few exons in the genome. ECM proteins represent one of the earliest recognized and most elaborate examples of exon (domain) shuffling during evolution (Naba et al. 2012b). This characteristic feature of ECM proteins allows bioinformatic identification of the proteome encoded by any given genome, using around 50 domains to establish a list of ECM protein candidates (Hynes and Naba 2012). Using such methods combined with manual annotation, Hynes and Naba groups have built an in-silico matrisome data base and generated a robust list of the proteins defining the mammalian matrisome by analysis of the human, mouse, and zebrafish genomes (Nauroy et al. 2018). Thus, by definition, the matrisome is a subset of the entire proteome dedicated to ECM. The matrisome is divided into two main categories: core- and associated-matrisome (Figure 17).

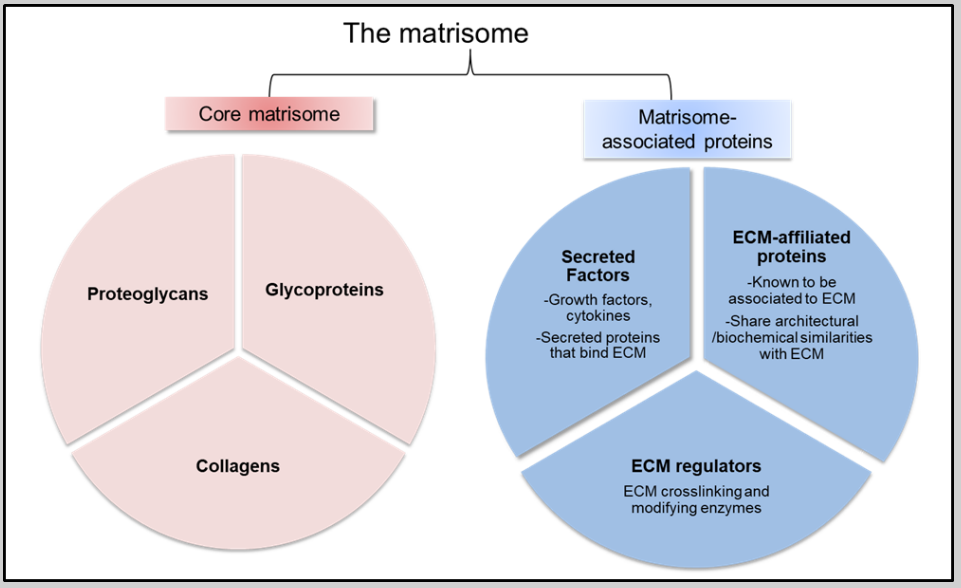


Figure 17 | The matrisome divisions and categories.
(Ouni. Unpublished).

The core-matrisome is the set of high molecular weight and structural proteins synthesized by cells to form ECMs. The human genome encodes 44 collagen genes, 195 ECM glycoproteins and 35 proteoglycans, forming the core-matrisome (Nauroy et al. 2018). The associated-matrisome encompasses proteins secreted and either localized to the ECM or remodeling the ECM. Thus, the associated-matrisome is further divided into secreted factors localizing to ECMs (344 proteins), ECM-regulators (238 proteins), and ECM-affiliated (171 proteins) (Nauroy et al. 2018). Overall, the matrisome of humans includes 1027 genes representing about 4% of the human's protein-encoding genome (Hynes and Naba 2012).

Collagens

The name 'collagen' is derived from the Greek for 'glue-producing' ('kolla' means glue, 'gen' means producing). This refers to collagen's early use in creating glue from boiling the skin and tendons of horses and other animals (Ewald 2020).

In the vertebrates, 46 distinct collagen chains have been identified and assembled to form 28 collagen types (Yue 2014). Collagens are typified by the presence of repeats of the triplet Gly-X-Y, where X is frequently proline and Y is often 4-hydroxyproline. This repeating structure forms stable rod-like, trimeric coiled coils, which can be of varying lengths. However, except for the fibril-forming collagens, most other collagens have frequent interruptions of the (Gly-Pro-Hyp) triple-helical region, which allows them to form more flexible (e.g. network [type IV and others] or chain-like microfibrillar supramolecular organization [type VI and others]) structures (Karsdal et al. 2017; Ricard-Blum 2011). Accordingly, the collagens can be subdivided into six different classes: fibrillar collagens, network-forming collagens, fibril-associated collagens with interrupted triple helices (FACIT), transmembrane

collagens, multiplexins, and collagens that do not fall into these categories (Ricard-Blum 2011). The function of each collagen type depends on its supramolecular organization and its constituent chains.

During collagen maturation, specific proline residues in procollagens are hydroxylated by prolyl 4-hydroxylase and prolyl 3-hydroxylase. Selected lysine residues are also hydroxylated by lysyl hydroxylase. Following processing, the fibrillar procollagens are secreted into the extracellular space where their propeptides are removed. The resulting collagens then assemble into fibrils via covalent crosslinks formed between lysine residues of two collagen chains by a process catalyzed by extracellular enzyme lysyl oxidases (LOX) (Gjaltema and Bank 2017) (Figure 18).

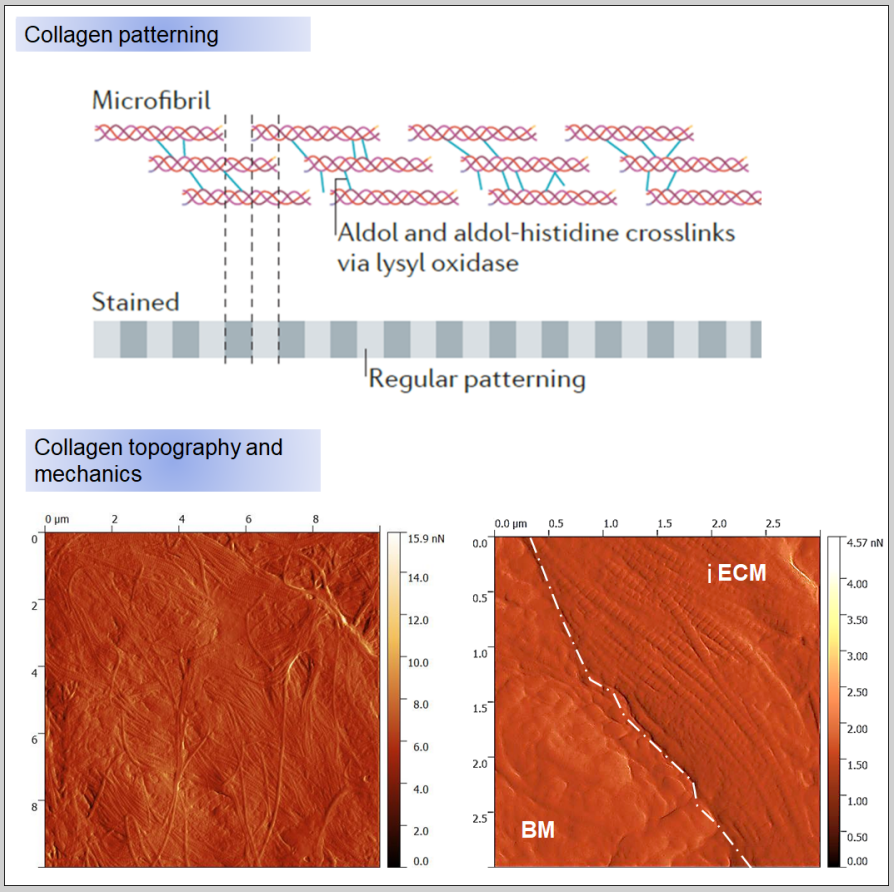


Figure 18 | Collagen crosslinking and impact on ECM topography and mechanics in the human ovarian tissue. Collagen crosslinking and assembly confers accordingly to the ECM (interstitial [iECM] and basement membrane [BM]) different surface patterns, as observed on AFM imagery, where collagen fibers are observed in concentric rings due to their local overlapping microfibrils (top).

These different patterns also contribute to ECM mechanical heterogeneity (Young's modulus described in color scale).

Extracellular lysyl oxidase catalyses and facilitates the oxidative deamination of targeted peptidyl lysine residues, which results in the formation of aldols by reacting with aldehydes or amino groups on lysines between collagen monomers to form intramolecular and intermolecular covalent crosslinks. The N- and C-terminals of neighbouring collagen monomers interact with each other and are covalently crosslinked *(Ouni. Unpublished).*

The collagenous backbone dictates the tissue architecture, shape, and organization (Figure 18). Therefore, an aberration in collagen expression, post-translational modification, or deposition is linked to fibrosis (Karsdal et al. 2020), aging (Ewald 2020) and even cancer (Xu et al. 2019).

Proteoglycans

Proteoglycans are composed of GAG chains covalently linked to a specific protein core (except for hyaluronic acid) (Iozzo and Murdoch 1996). Proteoglycans have been classified according to their core proteins, localization, and GAG composition and are divided into three main families: small leucine-rich (SLRPs), modular and cell-surface proteoglycans (Schaefer and Schaefer 2010). Many genetic diseases have been linked to mutations in proteoglycan genes (Jarvelainen et al. 2009; Schaefer and Iozzo 2008). SLRPs have been involved in multiple signaling pathways, including binding to and activation of epidermal growth factor receptor (EGFR), insulin-like growth factor 1 receptor (IGFIR) and low-density lipoprotein-receptor related protein 1 (LRP1), regulation of inflammatory response reaction, binding to and activation of TGFβ (Schaefer and Iozzo 2008). Modular proteoglycans can modulate cell adhesion, migration, and proliferation

(Schaefer and Schaefer 2010). Basement membrane modular proteoglycans (perlecan and agrin) have a dual function as pro- and anti- angiogenic factors (Iozzo et al. 2009). Moreover, cell-surface proteoglycans (syndecans and glypicans) can act as co-receptor facilitating ligand encounters with signaling receptors (Schaefer and Schaefer 2010).

GAGs, the specific hallmark of proteoglycans, are linear, anionic polysaccharides made up of repeating disaccharide units. There are four groups of GAGs: hyaluronic acid, keratan sulfate; chondroitin/dermatan sulfate, and heparan sulfate, including heparin. All except hyaluronic acid are sulfated (Yue 2014). The highly negatively charged GAG chains allow the proteoglycans to sequester water and divalent cations, conferring space-filling and lubrication functions (Figure 19). Secreted proteoglycans include large proteoglycans, such as aggrecan and versican, small leucine-rich proteoglycans, like decorin and lumican, and basement membrane proteoglycans, such as perlecan. The molecular diversity of proteoglycans provides a structural basis for many biological functions, from regulating collagen fiber assembly to modulating growth factors and interacting with growth factor receptors (Hynes 2009) (Figure 19).

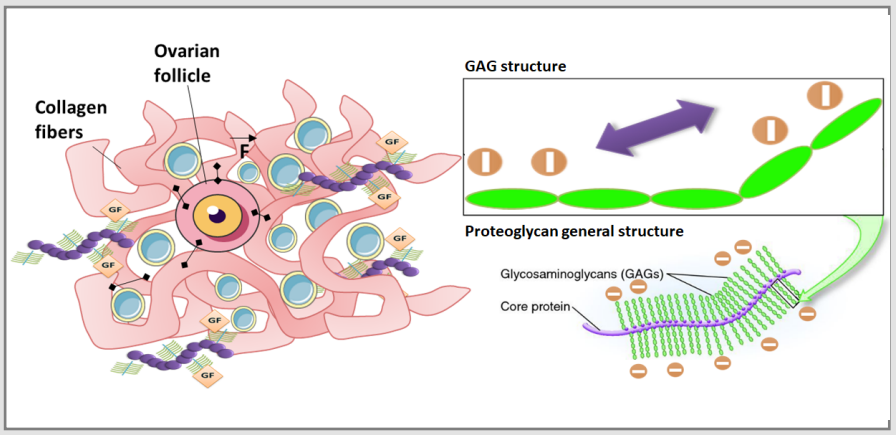


Figure 19 | Glycosaminoglycans (GAGs) interaction with collagen network. Sulfated GAG commonly linked to proteoglycans another major component of ECM, contribute to tissue elasticity since thanks to its high negative charge it is able to retain water within the ECM thus contributing to its elasticity by inflating the collagen network and causing tensile stress that allows the ECM to resist shear deformation. GAGs also sequester numerous growth factors (GF) and regulate their activity. *(Ouni. Unpublished).*

Glycoproteins

A glycoprotein is a compound containing carbohydrate (or glycan) covalently linked to protein (Berg et al. 2002). However, what differentiates them from proteoglycans, is that proteoglycans are a subclass of glycoproteins in which the carbohydrate units are GAGs (Hynes and Naba 2012).

Glycoproteins can be divided into two categories, N-linked and O-linked. Carbohydrates added to the amide nitrogen of asparagine are considered to

be N-linked, and carbohydrates added to the OH group of serine or threonine are considered O-linked. N-linked glycoproteins are the most common. The N-linked glycosylation' functional roles include the targeting of lysosomal enzymes, determination of polypeptide folding patterns, and providing specific cellular recognition targets (Samuel and Young 2002).

In addition to the collagens and proteoglycans that provide strength and space-filling functions (among others), glycoproteins confer numerous functions, including interactions allowing ECM assembly, domains and motifs promoting cell adhesion and growth factor anchorage. The bound growth factors can serve as reservoirs that can be released (e.g., by proteolysis) or presented as solid-phase ligands by the ECM proteins (Hynes 2009).

An interesting point is that, unlike collagen, no evidence exists for direct glycosylation of elastin although it is considered as a glycoprotein in the matrisome project http://matrisomeproject.mit.edu. It is synthesized and secreted by cells as a tropoelastin monomer, that is soluble, non-glycosylated and highly hydrophobic. It has been postulated that the interaction between tropoelastin and cell surface proteoglycans is part of the assembly process of elastin before it is deposited on microfibrils, namely fibrillins (Oszar et al. 2021).

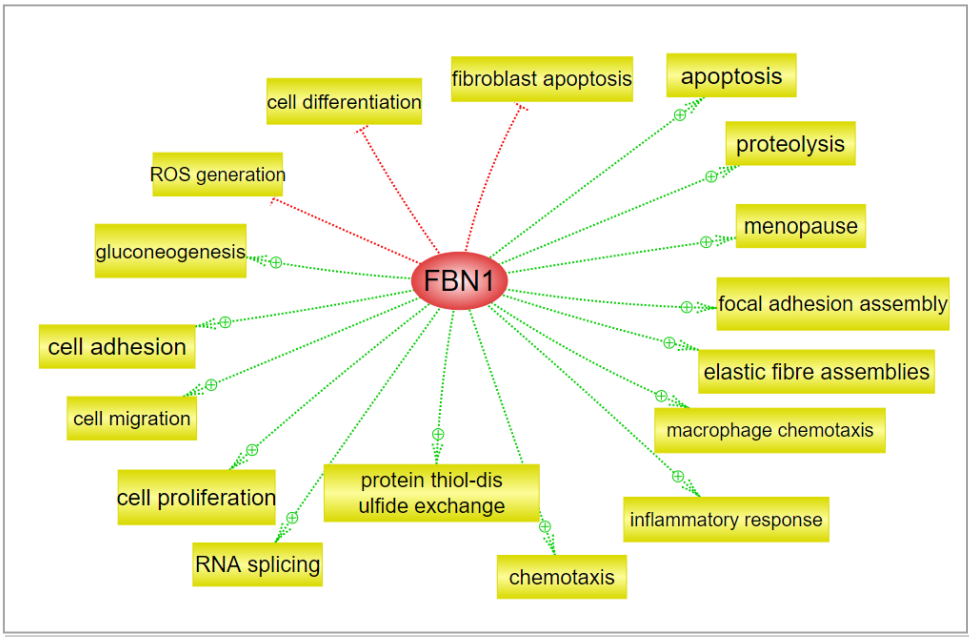


Figure 20 | Bioprocesses where fibrillin-1 (FBN1) is implicated. *Text-mining of literature using Pathway Studio software.*

Fibrillins (Figure 20) and latent transforming growth-factor β-binding proteins (LTBPs) are some of the groups of ECM glycoproteins that have been studied in the context of disease and regulation of TGFβ functions (Munger and Sheppard 2011; Ramirez and Dietz 2009; Ramirez and Rifkin 2009). However, there are multiple other ECM glycoproteins about which much less is known. These include some enormous glycoproteins with impressive arrays of domains, such as SCO-spondin (59 domains of seven types) and hemicentin-1, also known as fibulin-6 (61 domains of six types), and many that are affected in pathological conditions (Aszodi et al. 2006; Bateman et al. 2009; Nelson and Bissell 2006).

ECM secreted factors

Many growth factors bind to ECM proteins and are therefore considered as constituents of ECMs (Hynes 2009). In addition to growth factor interaction with GAGs, there are clear examples of growth factors binding to specific domains of ECM proteins. Fibronectin binds specifically to a variety of growth factors (VEGF, HGF, PDGF, etc.) (Rahman et al. 2005) and the von Willebrand factor C/chordin and follistatin domains found in many ECM proteins are known to bind BMPs (Banyai et al. 2010; Wang et al. 2008). TGF binds specifically to TB domains in LTBPs, which bind in turn to fibrillins and fibronectin-rich matrices (Munger and Sheppard 2011; Ramirez and Rifkin 2009). These ECM-TGF interactions have significant consequences for genetic diseases. For instance, mutations in fibrillins affect the regulation of TGFβ function in Marfan's syndrome among others (Ramirez and Dietz 2009).

ECM regulators

ECM is continuously subjected to remodeling and turnover, marked by significant matrisome protein modifications. In addition to collagen crosslinking by disulfide bonding, transamidation by transglutaminase, and through the action of lysyl oxidases and hydroxylases (Eyre et al. 2008; Ricard-Blum 2011; Robins 2007), laminins and other basement membrane proteins also become crosslinked by disulfide bonding (Choi and Hynes 1979), and the same is true for fibronectin, which also undergoes further processing to a state characterized by insolubility in deoxycholate (Schwarzbauer and DeSimone 2011).

The exact basis for this insolubility is unknown. However, fibronectin and other ECM proteins are also substrates for transglutaminase, which undoubtedly contributes to the insolubility of ECM (Iismaa et al. 2009; Lorand and Graham 2003).

Collagens and other ECM proteins are also substrates for MMPs (Cawston

and Young 2010; Page-McCaw et al. 2007), A disintegrin and metalloproteinases (ADAMs) (Murphy 2008) and A disintegrin and metalloproteinases with thrombospondin motif (ADAMTS) proteases (Apte 2009; Porter et al. 2005). Many other proteolytic enzymes (elastases, cathepsins, various serine esterase proteases, etc.) can also target ECM proteins (Li et al. 2011). These proteolytic processes participate in ECM turnover. They are thought to release ECM-bound growth factors and expose cryptic activities in the ECM (Mott and Werb 2004), including the release of angiogenic inhibitors (Bix and Iozzo 2005; Hynes 2007; Nyberg et al. 2005). Similarly, enzymes that degrade GAGs, such as heparanases and sulfatases, can also alter the properties of ECM proteoglycans (Lu et al. 2011b). The remodeling of ECM by these various processes has significant effects on development and pathology (Daley et al. 2008; Kessenbrock et al. 2010; Lu et al. 2011b). Therefore, all proteins regulating ECM structure and crosslinking belongs to the matrisome.

ECM-affiliated proteins

ECM-affiliated proteins are proteins associated with the core matrisome either structurally or physically. In other words, they share some architectural or biochemical similarities with ECM proteins (ficolins, mucins, etc.) or that are known to be associated with ECM proteins, based on prior information (literature) or based on proteomic analyses in which they repeatedly appeared in ECM enriched samples.

The potential impact of these proteins on the rest of the matrisome is still to be deciphered, especially when considering that their detection in ECM enriched samples does not necessarily prove their association with the matrisome proteins (Naba et al. 2012b).

II.4.1.2. ECM during aging and longevity

During aging, ECM components become damaged through fragmentation, glycation, crosslinking, and accumulation of protein aggregation, all of which contribute to the decline of ECM integrity and result in age-related pathologies (Bonnans et al. 2014; Lu et al. 2011b). Intriguingly, some teams reported that placing senescent cells into a young ECM rejuvenates them (Choi et al. 2011). Furthermore, others found that many longevity-assurances pathways re-activate de-novo synthesis of ECM proteins during aging. This highlights the presence of possible ECM components responsible for its homeostasis, longevity, and aging reversal.

Either through collagen fragmentation or loss of adherence proteins (Fisher et al. 2009), cells detach from the ECM likely leading to cell dysfunction and loss of ECM synthesis and turnover during aging. Another modification that significantly affects the core matrisome is the non-enzymatic glycation. The Maillard reaction is the major non-enzymatic glycation pathway for advanced glycation end-products (AGE) formation (Birch 2018). The reaction is defined by the interaction of glucose with lysine and arginine side chains of a protein (e.g., collagen) to form reversible Schiff base products within hours, which are stabilized to keto amine (Amadori products) within days. Within weeks to months, in a series of chemical reactions, these products are transformed into AGE, such as carboxymethyl-lysine, 3-deoxyglucosone-lysine dimer, glyoxal, glucosepane, pentosidine, etc. (Birch 2018). These AGEs are able to crosslink and thus stiffen collagen structures. Glycation and crosslinking of collagens impair wound healing and is a major problem for diabetes patients with high blood sugar levels (Birch 2018). Cells sense this increase in ECM stiffness and respond by expressing ECM-remodeling enzymes to adjust to their preferred matrix stiffness (Humphrey et al. 2014). However, AGEs or crosslinks hinder enzymatic cleavage, potentially leaving these stiffer matrix parts, but cleave the surrounding intact matrix, resulting in

collateral damage. Thus, certain parts of the ECM become stiffer through crosslinking, and others become mechanically weaker through collagen fragmentation during aging. Ultimately, aged ECMs are categorically stiffer but also mechanically weaker.

During development and growth, cells constantly remodel the ECM by degrading parts of it and through de-novo synthesis of matrisome components in order to maintain homeostasis. This dynamic and energy-intensive process might decline after reproduction. Either because natural selection, as defined as reproductive fitness, is ineffective after reproduction or because of a shift in resource allocation from somatic to germline tissue during the onset of reproduction. Irrespective of the etiology, this predicts that after reproduction, the homeostasis of matrisome components, i.e., de- novo synthesis and ECM remodeling, would decline. Thus, one would expect that a young ECM is different from an old ECM.

II.4.1.3. ECM characterization using proteomics

Biochemical understanding of native ECM has been impeded by the high insolubility of ECM proteins, which are frequently crosslinked. Although mRNA levels might be indicative for the synthesis of ECM proteins, mRNA expression levels mainly do not reflect protein levels, which is very likely to be true for ECM proteins. Conversely, mass spectrometry (MS)-based proteomics (Aebersold and Mann 2016) has emerged in the past decade as the method of choice to characterize, in an unbiased manner, the protein composition of the ECM of normal and pathological tissues (Byron et al. 2013; Lindsey et al. 2018; Socovich and Naba 2019). This was made possible by the development of novel experimental and bioinformatic approaches to overcome the challenging biochemical nature of ECM and to annotate and mine matrisome proteomic data (Naba et al. 2012a; Naba et al.

2016; Socovich and Naba 2019).

For instance, the high insolubility of the ECM can be deturned to reduce the complexity of tissue samples and detect scarce proteins in the ECM. To this end, it is first necessary to eliminate the sample's intracellular proteins, which are much more soluble, without losing the rest of the proteins in the ECM. This can be achieved by varying salt concentrations and the pH of the tissue homogenate solution (Ouni et al. 2019). Once the intracellular proteins have been extracted and removed, we must ensure that total solubilization has been obtained since only soluble proteins can be analyzed by MS. Incomplete solubilization results in partial characterization. Although many groups use very strong solvents and detergents to solubilize the matrix, with sodium dodecyl sulfate (SDS) the most common of them, these reagents are difficult to remove from samples and are responsible for serious artefacts in the mass spectrometer, even at very low concentrations (<0.01% SDS) (Wu and Yates 2003). Therefore, there is a real need to develop appropriate techniques with reproducible and reliable MS-compatible reagents for proteomic characterization of the ECM and biomarker investigation, in order to allow extrapolation of this technology to a clinical setting.

II.4.2. ECM nano and microarchitectural features: more than pretty fibrils

In the middle ages, it was believed that living organisms were composed of different types and arrangements of 'fibers' and that life arose spontaneously from them under certain conditions (Piez 1997). Overlooking the reference to spontaneous generation, this 'fibre theory' could be construed as extraordinarily insightful given what we know about the ECM's importance today. In fact, the belief that fibres were the basis of animal life persisted for

some time. The first scientific accounts on the effect of ECM geometry on cell growth and function date back to the late 1950s (Howarth and Dourmashkin 1958). Decades after, ECM architecture is still intriguing researchers and prompting more studies.

In vivo, cells encounter a broad range of ECM topologies, such as isotropic collagen networks in connective tissue or aligned collagen bundles in the dermis. These have a significant impact on the regulation of cellular processes by providing spatial and mechanical cues to which cells respond (Fort et al. 2011) (Figure 21).

The increasing progress in imaging technologies enabled a better characterization of ECM architecture at the micro and nanoscale to describe ECM porosity, fiber morphology, alignment, and orientation (Ganeva and Kukulski 2020; Mayorca-Guiliani et al. 2017). In the last decade, geometric shape (Padiolleau et al. 2020), matrix porosity (Kilian et al. 2010), ECM fiber diameter, and alignment (Taufalele et al. 2019) have been critical players in stem cell differentiation, which prompts bioengineers to design scaffolds with tailored ultrastructure.

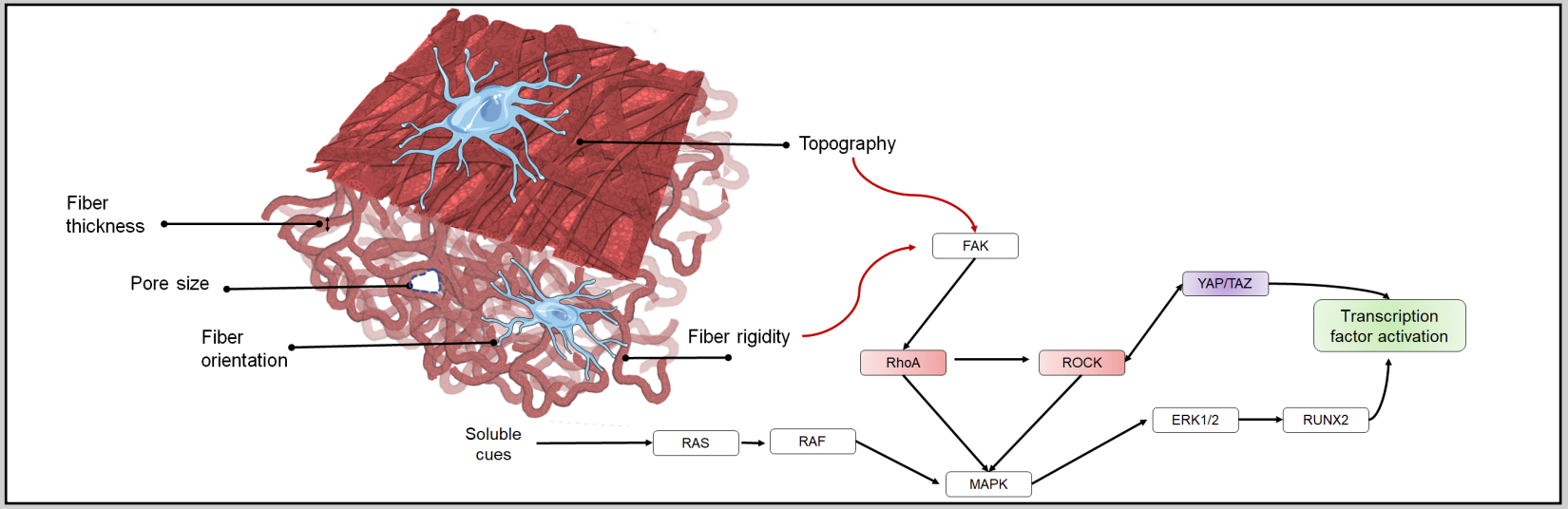


Figure 21 | Examples of physical ECM properties affecting cell signalling. Cells share common mechanisms to respond to physical, architectural, and topographical cues, which leads in some cases to changes in gene transcription. Key molecular players include integrins, focal adhesion-associated proteins (FAK and others), RhoA/ROCK, MAPK, and YAP/TAZ. Actomyosin-driven tractional forces, which enable cells to mechanically probe their physical microenvironment, also appear to play a critical and conserved role in cells' responses to ECM elasticity and topography.

ECM rigidity and topography induce differential activation of FAK that triggers downstream signaling to MAPK cascade, which conveys information about the extracellular environment to the cell nucleus and plays an important role in normal and pathologic development (Khatiwala et al. 2009). Changes in substrate elasticity alter the ROCK pathway upstream of changes in the MAPK cascade (Khatiwala et al. 2009). Then, this pathway influences the transcription factor RUNX2 to control cell differentiation (ie. osteoblast differentiation and matrix mineralization). Collectively, these findings suggest that activation of a FAK/RhoA/ROCK/MAPK signaling axis via changes in ECM elasticity and topography may play a central role in the ECM's ability to control cell fate decisions. ROCK, Rho-associated protein kinase; RhoA; MAPK, Mitogen-activated protein kinase; YAP, Yes-associated protein; TAZ, Transcriptional coactivator with PDZ- binding motif; ERK1/2, Extracellular signal-regulated kinase 1/2; RUNX2, Runt-related transcription factor 2. *(Ouni. Unpublished).*

For instance, cell adhesion and motility depend on ECM porosity (Fratzl 2008), which modulate ECM permeability. Hence, it defines accessibility of small (nutrients, hormones, and oxygen) and large molecules (e.g., that is a function of basement membranes), cell processes (e.g., axons), or cells (vascularization). ECM permeability to cell migration is important for regenerative processes. Low permeability for cells, such as in scarred tissues, results in poor regeneration. Permeability for fluid flows and molecular diffusion is essential for cell survival, since low permeability may result in lack of nutrients and ischemia (Akhmanova et al. 2015). Thus, the intertwined ECM fibers act as a mechanical hindrance for fluid flow, diffusion, and cell displacement (Ramanujan et al. 2002). Reduced pore sizes, which may be restricted by excess collagen deposition (Carey et al. 2012; Wolf et al. 2013), have been shown to hinder 3D cell migration (Wolf et al. 2013) and may require cells to remodel the ECM via matrix-degrading enzymes, such as MMPs, to navigate the ECM (Harjanto et al. 2011). Interestingly, fibril straightness may regulate MMP activity in the matrix. For instance, MMP-1, the interstitial collagenase that plays a role in specific regenerative processes, degrades collagen fibrils at a 100 times higher rate when the fibrils are stretched (Adhikari et al. 2011).

The ECM fibrous structure also contributes to its macroscale elastic nonlinearity and force transmission owing to fiber reorganization under applied loading, resulting in fiber alignment and densification (Babu et al. 2019). Previous experimental studies have demonstrated that the nonlinear elasticity of the ECM facilitates long-range transmission of loads, enabling cells to sense and respond to mechanical signals sent by other cells located at far distances.

Loss of tissue architecture is a prerequisite for, and one of the defining characteristics of, most cancers. Conversely, normal organ architecture can act as a powerful tumor suppressor, preventing malignant phenotypes even in cells stricken with gross genomic abnormalities (Howlett et al. 1995; Kirshner et al. 2003; Mintz and Illmensee 1975; F. Wang et al. 2002). Indeed, aligned collagen architecture is a characteristic feature of the tumor ECM and has been shown to facilitate cancer metastasis using 3D in vitro models.
ECM architecture has also been suggested as a predictive tool for ovarian (K. R. Campbell and Campagnola 2017; Khatiwala et al. 2009) and breast cancer (Bredfeldt et al. 2014a; Majeed et al. 2017), opening to ECM topology new avenues in clinical and pharmaceutical applications.

II.4.3. ECM topography and its role in cell signaling

ECM fibrous proteins have micro- and nano-scale features shaping tissue topography. ECM topography in completion to ECM elasticity synergizes with biomolecular cues to influence normal homeostasis and tissue phenotype by playing a role in a plethora of biological processes: cell differentiation (Huanget al. 2019), cell shape and morphology (Abagnale etal. 2017; Yim et al. 2005), cell adhesion (Karuri et al. 2004), mechanotransduction (Lim et al. 2007), tumor propagation (Zhou et al. 2017) and dormancy (Chaudhuri et al. 2016) and even ECM composition, described in this section (Figure 21).

Paralleling the increased focus on ECM elasticity in the recent literature, the past 10-15 years have witnessed a very large number of studies investigating the effects of physical topographical features (e.g., lines, gratings, holes, pillars, etc.) and/or chemical topographical features (e.g.,‘tracks’ or ‘islands’of printed or adsorbed ECM proteins). The fact that many cell types are naturally adapted to function within a complex nanotopographical environment has facilitated a series of studies investigating cellular responses toward the

phenomenon of nanotopographically mediated mechanotransduction, with studies indicating that most cells do react significantly to nanotopographical cues in vitro (Janson and Putnam 2015). For instance, the influence of nanotopography on cell differentiation and cell stemness has mainly been investigated and prompted more research on this physical factor. Indeed, in one study with mesenchymal stem cells (MSCs), arrangements of 120-nm diameter, 100-nm deep nanopits in poly(methyl methacrylate) that were asymmetric and more disordered (i.e., deviated from perfectly square or hexagonal arrays) were found to enhance the expression of osteogenic genes and proteins, even in the absence of soluble osteogenic supplements (Dalby et al. 2007). The same research group later demonstrated that regular square arrays of these nanopits embossed in polycaprolactone promote MSC stemness (McMurray et al. 2011). By contrast, topographical contact guidance has been associated to adipocyte phenotypic differentiation when MSC were cultured on micro-scale grooves (Xie et al. 2017). Other groups have also examined the role of nanotopography in the maintenance and differentiation of human embryonic stem cells (Kong et al. 2013; Lu et al. 2014).

Cell polarity is also influenced by micro- and nano-topographies. One study demonstrated that nanogratings could alter the polarization of smooth muscle cells in a wound-healing migration assay, with the orientation of the microtubule-organizing center towards the wound on unpatterned surfaces and along the axis of cell alignment in cells cultured on patterns (Yim et al. 2005). Similarly, chemical and physical microtopographies are linked to cell shape and morphology, and topography-based methods to control shape have been widely used in the literature for the past two decades (Biela et al. 2009; Yim et al. 2005) to understand the influence of topographical cues. The rationale to explore this linkage is that native ECM contains nanoscale

physical topographies, and thus features of similar size on engineered substrates may better mimic the native ECM (Biela et al. 2009). Early examples from the literature used substrates with various nanoscale features to investigate the adhesive characteristics of fibroblasts and endothelial cells (Dalby et al. 2002; Dalby et al. 2007). In a recent study, human MSC adhesion was examined on roughened titanium surfaces and found to be enhanced on those with 150 and 450 nm features compared to 20 nm features (Khang et al. 2012). However, similar nanoscale patterns on roughened titanium reportedly had no differential effects on osteoblast cell adhesion (Cai et al. 2006). Such discrepancies support the idea that different cell types respond differently to topography.

Chaudhuri et al. (2016) have further reinforced this principle in the context of cancer cells. This group examined the effect of topographic cues on cancer cell proliferation using micron-scale topographic features and observed that anisotropic features like micrograting at specific dimensions could reduce the proliferation of non-cancer breast epithelial cells (MCF-10A) but not that for malignant breast cancer cells (MDA-MB-231 and MCF-7). However, isotropic features, such as micropillars, did not affect proliferation of MCF-10A, indicating that the anisotropic environmental cues are essential for this process (Chaudhuri et al. 2016). They pioneered the concept of mechanically-induced dormancy (MID), where topographic cues could activate Rho-ROCK-Myosin signaling to suppress the proliferation of non-cancerous cells. In contrast, malignant cells were resistant to this inhibitory barrier and therefore continued their uncontrolled proliferation (Chaudhuri et al. 2016).

The mechanisms underlying the interaction of cells with the ECM topography are still poorly understood. Changes in substrate topography seem to affect not only cells but also their ECM composition, namely the stimulation of

elastogenesis of human coronary artery smooth muscle cells (Lin et al. 2011). From a therapeutic point of view, a better mechanistic understanding of how the presence of myriads of physical cues in the proliferative and metastatic niche contributes to the progression of tumorigenesis and metastasis will lead to the development of mechanobiologically-inspired anti-cancer treatments. Promising chemotherapeutic agents are targetting cellular contractility and adhesion machineries including integrin inhibitors and FAK antagonists has already started to emerge, and more are expected to come (Chaudhuri et al. 2016) (Figure 21). A similar application on ovarian tissues and cells might open a new era of therapies and research in reproductive biology. However, the topographical studies on ovarian tissue have not yet started.

II.5. How to build a road map to construct a functional biomimetic TAO

From the dawn of time, literature and the arts have mirrored the human desire to be able to create by themselves living individuals or at least parts of individuals. Such practice is known as ‘tissue engineering’. Driven by surgeons, this term was up to the mid-1980s loosely applied in the literature in cases of surgical manipulation of tissues and organs or in a broader sense when prosthetic devices or biomaterials were used (Skalak 1993). The term as we know it today was only introduced in medicine in 1987. The definition that was agreed on was: ‘tissue engineering is the application of the principles and methods of engineering and life sciences toward the fundamental understanding of structure-function relationships in normal and pathologic mammalian tissue and the development of biological substitutes to restore, maintain, or improve function (Meyer 2009). Despite the historical origins of tissue engineering, medical science has failed to translate promising bench research on engineered tissues and organs into clinical practice (Badylak 2016).

The original, and still dominant, template for creating replacement tissues established in the 1980s, still involve cell culture on a degradable scaffold in the shape of the target body part, which is then implanted into the recipient. Numerous reports of human ears, blood vessels, bladders, and other body parts manufactured using this approach have generated a great deal of enthusiasm. Although the field has seen significant advances recently with the 3D and even 4D printing, serious challenges remain, stemming primarily from the inherent complexity of the human organs, like the ovary, and the fact that the tissues created by the applied generic approach mentioned above, lack many of the supportive elements that sustain the viability and function of the cells (Badylak 2016). Tissue engineers have also failed to consider the cells' microenvironment, i.e. their native ECM and the cell-ECM dynamic interaction.

In the last years, our group has demonstrated the feasibility of the TAO concept (Amorim and Shikanov 2016; Cho et al. 2019; Luyckx et al. 2013). However, we have also revealed that the development of such a construct requires a deep understanding of the heterogeneous nature of the native ovary. On the other hand, the composition, architecture, biomechanical properties, and organization of the ovary biological, structural, and functional components have not yet been sufficiently elucidated.

Therefore, as a roadmap to construct a TAO, the objective of my project is to draw the most accurate description of the human ovarian ECM facets to date. We aim to describe as faithful as possible its composition, architecture, and biomechanics. Aware of the complexity of ovarian ECM, we came up with selection criteria that will enable us to prioritize key features that need to be absolutely reproduced in the TAO. All our characterizations of the human ovary were conducted based on comparative studies between different age groups.

The aim is to spot specific features of the ovary at reproductive age, which is more prone than its counterparts for follicle survival and development.

To build a road map to construct a functional bioinspired TAO, the following steps had to be conducted:

II.5.1. ECM proteomic characterization

Mimicking the ovarian tissue is crucial to supporting follicle survival in a TAO, as the ovarian ECM plays a primordial role in follicle growth and cell proliferation, and differentiation. Our laboratory's previous findings on transplantation of isolated human and mouse preantral follicles using natural polymers (Amorim and Shikanov 2016; Cho et al. 2019; Luyckx et al. 2013) convinced us that if we are to improve follicle survival in the TAO to achieve fertility restoration, we need to develop a matrix tailored specifically to human follicles. It was encouraging to obseve ECM synthesis after follicle isolation and cells grafting in natural polymers (Amorim and Shikanov 2016; Cho et al. 2019; Luyckx et al. 2013). Although the general aspect of this new ECM appears similar to the native ovarian tissue, we have not yet analyzed its composition, mainly because we do not have clear parameters to draw any comparisons. Indeed, the composition of the human ovarian ECM has never been properly defined. This is partly due to the difficulty of obtaining samples of human ovarian tissue to conduct such an extensive study, a limitation faced by most research centers worldwide. In addition, the biochemical properties of ECM proteins (large size, insolubility, crosslinking, etc.) render ovarian ECM characterization very challenging, mainly by MS (Byron et al. 2013). Therefore, this project provides a thorough characterization of the human ovarian ECM proteomics. To undertake such a comprehensive task, we developed a new advanced protocol tailored for matrisome proteomics (DC-MaP),

which can also be applied to a broad range of biological tissues with scarce availability, like the human ovarian biopsies. Our protocol enabled us to overcome these limitations: unfriendly-MS detergents, irreproducibility, labor-intensive processing, and consequent loss of low abundant proteins. This was achieved through setting up a sequence of optimized procedures from sample collection and homogenization with an MS-compatible detergent to a two-step fractionation and data analysis. To our knowledge, this protocol launched the first use of MS-compatible detergents in matrisome proteomics, representing a pioneering work on human ovarian tissue that can fasten not only TAO development, but also the transition of proteomics to the clinical practice and enable biomarker discovery in an unbiased fashion.

Using DC-MaP, we applied a quantitative proteomic strategy relying on tandem mass tags (TMT) (Zhang and Elias 2017), to create the most complete map of ovarian ECM proteins using highly advanced computational methods to select only high-quality spectra for protein relative quantification and reliable protein identification. With this technique, up to 15 samples could be analyzed in a single experiment, which significantly decreases experimental variability between sample preparations, normalizes protein detection and allows the study of larger sample numbers (Zhang and Elias 2017). Since the human ovarian ECM is a complex and dynamic meshwork of crosslinked proteins that evolve throughout a woman's life, we investigated ovarian biopsies from women before (prepubertal, n=5), during (pubertal, n=5), and after (menopausal, n=5) their reproductive lifespan in order to find fertility biomarkers at the matrisome level, which must be reproduced in the TAO. Each group includes samples to create proteomic profiles of ovarian tissue specific to each stage of reproductive life, which will be correlated to age-specific folliculogenesis. Clearing, light-sheet microscopy, 3D imaging,

and volumetric rendering were performed after labeling established biomarkers to identify the localization and distribution of differently expressed proteins and monitor their spatiotemporal deposition.

Our results provide a benchmark against which we can evaluate the ECM synthesized by ovarian cells and preantral follicles after grafting of the TAO, and will guide us during the assessment of the ovary-like structure obtained after TAO transplantation. In a near future, the collected proteomic data will also be exploited by our group to construct an online database devoted to human ovarian ECM proteomics to help research groups worldwide enrich our built-on knowledge and fasten the transition of TAO to the clinical setting.

II.5.2. Characterization of ovarian biomechanics

Mimicking the biomechanical properties of ovarian tissue is the key to supporting follicle survival in the TAO, as these mechanical properties, the heterogeneity of the ovary, and matrix degradability all have a significant impact on follicle survival and growth. When isolated human ovarian follicles were xenografted in a stiffer fibrin matrix, a positive correlation was observed between matrix rigidity and follicle recovery rates (Paulini et al. 2016). However, since there is no available information on the mechanical properties of the human ovary, our goal in this project was to identify the micromechanical characteristics of the human ovarian ECM in order to mimic these features when developing the TAO's physical support.

Ovarian samples from prepubertal, reproductive age, and menopausal patients were used for atomic force microscopy (AFM) to measure their elasticity. AFM was chosen thanks to its high sensitivity and effectiveness in distinguishing small mechanical changes between and within tissues at microscale resolution, hence adequately assessing the microenvironment surrounding the cells (Kao et al. 2016).

The evolution of ovarian biomechanics with age are also related to peculiar spatiotemporal changes in mechanical matrisome components that needs to be studied to understand the real players orchestrating mechanical behavior in the ovary at the perifollicular and interstitial space. The mechanical matrisome components encompass elastic fibers, which are large ECM structures that provide tissues with recoil needed to undergo repeated stretching and complement the tensile strength of fibrillar collagens. Elastic fibers reside in tissues as a large network composed of two discrete components, namely elastin, the principal constituent, and associated microfibrils, mainly fibrillin-1. Elastin microfibril interface-located protein 1 (EMILIN-1) is another glycoprotein present at the interface between amorphous elastin and microfibrils (Colombatti et al. 2011; Levillain et al. 2016; Thomson et al. 2019). GAGs also need to be evaluated since they confer elasticity to biological tissues by water immobilization (Kurylo et al. 2016).

II.5.3. Elucidation of the architectural and topographical features of the ovary

As discussed above, ECM multiscale architecture and topography play critical roles in tissue function and homeostasis. Although these aspects have never been related to ovarian function in vivo, we foresee their significant implication in fertility and their paramount characterization to build a biomimetic TAO.

To provide the first description of these structural features, ovarian tissues from prepubertal, reproductive-age, and menopausal patients were analysed by fluorescent microscopy to capture collagen autofluorescence in order to characterize collagen orientation and straightness in interstitial and perifollicular space. Scanning electron microscopy (SEM) was used at

different magnifications to capture: fibril (nanoscale), fiber (microscale), and fiber-bundle (mesoscale) organization and diameters, as well as pore number and area, as a reflection of ECM network tightness. Image analyses relied on advanced computed segmentation of fibers (Curvelet transform) and automated calculation based on well-established mathematical models. Moreover, using stereoscopic reconstruction of tilted SEM captions and 3D rendering, we were able to extract surface topography. In the course of these analyses, the mechanical features of ovarian tissue could be linked to its nanotopography, ultrastructure, and organization.

Overall, engineering a TAO is indeed quite complex. Only through investigating the multiple facets of the native ovarian matrisome and adopting a comparative approach, as we did by comparing the gold standard, which is the reproductive-age ovary, with its counterparts, we can limit and refine the list of components to reproduce. Moreover, by having a reliable reference of the ovarian matrisome, we can evaluate the engineered models and their convenience and even build from scratch new biomimetic constructs.

CHAPTER 3

Personal contribution

While tissue engineering strategies for most organs stems primarily from a limited number of organ donors and side effects of immunosuppressive treatments, the demand for a TAO emerges as a procedure for fertility restoration in cancer survivors. Indeed chemo- and radiotherapy can potentially be toxic for the ovaries, ultimately leading to sterility. The increased survival rates of cancer patients due to early diagnosis and improved treatments have shifted the discussion of cancer care to issues related to the quality of life after cancer, including the ability to have a family. Cryopreservation and transplantation of ovarian tissue have proved to be a promising technique to safeguard fertility in cancer patients (Dolmans and Donnez 2021). However, with some types of cancer potentially metastasizing to the ovary, there is a significant risk of transmitting malignant cells present in the cryopreserved ovarian fragments since they were not submitted to the cancer treatment. Transplantation of ovarian tissue in these patients is therefore not allowed, which effectively puts an end to their dreams of generating biologically related children. For these patients, a safer alternative could be the transplantation of isolated preantral follicles. To encapsulate and protect isolated follicles, a TAO needs to be created. The TAO consists of the isolation of follicles from ovarian tissue cryopreserved before cancer treatment, and their embedding into a 3D matrix along with fresh stromal cells retrieved from the patient once she is cured. Then, the ensemble is grafted to restore the patient's fertility. However, one of our most significant drawbacks when isolating the follicles and cells is the destruction of the native ECM. As discussed in the previous chapter, the ECM is a critical component that defines the microenvironment of the cells and follicles.

As it will be virtually impossible, in the short term, to create a matrix with the same composition and complexity of the ovarian ECM, our mission is to develop a biomimetic artificial ECM that offers a familiar microenvironment

for the follicles and cells, which will allow them to reconstruct the original ECM.

Studies on developing the TAO physical structure, i.e., the 3D matrix, have already been started in our laboratory (Amorim et al. 2009; Chiti et al. 2016; Luyckx et al. 2013). Despite our promising results, we believe that in order to improve follicle survival in an artificial ovary to ensure fertility restoration, we need to develop a matrix specifically tailored to isolated human follicles. To do so, it is crucial first to acquire sufficient knowledge of the human ovarian ECM and its interaction with preantral follicles. Therefore, the general goal of my project is to deconstruct the natural human ovary to understand the follicle environment in order to mimic it in the TAO. To this end, my project is divided into three specific aims:

(1) Biochemical characterization of the human ovarian matrisome

- *Pilot study*

  A draft map of the human ovarian proteome for tissue engineering and clinical applications

- *ECM tailored proteomic methodology*

  Divide-and-Conquer Matrisome Protein (DC-MaP) Strategy: An MS- Friendly Approach to Proteomic Matrisome Characterization

- *Reproductive age and aging biomarker discovery at the matrisome level*

Proteome-wide and matrisome-specific atlas of the human ovary from prepuberty to menopause

Spatiotemporal changes in mechanical matrisome components of the human ovary from prepuberty to menopause

(2) Elucidation of the topology and topography of the interstitial and perifollicular ECM

(3) Biomechanical characterization of the human ovarian tissue

Multi-scale study of the architecture, topography and mechanics of the human ovary from prepuberty to menopause: a blueprint for next- generation bioengineering and diagnosis

A draft map of the human ovarian proteome for tissue engineering and clinical applications

In order to mimic the natural ovary, we must acquire a better knowledge of its composition and regulation. To this end, we turned to literature to search for more details, but we faced significant limitations regarding human ovary characterization. For this reason, we decided to conduct a proteomic portrayal of the human ovarian tissue by MS. Therefore, we collected fresh cortex samples, which we divided into two groups: (1) fresh and (2) frozen from the same patient. The frozen samples were cryopreserved using the slow freezing procedure routinely applied in our laboratory. To digest the tissue samples, we used a modified version of our follicle isolation protocol. In the end, after centrifugation, instead of taking the pellet comprising the isolated follicles, we collected the supernatant containing the solubilized proteins. The suspensions were then analyzed with a two-dimensional-liquid chromatography-mass spectrometry (2D-LC-MS); an MS technique developed to characterize complex proteomic samples with a wide dynamic range without affecting the quality of proteins detection (Figure 22). First, we meticulously searched all the proteins that belong not only to the ECM but to the matrisome, by the comparison of our data with an in silico developed matrisome protein list (Naba et al. 2016).

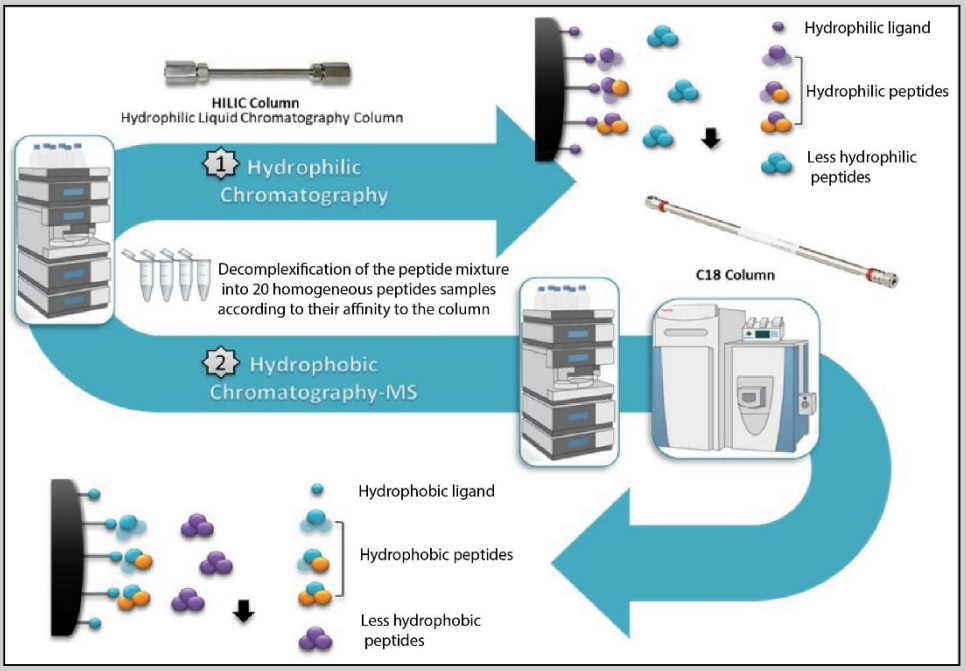


Figure 22 | 2D-LC/MS illustration. 2D stands for the use of 2 different types of orthogonal chromatography with different column properties. First, tryptic peptides obtained from the sample's enzymatic digestion are injected into the first high-performance liquid chromatography (HPLC) containing the hydrophilic stationary phase (HILIC), which will separate the peptides according to their hydrophilicity. This first HPLC enables us to divide our sample into 20 homogeneous fractions. The less hydrophilic peptides will be eluted first, and the most hydrophilic will be eluted at the end. The 20 resulting fractions are then analyzed one by one, by a second HPLC containing a hydrophobic C18 stationary phase that will separate the peptide according to their hydrophobicity. This second HPLC is coupled to MS to analyze the peptides. *(Ouni. Unpublished).*

After analyzing the proteomic results, we succeeded to identify and categorizing 84 ovarian matrisome components out of more than 1500 confidently detected proteins in the ovarian tissue.
The collagen was the most abundant protein type of the matrisome while proteoglycans presented only 7%, and ECM glycoproteins presented 15%; these three types of proteins constitute the core matrisome. ECM regulators, ECM secreted factors, and ECM affiliated proteins are the soluble ECM fraction and were, as expected, less abundant.

In the category of glycoproteins, we identified many fundamental basement membrane proteins. We report the first detection in the human ovary of the insulin-like growth factor-binding protein (IGFALS), which plays an essential role as a modulator of insulin-like growth factor (IGF) activity thanks to their high affinity. Indeed, they can stimulate or inhibit IGF signaling depending on circumstances by either concentrating IGF close to its receptors or, conversely, hampering sterically their binding. This process is critical given the IGF involvement in follicle growth regulation, selection, atresia, cellular differentiation, steroidogenesis, oocyte maturation, and cumulus expansion evidenced in animal models and humans. We also detected around 11 subtypes of collagen. Among them, the most abundant being collagen VI.

We detected different types of proteoglycans, such as heparan sulfate proteoglycan 2 (HSPG2), fibromodulin (FMOD) and osteoglycin (OGN). Proteoglycans are essential since they bind many secreted and growth factors to ECM through their attached GAGs.

Most ECM-affiliated proteins have seldom been studied, especially in the human ovary. Here, we detected many interesting proteins, such as galectins, which have been associated with the inhibition of steroidogenic activity and a loss of progesterone synthesis in pig and mouse ovaries

respectively.

In the category of ECM regulators, we found different protease inhibitors ensuring the integrity and stability of the ECM, such as serpins. We also detected proteins, such as cathepsin and plasmin, that have proteolytic activity and ensure the ECM dynamic degradation during follicular development and ovulation.

In the last category of matrisome proteins, we detected interesting calcium-binding proteins but with unknown functions in the ovary.

Then, we performed a more extended analysis of all the proteins detected in our samples within or out of the matrisome; by first investigating their localization and distribution among cellular compartments through webgestalt database. Pathways of great interest in which our proteins are involved were also detected, such as Pi3k-Akt pathway, related to follicle activation, and cyclic cGMP/PKG, implicated in oocyte meiotic arrest, in addition to renin-angiotensin system (RAS) that has been suspected to regulate oocyte maturation and quality. Moreover, other pathways associated to the regulation of the dynamic interaction between follicles and their microenvironment were further detected, like oocyte meiosis, tight and gap junction mediated pathways.

To our knowledge, this is the first time that fresh human ovarian cortex was analyzed by MS and compared with cryopreserved tissue. By comparing the total detected proteins within fresh and frozen samples, we found that more than 70% were seen in both. Comparing the matrisome proteins among fresh and frozen tissue, revealed an overlap in protein type and quantity. Thus, no significant differences were noticed between fresh and frozen samples. This was also confirmed by additional immunoblotting and immunohistochemical

tests.

To summarize, our study provided the most complete available proteomic analysis on the human ovary, with detailed ovarian matrisome description, and proved the suitability of cryopreserved tissue to accurately represent the proteomic composition of fresh tissue for future more extensive studies. These data will be used to enrich the manufactured matrices with structural proteins from the ovarian matrisome and enhance follicle viability and development with suitable cellular regulators. In this context, we may also take advantage of the ability of proteoglycans to attach growth factors to the ECM.

In the end, through proteomics, we hope to complement available ovarian data by providing further insights into folliculogenesis and ovarian biomarkers and open the door to bioengineers for the creation of better biomimetic scaffolds to restore female's fertility.

Research

⌘ *Author's Choice*

© 2019 by The American Society for Biochemistry and Molecular Biology, Inc.
This paper is available on line at http://www.mcponline.org

A Draft Map of the Human Ovarian Proteome for Tissue Engineering and Clinical Applications

Emna Ouni‡, Didier Vertommen§, Maria Costanza Chiti‡, Marie-Madeleine Dolmans‡¶, and Christiani A. Amorim‡‖

Fertility preservation research in women today is increasingly taking advantage of bioengineering techniques to develop new biomimetic materials and solutions to safeguard ovarian cell function and microenvironment *in vitro* and *in vivo*. However, available data on the human ovary are limited and fundamental differences between animal models and humans are hampering researchers in their quest for more extensive knowledge of human ovarian physiology and key reproductive proteins that need to be preserved. We therefore turned to multi-dimensional label-free mass spectrometry to analyze human ovarian cortex, as it is a high-throughput and conclusive technique providing information on the proteomic composition of complex tissues like the ovary. In-depth proteomic profiling through two-dimensional liquid chromatography-mass spectrometry, Western blotting, histological and immunohistochemical analyses, and data mining helped us to confidently identify 1508 proteins. Moreover, our method allowed us to chart the most complete representation so far of the ovarian matrisome, defined as the ensemble of extracellular matrix proteins and associated factors, including more than 80 proteins. In conclusion, this study will provide a better understanding of ovarian proteomics, with a detailed characterization of the ovarian follicle microenvironment, in order to enable bioengineers to create biomimetic scaffolds for transplantation and three-dimensional *in vitro* culture. By publishing our proteomic data, we also hope to contribute to accelerating biomedical research into ovarian health and disease in general. ***Molecular & Cellular Proteomics 18: 10.1074/mcp.RA117.000469, S159–S173, 2019.***

The World Health Organization has ranked infertility in women as the fifth highest serious global disability (1). Based on this critical assessment, several strategies have been developed to preserve and even restore fertility in women.

Although the human ovary is relatively well understood in terms of secretory patterns of ovarian hormones and the pathogenesis of ovarian diseases, little is known about the molecular composition and regulation of the microenvironment that directs the development and function of ovarian follicles, the functional units that mainly reside in the ovarian cortex and play an important role in oogenesis and gonadal hormone secretion. A few studies have focused on mRNA expression to provide a complete characterization of gene expression in the ovary. However, study of gene expression at the mRNA level yields no information about post-transcriptional modifications (2). Moreover, even abundant mRNA transcripts may be translated inefficiently or degrade rapidly, resulting in lower than expected levels of protein expression (3).

On the other hand, by focusing on final gene products, a proteomic approach has the advantage of investigating complex biological events and diseases, providing more conclusive information.

For several years now, ovarian proteomic studies have concentrated on characterizing follicular fluid composition in human preovulatory follicles (4–5), emphasizing the functional selectivity of the basement membrane toward plasma proteins (6). Efforts have also been made to identify ovary-related transcription in different species to explore the complex functions of the ovary in an integrated manner. This is necessary because of obvious difficulties in obtaining human ovaries, as well as the feasibility of conducting experimental research in humans because of ethical and logistical constraints. He *et al.* (2015). described ovarian proteomics in rhesus monkeys through identification of 4325 proteins to provide a basis for future studies of human reproductive disorders using this

From the ‡Pôle de Recherche en Gynécologie, Institut de Recherche Expérimentale et Clinique, Université Catholique de Louvain, Brussels, Belgium; §de Duve Institute, Université Catholique de Louvain, Brussels, Belgium; ¶Gynecology Department, Cliniques Universitaires Saint-Luc, Brussels, Belgium

⌘ *Author's Choice*—Final version free via Creative Commons CC-BY license.

Received November 15, 2017, and in revised form, February 15, 2018
Published, MCP Papers in Press, February 23, 2018, DOI 10.1074/mcp.RA117.000469
Author contributions: E.O. and C.A.A. designed research; E.O. performed research; E.O. and D.V. analyzed data; E.O. wrote the paper; D.V. contributed new reagents/analytic tools; M.C.C. participated in experimental procedures; M.-M.D. controlled the clinical aspect of the study and revised critically the manuscript; C.A.A. helped in result interpretation and revised critically the manuscript.

animal as a model (7). To our knowledge, the only proteomic analysis of human ovaries performed to date was conducted by Wang *et al.* (2005) (8). The study identified 138 proteins by two-dimensional (2D) electrophoresis and MALDI-TOF mass spectrometry, but without differentiation of ovarian extracellular matrix (ECM)[1] proteins, despite the ECM's important role in defining the follicular environment and orchestrating cellular organization and function. Indeed, the only aspect of the ovarian ECM to have been investigated so far is the basement follicular membrane, and this was done through immunohistochemical tests, which only offer a limited characterization restricted by the type and number of antibodies used (9–10).

The goal of this study was therefore to provide a draft map of functional proteins identified in human ovarian cortex and complement available ovarian ECM data. By using 2D liquid chromatography-mass spectrometry (2D-LC/MS) and ensuring adequate sample preparation, we aimed to shed light on potential key intra- and extracellular proteins in reproduction, to form a basis for comparative studies between normal and pathological ovaries and open the door to improved bioengineering techniques for creation of better biomimetic scaffolds.

EXPERIMENTAL PROCEDURES

Experimental Design and Statistical Rationale—This study involved six 2D-LC/MS experiments using human ovarian cortex from three patients undergoing laparoscopic surgery for benign gynecologic disease. Fresh and cryopreserved samples derived from the same biopsy were analyzed. Each biopsy from each of the patients was initially divided into two fragments; one was immediately analyzed (fresh tissue) and the other was frozen and thawed before analysis (frozen), totaling six experiments. Because the ovarian biopsies were obtained from patients with healthy ovaries, only a small portion of their ovarian tissue was taken ($\leq$9 mm^2) so as not to impact their ovarian activity. For this reason, we could not carry out technical replicates. Moreover, the scarcity of fresh human ovarian biopsies limited the number of samples available for analysis.

To provide a descriptive draft map of ovarian tissue, a threshold was maintained to select the most confidently detected proteins. This threshold included proteins with a Sequest HT score $\geq$10 in any of the 6 samples for gene ontology and pathway analyses. Each protein score was calculated by the Proteome Discoverer application as follows: *protein score = (sum of all cross-correlation factors of 0.8 or above) + (peptide charge × peptide relevance factor),* the default value for the peptide relevance factor being 0.4.

To establish a draft map of the ovarian matrisome, only proteins with a score $\geq$10 in any of the 6 samples and identified by at least two unique peptides in three or more samples were considered.

Fresh and frozen sample compositions were compared based on spectral counts for each detected matrisome protein. A formal quantitative approach was first attempted to carry out comparisons through a paired *t* test. However, a number of issues emerged with this type of test, making it hard to draw any conclusions: (1) small sample size because of limited availability of patients; (2) inability to justify the normality of data, possibly warranting use of non-parametric tests; and (3) need for multiple testing, requiring adequate adjustment (inflation) of *p* values. The first preliminary results pointed to only a few significant ($p < 0.05$) outcomes (proteins) before adjustment, whereas after adjustment (Benjamini-Hochberg), none of the proteins remained significant. It would therefore be naive to conclude that this somehow proves equivalence. In view of the small sample size and the fact that multiplicity corrections typically suppress detection to avoid false positives, we did not feel that this quantitative argument was sound enough to yield any conclusions. A qualitative, more descriptive approach was therefore pursued, considering the importance of comparing protein content and immunohistochemistry results between fresh and frozen tissues.

Collection of Ovarian Tissue and Biopsy Processing—Use of human ovarian cortex was approved by the Institutional Review Board of the Université Catholique de Louvain on November 28, 2016 (IRB reference 2012/23MAR/125, registration number B403201213872). Ovarian biopsies were taken from 3 women (30, 49, and 59 years of age) after obtaining their informed consent. All patients were undergoing laparoscopic surgery for benign gynecologic disease not related to the ovaries (supplemental Table S2). Biopsies were immediately transported on ice to the laboratory in minimal essential medium (MEM)-Glutamax (Gibco, Invitrogen, Merelbeeke, Belgium) and rigorously washed in Dulbecco's phosphate-buffered saline (DPBS) (Gibco) to remove blood remains.

The cortical area of the ovary was selected for analysis, as it is the reservoir of most of the follicle population and would therefore provide the greatest insights into the follicular microenvironment and regulatory factors. Hence, the medullary part of the biopsy was removed, and the cortex was cut into small fragments. A small piece of each biopsy was fixed in formalin and the remaining fragments were either immediately digested or cryopreserved.

Tissue Preparation for Fresh Ovarian Cortex—For extraction of intra- and extracellular proteins, including ECM proteins, we applied a modified version of our isolation protocol for human preantral follicles (11). Ovarian cortical fragments were first subjected to mechanical digestion using a tissue chopper (McIlwain Tissue Chopper; Mickle Laboratory, Guilford, UK), before being, incubated with 0.28 Wünsch units/ml Liberase DH (Roche Diagnostics, GmbH, Mannheim, Germany) diluted in 5 ml DPBS in a water bath at 37 °C with mild agitation. After 30 min, the suspension was centrifuged at 260 × *g* for 15 min at 4 °C, the supernatant was collected, and the action of Liberase was inhibited with 20 mM EDTA (Sigma, Bornem, Belgium). The sample was then stored at −80 °C until MS analysis.

Tissue Preparation for Frozen Ovarian Cortex—Freezing of ovarian cortex was performed using our routine protocol (12). Briefly, the ovarian fragments were suspended in a cryoprotective solution consisting of MEM-Glutamax (Gibco) supplemented with 4 mg/ml human serum albumin (HSA, Bornem, Belgium) at 4 °C, and transferred to 2 ml cryovials (Simport, Quebec City, Canada) containing 0.8 ml cryoprotective solution. The cryovials were cooled in a programmable freezer (Freezer Control CL-8800i, CryoLogic, Victoria, Australia) us-

[1] The abbreviations used are: ECM, extracellular matrix; 2D-LC/MS, two-dimensional liquid chromatography mass spectrometry; bFGF, basic fibroblast growth factor; BMP-2, bone morphogenetic protein 2; CGMP-PKG, cyclic GMP-protein kinase G; DAB, 3,3′-diaminobenzidine; EGF, epithelial growth factor; FDR, false discovery rate; GAPDH, glyceraldehyde-3-phosphate dehydrogenase; HILIC, hydrophilic interaction liquid chromatography; HSA, human serum albumin; HSPG2, perlecan; IGF, insulin-like growth factor; IGFALS, insulin-like growth factor-binding protein acid-labile subunit; MEM, minimal essential medium; MMP, matrix metalloproteinase; OGN, mimecan; ORA, overrepresentation enrichment analysis; PARS, platelet-associated regulatory system; PCNA, proliferating cell nuclear antigen; PEDF, pigment epithelium-derived factor; PI3K-Akt, phosphoinositide 3-kinase serine/threonine kinase Akt; PSM, peptide spectrum match; RAS, renin-angiotensin system; SLRP, small leucine-rich proteoglycan; TBS, tris-buffered saline; VEGF, vascular endothelial growth factor; αSMA, alpha-smooth muscle actin.

ing the following program: (1) cooled from 0 °C to −8 °C at −2 °C/min; (2) seeded manually; (3) cooled to −40 °C at −0.3 °C; and (4) cooled to −140 °C at −30 °C/min before being transferred to liquid nitrogen (−196 °C) for storage. After 24 h in liquid nitrogen, the cryovials were exposed to room temperature for 2 min and immersed in a water bath at 37 °C until the ice completely melted. To remove the cryoprotective solution, the ovarian cortical pieces were immediately transferred from the cryovials to plastic Petri dishes containing MEM, where they were washed three times (5 min per bath). A fragment from each sample was then fixed in formalin and the rest was digested and stored at −80 °C, as described above for fresh tissue.

Sample Preparation for Mass Spectrometry Analysis—Total protein content was quantified by the Bradford assay. Three hundred μg of proteins was reduced using 5 mM DTT and incubated at 56 °C for 20 min. After cooling to room temperature, cysteines were alkylated by addition of 30 mM chloroacetamide for 25 min.

Proteins were then precipitated by adding TCA to a final concentration of 10% [w/v]. After centrifugation at 14000 rpm for 5 min at 4 °C, the pellet was resuspended in 100 mM ammonium bicarbonate (pH 8.0) and 0.5 M urea, with continuous vortexing and sonication. Protein digestion was performed using trypsin at an enzyme/substrate ratio of 1:100 [wt/wt] overnight at 30 °C (Promega, Madison, WI). The reaction was halted by adding TFA to a final concentration of 0.1% [v/v] and the sample was stored at −20 °C.

Label-free Differential 2D-LC/MS—Tryptic digests were first desalted and concentrated on HyperSep C18 cartridges (50 mg/ml, Thermo Scientific, San Jose, CA) according to the manufacturer's instructions. Peptides were then loaded onto a hydrophilic interaction liquid chromatography (HILIC) TSKgel amide-80 column (4.6 mm by 25 cm; Tosoh Bioscience, Stuttgart, Germany) equilibrated with solvent B (98% ACN [v/v], 0.1% TFA [v/v] in water) and connected to an Agilent 1100 HPLC system. The peptides were separated using a 70-min elution gradient that consisted of 5% to 45% solvent A (2% ACN [v/v], 0.1% TFA [v/v] in water) at a flow rate of 500 μl/min. Absorbance was monitored at 214 nm to ensure that all samples contained similar amounts of material. Fractions were collected at 2-min intervals (starting at 30-min elution, 20 in total) and dried using a Speedvac. Peptides were resuspended in 10 μl of solvent C (3.5% ACN [v/v], 0.1% TFA [v/v] in water) and analyzed by LC-MS/MS. The LC-MS/MS system consisted of an LTQ XL IT mass spectrometer (Thermo Scientific) equipped with a microflow ESI source. Samples (6.5 μl) were injected and desalted on a peptide trap (C18 Pepmap 0.30 × 5 mm, ThermoScientific) equilibrated with solvent C (3.5% ACN [v/v], 0.1% TFA [v/v] in water) at a flow rate of 30 μl/min. After valve switching, peptides were eluted in backflush mode from the trap onto the analytical column (BioBasic C18 0.18 × 150 mm, ThermoScientific) equilibrated in solvent D (5% ACN [v/v], 0.05% formic acid [v/v] in water) and separated using a 70-min gradient from 0% to 70% solvent E (80% ACN [v/v], 0.05% formic acid [v/v] in water) at a flow rate of 1.5 μl/min. The MS scan routine was set to analyze, by MS/MS, the five most intense ions of each full MS scan, with dynamic exclusion enabled to ensure detection of co-eluting peptides.

Protein Identification and Quantitation—Protein identification was performed with Sequest HT. More specifically, peak lists were generated by Extract-MSn (Thermo Scientific) within Proteome Discoverer 1.4.2. From raw files, MS/MS spectra were exported using the following settings: peptide mass range 350–5000 Da, minimal total ion intensity 500. The resulting peak lists were searched using Sequest HT against a human protein database obtained from UniProt (March 1, 2014, 87,489 entries). The following parameters were applied: trypsin was selected with proteolytic cleavage only after arginine and lysine; the number of internal cleavage sites was set to 1; mass tolerance for precursors and fragment ions was 1.0 Da; and considered dynamic modifications were +15.99 Da for oxidized methionine and +57.00 for carbamidomethyl cysteine. Peptide matches were filtered using the q-value and posterior error probability calculated by the Percolator algorithm, ensuring an estimated false discovery rate (FDR) below 5%. Filtered Sequest HT output files for each peptide were grouped according to the protein from which they were derived, and their individual peptide spectrum match (PSM) score was taken as an indicator of protein abundance. No normalization procedure was required because sampling rates (*mean PSM ÷ number of detected proteins*) were similar between all samples (17 ± 0.57 in fresh samples and 16 ± 0.44 in frozen samples). These MS proteomic data were deposited in the ProteomeXchange Consortium database via the PRIDE partner repository with the data set identifier PXD008183.

Bioinformatics—Gene ontology (biological process and cellular component) analysis of the ensemble of detected proteins was performed through WebGestalt (http://www.WebGestalt.org) and DAVID (https://david.ncifcrf.gov) online databases. Pathway analysis was conducted via the KEGG pathway (http://www.genome.jp/kegg/pathway.html). Identification of matrisome proteins was achieved by comparison against matrisome atlas proteins (13). JMP® 12.2.0 was used to generate qualitative analysis graphs to compare fresh and frozen samples.

Histological and Immunohistochemical Analyses—Histological analysis was performed on fresh and frozen-thawed samples of ovarian cortex. After fixation, the ovarian fragments were dehydrated, embedded in paraffin and serially sectioned (5 μm-thick sections). Every fourth slide was stained with hematoxylin-eosin (Merck, Darmstadt, Germany) for histological evaluation; the other slides (Superfrost® Plus slides, Menzel-Glaser, Braunschweig, Germany) were kept for immunostaining.

Paraffin sections were deparaffinized with Histosafe (Yvsolab SA, Beerse, Belgium) and rehydrated in alcohol series. After blocking endogenous peroxidase activity with 3% H_2O_2 [v/v], epitope unmasking was performed with use of citrate buffer (0.01 M) at 98 °C for 75 min in a water bath or Tris-EDTA-Tween buffer (Tris 10 mM, EDTA 1 mM pH 9.0, Tween 20) at 96 °C for 20 min. Slides were incubated for 30 min with 10% goat serum and 1% BSA to block nonspecific binding sites and then analyzed using primary antibodies to proliferating cell nuclear antigen (PCNA) (1/4000 dilution, Dako, Glostrup, Denmark), desmin (1/50 dilution, Dako), alpha-smooth muscle actin (αSMA) (1/100 dilution, Dako), β-catenin (1/15000 dilution, BD Biosciences, San Diego, USA), emilin-1 (1/50 dilution, Sigma), fibrillin-1 (1/100 dilution, Sigma), collagen IV (1/25 dilution, Dako) and VI (1/100 dilution, Acris, Tokyo, Japan).

Immunohistochemical staining was carried out using 3,3′-diaminobenzidine (DAB) horseradish peroxidase chromogen-based system (EnVision™+, Dako) and hematoxylin as a counterstain. Slides were then mounted with DPX mounting medium (Sigma). Negative control samples were obtained by omission of the primary antibody, whereas placenta was used as a positive control for collagen VI, endometrium as a positive control for PCNA, desmin, αSMA, β-catenin and fibrillin-1, and uterine myoma tissue as a positive control for emilin-1 and collagen IV. Glycosaminoglycans were identified by alcian blue staining at pH 2.5 (Bio-Optica, Milan, Italy) to label carboxylated and sulfated proteoglycans (14). Images were taken with a Nikon Eclipse Ci microscope equipped with a Leica DFC450 camera interfaced to Leica Application Suite V4.5 software.

Western Blotting—Proteins (25 μg) in each sample were precipitated using the methanol:chloroform method, then boiled in 2X Laemmli buffer and loaded onto polyacrylamide gels. Following SDS-PAGE, the proteins were transferred onto PVDF membranes, which were then blocked in Tris-buffered saline (TBS) containing 0.1% [v/v] Tween and 3% [w/v] BSA. Membranes were incubated overnight at

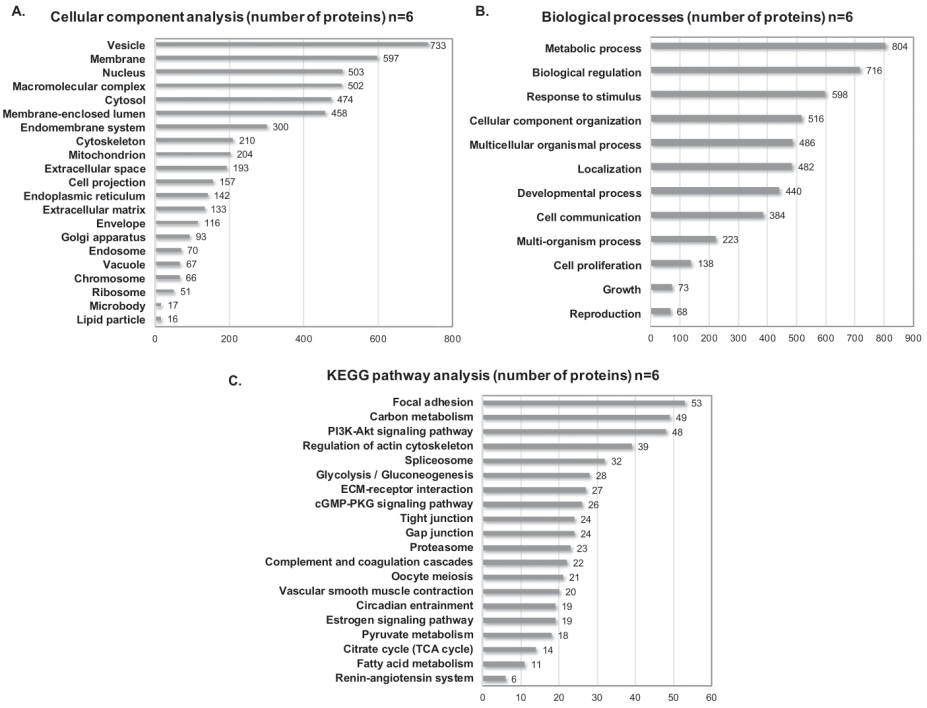


FIG. 1. **Gene ontology and pathway analysis of the ovarian proteome.** *A*, Cellular component analysis. *B*, Biological process analysis. Enriched biological processes and protein localization were achieved using WebGestalt database. *C*, KEGG pathway analysis. Proteins were identified based on conversion of their UniProt accession ID to Entrez Gene.

4 °C with primary antibodies against mimecan (OGN, 1/4000 dilution, Invitrogen, CA, USA) and insulin-like growth factor-binding protein complex acid labile subunit (IGFALS, 1/1000 dilution, OriGene, Rockville, USA), diluted in blocking buffer, then washed extensively in TBS containing 0.1% [v/v] Tween before and after incubation for 1 h with HRP-conjugated secondary antibodies (1/20,000 dilution). Glyceraldehyde-3-phosphate dehydrogenase (GAPDH, 1/10,000 dilution, Merck) was used as a loading control. Immunodetection was achieved with ECL Classico substrate (Merck).

RESULTS

Total Ovarian Proteome Analysis—A total of 5,253 proteins were detected with an FDR $<5\%$, out of which 1508 unique proteins were confidently identified based on a score ≥ 10. These 1508 proteins were kept for further bioinformatic analysis.

Functional Classification of the Ovarian Proteome and Pathway Analysis—To obtain an extended evaluation of the pool of proteins identified within our samples, we conducted cellular component, biological process and KEGG pathway analyses online using WebGestalt (http://WebGestalt.org) on all detected proteins within the threshold, after converting their UniProt accessions into Entrez Gene and removing duplicates. The following settings were selected to carry out the functional classification: genome protein-coding as a reference set for enrichment analysis, and overrepresentation enrichment analysis (ORA) as a method of reference. We thus obtained a better understanding of the gene ontology of detected proteins within our samples (Fig. 1).

Cellular component analysis revealed, at a glance, the localization of proteins detected by MS and their distribution among cellular compartments (Fig. 1*A*). It is worth mentioning that whereas membrane proteins represented most of detected proteins, it was also possible to extract proteins from different cellular compartments. Indeed, our protein extraction method enabled us to extract and detect, with a high degree of confidence, extracellular as well as intracellular proteins, transmembrane proteins and cell receptors, such as mem-

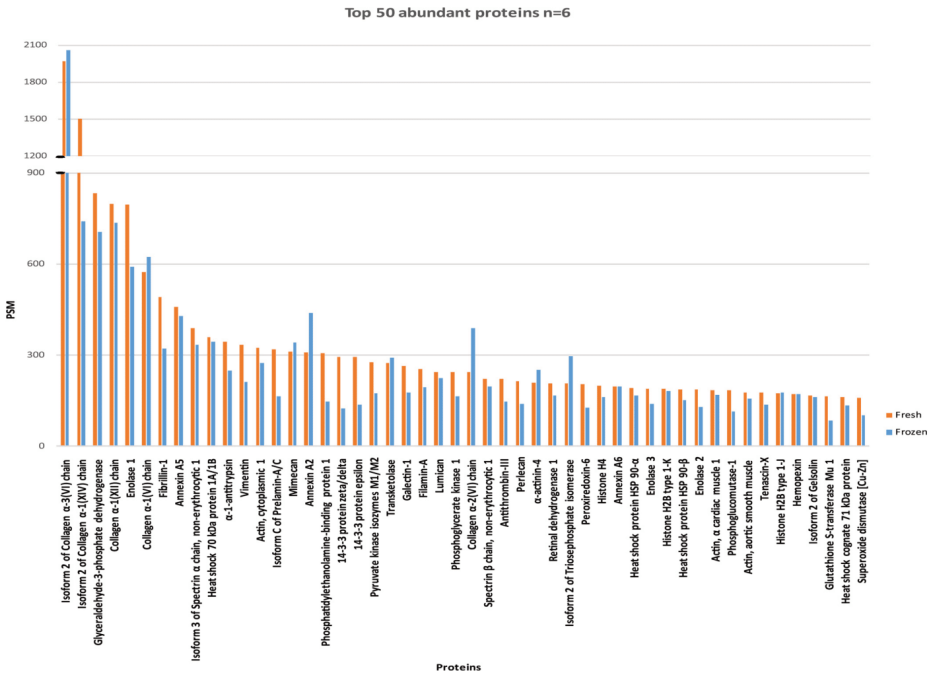


FIG. 2. **TOP 50 most abundant proteins.** After retrieval of the top contaminating plasma proteins from the proteome data set, the most abundant proteins in all samples were classified based on their PSM.

brane-associated progesterone receptor component 1, ryanodine receptor 1 and prolow-density lipoprotein receptor-related protein 1.

Biological process analysis showed many detected proteins to be implicated in metabolic processes, growth, proliferation and communication (Fig. 1*B*). Despite limited available information on ovarian proteomics, 68 proteins were confidently assessed as being involved in reproduction, whereas others were responsive to endogenous and exogenous stimulation, including photosensitive and mechanosensitive proteins.

Relevant biological processes related to reproduction were further investigated through pathway analysis using the KEGG database (Fig. 1*C*), which highlights proteins involved in the phosphoinositide 3-kinase serine/threonine kinase Akt (PI3K-Akt) signaling pathway and oocyte meiosis pathway. Among our proteomic data, we also detected other pathways linked to ovarian activity, such as cyclic GMP-protein kinase G (cGMP/PKG), gap junctions, and estrogen signaling (supplemental Data S1*A*).

Different mechano-regulating pathways chiefly related to smooth muscle contraction and relaxation, like the actin cytoskeleton organization pathway, were also identified. Moreover, because cells function in mutual interaction with the surrounding ECM for ECM regulation, cellular adhesion and activity modulation, we detected ECM-interaction receptors and focal adhesion proteins. Interaction between the ECM and ovarian cells is also governed by matrix metalloproteinases (MMPs), which were encountered, but with a very low PSM and score, reflecting their small proportion compared with other proteins found in our samples. Nevertheless, some ECM degradation proteases were clearly discernible, namely cathepsin G, cathepsin D and plasmin.

Top 50 Detected Proteins—High expression of some proteins in the ovary suggested that they may play specific roles in the maintenance of normal ovarian function (Fig. 2). The 50 most abundant proteins observed in our fresh ($n = 3$) and frozen ($n = 3$) samples were pooled and ranked based on the number of PSMs after retrieval of hemoglobin subunits and top plasma-contaminating proteins: serum albumin, sero-

transferrin, ceruloplasmin, transthyretin, immunoglobulin, complement factors and apolipoprotein A-I (inspired by commercial kits available for plasma protein retrieval from analyzable samples). Around 76% of ranked proteins were recorded among the 50 most commonly found proteins in each individual sample. Collagens, as expected, were the most abundant proteins, mainly collagen VI, followed by cytoskeleton organization proteins (vimentin, α-filamin, actin, actinin) and ECM (annexins, fibrillin-1, galectin, lumican) and cellular regulators (GAPDH, transketolase, 14-3-3 protein zeta/delta) from different cellular compartments. Certain proteogylcans were also widely detected, such as mimecan and perlecan.

Ovarian ECM Proteome Map—Although gene ontology can offer us a preliminary understanding of the cellular compartments, functions and biological processes of proteins, it has clear limitations with respect to ECM protein differentiation and classification, which is why we needed to clearly establish which proteins should be considered part of the ECM. To this end, all proteins detected by MS were compared against the Matrisome Project data (13) to identify all ECM proteins within our samples. Hence, we were able to provide an extended definition of the ovarian ECM, including not only all structural ECM components, but also proteins able to regulate and remodel the ECM. We subsequently categorized our proteins following Naba *et al.* 's (2016) classification (13):

1 Core matrisome proteins: ECM glycoproteins, collagens and proteoglycans.

2 ECM-associated proteins.

- ECM-affiliated proteins: proteins showing biochemical and architectural analogy with ECM proteins or known to be associated.
- ECM regulators: proteins responsible for ECM turnover.
- Secreted factors interacting with core ECM proteins.

The ensemble above forms the matrisome (Fig. 3). Subsequently, only matrisome proteins that were confidently detected based on score and number of unique peptides were retained and their distribution among samples was evaluated and compared between tests, using their PSM values as an estimate of protein abundance. This approach allowed us to constitute the ovarian matrisome draft map consisting of: (1) the core matrisome, including 28 glycoproteins, 11 subtypes of collagen and 7 proteoglycans, representing 15%, 49% and 7% of the total matrisome proteins respectively (Fig. 3 and 4); and (2) matrisome-associated proteins, including 12 ECM-affiliated proteins, 23 ECM regulators and 4 secreted factors, representing around 18%, 10%, and 1% of the total matrisome proteins respectively. This percentage calculation was based on the sum of PSM means of all proteins within the same category (*e.g.* collagens), divided by the sum of PSM means of all matrisome proteins (Fig. 3). Thus, the ECM of human ovarian cortex comprises 85 matrisome proteins in total: 46 core matrisome proteins and 39 matrisome associated-proteins.

As expected, secreted factors and ECM modification enzymes were less abundant than structural proteins and, consequently, less well represented in our data set (Fig. 3).

Comparison Between Fresh and Frozen-Thawed Ovarian Cortex Proteomic Data—In order to evaluate the ability of cryopreserved tissue to reflect fresh tissue proteomic composition, we compared proteomic data from fresh and cryopreserved samples. A comparison of total proteins within each group showed similar variability between fresh and frozen samples (Fig. 5*A*) and, interestingly, an overlap of more than 70% in detected proteins between the two sample types (Fig. 5*B*). Considering only matrisome proteins, analysis of PSM means revealed no clear difference between fresh and frozen-thawed samples among highly abundant proteins. However, the curve showed some differences among less abundant proteins, which are very difficult to detect by MS in complex samples such as ours (Fig. 6).

Histological and Immunohistochemical Analyses—To assess the localization and distribution of detected proteins of interest by MS, 8 proteins from different cellular components with relevant functions in ovarian tissue were analyzed. Fresh and frozen-thawed samples collected from all patients were evaluated and compared by immunohistochemical staining (Fig. 7). It is important to stress that no visible differences between fresh and frozen-thawed tissue samples were observed in any of the selected proteins.

First, to confirm MS data on the dominant type of collagen in ovarian cortex, collagen VI was stained and compared with collagen IV, because it is the most widely characterized collagen type in the ovary (10-15-17). Positive staining for collagen IV was predominantly found in the follicular basement membrane, whereas collagen VI was detected throughout the interstitial ECM, and often close to the basement membrane. Collagen VI has different roles in tissues where it is expressed, ranging from mechanical roles, which are typical of collagen components of the ECM, to more specific cytoprotective functions, counteracting apoptosis and oxidative damage and regulating cell autophagy and differentiation (18).

Mechanical tissue features related to ovarian cyclic evolvement were evaluated using desmin and αSMA as markers of muscle contraction. Although ovarian cortex was highly immunopositive for desmin, it contained lower levels of αSMA, which was mainly present around blood vessels in all analyzed samples.

ECM proteins emilin-1 and fibrillin-1 were investigated as elasticity markers (19–20). Immunostaining results showed broad distribution of both glycoproteins within ovarian cortex in all patient samples with similar localizations, emphasizing the close relationship between structural and regulatory properties of emilin-1 and fibrillin-1 in connective tissue. Emilin-1 is usually distributed in tissues where resilience and elastic recoil are prominent, is known to interact with integrins, and

Core matrisome

Glycoproteins

PSM: Low — High

ENTREZ GENE Accession	Protein name	P1 fresh	P1 frozen	P2 fresh	P2 frozen	P3 fresh	P3 frozen	PSM mean
1805	Dermatopontin (DPT)	9	10	17	21	15	12	14
10516	Fibulin 5 (FBLN5)	33	33	18	14	24	21	24
2200	Fibrillin 1 (FBN1)	321	175	214	281	490	321	300
2243	Fibrinogen alpha chain (FGA)	41	25	12	11	19	14	20
2244	Fibrinogen beta chain (FGB)	90	48	67	68	73	38	64
2266	Fibrinogen gamma chain (FGG)	63	65	47	50	55	25	51
3483	Insulin-like growth factor-binding protein acid labile subunit (IGFALS)			7	3	7		6
3908	Laminin subunit alpha 2 (LAMA2)	3	2	1	5	9	4	4
3910	Laminin subunit alpha 4 (LAMA4)	11	7	1	1	2	2	4
3911	Laminin subunit alpha 5 (LAMA5)	115	78	12	26	4	4	40
3912	Laminin subunit beta 1 (LAMB1)	22	15	4	3	2	3	8
3913	Laminin subunit beta 2 (LAMB2)	117	83	32	47	19	20	53
3915	Laminin subunit gamma 1 (LAMC1)	98	78	33	48	14	14	48
4237	Microfibrillar-associated protein 2 (MFAP2)	10	7	11	11	11	17	11
4239	Microfibrillar-associated protein 4 (MFAP4)	35	29	100	102	25	31	54
4811	Nidogen 1 (NID1)	28	18	8	10	4	6	12
22795	Nidogen 2 (NID2)	70	44	21	21	5	6	28
5118	Procollagen C-endopeptidase enhancer (PCOLCE)		1	13	5		2	5
7057	Thrombospondin 1 (THBS1)	7	3	4	4	2	2	4
7448	Vitronectin (VTN)	17	14	25	60	42	29	31
7450	Von Willebrand factor (VWF)	13	9	2	6	2	3	6
11117	Elastin microfibril interfacer 1 (EMILIN1)	44	31	115	104	102	47	74
64129	Isoform 3 of Tubulointerstitial nephritis antigen-like (TINAGL1)	8	7	5	9	2	1	5
148113	Cartilage intermediate layer protein 2 (CILP2)			13	32	9	6	15
2335	Isoform 10 of Fibronectin (FN1)	81	49	78	63	36	6	52
7045	Transforming growth factor beta induced (TGFBI)	79	37	56	75	30	36	52
7148	Tenascin XB (TNXB)	131	79	179	139	112	29	112
UniProt accession								
B4DW75	EGF-containing fibulin-like extracellular matrix protein 1 (EFEMP1)	14	8	6	9	4	2	7

Glycoproteins			
Sum of PSM means	1104	%	15

Collagens

ENTREZ GENE Accession	Protein name	P1 fresh	P1 frozen	P2 fresh	P2 frozen	P3 fresh	P3 frozen	PSM mean
1277	Collagen type I alpha 1 chain (COL1A1)	1		3	13	5		6
1278	Collagen type I alpha 2 chain (COL1A2)	2		4	6	8	4	5
1282	Collagen type IV alpha 1 chain (COL4A1)	28	13	6	37	2		17
1284	Collagen type IV alpha 2 chain (COL4A2)	22	22	11	12	11	3	14
1291	Collagen type VI alpha 1 chain (COL6A1)	462	367	573	624	318	236	430
1292	Collagen type VI alpha 2 chain (COL6A2)	196	182	244	389	186	138	223
1293	Collagen type VI alpha 3 chain (COL6A3)	1303	1217	1967	2058	1174	1094	1469
1295	Collagen type VIII alpha 1 chain (COL8A1)	4	4	4	3	1		3
1303	Collagen type XII alpha 1 chain (COL12A1)	254	245	798	735	397	241	445
7373	Collagen type XIV alpha 1 chain (COL14A1)	686	652	1309	1280	1500	740	1028
80781	Collagen type XVIII alpha 1 chain (COL18A1)	17	16	35	40	22	22	25

Collagens			
Sum of PSM means	3664	%	49

Proteoglycans

ENTREZ GENE Accession	Protein name	P1 fresh	P1 frozen	P2 fresh	P2 frozen	P3 fresh	P3 frozen	PSM mean
1634	Decorin (DCN)	8		37	27	17	4	19
2331	Fibromodulin (FMOD)	19	18	51	68	28	22	34
3339	Heparan sulfate proteoglycan 2 (HSPG2)	215	140	114	144	38	38	115
4060	Lumican (LUM)	98	73	245	224	186	108	156
4969	Osteoglycin (OGN)	155	103	311	341	168	220	216
5549	Proline and arginine rich end leucine rich repeat protein (PRELP)	2		3	6	3	2	3
127435	Podocan (PODN)	1	2	1	2	8	6	3

Proteoglycans			
Sum of PSM means	546	%	7

FIG. 3. **Ovarian matrisome proteins.** Core matrisome proteins (glycoproteins, collagens and proteoglycans) and matrisome-associated proteins (ECM-affiliated proteins, ECM regulators and secreted factors) detected with a score ≥10 in at least one sample and identified with at least 2 unique peptides in 3 or more samples were taken into consideration. The color code represents protein abundance among fresh and frozen ovarian tissues according to their PSMs. The figure explains how percentages in Fig. 4 were estimated to illustrate matrisome protein distribution in human ovarian tissue (*e.g.* glycoproteins (%) = (sum of PSM means in detected glycoproteins/total PSM mean sum of all categories)*100 = (1104/7423)*100 ≈ 15%).

Matrisom-associated proteins

ECM-affiliated proteins

ENTREZ GENE Accession	Protein name	P1 fresh	P1 frozen	P2 fresh	P2 frozen	P3 fresh	P3 frozen	PSM mean
3263	Hemopexin (HPX)	40	24	173	173	87	33	88
3956	Galectin 1 (LGALS1)	95	31	257	301	265	177	188
3958	Galectin 3 (LGALS3)	13	16	31	25	14	16	19
7123	C-type lectin domain family 3 member B (CLEC3B)	8	3	8	9	10	3	7
23654	Plexin B2 (PLXNB2)	1		4	6	2	3	3
301	Annexin A1 (ANXA1)	58	72	149	161	58	123	104
302	Annexin A2 (ANXA2)	302	250	308	440	284	483	345
307	Annexin A4 (ANXA4)	33	41	43	42	52	59	45
308	Annexin A5 (ANXA5)	200	207	459	430	385	379	343
309	Annexin A6 (ANXA6)	123	123	206	202	184	303	190
UniProt accession								
B4DT77	Annexin 7 (ANXA7)	4	6	8	15	14	13	10
B4DVE7	Annexin 11 (ANXA11)	6	15	14	18	12	17	14

ECM-affiliated proteins			
Sum of PSM means	1355	%	18

ECM regulators

ENTREZ GENE Accession	Protein name	P1 fresh	P1 frozen	P2 fresh	P2 frozen	P3 fresh	P3 frozen	PSM mean
2	Alpha-macroglobulin (A2M)	75	46	49	28	87	40	54
183	Angiotensinogen (AGT)	3	3	19	9	8	1	7
1476	Cystatin B (CSTB)	9	3	16	11	11	18	11
3273	Histidine-rich glycoprotein (HRG)	6	10	24	11	9	19	13
3697	Inter-alpha-trypsin inhibitor heavy chain 1 (ITIH1)	3	1	9	4	7	3	5
3698	Inter-alpha-trypsin inhibitor heavy chain 2 (ITIH2)	3	2	3	2	1	2	2
3700	Inter-alpha-trypsin inhibitor heavy chain family member 4 (ITIH4)	8	4	29	20	19	5	14
5265	Serpin family A member 1 (SERPINA1)	168	76	298	213	344	249	225
12	Serpin family A member 3 (SERPINA3)	8	13	30	28	5	3	15
5267	Serpin family A member 4 (SERPINA4)		2	4	2	2	1	2
1992	Serpin family B member 1 (SERPINB1)	6	1	24	15	14	13	12
5269	Serpin family B member 6 (SERPINB6)	6	5	77	59	126	43	53
462	Serpin family C member 1 (SERPINC1)	165	113	221	147	184	84	152
3053	Serpin family D member 1 (SERPIND1)	7	4	21	11	2	2	8
5270	Serpin family E member 2 (SERPINE2)	7		8	11	6	1	7
5176	Serpin family F member 1 (SERPINF1)	19	10	47	36	20	14	24
5345	Serpin family F member 2 (SERPINF2)	1	2	5	10	2		4
871	Serpin family H member 1 (SERPINH1)	33	28	28	35	33	47	34
5340	Plasminogen (PLG)	8	2	7	9	10	5	7
1508	Cathepsin B (CTSB)	5	3	3	1			3
1509	Cathepsin D (CTSD)	20	8	18	20	28	22	19
259	Alpha-1-microglobulin/bikunin precursor (AMBP)	1	4	66	22	53	27	29
UniProt accession								
B4E1H2	Plasma protease C1 inhibitor (SERPING1)	13	12	31	20	6	7	15

ECM regulators			
Sum of PSM means	715	%	10

Secreted factors

ENTREZ GENE Accession	Protein name	P1 fresh	P1 frozen	P2 fresh	P2 frozen	P3 fresh	P3 frozen	PSM mean
3054	Host cell factor C1 (HCFC1)	2		8	10	4	3	5
6277	S100 calcium binding protein A6 (S100A6)	4	1	14	12	5		7
6282	S100 calcium binding protein A11 (S100A11)	12	5	29	31	35	6	20
6284	S100 calcium binding protein A13 (S100A13)	2		5	10	11	9	7

Secreted factors			
Sum of PSM means	40	%	1

FIG. 3.—*continued*

may connect cells to elastic fibers by providing them with specific cell adhesion features (21); Fibrillin-1 has been shown to provide long-term force-bearing structural support to connective tissues and contains calcium-binding EGF-like domains, integrin-binding Arg-Gly-Asp (RGD) sequences, as well as heparin-binding domains capable of binding cell surface HSPGs (22). The presence of such structural motifs suggests that fibrillin may direct not only cell signaling, but also assembly of elastic microfibers.

Proteins related to meiosis and follicular endowment were also evaluated, namely PCNA and β-catenin as a core molecule of the WNT/β-catenin pathway and major component of cellular junctions involved in cellular communication and signal transduction. Immunohistochemical

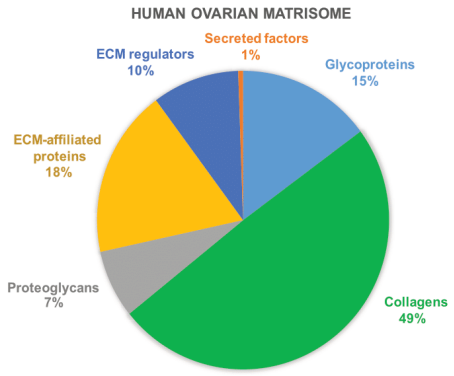


FIG. 4. **Pie chart of matrisome protein categories.**

analysis revealed PCNA-positive cells at the nuclear level in both fresh and frozen samples, as it showed positive β-catenin staining localized in the cell cytoplasm and junctions.

Because glycosaminoglycans are key components of the ECM, ensuring its homeostasis and growth factor sequestering by proteoglycans, their presence was evaluated by alcian blue staining. It revealed their diffuse distribution throughout the ovarian cortex of all patients (Fig. 7).

Western Blotting—Western blotting confirmed detection of two ECM proteoglycans; OGN and IGFALS, in the same samples analyzed by MS (Fig. 8). This is the first time that the presence of these proteins has been reported in human ovarian cortex.

Insulin-like growth factor-binding proteins such as IGFALS are known to play an important role as modulators of insulin-like growth factor (IGF) activity thanks to their high affinity (23). Indeed, they can stimulate or inhibit IGF signaling depending on circumstances by either concentrating IGF close to its receptors or, conversely, hampering sterically their binding (23). This process is of a high importance given the involvement of IGF in follicle growth regulation, selection, atresia, cellular differentiation, steroidogenesis, oocyte maturation, and cumulus expansion evidenced in animal models and humans (24–25).

Western blotting results highlighted the abundance of OGN in ovarian tissue. This protein belongs to a small leucine-rich proteoglycan (SLRP) family, a collagen-associated class of proteins that have an impact on collagen fibrillogenesis and an indirect effect on cell growth. This protein is mainly associated with bone formation and negative regulation of smooth muscle proliferation (26), but its involvement in ovarian tissue is still unknown.

DISCUSSION

The present study confidently identified 1508 proteins in fresh and frozen human ovarian cortex by 2D-LC/MS. Using bioinformatic tools and data mining analysis, we gained a deeper understanding of the function, cellular distribution and signaling role of these proteins. Although we do not yet fully discern the implication of all of them in the ovarian function, we report the most complete proteomic characterization of human ovarian cortex made to date, including a detailed description of the human ovarian ECM composition, which will lead to a better understanding of the follicle environment.

The technique described can be broadly applied to different tissues of unknown composition to provide a basic understanding of their most abundant proteins and ECM characteristics in one fraction analysis without ECM enrichment. Tissue digestion with Liberase before sample preparation for MS enabled solubilization of major fibrous proteins and thus facilitated analysis of attached molecules and characterization of the ECM. An enzymatic tissue digestion method was chosen because of the high insolubility of ECM proteins, even in strong detergents, which might hinder their detection by MS. Moreover, enzymatic digestion led to rupture of some cellular membranes, which yielded further information on intracellular proteins.

A large panel of proteins was identified within our data set, some of which had only been demonstrated *in vitro* or in animal models, but never in humans. We therefore turned to gene ontology and pathway analysis to better understand their biological role in ovarian tissue, as well as their interactions.

Fundamental cellular biological processes and several oocyte-related events were detected, namely cell communication pathways involving ECM-receptor interaction, focal adhesion and gap junctions, emphasizing the primordial functional importance of ovarian cell interaction and communication. Focal adhesion proteins made up the second largest group. Proteins included in this category were considered important for ovarian function, because focal adhesion is a key means by which cells sense and respond to the extracellular environment. Conformation of these proteins can vary in response to physical forces, and hence their function (27). This fact can be correlated with the importance of biomechanical regulation mechanisms within the ovary and the impact of the mechanical properties of scaffolds used in 3D culture on ovarian cell fate *in vitro* (28–29). Thus, greater awareness of ovarian focal adhesion proteins might provide more insights into ovarian cell communication and implication in reproduction. Gap junction channels, another detected protein category, allow direct cell-cell communication and diffusion of fundamental nutrients and chemical cues essential for follicular development (30). Their assembly is promoted by the WNT/β-catenin pathway of gap junction proteins, wherein β-catenin, a protein documented in our MS data and immu-

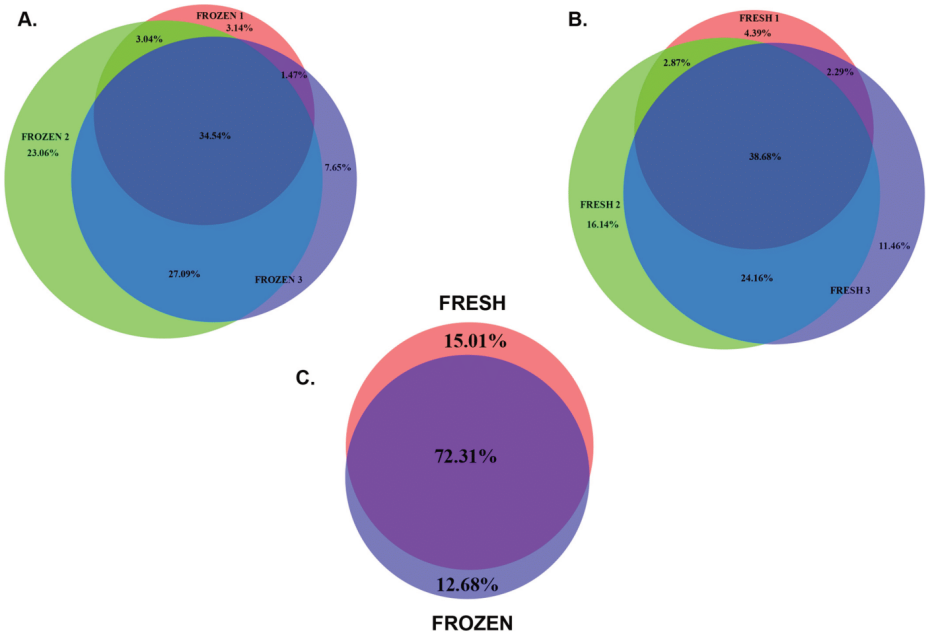


FIG. 5. **Fresh and frozen sample comparison showing the overlap of shared and unique proteins among analyzed samples from the three patients.** *A*, Overlap of fresh samples. *B*, Overlap of frozen samples. *C*, Overlap of all fresh and frozen samples. The comparison was made based on the 1508 confidently identified proteins.

nohistochemical results, plays a key role in reproduction by influencing estradiol synthesis and adversely affecting follicular development (31–32) (Fig. 7*D*).

Other pathways of interest were also detected, such as cyclic GMP-protein kinase G (cGMP/PKG) (supplemental Data S1*B*) implicated in oocyte meiotic arrest (33), and the renin-angiotensin system (RAS) that is presumed to regulate oocyte maturation and quality. Up to day, RAS involvement in hormonal regulation remains unclear because of significant differences between species (34). Hence, by means of our data set acquired by MS, we hope to contribute to the elucidation of unexplored proteins in the RAS pathway in the human ovary (supplemental Data S1*C*).

Numerous coagulation- and angiogenesis-related proteins were identified and further elucidated by KEGG pathway analysis, such as coagulation factors (*e.g.* fibrinogen, prothrombin and plasminogen), as well as those linked to the coagulation and platelet-associated regulatory system (*e.g.* antithrombin, von Willebrand factor, platelet-activating factor acetylhydrolase IB and serpins), revealing their potential function in reproduction. In 2014, Bódis *et al.* suggested the role of the platelet-associated regulatory system (PARS) in regulating activity of the hypothalamo-hypophyseal ovarian system and its function in inducing and stimulating follicular and oocyte maturation and steroid hormone secretion in the ovary (35). In the light of recent discoveries, coagulation proteins in the ovary appear to occupy new roles beyond plugging blood leakage that go as far as stem cell awakening in the ovary and ovarian rejuvenation (36–37), clearly requiring further investigation.

Although pro-angiogenic factors have been widely explored in the ovary, mainly vascular endothelial growth factor (VEGF), anti-angiogenic factors are still under-investigated. Among identified growth factors, we report detection of pigment epithelium-derived factor (PEDF), a glycoprotein known to have potent physiologic anti-angiogenic activity that negates VEGF action (38), and thus plays a potential anti-tumoral role (39). PEDF may also function as a gonadal protectant thanks to its anti-inflammatory and anti-oxidative abilities (40–41), which are two important functions in reproduction, considering that oxidative stress and inflammation have been correlated with infertility in women (38). Moreover, high levels of PEDF secreted before ovulation may induce apoptosis in ovarian sur-

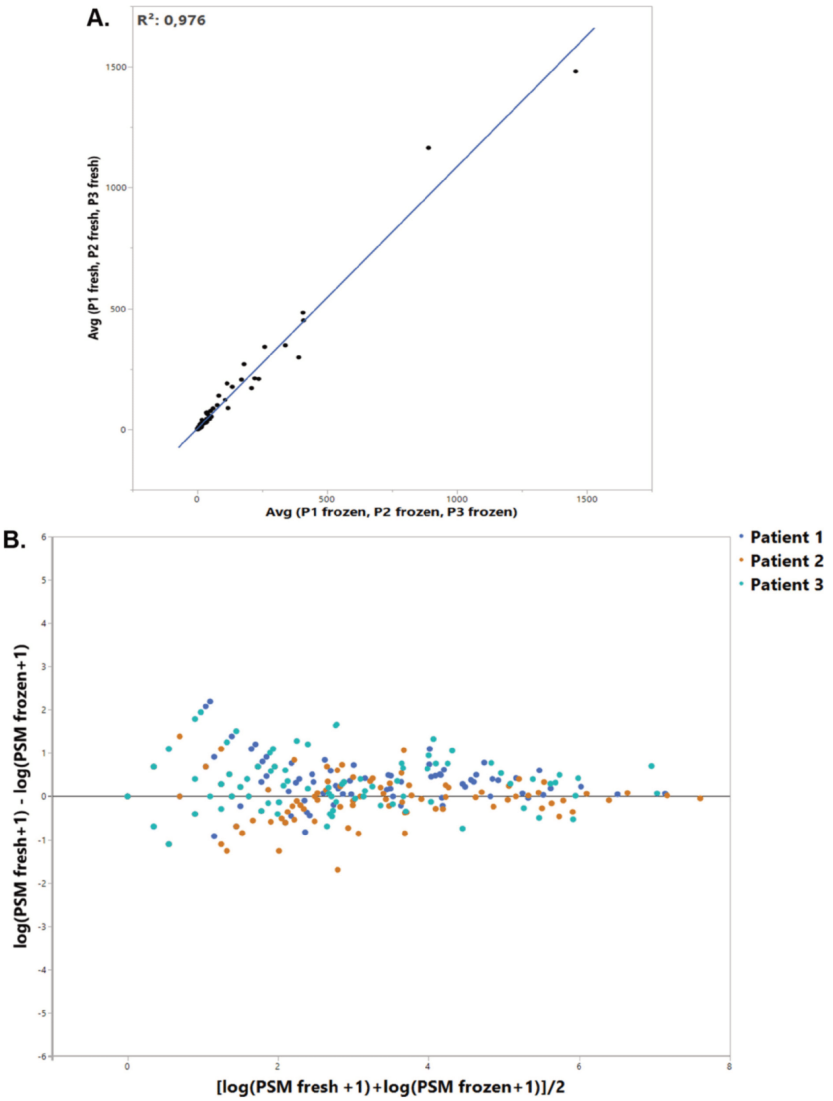


FIG. 6. **Comparison of matrisome proteins in fresh and frozen-thawed ovarian cortex samples.** *A*, Representation of the average abundance (PSMs) of each matrisome protein in both fresh and cryopreserved samples. *B*, Representation of log(PSM fresh+1) − log(PSM frozen+1) per protein in terms of log(PSM+1) mean in both samples as an abundance indicator. The extent of point deviation from the Y = 0 axis translates the difference in protein presence between fresh and frozen samples.

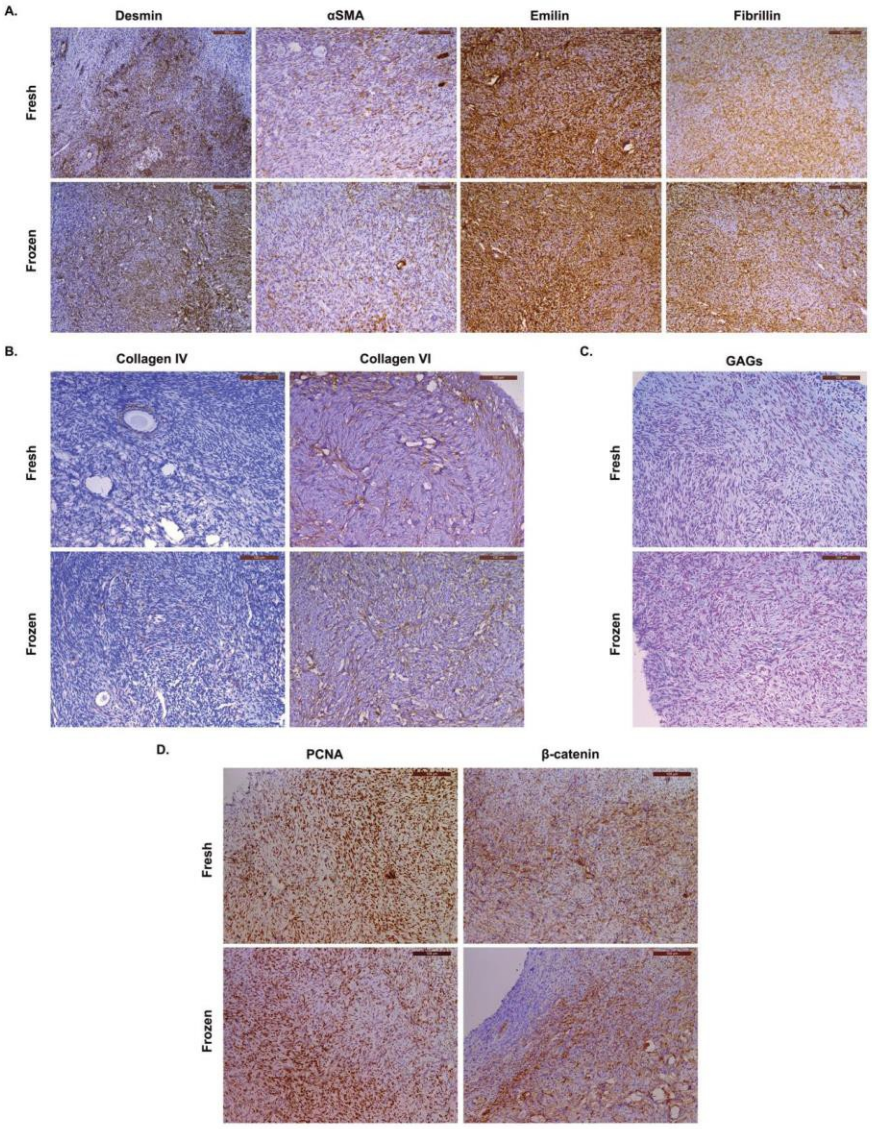


FIG. 7. **Immunohistochemical staining in fresh and cryopreserved ovarian cortex.** *A*, Desmin and αSMA were chosen as muscle contraction markers in the ovary. Emilin-1 and fibrillin-1, both ECM proteins, were selected as elasticity markers. *B*, Collagen VI, the dominant collagen type in ovarian cortex as demonstrated by MS, was analyzed to confirm proteomic results and compared with collagen IV, the most widely characterized collagen type in ovarian cortex in the literature. *C*, GAGs were stained by alcian blue at pH = 2.5 to identify carboxylated and sulfated proteoglycans. *D*, PCNA and β-catenin staining in ovarian cortex are essential proteins for meiosis and cell proliferation.

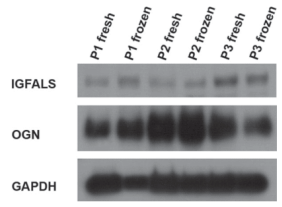


FIG. 8. **Western blotting for MS result confirmation.** Some proteins were detected for the first time in ovarian cortex during this study by MS, namely OGN and IGFALS. Western blotting was used to confirm their detection.

face epithelium cells surrounding the follicle to facilitate release of oocyte (42).

Other rarely explored proteins in human ovaries were documented in our data set, namely 14-3-3 protein isoforms delta and epsilon, which are among the top 50 most abundant proteins. 14-3-3 proteins are known to be central mediators modifying cell-signaling processes, including cell cycle regulation and apoptosis (43–46). It has been suggested that these proteins are involved, at least in the *Xenopus* genus, in maintaining prophase I arrest in germinal vesicle-intact oocytes by sequestering the key phosphatase, in meiosis resumption M-phase inducer phosphatase 2 (CDC25B), in an inactive state (47).

In view of the lack of knowledge of the follicular environment, particularly ECM proteins, this study provides the most comprehensive description available of healthy human ovarian ECM. ECM protein recognition in raw MS data was achieved by comparison of confidently detected proteins with the Matrisome Project data set (13), an *in silico* identified ECM protein set, founded on the characteristic domain-based organization of ECM proteins (48). Hence, we were able to define not only the ovarian ECM, but also the matrisome: an extended definition of the ECM and associated proteins. The dominant collagen type in the ovaries was revealed to be collagen VI, which we showed to be ubiquitously expressed throughout the ECM by immunohistochemistry. It is a basement membrane-anchoring molecule that interacts with collagen IV and may have additional cytoprotective and regulatory functions (18). In addition, it has been suggested that type VI collagen microfibrils are resistant to MMPs but are susceptible to degradation by serine proteases, which are enzymes secreted by granulocytes and neutrophils and known to be present in the ovary during the inflammatory phase preceding ovulation (49).

Within the category of glycoproteins, we identified laminin, fibrillin and thrombospondin, fundamental proteins of the basement membrane, of key importance for cellular attachment, cell proliferation and ECM organization. Most importantly, however, they share EGF-like intrinsic domains, which might bind to EGF receptors and modulate its signaling following their release by ECM proteolysis.

Within the category of proteoglycans, perlecan (HSPG2) was of interest. Like many proteoglycans, HSPG2 is able to bind growth factors and cytokines and sequester them in the ECM and may be crucially important in the action of basic fibroblast growth factor (bFGF), a key growth factor with pro-angiogenic and anti-apoptotic effects in the ovary. Localized in the basement membrane, HSPG2 provides a barrier, which is both size- and charge-selective, and promotes cell adhesion, endothelial cell growth and regeneration. In the ovary, it has been identified as a major estrogen-binding protein in follicular fluid (50).

Another proteoglycan that was unexpectedly detected is OGN, also known as osteoglycin. Its down-regulation in vascular smooth muscle cells results in an increased cell proliferation (51), which can provide insights into possible vascular stimulation of the ovarian tissue grafting site by controlling OGN expression.

In osteoblasts, bone morphogenetic protein 2 (BMP-2) increases OGN expression, whereas in the ovary, the same protein is implicated in primordial follicle assembly during fetal life (52), which might suggest the possible involvement of OGN in ovarian fetal remodeling and follicular assembly under the action of BMP-2. Further research is nevertheless needed to elucidate its function in the ovary, especially in adult life.

In the ovary, enzymatic ECM degradation is required to allow activated follicle expansion. However, to protect surrounding cells from proteolysis, different protease inhibitors appear to be secreted in the ovary, such as protein AMBP, alpha-2-macroglobulin and serpins. The latter is the most widely detected ECM regulator protein family and its expression is closely related to ovarian function (53). Indeed, folliculogenesis stage-specific expression of serpins seems to participate in the growth and atresia of follicles (54), as it may control ECM remodeling (55).

Most of ECM-affiliated proteins have seldom been studied, especially in the human ovary, where we detected galectin-1 and galectin-3. Galectins are a family of β-galactoside-binding proteins implicated in modulating cell-cell and cell-matrix interactions. In 2004, Walzel H *et al.* demonstrated the inhibitory effect of galectin-1 on the steroidogenic activity of granulosa cells, interfering with hormone-receptor interaction and resulting in decreased responses to FSH stimulation in pigs (56). Although galectin-3 has similar functions to galectin-1, it has been associated with loss of progesterone synthesis in the mouse ovary, showing increased presence in atretic preantral follicles and the later stages of luteolysis (57). This protein been described in a variety of tissues, but not explicitly in healthy human ovarian cortex. It plays a role in diverse biological events, such as embryogenesis, angiogenesis, adhesion, cellular proliferation, apoptosis and modulation of immunity and inflammatory processes (58). Overexpression of both galectins is related to ovarian carcinoma; therefore, un-

raveling the regulatory mechanisms might provide therapeutic solutions.

The third category of matrisome-associated proteins includes ECM-secreted factors. Proteins in this group were the least abundant, as expected, but several S100 proteins emerged as the most abundant protein type in this category. In fact, binding of calcium to the S100 protein causes structural rearrangement, exposing a target-binding surface. Target-binding results in a range of responses, from inflammation (S100A13) and cytoskeletal reorganization (S100A10), to cell growth control (S100A9) and tumor suppression (59–60). However, little is known about the action of these calcium-binding proteins in the ovary.

To our knowledge, this is the first time that fresh human ovarian cortex has been analyzed by MS and compared with frozen tissue cryopreserved using the protocol that has so far generated 13 live births after transplantation in our hospital. This comparison demonstrates the suitability of cryopreserved tissue to accurately represent the proteomic composition of fresh tissue, proving that it can be used to conduct more extended MS analyses.

In conclusion, our study provides an accurate first draft map of human ovarian cortex, with identification of its ECM proteins. It represents the first step in human ovary characterization, essential for development of a biomimetic artificial ovary and greater understanding of fertility in women.

Acknowledgments—We thank Olivier Van Kerk and Gaëtan Herinckx for their technical assistance, and Lieven Desmet for his advice on biostatistical evaluation. We also thank Mira Hryniuk, BA, for reviewing the English language of the manuscript.

DATA AVAILABILITY

Raw MS proteomic data were deposited in the ProteomeXchange Consortium database via the PRIDE partner repository with the data set identifier PXD008183 (https://www.ebi.ac.uk/pride/archive/projects/PXD008183).

* This study was supported by grants from the Fonds National de la Recherche Scientifique de Belgique (FNRS) (C. A. Amorim is a Research Associate, FRS - FNRS; grant M 4/1/2/5 awarded to C. A. Amorim; grant 5/4/150/5 awarded to M.-M. Dolmans).

S This article contains supplemental material.

‖ To whom correspondence should be addressed: Pôle de Recherche en Gynécologie, Université Catholique de Louvain, 52 Avenue Mounier, Bte. B1.52.02, 1200 Brussels, Belgium. Tel.: +322-764-5237; E-mail: christiani.amorim@uclouvain.be.

Authors' mailing addresses: Emna Ouni: emna.ouni@uclouvain.be; Didier Vertommen: didier.vertommen@uclouvain.be; Maria Costanza Chiti: maria.chiti@uclouvain.be; Marie-Madeleine Dolmans: marie-madeleine.dolmans@uclouvain.be; Christiani A. Amorim: christiani.amorim@uclouvain.be.

REFERENCES

1. World report on disability. (2011) *Lancet,* **377,** 1977
2. Vogel, C., and Marcotte, E. M. (2012) Insights into the regulation of protein abundance from proteomic and transcriptomic analyses. *Nat. Rev. Genet.* **13,** 227–232
3. Ghaemmaghami, S., Huh, W. K., Bower, K., Howson, R. W., Belle, A., Dephoure, N., O'Shea, E. K., and Weissman, J. S. (2003) Global analysis of protein expression in yeast. *Nature* **425,** 737–741
4. Jarkovska, K., Martinkova, J., Liskova, L., Halada, P., Moos, J., Rezabek, K., Gadher, S. J., and Kovarova, H. (2010) Proteome mining of human follicular fluid reveals a crucial role of complement cascade and key biological pathways in women undergoing in vitro fertilization. *J. Proteome Res.* **9,** 1289–1301
5. Ambekar, A. S., Kelkar, D. S., Pinto, S. M., Sharma, R., Hinduja, I., Zaveri, K., Pandey, A., Prasad, T. S., Gowda, H., and Mukherjee, S. (2015) Proteomics of follicular fluid from women with polycystic ovary syndrome suggests molecular defects in follicular development. *J. Clin. Endocrinol. Metab.* **100,** 744–753
6. Angelucci, S., Ciavardelli, D., Di Giuseppe, F., Eleuterio, E., Sulpizio, M., Tiboni, G. M., Giampietro, F., Palumbo, P., and Di Ilio, C. (2006) Proteome analysis of human follicular fluid. *Biochim. Biophys. Acta.* **1764,** 1775–1785
7. He, H., Teng, H., Zhou, T., Guo, Y., Wang, G., Lin, M., Sun, Y., Si, W., Zhou, Z., Guo, X., and Huo, R. (2014) Unravelling the proteome of adult rhesus monkey ovaries. *Mol. Biosyst.* **10,** 653–662
8. Wang, L., Zhu, Y. F., Guo, X. J., Huo, R., Ma, X., Lin, M., Zhou, Z. M., and Sha, J. H. (2005) A two-dimensional electrophoresis reference map of human ovary. *J. Mol. Med.* **83,** 812–821
9. Heeren, A. M., van Iperen, L., Klootwijk, D. B., de Melo Bernardo, A., Roost, M. S., Gomes Fernandes, M. M., Louwe, L. A., Hilders, C. G., Helmerhorst, F. M., van der Westerlaken, L. A., Chuva de Sousa Lopes, S. M. (2015) Development of the follicular basement membrane during human gametogenesis and early folliculogenesis. *BMC Dev. Biol.* **15**, 4
10. Rodgers, R. J., Irving-Rodgers, H. F., and Russell, D. L. (2003) Extracellular matrix of the developing ovarian follicle. *Reproduction* **126,** 415–424
11. Vanacker, J., Camboni, A., Dath, C., Van Langendonckt, A., Dolmans, M. M., Donnez, J., Amorim, C. A., (2011) Enzymatic isolation of human primordial and primary ovarian follicles with Liberase DH: protocol for application in a clinical setting. *Fertil. Steril.* **96,** 379–383.e3
12. Amorim, C. A., Van Langendonckt, A., David, A., Dolmans, M. M., and Donnez, J. (2009) Survival of human pre-antral follicles after cryopreservation of ovarian tissue, follicular isolation and in vitro culture in a calcium alginate matrix. *Hum. Reprod.* **24,** 92–99
13. Naba, A., Clauser, K. R., Ding, H., Whittaker, C. A., Carr, S. A., and Hynes, R. O. (2016) The extracellular matrix: Tools and insights for the "omics" era. *Matrix Biol* **49,** 10–24
14. Quintarelli, G., and Dellovo, M. C. (1965) The chemical and histochemical properties of alcian blue. IV. Further studies on the methods for the identification of acid glycosaminoglycans. *Histochemie* **5,** 196–209
15. Smith, R. M., Woodruff, T. K., and Shea, L. D. (2010) Designing follicle-environment interactions with biomaterials. *Cancer Treat. Res.* **156,** 11–24
16. Woodruff, T. K., and Shea, L. D. (2007) The role of the extracellular matrix in ovarian follicle development. *Reprod. Sci.* **14,** 6–10
17. Irving-Rodgers, H. F., and Rodgers, R. J. (2005) Extracellular matrix in ovarian follicular development and disease. *Cell Tissue Res.* **322,** 89–98
18. Cescon, M., Gattazzo, F., Chen, P., Bonaldo, P., and Collagen, V. I. (2015) at a glance. *J. Cell Sci.* **128,** 3525–3531
19. Zhang, H., Apfelroth, S. D., Hu, W., Davis, E. C., Sanguineti, C., Bonadio, J., Mecham, R. P., and Ramirez, F. (1994) Structure and expression of fibrillin-2, a novel microfibrillar component preferentially located in elastic matrices. *J. Cell Biol.* **124,** 855–863
20. The UniProt Consortium. (2017) UniProt: the universal protein knowledgebase. *Nucleic Acids Res.* **45,** D158–D169
21. Danussi, C., Petrucco, A., Wassermann, B., Pivetta, E., Modica, T. M., Del Bel. (2011) Belluz, L., Colombatti, A., Spessotto, P., EMILIN1-alpha4/alpha9 integrin interaction inhibits dermal fibroblast and keratinocyte proliferation. *J. Cell Biol.* **195,** 131–145
22. Theocharis, A. D., Skandalis, S. S., Gialeli, C., and Karamanos, N. K. (2016) Extracellular matrix structure. *Adv. Drug Deliv. Rev.* **97,** 4–27
23. Bach, L. A. (2015) Insulin-like growth factor binding proteins 4–6. *Best Pract. Res. Clin. Endocrinol. Metab.* **29,** 713–722
24. Sirotkin, A. V. (2011) Growth factors controlling ovarian functions. *J. Cell. Physiol.* **226,** 2222–2225
25. Wandji, S. A., Gadsby, J. E., Simmen, F. A., Barber, J. A., and Hammond, J. M. (2000) Porcine ovarian cells express messenger ribonucleic acids for the acid-labile subunit and insulin-like growth factor binding protein-3

during follicular and luteal phases of the estrous cycle. *Endocrinology* **141,** 2638–2647
26. Funderburgh, J. L., Funderburgh, M. L., Mann, M. M., Corpuz, L., and Roth, M. R. (2001) Proteoglycan expression during transforming growth factor beta -induced keratocyte-myofibroblast transdifferentiation. *J. Biol. Chem.* **276,** 44173–44178
27. Wu, C. (2007) Focal adhesion: a focal point in current cell biology and molecular medicine. *Cell Adh. Migr.* **1,** 13–18
28. Wood, C. D., Vijayvergia, M., Miller, F. H., Carroll, T., Fasanati, C., Shea, L. D., Brinson, L. C., and Woodruff, T. K. (2015) Multi-modal magnetic resonance elastography for noninvasive assessment of ovarian tissue rigidity in vivo. *Acta Biomater.* **13,** 295–300
29. West, E. R., Xu, M., Woodruff, T. K., and Shea, L. D. (2007) Physical properties of alginate hydrogels and their effects on in vitro follicle development. *Biomaterials* **28,** 4439–4448
30. McGinnis, L. K., and Kinsey, W. H. (2015) Role of focal adhesion kinase in oocyte-follicle communication. *Mol. Reprod. Dev.* **82,** 90–102
31. DaganWells, Z. H. a., Molecular aspects of follicular development. In *Principles and Practice of Fertility Preservation*, Cambridge University Press: Cambridge, 2011; pp 114–128
32. Parakh, T. N., Hernandez, J. A., Grammer, J. C., Weck, J., Hunzicker-Dunn, M., Zeleznik, A. J., and Nilson, J. H. (2006) Follicle-stimulating hormone/cAMP regulation of aromatase gene expression requires beta-catenin. *Proc. Natl. Acad. Sci. U.S.A.* **103,** 12435–12440
33. Vaccari, S., and Weeks, J. L. (2009) 2nd; Hsieh, M., Menniti, F. S., Conti, M., Cyclic GMP signaling is involved in the luteinizing hormone-dependent meiotic maturation of mouse oocytes. *Biol. Reprod.* **81,** 595–604
34. Herr, D., Bekes, I., Wulff, C. (2013) Local Renin-Angiotensin system in the reproductive system. *Front. Endocrinol.* **4**, 150
35. Bodis, J., Papp, S., Vermes, I., Sulyok, E., Tamas, P., Farkas, B., Zambo, K., Hatzipetros, I., and Kovacs, G. L., (2007) "Platelet-associated regulatory system (PARS)" with particular reference to female reproduction. *J. Ovarian Res.* **7,** 55
36. Bukovsky, A. (2015) Novel methods of treating ovarian infertility in older and POF women, testicular infertility, and other human functional diseases. *Reprod. Bio.l Endocrinol.* **13,** 10
37. Hirota, Y., Osuga, Y., Yoshino, O., Koga, K., Yano, T., Hirata, T., Nose, E., Ayabe, T., Namba, A., Tsutsumi, O., and Taketani, Y. (2003) Possible roles of thrombin-induced activation of protease-activated receptor 1 in human luteinized granulosa cells. *J. Clin. Endocrinol. Metab.* **88,** 3952–3957
38. Chuderland, D., Ben-Ami, I., Bar-Joseph, H., and Shalgi, R. (2014) Role of pigment epithelium-derived factor in the reproductive system. *Reproduction* **148,** R53–R61
39. Cheung, L. W., Au, S. C., Cheung, A. N., Ngan, H. Y., Tombran-Tink, J., Auersperg, N., and Wong, A. S. (2006) Pigment epithelium-derived factor is estrogen sensitive and inhibits the growth of human ovarian cancer and ovarian surface epithelial cells. *Endocrinology* **147,** 4179–4191
40. Yamagishi, S., Nakamura, K., Ueda, S., Kato, S., and Imaizumi, T. (2005) Pigment epithelium-derived factor (PEDF) blocks angiotensin II signaling in endothelial cells via suppression of NADPH oxidase: a novel anti-oxidative mechanism of PEDF. *Cell Tissue Res.* **320,** 437–445
41. Wang, J. J., Zhang, S. X., Mott, R., Chen, Y., Knapp, R. R., Cao, W., and Ma, J. X. (2008) Anti-inflammatory effects of pigment epithelium-derived factor in diabetic nephropathy. *Am. J. Physiol. Renal Physiol.* **294,** F1166–F1173
42. Auersperg, N., Wong, A. S., Choi, K. C., Kang, S. K., and Leung, P. C. (2001) Ovarian surface epithelium: biology, endocrinology, and pathology. *Endocr. Rev.* **22,** 255–288
43. Pozuelo Rubio, M., Geraghty, K. M., Wong, B. H., Wood, N. T., Campbell, D. G., Morrice, N., and Mackintosh, C. (2004) 14-3-3-affinity purification of over 200 human phosphoproteins reveals new links to regulation of cellular metabolism, proliferation and trafficking. *Biochem. J.* **379,** 395–408
44. Aitken, A. (2006) 14-3-3 proteins: a historic overview. *Semin. Cancer Biol.* **16,** 162–172
45. Morrison, D. K. (2009) The 14-3-3 proteins: integrators of diverse signaling cues that impact cell fate and cancer development. *Trends Cell Biol.* **19,** 16–23
46. Freeman, A. K., and Morrison, D. K. (2011) 14-3-3 Proteins: diverse functions in cell proliferation and cancer progression. *Semin. Cell Dev. Biol.* **22,** 681–687
47. Duckworth, B. C., Weaver, J. S., and Ruderman, J. V. (2002) G2 arrest in Xenopus oocytes depends on phosphorylation of cdc25 by protein kinase A. *Proc. Natl. Acad. Sci. U.S.A.* **99,** 16794–16799
48. Naba, A., Clauser, K. R., Hoersch, S., Liu, H., Carr, S. A., Hynes, R. O. (2012) The matrisome: in silico definition and in vivo characterization by proteomics of normal and tumor extracellular matrices. *Mol. Cell. Proteomics* **11,** M111.014647
49. Iwahashi, M., Muragaki, Y., Ooshima, A., Nakano, R., and Type, V. I. (2000) collagen expression during growth of human ovarian follicles. *Fertil. Steril.* **74,** 343–347
50. Bentov, Y., Jurisicova, A., Kenigsberg, S., and Casper, R. F. (2016) What maintains the high intra-follicular estradiol concentration in pre-ovulatory follicles? *J. Assist. Reprod. Genet.* **33,** 85–94
51. Deckx, S., Heggermont, W., Carai, P., Rienks, M., Dresselaers, T., Himmelreich, U., van Leeuwen, R., Lommen, W., van der Velden, J., Gonzalez, A., Diez, J., Papageorgiou, A. P., and Heymans, S. (2017) Osteoglycin prevents the development of age-related diastolic dysfunction during pressure overload by reducing cardiac fibrosis and inflammation. *Matrix Biol.* **66,** 110–124
52. Chakraborty, P., and Roy, S. K. (2015) Bone morphogenetic protein 2 promotes primordial follicle formation in the ovary. *Sci. Rep.* **5,** 12664
53. Ny, T., Wahlberg, P., and Brandstrom, I. J. (2002) Matrix remodeling in the ovary: regulation and functional role of the plasminogen activator and matrix metalloproteinase systems. *Mol. Cell. Endocrinol.* **187,** 29–38
54. Hayashi, K. G., Ushizawa, K., Hosoe, M., and Takahashi, T. (2011) Differential gene expression of serine protease inhibitors in bovine ovarian follicle: possible involvement in follicular growth and atresia. *Reprod. Biol. Endocrinol.* **9,** 72
55. Law, R. H., Zhang, Q., McGowan, S., Buckle, A. M., Silverman, G. A., Wong, W., Rosado, C. J., Langendorf, C. G., Pike, R. N., Bird, P. I., and Whisstock, J. C. (2006) An overview of the serpin superfamily. *Genome Biol* **7,** 216
56. Walzel, H., Brock, J., Pohland, R., Vanselow, J., Tomek, W., Schneider, F., and Tiemann, U. (2004) Effects of galectin-1 on regulation of progesterone production in granulosa cells from pig ovaries in vitro. *Glycobiology* **14,** 871–881
57. Nio, J., and Iwanaga, T. (2007) Galectins in the mouse ovary: concomitant expression of galectin-3 and progesterone degradation enzyme (20alpha-HSD) in the corpus luteum. *J Histochem Cytochem* **55,** 423–432
58. Devouassoux-Shisheboran, M., Deschildre, C., Mauduit, C., Berger, G., Mejean-Lebreton, F., Bouvier, R., Droz, J. P., Fenichel, P., and Benahmed, M. (2006) Expression of galectin-3 in gonads and gonadal sex cord stromal and germ cell tumors. *Oncol. Rep.* **16,** 335–340
59. Donato, R. (2001) S100: a multigenic family of calcium-modulated proteins of the EF-hand type with intracellular and extracellular functional roles. *Int. J. Biochem. Cell Biol.* **33,** 637–668
60. Santamaria-Kisiel, L., Rintala-Dempsey, A. C., and Shaw, G. S. (2006) Calcium-dependent and -independent interactions of the S100 protein family. *Biochem. J.* **396,** 201–214

Divide-and-Conquer Matrisome Protein (DC-MaP) Strategy: An MS-Friendly Approach to Proteomic Matrisome Characterization

Extracellular proteins present an analytical challenge because of their highly crosslinked biochemical properties, and therefore insoluble molecules, even in the strongest organic detergents and denaturants. Nevertheless, theECM high insolubility could be exploited to reduce the complexity of tissue samples and detect scarce proteins at the ECM level.
So far, numerous alternatives have been proposed to address ECM proteins enrichment for proteomic analysis, mainly using high concentrations ofstrong chemical denaturants or surfactants. The drawback of these approaches is that they reduce the proteolytic activity of enzymes used in bottom-up proteomics and interfere with MS and liquid chromatography (LC).Therefore, sample cleanup is often necessary before LC, MS, or LC-MS analysis. Various sample preparation methods were developed, including dialysis, solid-phase extraction sample cleanup using reversed-phase, hydrophilic interaction chromatography, or surfactant precipitation. These methods are time-consuming, only partially efficient, and often lead to protein degradation. Moreover, upon denaturant/surfactant depletion, most protein sample reaggregates and resists digestion, which leads to poor ECM protein recovery and detection.

In our study, we set out to overcome the major issues hampering our ability to characterize the matrisome accurately: unfriendly-MS detergents, irreproducibility, labor-intensive processing, and consequent loss of low abundant proteins (Figure 23).

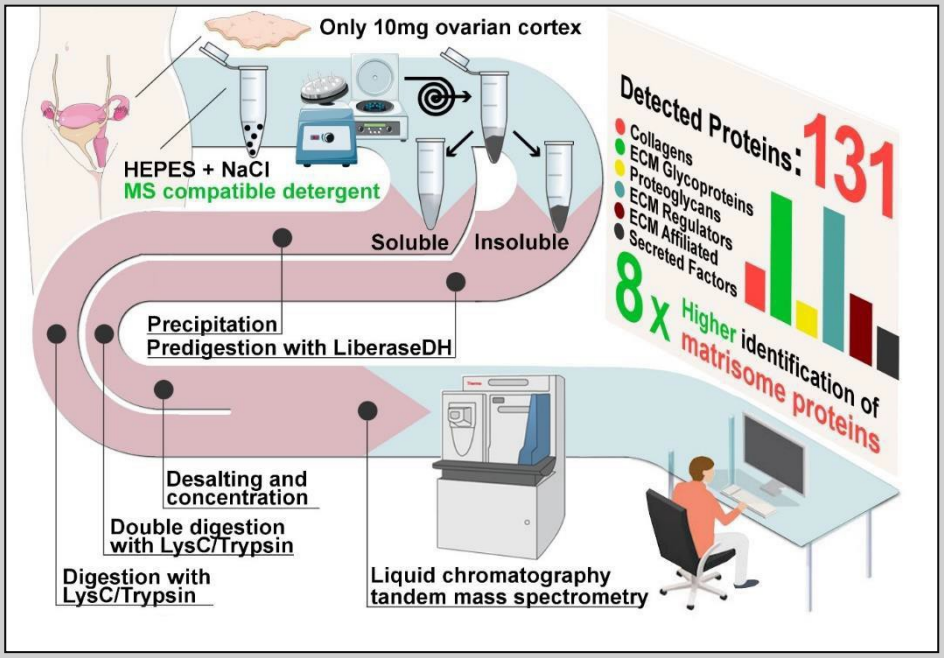


Figure 23 | Graphical summary of the divide and conquer matrisome protein (DC-MaP) technique.

Cleavable detergents have the added benefit that when they are no longer necessary, upon addition of acid to the surfactant-containing sample, the surfactant quickly degrades into innocuous non-surfactant byproducts that can be removed by centrifugation, eliminating the need to remove the detergent before MS analysis. However, these surfactants have not yet been tested for their performance in matrisome proteomics. We chose to test these surfactants on over 50-year old ovaries as being the most challenging in extracting and solubilizing ECM proteins due to their high level of collagen and fibrosis. With mass-limited samples like ovarian biopsies, it can be challenging to obtain sufficient amounts of proteins to generate high-quality mass spectrometric data. Therefore, we gave special care to sampling standardization and screened different mechanical disruption matrices to choose the one that yielded the

highest protein amount, which was the stainless steel beads with 0.3 mm diameter. This method overcame handy, time-consuming, partial mechanical lysis and possible cross-contamination encountered by other applied methods (e.g. pestle, grinder). Protein extraction, including the lysis of cells, the release of proteins from different cell compartments, and solubilization of proteins into extraction buffer, is the first step of protein sample preparation. In this context, the addition of 300 mM NaCl to HEPES buffer and its use to resuspend the tested detergents proved effective in solubilizing mainly cellular proteins and enhanced detergent efficiency. Our approach combining centrifugation and MS-compatible detergent along with LC- MS/MS successfully revealed the highest number of ECM proteins that have ever been described before in the human ovary. This was thanks to the use of 0.2% RP with a simple 2-step fractionation, which showed the highest number/quantity of identified matrisome proteins with the highest reproducibility (Figure 23). Moreover, RP has a major advantage over its commercialized competitors; its cleavage does not result in amine containing byproducts. Thus, our proposed method is compatible with the isobaric amine-reactive tandem mass tag labeling reagents, such as TMT or isobaric tags for relative and absolute quantitation (iTRAQ).

We believe that accurate characterization of ECM proteins from different tissue types can be achieved with our DC-Map method to help advance organ engineering efforts by generating a molecular readout that can be correlated with a functional outcome to drive the next generation of engineered organs and catalyze biomarker discovery. To overcome these problems, we developed the first quantitative MS-compatible protocol for ECM characterization, tailored for ECM extraction from small biological samples (~10 mg) and its solubilization. Upon development, this method was applied

in the following study described in my 5th article by comparing ovarian tissue from patients with different reproductive status: prepubertal, reproductive, and menopausal (n=5/age group) to identify and quantify the proteins that are differently expressed in each stage and elucidate the key proteins specific to the human ovary in the reproductive age. These will be integrated into the artificial ovary construct since they represent optimal microenvironment cues for functional follicles.

International Journal of
Molecular Sciences

MDPI

Article

Divide-and-Conquer Matrisome Protein (DC-MaP) Strategy: An MS-Friendly Approach to Proteomic Matrisome Characterization

Emna Ouni [1], Sébastien Pyr dit Ruys [2], Marie-Madeleine Dolmans [1,3], Gaëtan Herinckx [2], Didier Vertommen [2] and Christiani A. Amorim [1,*]

1 Pôle de Recherche en Gynécologie, Institut de Recherche Expérimentale et Clinique, Université Catholique de Louvain, 1200 Brussels, Belgium; emna.ouni@uclouvain.be (E.O.); marie-madeleine.dolmans@uclouvain.be (M.-M.D.)
2 de Duve Institute, Université Catholique de Louvain, 1200 Brussels, Belgium; sebastien.pyrditruys@uclouvain.be (S.P.d.R.); gaetan.herinckx@uclouvain.be (G.H.); didier.vertommen@uclouvain.be (D.V.)
3 Gynecology and Andrology Department, Cliniques Universitaires Saint-Luc, 1200 Brussels, Belgium
* Correspondence: christiani.amorim@uclouvain.be; Tel.: +32-(0)2-764-5287

Received: 28 October 2020; Accepted: 25 November 2020; Published: 30 November 2020

check for updates

Abstract: Currently, the extracellular matrix (ECM) is considered a pivotal complex meshwork of macromolecules playing a plethora of biomolecular functions in health and disease beyond its commonly known mechanical role. Only by unraveling its composition can we leverage related tissue engineering and pharmacological efforts. Nevertheless, its unbiased proteomic identification still encounters some limitations mainly due to partial ECM enrichment by precipitation, sequential fractionation using unfriendly-mass spectrometry (MS) detergents, and resuspension with harsh reagents that need to be entirely removed prior to analysis. These methods can be technically challenging and labor-intensive, which affects the reproducibility of ECM identification and induces protein loss. Here, we present a simple new method applicable to tissue fragments of 10 mg and more. The technique has been validated on human ovarian tissue and involves a standardized procedure for sample processing with an MS-compatible detergent and combined centrifugation. This two-step protocol eliminates the need for laborious sample clarification and divides our samples into 2 fractions, soluble and insoluble, successively enriched with matrisome-associated (ECM-interacting) and core matrisome (structural ECM) proteins.

Keywords: ECM; proteomics; ovary

1. Introduction

Identification and quantification of the components of distinct extracellular matrix (ECM) proteins and comprehension of their underpinning network interactions represent key steps towards elucidating the role of the ECM in health and pathological conditions [1,2]. Proteomics offers an opportunity to address these challenges in a global and unbiased manner, without the need for hypothesis-driven molecular candidates. Indeed, the past decade has seen the emergence of mass spectrometry (MS)-based proteomics [3] as the method of choice to characterize the protein composition of the ECM [4–8].

Despite the significant development in data acquisition and identification of post-translational ECM modifications [9–14], extracellular proteins still present analytical difficulties in proteomic strategies due to the biochemical characteristics of these molecules, which are highly cross-linked, often glycosylated and hence insoluble even in strong detergents and organic denaturants [8]. Obtaining the fullest picture of ECM protein composition is still hampered by its complex biochemical nature and wide

dynamic range. Nevertheless, in recent years, different techniques have been proposed in an attempt to complete our understanding of the human matrisome in health and disease [2]. The matrisome is a contemporary extended definition of the ECM and is composed of 2 major protein categories: (i) core matrisome proteins, including ECM glycoproteins, collagens and proteoglycans; and (ii) ECM-associated proteins, consisting of ECM-affiliated proteins that show biochemical and architectural analogy with the ECM or are known to be associated, ECM regulators that are proteins responsible for ECM turnover, and secreted factors that interact with core ECM proteins [8].

Since only the most abundant proteins are identified in non-targeted proteomics, the ability to selectively enrich for ECM proteins is the first key step of dedicated proteomic pipelines. Recent papers have reported the use of buffers with defined salt and detergent concentrations and increased stringency to sequentially extract (or fully deplete) intracellular components and thereby enrich for less soluble components, mainly core matrisome proteins, and improve ECM-associated protein detection [15]. In this context, ionic, non-ionic, and zwitterionic detergents have been used to solubilize ECM-enriched samples [16]. However, their use in MS presents some limitations. Although SDS is the most widely used detergent [17–19], even at low concentrations (<0.01%) it can severely suppress the ionization of proteins/peptides and hamper their identification. Non-ionic surfactants mostly considered as mild surfactants such as Triton X-100 and NP-40 can cause significant signal suppression and high polymer background in addition to the formation of adducts with the proteins [20]. Zwitterionic surfactants such as CHAPS, characterized by intermediate protein solubilizing abilities, being stronger than non-ionic detergents but not as strong as ionic surfactants (e.g., SDS) have been also used in MS, despite causing adduct formation and signal suppression [20].

As an alternative to detergents, resuspension of ECM-enriched protein samples prior to digestion can also be achieved by the use of high concentrations of chaotropic agents such as urea or guanidinium chloride (GdnHCl) [21] and concomitant use of reducing agents. The currently accepted and widely used solubilization method to obtain ECM-enriched pellets for bottom-up proteomic analysis relies on two reagents: cyanogen bromide (CNBr), which cleaves peptide bonds at the C-terminus of methionine [22]; and hydroxylamine (NH_2OH), which cleaves at the C-terminus of asparagine and the N-terminus of glycine [2,21]. Comparison of these two non-enzymatic cleavage approaches by Hansen's group revealed that hydroxylamine reduced analytical variability compared to CNBr digestion and avoided CNBr toxicity and labor-intensive handling [21,23]. While the NH_2OH method yielded higher concentrations of ECM components and more reproducible measures between replicates, the cleavage specificity of the two chemical approaches presented some limitations that needed further consideration when conducting database searches [21]. The authors also mentioned that quantification of peptides containing asparagine residues should be performed with caution since the NH_2OH cleavage site is not strictly asparagine-specific [21].

Despite some success in overcoming solubility issues of ECM molecules, dialysis, gel filtration, or filter-aided sample preparation (FASP) are required before protein digestion and MS detection for removal of excess detergents, salts and chemicals [18]. Unfortunately, these processes of sample clarification usually induce significant protein sample loss due to buffer exchange and redissolving steps, compromising the sensitivity, reliability and accuracy of proteomic analysis and, more specifically, identification of matrisome composition [24]. With only micrograms of samples available from human biopsies, fractionation becomes an even greater challenge. Successive sample loss can be crippling, and dilution of highly complex mixtures can lead to a deficit of low-abundance protein species below signal-to-noise thresholds.

Decellularization offers another option to enrich ECM proteins while removing intracellular material. However, complete decellularization requires several hours to days of extensive physical and chemical treatment. This may lead to protein degradation and loss of matrisome-associated proteins due to buffer exchanges during the whole process, which could in turn cause poor reproducibility and low recovery [25].

Recently, MS-compatible surfactants have been developed to overcome common limitations of standard detergents described above, namely RapiGest (RP), ProteaseMax (PM), and 3273 (also known as MaSDeS) [16,26,27]. These molecules contain an acid-labile functional group, which quickly degrades into innocuous non-surfactant byproducts upon addition of acid, eliminating the need to remove the detergent prior to MS analysis (effectively rendering it MS-compatible). In addition to these acid-labile surfactants, non-ionic saccharide surfactants such as n-dodecyl β-D-maltoside (DDM) are described as MS-compatible at relatively low concentrations and have been applied for many years for insoluble membranous protein characterization [28,29], but they have never been used for matrisome characterization.

Here, we describe the first application of MS-compatible detergents in matrisome proteomics and propose a novel method of optimized tissue sampling and mechanical digestion adapted to small biological samples before initiating a fractionated extraction. Our protocol is tailored to matrisome proteomics to overcome current limitations in the field and provide a reliable screening, not only of the structural ECM, but also of associated proteins able to regulate and remodel the ECM, through a simple and reproducible workflow.

2. Results

2.1. Stainless Steel Beads Allow Optimal Mechanical Lysis

Ovarian tissue is inherently mechanically resilient. Therefore, to successively homogenize our samples, we chose to apply a mechanical disruption method using 5 different commercial lysing matrices, which yielded different amounts of proteins (Figure 1A). None of the lysing matrices tested left behind any tissue clumps. Based on total extracted protein amounts, we could eliminate condition Cd4, a garnet matrix with one 6.3 mm ceramic sphere that extracted the lowest amount of proteins with a muddy homogenate aspect. While the Cd5 lysing matrix, 1.4 mm ceramic beads delivered promising outcomes in terms of total protein amounts, it showed high variability explained by the more elaborate and time-consuming two-step process: (i) tissue chopping and (ii) disruption of the tissue clumps with 1.4 mm ceramic spheres. Cd3, 0.5 mm zirconium oxide beads extracted the highest protein yield, but the quality profile visualized by total protein labeling on SDS-PAGE revealed poor protein quality (faint and diffuse bands) affected by the mechanical disruption (Figure 1B). Immunoblotting was conducted on supernatants of the pass-throughs, which are composed of soluble proteins, in order to detect any potential impact of lysing matrices on ECM protein solubilization. We observed ECM solubilization under the influence of Cd3, highlighted by a high detected level of fibronectin in the soluble fraction (fraction 1) (Figure 1C). This could later harm the fractionation process and impact the dynamic range.

Two options were left: Cd1 and Cd2. Cd2, 2.8 mm stainless steel beads occasionally led to the fracture of the lysis tube during homogenization and loss of samples, but Cd1 yielded more reproducible results and ease of handling. In addition, it showed a better protein quality profile and good preservation of ECM proteins in the insoluble fraction (fraction 2), highlighted by weak band intensity of fibronectin and undetected osteoglycin (OGN, aka mimecan) in fraction 1 (Figure 1B,C). Thus, Cd1, composed of stainless steel beads measuring 0.3 mm in diameter, enabled optimal mechanical lysis of human ovarian tissue and was therefore used in all downstream procedures.

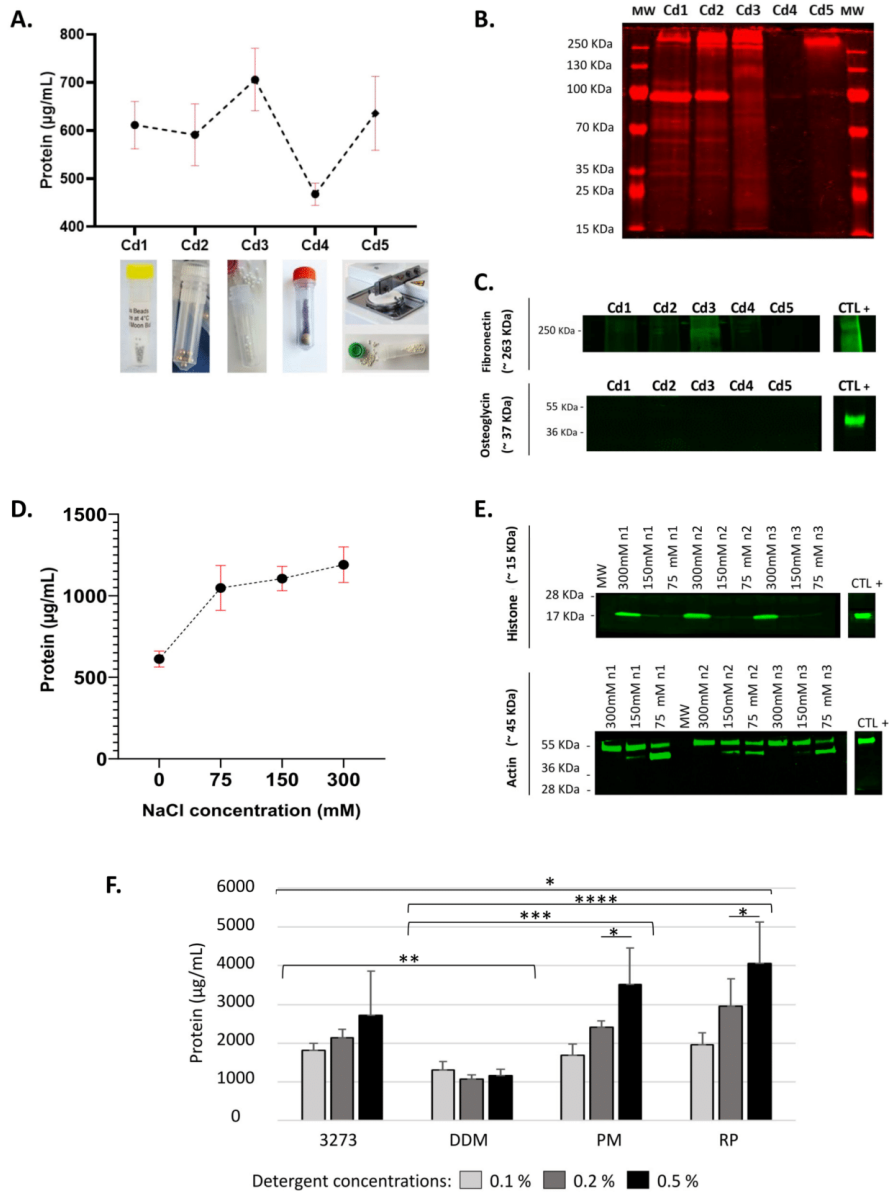


Figure 1. Choice of mechanical lysing matrix and buffer formulation. (**A**) Comparison of 5 lysis beads (n = 3) based on the total amount of soluble extracted proteins (± SD, red lines) from 10 mg samples. The size and nature of lysis matrices is described as follow: Cd1, 0.3 mm stainless steel beads; Cd2, 2.8 mm stainless steel beads; Cd3, 0.5 mm zirconium oxide beads; Cd4, a garnit matrix with a 6.3 mm

ceramic sphere; and Cd5, 1.4 mm ceramic beads. Twenty micrograms of total proteins and a molecular weight marker (MW) were loaded per gel, (**B**) their quality evaluated by electrophoresis, and (**C**) preservation of core matrisome proteins was estimated by Western blot. Ovarian tissue homogenate was used as a positive control (CTL+). (**D**) Three concentrations of NaCl were used to enrich HEPES lysis buffer (n = 3): 75 mM, 150 mM and 300 mM with Cd1 lysis beads. Their evaluation was based on the total amount of extracted proteins (± SD, red lines) and (**E**) their cellular compartment (histone, nucleus; actin, cytoskeleton) in all biological replicates (n1, n2, n3). (**F**) Protein yield obtained by use of Cd1 as a lysing matrix, and 25 mM HEPES and 300 mM NaCl as the optimal lysis buffer to resuspend mass spectrometry-compatible detergents. Two-way ANOVA was applied to compare detergent performance independently of the concentration used, before comparing outcomes with the same detergent at different concentrations (* $p < 0.05$, ** $p < 0.01$, *** $p < 0.001$, **** $p < 0.0001$).

2.2. Potentialization of Protein Extraction Using 300 mM NaCl

Using Cd1 lysis beads, we investigated the extraction efficiency of HEPES lysis buffer containing different NaCl concentrations. Controlling salt concentrations in protein extraction buffers has a great impact on protein extraction yields [30,31]. Concentrations were carefully selected to enhance protein salting without rendering the residual pellet in fraction 2 more insoluble. Indeed, at low salt concentrations (<0.5 M), protein solubility increases along with ionic strength [32].

Higher salt concentrations extracted more soluble proteins (Figure 1D). Primarily, we noted an increase of total protein amount of around 2-fold with 300 mM NaCl yielding the highest amount of extracted proteins. Western blot of histone H3 and actin revealed a difference in extraction of nuclear and cytoskeleton proteins among tested concentrations (Figure 1E). A 300 mM NaCl concentration enabled better extraction of nuclear and cytoskeleton proteins than all other conditions.

A final lysis buffer containing 300 mM NaCl in HEPES was therefore used to resuspend MS-compatible detergents. Quantification of soluble proteins in fraction 1 revealed that RP enabled the best extraction, showing a significantly higher yield with all 3 concentrations (0.1%, 0.2% and 0.5%) than 3273 ($p < 0.05$) or DDM ($p < 0.00001$) (Figure 1F). DDM delivered the poorest protein extraction, with no visible difference between tested concentrations. Most importantly, following addition of RP to the lysis buffer, we succeeded to obtain higher amounts of extracted proteins than with NaCl buffer alone, reaching 4000 µg/mL from 10 mg wet weight tissue.

2.3. Differential Protein Enrichment Favors Matrisome-Associated Protein Detection

Our MS-compatible detergents, 3273, DDM, RP, and PM, were resuspended in the lysis buffer to achieve 0.1%, 0.2%, and 0.5% (w/v) concentrations and used during the mechanical lysis step to homogenize ovarian tissue. The obtained homogenate was centrifuged to recover the soluble supernatant labeled as "fraction 1" and the remaining pellet labeled as "fraction 2". To be able to evaluate our fractionation procedure and follow the distribution of each protein between the two fractions, we assumed total amounts of each protein present within the same tissue sample to be equal to the sum of its normalized abundance (sampling rate normalization) in fractions 1 and 2, both expressed in peak integration of extracted ion chromatograms (XICs, area under the curve). To facilitate interpretation, we duly converted the data into percentages to evaluate how much of the same protein was extracted in fraction 1 and how much remained in fraction 2. By plotting all the quantitative data of each protein detected per condition, we were able to observe the ability of this procedure to isolate the majority of cellular proteins in fraction 1, as well as matrisome-associated proteins (Figure 2A), which are known to be soluble. Fraction 2 (the insoluble fraction), on the other hand, was more enriched in glycoproteins and collagens (Figure 2B). Such fractionation allowed better detection of low-abundance matrisome-associated proteins and reduced the dynamic range. Indeed, the total number of spotted matrisome-associated proteins reached 73 ± 2 (Figure 3 and Supplementary Table S1), among which 41 ± 1 ECM regulators, 19 ± 1 ECM affiliated proteins as well as 13 ± 0 secreted factors were confidently detected in all conditions, but with different detection levels in XICs.

Int. J. Mol. Sci. **2020**, *21*, 9141

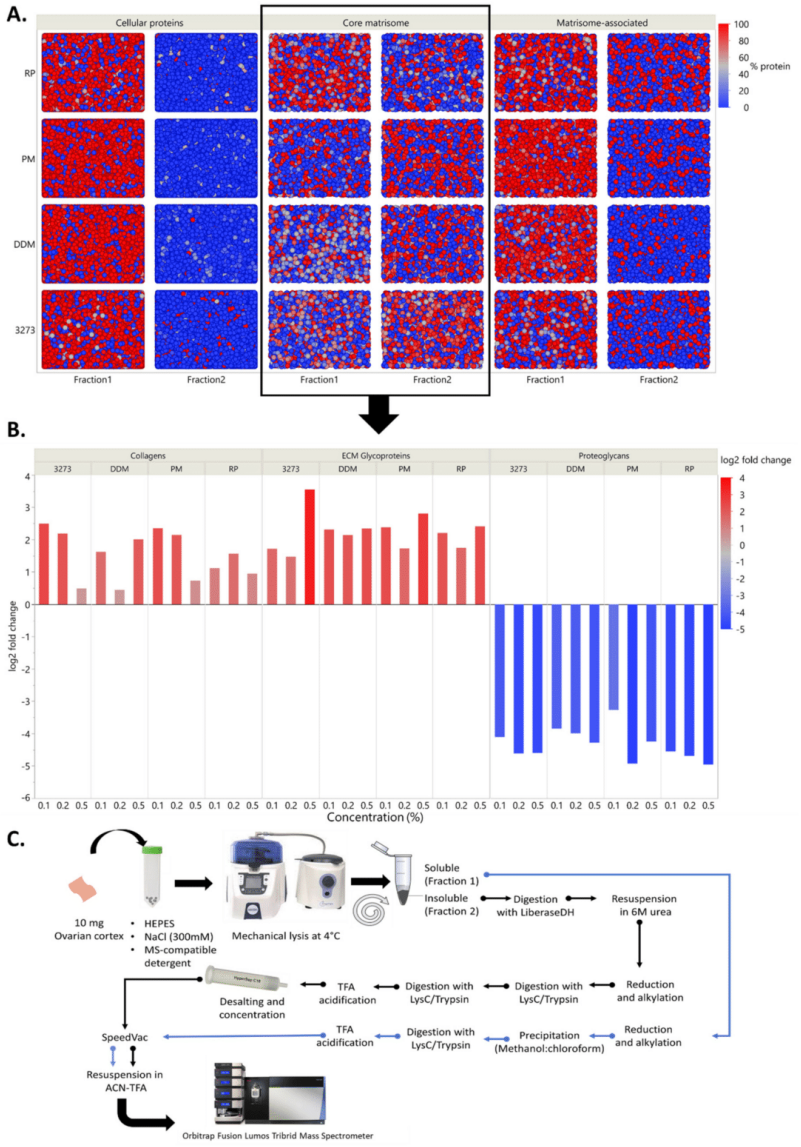


Figure 2. Two-step fractionation impact on the segregation of cellular protein, core matrisome and matrisome-associated proteins. (**A**) Scatter plot of proteomic data according to the protein percentage in each fraction; each dot represents a protein and the color key reflects its relative abundance per fraction. Matrisome data (framed) have been explored deeper in B. (**B**) Enrichment of collagen and glycoproteins in all conditions in fraction 2 expressed as the log2 fold change in XICs. (**C**) Summary of the two-step fractionation approach (DC-MaP technique).

Int. J. Mol. Sci. **2020**, *21*, 9141

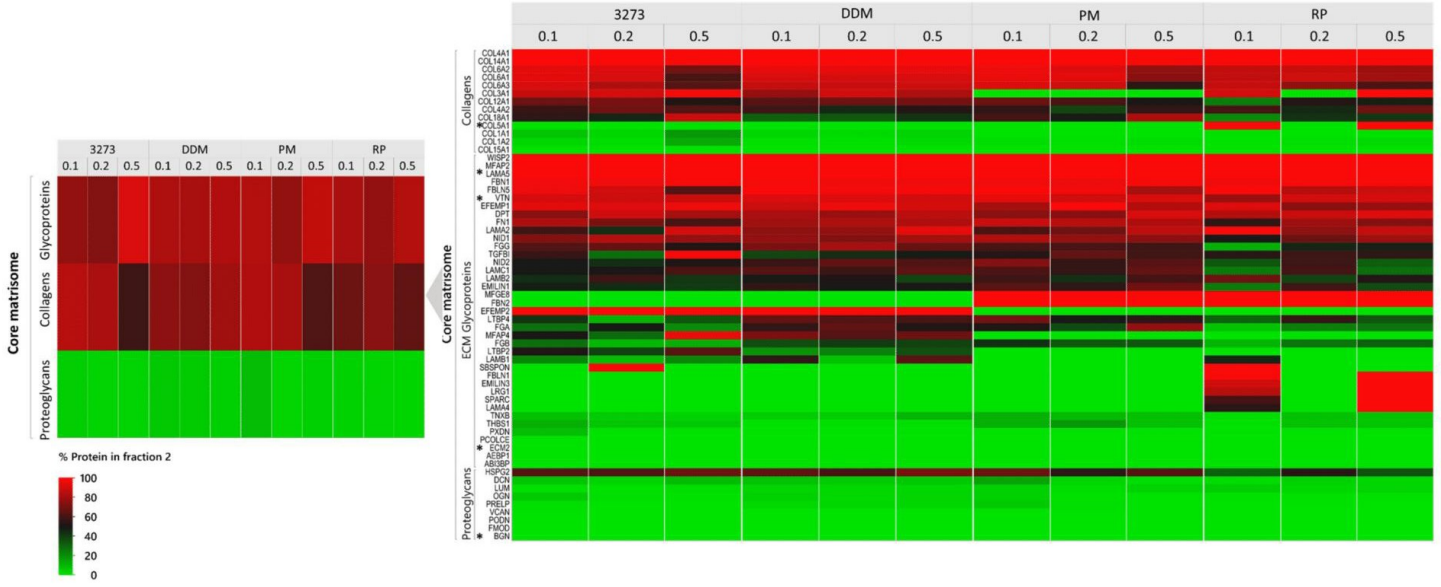


Figure 3. *Cont.*

Int. J. Mol. Sci. **2020**, *21*, 9141

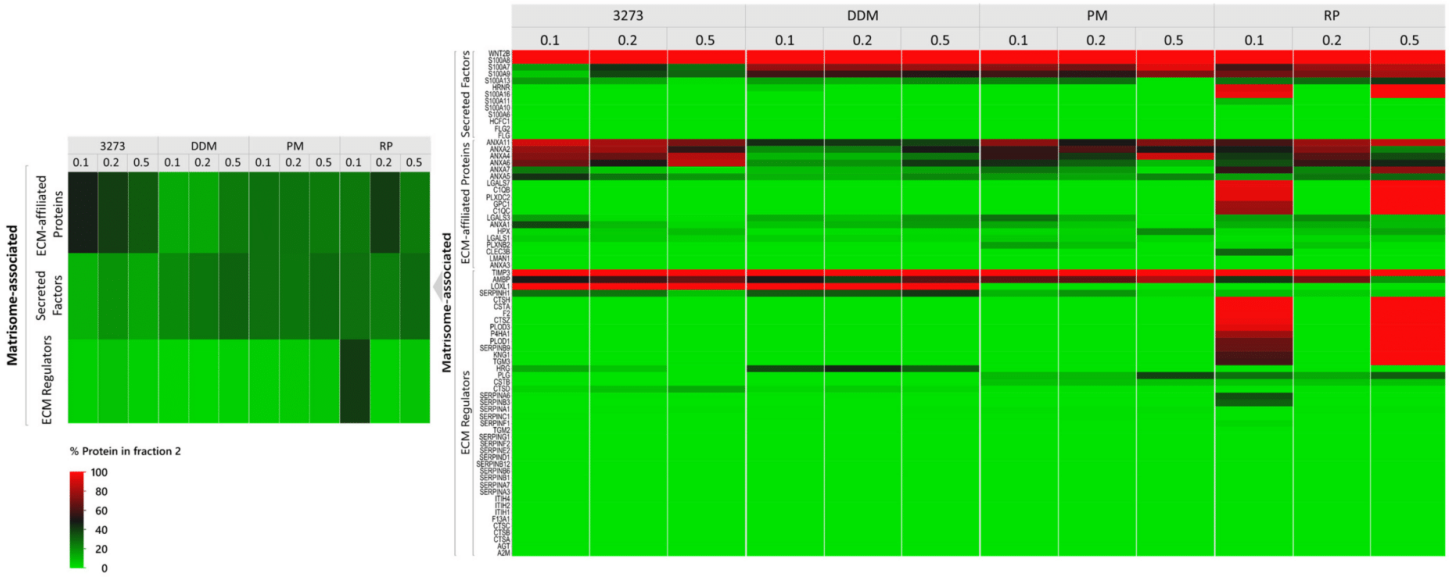


Figure 3. Heatmap of matrisome proteins detected in each condition. Protein abundance is expressed as the protein percentage detected in fraction 2 for each matrisome protein (**right side**) and averaged per category (**left side**). Proteins cited in the text are labeled with asterisks.

By adopting 2-step fractionation using MS-compatible detergents (Figure 2C), we noted that 0.2% 3273 yielded the best matrisome protein enrichment in fraction 2 (>70% enrichment of proteoglycans and >80% enrichment of ECM regulators and secreted factors) (Figure 3). Nevertheless, optimal enrichment of all matrisome proteins in just one fraction was not attainable, since in all conditions, some ECM proteins were 100% present in fraction 1 (BGN, ECM 2 and COL5A1), while others were 100% in fraction 2 (TIMP3, LAMA5, and VTC) (Figure 3 and Supplementary Data S1). To overcome this unavoidable limitation, we chose to combine matrisome protein detection in fractions 1 and 2 during post-acquisition, which revealed promising ECM protein discovery with 3273 and RP (Supplementary Datas S2 and S3). Overall, RP yielded a better identification than 3273 of core matrisome proteins, such as FBN2, an important elastic ECM protein that regulates the early process of elastic fiber assembly and has not been detected before in human premenopausal or menopausal ovaries. RP allowed better detection of MFGE8, another core matrisome protein that plays a pivotal role in the human ovary by mediating the regression process of atretic ovarian follicles [33]. With RP, detection of FBN2 and MFGE8 was 2-fold higher (based on log10 [quantile normalized abundance]) than with 3273 (Supplementary Data S3).

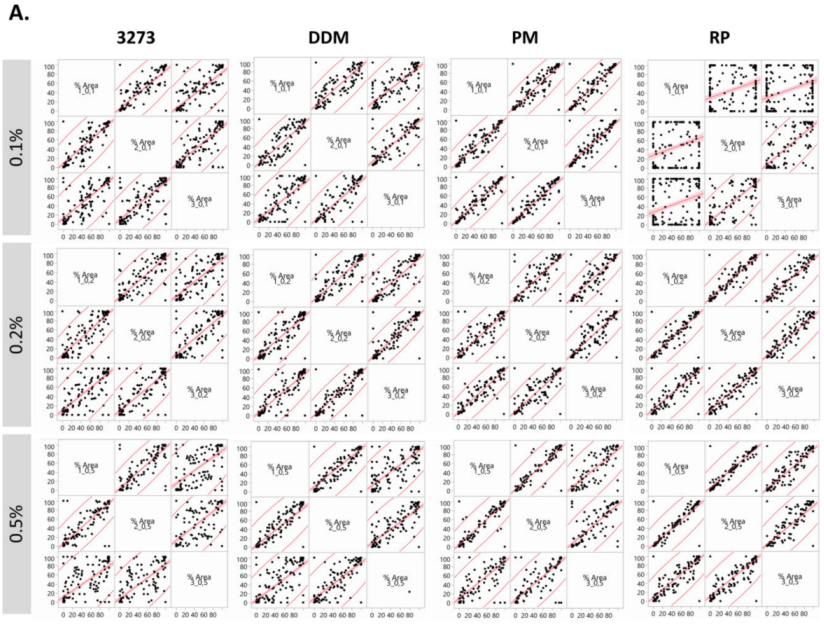
Matrisome-associated protein detection is quite challenging due to the high solubility of this category of proteins, which are embedded within the highly abundant core matrisome components (like collagen) that hamper their detection. Nevertheless, detection was improved with RP compared to 3273, where we saw cathepsins that participate in ECM degradation and turnover [34]. In this protein family, C1QC, C1QB, and CTSH were identified twice as often with RP (Supplementary Data S3). Moreover, among secreted factors, RP enabled greater identification of S100A16, a member of the serpin family, which plays an important role in ovarian function [35–37] and has prognostic value in ovarian cancer [38]. Conversely, 3273 produced a slightly higher collagen yield at all tested concentrations mainly, COL6A1/A2/A3 and COL12A1 (Supplementary Figure S3). Nevertheless, all collagens identified with 3273 were also identified with RP, so 2-step fractionation using RP is the most sensitive method for matrisome protein identification, especially at 0.2% and 0.5% when summing the XICs of both fractions during post-acquisition. On the other hand, fractionation enhanced detection of low-abundance soluble proteins in fraction 1 by sending glycoproteins and collagens to fraction 2 (Figure 2B). Consequently, combining the results obtained from both fractions as described above enabled to capture the full picture of the ovarian matrisome (Figure 3, Supplementary Data S3).

2.4. Highest Reproducibility at 0.2% Detergent Concentration

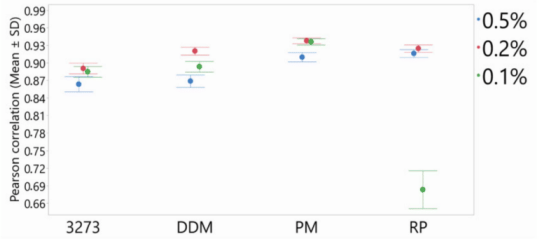
To obtain a reliable readout of the ovarian matrisome, reproducibility of protein identification is essential for clinical research and tissue engineering. Therefore, in order to select the most reproducible method, we used Pearson's correlation between biological replicates in each condition (Figure 4). At 0.1%, correlation coefficient r of RP was the weakest relative to the rest of the tested conditions, but it reached a peak at 0.2% (Figure 4A,B). It is worth mentioning that at 0.5%, 3273 became more viscous, which could account for its relatively weak reproducibility at this concentration. Similarly, the highest tested concentration of DDM and RP gave the least reproducible outcomes. These results are further reflected in intraclass correlation coefficients (ICCs), and their delimited 95% confidence interval confirms the consistency of our methods (Figure 4C). ICCs assess the extent to which measurements can be replicated by reflecting not only the degree of correlation between replicates, but also agreement between measurements. This test was therefore conducted between replicates to further evaluate the reproducibility of each method. ICCs are measured on a scale of 0 to 1; 1 represents perfect consistency (reproducibility) with no measurement/technical error, while 0 indicates no reliability.

Int. J. Mol. Sci. **2020**, *21*, 9141

A.



B.



C.

Concentration	3273				DDM			PM			RP		
	Intra Class Correlation	95% Confidence Interval		ICC	95% Confidence Interval		Intra Class Correlation	95% Confidence Interval		Intra Class Correlation	95% Confidence Interval	
		Lower Bound	Upper Bound		Lower Bound	Upper Bound		Lower Bound	Upper Bound		Lower Bound	Upper Bound
0.10%	0.827	0.793	0.857	0.840	0.809	0.868	0.904	0.884	0.921	0.527	0.459	0.593
0.20%	0.836	0.803	0.864	0.880	0.856	0.902	0.907	0.887	0.924	0.887	0.864	0.907
0.50%	0.796	0.757	0.830	0.803	0.765	0.836	0.865	0.837	0.888	0.874	0.849	0.896

Figure 4. Reproducibility evaluation. (**A**) All biological replicates in each condition were compared and correlated two by two using Pearson's correlation. (**B**) Plot of means of correlation coefficients calculated for each detergent at the 3 tested concentrations: 0.1%, 0.2%, and 0.5% (mean ± SD). (**C**) The intraclass correlation coefficient (ICC) was calculated per condition to further assess the consistency of each method, which proved the reliability of RP at 0.2%.

Considering sensitivity (defined as high qualitative and quantitative detection of matrisome proteins) in association with high reproducibility, 0.2% RP outperformed all the other MS-compatible detergents.

2.5. Optimal RP Performance in the Presence of Salt and Minimal Sample-Surface Contact

Once RP was selected as the most reliable MS-compatible detergent, we chose to add a third fractionation step to exclude the possibility of interference of high salt (NaCl) levels in the lysis buffer with the action of the surfactant and evaluate its impact on ECM detection (Figure 5). While 2-step fractionation starts with mechanical lysis in lysis buffer containing 300 mM NaCl and MS-compatible detergent, the 3-step procedure starts with mechanical lysis in the lysis buffer free of any detergents, and only the pellet is treated with MS-compatible detergent in a low-concentration NaCl buffer.

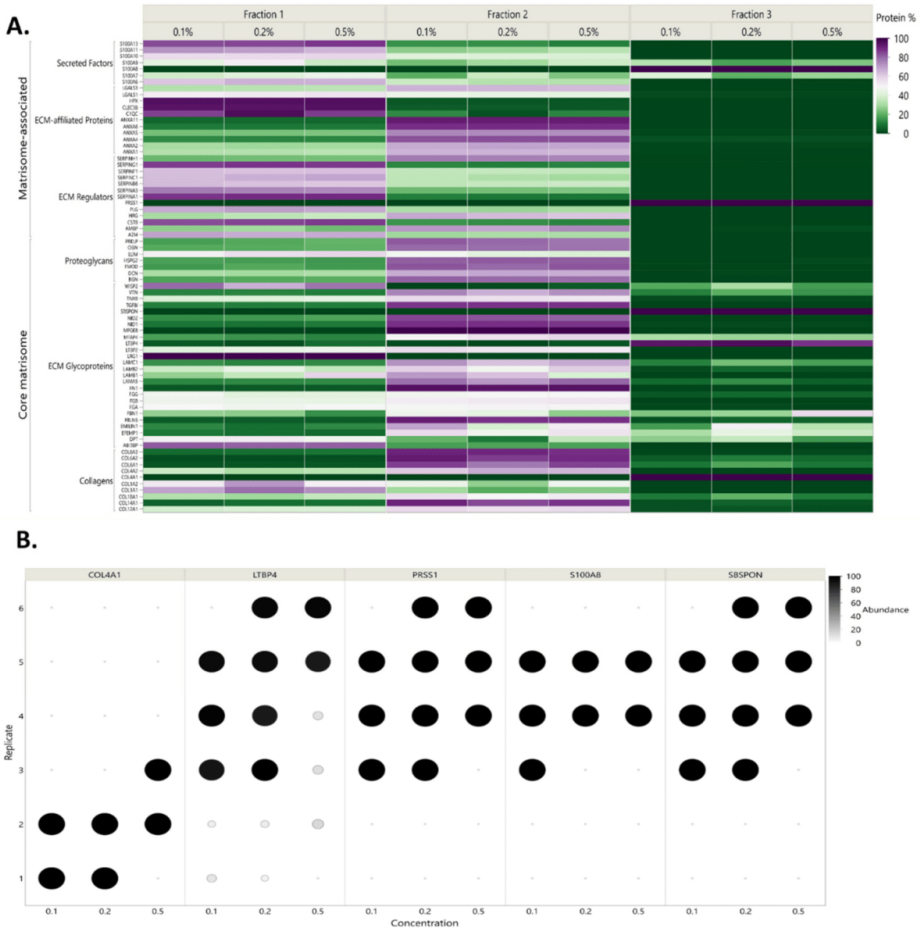


Figure 5. *Cont.*

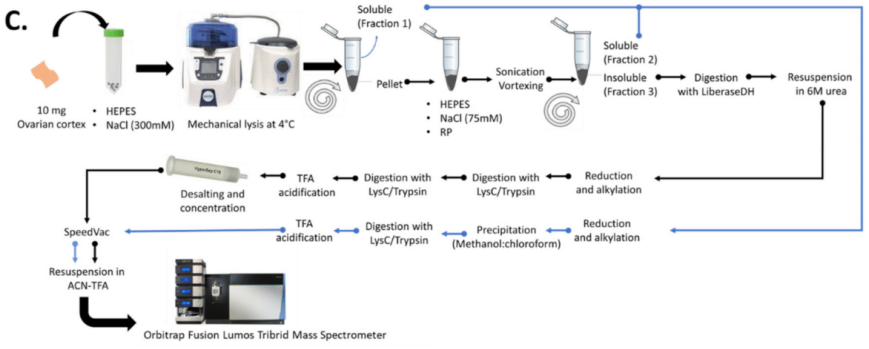


Figure 5. Three-step fractionation procedure outcomes. (**A**) Heatmap of matrisome protein abundance within the 3 obtained fractions highlights the localization of the majority of identified proteins in fractions 1 and 2. (**B**) Some proteins were exclusively detected in fraction 3, but their detection (abundance as a percentage in fraction 3) was very variable between the 6 tested replicates, as shown by the color and size of markers. (**C**) Summary of the three-step fractionation approach.

Contrary to our assumptions, RP action appeared to be optimal in contact with NaCl at 300 mM. Although 3 fractions were recovered in the 3-step procedure, only fraction 1 (HEPES pH 7.6, 300 mM NaCl) and fraction 2 (HEPES pH 7.6, 75 mM, RP) could accommodate the total amount of identified matrisome proteins (Figure 5A). The only proteins 100% present in fraction 3 (COL4A1, LTBP4, PRSS1, S100A8, and SBSPON) showed high variance between biological replicates (Figure 5B). Comparison of 2-step and 3-step fractionation also aimed to evaluate the possibility of further improving the dynamic range and washing away cellular proteins from ECM-containing fractions. Nevertheless, the results revealed the solubility of portions of matrisome proteins following mechanical lysis, even in HEPES with 75 mM NaCl, exposing the limitations of 3-step fractionation (Figure 6A). We observed that an increase in sample processing steps and surfaces harmed protein recovery and particularly matrisome proteins.

Indeed, this method includes vigorous agitation and long vortexing, which causes protein adsorption and loss with increased exposure to surfaces. The 2-step fractionation method enabled the exclusive identification of 63 matrisome proteins in addition to the detection of all proteins identified with the 3-step method (Figure 6B, Supplementary Data S3).

Hence, the 2-step fractionation procedure using 0.2% RP in the presence of 300 mM NaCl is the most tailored approach to matrisome proteomics.

2.6. To Fractionate or Not to Fractionate

To comprehensively characterize the human ovarian ECM, we previously developed a proteomic method with no centrifugal fractionation using two-dimensional liquid chromatography mass spectrometry (2D-LC/MS). This method, based on in silico matrisome identification, allowed confident identification of more than 80 matrisome proteins from a bulk of cellular proteins [39]. It was therefore essential to compare this technique with the current 2-step fractionation method using 0.2% RP in the same MS conditions (Figure 6B,C). The results revealed an 8-fold increase in the detected number of matrisome proteins, with around a 15-fold upturn in core matrisome abundance and 13-fold increase in matrisome-associated proteins. Thus, our new technique of 2-step fractionation using 0.2% RP clearly yields superior extraction and identification of ovarian matrisome proteins without the need to go through time-consuming 2D-LC/MS analysis.

Int. J. Mol. Sci. 2020, 21, 9141

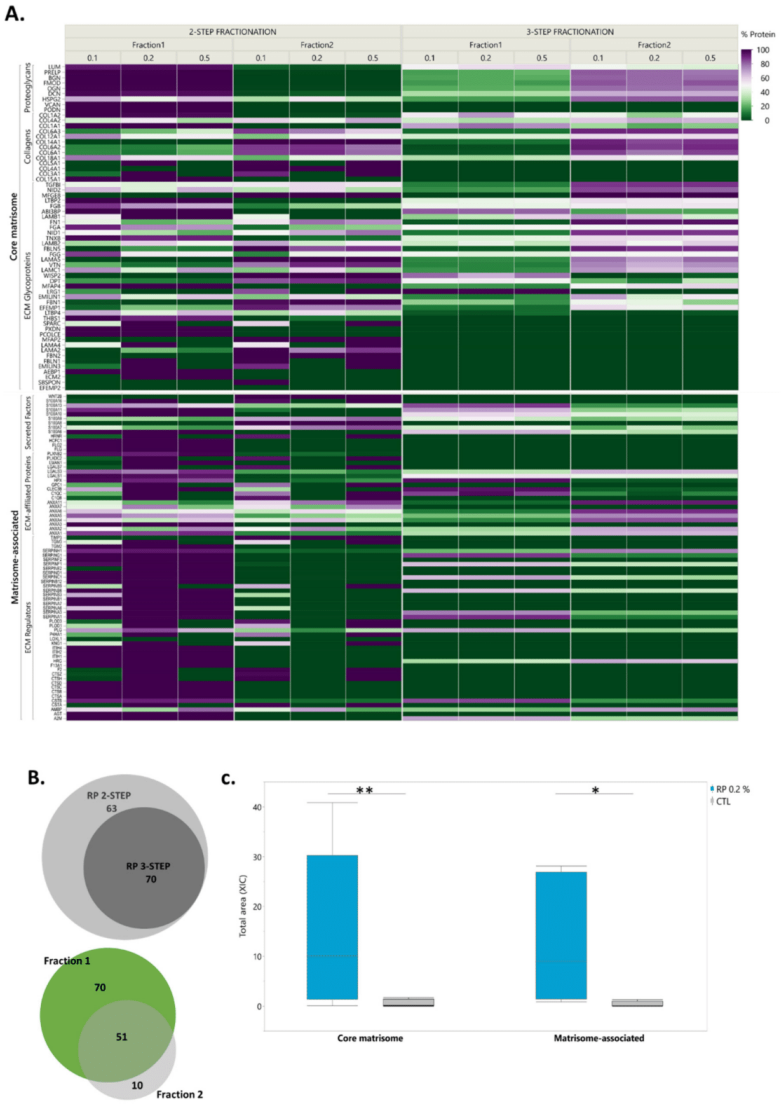


Figure 6. Superiority of the DC-MaP technique. (**A**) Comparison of the DC-MaP technique with the 3-step fractionation approach. Protein abundance is expressed as a percentage of each protein per fraction in each condition (**B**) Venn diagrams show unique and shared identified matrisome proteins between fractions 1 (soluble) and 2 (insoluble) using the DC-MaP technique and between both fractionation approaches using 0.2% RP. (**C**) Box plots of core matrisome and matrisome-associated protein levels identified with DC-MaP and a non-fractionated sample (CTL). A paired t-test and Wilcoxon's test were used to compare the abundance of core matrisome and matrisome-associated proteins respectively (* $p < 0.05$, ** $p < 0.01$).

3. Discussion

In our study, we set out to overcome the major challenges hampering our ability to accurately characterize the matrisome: MS-unfriendly detergents, irreproducibility, labor-intensive processing, and consequent loss of low-abundance proteins. To this end, we used the non-ionic saccharide surfactant DDM and acid-labile detergents 3273, RP, and PM, which are MS-friendly reagents that have similar properties to conventional detergents [40] and have been described as trypsin enhancers [41]. Cleavable detergents have the added benefit of quickly degrading into innocuous non-surfactant by-products when they are no longer required upon addition of acid, eliminating the need to remove them prior to MS analysis. However, these surfactants have not yet been tested for their performance in matrisome proteomics. We chose to test them on ovaries from women aged over 50 years, which could be considered the most challenging samples to use for extracting and solubilizing ECM proteins due to their high levels of collagen and fibrosis-like aspect [42]. With scarce samples of healthy ovarian biopsies, it can be difficult to obtain sufficient amounts of proteins to generate high-quality MS data. We therefore paid special attention to sampling standardization and screened different mechanical disruption lysis matrices to select the one that yielded the highest amounts of protein. This turned out to be the stainless-steel beads measuring 0.3 mm in diameter. This approach overcame ill-adapted, time-consuming, partial mechanical lysis and possible cross-contamination encountered when using other methods (e.g., pestle and grinder).

Protein extraction, including lysis of cells, release of proteins from different cell compartments, and solubilization of proteins into extraction buffer, is the first step in protein sample preparation. In this context, addition of 300 mM NaCl to HEPES buffer and its concomitant use with detergents proved to be effective in solubilizing mainly cellular proteins and enhancing detergent efficiency. Our approach, combining centrifugation and MS-compatible detergent along with LC-MS/MS successfully identified 131 matrisome proteins with good reproducibility, which is the highest number of ECM proteins to have ever been described in the human ovary thanks to the use of RP at 0.2% with simple 2-step fractionation [39]. Moreover, RP has a major advantage over its commercialized competitors, as its cleavage does not result in amine products following degradation (Supplementary Figure S4). Our proposed method is therefore compatible with isobaric amine-reactive tandem mass tag labeling reagents, such as tandem mass tag (TMT) and isobaric tags for relative and absolute quantitation (iTRAQ) [16,26].

To avoid the above-mentioned caveats associated with chemical digestion of insoluble ECM pellets, we chose to use Liberase DH for pre-enzymatic digestion. Liberase DH is a mixture of highly purified collagenase I and II and neutral protease dispase produced successively by *Clostridium histolyticum* and *Bacillus polymyxa*, and formulated for efficient, gentle, and reproducible dissociation of tissue from a wide variety of sources [43]. While collagenase cleaves specifically helical regions in native collagen preferentially at the X-Gly bond in the sequence Pro-X-Gly-Pro, where X is most commonly a neutral amino acid, dispase cleaves peptide bonds containing leucine and phenylalanine (e.g., fibronectin). Use of Liberase DH decreased insoluble protein agglomeration and cleaved collagen as the most abundant substrate, allowing better detection of low abundance proteins. Moreover, Kuljanin et al. [44] already demonstrated that collagenase preferentially cleaves collagen, with minor off-target effects, and described the advantages of its use in proteomics.

In line with the literature, our previously published proteomic method using Liberase did not spot any interference with non-collagenous protein detection [39]. Following its use and upon double trypsin/Lys-C digestion, we did not observe any residual undigested material in our samples, which could easily be left behind and discarded in widely accepted proteomic methods.

Our study also revealed that a high percentage of ECM proteins could be lost, even in detergent-free buffers in intermediate fractions, which are not considered for analysis in most published ECM proteomic studies [15]. This observation is another key element behind our matrisome-tailored proteomic pipeline based on the principle of divide-and-conquer matrisome proteins (DC-MaP). While centrifugation enabled us to separate the soluble fraction from the insoluble fraction enriched

with collagens and glycoproteins, pre-enzymatic Liberase DH digestion of the resulting pellet optimized identification of low-abundance matrisome-associated proteins entrapped in insoluble protein agglomerates. Only through combined analysis of both fractions could we capture the full picture of the ovarian matrisome in our samples without jeopardizing detection of soluble ECM-associated proteins that could easily be overlooked in standard enrichment procedures (Supplementary Data S3). Moreover, we foresee a possible application of our fractionation method in monitoring changes in solubility and crosslinking of ECM proteins, in different experimental conditions for example between healthy and fibrotic tissues or between normal and cancerous tissues [45–47].

Our comparison between 3- and 2-step fractionation demonstrated the superiority of the shorter procedure, leading us to conclude that more elaborate fractionation and multiple surface contact with the protein sample can lead to huge matrisome protein loss. Thus, DC-MaP is a combination of optimal extraction conditions for a high throughput matrisome proteomics designed to overcome encountered difficulties with conventional methods.

Our DC-MaP technique using 2-step fractionation with 0.2% RP complemented by insoluble pellet digestion with Liberase DH is the first validated application of an MS-compatible detergent in matrisome proteomics, representing a robust, affordable (Supplementary Data S5) and straightforward proteomic procedure tailored to matrisome protein discovery. Furthermore, our technique could be safely applied with isobaric amine-reactive tandem mass tag labeling reagents in comparative studies, since RP cleavage does not release primary amines (Supplementary Data S4). We believe the most accurate characterization of ECM proteins from different tissue types and even those with limited availability can be achieved with our DC-MaP method. This will help advance organ engineering efforts by generating a molecular readout that can be correlated with functional outcomes to drive the next generation of engineered organs (e.g., the artificial ovary) and fasten the transition of proteomics to clinical practice through enabling biomarker discovery at the level of ECM in an unbiased fashion.

4. Materials and Methods

4.1. Collection of Ovarian Tissue and Biopsy Processing

Use of human ovarian cortex was approved by the Institutional Review Board of the Université Catholique de Louvain on 13 May 2019 (IRB reference 2012/23MAR/125, registration number B403201213872). Ovarian biopsies were taken from adult patients (n = 6; mean age [±SD] = 58 ± 9 years) after obtaining their informed consent. All women were undergoing laparoscopic surgery for benign gynecological diseases not related to the ovaries. Biopsies were immediately transported on ice to the laboratory in minimal essential medium (MEM)-GlutaMAX (Gibco, Invitrogen, Merelbeeke, Belgium). Fresh biopsies were cut into fragments and cryopreserved [48]. On the day of biopsy processing for protein extraction, all samples were thawed [48] and cut into 3 × 3 × 1 mm fragments using graph paper. Excess medium was removed with gauze and 10 mg wet weight of each sample was processed as described below.

4.2. Selection of Lysing Matrix

Lysing matrices were used to supersede ill-adapted, time-consuming, partial mechanical lysis procedures and avoid possible cross-contamination encountered in other applied methods (e.g., pestle and grinder). Outcomes of five mechanical lysis conditions (Cd) using different bead types were compared: Cd1 (Full Moon, BioSystems, Sunnyvale, CA, USA), Cd2 (Precellys Lysing Kit MK28, Bertin Technologies, Aix en Provence, France), Cd3 (Lysing Matrix Z, MP Biomedicals, Illkirch-Graffenstaden, France), Cd4 (Lysing Matrix A, MP Biomedicals) and Cd5 (Lysing Matrix D, MP Biomedicals), which was preceded by a tissue chopping step (McIlwain Tissue Chopper, Mickle Laboratory, Guildford, UK).

A tissue fragment from each patient (n = 3/condition) was transferred to an empty 2 mL FastPrep® Lysing matrix tube (MP Biomedicals) filled with one of the different bead types. As lysis buffer, we used

a 25 mM HEPES solution (pH = 7.6) supplemented with protease inhibitors (1× complete tablet, 50 mM sodium fluoride [NaF], 0.25 mM sodium orthovanadate and 0.25 mM phenylmethylsulfonyl fluoride [PMSF]). Each 2 mL lysis tube was filled with 200 µL lysis buffer and homogenized at 4 °C with Precellys Evolution (Bertin Technologies) at the following settings: speed 9500 rpm, cycle 4 × 20 s, pause 15 s. After homogenization, the tubes were kept on ice until elution. The tubes' bottoms were inverted and pierced with a clean needle, then the cap was slightly loosened and placed in a Falcon tube. The Falcon tubes were centrifuged at 3000× *g* for 5 min at 4 °C. Pass-throughs were subsequently transferred to 1.5 mL conical bottom centrifuge tubes and centrifuged again at 16,000× *g* for 30 min at 4 °C, before analyzing the supernatants. Comparisons between lysing matrices were based on the total amount of extracted soluble proteins, their quality, preservation of core matrisome proteins, and method reproducibility, as described below.

BCA assay (Thermo Scientific™, San José, CA, USA) was used for quantification of total extracted soluble proteins. Their quality was monitored by SDS-PAGE using the Mix-n-Stain™ Total Protein Prestain Kit (Biotium, Fremont, CA, USA). Preservation of core matrisome proteins in the insoluble fraction was monitored in the supernatant by near-infrared western blot using two ECM antibodies, anti-osteoglycin (Invitrogen, Carlsbad, CA, USA) and anti-fibronectin (Abcam, Cambridge, MA, USA), and revealed by donkey anti-rabbit secondary antibody CF®770 (Biotium).

4.3. Formulation of Lysis Buffer

Starting from a limited sample size could be a burden to full matrisome detection. Therefore, it was essential to maximize the amount of total proteins from the beginning and wash out as many intracellular proteins as possible from the insoluble ECM to decrease the dynamic range and improve matrisome detection by MS. In this context, three concentrations of NaCl were used to supplement the HEPES lysis buffer (n = 3), 75 mM, 150 mM, and 300 mM, using the selected lysis matrix as described above. Supernatants were separated from the homogenates and the amount of total soluble proteins extracted with each NaCl concentration was evaluated by BCA assay (Thermo Scientific). Near-infrared western blot was used to evaluate the impact of each NaCl concentration on intracellular protein extraction, namely histone (nucleus) and actin (cytoskeleton) using anti-histone (Abcam) and anti-actin (Abcam) antibodies, respectively, before being revealed by donkey anti-rabbit secondary antibody CF®770 (Biotium).

4.4. Deciphering Matrisome Composition Using 2-Step Fractionation and MS-Compatible Detergents

4.4.1. Sample Fractionation

Ovarian tissue samples (10 mg) were mechanically lysed using the selected lysing matrix. At this point, optimized lysis buffer was used to resuspend MS-compatible detergents, namely 3273, DDM, RP, and PM, to achieve 0.1%, 0.2%, and 0.5% concentrations. The homogenate was eluted with the needle technique (described above) by centrifugation at 3000× *g* for 5 min at 4 °C. The eluate was then centrifuged again at 16,000× *g* for 30 min at 4 °C to recover the supernatant labeled as "fraction 1" (soluble) and the remaining pellet obtained labeled as "fraction 2" (insoluble).

4.4.2. Yield of Extracted Proteins

Total protein concentration measurement (BCA) was conducted on fraction 1 to evaluate the effect of detergent type and concentration on the yield of extracted proteins. To avoid possible interference of used detergents with BCA quantification, lysis solutions containing the detergents were used as blank.

4.4.3. Western Blot

A total of 20 µg of fractions 1 and 2 obtained with each detergent were loaded onto 4–15% gradient bis-acrylamide gels (Biorad, Hercules, CA, USA), using n = 3 per condition for immunoblotting. Since fraction 2 is insoluble, it was first solubilized using 100 µL of 1% SDS and incubated for 1 h in the

thermomixer at 60 °C under 1400 rpm agitation. Ceramic beads were added to the vial to improve protein solubilization. The obtained homogenate was centrifuged at 3000× *g* for 5 min. Another 100 µL of 1% SDS was added to the remaining insoluble pellet and incubated for 1 h in thermomixer at 37 °C under agitation at 1400 rpm. Both solubilized homogenates were pooled, spun, and quantified by BCA assay for SDS-PAGE. Electrophoresis migration was run at a voltage of 55 V for 30 min and 170 V for 1 h. An adapted Laemmli buffer formulation was used at 1× final concentration for protein denaturation: 0.44% [*wt/vol*] SDS, 12.4 mM Tris-HCl pH 6.8, 1% [*vol/vol*] 2-mercaptoethanol, 4% [*vol/vol*] glycerol, 0.00125% [wt/vol] bromophenol blue, supplemented with 100 mM dithiothreitol (DTT). Proteins were then transferred to immobilon-FL membrane (Biorad) in an 18% methanol transfer buffer and blocked with SuperBlock™ (TBS) Blocking Buffer (Thermo Scientific). The blocking solution was diluted 2× in 1× Tris-Buffered Saline and 0.1% Tween® 20 Detergent (TBST) to dilute antibodies and secondary antibodies (Supplementary Data S2). Representative primary antibodies for each of the cellular (β1-integrin, histone, and actin) and ECM (osteoglycin and fibronectin) proteins were used to monitor protein fractionation. Following primary antibody incubation at 4 °C overnight under mild agitation, 6 repeated 5 min washes of the membrane were carried out before and after secondary antibody incubation (6 with TBST before incubation, and 3 with TBST followed by 3 with PBS after incubation). Each antibody was tested with a total protein extract obtained from a pool of ovarian tissue fragments from the group of patients whose tissue was solubilized similarly to fraction 2 before loading. This control sample was included in each western blot. To enable reliable quantification of the staining, all tested samples were also loaded in parallel SDS-PAGE gel and labeled with PageBlueTM protein staining (Thermo Scientific) to allow densitometry normalization per total loaded protein. All membranes were scanned with an infrared imaging system (Odyssey, Li-Cor Biosciences, Lincoln, NE, USA) and analyzed using Licor Image Studio Lite software (Li-Cor Biosciences).

4.5. Impact of a Third Fractionation Step on ECM Recovery

4.5.1. Sample Fractionation

A supplemental experiment was conducted to check the reliability of the 2-step fractionation procedure, exclude the possibility that high salt (NaCl) levels in the lysis buffer might interfere with the action of the selected MS-compatible surfactant, and evaluate its impact on ECM detection. For this, ovarian fragments (n = 6) were first mechanically lysed in 200 µL of a detergent-free lysis buffer containing 25 mM HEPES solution (pH = 7.6) with 300 mM NaCl, supplemented with protease inhibitors (1× complete tablet, 50 mM NaF, 0.25 mM sodium orthovanadate and 0.25 mM PMSF). The previously selected lysis matrix was used following the same mechanical lysis settings. Eluted homogenates were centrifuged at 16,000× *g* for 30 min at 4 °C and the supernatants were labeled as "fraction 1" (soluble). The remaining pellets were resuspended in 60 µL MS-compatible detergent prepared in low-salt buffer containing 25 mM HEPES solution (pH = 7.6) and 75 mM NaCl with protease inhibitors. The samples were then sonicated for 30 min at 37 °C with regular vortexing every 5 min and centrifuged at 16,000× *g* for 30 min at 4 °C. The remaining supernatant formed "fraction 2" (soluble), while the final pellet constituted "fraction 3" (insoluble).

4.5.2. Comparison of 2-Step and 3-Step Procedures

Qualitative and quantitative differences were evaluated between matrisome proteins detected in the 2- and 3-step procedures. For qualitative comparisons, we considered the type and category of matrisome proteins and the number of fractions that yielded the most complete description of the human ovarian matrisome. On the other hand, quantitative comparisons took into account the number and abundance of detected matrisome proteins and their recovery.

4.6. Sample Preparation for MS Analysis

Ovarian tissue fragments (n = 3) were mechanically lysed in the presence of MS-compatible detergents to obtain soluble and insoluble fractions by the 2-step and 3-step fractionations, as described above. Insoluble fractions were enzymatically digested using 1.35 mg/mL Liberase^{TM} DH (Roche Diagnostics, GmbH, Mannheim, Germany) in 100 mM triethylamonium bicarbonat (TEAB) and 5 mM calcium chloride ($CaCl_2$). The samples were incubated at 37 °C for 2 h under agitation (140 rpm) with regular 30-s vortexing every 30 min. The enzymatic reaction was halted by the addition of 20 mM EDTA. BCA assay was used to quantify total proteins by subtracting Liberase^{TM} DH amounts from the insoluble fractions.

4.6.1. Soluble Fraction Processing

Thirty µg of total soluble proteins were reduced with a 10 mM final concentration of DTT and incubated for 30 min at 56 °C, and subsequently alkylated with a 60 mM final concentration of chloroacetamide for 25 min at room temperature (RT) in the dark. The proteins were then precipitated using the methanol-chloroform method, before being resuspended in 100 mM TEAB (pH 8) and further digested with Lys-C/trypsin at an enzyme:substrate ratio of 1:25 [*wt/wt*] overnight at 37 °C. The reaction was halted by adding fresh TFA to a final concentration of 0.2% [*vol/vol*] (pH < 2). The samples were then centrifuged at 16,000× *g* for 10 min at 4 °C. Recovered peptides were dried in a speedvac, resuspended in 50 µL of 3.5% acetonitrile (ACN) [*vol/vol*] and 0.1% TFA [vol/vol] in water, and quantified by Pierce™ Quantitative Colorimetric Peptide Assay (#23275, Thermo Scientific) according to the manufacturer's instructions.

4.6.2. Insoluble Fraction Processing

Fifty µg of total insoluble proteins were resuspended in a 6 M final concentration of urea in 100 mM TEAB, with continuous vortexing and sonication. Proteins were reduced in a 5 mM final concentration of DTT and incubated for 1 h at 37 °C. After cooling to RT, cysteines were alkylated by addition of 25 mM chloroacetamide for 30 min at RT in the dark. No precipitation was conducted during insoluble fraction processing to avoid resolubilization problems and to get advantage of the trypsin-enhancing action of MS-compatible detergents. Protein digestion was performed using Lys-C/trypsin at an enzyme:substrate ratio of 1:50 [*wt/wt*] and incubation for 2 h at 37 °C under 1000 rpm agitation. After reducing urea concentration to 1 M by addition of 100 mM TEAB, a second aliquot of trypsin was added to the sample at an enzyme:substrate ratio of 1:100 [*wt/wt*] and incubated overnight at 37 °C with continuous agitation at 1000 rpm. The reaction was halted by the addition of freshly prepared 50% TFA [*vol/vol*], pH < 2. The acidified sample was centrifuged at 16,000× *g* for 10 min at RT to eliminate MS-compatible detergents. Digests were first desalted and concentrated on HyperSep C18 cartridges (50 mg/mL, Thermo Scientific, San Jose, CA, USA) according to the manufacturer's instructions, and then dried using a speedvac. Peptides were resuspended in 50 µL of 3.5% ACN [*vol/vol*] and 0.1% TFA [*vol/vol*] in water and quantified by the Pierce™ Quantitative Colorimetric Peptide Assay following the manufacturer's instructions.

4.6.3. Liquid Chromatography-Tandem-Mass-Spectrometry (LC-MS/MS)

One µg of peptides dissolved in solvent A (0.1% TFA in 2% ACN) was directly loaded onto a reversed-phase pre-column (Acclaim PepMap 100, Thermo Scientific) and eluted in backflush mode. Peptide separation was achieved using a reversed-phase analytical column (Acclaim PepMap RSLC, 0.075 × 250 mm, Thermo Scientific) with a 140 min linear gradient of 4%–32% solvent B (0.1% TFA in 80% ACN) for 99 min, 32%–60% solvent B for 10 min, 60%–95% for 1 min and holding at 95% for the last 10 min at a constant flow rate of 300 nL/min on an Ultimate 3000 RSLN nanoHPLC system (Thermo Scientific). The peptides were analyzed by an Orbitrap Fusion Lumos tribrid mass spectrometer (Thermo Fisher Scientific) with enabled advanced peak determination (APD). The peptides

were subjected to a nanospray ionization source, followed by MS/MS in the Fusion Lumos coupled online to the UPLC. Intact peptides were detected in the Orbitrap at a resolution of 120,000 and MS/MS spectra were acquired in the IT after HCD fragmentation at 30%. A data-dependent procedure of MS/MS scans was applied for the top precursor ions above a threshold ion count of 5.0×10^3 in the MS survey scan with 30 s dynamic exclusion. The total cycle time was set to 4 s. MS1 spectra were obtained with an AGC target of 4×10^5 ions and a maximum injection time of 50 ms. MS2 spectra were acquired with an AGC target of 1×10^4 ions and a maximum injection time of 35 ms. For MS scans, the m/z scan range was 350 to 1800. MS/MS spectra were exported using the following settings: peptide mass range: 350–5000 Da, minimal total ion intensity: 500.

4.6.4. Protein Identification and Quantification

Resulting MS/MS data were processed using Sequest HT search engine within Proteome Discoverer 2.3 against a human protein reference target-decoy database obtained from Uniprot (1 March 2020, 87,489 forward entries). Trypsin was specified as the cleavage enzyme, allowing up to 2 missed cleavages, 4 modifications per peptide, and up to 3 charges. Mass error was set to 10 ppm for precursor ions and 0.1 Da for fragment ions, and considered dynamic modifications were +15.99 Da for oxidized methionine and +57.00 for carbamidomethyl cysteine. The false discovery rate (FDR) was investigated using Percolator, and thresholds for protein, peptide, and modification sites were specified at 1%.

4.7. Data Mining and Data Visualization

Matrisome protein recognition in raw MS data was achieved by comparison of confidently detected proteins with the Matrisome Project data set [49], an in silico-identified ECM protein set founded on the characteristic domain-based organization of ECM proteins. JMP® 14 was used to manage data, conduct correlations, and generate qualitative analysis graphs.

4.8. Experimental Design and Statistical Rationale

All experiments included $n = 3$ biological replicates of menopausal ovarian tissue per each tested condition, except in the 3-step fractionation where the number of replicates was elevated to $n = 6$. A threshold was maintained to pinpoint the most confidently detected proteins to consider in our interpretation of results. This threshold included proteins with an FDR < 1% and unique peptides ≥ 2 for each sample. XICs were performed by label-free quantification using Proteome Discoverer 2.3 (Thermo Fisher Scientific) and were regarded as an indicator of protein abundance. Sampling rate normalization was applied to all our data (mean XICs/number of detected proteins). After confirming data normality, two-way ANOVA was used to first compare the overall performance of detergents irrespective of their used concentrations, and then the outcomes of the same detergent at different concentrations. To evaluate the reproducibility of each procedure between replicates, Pearson's correlation was used to calculate the correlation coefficient, r. ICCs were also acquired between replicates to further evaluate the consistency of each method using IBM SPSS Statistics 24 software (IBM Corp, Armonk, NY, USA), as described by Richard Landers [50]. Briefly, ICC is measured on a scale of 0 to 1; 1 represents perfect consistency (reproducibility) with no measurement/technical error, while 0 indicates no reliability.

Total abundance of a protein was considered as the sum of its XICs in all fractions, and the percentage per fraction was accordingly calculated. Log2 fold change of XICs between fraction 2 per fraction 1 was used to identify the most enriched protein matrisome categories in each fraction. To evaluate the total amount of identified matrisome proteins in all fractions, we used quantile normalization of the XIC sum in all fractions, as well as Log10 transformation.

To compare the identification of matrisome proteins using DC-MaP with a fractionation-free technique, we applied a paired *t*-test (core matrisome) and Wilcoxon's test (matrisome-associated) according to data distribution in each matrisome category. In this comparison, only proteins confidently identified with both techniques were considered.

4.9. Data Availability

The mass spectrometry proteomics data have been deposited to the ProteomeXchange Consortium via the PRIDE [51] partner repository with the dataset identifier PXD020823 (https://www.ebi.ac.uk/pride/archive/projects/PXD020823). XLS file with quantification data is provided in Supplementary Table S2.

Supplementary Materials: Supplementary Materials can be found at http://www.mdpi.com/1422-0067/21/23/9141/s1.

Author Contributions: Conceptualization and methodology, E.O., G.H., S.P.d.R. and D.V.; software, E.O. and D.V.; validation, C.A.A.; resources, C.A.A. and M.-M.D.; writing—original draft preparation, E.O.; writing—review and editing, D.V. and C.A.A.; visualization, E.O.; supervision, D.V. and C.A.A.; funding acquisition, C.A.A., M.-M.D. and E.O. All authors have read and agreed to the published version of the manuscript.

Funding: This study was supported by grants from the Fonds National de la Recherche Scientifique de Belgique (FNRS) (C.A.A. is an FRS-FNRS research associate; grant MIS #F4535 16 awarded to C.A.A.; EOS grant 30443682 awarded to M.-M.D. and C.A.A.; grant 5/4/150/5 awarded to M.-M.D.) and the Université Catholique de Louvain (PhD grant 'Coopération au développement' awarded to E.O.).

Acknowledgments: We thank Céline Bugli (Louvain Institute of Data Analysis and Modeling in Economics and Statistics, Université Catholique de Louvain) for her contribution to statistical evaluation in the primary steps of the project. We also thank Ying Ge for her guidance on 3273 use and Sergei Saveliev and Marylene Focant from Sigma for their technical support and generous offer of free 3273 samples. Some of the lysing matrices tested in this study were also generously donated by Bertin Technologies, MP Biomedicals and Full Moon BioSystems. Data mining using JMP software was achieved thanks to considerable assistance from Paolo Chiappa and Valérie Nedbal. Finally, we thank Mira Hryniuk, for reviewing the English language of the manuscript.

Conflicts of Interest: The authors declare no conflict of interest.

Abbreviations

ACN	Acetonitrile
APD	Advanced peak determination
Cd	Condition
CNBr	Cyanogen bromide
DC-MaP	Divide-and-conquer matrisome protein
DDM	*N*-dodecyl β-D-maltoside
DTT	Dithiothreitol
ECM	Extracellular matrix
FASP	Filter-aided sample preparation
FDR	False discovery rate
GdnHCl	Guanidinium chloride
ICC	Intra-class correlation coefficient
iTRAQ	Isobaric tags for relative and absolute quantitation
MEM	Minimal essential medium
NaCl	Sodium chloride
NaF	Sodium fluoride
NH_2OH	Hydroxylamine
PM	ProteaseMax
PMSF	Phenylmethylsulfonyl fluoride
RP	RapiGest
RT	Room temperature
TMT	Tandem mass tag

References

1. Randles, M.J.; Lennon, R. Applying Proteomics to Investigate Extracellular Matrix in Health and Disease. *Co Transp. Syst.* **2015**, *76*, 171–196. [CrossRef]
2. Taha, I.N.; Naba, A. Exploring the extracellular matrix in health and disease using proteomics. *Essays Biochem.* **2019**, *63*, 417–432. [CrossRef] [PubMed]

3. Aebersold, R.; Mann, M. Mass-spectrometric exploration of proteome structure and function. *Nature* **2016**, *537*, 347–355. [CrossRef]
4. Socovich, A.M.; Naba, A. The cancer matrisome: From comprehensive characterization to biomarker discovery. *Semin. Cell Dev. Biol.* **2019**, *89*, 157–166. [CrossRef] [PubMed]
5. Byron, A.; Humphries, J.D.; Humphries, M.J. Defining the extracellular matrix using proteomics. *Int. J. Exp. Pathol.* **2013**, *94*, 75–92. [CrossRef] [PubMed]
6. Lindsey, M.L.; Jung, M.; Hall, M.E.; DeLeon-Pennell, K.Y. Proteomic analysis of the cardiac extracellular matrix: Clinical research applications. *Expert Rev. Proteom.* **2018**, *15*, 105–112. [CrossRef] [PubMed]
7. Barallobre-Barreiro, J.; Lynch, M.; Yin, X.; Mayr, M. Systems biology-opportunities and challenges: The application of proteomics to study the cardiovascular extracellular matrix. *Cardiovasc. Res.* **2016**, *112*, 626–636. [CrossRef] [PubMed]
8. Naba, A.; Clauser, K.R.; Ding, H.; Whittaker, C.A.; Carr, S.A.; Hynes, R.O. The extracellular matrix: Tools and insights for the "omics" era. *Matrix Biol.* **2016**, *49*, 10–24. [CrossRef] [PubMed]
9. Ludwig, C.; Gillet, L.; Rosenberger, G.; Amon, S.; Collins, B.C.; Aebersold, R. Data-independent acquisition-based SWATH-MS for quantitative proteomics: A tutorial. *Mol. Syst. Biol.* **2018**, *14*, e8126. [CrossRef]
10. Hosseininia, S.; Onnerfjord, P.; Dahlberg, L.E. Targeted proteomics of hip articular cartilage in OA and fracture patients. *J. Orthop. Res.* **2019**, *37*, 131–135. [CrossRef]
11. Liu, F.; Rijkers, D.T.; Post, H.; Heck, A.J. Proteome-wide profiling of protein assemblies by cross-linking mass spectrometry. *Nat. Methods* **2015**, *12*, 1179–1184. [CrossRef] [PubMed]
12. Schmitt, L.R.; Henderson, R.; Barrett, A.; Darula, Z.; Issaian, A.; D'Alessandro, A.; Clendenen, N.; Hansen, K. Mass spectrometry-based molecular mapping of native FXIIIa cross-links in insoluble fibrin clots. *J. Biol. Chem.* **2019**, *294*, 8773–8778. [CrossRef] [PubMed]
13. Yalak, G.; Shiu, J.-Y.; Schoen, I.; Mitsi, M.; Vogel, V. Phosphorylated fibronectin enhances cell attachment and upregulates mechanical cell functions. *PLoS ONE* **2019**, *14*, e0218893. [CrossRef] [PubMed]
14. Basak, T.; Vega-Montoto, L.; Zimmerman, L.J.; Tabb, D.L.; Hudson, B.G.; Vanacore, R.M. Comprehensive Characterization of Glycosylation and Hydroxylation of Basement Membrane Collagen IV by High-Resolution Mass Spectrometry. *J. Proteome Res.* **2016**, *15*, 245–258. [CrossRef]
15. Naba, A.; Clauser, K.R.; Hynes, R.O. Enrichment of Extracellular Matrix Proteins from Tissues and Digestion into Peptides for Mass Spectrometry Analysis. *J. Vis. Exp.* **2015**, *101*, e53057. [CrossRef]
16. Chang, Y.-H.; Gregorich, Z.R.; Chen, A.J.; Hwang, L.; Guner, H.; Yu, D.; Zhang, J.; Ge, Y. New Mass-Spectrometry-Compatible Degradable Surfactant for Tissue Proteomics. *J. Proteome Res.* **2015**, *14*, 1587–1599. [CrossRef]
17. Wu, C.C.; Yates, J.R. The application of mass spectrometry to membrane proteomics. *Nat. Biotechnol.* **2003**, *21*, 262–267. [CrossRef]
18. Wiśniewski, J.R.; Zougman, A.; Nagaraj, N.; Mann, M. Universal sample preparation method for proteome analysis. *Nat. Methods* **2009**, *6*, 359–362. [CrossRef]
19. Masuda, T.; Tomita, M.; Ishihama, Y. Phase Transfer Surfactant-Aided Trypsin Digestion for Membrane Proteome Analysis. *J. Proteome Res.* **2008**, *7*, 731–740. [CrossRef]
20. Loo, R.R.O.; Dales, N.; Andrews, P.C. Surfactant effects on protein structure examined by electrospray ionization mass spectrometry. *Protein Sci.* **1994**, *3*, 1975–1983. [CrossRef]
21. Barrett, A.S.; Wither, M.J.; Hill, R.C.; Dzieciatkowska, M.; D'Alessandro, A.; Reisz, J.A.; Hansen, K.C. Hydroxylamine Chemical Digestion for Insoluble Extracellular Matrix Characterization. *J. Proteome Res.* **2017**, *16*, 4177–4184. [CrossRef]
22. Hill, R.C.; Calle, E.A.; Dzieciatkowska, M.; Niklason, L.E.; Hansen, K.C. Quantification of Extracellular Matrix Proteins from a Rat Lung Scaffold to Provide a Molecular Readout for Tissue Engineering. *Mol. Cell. Proteom.* **2015**, *14*, 961–973. [CrossRef] [PubMed]
23. Samyn, B.; Sergeant, K.; Van Beeumen, J. A method for C-terminal sequence analysis in the proteomic era (proteins cleaved with cyanogen bromide). *Nat. Protoc.* **2006**, *1*, 318–323. [CrossRef] [PubMed]
24. Krasny, L.; Paul, A.; Wai, P.; Howard, B.A.; Natrajan, R.C.; Huang, P.H. Comparative proteomic assessment of matrisome enrichment methodologies. *Biochem. J.* **2016**, *473*, 3979–3995. [CrossRef]

25. Gaetani, R.; Aude, S.; DeMaddalena, L.L.; Strassle, H.; Dzieciatkowska, M.; Wortham, M.; Bender, R.H.F.; Nguyen-Ngoc, K.-V.; Schmid-Schöenbein, G.W.; George, S.C.; et al. Evaluation of Different Decellularization Protocols on the Generation of Pancreas-Derived Hydrogels. *Tissue Eng. Part C Methods* **2018**, *24*, 697–708. [CrossRef] [PubMed]
26. Yu, Y.-Q.; Gilar, M.; Lee, P.; Bouvier, E.S.P.; Gebler, J.C. Enzyme-Friendly, Mass Spectrometry-Compatible Surfactant for In-Solution Enzymatic Digestion of Proteins. *Anal. Chem.* **2003**, *75*, 6023–6028. [CrossRef]
27. Chen, E.I.; McClatchy, D.; Park, S.K.; Yates, J.R. Comparisons of Mass Spectrometry Compatible Surfactants for Global Analysis of the Mammalian Brain Proteome. *Anal. Chem.* **2008**, *80*, 8694–8701. [CrossRef] [PubMed]
28. Zhang, X. Less is More: Membrane Protein Digestion Beyond Urea–Trypsin Solution for Next-level Proteomics. *Mol. Cell. Proteom.* **2015**, *14*, 2441–2453. [CrossRef] [PubMed]
29. Garavito, R.M.; Ferguson-Miller, S. Detergents as Tools in Membrane Biochemistry. *J. Biol. Chem.* **2001**, *276*, 32403–32406. [CrossRef]
30. Novák, P.; Havlíček, V. 4—Protein Extraction and Precipitation. In *Proteomic Profiling and Analytical Chemistry*, 2nd ed.; Ciborowski, P., Silberring, J., Eds.; Elsevier: Amsterdam, The Netherlands, 2016; pp. 51–62.
31. Novák, P.; Silberring, J. Protein Extraction and Precipitation. In *Proteomic Profiling and Analytical Chemistry*, 2nd ed.; Ciborowski, P., Silberring, J., Ed.; Elsevier: Amsterdam, The Netherlands, 2016; pp. 51–62.
32. Duong-Ly, K.C.; Gabelli, S.B. Salting out of Proteins Using Ammonium Sulfate Precipitation. *Methods Enzymol.* **2014**, *541*, 85–94. [CrossRef]
33. Naka, M.; Kusakabe, K.; Takeshita, A.; Nakagawa, H.; Ito, Y.; Shibata, M.-A.; Otsuki, Y. Phagocytosis mechanism of apoptotic granulosa cells regulated by milk-fat globule-EGF factor 8. *Med. Mol. Morphol.* **2009**, *42*, 143–149. [CrossRef] [PubMed]
34. Lohr, M.; Kaltner, H.; Lensch, M.; André, S.; Sinowatz, F.; Gabius, H.-J. Cell-type-specific expression of murine multifunctional galectin-3 and its association with follicular atresia/luteolysis in contrast to pro-apoptotic galectins—1 and 7. *Histochem. Cell Biol.* **2008**, *130*, 567–581. [CrossRef] [PubMed]
35. Ny, T.; Wahlberg, P.; Brändström, I.J.M. Matrix remodeling in the ovary: Regulation and functional role of the plasminogen activator and matrix metalloproteinase systems. *Mol. Cell. Endocrinol.* **2002**, *187*, 29–38. [CrossRef]
36. Hayashi, K.-G.; Ushizawa, K.; Hosoe, M.; Takahashi, T. Differential gene expression of serine protease inhibitors in bovine ovarian follicle: Possible involvement in follicular growth and atresia. *Reprod. Biol. Endocrinol.* **2011**, *9*, 72. [CrossRef] [PubMed]
37. Law, R.H.P.; Zhang, Q.; McGowan, S.; Buckle, A.M.; A Silverman, G.; Wong, W.; Rosado, C.J.; Langendorf, C.G.; Pike, R.N.; Bird, P.I.; et al. An overview of the serpin superfamily. *Genome Biol.* **2006**, *7*, 216. [CrossRef]
38. Bai, Y.; Li, L.-D.; Li, J.; Lu, X. Prognostic values of S100 family members in ovarian cancer patients. *BMC Cancer* **2018**, *18*, 1256. [CrossRef]
39. Ouni, E.; Vertommen, D.; Chiti, M.C.; Dolmans, M.-M.; Amorim, C.A. A Draft Map of the Human Ovarian Proteome for Tissue Engineering and Clinical Applications. *Mol. Cell. Proteom.* **2018**, *18*, S159–S173. [CrossRef]
40. Norris, J.L.; Porter, N.A.; Caprioli, R.M. Combination Detergent/MALDI Matrix: Functional Cleavable Detergents for Mass Spectrometry. *Anal. Chem.* **2005**, *77*, 5036–5040. [CrossRef]
41. Chen, E.I.; Cociorva, D.; Norris, J.L.; Yates, J.R. Optimization of Mass Spectrometry-Compatible Surfactants for Shotgun Proteomics. *J. Proteome Res.* **2007**, *6*, 2529–2538. [CrossRef]
42. Briley, S.M.; Jasti, S.; McCracken, J.M.; Hornick, J.E.; Fegley, B.; Pritchard, M.T.; Duncan, F.E. Reproductive age-associated fibrosis in the stroma of the mammalian ovary. *Reproduction* **2016**, *152*, 245–260. [CrossRef]
43. Bond, M.D.; Van Wart, H.E. Characterization of the individual collagenases from Clostridium histolyticum. *Biochemistry* **1984**, *23*, 3085–3091. [CrossRef] [PubMed]
44. Kuljanin, M.; Brown, C.F.; Raleigh, M.J.; Lajoie, G.A.; Flynn, L.E. Collagenase treatment enhances proteomic coverage of low-abundance proteins in decellularized matrix bioscaffolds. *Biomaterials* **2017**, *144*, 130–143. [CrossRef] [PubMed]

45. Schiller, H.B.; Mayr, C.H.; Leuschner, G.; Strunz, M.; Staab-Weijnitz, C.; Preisendörfer, S.; Eckes, B.; Moinzadeh, P.; Krieg, T.; Schwartz, D.A.; et al. Deep Proteome Profiling Reveals Common Prevalence of MZB1-Positive Plasma B Cells in Human Lung and Skin Fibrosis. *Am. J. Respir. Crit. Care Med.* **2017**, *196*, 1298–1310. [CrossRef]
46. Schiller, H.B.; Fernandez, I.E.; Burgstaller, G.; Schaab, C.; Scheltema, R.A.; Schwarzmayr, T.; Strom, T.M.; Eickelberg, O.; Mann, M. Time- and compartment-resolved proteome profiling of the extracellular niche in lung injury and repair. *Mol. Syst. Biol.* **2015**, *11*, 819. [CrossRef] [PubMed]
47. Barrett, A.S.; Maller, O.; Pickup, M.W.; Weaver, V.M.; Hansen, K.C. Compartment resolved proteomics reveals a dynamic matrisome in a biomechanically driven model of pancreatic ductal adenocarcinoma. *J. Immunol. Regen. Med.* **2018**, *1*, 67–75. [CrossRef]
48. Amorim, C.A.; Van Langendonckt, A.; David, A.; Dolmans, M.-M.; Donnez, J. Survival of human pre-antral follicles after cryopreservation of ovarian tissue, follicular isolation and in vitro culture in a calcium alginate matrix. *Hum. Reprod.* **2008**, *24*, 92–99. [CrossRef]
49. Naba, A.; Pearce, O.M.T.; Del Rosario, A.; Amanda, D.R.; Ding, H.; Rajeeve, V.; Cutillas, P.R.; Balkwill, F.R.; Hynes, R.O. Characterization of the Extracellular Matrix of Normal and Diseased Tissues Using Proteomics. *J. Proteome Res.* **2017**, *16*. [CrossRef]
50. Landers, R. Old Dominion University Computing Intraclass Correlations (ICC) as Estimates of Interrater Reliability in SPSS. *Winnower* **2015**, *2*, e143518.81744. [CrossRef]
51. Perez-Riverol, Y.; Csordas, A.; Bai, J.; Bernal-Llinares, M.; Hewapathirana, S.; Kundu, D.J.; Inuganti, A.; Griss, J.; Mayer, G.; Eisenacher, M.; et al. The PRIDE database and related tools and resources in 2019: Improving support for quantification data. *Nucleic Acids Res.* **2019**, *47*, D442–D450. [CrossRef]

Publisher's Note: MDPI stays neutral with regard to jurisdictional claims in published maps and institutional affiliations.

© 2020 by the authors. Licensee MDPI, Basel, Switzerland. This article is an open access article distributed under the terms and conditions of the Creative Commons Attribution (CC BY) license (http://creativecommons.org/licenses/by/4.0/).

Spatiotemporal changes in mechanical matrisome components of the human ovary from prepuberty to menopause

More than a century ago, it was proposed that mechanical forces could drive tissue formation and function, but only now we recognize that the mechanical forces generated within tissues can provide regulatory signals that are just as important as those conveyed by chemicals and genes. This fact is supported by numerous pertinent theories in the field of fertility preservation. However, the actual players orchestrating ovarian tissue plasticity are still undetermined. We therefore investigated the real elastic system components that confer intrinsic mechanical features to tissue and orchestrate a myriad of molecular signalization pathways, including collagen, elastin, EMILIN-1, fibrillin-1, and GAGs. First, we studied their spatiotemporal quantitative changes from puberty to menopause before conducting a closer analysis of the ECM around follicles from primordial to secondary stages in both prepubertal and reproductive-age tissue.

The study included ovarian cortical tissue from 68 patients from different groups: prepubertal (n=16), reproductive-age (n=21) and menopausal (n=31). The menopausal group was subdivided into two subgroups: with (n=7) and without hormone treatment (n=24).

Our results demonstrated the ECM deposition and turnover in an age- and follicular stage-related manner. While collagen levels climbed with age, all elastic components declined. Interestingly, higher levels of collagen, EMILIN-1, and elastin were noted in reproductive-age and menopausal women undergoing hormone treatment, suggesting a positive effect of secreted estrogen and hormonal therapy on collagen and elastin crosslinking and preservation. Excessive accumulation of GAGs with age further contributed

to the ovarian tissue stiffness due to high osmotic pressure linked to water retention by GAGs. In addition, high amounts of GAGs appeared to hamper the formation of the fibrillin-1 network, which explains its decline over time. Based on the same assumptions, exploration of the ECM surrounding follicles from the primordial to the secondary stage, both before and after puberty, points to high levels of mechanical stress placed on prepubertal follicles compared to the more compliant ECM around reproductive-age follicles. Such a stiff niche is nonpermissive to prepubertal follicle activation and growth and more favorable for quiescence.

From a biochemical perspective, our study revealed exciting changes to ECM composition, dictating the ovarian tissue elastic features, which is in line with the existing literature.

Our findings pave the way for possible therapeutic targets at the ECM level in the context of female fertility and ovarian rejuvenation. Our data will prove very useful in designing biomimetic scaffolds and tissue-engineered models like the artificial ovary. Indeed, they emphasize the importance of encapsulating each type of isolated follicles in an appropriate biomaterial that must replicate the corresponding functional perifollicular ECM and respect ovarian tissue heterogeneity to guarantee its biomimicry. Although our data disclose the complexity of this task, they also offer new opportunities to explore ovarian ECM synthesis de novo, which may reverse ovarian aging and help to develop reliable in vitro models to complement our knowledge of human ovary regulation.

Human Reproduction, pp. 1–27, 2020
doi:10.1093/humrep/deaa100

human reproduction

ORIGINAL ARTICLE ***Reproductive biology***

Spatiotemporal changes in mechanical matrisome components of the human ovary from prepuberty to menopause

E. Ouni[1], C. Bouzin[2], M.M. Dolmans[1,3], E. Marbaix[4,5], S. Pyr dit Ruys[6], D. Vertommen[6], and C.A. Amorim[1,*]

[1]Pôle de Recherche en Gynécologie, Institut de Recherche Expérimentale et Clinique, Université Catholique de Louvain, 1200 Brussels, Belgium [2]IREC Imaging Platform (2IP), Institut de Recherche Expérimentale et Clinique, Université Catholique de Louvain, 1200 Brussels, Belgium [3]Gynecology and Andrology Department, Cliniques Universitaires Saint-Luc, 1200 Brussels, Belgium [4]Pathology Department, Cliniques Universitaires Saint-Luc, 1200 Brussels, Belgium [5]Cell Biology Unit, de Duve Institute, Université Catholique de Louvain, 1200 Brussels, Belgium [6]de Duve Institute, Université Catholique de Louvain, Brussels, Belgium

*Correspondence address. Pôle de Recherche en Gynécologie, Institut de Recherche Expérimentale et Clinique, Université Catholique de Louvain, Avenue Mounier 52, bte B1.52.02, 1200 Brussels, Belgium. Tel: +32 (0)2 764 5287; E-mail: christiani.amorim@uclouvain.be

Submitted on November 29, 2019; resubmitted on April 15, 2020; accepted on April 22, 2020

STUDY QUESTION: How do elastic matrisome components change during the lifetime of the human ovary?

SUMMARY ANSWER: The deposition and remodeling of mechanical matrisome components (collagen, elastin, elastin microfibril interface-located protein 1 (EMILIN-1), fibrillin-1 and glycosaminoglycans (GAGs)) that play key roles in signaling pathways related to follicle activation and development evolve in an age- and follicle stage-related manner.

WHAT IS KNOWN ALREADY: The mechanobiology of the human ovary and dynamic reciprocity that exists between ovarian cells and their microenvironment is of high importance. Indeed, while the localization of primordial follicles in the collagen-rich ovarian cortex offers a rigid physical environment that supports follicle architecture and probably plays a role in their survival, ovarian extracellular matrix (ECM) stiffness limits follicle expansion and hence oocyte maturation, maintaining follicles in their quiescent state. As growing follicles migrate to the medulla of the ovary, they encounter a softer, more pliant ECM, allowing expansion and development. Thus, changes in the rigidity of the ovarian ECM have a direct effect on follicle behavior. Evidence supporting a role for the physical environment in follicle activation was provided in clinical practice by ovarian tissue fragmentation, which promoted actin polymerization and disrupted ovarian Hippo signaling, leading to increased expression of downstream growth factors, promotion of follicle growth and generation of mature oocytes.

STUDY DESIGN, SIZE, DURATION: We investigated quantitative spatiotemporal changes in collagen, elastin, EMILIN-1, fibrillin-1 and GAGs from prepuberty to menopause, before conducting a closer analysis of the ECM surrounding follicles, from primordial to secondary stages, in both prepubertal and tissue from women of reproductive age. The study included ovarian tissue (cortex) from 68 patients of different ages: prepubertal ($n = 16$; mean age [±SD]=8 ± 2 years); reproductive ($n = 21$; mean age [±SD]=27 ± 4 years); menopausal with estrogen-based HRT ($n = 7$; mean age [±SD]=58 ± 4 years); and menopausal without HRT ($n = 24$; mean age [±SD]=61 ± 5 years).

PARTICIPANTS/MATERIALS, SETTING, METHODS: Quantitative investigations of collagen and GAG deposition in ovarian tissue throughout a woman's lifetime were conducted by analyzing brightfield images. Characteristic features of collagen fiber content were based on polarized light microscopy, since polarized light changes with fiber thickness. To evaluate the deposition and distribution of elastin, fibrillin-1 and EMILIN-1, multiplex immunofluorescence was used on at least three sections from each patient. Image processing and tailored bioinformatic analysis were applied to enable spatiotemporal quantitative evaluation of elastic system component deposition in the human ovary over its lifetime.

MAIN RESULTS AND THE ROLE OF CHANCE: While collagen levels increased with age, fibrillin-1 and EMILIN-1 declined. Interestingly, collagen and elastin reached their peak in reproductive-age women compared to prepubertal ($P < 0.01$; $P = 0.262$) and menopausal subjects with ($P = 0.706$; $P < 0.01$) and without ($P = 0.987$; $P = 0.610$) HRT, indicating a positive impact of secreted estrogen and hormone treatment on collagen and elastin preservation. Interestingly, HRT appears to affect elastin presence in ovarian tissue, since a significantly higher ($P < 0.05$) proportion of elastin was detected in biopsies from menopausal women taking HRT compared to those not. Higher GAG levels were found in adult ovaries compared to prepubertal ovaries ($P < 0.05$), suggesting changes in tissue ultrastructure and elasticity with age. In this context, elevated GAG values are suspected to participate in hampering formation of the fibrillin-1 network

© The Author(s) 2020. Published by Oxford University Press on behalf of European Society of Human Reproduction and Embryology. All rights reserved.
For permissions, please email: journals.permissions@oup.com

($r = -0.2475$; $P = 0.04687$), which explains its decline over time. This decline partially accounts for the decrease in EMILIN-1 ($r = 0.4149$; $P = 0.00059$). Closer examination of the ECM surrounding follicles from the primordial to the secondary stage, both before and after puberty, points to high levels of mechanical stress placed on prepubertal follicles compared to the more compliant ECM around reproductive-age follicles, as suggested by the higher collagen levels and lower elastin content detected mainly around primordial ($P < 0.0001$; $P < 0.0001$, respectively) and primary ($P < 0.0001$; $P < 0.001$, respectively) follicles. Such a stiff niche is nonpermissive to prepubertal follicle activation and growth, and is more inclined to quiescence.

LARGE SCALE DATA: Not applicable.

LIMITATIONS, REASONS FOR CAUTION: The duration and form of administered HRT were not considered when studying the menopausal patient group undergoing treatment. Moreover, we cannot exclude interference from other nongynecological medications taken by the study patients on ovarian ECM properties since there is no information in the literature describing the impact of each medication on the ECM. Finally, since the ECM is by definition a very heterogeneous meshwork of proteins, the use of two-dimensional histology could be a limitation. Single time points on fixed tissues could also present limitations, since following ovary dynamics from prepuberty to menopause in the same patient is not feasible.

WIDER IMPLICATIONS OF THE FINDINGS: From a biomechanical perspective, our study revealed important changes to ECM properties dictating the mechanical features of ovarian tissue, in line with the existing literature. Our findings pave the way for possible therapeutic targets at the ECM level in the context of female fertility and ovarian rejuvenation, such as mechanical stimulation, antifibrotic treatments, and prevention or reversion of elastic ECM degradation. Our study also sheds light on the follicle-specific ECM composition that is dependent on follicle stage and age. These data will prove very useful in designing biomimetic scaffolds and tissue-engineered models like the artificial ovary. Indeed, they emphasize the importance of encapsulating each type of isolated follicle in an appropriate biomaterial that must replicate the corresponding functional perifollicular ECM and respect ovarian tissue heterogeneity in order to guarantee its biomimicry.

STUDY FUNDING/COMPETING INTEREST(S): This study was supported by grants from the Fonds National de la Recherche Scientifique de Belgique (FNRS) (C.A.A. is an FRS-FNRS research associate; grant 5/4/150/5 awarded to M.M.D.) and the Université Catholique de Louvain (PhD grant 'Coopération au développement' awarded to E.O.). None of the authors have any competing interests to declare.

Key words: ovary / extracellular matrix / hormone replacement therapy / aging / fertility preservation / mechanobiology

Introduction

The ovary contains a large number of dormant immature follicles, the organ's functional units, each accommodating a single oocyte and residing on the periphery of the ovary. Upon puberty, a group of immature follicles is sequentially activated to resume growth with every reproductive cycle and a single dominant follicle eventually emerges, ovulates, and then involutes to allow selection of the next group of follicles. This process, known as folliculogenesis, makes the human ovary one of the most dynamic tissues in the female body, undergoing repeated cycles of growth and involution throughout her reproductive life.

Although many hormonal and molecular analyses have been conducted to identify the mechanisms underlying ovarian development and folliculogenesis (Adhikari and Liu, 2009; Grive and Freiman, 2015; Hsueh *et al.*, 2015; Filatov *et al.*, 2017; Ford *et al.*, 2019), the role of the extracellular matrix (ECM) in these processes remains unclear. Nevertheless, this last decade has witnessed growing interest in the mechanobiology of the human ovary and the dynamic reciprocity that exists between ovarian cells and their microenvironment (Woodruff and Shea, 2011; Thorne *et al.*, 2015). Indeed, while the localization of primordial (dormant) follicles in the collagen-rich ovarian cortex offers a rigid physical environment that supports follicle architecture and probably plays a role in their survival, ovarian ECM stiffness limits follicle expansion and hence oocyte maturation, maintaining follicles in their quiescent state (Shah *et al.*, 2018). As growing follicles migrate to the medulla of the ovary, they encounter a softer, more pliant ECM, allowing expansion and development. Thus, changes in the rigidity of the ovarian ECM have a direct effect on follicle behavior. This hypothesis was first investigated in *in vitro* experiments (Xu *et al.*, 2006; Hornick *et al.*, 2012; Choi *et al.*, 2014) and substantiated by *in vivo* studies and clinical practice (Kawamura *et al.*, 2016). Evidence supporting a role for the physical environment in follicle activation was provided by Kawamura *et al.* (2013), who proved that ovarian tissue fragmentation promoted actin polymerization and disrupted ovarian Hippo signaling, leading to increased expression of downstream growth factors, promotion of follicle growth and generation of mature oocytes.

This strongly suggests that in addition to well-established biochemical cues (Hsueh *et al.*, 2015), follicle activation depends on the physical environment of the ovary, and any alterations to its normal physical aspects may be implicated in ovarian disorders, such as primary ovarian insufficiency and polycystic ovary syndrome (PCOS) (Wood *et al.*, 2015). Interestingly, therapies for PCOS have included ovarian wedge resection or laser drilling to induce follicle growth (Lunde *et al.*, 2001), but the underlying mechanisms of these disruptive procedures are unclear. So far, our characterization of the biomechanical regulation of the human ovary extends to use of terms such as rigid or soft microenvironment to describe the ovarian ECM, with little focus on the actual elastic system components that give the tissue its intrinsic mechanical features and orchestrate related downstream cell signaling.

The mechanical features of soft tissues are mainly governed by the content and organization of collagen and elastic fibers (Levillain *et al.*,

2016). Elastic fibers are large ECM structures that provide tissues with recoil needed to undergo repeated stretching and complement the tensile strength of fibrillar collagens. Elastic fibers reside in tissues as a large network composed of two discrete components, namely elastin, the major constituent, and associated microfibrils, mainly fibrillin-1. Elastin microfibril interface-located protein 1 (EMILIN-1) is another glycoprotein present at the interface between amorphous elastin and microfibrils. Glycosaminoglycans (GAGs) participate in the immobilization of water, conferring elasticity to biological tissues and contributing to their homeostasis and osmotic equilibrium (Kurylo *et al.*, 2016). Beyond elastogenesis and mechanical properties, these molecules are linked to a myriad of molecular signaling pathways (Afratis *et al.*, 2012). While they are probably involved in various processes in the ovary, to the best of our knowledge there are no existing studies defining their role in the human ovary and possible association with ovarian follicles.

The goal of this study was therefore to decipher the role of ECM fibers in the human ovary by comparing elastin, EMILIN-1, fibrillin-1 and GAGs in ovarian tissue from prepubertal girls, women of reproductive age and menopausal women both undergoing and not undergoing HRT. Comparisons were made by means of histological staining, immunofluorescence and tissue scanning. Image processing and tailored bioinformatic analysis were used to enable spatiotemporal quantitative evaluation of elastic system component deposition in the human ovary over its lifetime. We also conducted an in-depth analysis of the ECM surrounding preantral follicles before and after puberty in order to link mechanical cues involved in follicle activation with biochemical and hormone regulation.

Materials and methods

Human ovarian tissue

Sixty-eight ovarian tissue samples retrieved from patients of different ages were included in this study (Fig. 1): prepubertal ($n = 16$; mean age [±SD]=8 ± 2 years); reproductive-age ($n = 21$; mean age [±SD]=27 ± 4 years); menopausal with estrogen-based HRT ($n = 7$; mean age [±SD]=58 ± 4 years) and without HRT ($n = 24$; mean age [±SD]=61 ± 5 years). All participating adult patients were undergoing laparoscopic surgery for benign gynecologic diseases not affecting the ovaries. Prepubertal tissue was derived from young cancer patients scheduled for ovarian cortex cryopreservation as a fertility preservation strategy, before being subjected to acute gonadotoxic cancer treatments. Sample storage in the biobank of St-Luc's Hospital involved tissue fixation, dehydration and embedding in several paraffin blocks for further investigation by the anatomic pathology department of the institution. Enrolled subjects did not show any alterations to any of the ovaries included in our study, allowing use of residual material (Supplementary Table SI).

Ethics

Use of human ovarian cortex was approved by the Institutional Review Board of the Université Catholique de Louvain on 13 May 2019 (IRB reference 2012/23MAR/125, registration number B403201213872). After obtaining informed consent from all parties, fragments of ovarian tissue were collected.

Morphological selection criteria

All samples used in this study were fixed in 10% neutral buffered formalin overnight at 4°C, before being directly dehydrated and embedded in paraffin. Biopsies were kept in paraffin blocks during collection of study samples and sectioned (serial sections of 5 µm) just before analysis to better preserve their antigen epitopes. The cortical layer of each ovarian sample was evaluated, and every fourth slide was stained with hematoxylin-eosin (Merck, Darmstadt, Germany) for morphological analysis and follicle classification. This step enabled selection of tissue sections with high and comparable follicle numbers within prepubertal and reproductive-age group for further comparative analysis. A total of three to five slides were examined from each sample.

Hematoxylin-eosin staining was also used to select only cortical sections and exclude slides containing the tunica albuginea or medullary compartment to avoid any bias in ECM characterization. The medulla contains many large blood vessels and lacks the swirling, highly cellular appearance typical of the ovarian cortex. These characteristic features, in addition to assistance from an experienced histologist, helped ensure that the tissue analyzed was solely from the cortex. The remaining slides (Superfrost® Plus slides, Menzel-Glaser, Braunschweig, Germany) were kept for immunofluorescence and additional histological staining (Fig. 1)

Follicle classification was based on the following criteria defining: primordial follicles containing flattened granulosa cells surrounding the oocyte; primary follicles with one layer of cuboidal granulosa cells; and secondary follicles with at least two layers of granulosa cells and no antrum. Follicles with binuclear oocytes and those showing disrupted integrity and signs of degeneration (pyknotic oocyte nuclei, shrunken ooplasm and/or disorganized granulosa cells) were all excluded from the study.

Histological staining

Five-µm-thick paraffin sections were deparaffinized, rehydrated and treated with a saturated picric acid solution containing 1.3% Sirius Red for 1 h at room temperature. GAGs were identified by Alcian blue staining at pH 2.5 (Bio-Optica, Milan, Italy), as described (Hayat, 1993). Alcian blue staining at pH 2.5 selectively labels carboxylated and sulfated GAGs, based on its positive charge attracted to negative structures (e.g. acidic sugars forming the GAGs). Its bulkiness prevents its diffusion toward other highly negative structures in tissue, such as chromatin and Nissl substance (Kiernan, 2006).

Human small intestine was used as a positive control to monitor Alcian blue staining quality (Supplementary Fig. S1). Slides were digitized at X20 magnification with a Leica SCN400 Slide Scanner (Leica, Heerbrugg, Switzerland).

Acquisition of collagen birefringence

In addition to brightfield observations, sections stained with Sirius Red were observed under polarized light using a Nikon Eclipse Ci microscope, and captured with a Leica DFC450 camera equipped with filters to provide circularly polarized illumination. Filters were aligned so that the background in the field of view was as dark as possible, as

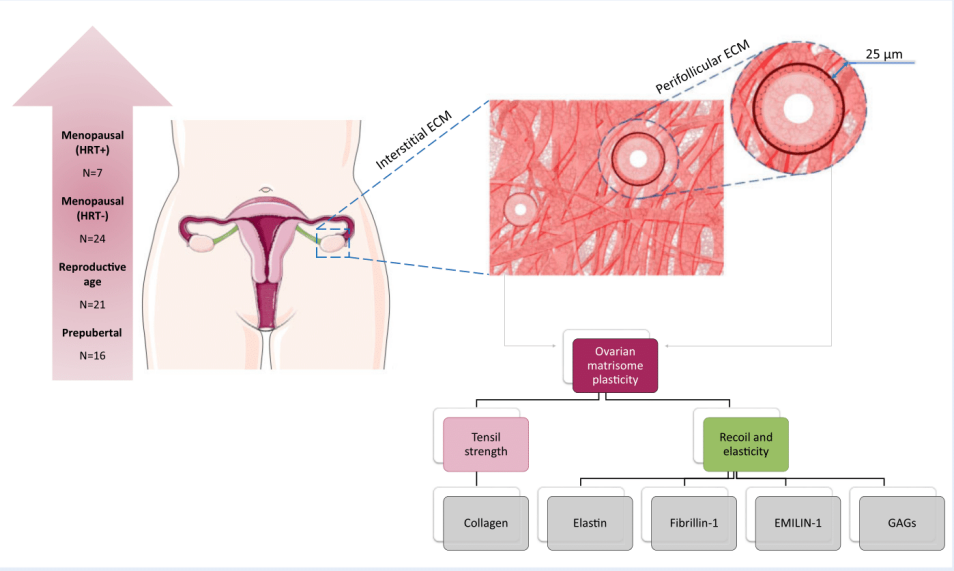


Figure 1 Schematic of the study of elastic matrisome components in human ovary. This study investigates the elastic matrisome components that control ovarian tissue plasticity: collagen, which is associated with tensile strength; and elastin, elastin microfibril interface-located protein (EMILIN-1), fibrillin-1 and glycosaminoglycans (GAGs), which are all associated with tissue recoil and elasticity. First, we studied their quantitative spatiotemporal changes from prepuberty to menopause (with and without HRT [HRT+/HRT−]) in the interstitial extracellular matrix (ECM), before conducting a closer analysis of the perifollicular ECM surrounding follicles from primordial to secondary stages in both prepubertal and reproductive-age tissue. The female genital apparatus illustration was created using Servier Medical Art templates, which are licensed under a Creative Commons Attribution 3.0 Unported License (https://smart.servier.com).

previously reported (Rich and Whittaker, 2005). Objective lenses set at X20 and X40 magnification were used to capture global and perifollicular ECM, respectively.

Each area of interest was captured under polarized and brightfield light in order to obtain a morphological readout and enable identification of follicle developmental stage. Pictures at the same magnification were taken under the same conditions (exposure, gain, saturation and gamma).

Immunofluorescence

To evaluate elastin, fibrillin-1 and EMILIN-1 deposition and distribution, multiplex immunofluorescence was used on at least three sections from each patient, following a previously described protocol (Aboubakar Nana *et al.*, 2019). All antibodies were tested separately with 3,3′-diaminobenzidine (DAB) and immunofluorescence on successive slides, before conducting multiplex immunofluorescence to ensure that no cross-reactivity between antibodies is present and the signal is not affected by the tissue processing steps (Supplementary Fig. S2).

After deparaffinization in Histosafe (Yvsolab SA, Beerse, Belgium) and ethanol, autofluorescence was quenched by 10-min incubation in 50 mM NH_4Cl, and endogenous peroxidase inhibition was achieved after 30 min in 0.3% H_2O_2. Sections were then subjected to water bath antigen retrieval in 10 mM citrate buffer (pH 5.7) containing 0.1% Triton or Tris-EDTA buffer (pH9.0), before blocking of nonspecific antigen binding sites (Tris-buffered saline (TBS) solution containing 10% normal goat serum and 1% bovine serum albumin (BSA)). The first primary antibody was incubated overnight at 4°C in a humid chamber in TBS containing 1% BSA and 0.1% Tween-20 and detected by corresponding horseradish peroxidase (HRP)-conjugated secondary antibodies (Envision, Dako, Glostrup, Denmark) for 1 h at room temperature. HRP was then visualized by tyramide signal amplification using Alexa Fluor-conjugated tyramides (Invitrogen Carlsbad, CA, USA). After one more citrate buffer antigen retrieval step, the same protocol was applied with other primary antibodies and different Alexa Fluor-conjugated tyramides. In all, three sequential reactions were performed with anti-elastin, anti-fibrillin-1 and anti-EMILIN-1 (Table I). Finally, nuclei were counterstained with Hoechst 33342 (Thermo Fisher Scientific, Waltham, MA, USA) and mounted with HIGHDEF IHC fluoromount (Enzo, New York, USA). Negative controls were conducted by adding rabbit IgG (Dako, Carpinteria, USA) instead of the primary antibody, while human testis was used for positive controls of all tested antibodies (Supplementary Fig. S2). Stained slides

Table I Primary antibodies and respective parameters.

Antigen	Primary antibody				Secondary antibody			TSA Fluochrome
	Concentration (µg/ml)	Incubation	Company	Catalog number	Polymer HRP	Company	Catalog number	
Elastin	2.20 (1/250)	O/N 4°C	Abcam	EPR 20603	Anti-rabbit	Agilent/Dako	K4003	AF488
Fibrillin-1	0.50 (1/200)	O/N 4°C	Sigma	HPA 017759				AF555
EMILIN-1	3 (1/100)	O/N 4°C	Sigma	HPA 002822				AF647

HPR, horseradish peroxidase; TSA, tyramine signal amplification; EMILIN-1, elastin microfibril interface 1.

Table II Number of follicles selected for analysis of the perifollicular extracellular matrix.

	Primordial follicles		Primary follicles		Secondary follicles	
	Prepubertal tissue	Reproductive age tissue	Prepubertal tissue	Reproductive age tissue	Prepubertal tissue	Reproductive age tissue
Collagen (BF)	841	241	196	161	30	48
Collagen (PL)	128	64	39	39	11	23
Elastin	826	260	310	198	25	13
Fibrillin-1	826	260	310	198	25	13
EMILIN-1	826	260	310	198	25	13
GAGs	217	238	182	160	18	30

Number of human follicles selected for analysis of the perifollicular extracellular matrix. Brightfield (BF) and polarized light (PL) microscopy were used for detection of collagen. Elastin, fibrillin-1 and EMILIN-1 were detected by multiplex immunofluorescence, so their evaluation was conducted over the same perifollicular areas, explaining the identical number of selected follicles. Carboxylated and sulfated glycosaminoglycans (GAGs) were selectively labeled by Alcian blue staining (pH 2.5).

were digitized by automated whole-slide image capture with a Pannoramic 250 Flash III scanner (3DHISTECH Ltd, Budapest, Hungary).

Digital image analysis

To ensure reproducible and objective results, computer-assisted quantification of immunofluorescence labeling and histological staining was carried out with Oncotopix, version 2017.2 (Visiopharm, Hoersholm, Denmark) (Supplementary Fig. S3). Tailored software applications were developed by our team to detect tissue regions of interest (ROIs); quantify ROI area; and measure the stained area within a given ROI. Vessels, oocytes and artifacts were manually discarded from ROIs.

Computer-assisted quantification of staining (brightfield: GAGs, Sirius Red) and immunostaining (fluorescence: elastin, EMILIN-1, fibrillin-1) was based on the following equation:

$$\% \text{ stained area} = \text{stained area} \times 100/\text{ROI area}.$$

The same quantification was applied in a concentric region (25-µm-thick) surrounding follicles after their manual delineation and separation into primordial, primary and secondary, based on criteria described in the 'Morphological selection criteria' section (Supplementary Fig. S3, Table II).

Collagen content characterization was based on the birefringence of Sirius Red stained sections under polarized light. It is known that the color of collagen fibers stained with Sirius Red and viewed under polarized light depends on fiber thickness and packing, with polarization colors ranging from green to yellow, orange and red according to their increase in diameter and packing density (Dayan *et al.*, 1989).

To establish proportions of different polarization colors, we used a macro program developed in-house on Fiji software (Schindelin *et al.*, 2012) to automate the quantification (Supplementary Fig. S4, Table II). This macro program determines the total area of polarized pixels using the color threshold tool on Fiji and classifies them into three categories based on the hue histogram. We used a modification of hue definitions applied by MacKenna *et al.* (1994): red 2–9, yellow/orange 10–38, green 24–135. Results were expressed as:

$$\% \text{ polarized collagen} = \text{green}-, \text{ yellow/orange} - \text{ or red} - \text{positive area} \times 100/\text{total positive area}.$$

All quantifications were performed blinded to group assignment.

Statistical analysis

Data are presented as mean ± SEM and were calculated using the GraphPad Prism software package, version 8.0 (San Diego, CA, USA).

Descriptive analyses of values (Dagostino and Pearson or Shapiro–Wilk normality tests) were conducted before each evaluation to select the appropriate statistical test. One-way ANOVA or the Kruskal–Wallis test followed by *post hoc* multiple comparisons using Dunn's test were applied when required to compare interstitial ECMs. Differences in perifollicular ECMs in each of the prepubertal and reproductive-age ovaries were evaluated based on two-way ANOVA or Kruskal–Wallis tests, depending on data distribution. The multiple Student's *t*-test or Mann–Whitney test were used to compare prepubertal and reproductive-age perifollicular ECMs at the same developmental stage. Differences were considered significant at values of $P < 0.05$. Spearman's correlation was applied to measure EMILIN-1/fibrillin-1 and GAG/fibrillin-1 interdependence.

Results

Collagen

Quantitative investigation of collagen deposition in ovarian tissue throughout a woman's lifetime was carried out by analyzing brightfield images. Characteristic features of collagen fiber content were based on polarized light microscopy, since polarized light changes with fiber thickness, as described above.

Collagen levels increase with age

Digital image analysis of ovarian tissue from prepubertal, reproductive-age and menopausal women with or without HRT allowed comparison of collagen deposition levels. Quantification was based on Sirius Red staining acquired on brightfield images (Supplementary Fig. S3). Our results showed a continual increase in collagen levels from prepuberty to menopause, with a significant difference between prepubertal tissue and reproductive-age subjects ($P < 0.01$) as well as with menopausal subjects under HRT ($P < 0.05$) (Fig. 2A and B). Maintenance of collagen levels between reproductive-age subjects and menopausal women without HRT and the absence of any statistically significant difference ($P = 0.706$) clearly demonstrate that collagen reaches its peak at reproductive age (Fig. 2A and B).

Collagen fibers evolve with age

While analyses of Sirius Red staining with brightfield microscopy showed rising collagen fiber deposition with age, it was paramount to look more closely at collagen fiber thickness and its evolution with age. Polarized light microscopy was used once again to inspect the same slides stained with Sirius Red, and revealed that red fibers (the thickest) are the least abundant in human ovarian cortex at any age and represent <7% of total collagen. Interestingly, the reproductive-age group retained the highest proportion of thick collagen fibers of all groups. Thin fibers (green) and average-size fibers (orange and yellow) were found at equivalent rates (~48%) in all groups except prepubertal, where we detected the highest percentage of thin fibers ($61 \pm 3.1\%$) and the lowest percentage of average fibers ($35 \pm 2.8\%$) (Fig. 2A–C).

ECM surrounding prepubertal follicles is the richest in collagen

Although collagen levels do not appear to change with follicle development in either young or adult patients, we encountered significantly higher collagen content in the microenvironment of both primordial ($P < 0.0001$) and primary ($P < 0.0001$) follicles derived from prepubertal ovarian tissue compared to reproductive-age tissue (Fig. 3A and B).

Collagen fiber content in ECM surrounding primordial follicles differs between prepubertal and reproductive-age ovaries

Closer investigation of the microenvironment of primordial follicles at different ages revealed a significantly higher proportion of thick fibers ($P < 0.001$) and lower levels of intermediate ($P < 0.001$) and thin ($P < 0.001$) fibers at prepuberty. High levels of thick collagen fibers seen in perifollicular areas of prepubertal ovaries do not appear to significantly change during early folliculogenesis. On the other hand, a significant decrease in thick collagen fibers was observed in the perifollicular ECM of reproductive-age ovaries, from primary to secondary follicles (Fig. 3A–C).

Elastin

It is known that elastin fibers enable tissues to go through repeated stretching and contraction, so we could hypothesize that elastin plays a major role in a dynamic organ like the ovary. For this reason, we studied its presence and localization in the ECM of different ovary age groups.

Elastin concentrations are affected by aging and HRT

Levels of elastin were as high as 5% in human ovarian tissue, but its density varies according to age. Although we saw a moderate increase from prepubertal to reproductive-age tissue, elastin levels fell dramatically in menopausal women not using HRT ($P < 0.01$) (Fig. 4). Interestingly, hormone substitutes appear to affect elastin presence in ovarian tissue, since a significantly higher ($P < 0.05$) proportion of elastin was detected in biopsies from menopausal women taking HRT compared to those who were not (Fig. 4).

Perifollicular ECM in prepubertal ovaries contains the least elastin

In-depth analysis of the perifollicular ECM revealed significantly lower elastin content around primordial ($P < 0.0001$) and primary ($P < 0.001$) follicles in prepubertal ovarian tissue compared to reproductive-age counterparts (Fig. 5).

Fibrillin-1

Fibrillin-1 microfibrils are associated with elastin and play an important role in the mechanical properties of biological tissues, with implication in biochemical pathways. Fibrillin-1 levels were therefore investigated in ovarian ECM and related to age, follicle stage and hormones.

Fibrillin-1 levels are age-dependent

Fibrillin-1 levels do not change from prepuberty to reproductive age, but drop by half upon menopause. However, by contrast with elastin, fibrillin-1 deposition was not found to be affected by HRT administration (Fig. 6).

Fibrillin-1 levels do not vary in a similar manner in the perifollicular ECM of prepubertal and reproductive-age ovarian tissue

While fibrillin-1 levels did not significantly change during reproductive age in the perifollicular ECM overall, levels rose in prepubertal ovarian tissue following follicle activation ($P < 0.001$). A higher proportion of fibrillin-1 was detected in the ECM surrounding primary ($P < 0.001$)

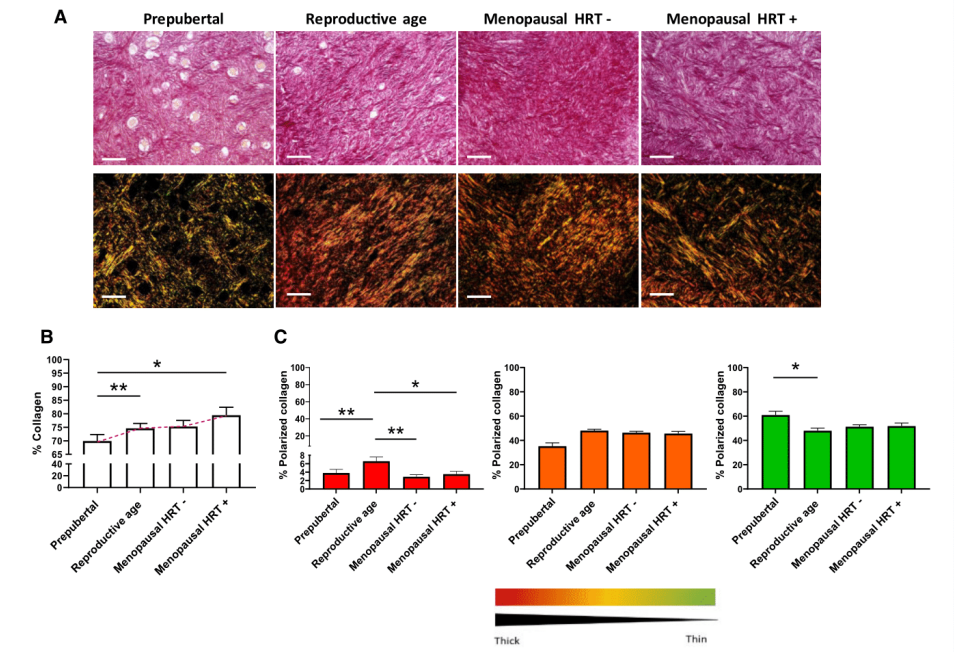


Figure 2 Spatiotemporal evolution of collagen deposition in the ovarian interstitial ECM under brightfield and polarized light microscopy. (**A** and **B**) Quantitative investigation of collagen deposition in ovarian tissue throughout a woman's lifetime was carried out by analyzing brightfield images, which revealed that collagen levels in the human ovary reach a peak at reproductive age (75% ± 1.8). (**C**) Characteristic features of collagen fiber content were based on collagen birefringence observed under polarized light microscopy, since polarized light changes according to fiber thickness: thick fibers (red); average-size fibers (yellow/orange); and thin fibers (green). Thin fibers and average-size fibers were found at equivalent rates (~48%) in all groups except prepubertal tissue, where we detected the lowest rate of average-size fibers (35% ± 2.8) and the highest rate of thin fibers (61% ± 3.1). These decrease in reproductive-age subjects in favor of thicker collagen fibers. The represented data included analysis of ovarian tissue from 68 patients: prepubertal ($n = 16$); reproductive ($n = 21$); menopausal with estrogen-based HRT ($n = 7$); and menopausal without HRT ($n = 24$). One-way ANOVA (*post hoc*: Tukey) and Kruskal–Wallis (*post hoc*: Dunn) tests were, respectively, used to compare collagen content and fiber thickness between groups (*$P < 0.05$ and **$P < 0.01$). Results are presented as mean ± SEM. Scale bars: 100 µm.

follicles in prepubertal ovaries compared to reproductive-age tissue (Fig. 7).

Elastin microfibril interface-located protein 1

EMILIN-1 is a key glycoprotein associated with the ECM elastic system and implicated in elastogenesis, among other functions (Zanetti *et al.*, 2004). It is therefore another pivotal element in the elastic system, whose spatiotemporal deposition in the human ovary needed investigation.

EMILIN-1 levels fluctuate with age

At prepuberty, around 30% of the ovarian ECM surface area is composed of EMILIN-1, which increases slightly after puberty, only to decrease again at menopause (Fig. 8). Contrary to the positive effect that HRT has on elastin at menopause, no significant difference in EMILIN-1 levels was found between menopausal patients with or without HRT ($P = 0.683$). It is important to stress that the distribution of EMILIN-1 was highly heterogeneous in ovarian tissue and between patients, which hampered detection of statistically significant results, despite a clear tendency. Indeed, the ECM is a very heterogeneous protein meshwork that varies even within the same biological sample (Malandrino *et al.*, 2018). Therefore, it was no surprise to find a wide range of expression of EMILIN-1 in large tissue areas like interstitial ECM.

Perifollicular ECM in prepubertal ovaries contains low levels of EMILIN-1

The limited area of perifollicular ECM (25-µm-thick perimeter) showed considerably less heterogeneity in perifollicular ROIs compared to

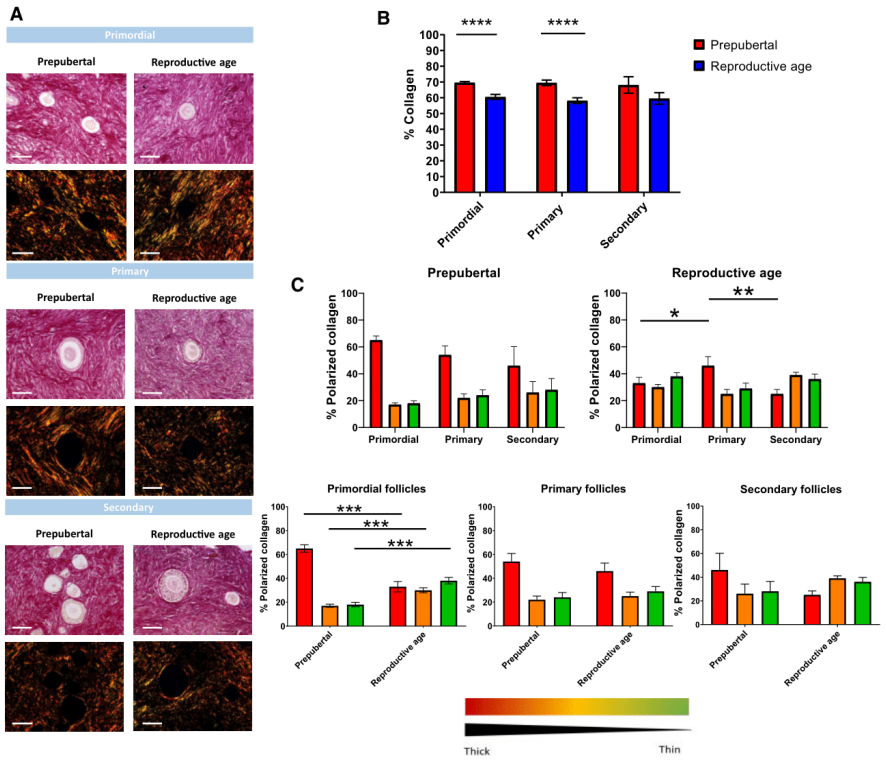


Figure 3 Comparison of collagen content and cross-linking between prepubertal and reproductive-age perifollicular ECM during early folliculogenesis. (**A** and **B**) Greater accumulation of collagen was detected in the microenvironment of both primordial and primary follicles derived from prepubertal ovarian tissue compared to reproductive-age tissue. (**C**) Investigation of the microenvironment of primordial follicles at different ages under polarized light revealed a significantly higher proportion of thick fibers and lower levels of intermediate and thin fibers at prepuberty. A significant decrease in thick collagen fibers was also observed around reproductive-age ovaries, from the primary to the secondary follicle stage. The Kruskal–Wallis test and multiple Student's *t*-test with the Holm–Sidak method for multiple comparison correction were, respectively, used to compare collagen amounts and fiber thickness between groups. The represented data included analysis of follicles from prepubertal ($n = 16$) and reproductive age tissues ($n = 21$). The comparison of perifollicular ECM at prepubertal versus reproductive age under bright field included primordial ($n = 841$ vs $n = 241$), primary ($n = 196$ vs $n = 161$) and secondary ($n = 30$ vs $n = 48$) follicles. The comparison of perifollicular ECM at prepubertal versus reproductive age under polarized light included primordial ($n = 128$ vs $n = 64$), primary ($n = 39$ vs $n = 39$) and secondary ($n = 11$ vs $n = 23$) follicles. Two-way ANOVA (*post hoc*: Tukey) was used to compare collagen thickness between follicle stages in each group (**$P<0.01$, ***$P<0.001$ and ****$P<0.0001$). Results are presented as mean ± SEM. Scale bars: 50 µm.

interstitial ECM. Indeed, lower amounts of EMILIN-1 were detected in the perifollicular ECM of prepubertal ovarian tissue, reaching statistical significance in primordial follicles ($P < 0.05$). In both prepubertal and reproductive-age patients, we observed a decline in EMILIN-1 levels following follicle activation (Fig. 9), but it was only significant in reproductive-age ovaries ($P < 0.01$).

Glycosaminoglycans

Thanks to their affinity for water, GAGs provide a mechanism of resistance to deformation. We therefore investigated their density in ovarian tissue in order to understand their involvement in the mechanical properties of the human ovary.

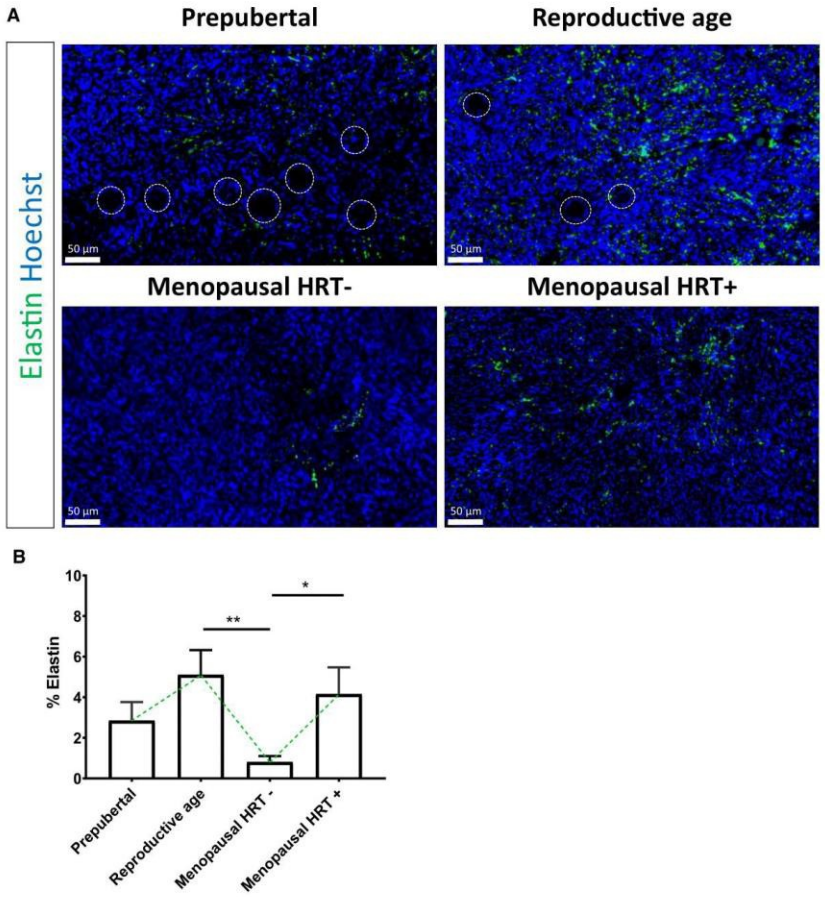


Figure 4 Spatiotemporal elastin synthesis and coacervation in the ovarian interstitial ECM. (**A**) Immunofluorescent staining of tissue sections for elastin (green) and counterstaining with Hoechst (blue) for nuclear observation. (**B**) Levels of elastin were as high as 5% in human ovarian tissue, but its density is known to vary according to age and reaches its peak at reproductive age, before drastically declining at menopause (HRT−) when estrogen levels are almost zero. On the other hand, elastin levels remained comparable to those at reproductive age in menopausal women taking hormone replacement therapy (HRT+), revealing possible *de novo* synthesis of elastin under estrogen. The represented data included analysis of ovarian tissue from 68 patients: prepubertal ($n = 16$); reproductive ($n = 21$); menopausal with estrogen-based HRT ($n = 7$); and menopausal without HRT ($n = 24$). The Kruskal–Wallis (*post hoc*: Dunn) test was used to compare elastin levels between age groups (*$P < 0.05$, **$P < 0.01$). Drawn circles highlight the presence of preantral follicles. Results are presented as mean ± SEM. Scale bars: 50 µm.

GAG levels increase with age

Comparison between different groups revealed a significant difference between prepubertal ovarian ECM and both reproductive-age ($P < 0.01$) and menopausal ovarian ECM with ($P < 0.001$) and without ($P < 0.05$) HRT (Fig. 10).

GAG content is different in the perifollicular ECM of prepubertal and reproductive-age ovarian tissue

While levels of GAGs fell significantly ($P < 0.001$) in the perifollicular microenvironment of prepubertal patients during early folliculogenesis, they remained stable at reproductive age from the primary to the

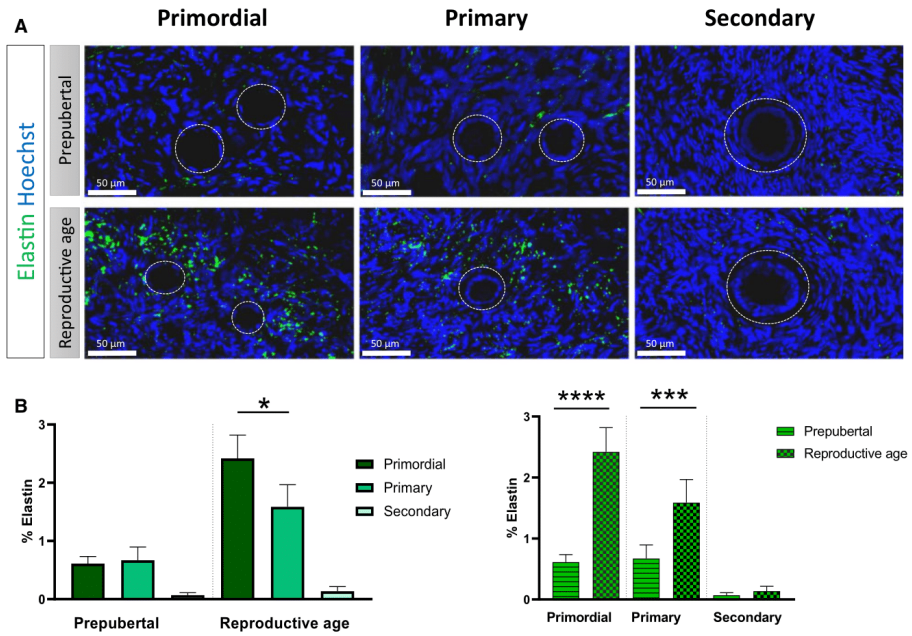


Figure 5 Comparison of elastin distribution and deposition between prepubertal and reproductive-age perifollicular ECM during early folliculogenesis. (**A**) Immunofluorescent staining of tissue sections for elastin (green) and counterstaining with Hoechst (blue) for nuclear observation. (**B**) Lower elastin content was observed around prepubertal primordial and primary follicles compared to their reproductive-age counterparts, indicating a less compliant environment. The represented data included analysis of follicles from prepubertal ($n = 16$) and reproductive age tissues ($n = 21$). The comparison of perifollicular ECM at prepubertal versus reproductive age included primordial ($n = 826$ vs $n = 260$), primary ($n = 310$ vs $n = 198$) and secondary ($n = 25$ vs $n = 13$) follicles. The Kruskal–Wallis (*post hoc*: Dunn) test was used to compare elastin levels between follicle stages in each group, and the Mann–Whitney test to compare prepubertal and reproductive-age follicles at the same developmental stage (*$P<0.05$, ***$P<0.001$, ****$P<0.0001$). Drawn circles highlight the presence of preantral follicles. Results are presented as mean ± SEM. Scale bars: 50 µm.

secondary stage. By comparing follicles of the same stage from prepubertal and adult patients, we found a significantly higher GAG content in the microenvironment of primary ($P < 0.0001$) and secondary ($P < 0.0001$) follicles in ovarian tissue from reproductive-age women. However, at the primordial stage, no difference was detected between young and adult ovarian tissue (Fig. 11).

Discussion

In recent years, we have witnessed a new dawn in mechanobiology dictating that mechanical forces generated within tissues can provide regulatory signals that are just as important as those conveyed by chemicals and genes (Mammoto *et al.*, 2013). This fact is reflected in the field of fertility preservation by numerous theories (Woodruff and Shea, 2011; Choi *et al.*, 2014; Thorne *et al.*, 2015), and lately by the work of Kawamura *et al.* (Kawamura *et al.*, 2013; Kawashima and Kawamura, 2018), which associates ovarian follicle activation to mechanical stress release. However, the real players orchestrating mechanical behavior in the ovary remain unknown. In this study, we investigated quantitative spatiotemporal changes in microstructural elastic components in interstitial and perifollicular ECM, looking to establish a potential connection between these molecules, follicle activation and early development.

What is behind the biomechanical properties of human ovarian tissue?

Our quantification of collagen and elastin deposition in the ovary throughout a woman's lifetime revealed progressive accumulation of these proteins in the ovarian ECM of prepubertal to reproductive-age subjects, as expected in late-stage tissue development (Oomen *et al.*, 2018). Our data demonstrate that collagen reaches its peak during

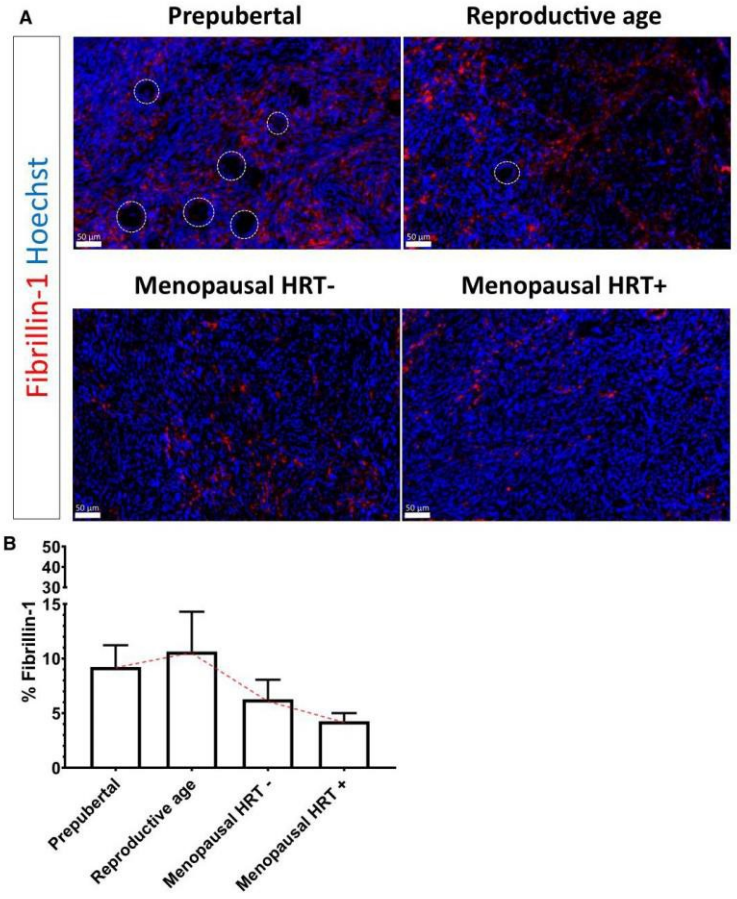


Figure 6 Spatiotemporal evolution of fibrillin-1 deposition in the ovarian interstitial ECM. (**A**) Immunofluorescent staining of tissue sections for fibrillin-1 (red) and counterstaining with Hoechst (blue) for nuclear observation. (**B**) Fibrillin-1 levels did not change from prepuberty to reproductive age, but dropped by half upon menopause. By contrast with elastin, fibrillin-1 deposition is not affected by HRT administration. The represented data included analysis of ovarian tissue from 68 patients: prepubertal ($n = 16$); reproductive ($n = 21$); menopausal with estrogen-based HRT ($n = 7$); and menopausal without HRT ($n = 24$). The Kruskal–Wallis (*post hoc*: Dunn) test was used to compare fibrillin-1 levels between age groups (*$P < 0.05$). Drawn circles highlight the presence of preantral follicles. Results are presented as mean ± SEM. Scale bars: 50 µm.

reproductive age in healthy ovaries. Interestingly, we observed a significant difference in collagen levels in the ovary before and after puberty, and also within menopausal ovarian tissue under HRT, pointing to the involvement of steroids in collagen deposition (Supplementary Video). We can speculate that estrogen is implicated in the activation of lysyl oxidase (LOX) and lysyl oxidase-like 1 (LOXL1), two enzymes governing collagen cross-linking and leading to dense deposition of collagen (Sanada *et al.*, 1978). Our results using polarized light microscopy also corroborate our hypothesis that estrogen is involved in collagen cross-linking in ovarian tissue, as demonstrated by the decrease in thin fibers

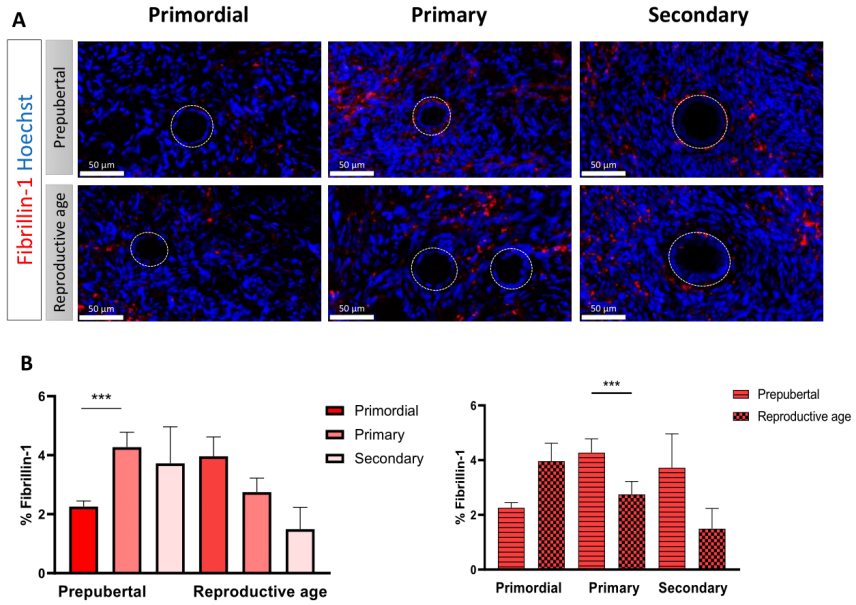


Figure 7 Comparison of fibrillin-1 distribution and deposition between prepubertal and reproductive-age perifollicular ECM during early folliculogenesis. (**A**) Immunofluorescent staining of tissue sections for fibrillin-1 (red) and counterstaining with Hoechst (blue) for nuclear observation. (**B**) While fibrillin-1 levels did not significantly change during reproductive age in the perifollicular ECM overall, during early folliculogenesis its levels increased in prepubertal ovarian tissue, mainly following follicle activation. The represented data included analysis of follicles from prepubertal ($n = 16$) and reproductive age tissues ($n = 21$). The comparison of perifollicular ECM at prepubertal versus reproductive age included primordial ($n = 826$ vs $n = 260$), primary ($n = 310$ vs $n = 198$) and secondary ($n = 25$ vs $n = 13$) follicles. The Kruskal–Wallis (*post hoc*: Dunn) test was used to compare fibrillin-1 levels between follicle stages in each group, and the Mann–Whitney test to compare prepubertal and reproductive-age follicles at the same developmental stage (***$P < 0.001$). Drawn circles highlight the presence of preantral follicles. Results are presented as mean ± SEM. Scale bars: 50 µm.

and increase in thick fibers, mainly in reproductive-age ovaries, that are modulated by physiological estrogen levels. Estrogen also has a role in the mechanical properties of ovarian tissue through its impact on elastin production, as evidenced by the significant decline in elastin in menopausal ovaries without HRT. It is widely acknowledged that elastin synthesis in human starts from late fetal stages to the early postnatal period, gradually decreasing and ceasing in adults (Swee *et al.*, 1995). However, our study indicates that when estrogen is present, elastin continues to be synthesized. Immunofluorescence analyses demonstrate that elastin not only remains at similar levels in adult ovaries compared to their prepubertal counterparts, but also can be synthesized *de novo* under the influence of HRT in menopausal ovaries. Although ovarian tissue is known to be very elastic, especially at reproductive age, our results on elastin provide more insights into this common belief. Indeed, elastin levels in the ovarian cortex do not exceed 5%, while elastin constitutes about 28–32% of major blood vessels, 30–57% of the aorta, 50% of elastic ligaments, 3–7% of lung tissue and 2–3% of the dry weight of skin, where elasticity and flexibility are of major importance (Lescan *et al.*, 2018).

In addition to collagen and elastin, microfibrils play a key role in mechanoregulation and contribute significantly to the long-term stability of elastic fibers, serving as a scaffold for elastin deposition (Marque *et al.*, 2001). Among the three known fibrillin isoforms, fibrillin-1 is the most abundant microfibril isoform in mature tissues, specifically in the human ovary (Bastian *et al.*, 2016; Ouni *et al.*, 2019). Our spatiotemporal follow-up of fibrillin-1 showed a tendency toward a progressive downturn in availability from prepuberty to menopause (with and without HRT), which may be one of the reasons for elastin decline with age. Hence, in contrast to its impact on collagen and elastin, HRT does not have any effect on fibrillin-1 synthesis or coacervation, which might harm the integrity of elastin synthesized by menopausal women taking HRT.

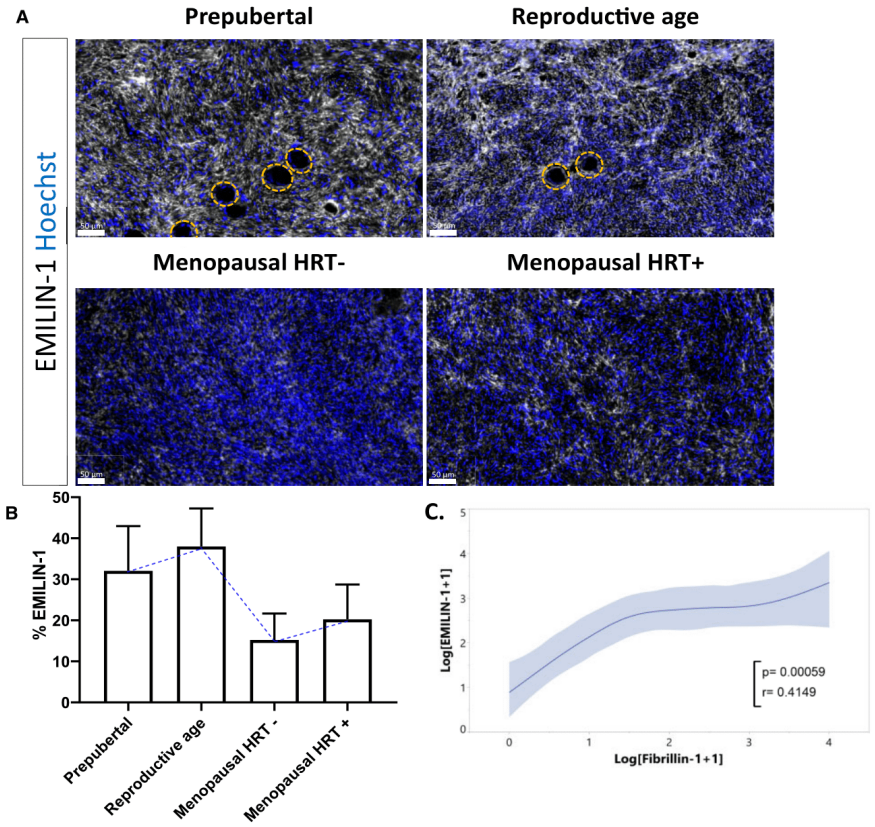


Figure 8 Spatiotemporal evolution of EMILIN-1 deposition in the ovarian interstitial ECM. (**A**) Immunofluorescent staining of tissue sections for EMILIN-1 (white) and counterstaining with Hoechst (blue) for nuclear observation. (**B**) At prepuberty, around 30% of the ovarian ECM surface area was found to be composed of EMILIN-1. This level increases slightly after puberty, only to decrease again at menopause. EMILIN-1 deposition is therefore not affected by HRT administration. (**C**) Positive correlation between EMILIN-1 and fibrillin-1. The represented data included analysis of ovarian tissue from 68 patients: prepubertal ($n = 16$); reproductive ($n = 21$); menopausal with estrogen-based HRT ($n = 7$); and menopausal without HRT ($n = 24$). The data plot fits a smoothing spline with a lambda value of 2.3. The curves also include the bootstrap confidence region for each fit generated by JMP® Pro 14.3.0. The Kruskal–Wallis (*post hoc*: Dunn) test was used to compare EMILIN-1 levels between age groups ($^*P < 0.05$). Drawn circles highlight the presence of preantral follicles. Results are presented as mean ± SEM. Scale bars: 50 µm.

At the interface between elastin and fibrillin-1 (Colombatti *et al.*, 2000), EMILIN-1 plays a niche role in elastin fiber biogenesis by aiding with fusion of elastin fibers, making them more organized (Randell and Daneshtalab, 2017). EMILIN-1 was also detected in the human ovarian matrisome of adult patients by a proteomic approach (Ouni *et al.*, 2019), and recently in porcine ovarian tissue (Henning *et al.*, 2019). EMILIN-1 deposition is highly dependent on fibrillin-1 expression, as evidenced in fibrillin-1 knock-out mice, which were unable to synthesize EMILIN-1 (Schiavinato *et al.*, 2016). In view of these findings in mice and based on the weak but significant correlation established

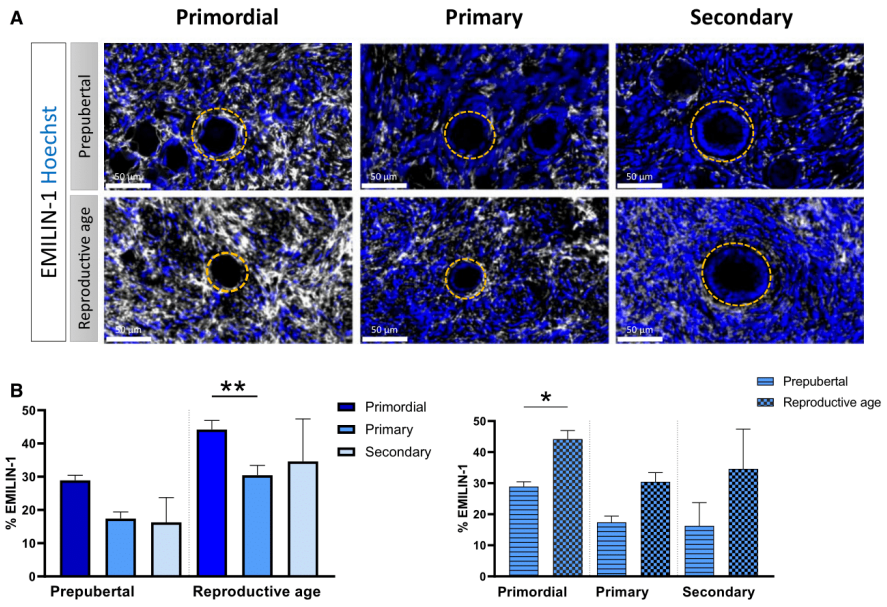


Figure 9 Comparison of EMILIN-1 distribution and deposition between prepubertal and reproductive-age perifollicular ECM during early folliculogenesis. (**A**) Immunofluorescent staining of tissue sections for fibrillin-1 (white) and counterstaining with Hoechst (blue) for nuclear observation. (**B**) In both prepubertal and reproductive-age patients, we observed a decrease in EMILIN-1 as folliculogenesis advanced. However, prepubertal perifollicular ECM showed the lowest EMILIN-1, especially at the primordial stage. The represented data included analysis of follicles from prepubertal ($n = 16$) and reproductive age tissues ($n = 21$). The comparison of perifollicular ECM at prepubertal versus reproductive age included primordial ($n = 826$ vs $n = 260$), primary ($n = 310$ vs $n = 198$) and secondary ($n = 25$ vs $n = 13$) follicles. The Kruskal–Wallis (*post hoc*: Dunn) test was used to compare EMILIN-1 levels between follicle stages in each group, and the Mann–Whitney test to compare prepubertal and reproductive-age follicles at the same developmental stage (*$P < 0.05$, **$P < 0.01$). Drawn circles highlight the presence of preantral follicles. Results are presented as mean ± SEM. Scale bars: 50 µm.

between EMILIN-1 and fibrillin-1, we can confirm the interdependence between EMILIN-1 and fibrillin-1 in the human ovary (Fig. 8C). Clearly, EMILIN-1 does not only depend on fibrillin-1 levels ($r = 0.4149$; $P = 0.00059$), but also other possible variables, such as age, menstrual phase and cellular signaling context (Kielty *et al.*, 2005; Wagenseil and Mecham, 2007; Colombatti *et al.*, 2011). Our results point to a lack of two fundamental elastogenesis-associated proteins (Shen *et al.*, 2016) at menopause, namely EMILIN-1 and fibrillin-1, which may produce elastic fiber abnormalities even after HRT, as explained by Zanetti *et al.* (2004).

Interestingly, both EMILIN-1 and fibrillin-1 serve as negative regulators of transforming growth factor beta (TGF-β) (Zacchigna *et al.*, 2006; Olivieri *et al.*, 2010). Consequently, and in line with the available literature, we can hypothesize that the growing lack of EMILIN-1 and fibrillin-1 in interstitial ovarian ECM with age may lead to an upturn in TGF-β (Isogai *et al.*, 2003; Neptune *et al.*, 2003; Zacchigna *et al.*, 2006), responsible for greater tissue rigidity and age-related fibrosis (Hayward and Brock, 1997; Briley *et al.*, 2016; McCloskey *et al.*, 2019).

All the elastic network components mentioned above are embedded in a hydrogel of GAG chain-containing proteoglycans (Frantz *et al.*, 2010). The innate polyanionic nature of GAGs is pivotal to maintaining water retention, hydrostatic pressure, nutrient transport, cell migration, cell differentiation, matrix structure and mechanical integrity (Kurylo *et al.*, 2016). From a mechanical point of view, GAGs enable healthy tissue to resist compressive stress thanks to their binding to fibrous ECM molecules (Scott, 2003). Thereby, GAGs act by inflating the collagen network and causing tensile stress that allows the ECM to resist shear deformation (Jin and Grodzinsky, 2001). Although a quantitative change in GAGs with age was expected, our data demonstrate maintenance of significantly higher GAG levels in adult ovaries than in prepubertal ones. In accordance with *in vitro* findings linking GAGs to disruption of fibrillin-1 aggregation (Kielty *et al.*, 1996; Tiedemann *et al.*, 2001), our *in vivo* study of GAG levels in human

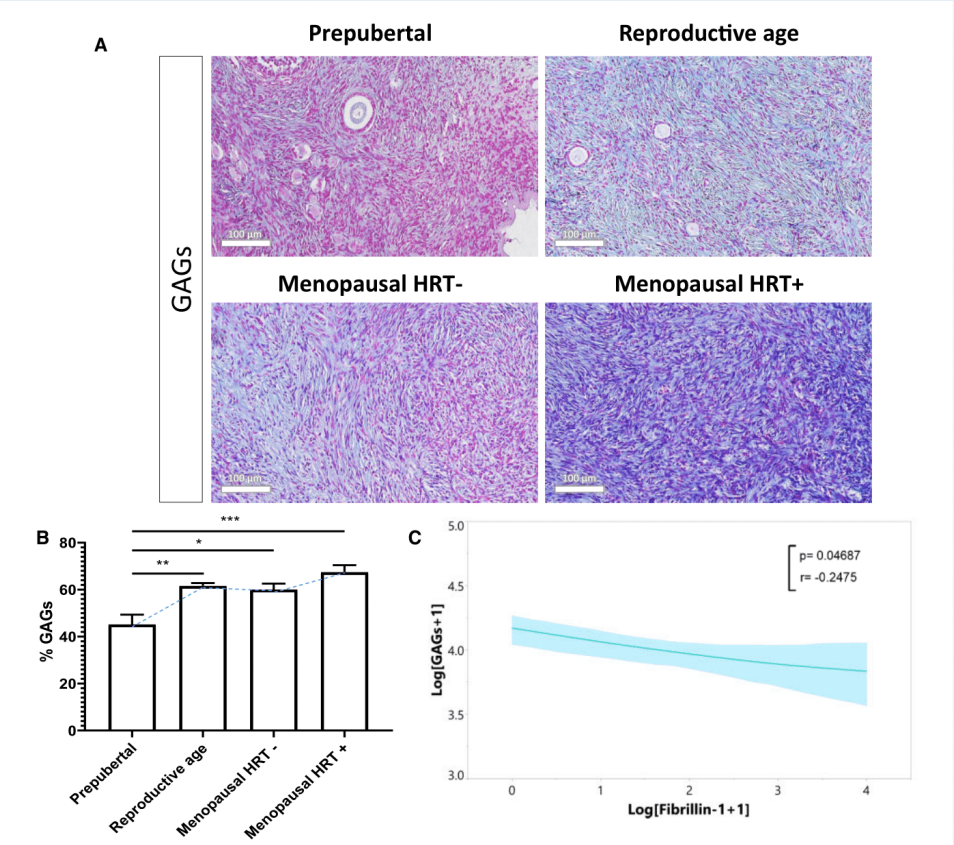


Figure 10 Age-dependent GAG accumulation in the ovarian interstitial ECM. (**A**) Alcian blue staining of sulfated and carboxylated GAGs (blue) in ovarian tissue, showing nuclear counterstaining with Mayer's carmalum (red). (**B**) Progressive accumulation of GAGs with age was observed within the interstitial ECM. (**C**) Negative correlation between GAGs and fibrillin-1. The data plot fits a smoothing spline with a lambda value of 2.3. The curves also include the bootstrap confidence region for each fit generated by JMP® Pro 14.3.0. The represented data included analysis of ovarian tissue from 68 patients: prepubertal ($n = 16$); reproductive ($n = 21$); menopausal with estrogen-based HRT ($n = 7$); and menopausal without HRT ($n = 24$). The Kruskal–Wallis (*post hoc*: Dunn) test was used to compare GAG levels between age groups (*$P < 0.05$, **$P < 0.01$ and ***$P < 0.001$). Results are presented as mean ± SEM. Scale bars: 100 µm.

ovaries revealed that the decrease in fibrillin-1 with age is weakly but significantly correlated to an increase in GAGs ($r = 0.2475$; $P = 0.04687$, Fig. 10C). This weak correlation indicates that fibrillin-1 and GAG deposition are dependent on other factors in the human ovary that require further investigation. More qualitative GAG studies are therefore needed to decipher the age-dependent effect on available GAG types in the ovary, which might further explain the GAG-fibrillin-1 interaction (Cain *et al.*, 2005).

Perifollicular ECM as a starting point for follicle development and biomechanical regulation

Our results showed perifollicular ECM changes with age to be very distinct from the rest of the interstitial ECM, which reinforces the dynamic reciprocity theory between ovarian follicles and their microenvironment (Woodruff and Shea, 2011; Thorne *et al.*, 2015).

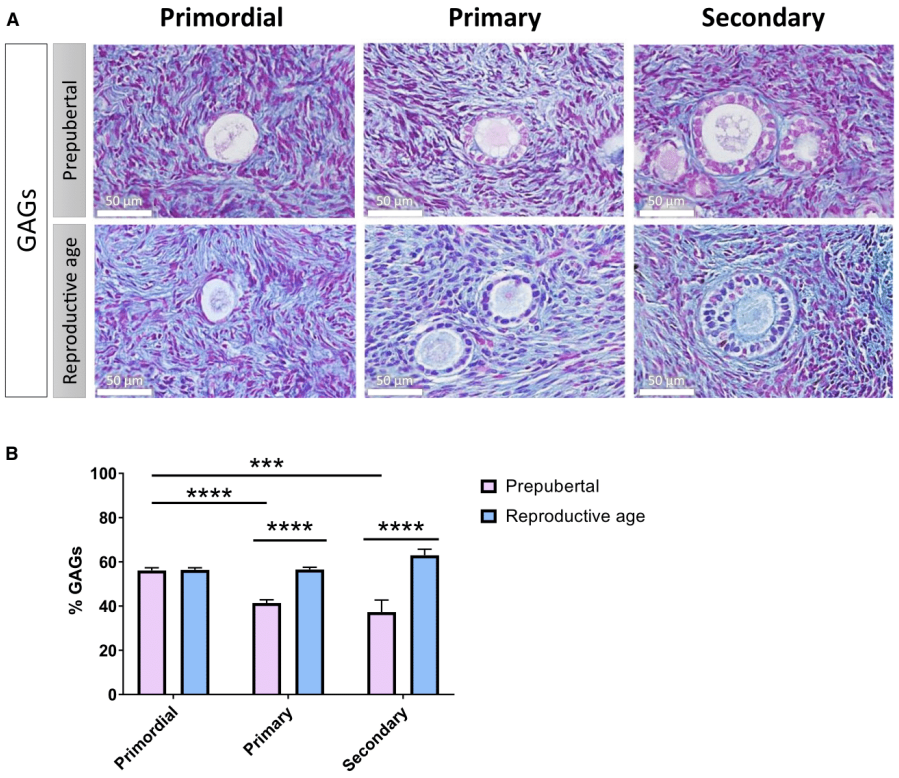


Figure 11 Comparison of GAG accumulation in the perifollicular ECM according to age and follicle stage. (**A**) Close-up of GAG content (blue) in the perifollicular ECM using Alcian blue staining. (**B**) While levels of GAGs fell significantly in the perifollicular microenvironment of prepubertal patients during early folliculogenesis, they remained stable at reproductive age from the primary to the secondary stage. Following follicle activation, the prepubertal perifollicular ECM was poorest in GAGs. (**C**) Negative correlation between GAGs and fibrillin-1 levels. The represented data included analysis of follicles from prepubertal ($n = 16$) and reproductive age tissues ($n = 21$). The comparison of perifollicular ECM at prepubertal versus reproductive age included primordial ($n = 217$ vs $n = 238$), primary ($n = 182$ vs $n = 160$) and secondary ($n = 18$ vs $n = 30$) follicles. Two-way ANOVA (*post hoc*: Tukey) was used to compare GAG content at all follicle stages in and between groups (***$P < 0.001$ and ****$P < 0.0001$). Results are presented as mean ± SEM. Scale bars: 50 µm.

Intriguingly, while higher collagen proportions were found in ovarian tissue from reproductive-age women than prepubertal girls, more collagen was actually accumulated in the ECM surrounding preantral follicles in the latter group. A closer look at fiber thickness by polarized light microscopy revealed that primordial follicles in prepubertal ovaries are surrounded by a higher proportion of thick collagen fibers. Thicker collagen fibers are less elastic and offer great resistance to tension forces, which could account for the preservation of primordial follicles in a resting state (Jorge *et al.*, 2014). After puberty, on the other hand, concomitant with the decrease in thicker fibers following follicle activation, there is a significant increase in thinner collagen fibers, probably due to enzymatic degradation. These findings highlight a profound difference in collagen deposition between young and adult perifollicular ECM, which is most pronounced in primordial follicles, and demonstrate that perifollicular ECM remodeling is vital for follicle growth (Hornick *et al.*, 2012). Elastin findings also support this theory, with perifollicular ECM showing less elastin deposition in prepubertal ovarian tissue at all follicle stages. Interestingly, in both groups, there is a

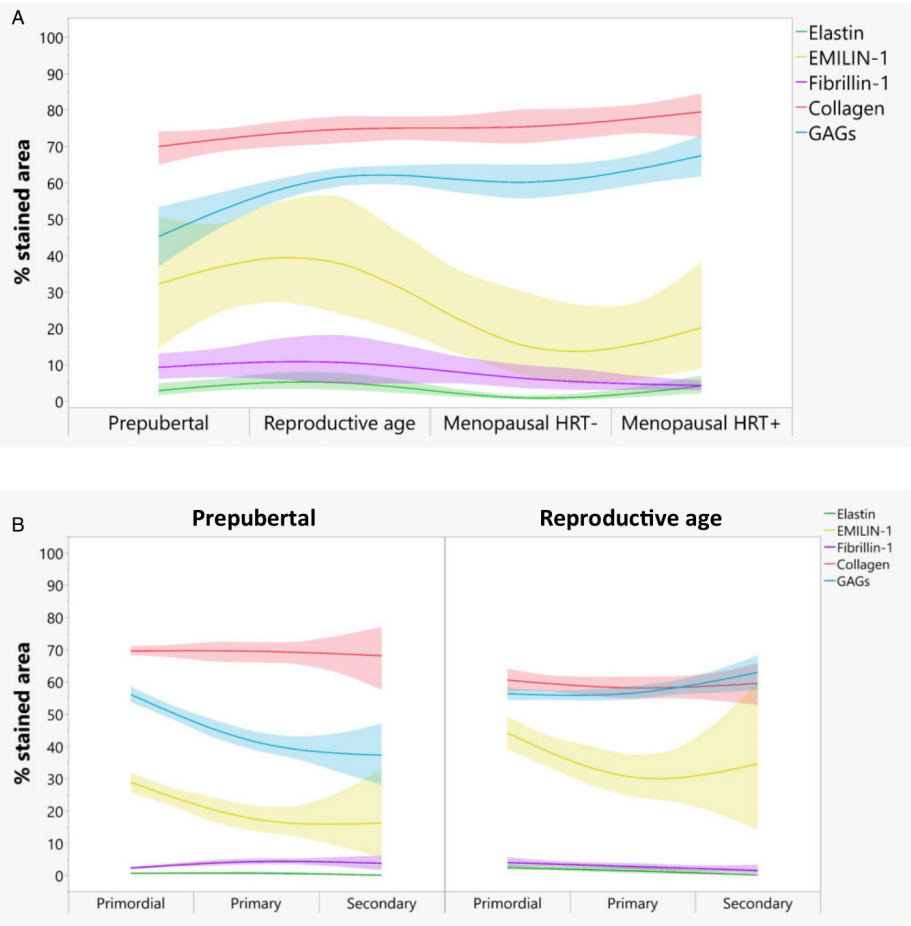


Figure 12 Summary of the spatiotemporal deposition of elastic matrisome components in the human ovary. (**A**) Summary of all studied elastic matrisome proteins in interstitial and (**B**) perifollicular ECM. The represented data included analysis of ovarian tissue from 68 patients: prepubertal ($n = 16$); reproductive ($n = 21$); menopausal with estrogen-based HRT ($n = 7$); and menopausal without HRT ($n = 24$). The curves represent average levels of the matrisome components in all groups and follicle stages at both prepuberty and reproductive age, fitting a smoothing spline with a lambda value of 0.05. The curves also include the bootstrap confidence region for each fit generated by JMP® Pro 14.3.0.

dramatic decline in this protein during follicle development from the primordial to the secondary stage, which is likely due to ECM digestion to support follicle growth. Whether based on collagen or elastin perifollicular ECM levels, our findings predict a stiffer microenvironment around prepubertal follicles, mainly at primordial and primary stages. These differences tend to diminish once follicles reach the secondary stage.

Besides their mechanical roles in ovarian tissue, fibrillin-1 and EMILIN-1 modulate important signaling pathways for ovarian homeostasis and follicle development (John *et al.*, 2008; Guo and Wang, 2009; Ernst *et al.*, 2017). EMILIN-1 is a negative regulator of cell proliferation (Colombatti *et al.*, 2011). Thus, the declining tendency of perifollicular EMILIN-1 levels with the progress of folliculogenesis in both prepubertal and reproductive age groups is consistent with granulosa

cell proliferation in preantral follicles (Bax *et al.*, 2003; Conti and Chang, 2016). On the other hand, a lack of fibrillin-1 leads to tissue stiffening as a result of TGF-β signaling overactivation (MacFarlane *et al.*, 2017). Our findings and the available literature on folliculogenesis (McGee and Raj, 2015) suggest similar effects of fibrillin-1 in the ovary, pointing to a stiffer ECM around primordial follicles at prepuberty (Marque *et al.*, 2001; Alper, 2002; Kielty *et al.*, 2002; MacFarlane *et al.*, 2017; Abbas *et al.*, 2019). However, in prepubertal perifollicular ECM, there was a surge in fibrillin-1 after follicle activation, which was not observed in adult tissue. This might suggest ECM remodeling by way of increasing its elasticity and releasing growing follicles from their mechanical retention (Woodruff and Shea, 2011; Nagamatsu *et al.*, 2019). Knowing that GAGs also contribute to tissue elasticity, comparison of GAGs in perifollicular ECM revealed lower levels of GAGs surrounding prepubertal follicles, which complements our theory of greater mechanical retention of prepubertal follicles. Although we did not observe significant changes in GAG levels in reproductive-age tissue during the same period, we cannot exclude the possibility of qualitative GAG differences (Hatzirodos *et al.*, 2012; Takahashi *et al.*, 2014) between ages and follicular stages, calling for further GAGOme studies (Chen *et al.*, 2018).

Taken together, these results clearly illustrate ECM deposition and remodeling in an age- and follicle stage-related manner (Fig. 12, Supplementary Video and Fig. S5). More precisely, our findings point to a more elastic ECM surrounding reproductive-age follicles compared to the less compliant perifollicular ECM of prepubertal tissue. However, menstrual cycle phase and age-related changes to the stroma, follicle density and vascularization can also impact ECM composition. Advanced combinational analysis will therefore be needed in the future to calculate the contribution of each matrisome component to ovarian plasticity.

In conclusion, from a biochemical perspective, our study revealed interesting changes to ECM composition, dictating the elastic features of ovarian tissue, in line with the existing literature. Our findings pave the way for possible therapeutic targets at the ECM level in the context of female fertility and ovarian rejuvenation. Our data will prove very useful in designing biomimetic scaffolds and tissue-engineered models, such as the artificial ovary (Amorim and Shikanov, 2016; Dolmans and Amorim, 2019). Indeed, they emphasize the importance of encapsulating each type of isolated follicle in an appropriate biomaterial that must replicate the corresponding functional perifollicular ECM and respect ovarian tissue heterogeneity (Choi *et al.*, 2014) to guarantee its biomimicry. Although our data disclose the complexity of this task, they also offer new opportunities to explore ovarian ECM synthesis *de novo*, which may reverse ovarian aging, and help us to develop reliable *in vitro* models to complement our knowledge of human ovary regulation.

Supplementary data

Supplementary data are available at *Human Reproduction* online.

Acknowledgments

We thank Olivier Van Kerk and Sarah Storder for their technical assistance, as well as Thuy Tran and Soulaima Cherkaoui for their contribution to experimental procedures. We also thank Lieven Desmet (Louvain Institute of Data Analysis and Modeling in Economics and Statistics, Université Catholique de Louvain) for his advice on biostatistical evaluation, and Mira Hryniuk, BA, for reviewing the English language of the manuscript. Holotomography acquisitions were achieved thanks to the invaluable contribution of Sanela Vellino and Thibault Courthéoux from Nanolive. Finally, we are very grateful to Omar Rhouma for graphic illustration.

Authors' roles

E.O.: conception and design, experimental procedures, analysis of results and article preparation; C.B.: design of digital image analysis; M.M.D.: clinical inspection of patient records and critical manuscript revision; E.M.: inspection of histological descriptions and classifications; S.P.D.R.: text-mining; D.V.: critical manuscript revision from a proteomic point of view; and C.A.A.: conception and design, discussion contribution and critical manuscript revision.

Funding

This study was supported by grants from the Fonds National de la Recherche Scientifique de Belgique (FNRS) (C.A.A. is an FRS-FNRS research associate; grant 5/4/150/5 awarded to M.M.D.) and the Université Catholique de Louvain (PhD grant 'Coopération au développement' awarded to E.O.).

Conflict of interest

The authors report no conflict of interest and have nothing to disclose.

References

Abbas Y, Carnicer-Lombarte A, Gardner L, Thomas J, Brosens JJ, Moffett A, Sharkey AM, Franze K, Burton GJ, Oyen ML. Tissue stiffness at the human maternal-fetal interface. *Hum Reprod* 2019; **34**:1999–2008.

Aboubakar Nana F, Hoton D, Ambroise J, Lecocq M, Vanderputten M, Sibille Y, Vanaudenaerde B, Pilette C, Bouzin C, Ocak S. Increased expression and activation of FAK in small-cell lung cancer compared to non-small-cell lung cancer. *Cancers* 2019;**11**: 1526.

Adhikari D, Liu K. Molecular mechanisms underlying the activation of mammalian primordial follicles. *Endocr Rev* 2009;**30**:438–464.

Afratis N, Gialeli C, Nikitovic D, Tsegenidis T, Karousou E, Theocharis AD, Pavao MS, Tzanakakis GN, Karamanos NK. Glycosaminoglycans: key players in cancer cell biology and treatment. *FEBS J* 2012;**279**:1177–1197.

Alper J. Protein structure. Stretching the limits. *Science* 2002;**297**: 329–331.

Amorim CA, Shikanov A. The artificial ovary: current status and future perspectives. *Future Oncol* 2016;**12**:2323–2332.

Bastian NA, Bayne RA, Hummitzsch K, Hatzirodos N, Bonner WM, Hartanti MD, Irving-Rodgers HF, Anderson RA, Rodgers RJ. Regulation of fibrillins and modulators of TGFbeta in fetal bovine and human ovaries. *Reproduction* 2016;**152**:127–137.

Bax DV, Bernard SE, Lomas A, Morgan A, Humphries J, Shuttleworth CA, Humphries MJ, Kielty CM. Cell adhesion to fibrillin-1 molecules and microfibrils is mediated by alpha 5 beta 1 and alpha v beta 3 integrins. *J Biol Chem* 2003;**278**:34605–34616.

Briley SM, Jasti S, McCracken JM, Hornick JE, Fegley B, Pritchard MT, Duncan FE. Reproductive age-associated fibrosis in the stroma of the mammalian ovary. *Reproduction* 2016;**152**:245–260.

Cain SA, Baldock C, Gallagher J, Morgan A, Bax DV, Weiss AS, Shuttleworth CA, Kielty CM. Fibrillin-1 interactions with heparin. Implications for microfibril and elastic fiber assembly. *J Biol Chem* 2005;**280**:30526–30537.

Chen YH, Narimatsu Y, Clausen TM, Gomes C, Karlsson R, Steentoft C, Spliid CB, Gustavsson T, Salanti A, Persson A *et al*. The GAGOme: a cell-based library of displayed glycosaminoglycans. *Nat Methods* 2018;**15**:881–888.

Choi JK, Agarwal P, Huang H, Zhao S, He X. The crucial role of mechanical heterogeneity in regulating follicle development and ovulation with engineered ovarian microtissue. *Biomaterials* 2014;**35**: 5122–5128.

Colombatti A, Doliana R, Bot S, Canton A, Mongiat M, Mungiguerra G, Paron-Cilli S, Spessotto P. The EMILIN protein family. *Matrix Biol* 2000;**19**:289–301.

Colombatti A, Spessotto P, Doliana R, Mongiat M, Bressan GM, Esposito G. The EMILIN/multimerin family. *Front Immunol* 2011;**2**: 93.

Conti M, Chang RJ. Folliculogenesis, ovulation, and luteogenesis. In J Larry Jameson, DM de Kretser, LC Giudice, AB Grossman, S Melmed, JT Potts, GC Weir (ed). *Endocrinology: Adult and Pediatric*. 7th edn. Philadelphia, USA: Elsevier, 2016, 2179–2191.e2173.

Dayan D, Hiss Y, Hirshberg A, Bubis JJ, Wolman M. Are the polarization colors of picrosirius red-stained collagen determined only by the diameter of the fibers? *Histochemistry* 1989;**93**:27–29.

Dolmans MM, Amorim CA. Construction and use of artificial ovaries. *Reproduction* 2019;**158**:F15-F25.

Ernst EH, Grondahl ML, Grund S, Hardy K, Heuck A, Sunde L, Franks S, Andersen CY, Villesen P, Lykke-Hartmann K. Dormancy and activation of human oocytes from primordial and primary follicles: molecular clues to oocyte regulation. *Hum Reprod* 2017;**32**: 1684–1700.

Filatov M, Khramova Y, Parshina E, Bagaeva T, Semenova M. Influence of gonadotropins on ovarian follicle growth and development in vivo and in vitro. *Zygote* 2017;**25**:235–243.

Ford E, Beckett EL, Roman S, McLaughlin EA, Sutherland J. Advances in human primordial follicle activation and premature ovarian insufficiency. *Reproduction* 2020;**159**:R15-R29.

Frantz C, Stewart KM, Weaver VM. The extracellular matrix at a glance. *J Cell Sci* 2010;**123**:4195–4200.

Grive KJ, Freiman RN. The developmental origins of the mammalian ovarian reserve. *Development* 2015;**142**:2554–2563.

Guo X, Wang XF. Signaling cross-talk between TGF-beta/BMP and other pathways. *Cell Res* 2009;**19**:71–88.

Hatzirodos N, Nigro J, Irving-Rodgers HF, Vashi AV, Hummitzsch K, Caterson B, Sullivan TR, Rodgers RJ. Glycomic analyses of ovarian follicles during development and atresia. *Matrix Biol* 2012;**31**: 45–56.

Hayat MA. *Stains and Cytochemical Methods*. 1st edn. New York, USA: Plenum Press, 1993.

Hayward C, Brock DJ. Fibrillin-1 mutations in Marfan syndrome and other type-1 fibrillinopathies. *Hum Mutat* 1997;**10**:415–423.

Henning NF, LeDuc RD, Even KA, Laronda MM. Proteomic analyses of decellularized porcine ovaries identified new matrisome proteins and spatial differences across and within ovarian compartments. *Sci Rep* 2019;**9**:20001.

Hornick JE, Duncan FE, Shea LD, Woodruff TK. Isolated primate primordial follicles require a rigid physical environment to survive and grow in vitro. *Hum Reprod* 2012;**27**:1801–1810.

Hsueh AJ, Kawamura K, Cheng Y, Fauser BC. Intraovarian control of early folliculogenesis. *Endocr Rev* 2015;**36**:1–24.

Isogai Z, Ono RN, Ushiro S, Keene DR, Chen Y, Mazzieri R, Charbonneau NL, Reinhardt DP, Rifkin DB, Sakai LY. Latent transforming growth factor beta-binding protein 1 interacts with fibrillin and is a microfibril-associated protein. *J Biol Chem* 2003;**278**: 2750–2757.

Jin M, Grodzinsky AJ. Effect of electrostatic interactions between glycosaminoglycans on the shear stiffness of cartilage: a molecular model and experiments. *Macromolecules* 2001;**34**:8330–8339.

John GB, Gallardo TD, Shirley LJ, Castrillon DH. Foxo3 is a PI3K-dependent molecular switch controlling the initiation of oocyte growth. *Dev Biol* 2008;**321**:197–204.

Jorge S, Chang S, Barzilai JJ, Leppert P, Segars JH. Mechanical signaling in reproductive tissues: mechanisms and importance. *Reprod Sci* 2014;**21**:1093–1107.

Kawamura K, Cheng Y, Suzuki N, Deguchi M, Sato Y, Takae S, Ho CH, Kawamura N, Tamura M, Hashimoto S *et al*. Hippo signaling disruption and Akt stimulation of ovarian follicles for infertility treatment. *Proc Natl Acad Sci USA* 2013;**110**:17474–17479.

Kawamura K, Kawamura N, Hsueh AJ. Activation of dormant follicles: a new treatment for premature ovarian failure? *Curr Opin Obstet Gynecol* 2016;**28**:217–222.

Kawashima I, Kawamura K. Regulation of follicle growth through hormonal factors and mechanical cues mediated by Hippo signaling pathway. *Syst Biol Reprod Med* 2018;**64**:3–11.

Kielty CM, Sherratt MJ, Marson A, Baldock C. Fibrillin microfibrils. *Adv Protein Chem* 2005;**70**:405–436.

Kielty CM, Sherratt MJ, Shuttleworth CA. Elastic fibres. *J Cell Sci* 2002;**115**:2817–2828.

Kielty CM, Whittaker SP, Shuttleworth CA. Fibrillin: evidence that chondroitin sulphate proteoglycans are components of microfibrils and associate with newly synthesised monomers. *FEBS Lett* 1996; **386**:169–173.

Kiernan JA. Dyes and other colorants in microtechnique and biomedical research. *Color Technol* 2006;**122**:1–21.

Kurylo MP, Grandfield K, Marshall GW, Altoe V, Aloni S, Ho SP. Effect of proteoglycans at interfaces as related to location, architecture, and mechanical cues. *Arch Oral Biol* 2016;**63**:82–92.

Lescan M, Perl RM, Golombek S, Pilz M, Hann L, Yasmin M, Behring A, Keller T, Nolte A, Gruhn F *et al*. De novo synthesis of elastin by exogenous delivery of synthetic modified mRNA into skin and elastin-deficient cells. *Mol Ther Nucleic Acids* 2018;**11**:475–484.

Levillain A, Orhant M, Turquier F, Hoc T. Contribution of collagen and elastin fibers to the mechanical behavior of an abdominal connective tissue. *J Mech Behav Biomed Mater* 2016;**61**:308–317.

Lunde O, Djoseland O, Grottum P. Polycystic ovarian syndrome: a follow-up study on fertility and menstrual pattern in 149 patients

15-25 years after ovarian wedge resection. *Hum Reprod* 2001;**16**: 1479–1485.

MacFarlane EG, Haupt J, Dietz HC, Shore EM. TGF-beta family signaling in connective tissue and skeletal diseases. *Cold Spring Harb Perspect Biol* 2017;**9**:a022269.

MacKenna DA, Omens JH, McCulloch AD, Covell JW. Contribution of collagen matrix to passive left ventricular mechanics in isolated rat hearts. *Am J Physiol* 1994;**266**:H1007–H1018.

Malandrino A, Mak M, Kamm RD, Moeendarbary E. Complex mechanics of the heterogeneous extracellular matrix in cancer. *Extreme Mech Lett* 2018;**21**:25–34.

Mammoto T, Mammoto A, Ingber DE. Mechanobiology and developmental control. *Annu Rev Cell Dev Biol* 2013;**29**:27–61.

Marque V, Kieffer P, Gayraud B, Lartaud-Idjouadiene I, Ramirez F, Atkinson J. Aortic wall mechanics and composition in a transgenic mouse model of Marfan syndrome. *Arterioscler Thromb Vasc Biol* 2001;**21**:1184–1189.

McCloskey CW, Cook DP, Kelly BS, Azzi F, Allen CH, Forsyth A, Upham J, Rayner KJ, Gray DA, Boyd RW *et al*. Metformin abrogates age-associated ovarian fibrosis. *Clin Cancer Res* 2020;**26**: 632–642.

McGee EA, Raj RS. Regulators of ovarian preantral follicle development. *Semin Reprod Med* 2015;**33**:179–184.

Nagamatsu G, Shimamoto S, Hamazaki N, Nishimura Y, Hayashi K. Mechanical stress accompanied with nuclear rotation is involved in the dormant state of mouse oocytes. *Sci Adv* 2019;**5**:eaav9960.

Neptune ER, Frischmeyer PA, Arking DE, Myers L, Bunton TE, Gayraud B, Ramirez F, Sakai LY, Dietz HC. Dysregulation of TGF-beta activation contributes to pathogenesis in Marfan syndrome. *Nat Genet* 2003;**33**:407–411.

Olivieri J, Smaldone S, Ramirez F. Fibrillin assemblies: extracellular determinants of tissue formation and fibrosis. *Fibrogenesis Tissue Repair* 2010;**3**:24.

Oomen PJA, Holland MA, Bouten CVC, Kuhl E, Loerakker S. Growth and remodeling play opposing roles during postnatal human heart valve development. *Sci Rep* 2018;**8**:1235.

Ouni E, Vertommen D, Chiti MC, Dolmans MM, Amorim CA. A draft map of the human ovarian proteome for tissue engineering and clinical applications. *Mol Cell Proteomics* 2019;**18**:S159–S173.

Randell A, Daneshtalab N. Elastin microfibril interface-located protein 1, transforming growth factor beta, and implications on cardiovascular complications. *J Am Soc Hypertens* 2017;**11**:437–448.

Rich L, Whittaker P. Collagen and picrosirius red staining: a polarized light assessment of fibrillar hue and spatial distribution. *Braz J morphol Sci* 2005;**2**:97–104.

Sanada H, Shikata J, Hamamoto H, Ueba Y, Yamamuro T, Takeda T. Changes in collagen cross-linking and lysyl oxidase by estrogen. *Biochim Biophys Acta* 1978;**541**:408–413.

Schiavinato A, Keene DR, Wohl AP, Corallo D, Colombatti A, Wagener R, Paulsson M, Bonaldo P, Sengle G. Targeting of EMILIN-1 and EMILIN-2 to fibrillin microfibrils facilitates their incorporation into the extracellular matrix. *J Invest Dermatol* 2016; **136**:1150–1160.

Schindelin J, Arganda-Carreras I, Frise E, Kaynig V, Longair M, Pietzsch T, Preibisch S, Rueden C, Saalfeld S, Schmid B *et al*. Fiji: an open-source platform for biological-image analysis. *Nat Methods* 2012;**9**:676–682.

Scott JE. Elasticity in extracellular matrix 'shape modules' of tendon, cartilage, etc. A sliding proteoglycan-filament model. *J Physiol* 2003; **553**:335–343.

Shah JS, Sabouni R, Cayton Vaught KC, Owen CM, Albertini DF, Segars JH. Biomechanics and mechanical signaling in the ovary: a systematic review. *J Assist Reprod Genet* 2018;**35**:1135–1148.

Shen S, Hinderer S, Schenke-Layland K. Scaffold and biomechanical transductive approaches to elastic tissue engineering. In CK Anand Ramamurthi (ed). *Elastic Fiber Matrices*. Boca Raton, USA: CRC Press, 2016, 24.

Swee MH, Parks WC, Pierce RA. Developmental regulation of elastin production. Expression of tropoelastin pre-mRNA persists after down-regulation of steady-state mRNA levels. *J Biol Chem* 1995; **270**:14899–14906.

Takahashi N, Tarumi W, Ishizuka B. Involvement of hyaluronan synthesis in ovarian follicle growth in rats. *Reproduction* 2014;**147**: 189–197.

Thorne JT, Segal TR, Chang S, Jorge S, Segars JH, Leppert PC. Dynamic reciprocity between cells and their microenvironment in reproduction. *Biol Reprod* 2015;**92**:25.

Tiedemann K, Batge B, Muller PK, Reinhardt DP. Interactions of fibrillin-1 with heparin/heparan sulfate, implications for microfibrillar assembly. *J Biol Chem* 2001;**276**:36035–36042.

Wagenseil JE, Mecham RP. New insights into elastic fiber assembly. *Birth Defects Res C Embryo Today* 2007;**81**:229–240.

Wood CD, Vijayvergia M, Miller FH, Carroll T, Fasanati C, Shea LD, Brinson LC, Woodruff TK. Multi-modal magnetic resonance elastography for noninvasive assessment of ovarian tissue rigidity in vivo. *Acta Biomater* 2015;**13**:295–300.

Woodruff TK, Shea LD. A new hypothesis regarding ovarian follicle development: ovarian rigidity as a regulator of selection and health. *J Assist Reprod Genet* 2011;**28**:3–6.

Xu M, West E, Shea LD, Woodruff TK. Identification of a stage-specific permissive in vitro culture environment for follicle growth and oocyte development. *Biol Reprod* 2006;**75**:916–923.

Zacchigna L, Vecchione C, Notte A, Cordenonsi M, Dupont S, Maretto S, Cifelli G, Ferrari A, Maffei A, Fabbro C *et al*. Emilin1 links TGF-beta maturation to blood pressure homeostasis. *Cell* 2006;**124**:929–942.

Zanetti M, Braghetta P, Sabatelli P, Mura I, Doliana R, Colombatti A, Volpin D, Bonaldo P, Bressan GM. EMILIN-1 deficiency induces elastogenesis and vascular cell defects. *Mol Cell Biol* 2004;**24**: 638–650.

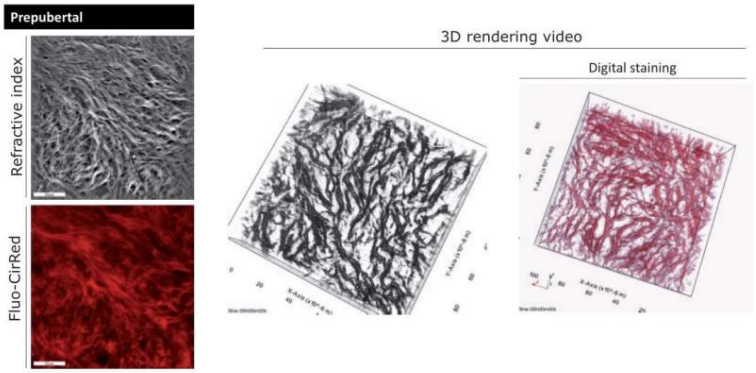
human reproduction SUPPLEMENTARY DATA

Supplementary Table SI **Clinical characteristics of the patient cohort.**

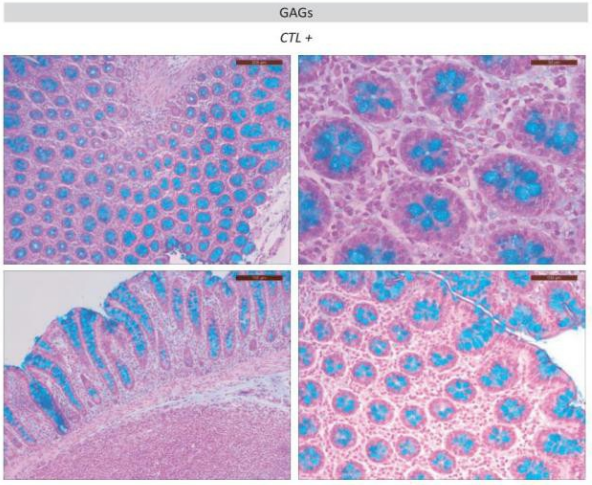
Prepubertal		Reproductive age			Menopausal HRT−		Menopausal HRT+		
Age (years)	Diagnosis	Age (years)	Diagnosis	Oral contraceptives	Age (years)	Diagnosis	Age (years)	Diagnosis	HRT
6	Orbital rhabdomyosarcoma	22	Retrocervical endometriosis	YES	62	Mucinous cystadenoma	55	Urinary incontinence	Femoston
6	Neurofibromatosis type I	22	Rectovaginal endometriosis	YES	63	Endometrial neoplasia	54	Prophylaxis (family history of ovarian cancer)	Oestrogel/utrogestan
7	Cutaneous Ewing sarcoma	33	Adenomyosis	YES	67	Endometrial polyp	54	Prophylaxis (family history of ovarian cancer)	Estalis
7	Ewing Sarcoma	33	Endometriosis in the left uterosacral ligament	NO	59	Triple-negative breast cancer	66	Ovarian cyst	Oestrogel
8	Brain tumor	20	Peritoneal carcinomatosis	YES	57	Ovarian cyst	64	Ovarian cyst	Femoston
6	Lymphoblastic lymphoma	30	Peritoneal endometriosis	YES	56	BRCA1 mutation	54	Prophylaxis	Oestrogel/utrogestan
8	Anaplastic astrocytoma	25	Sarcoma	YES	72	Urogenital prolapse	60	Cervical dysplasia	Oestrogel/utrogestan
7	Adrenal tumor	25	Sarcoma	NA	56	BRCA1 mutation			
6	Hodgkin's lymphoma	33	Borderline ovarian tumor	NA	62	Ovarian cyst			
6	Sarcoma	27	Breast cancer	YES	60	Urogenital prolapse			
12	Sarcoma	24	Hodgkin's Lymphoma	NA	54	Ovarian cyst			
11	Sarcoma	21	Hodgkin's lymphoma	YES	55	Hydrosalpinx			
9	Sarcoma	33	Ovarian cyst	YES	54	BRCA2 mutation			
12	Sarcoma	30	Pelvic endometriosis	NO	55	Prophylaxis (family history of breast cancer)			
9	Bone marrow tumor	28	Rectovaginal nodule	YES	58	BRCA1 mutation			
9	Osteosarcoma	27	Endometriosis	YES	61	Cervical dysplasia			
		27	Endometriosis	YES	63	BRCA1 mutation			
		21	Ovarian cyst	YES	65	Breast cancer			
		22	Ovarian cyst	YES	65	Mammary neoplasia			
		27	Breast cancer	NA	67	Peritoneal carcinomatosis			
		29	Ewing sarcoma	YES	70	Uterine prolapse			
					73	Uterine prolapse			

None of the selected ovarian tissues with benign gynecological pathologies presented any potential confounders in this study, as confirmed by the anatomic pathology department of the UCLouvain institution. More than 70% of enrolled reproductive-age women were taking oral contraceptives.
NA, not available.

human reproduction SUPPLEMENTARY DATA

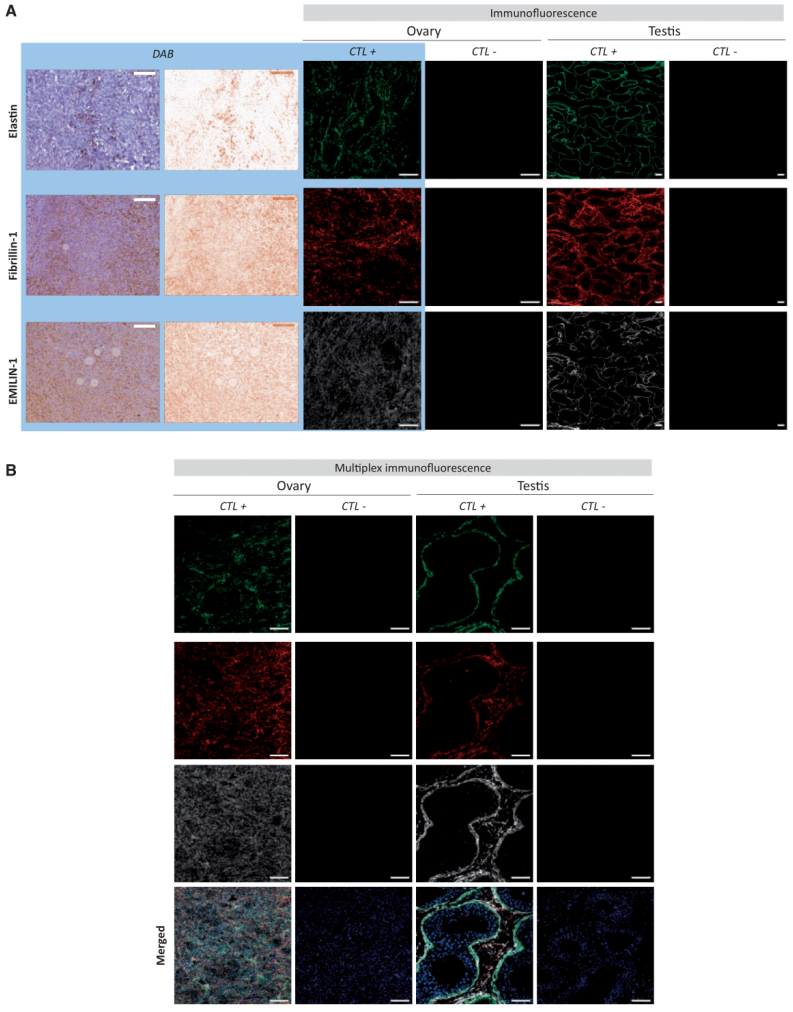


Supplementary Video **Ovarian tissue imaging under a holotomographic microscope (Nanolive, Lausanne, Switzerland) with and without Sirius Red staining to observe structural features.**



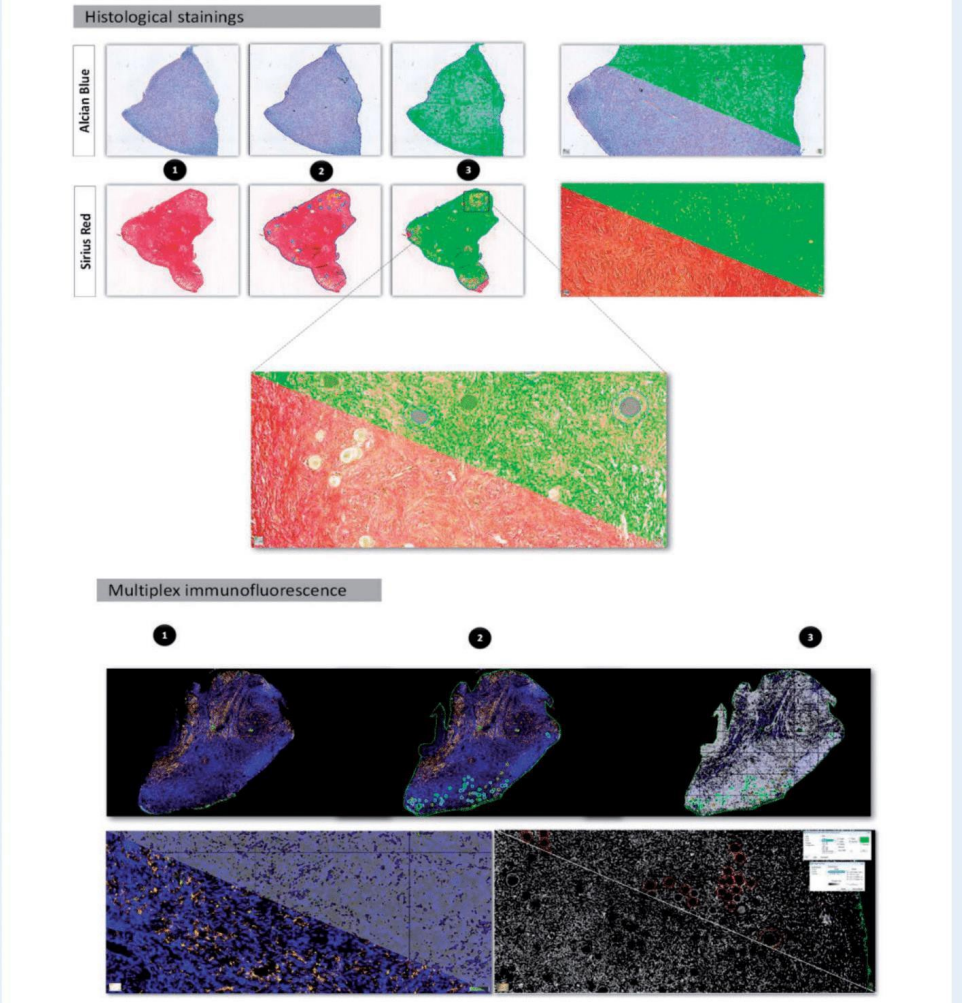
Supplementary Figure S1 **Glycosaminoglycan positive control.** Human small intestine was used as a positive control to monitor Alcian blue staining quality.

human reproduction SUPPLEMENTARY DATA



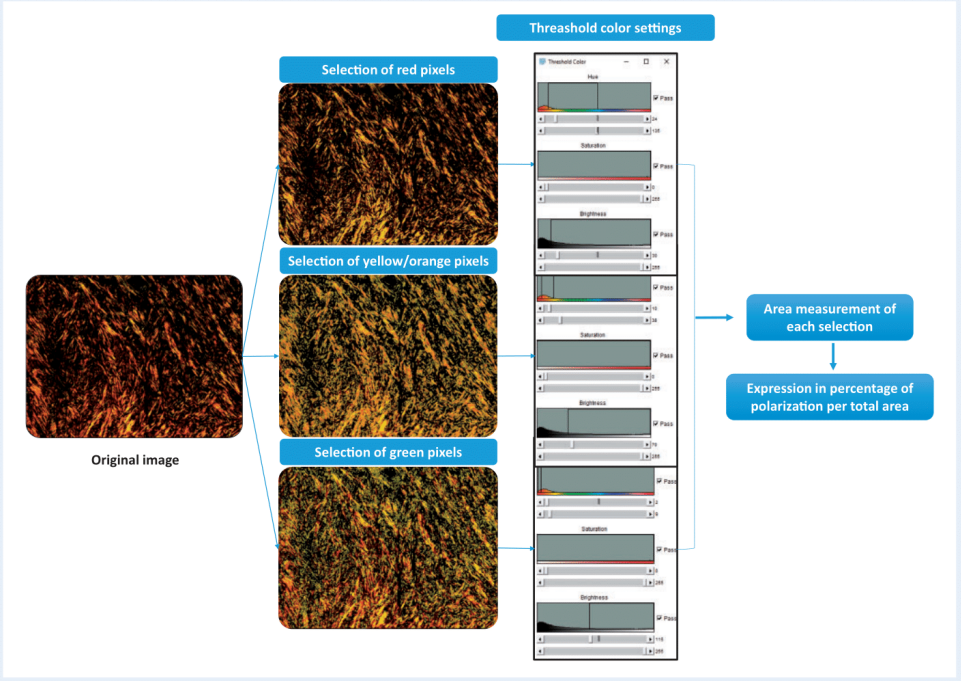
Supplementary Figure S2 Positive and negative controls for multiplex immunofluorescence. (**A**) Each antibody was first tested separately by DAB (Ouni *et al.*, 2019) and immunofluorescence. Digital color separation was applied to better distinguish DAB from hematoxylin staining using Fiji software. (**B**) Simple and multiplex immunofluorescence tests were subsequently compared in order to ensure no cross-reactivity between antibodies and that the signal was not affected by tissue processing steps. Comparison of simple immunofluorescence and multiplex immunofluorescence using the same antibodies revealed no difference in the detected signal between the two techniques. Human testicular and ovarian tissues were used for negative controls (CTL−), with rabbit IgG instead of primary antibodies. Scale bar: 100 µm.

human reproduction SUPPLEMENTARY DATA



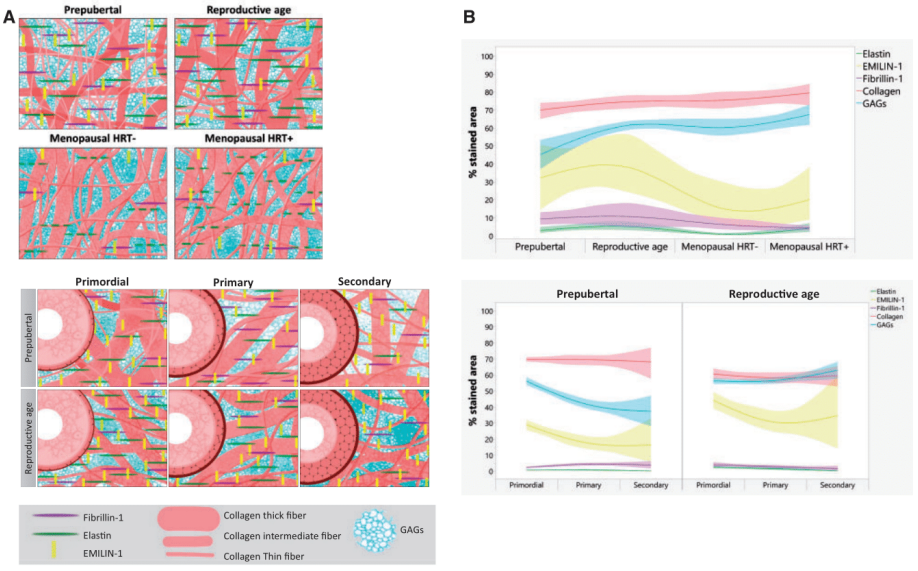
Supplementary Figure S3 Summary of the workflow using Oncotopix, version 2017.2. For immunofluorescence and histological staining, we can summarize the workflow in three main steps: (1) Visualization of scanned slides. (2) Delineation of regions of interest (ROIs) and elimination of artifacts. Ovarian follicles were also delineated and labeled according to their developmental stage. A 25-µm-thick perimeter was defined around each follicle to create new ROIs that served for analysis of each follicular microenvironment [perifollicular extracellular matrix (ECM)]. (3) Calculation of stained areas according to an optimized threshold.

human reproduction SUPPLEMENTARY DATA



Supplementary Figure S4 Collagen birefringence workflow. Polarized light depends upon fiber thickness. As fiber thickness increases, the color changes from green to yellow to orange to red. To determine the proportion of different colored collagen fibers, we resolved the subtracted image into its hue, saturation and value components using a home-made macro program that we developed using Fiji software. The number of pixels within each hue range was determined and expressed as a percentage of the total number of collagen pixels, which in turn was expressed as a percentage of the total number of polarized pixels in the image.

human reproduction SUPPLEMENTARY DATA



Supplementary Figure S5 Illustration and summary of the spatiotemporal deposition of elastic matrisome components in the human ovary. (**A**) Graphic illustration of results. (**B**) Summary of all studied elastic matrisome proteins in perifollicular and interstitial ECM. The curves represent average levels of studied matrisome components in all groups and follicle stages at both prepuberty and reproductive age, fitting a smoothing spline with a lambda value of 0.05. The curves also include the bootstrap confidence region for each fit generated by JMP® Pro 14.3.0.

Proteome-wide and matrisome-specific atlas of the human ovary from prepuberty to menopause

Emna Ouni[1], Valerie Nedbal[2], Marta Da Pian[3], Hangbao Cao[4], Kalina T. Haas[5], Alexis Peaucelle[5], Olivier Van Kerk[1], Gaetan Herinckx[6], Etienne Marbaix[7,8], Marie-Madeleine Dolmans[1,8], Timo Tuuri[9], Marjut Otala[9], Didier Vertommen[6,¥], Christiani A. Amorim[1,¥,*]

[1]Pôle de Recherche en Gynécologie, Institut de Recherche Expérimentale et Clinique, Université Catholique de Louvain, 1200 Brussels, Belgium
[2]Global Technical Enablement, SAS Institute GmbH, In der Neckarhelle 162, 69118 Heidelberg, Germany
[3]Elsevier Life Sciences, 35131 Padova, Italy
[4]Elsevier Biology Solution, Washington DC, USA
[5]Institut Jean-Pierre Bourgin, INRAE, AgroParisTech, Université Paris-Saclay, 78000 Versailles, France
[6]PHOS Unit & MASSPROT platform de Duve Institute, Université Catholique de Louvain, 1200 Brussels, Belgium
[7]Cell Biology Unit, de Duve Institute, Université Catholique de Louvain, 1200 Brussels, Belgium
[8]Gynecology and Andrology Department, Cliniques Universitaires Saint-Luc, 1200 Brussels, Belgium
[9]Department of Obstetrics and Gynecology, Helsinki University Hospital, University of Helsinki, 00029 Helsinki, Finland

*Corresponding author
¥ Co-last authors

Abstract

Our modern era is witnessing an increasing infertility rate worldwide. Although some of the causes can be attributed to our modern lifestyle (e.g., persistent organic pollutants, late pregnancy), our knowledge of the human ovarian tissue has remained limited and insufficient to reverse the infertility statistics. Indeed, all efforts have been focused on the endocrine and cellular function in support of the cell theory that dates back to the 18th century, while the human ovarian matrisome is still under-described. Therefore, hereby we provide the first systematic study focusing on the human ovarian matrisome and its remodeling during a woman's lifetime, from prepuberty until menopause. We have applied our matrisome tailored fractionation method, the DC-MaP strategy and mass spectrometry-based quantitative proteomics using TMT pro16-plex isobaric labeling to delineate proteome- wide and extracellular matrix (ECM)-specific shifts between prepubertal, reproductive-age and menopausal stages. Post-translational modifications, namely proline hydroxylation and advanced glycation end products, have also been detected at different intensities according to age.

Matrisome age-biomarkers have been validated with light-sheet microscopy-based-3D imaging, following immunofluorescence and tissue clearing with an ovary-tailored protocol. We used machine learning and statistics to build a neural network that predicts the probability of a specific ovarian tissue matrisome to resemble to prepubertal, reproductive-age, or menopausal tissue and potentially conclude its fertility potency or evaluate in the future the efficiency of ovarian rejuvenation treatments. We also used Nature Language Processing (NLP) medscan technology for advanced literature text-mining to predict all possible connections between the extra- and intracellular compartments and how chemotherapy, known for its gonadotoxicity, can also affect key matrisome proteins.

This comprehensive proteomics analysis represents the ovarian proteomic codex and contributes to an improved understanding of the critical roles that ECM plays throughout the ovarian life span. By publishing our proteomic data, we hope to open new avenues in fertility restoration, ovarian rejuvenation, and reproductive tissue bioengineering.

Introduction

Before the early 1800s, the "fibers" of connective tissue were thought to be somehow alive, where life arose by spontaneous generation (1). Indeed, extracellular matrix (ECM) composed of "fibers" of different kinds and in various arrangements, known under a variety of other names at that era, preceded the discovery of cells by centuries, even thousands of years (2). Nevertheless, the fiber theory was later argued and attacked by Rudolf Virchow in the middle 1800s (3), and was finally replaced by the cellular theory, which states that cells arise only from cells (omnis cellula excellula) (4). This is a remarkable turnaround from fibers are and make life, to cells are life and make fibers. Along with the pursuit of the origins of life, reproduction and how a new individual is generated have long fascinated mankind. At that time, Theodore Schwann proposed that the ovum was also a cell, yet more than 20 years elapsed before Karl Gegenbaur, in 1861, demonstrated convincingly that the ova of all vertebrates are cells. William Harvey's dictum (Ex ovo omnia) that all living creatures come from an egg was, therefore, ready to be confirmed more than 200 years after it was conceived (5).

Until today, the ovarian cells and the ovum have remained the center of many research interests, putting the implication of the ECM in reproduction as a secondary matter. Although cells undoubtedly make the ECM, they are in turn dependent on it. Indeed, the biological interactions that constitute life and disease - take place in a continuum throughout cellular and extracellular space (1). However, our knowledge of the human ovarian ECM is still limited. Most data on human ovarian tissue and its ECM have been obtained through immunohistological staining (6-8), and thus have not comprehensively identified the compositional profile of ECM proteins neither their evolution and remodeling with age. Moreover, the scarcity of healthy human ovarian

biopsies has prompted the use of animal models. However, substantial differences between animal and human reproductive systems may question our fundamental understanding of homeostatic ovarian function in our specie (9). Despite these limitations, ECM biology is now starting to gain momentum in the reproductive medicine, mainly in the pathological context such as primary ovarian insufficiency, ovarian aging, polycystic ovary syndrome (PCOS), and clinical applications of fertility preservation. Therefore, it is high time we revealed more insights on ECM-cell interactions in the human ovary, integrating all components of the essence of life that have been defined so far: fibers, cells, and ovum.

Here, we used an untargeted mass spectrometry (MS) based method to compare ovarian matrisome of prepubertal, reproductive-age, and menopausal women. MS has become the gold standard for identifying and quantifying matrisomics and shows great potential for the sensitive and large-scale analysis of complex biological systems (10). Despite the significant development in data acquisition and identification of post-translational ECM modifications (11-15), extracellular proteins still present analytical difficulties in proteomic strategies due to the biochemical characteristics of these molecules, which are highly crosslinked, often glycosylated, and hence insoluble even in strong detergents and organic denaturants (16). Thus, obtaining the most detailed picture of ECM protein composition is still hampered by its complex biochemical nature and wide dynamic range. Therefore, we set out to overcome the major technical hurdles: unfriendly-MS detergents, irreproducibility, labor-intensive processing, and consequent loss of low abundant proteins by using our previously described DC-MaP method tailored for unbiased ECM proteomics (17). Our protocol is compatible with the isobaric amine-reactive tandem mass tag labeling reagents, such as tandem mass tags (TMTs), which we used in our quantitative proteomics. This method overcomes run-to-run variations and

enables to achieve accurate and multiplexing quantitative analysis.

By applying our DC-MaP approach and adopting a tailored experimental design of TMT labeling to compare the matrisome of prepubertal, reproductive-age, and menopausal ovarian tissue, we unraveled for the first time 26 potential biomarkers phenotyping ovarian ECM at each age phase of female reproductive life. These biomarkers were validated by a clearing method tailored for human ovarian tissue that we developed to unravel their 3D-spatial distribution and localization. Beyond descriptive analyses, this study relied on advanced text-mining to relate ECM proteins of interest to cellular biological processes regulating ovarian activity and follicle quiescence, activation, and development to complement our knowledge of the human ovary and create new interconnections between intra- and extracellular regulators (18). We also used machine learning and statistics to build a neural network that can predict all ovarian matrisome quantities of any ovarian tissue starting from one quantification of a specific matrisome component. Moreover, our model could be used to predict the probability of a specific ovarian tissue matrisome to resemble prepubertal, reproductive-age, or menopausal tissue. In the future, this could be a predictor of fertility potential, premature aging, or even an evaluation tool of the efficiency of ovarian rejuvenation or fertility restoration strategies acting at the level of the ECM. Beyond data mining and visualization, this project presents a unique approach to understanding the data and depict the ECM remodeling with age through listening to the data, a recently growing discipline known as data sonification. We believe that this technique could help scientists identify ovarian anomalies in proteins more easily by listening to them and can even catalyze the transition of MS to clinical use.

These results represent an unprecedented knowledge base in understanding the significant remodeling and alterations that occur in the ovarian matrisome

throughout the human life cycle. They also provide a valuable reference for comparative studies between healthy and pathological conditions, as they represent a trustful basis for tissue engineering applications such as the transplantable artificial ovary (19).

Materials and methods

Ovarian biopsies included in this study

The use of human ovarian cortex was approved by the Institutional Review Board of the Université Catholique de Louvain on May 13, 2019 (IRB reference 2012/23MAR/125, registration number B403201213872). Ovarian cortex biopsies were taken from prepubertal (mean age [±SD]=7±3 years; n=5), reproductive-age (mean age [±SD]=26±5 years; n=5) and menopausal (mean age [±SD]=59±8 years; n=5) patients after obtaining their informed consent. All participating adult subjects were undergoing laparoscopic surgery for benign gynecological diseases not affecting the ovaries. Prepubertal tissue was derived from young cancer patients scheduled for ovarian cortex cryopreservation as a fertility preservation strategy before being subject to acute gonadotoxic cancer treatments. All samples used in mass spectrometry analyses were cryopreserved by slow freezing (20) and kept frozen until the day of their analysis. Samples used in imagery analyses were obtained from the pathology department of Université Catholique de Louvain St-Luc's Hospital after overnight fixation in 4% paraformaldehyde. They were kept in 70% ethanol until the day of their processing, as described below.

Protein extraction

All samples were processed throughout the full procedure simultaneously the same day to avoid batch effects. First, cryopreserved samples were thawed (20) and cut into 3 x 3 x 1 mm fragments using graph paper. The excess

medium was removed with gauze, and 10 mg wet weight of each sample was processed following our DC-MaP technique (17). Briefly, each 10 mg- ovarian tissue was transferred to an empty 2 mL FastPrep®Lysing matrix tube (MP Biomedicals) filled with 200 µL lysis buffer (0.2% RapiGest [Waters Corp., Milford, MA], 300 mM NaCl 25mM HEPES, 0.25 mM sodium orthovanadate, 50 mM NaF, 0.25 mM PMSF, 1X halt protease inhibitor cocktail [Thermo Scientific, San José, USA] and 5 mM EDTA) and mechanically lysed using 0.3 mm-diameter stainless steel beads (Full Moon,BioSystems, Sunnyvale, CA, USA). Homogenization was carried at 4°C withPrecellys Evolution (Bertin Technologies, Montigny-le-Bretonneux, France).The homogenate was eluted with the needle technique (17) by centrifugationat 3,000 g for 5 min at 4°C. The eluate was then centrifuged again at 16,000gfor 30 min at 4°C to recover the supernatant, representing the soluble fraction.

The remaining pellet representing the insoluble fraction, was enzymatically digested using 1.35 mg/mL LiberaseTM DH (Roche Diagnostics, GmbH, Mannheim, Germany) in 100 mM triethylamonium bicarbonat (TEAB, pH 8) and 5 mM CaCl2. Each sample was subsequently incubated at 37°C for 2 h under agitation (140 rpm) with regular 30-s vortexing every 30 min. The enzymatic reaction was halted by the addition of 20 mM EDTA. Both soluble and insoluble fractions were processed as described below.

Soluble Fraction Processing

One hundred µg of total soluble proteins were reduced with 5 mM 1,4-Dithiothreitol (DTT), incubated for 30 min at 56 °C and subsequently alkylated with a 25 mM final concentration of chloroacetamide for 25 min at room temperature in the dark. The proteins were then precipitated using methanol-chloroform, resuspended in 100 mM TEAB (pH 8) and further digested with Lys-C/trypsin at an enzyme:substrate ratio of 1:25 [wt/wt] overnight at 37 °C. The samples were centrifuged at 16,000 g for 10 min at 4 °C. Recovered

peptides were quantified by Pierce™ Quantitative Colorimetric Peptide Assay (#23275, Thermo Scientific) according to the manufacturer's instructions.

Insoluble Fraction Processing

One hundred µg of total insoluble proteins were resuspended in a 6 M final concentration of urea in 100 mM TEAB, with continuous vortexing and sonication. Proteins were then reduced in 5 mM DTT and incubated for 1 h at 37 °C. After cooling to RT, cysteines were alkylated by adding 25 mM chloroacetamide for 25 min at RT in the dark. No precipitation was conducted during insoluble fraction processing to avoid resolubilization problems and take advantage of the trypsin-enhancing action of RapiGest. Protein digestion was performed using Lys-C/trypsin at an enzyme:substrate ratio of 1:50 [wt/wt] and incubation for 2 h at 37°C under 1,000 rpm agitation. After reducing urea concentration to 1 M by adding 100 mM TEAB, a second aliquot of trypsin was added to the sample at an enzyme:substrate ratio of 1:100 [wt/wt] and incubated overnight at 37°C with continuous agitation at 1,000 rpm. The reaction was stopped and the detergents hydrolyzed by the addition of freshly prepared 50% trifluoroacetic acid (TFA) [vol/vol] to a final concentration of 1% TFA [vol/vol], pH < 2. The acidified sample was centrifuged at 16,000× g for 10 min at RT to eliminate the insoluble MS-compatible detergents. Digests were then desalted and concentrated on HyperSep C18 cartridges (50 mg/mL, Thermo Scientific, San Jose, CA, USA) according to the manufacturer's instructions, and then dried using a speedvac. Peptides were resuspended in 50 µL of 100 mM TEAB and quantified by the Pierce™ Quantitative Colorimetric Peptide Assay following the manufacturer's instructions.

TMTpro Labelling

Thirty µg of peptides were prepared in one hundred µl of 100mM TEAB. In addition, a bridge sample, which contains an equal amount (1µg) of each soluble and insoluble fraction, for a total of thirty µg, was prepared in one hundred µl of 100 mM TEAB. All were labeled with TMTpro™ 16plex Label (A44521, Thermo Scientific) according to the manufacturer's instructions (Fig. 1). One label reagent (reporter ion) was used for the bridge sample, and the fifteen other labels were used to label an equal amount of peptides from the soluble and insoluble fractions. After labeling with the TMT tags and quenching the reaction with 5 µL of 5% hydroxylamine, an equal amount of each soluble fraction and bridge sample were combined on one side. And the same equal amount of each insoluble fraction and the bridge were combined on the other side. Both combined samples were dried in a speedvac, resuspended in 3.5% acetonitrile (ACN) [vol/vol] and 0.1% TFA [vol/vol] in water, then cleaned up with C18 cartridges (200 mg/mL, Thermo Scientific) according to the manufacturer's instructions then dried again and resuspended in 3.5% ACN [vol/vol] and 0.1% TFA [vol/vol] in water.

Liquid chromatography-tandem-mass-spectrometry (LC-MS/MS)

One µg of peptides dissolved in solvent A (0.1% TFA in 2% ACN) was directly loaded onto a reversed-phase pre-column (Acclaim PepMap 100, ThermoScientific) and eluted in backflush mode. Peptide separation was achieved using a reversed-phase analytical column (Acclaim PepMapRSLC, 0.075 × 250 mm, Thermo Scientific) with a 140 min linear gradientof 4%–32% solvent B (0.1% TFA in 80% ACN) for 99 min, 32%–60% solvent B for 10 min, 60%–95% for 1 min and holding at 95% for the last 10min at a constant flow rate of 300 nL/min on an Ultimate 3000 RSLN nanoHPLC system (Thermo Scientific). The peptides were analyzed by an Orbitrap Fusion Lumos tribrid mass spectrometer (Thermo Fisher Scientific) with

enabled advanced peak determination (APD) and relative quantification either by MS2 or SPS MS3. The peptides were subjected to a nanospray ionization source, followed by MS/MS in the Fusion Lumos coupled online to the UPLC. Intact peptides were detected in the Orbitrap at a resolution of 120,000 with a scan range m/z from 375 to 1500 and an AGC target of 4x105, maximum injection time was set to 50 ms. A data-dependent procedure of MS/MS scans was applied for the top precursor ions above a threshold ion count of 5.0 × 103 in the MS survey scan with60 s dynamic exclusion. The total cycle time was set to 3 s.

For MS2 quantification of the TMT reporter ions, MS/MS spectra were acquired in the Orbitrap at a resolution of 50,000 after HCD fragmentation at 35% with an AGC target of 1 × 105 ions and a maximum injection time of 120 ms. For MS3 quantification, MS/MS spectra were first acquired in the Ion Trap after CID fragmentation at 30%, 10 precursors were synchronously selected (SPS MS3) for HCD fragmentation at 55%, and the MS3 spectra was acquired in the Orbitrap at a resolution of 50,000 with an AGC of 2 x 105 and a maximum injection time of 120 ms. MS/MS spectra was exported using the following settings: peptide mass range: 350–5000 Da, minimal total ion intensity: 500.

Protein Identification and quantification

Resulting MS/MS data were processed using the Sequest HT search engine within Proteome Discoverer 2.4 against a human protein reference target-decoy database obtained from Uniprot (March 1, 2020, 87,489 forward entries). Trypsin was specified as the cleavage enzyme, allowing up to 2 missed cleavages, 4 modifications per peptide, and up to 3 charges. The mass error was set to 10 ppm for precursor ions and 0.1 Da for fragment ions, and considered dynamic modifications were +15.99 Da for oxidized methionine or proline, +21.984 Da for glyoxal on arginine, +114.042 Da for

3-deoxyglucosone on arginine and +42.011 Da for acetylation of the protein N-term. Fixed modifications were TMTpro (+304.207 Da) for lysine and peptide N-termini, and +57.00 Da for carbamidomethyl cysteine. The false discovery rate (FDR) was calculated using Percolator, and thresholds for protein, peptide, and modification sites were specified at 1%. Relative quantification was performed with the MS2 or MS3 signal from TMT reporters' ions.

Quan value corrections for isotopic impurities were applied, and co-isolation threshold was set at 50 or 65 for MS2 and MS3 data respectively. Two different ways of normalization were used: none with a scaling mode set on "controls average" or "all average"; or with normalization against a specific protein database containing liberase.

Proteomic data post-processsing and statistical analysis

Only proteins that have been identified with at least 2 unique peptides per protein have been taken into consideration. Since our DC-Map technique leads to the obtention of two fractions, soluble and insoluble, to have an optimal quantification of the total amount of a protein per ovarian tissue, we summed its intensity in both fractions. Missing intensities from MS2 were replaced by MS3 for all compared samples. Matrisome protein recognition in Sequest result files was achieved by comparison of confidently detected proteins with the Matrisome Project data set (http://matrisomeproject.mit.edu/), an in silico-identified ECM protein set founded on the characteristic domain-based organization of ECM proteins. Quantile normalization has been used to normalize cellular and extracellular data distribution. Bioinformatics analyses, including Pearson's correlation analysis, hierarchical clustering, parallel plots, and volcano plots have been conducted on JMP Genomics 10. For biomarker discovery, a one-way ANOVA analysis with an FDR cutoff of 0.05 was used and carried on

JMP Genomics 10. Biological processes and pathways were enriched with Pathway Studio using GSEA. At least two selected terms with $p<0.05$ were shown for each cellular process.

Data-mining

Pathway Studio was used to examine possible interactions of matrisome proteins of interest with other cellular proteins, explore the biological processes they are involved in, and elucidate the impact of FDA-approved anticancer drugs (21) on ovarian matrisome proteins. Pathway Studio (www.pathwaystudio.com) is an Elsevier-associated text-mining software that collects more than 13.5 million biological relationships between different entity types including genes, diseases, drugs and cells. It covers over 32 million PubMed abstracts and 5.3+ Elsevier and third-party full-text articles, which gets updated weekly. The database was compiled using a Nature Language Processing (NLP) technology called MedScan (22).

Machine learning (Neural network)

Using the 26 matrisome biomarkers differently distinguishing each age group, we constructed a neural network via JMP genomics by building a model predicting the interdependence of matrisome protein intensities.

The constructed model also calculates the probability of an ovarian tissue matrisome analyzed with our described pipeline to resemble prepubertal, reproductive-age, or menopausal tissue. Through its interactive interface, the model demonstrates how by shifting the expression level of one or several matrisome proteins, the biological tissue age might be changed. To do so, the dataset was split into training (60% of total data), validation (20%), testing (20%) following the Holdback validation method to ensure the model performance.

Data sonification

Sonification translates data into a sound signal that helps integrate multi-parameter data. The following parameters could be used simultaneously to generate a soundtrack: pitch level, intensity, and rhythm.

To illustrate the evolution of relative protein representation in the tissue, we focused on pitch to represent the level of protein expression: the higher the pitch, the higher the relative expression. We will not use the intensity as a marker as our ear interpret pitch and intensity in a nonlinear relation. Thus, this parameter could lead to misinterpretation of the data. Played one by one, we could follow the melody of 3 soundtracks describing the evolution of matrisome composition from prepubertal toward menopausal age that we name "expression melodies." We could then play together several "expression melodies" combining similar matrisome categories (eg., proteoglycans, collagens) corresponding to each age. The diversity in pitch or the richness of the obtained choir will represent the diversity in expression levels within this category. The evolution will pinpoint global changes affecting part or all the quantified matrisome components. To facilitate the audition, we used a rhythm-based on three beats (3-time points) to express the movement from one type of category to the other at each step. This way, we can hear the orchestration of the biochemical evolution of ECM during aging.

Immunofluorescence and tissue clearing

For validation and localization of ECM biomarkers detected by MS, we used a technique we developed, tailored for 3D immunofluorescene of intact human ovarian ECM of few hundreds of microns (thickness of ovarian cortex) to observe targeted proteins in their inherent 3D configuration and distribution. The workflow is subdivided into five main steps: 1) permeabilization; 2) autofluorescence quenching; 3) non-specific reaction

blocking; 4) immunofluorescence labeling; 5) clearing; 6) refractive index balance. At all steps, samples were protected from light.

The permeabilization step consists of washing fixed ovarian tissues (previously kept in 70% ethanol) in PBS for 3 h at RT. Fresh PBS was renewed each hour. The samples were then transferred to a new solution composed of 0.2% Triton-x100 in PBS for 2 h at RT followed by another incubation in 0.2% Triton-x100 and 20% DMSO in PBS overnight at 37°C. Samples were then rinsed in 0.2% Triton-x100 prepared in PBS for 1 h at RT. All these steps were carried out under radial agitation. Autofluorescence quenching was achieved through sample incubation in 1 mg/mL sodium borohydride dissolved in PBS, overnight at RT, and under agitation. The samples were then rinsed in PBS for 90 min with solution renewal every 30 min at RT and under radial agitation. To block non-specific antibody binding, the samples were incubated in 10% fetal bovine serum (FBS), 1% bovine serum albumin (BSA), 1% Triton-x100, and 0.2% Azide at 4°C for 2 days, under radial agitation. After these steps, the samples were ready for antibody labeling. One of the hurdles of conducting immunofluorescence on thick tissue samples, is the limited diffusion of antibodies, especially in fibrous samples, such as human ovarian tissue. Therefore, antibodies were resuspended in 10X diluted blocking solution to achieve the required concentration (Table 1) with 500 µL final volume and were transferred to 1 mL syringes (Baxter Inc, McGaw Park, IL, USA), after hermetically sealing the tips. The samples were subsequently placed into the syringes, and the syringe plunger was put in place. To ensure constant pressure during incubation, the syringes were then packed inside slide staining jars. Incubation with primary antibodies was carried at 4°C under rocking agitation for 5 days under pressure (in syringes). Samples are then transferred to Petri

dishes and washed for 2 days in 3% NaCl, 0.2% Triton-x100, and PBS at 4°C under rocking agitation. Like primary antibodies, secondary antibody incubation was carried under pressure at 4°C under rocking agitation, but for only 3 days, followed by a washing step. Nuclear staining was then conducted under pressure in 500x diluted Hoechst in PBS, overnight at 4°C under rocking agitation and rinsed after in PBS for 3 days at 4°C, under orbital agitation.

Following immunofluorescence, the samples were placed in a 96-well plate and incubated in 100µL RapiClear 1.49 solution (Sunjin Lab, Hsinchu City, Taiwan), at 37°C overnight to achieve transparency. The samples were then kept at 4°C in our in-home developed POTATO (Preservation Of Transparency And Tissue Observation) imaging medium composed of 39% antipyrine, 26% nicotinamide in distilled water, to balance their refractive index (RI), until the day of their analysis.

3D imaging and rendering

With a RI equal to 1.48, the POTATO solution preserves the transparency of ovarian samples perfectly, limits light scattering, offers a cost-effective alternative to expensive commercial solutions, as it is also compatible with most 20X objectives of light-sheet microscopes such as the one we used, a 20x1.0 Clr Plan Neofluar (WD 5.6 mm). On the day of acquisition on Lightsheet.z1 LSFM (Zeiss Inc,Germany), samples were embedded in 1% of low melting agar and pumped in 2.5 mm-diameter capillaries as described by the manufacturer. Cross-linked agar capillaries are then transferred to the imaging chamber filled with POTATO solution and kept at least one hour at RT for RI matching of all imaging system components (sample-media-lens). RI-matched samples were acquired with 408nm, 488nm, and 660nm lasers. Z stack images (optical slices) were pre-processed and normalized using Zen (black edition) (Zeiss). Video animations were achieved through Arivis 4D

(rivis AG, Rostock, Germany).

Data availability

The mass spectrometry proteomics data have been deposited to the ProteomeXchange Consortium via the PRIDE (22) partner repository with the dataset identifier PXD (Username: reviewer_pxd025940@ebi.ac.uk; Password: 0K9w3nwz).

All supplementary data can be accessed via the Mendeley depository: https://data.mendeley.com/datasets/nvjsyyg43h/draft?a=2565d0c7-4e1b-46a1-9de2-2a96546c5f5d

Results

Overview of detected proteins in numbers

We confidently (unique peptides ≥ 2; FDR<1%) identified 120 matrisome proteins among which 98 proteins were quantified in all samples and included: 16 collagen types; 27 glycoproteins; 8 proteoglycans; 16 ECM-affiliated proteins; 22 ECM regulators and 9 secreted factors. In addition, 1045 cellular proteins were also confidently detected including 825 quantified proteins.

Ovarian matrisome remodeling from prepuberty until menopause

Thanks to our DC-MaP strategy complemented by 16-plex pro TMT labelling (Fig. 1), we could confidently detect and quantify 98 matrisome proteins within human ovarian tissue over the three investigated groups, which makes it the first dataset of the temporal remodeling of the human ovarian tissue during a woman's life. Interestingly, using one-way ANOVA (FDR<0.05), we revealed that 26 matrisome proteins were expressed differently among prepubertal, reproductive-age, and menopausal ovarian tissues and

delineated a peculiar matrisomal fingerprint at each age (Fig. 2). Hierarchical clustering enabled the determination of 5 distinct clusters designating upregulated proteins: i) at prepuberty and downregulated inreproductive age; ii) at prepuberty and downregulated in menopause; iii) at reproductive age; iv) similarly expressed in reproductive and menopausal age and v) at menopause.

To decipher the main cellular processes where each cluster is implicated, we used GSEA with a $p \leq 0.05$. Selected biological processes were annotated for each cluster. Thus, we were able to spot enriched cellular- processes in an age-related manner.

Prepuberty

Prepubertal ovarian tissue has the highest number of unique matrisome proteins reaching 13 upregulated biomarkers. Although collagen type VI is revealed to be the dominant collagen type in human ovarian tissue at all ages, its highest levels were detected during prepuberty (Fig. 2.A). At this stage, the enriched cellular processes describe the ovarian ECM as under fundamental remodeling and construction (Fig. 2.B). Indeed, proteins implicated in elastic fiber assembly (FBLN5 and POSTN) and ECM fiber polymerization (TNXB) were overexpressed. Moreover, proteins involved particularly in basement membrane assembly (COL4 and NID1) and repair (ANXA7) were significantly highly abundant compared to adult ovaries.

Beyond matrisome protein structural role, fundamental cellular processes related to follicular atresia and quiescence could be linked to prepubertal matrisome hallmarks (Figure 2.B). On one side, primordial follicles (dormant follicles) are dominant during prepuberty and present original features of quiescence and long survival. This could be in part regulated by COL14A1, which promotes quiescence in corroboration with anti-apoptotic matrisome

proteins, such as HRNR (23). On the other side, the infant ovary is also characterized by an increasing follicle loss preceding puberty, which could be assigned for high expression of pro-apoptotic proteins (24): OGN and TGFBI.

Reproductive age

At reproductive age, all matrisomal hallmarks of prepuberty have declined, and only two proteins appear to be exceptionally highly expressed in this age group: AGT and GPC6 (Fig. 2.A,C). AGT has been enriched in the renin angiotensinogen system (RAS), which is presumed to regulate oocyte maturation and quality, promote angiogenesis and lipid storage (25, 26). GPC6 is a positive regulator of cell proliferation, a paramount process for follicle development (27, 28).

Menopause

Seven matrisomal proteins weakly expressed during prepuberty, increase progressively at reproductive age, and reach their peak upon menopause and have been enriched in several cell processes (Fig. 2.A,B).

The only collagen type upregulated at menopause is non-fibrillar, COL18A1. This endostatin-producing collagen has been known as an inhibitor of endothelial cell migration and angiogenesis (29, 30). Among menopause matrisomal biomarkers, we could find upregulated proteins responsible for (Fig. 2.B): ECM production, polymerization and fibrosis (ANXA5, F2, ITIH4 and SERPINA1). Interestingly, almost the same proteins active in fibrosis play an important role in promoting cell survival (ANXA5, F2, HPX, SERPINA1), preventing cell damage (HPX, SERPINA1), inhibiting reactive oxygen species (ROS) generation (F2, HPX, SERPINA1, and CSTB), and are implicated in hemolysis inhibition (ANXA5) and protection against heme toxicity (HPX), as depicted by GSEA. In conjunction with their cytoprotective

effects, ANXA5, SERPINA1, and F2 are also associated to senescence (31-33).

Although we would expect a large panel of differences compared to reproductive-age ovarian tissue (the gold standard of fertility), hierarchical clustering of quantified ECM proteins revealed common matrisomal features (Fig. 2). While it was not surprising to find a higher plasminogen activation in reproductive tissue since it is one of the major ECM degradation and remodeling processes during ovarian cycle enabling ovulation (34), we noticed that plasminogen stimulator, CLEC3B, remains highly expressed in the human ovary even after menopause, concommitantly with the expression of the anti-inflammatory and anti-oxidative ECM proteins ANXA1 and SERPINC1. This may mirror the presence of a peculiar inflammation process at menopause even in the absence of ovulation occurring during ovarian aging and further highlights the plethora of roles that matrisome proteins may play.

Changes in collagen hydroxylation level with age

Proline hydroxylation of all quantified proteins with our DC-Map TMT-based workflow has been screened (Fig. 3.A, Supp Table 1). In the matrisome, we found 13 collagens and one proteoglycan (lumican) differently hydroxylated between age groups at 253 locations (peptide sequences). Proline hydroxylation may regulate the flexibility of collagen molecules and make functional sites available for interacting proteins and receptors (35). With the value of this post-translational modification in mind, our results revealed that menopausal ovarian collagen is the least hydroxylated compared to younger ones, which might reflect an abnormal and unstable collagen assembly with limited interaction with cell receptors and other matrisome proteins at such stage. By contrast, reproductive-age ovaries are characterized by the highest hydroxylation of fibril forming collagen such as COL1A1, COL1A2, COL5A1

and COL5A2. Among matrisomal hallmarks of prepuberty, we found the highest hydroxylation of non-fibrillar COL6 and COL14 at this group with a remarkable hydroxylation of the fibrillar COL3 (Fig. 3.A).

In addition to collagen hydroxylation, lumican was also hydroxylated. Lumican is a small leucine-rich proteoglycan that colocalizes with fibrillar collagen and regulates the assembly and diameter of collagen fibers (36). Despite the presence of lumican and other fibrillar collagen types, namely type I, II, III, and V at equivalent levels in ovarian tissue at all stages (Fig. 2), the depicted differences in their hydroxylation may impact ECM architecture (37) and suggest a possible collagen synthesis by different cell populations within the studied groups (38).

Machine learning (Neural network)

Our collected proteomic data on ovarian matrisome temporal remodeling from prepuberty til menopause were used to build a neural network. Ordinary least-squares gave us a model with an R-square value of 0.96 and a small RMSE=0.20 on the testing set, which proves the goodness of fit of our model. Based on the TanH hyperbolic tangent function, the neural network relied on 3 nodes. The results of our model can be seen (.html format) or interactively tested to evaluate different possible theoretical ovarian profiles (eg. pathological conditions) by downloading the source data on (.jrp format):

https://data.mendeley.com/datasets/nvjsyyg43h/draft?a=2565d0c7-4e1b-46a1-9de2-2a96546c5f5d and opening the jrp file using JMP software (accessible demo): https://www.jmp.com/en_us/download-jmp-free-trial.html

We noticed that variations in GPC6, ITIH4, ANXA5, or TNXB levels lead to high variability in the response, which reveals their important effect on the model and eventually on the rest of ovarian matrisome and encourage their

deeper investigation. The model has been built based on gathered data developed with our specific pipeline and thus for the moment only reflects ovarian matrisome detected with these experimental conditions. However, we forsee in the future the collection of larger data from several proteomic platforms that can enrich ours and overcome technical variabilities, which can benefit medical diagnostics and data analysis. Indeed, neural networks can tolerate up to 15% error and still produce a robust result (39). In some cases, introducing noise to the dataset can actually improve the performance of the network (39).

Intracellular proteome temporal dynamics

Prepuberty

Among the 825 confidently detected cellular proteins, around 182 ones are particularly upregulated during prepuberty (FDR<0.05) and were enriched in 3 main biological processes: mitochondrial damage, immune chemotaxis, aberrant RNA clearing (Fig. 4). Excessive follicle atresia in the ovary and significant loss of follicular reserve, especially during prepuberty (40), can be attributed to mitochondria, whether by promotion of mitochondrial damage (41) by the release of cytochrome C (PARP1, MIF, VDAC1, SLC25A4), mitochondrion autophagy (PPID, PHB2) or mitochondrion fission (UTRN, RALA, CS). All of which lead to cell death. An important activity of immune cell recruitment also appears to occur during prepuberty, namely, under the control of S100A8, S100A9, and PTGDR implicated in neutrophil recruitment and PPIB and MIF regulating macrophage migration and activation. Although immune cell implication in the ovarian function has been already described (42), our data further outline their possible involvement in releasing pivotal cytokines and growth factors. These proteins are necessary for the development of the ovary's functional aspects and release of chemokines that attract and activate additional monocytes and neutrophils into the ovary from circulation and secrete an array of proteases that degrade the ECM as

well as release/alter ECM- or membrane-bound proteins (43) (Fig. 4).

The central dogma of molecular biology posits that the genetic information encoded in DNA is transcribed into RNA and then translated into protein. RNA splicing is a process in eukaryotic gene expression where that genetic information is altered while in RNA form. In splicing, specific regions of the RNA transcript are cut out, and the flanking sequences are pasted together (44). The process of splicing fundamentally changes the information content of the RNA transcript, which directly impacts the translation of that genetic information into protein (44). Regulation of splicing therefore represents a critical step of gene expression. In prepubertal tissue, we have detected proteins that prevent RNA splicing and ensure homeostasis, such as DDX1, RPS3, RPL30, PTBP1 and RPS14 (Fig. 4).

Nonsense-mediated mRNA decay, which can be defined by the loss of mRNAs carrying premature stop codons, is a process by which cells recognize and degrade nonsense mRNAs to prevent possibly toxic effects of truncated peptides (Figure 4). This homeostatic process in prepubertal ovaries is promoted by the upregulation of SRSF1, SRSF2 and GPX1. Since nonsense mRNA can lead to ovarian insufficiency in adult life (45), it seems that nonsense-mediated mRNA catabolism proteins may play a fundamental role in the faith of ovarian reproductive potency during adult life.

Reproductive age

At reproductive age, nonsense mRNA decay continues through upregulated HNRNPL and TPI1, which complements the previously described prevention of the consequences of truncated peptides (Fig. 4). An additional cellular process related to the prevention of abnormal protein synthesis is enriched in reproductive age ovaries. It consists in the inhibition of endoplasmic reticulum stress, which occurs when proteins are not properly folded or

conformed (misfolded protein). Consequently, through the upregulation of P4HB, CALU, GPI, and CALR, reproductive-age ovaries are able to limit endoplasmic stress that interferes with normal physiological functions of cells. Among the 41 cellular proteins that are particularly upregulated at reproductive age, we found anti-senescence proteins, namely: TPI1, HNRNPD, ENO1, and FSCN1 (Fig. 4). While senescence could hamper fertility, follicular quiescence could also interfere with the growth and release of eggs from the ovaries (ovulation) such as the case for PCOS patients (28). Both processes can lead to infertililty and thus through identifying their regulators in healthy reproductive-age ovaries we can better target their disfunction in pathological conditions. One of the targets of the recent therapies under development for PCOS patients is actin, since its polymerization reestablishes follicle activation (46). Bearing this in mind, we found in healthy reproductive ovarian tissue proteins promoting actin polymerization, namely: TPM1, TPM2 and PGK1, which could be further investigated in the context of PCOS and present promising therapeutical targets.

Menopause

Among the 45 upregulated cellular proteins in menopausal ovarian tissue, two have been related to promoting DNA fragmentation: PRF1 and IAPP. Despite expected aging hallmarks such as mitochondrial damage (DBI) and ROS generation (AOX1, PRF1, and CLIC1), menopausal ovaries appear to have their own anti-oxidative stress shield controlled by PRDX6, preventing lipid peroxidation and DNA damage and PKM, DBI, GAPDH, and SLPI limiting ROS production (Fig. 4). Other proteins upregulated at menopause play an important cytoprotective role (mechanoprotection, neuroprotection), such as FLNA, YWHAQ, CSRP1, AFM, and GSTM2. On the other hand, autophagy is halted by the overexpression of TSPO and DAP. Limitation of

both cell death and autophagy processes may reinforce cell senescence in aging ovarian tissue. Indeed, senescence is also another enriched cell process promoted by upregulation of DBI and TSPO but also by ZYX, ARID4A, RNASEH1, RBP1, and PRDX6 (Fig. 4).

Despite significant differences between menopausal and reproductive-age ovarian tissues, both groups share common expression levels of 37 cellular proteins, downregulated in prepubertal ovaries, among which a high number of anti-oxidative stress proteins, such as ADH5, PEBP1, TALDO1, PSME1, MPST, and DDT, which complement the unique anti-oxidative proteins only upregulated during menopause as mentioned above (Fig. 4). The enriched cellular processes reflect a high cellular activity at menopause with common regulators with reproductive age tissue, such as nuclear import responsible for transporting transcriptional factors toward the nucleus (YWHAB, YWHAZ, YBX1, CFL1, and DCTN2) and cytokinesis (ARHGDIA, CRK, and DDT), which are operating via focal adhesion and cytoskeleton reorganization and influencing, consequently, cell shape, spreading and mechanosensing (RDX, CRKL, and DCTN2).

Among the shared enriched mechanisms between reproductive-age and menopausal ovaries, we also detected common promoters of cell-mediated cytotoxicity, which is a crucial process responsible for the host immune defense against pathogens localized within cells (47). In the context of the human ovary, many theories have related the immune system to follicle selection, degeneration of large follicles, and ovulation (48). These events usually are only present at the reproductive age ovary due to follicle reserve presence. However, the pro-cell-mediated cytotoxicity proteins shared with reproductive-age ovaries, TTR, EIF5A, CUTA, and B2M, might suggest their residual action even after menopause. Advanced glycation end products (AGEs) affecting exclusively cellular proteins and not matrisomal ones.

Advanced glycation end products (AGEs) are heterogeneous products of the non-enzymatic interaction between proteins and reducing sugars (49) and have been associated to aging. AGE is also considered as one of collagen post-transcriptional modifications that increase with age inducing higher cross-linking and thus stiffness of collagen structures (50), which is a biomechanical hallmark of aging human ovarian tissue (51). Nevertheless, our results reveal that AGE only reaches cellular proteins, namely: HDLBP, HSPA8, KIAA0319L, SLITRK4, and TBCK, over 5 distinct sites with variable levels between age groups, despite undetected significant differences in these protein expressions (Fig. 3.B, Supp Table 1). High AGE serum levels have been lately established to diagnose diminished fertility (52) and have been associated to infertility-related diseases (52). While our data disclose a significant positive correlation between age and AGE-tissue levels at TBCK (r= 0.766; p=0.0009), SLITRK4 (r=0.707; p=0.00032) and HSPA8 (r=0.554; p=0.0322), we also found an age-independant variation in AGE at HDLBP (r=-0.198; p=0.4800) and KIAA0319L (r=-0.317; p=0.2489). Thus our results reveal specifically potential targets affected by AGE during aging, which complements the depicted ovarian phenotype during menopause and may prompt more precise diagnosis of infertility and premature ovarian aging.

Matrisome and cellular protein interaction

We relied on pathway studio and its NLP technology to study all possible bidirectional regulation occurring between each of the 26 matrisome biomarkers and members of Hippo or mammalian target of rapamycin (mTOR) signaling pathways. This was necessary to understand the possible interaction of ovarian matrisome biomarkers with these key signaling pathways related to fertility and follicle activation and development. All connections were manually supervised and curated to select the most relevant relationships between the matrisome and cellular proteins.

The mTOR signaling, known as a regulator of cell growth and proliferation, is a crucial mediator of primordial follicle activation via the Akt pathway in mice (53-56). Activated mTOR works upstream of Akt and promotes Akt phosphorylation, leading to the suppression of FOXO3 nuclear transcription, responsible of follicle activation. MAPK3/1 signaling also participates in primordial follicle activation through downstream mTORC1-KITL. While these findings do not consider the implication of ovarian ECM, there is one study in mouse that bridges ECM to follicle activation signaling, through demonstrating that fragmentation of ovaries promotes follicle growth (46). This effect was correlated with Hippo pathway disruption due to increased actin polymerization (conversion of G-Actin to F-Actin), which results in accumulation of yes-associated protein (YAP) in the nucleus (46). The transcription factor YAP upregulates the expression of CCN growth factors that modulate follicle growth and oocyte maturation (46). Nevertheless, until our study, the Hippo pathway was not linked directly to matrisome proteins. Our analytical method revealed all the possible interactions between matrisomal biomarkers at each age and their targets at both Hippo and mTOR pathways.

Hippo pathway

In the prepubertal ovarian tissue, we found inhibitors of Hippo pathway (COL6A3 and FBLN5) at the matrisome level, possibly implicated in follicle activation, which stimulate YAP activation (Table 2, Supp Fig. 1, Supp Table 2). Interestingly, most ovarian matrisome proteins appear to interact with the Hippo pathway through E-cadherin, a major regulator of the Wnt/β-catenin signaling pathway. For instance, upregulated TGFBI and OGN during prepuberty lead to downregulation of E-cadherin and β-catenin stabilization and its nuclear localization, which stimulate Wnt/β-catenin activity. Knowing that Wnt/β-catenin has been previously described as hampering follicle activation and development (57, 58), TGFBI and OGN can be consequently

considered as potential inhibitors of follicle activation (Table 2, Supp Fig. 1, Supp Table 2).

Upon puberty, upregulation of GPC6 declines Wnt/β-catenin signaling, promoting follicle activation, while an upregulated AGT activates the renin-angiotensin system (RAS) that has been related to oocyte maturation and its quality regulation (59). Similarly, high levels of S100A6 and ANXA1 in reproductive-age and menopausal patients compared to prepubertal ones are linked to alterations in tight junction assembly and E-cadherin stability, which may weaken the interaction between E-cadherin and β-catenin at the membrane and leads to the translocation of the latter to the nucleus, consequently activating the repressive effect of Wnt/β-catenin signaling on follicles (Table 2, Supp Fig. 1, Supp Table 2).

In humans, this resting state could last for decades, and some follicles, although scarce, may stay in a dormant state even after menopause. Although upregulation of F2 can promote TAZ activation and consequently follicle recruitment, we noticed that SERPINA1 upregulation also alters tight junctions and E-cadherin as it activates PP2A too. PP2A, as one of the most complex Ser/Thr phosphatases (Table 2, Supp Fig. 1, Supp Table 2), was demonstrated to have promiscuous activity resulting in dephosphorylation of proteins involved in a diverse range of biological processes such as cell cycle progression and cell death (60). Since PP2A acts as an oncogenic or tumor suppressor, depending on its subunit and substrate, it is hard to predict whether the menopausal matrisome may have precursors of follicle activation.

mTOR pathway

During prepuberty, several matrisomal biomarkers (COL6A1, POSTN, and FBLN5) interact with the mTOR signaling pathway and activate Akt and

potentially participate in follicle activation (Table 2, Supp Fig. 2, Supp Table 2). In contrast, the interaction between OGN and mTOR signaling further proves that OGN is a negative regulator of follicle activation. Indeed, OGN negatively regulates Akt activity and blocks cytoskeletal remodeling, limiting the formation of F-actin, one of the hallmarks of follicle activation (46).

Upon puberty, mTOR activity is levitated under the overexpression of AGT. Common highly expressed ECM proteins between reproductive-age and menopausal patients such as S100A6 and ANXA1 appear to regulate follicle activation through pro and repressive actions by phosphorylation of MAPK, Akt, and FOXO3, and stimulation of actin-bundling on one side and activation of p53 (upstream repressor of mTOR) and downregulation of PI3K phosphorylation on the other (Table 2, Supp Fig. 2, Supp Table 2).

During menopause, p53 is also upregulated by ANXA5. Nevertheless, its action is restrained by COL18A1 (30). Another mTOR promoter during menopause is F2 which also activates its downstream target RPS6KB1 (p70) (Table 2, Supp Fig. 2, Supp Table 2).

Clearly, at each age, the human ovary has its intertwined processes for pro and anti-follicle activation, orchestrating ovarian homeostasis. Although the current results open a new world of opportunities for future investigations and possible clinical targets, experimental validation of the discussed processes will be paramount to decode activation of human ovarian follicles.

Localization and 3D distribution of matrisome biomarkers

To confirm the trends in the 26 ECM biomarker-expressions from the MS study and identify their 3D distribution and localization in the human ovarian tissue from prepuberty until menopause, we conducted immunofluorescence and tissue clearing with an ovary-tailored protocol, followed by light-sheet microscopy acquisition (Fig. 5). The 3D observations have revealed an

important heterogeneity in protein deposition within the same tissue (ANXA1, HPX) and between age groups (COL6A6). We noticed a markedly architectural remodeling in some ECM biomarkers (COL6A3, COL18A1, F2, ITIH4) and localization shifts (CSTB). Some proteins have been exclusively localized during prepuberty at the follicle level and appear to be expressed by oocyte or granulosa cells (AGT, SERPINC1, ANXA7), which delineate a local matrisomal homeostasis at the follicle periphery.

Overall, qualitatively, the immunofluorescence staining correlates well with and validates the MS data and further predicts possible ultrastructural changes in the 26 biomarkers with age that might reach protein function.

Clinical opportunities: matrisome proteins at the heart of precision medicineand fertility restoration

Chemotherapy has been known for its gonadotoxicity through several mecanisms by (i) having a direct detrimental effect on the DNA of primordial follicles constituting the ovarian reserve leading to apoptosis; (ii) induction of a massive growth of dormant follicles, which are then destroyed; or (ii) vascular ovarian damage (61). While our results highlight the involvement of matrisome proteins in the described cellular mechanisms (Fig. 2), chemotherapy gonadotoxicity has never been related to the follicle's microenvironment. Therefore, here we shed light on all the possible effects of chemodrugs on the 98 detected ovarian matrisomeproteins (detailed list of chemo-ECM interaction and drug's main targets andapplications could be found in Supp Table. 3). Thus, by improving our understanding of the mechanisms involved, we hope to mediate the development of solutions limiting the negative impact of chemotherapy on the ovarian reserve.

AGT is among the affected matrisome proteins with a characteristic expression level during reproductive-age. AGT expression could be

upregulated by Decitabine or Doxorubicin, both described as DNA-targeting drugs respectively prescribed for head and neck carcinoma, and breast cancer or neuroblastoma (62, 63) (Supp Table. 3). Conversely, AGT expression is inhibited by another DNA-targeting chemodrug, Actinomycin D (64), which is used for treating Ewing's sarcoma and uterine carcinoma. Clearly, chemodrugs have collateral effects beyond their main targets reaching matrisome proteins and leading to their abnormal expression which can affect ovarian homeostasis and negatively impact follicle reserve and fertility.

We have also studied all the possible interactions between the detected matrisome age fingerprints and drug-resistance, using again the NLP literature-mining technology (Fig. 8). We detected few ECM proteins that have been highly related to chemo-drug resistance (TGFBI, COL6A3, ANXA1/5/7, ITIH4, POSTN, F2). Moreover, these proteins have been upregulated at different ovarian stages (prepubertal, reproductive-age and menopausal), which reveals different responses of ovarian tissue to chemo-drugs according to these protein expression levels and prompts careful selection of cancer therapy according to patient age.

For instance, some studies have suggested that TGFBI, one of the matrisome proteins particularly upregulated during prepuberty, sensitizes ovarian cancer cells to Paclitaxel by inducing microtubule stabilization and that the loss of TGFBI induces drug resistance and mitotic spindle abnormalities in ovarian cancer cells (65). Another protein exclusively upregulated during prepuberty is POSTN, which has been associated to the induction of chemoresistance of colorectal cancer cells by activating Pi3k/Akt/survivin signalling pathway, while POSTN silencing could reverse chemoresistance in pancreatic cancer (66) (Fig. 2,8). During menopause, we

have detected a unique high level of ANXA5 expression. This protein was also associated to chemoresistance to Telozolomide in glioblastoma through a PI3K dependant mechanism (67).

In the light of current results, it is tempting to think of therapeutic solutions targeting the expression of matrisome proteins to counter chemo-drug toxicity at the follicle level or chemo-resistance. However, the over-expression of some ECM proteins beyond their homeostatic level during reproductive age may lead to ovarian pathologies such as PCOS (Fig. 8b), despite their upregulation during prepuberty or menopause (ANXA5, POSTN, SERPINA1). This points to potential risks related to ECM-targeted therapies and prompts in-depth validations and safety monitoring in vitro and in vivo.

Discussion

Due to the difficulty in obtaining human ovarian tissue, it has been challenging to determine the human ovarian cortex proteomics. Moreover, the fibrous nature of human ovarian ECM makes the pursuit of reliable proteomic characterization strewn with obstacles (17). Thanks to our DC-MaP protocol for TMT-based matrisome proteomics and our adopted reproducible workflow for analyzing extracted fractions, we could capture the fullest picture of intra- and extracellular proteins (17) (reproducibility of samples within each group is highlighted by pairwise Pearson's correlation analysis in Supp Fig. 3). Here, we present the first proteome-wide and matrisome-specific analysis of the human ovarian tissue at prepubertal, reproductive, and menopausal stages, providing unprecedented insights into the mechanisms by which human ovaries develop, reach reproductive competence, and age in normal conditions.

Among the main discoveries of our study is the dominant collagen type in

human ovarian tissue at all ages, COL6 (COL6A1, COL6A2, COL6A3 and COL6A6 identified respectively with 28, 22, 7 and 3 unique peptides), which confirms our previous label-free proteomic study of pre-menopausal ovarian tissue (68) and corrects an ancient thought, reporting that collagen type I was the dominant collagen type in human ovarian cortex (69, 70) and led to several related research using COL1A1 as a scaffold for 3D culture of ovarian follicles and cells (71-75). COL6 is an unusual member of the collagen family and has been studied in the past few years within the context of an extensive wide range of tissues. The distinctive feature of this protein is its unique supramolecular assembly, which is driven by a multi-step process that leads to the formation of the characteristic beaded microfilaments network in the ECM (76). COL6 exerts different roles in tissues, spanning from mechanical roles, typical of collagen components of the ECM, to more specific cytoprotective functions (mechanoprotection from compressive forces), including apoptosis and oxidative damage inhibition, cell differentiation and autophagic machinery regulation (77, 78). COL6 also has bridging and anchoring roles, facilitated through interactions with a wide variety of other ECM proteins, including other collagens, proteoglycans, fibronectin, and microfibril-associated proteins. Moreover, COL6 can bind to a range of cell surface receptors including integrins α1β1, α2β1, α3β1, α10β1 and αvβ1 (77) and thus regulate cell-ECM communication and may represent a communication platform between ovarian follicles and cells. Our temporal follow up of ovarian matrisome remodeling revealed COL6 as one of the matrisomal fingerprints of prepubertal ovarian tissue, where it is upregulated in synergy with autocrine and paracrine signaling accompanying prepubertal gonadal development. During prepuberty, the human ovarian tissue seems under high elastic structuration and remodeling by FBLN5, POST, TNXB, preparing the ovary for its later stages. While COL14A1, HRNR, NID1 and COL6 participate in ovarian follicle dormancy,

high expression of OGN, POSTN, and TGFBI stimulate atresia. Both events are characteristic of prepubertal ovaries: while follicle dormancy preserves the ovarian reserve for reproductive-age life, follicle atresia might be a selective process for keeping the most competent follicles (79). In addition, as we suggested before (80), prepubertal matrisome seems non-permissive to follicle activation from biochemical and mechanical perspectives. At the intracellular level, highly expressed proteins distinguishing the prepubertal ovaries from their age counterparts highlight an intense regulatory process for the elimination of abnormal cells through mitochondrial damage (PARP1, MIF, VDAC1, SLC25A4, and UTRN) and clearing of nonsense mRNA decay (DDX1, RPS3, RPL30, PTBP1, and RPS14).

Upon puberty, only two ECM proteins separate reproductive-age ovaries from infant and menopausal counterparts: AGT and GPC6. AGT is a member of RAS signaling, which regulates oocyte maturation and quality and participates in critical physiological events during ovulation and luteinization (59). Its production is strongly influenced by estrogens (81), highly secreted by growing follicles at reproductive-age. Naturally, deregulation in AGT expression might trigger pathological conditions. Indeed, while AGT deficiency is associated with a decreased fertility (82), RAS enhanced activity is associated with PCOS (83).

The second matrisomal fertility biomarker is the glycoprotein GPC6, a regulator of heparin-binding growth factors such as FGFs, BMPs, Wnts, Hhs and IGF and has been associated to development, morphogenesis and cell proliferation (84). It appears to be a very promising fertility biomarker, although its real implication in ovarian activity is still undercovered. Our neural network model further highlights the high influence of GPC6 quantitative variations on the rest of ovarian matrisome protein expression. At the intracellular level, among the 45 upregulated proteins during

reproductive age, many were implicated in nonsense mRNA decay (HNRNPL and TPI1), proper protein folding (P4HB, CALU, GPI, CALR and TPI1) and senescence prevention (HNRNPD, ENO1, and FSCN1), highlighting the necessity of ubiquitous transcriptional as well as translational corrections to maintain normal ovarian function.

During reproductive life, the ovary undergoes continuous cyclic changes related to follicular development, requiring, therefore, continual angiogenesis (85), a process also promoted by AGT and GPC6. Nevertheless, upon menopause, the upregulation of COL18 corroborates with an important feature of aging, which is the marked reduction of the ovarian vascular network (86). Indeed, a proteolytic fragment of COL18, endostatin, can downregulate VEGF-A and HIF-1α (upstream factor of VEGF-A), inhibiting endothelial cell proliferation and hence negatively regulating angiogenesis (87).

On the other side, processes related to ECM remodeling and fibrosis were enriched with upregulated menopausal biomarkers at the matrisome level. Indeed, at this stage, the human ovary contains very few remaining follicles. Hence, follicular space has been consequently replaced by neo- synthetized ECM, which sustains previous studies reporting age-relatedf ibrosis (ANXA5, F2, ITIH4 and SERPINA1) in the human ovary (35). Interestingly, the same matrisomal biomarkers of menopausal tissue implicated in fibrosis also play an essential protective role ranging from preventing ROS generation and cell damage to preventing heme toxicity (Fig. 6). Indeed, upregulated HPX during menopause plays a protectant role against hemoglobin (Hb)-derived heme toxicity resulting in ROS generation as well as mitigating heme-mediated effects on immune cells (88) that collectively contribute to driving inflammation (88) (Fig. 6). At the intracellular level, although markers of DNA fragmentation (PRF1 and IAPP),ROS generation (AOX1, PRF1, and CLIC1)

and senescence (ARID4A, ZYX, and RBP1) were detected, proteins with cytoprotective roles, preventing DNA damage (PKM and PRDX6), oxidative-stress and ROS generation were also quantified (DDT, DBI, PSME1 and SLPI) (Fig. 7). ROS has been considered as the most prominent molecular species involved in the aging process (89). Indeed, all studies describing aging process in different organs, including ovaries, have related aging to downregulation of anti-oxidative stress pathways and/or ROS upregulation (90). By contrast, our results reveal unique menopausal proteins with an anti-oxidative stress activity and highlight highly expressed proteins during adult life fighting ROS generation inside-out the cells that increase with age (Fig. 6 and 7). Although cytoprotective anti-oxidative stress proteins detected in menopausal group are more numerous than their antagonists, we still unaware of their appropriate activity and function to counterbalance the ROS generation also detected during aging, which prompts further investigations.

Inflamm-aging is another hypothesis relating ovarian aging to inflammation (91). In recent years, an increasing number of studies have found that inflammation is associated with the occurrence of aging, where tissues and organs are accompanied by a chronic, progressive proinflammatory state (92-94). Interestingly, ovulation is an inflammation-like process during which the ovarian balance is achieved through proinflammatory action mediated by cytokines and negative feedback from anti-inflammatory cytokines, accompanied by leukocyte recruitment (48). Hence, while it is not surprising to find proinflammatory proteins in reproductive age ovaries, some were equally expressed in menopausal ovaries (PSMB6, B2M) and others increased with age (CSRP1, IAPP, TSPO, PKM). In addition, detected high levels of AGEs at TBCK, SLITRK4 and HSPA8 activate intracellular multiple inflammatory signaling pathways (95), which corroborates to the inflamm-aging hypothesis.

More surprising about the menopausal ovarian tissue is the upregulation of proteins related to cytokinesis and cell proliferation, and even follicle activation. Thus, ovarian aging is not only associated with follicle senescence and prolonged dormancy of residual follicles, but it is also possibly related to inappropriate communication between menopausal microenvironment since follicles are hardly activated during menopause (96) despite the presence of several clues for their activation. This miscommunication can be attributed to collagen hypo-hydroxylation during menopause. Indeed, collagen hydroxylation promotes interactions with cellular collagen receptors, such as integrins and discoidin domain receptors, in both direct and indirect manners (38). Moreover, proline hydroxylation may regulate the flexibility of collagen molecules and make functional sites available for interacting proteins (38). Our previous findings also revealed that ovarian tissue aging is accompanied by tremendous architectural changes (51), limiting its porosity, which may hamper glucose, oxygen, and small molecule (cytokines, calcium) diffusion toward the ovarian cells. This would limit regulation of cellular processes that depend on these elements and bidirectional ECM-intracellular protein interactions.

At all stages of ovarian life, we have noted stimulatory and inhibitory proteins, mediating follicle activation or preventing it, namely at the level of mTOR and Hippo pathway to maintain homeostasis. Walter B. Cannon, originator of the concept of homeostasis, said in his book Wisdom of the Body, ‘‘when a factor is known which can shift a homeostatic state in one direction it is reasonable to look for a factor or factors having an opposing effect.’’ (97) But are these opposing factors at work all the time, or at least in some circumstances, might one factor prevail over the other and cause the rupture of homeostasis leading to pathology?

Indeed, overexpression of AGT, SERPINA1, SERPINC1, POSTN, ANXA5 or

F2 in PCOS compared to healthy patients is the best illustration of the importance of matrisome components harmonization at each age to comply with the ovarian physiological function at all stages of life (Fig. 8). This harmonization is described and effortlessly sensed by our data sonification technique orchestrating matrisome equilibrium and homeostatic remodeling from prepuberty til menopause. A disturbance of this equilibrium should change the generated expression melodies and alert of a potential pathological condition. Therefore, we forsee the potential of such sonification technique in propelling MS use from the laboratory to the operating room by overcoming the difficulty of complex data processing and interpretation. This technique can be complementary to the emerging in vivo-MS and may be used to pinpoint markers of cancer in a living patient's tissue during surgery, without having to wait for the pathology report that can take up to 45 risky minutes under anesthesia (98).

We believe that by dissecting the complexity of ovarian ECM in normal tissue throughout distinct developmental time points, our study provides important context for healthy ovarian physiology, identifying and characterizing disease states and recapitulating physiological tissues or development in vitro. To better understand the usefulness of ECM for regenerative medicine and tissue engineering applications, it is essential to have a more complete and comprehensive understanding of the ECM within normal, native tissue. Human ovarian matrisome until this day has remained incomplete and prevailed by knowledge built on animal models. Our data fill this gap and reveal potential biomarker candidates. Indeed, while highly expressed matrisome proteins at reproductive age can be promising candidates of fertility biomarkers at the ovarian tissue level, upregulated proteins during menopause could be considered as potential ovarian aging biomarkers.

This information may help the tremendous efforts that have been made to understand the increasing rate of female infertility, one of the top highest global disabilities of our era (99).

Currently, the expanding cure rate of cancer has led to a vast population of survivors facing the late adverse effects of oncological treatments, with fertility impairment being one of the most sensitive issues for patients (100). While ECM and intracellular mechanisms are tightly related, data on gonadotoxic effects of cancer therapies on ovarian tissue only describes intracellular signaling effects. Therefore, our study shows possible interactions between FDA-approved chemodrugs (21) and matrisome proteins based on NLP technology. Our goal is to help understanding how chemotherapy can affect differently ovarian cell microenvironment in an age-dependent manner, leading to different alterations depending on the treatment type and the patient age (Supp Table 3). Furthermore, many differently detected matrisome proteins have a chemoresistant-effect (TGFBI, COL6A3, ANXA7 and POSTN overexpressed in prepubertal tissue, ANXA1 equally expressed in reproductive-age and menopausal tissue and ITIH4, ANXA5, and F2 upregulated at menopause), which might jeopardize the efficacy of prescribed cancer-treatment depending on the patient-age and its corresponding matrisome (Fig. 8). Comprehensive knowledge of the possible mechanisms implicated in chemotherapy-induced ovarian damage will facilitate the development of new therapies, called fertoprotective agents (101), aimed at protecting the follicular reserve. In this context, our findings pave the way for better-personalized oncology treatments and open new possibilities in oncofertility by providing a blueprint of the ovarian tissue toward creating new fertility restoration treatments for cancer patients such as functional bio-inspired engineered ovary mimicking the features of healthy reproductive-age tissue, the gold standard of fertility. Moreover, we provide the first interactive model of ovarian matrisome that can predict the

probability of a specific ovarian tissue matrisome to resemble prepubertal, reproductive-age, or menopausal tissue. This could be in the future a predictor of fertility potential, premature aging, or even an evaluation tool of the efficiency of ovarian rejuvenation or fertility restoration solutions acting at the level of the ECM. This model represents the first sparkle in computed gynecology and could become more robust by gradually introducing a higher number of analyzed healthy ovarian tissue.

At the intersection of fiber and cell theories, our study complements our knowledge of the human ovary during the female life and open new avenues in gynecology research and oncofertility practice (Supp Table 4). Our analytical method can be easily adapted to achieve a large-scale and in-depth quantitative analysis of ECM-containing proteome in other biological systems with relatively straightforward operations and low cost.

References

1. K. A. Piez, History of extracellular matrix: a personal view. Matrix biology : journal of the International Society for Matrix Biology 16, 85-92 (1997).
2. P. Klemperer, The significance of the intermediate substances of the connective tissue in human disease. Harvey lectures 49, 100-123 (1953).
3. U. Rokitansky-Tilscher, Carl Freiherr von Rokitansky's Manual and Rudolf Virchow's criticism: The controversial subject of Rokitansky's doctrine of crases and dyscrases and the groundwork for modern humoral pathology. Wiener Medizinische Wochenschrift 170, 284-289 (2020).
4. D. Ribatti, An historical note on the cell theory. Experimental Cell Research 364, 1-4 (2018).
5. A. Lopata, History of the Egg in Embryology. Journal of Mammalian Ova Research, 2-9, 8 (2009).
6. H. M. Brown, K. R. Dunning, R. L. Robker, M. Pritchard, D. L. Russell, Requirement for ADAMTS-1 in extracellular matrix remodeling during ovarian folliculogenesis and lymphangiogenesis. Developmental Biology 300, 699-709 (2006).

7. C. Philippart, R. Masciangelo, A. Camboni, J. Donnez, M.-M. Dolmans, Basal lamina characterization in frozen-thawed and long-term grafted human prepubertal ovarian tissue. Reproductive BioMedicine Online 42, 859-869 (2021).

8. H. F. Irving-Rodgers, K. Hummitzsch, L. S. Murdiyarso, W. M. Bonner, Y. Sado, Y. Ninomiya, J. R. Couchman, L. M. Sorokin, R. J.Rodgers, Dynamics of extracellular matrix in ovarian follicles and corpora lutea of mice.Cell and Tissue Research 339, 613-624 (2010).

9. R. Jiménez, Ovarian Organogenesis in Mammals: Mice Cannot Tell Us Everything. Sexual Development 3, 291-301 (2009).

10. A. Naba, S. Ricard-Blum, in Extracellular Matrix Omics, S. Ricard- Blum, Ed. (Springer International Publishing, Cham, 2020), pp. 1-16.

11. C. Ludwig, L. Gillet, G. Rosenberger, S. Amon, B. C. Collins, R. Aebersold, Data-independent acquisition-based SWATH-MS for quantitative proteomics: a tutorial. 14, e8126 (2018).

12. S. Hosseininia, P. Önnerfjord, L. E. Dahlberg, Targeted proteomics of hip articular cartilage in OA and fracture patients. 37, 131-135 (2019).

13. F. Liu, D. T. S. Rijkers, H. Post, A. J. R. Heck, Proteome-wide profiling of protein assemblies by cross-linking mass spectrometry. Nature Methods 12, 1179-1184 (2015).

14. L. R. Schmitt, R. Henderson, A. Barrett, Z. Darula, A. Issaian, A. D'Alessandro, N. Clendenen, K. C. Hansen, Mass spectrometry–based molecular mapping of native FXIIIa cross-links in insoluble fibrin clots. Journal of Biological Chemistry 294, 8773-8778 (2019).

15. T. Basak, L. Vega-Montoto, L. J. Zimmerman, D. L. Tabb, B. G. Hudson, R. M. Vanacore, Comprehensive Characterization of Glycosylation and Hydroxylation of Basement Membrane Collagen IV by High-Resolution Mass Spectrometry. Journal of Proteome Research 15, 245-258 (2016).

16. A. Naba, K. R. Clauser, H. Ding, C. A. Whittaker, S. A. Carr, R. O. Hynes, The extracellular matrix: Tools and insights for the "omics" era. Matrix Biology 49, 10-24 (2016).

17. E. Ouni, S. P. d. Ruys, M.-M. Dolmans, G. Herinckx, D. Vertommen, C. A. Amorim, Divide-and-Conquer Matrisome Protein (DC-MaP) Strategy: An MS-Friendly Approach to Proteomic Matrisome Characterization. 21, 9141 (2020).

18. A. Nikitin, S. Egorov, N. Daraselia, I. Mazo, Pathway studio—the analysis and navigation of molecular networks. Bioinformatics 19, 2155-2157 (2003).

19. A. P. Amorim Andrade Christiani, Ouni Emna, Vilela Janice, Camboni Alexandra, Chiti Maria Costanza., in Female and Male Fertility Preservation, P. P. Grynberg Michael, Ed. (Springer, 2021).

20. C. A. Amorim, A. Van Langendonckt, A. David, M. M. Dolmans, J. Donnez, Survival of human pre-antral follicles after cryopreservation of ovarian tissue, follicular isolation and in vitro culture in a calcium alginate matrix. Hum Reprod 24, 92-99 (2009).

21. J. Sun, Q. Wei, Y. Zhou, J. Wang, Q. Liu, H. Xu, A systematic analysisof FDA-approved anticancer drugs. BMC systems biology 11, 87 (2017).

22. S. Novichkova, S. Egorov, N. Daraselia, MedScan, a natural language processing engine for MEDLINE abstracts. *Bioinformatics* **19**, 1699-1706 (2003).

23. Y. Perez-Riverol, A. Csordas, J. Bai, M. Bernal-Llinares, S. Hewapathirana, D. J. Kundu, A. Inuganti, J. Griss, G. Mayer, M. Eisenacher,E. Perez, J. Uszkoreit, J. Pfeuffer, T. Sachsenberg, S. Yilmaz, S. Tiwary, J. Cox, E. Audain, M. Walzer, A. F. Jarnuczak, T. Ternent, A. Brazma, J. A. Vizcaino, The PRIDE database and related tools and resources in 2019: improving support for quantification data. Nucleic AcidsRes 47, D442-D450(2019).

24. M. Ruehl, U. Erben, D. Schuppan, C. Wagner, A. Zeller, C. Freise, H.Al-Hasani, M. Loesekann, M. Notter, B. M. Wittig, M. Zeitz, W. Dieterich, R. Somasundaram, The elongated first fibronectin type III domain of collagen XIV is an inducer of quiescence and differentiation in fibroblasts and preadipocytes. J Biol Chem 280, 38537-38543 (2005).

25. T. W. Kelsey, P. Wright, S. M. Nelson, R. A. Anderson, W. H. Wallace,A validated model of serum anti-mullerian hormone from conception to menopause. PloS one 6, e22024 (2011).

26. K. Ozegowska, A. Bogacz, J. Bartkowiak-Wieczorek, A. Seremak-Mrozikiewicz, L. Pawelczyk, Association between the angiotensin converting enzyme gene insertion/deletion polymorphism and metabolic disturbances in women with polycystic ovary syndrome. Mol Med Rep 14, 5401-5407 (2016).

27. Y. Yoshimura, The ovarian renin-angiotensin system in reproductive physiology. Front Neuroendocrinol 18, 247-291 (1997).

28. L. Cuiling, Y. Wei, H. Zhaoyuan, L. Yixun, Granulosa cell proliferation differentiation and its role in follicular development. Chinese Science Bulletin50, 2665 (2005).

29. C. Zeng, R. Yan, G. Yang, S. Xiang, F. Zhao, Hedgehog signaling activation required for glypican-6-mediated regulation of invasion, migration,and epithelial-mesenchymal transition of gastric cancer cells. Bioscience reports 40, (2020).H. F. Irving-Rodgers, R. J. Rodgers, Extracellular matrix in ovarian follicular development and disease. Cell Tissue Res 322, 89-98 (2005).

30. A. G. Marneros, B. R. Olsen, Physiological role of collagen XVIII andendostatin. 19, 716-728 (2005).

31. K. Klement, C. Melle, U. Murzik, S. Diekmann, J. Norgauer, P. Hemmerich, Accumulation of annexin A5 at the nuclear envelope is a biomarker of cellular aging. Mechanisms of ageing and development 133, 508-522 (2012).

32. M. Mela, W. Smeeton, S. E. Davies, E. Miranda, C. Scarpini, N. Coleman, G. J. M. Alexander, The Alpha-1 Antitrypsin Polymer Load Correlates With Hepatocyte Senescence, Fibrosis Stage and Liver-Related Mortality. Chronic Obstr Pulm Dis 7, 151-162 (2020).

33. H. Hasan, S. H. Park, C. Auger, E. Belcastro, K. Matsushita, B. Marchandot, H. H. Lee, A. W. Qureshi, G. Kauffenstein, P. Ohlmann, V. B. Schini-Kerth, L. Jesel, O. Morel, Thrombin Induces Angiotensin II-Mediated Senescence in Atrial Endothelial Cells: Impact on Pro-Remodeling Patterns.J Clin Med 8, (2019).

34. H. F. Irving-Rodgers, K. D. Catanzariti, W. J. Aspden, M. J. D'Occhio, R. J. Rodgers, Remodeling of extracellular matrix at ovulation of the bovine ovarian follicle. Molecular Reproduction and Development 73, 1292-1302 (2006).

36. S. M. Briley, S. Jasti, J. M. McCracken, J. E. Hornick, B. Fegley, M. T. Pritchard, F. E. Duncan, Reproductive age-associated fibrosis in the stroma of the mammalian ovary. Reproduction 152, 245-260 (2016).

37. S. Chen, D. E. Birk, The regulatory roles of small leucine-rich proteoglycans in extracellular matrix assembly. FEBS J 280, 2120-2137Natl Acad Sci U S A 110, 17474-17479 (2013).

38. K. Musselmann, B. Kane, B. Alexandrou, J. R. Hassell, Stimulation of Collagen Synthesis by Insulin and Proteoglycan Accumulation by Ascorbatein Bovine Keratocytes In Vitro. Investigative Ophthalmology & Visual Science47, 5260-5266 (2006).

39. P. Rappu, A. M. Salo, J. Myllyharju, J. Heino, Role of prolyl hydroxylation in the molecular interactions of collagens. Essays in biochemistry 63, 325-335 (2019).

40. R. C. Wilson, A. Shenhav, M. Straccia, J. D. Cohen, The Eighty Five Percent Rule for optimal learning. Nat Commun 10, 4646 (2019).

41. R. A. Anderson, M. McLaughlin, W. H. Wallace, D. F. Albertini, E. E. Telfer, The immature human ovary shows loss of abnormal follicles and increasing follicle developmental competence through childhood and adolescence. Hum Reprod 29, 97-106 (2014).

42. J. Zhou, X. Peng, S. Mei, Autophagy in Ovarian Follicular Development and Atresia. Int J Biol Sci 15, 726-737 (2019).

43. I. M. Sheldon, J. J. Bromfield, Innate immunity in the human endometrium and ovary. Am J Reprod Immunol 66 Suppl 1, 63-71 (2011).

44. D. F. Boyd, P. G. Thomas, Towards integrating extracellular matrix and immunological pathways. Cytokine 98, 79-86 (2017).

45. M. S. Jurica, G. A. Roybal, in Encyclopedia of Biological Chemistry (Second Edition), W. J. Lennarz, M. D. Lane, Eds. (Academic Press, Waltham, 2013), pp. 185-190.

46. X. Jiao, H. Ke, Y. Qin, Z.-J. Chen, Molecular Genetics of Premature Ovarian Insufficiency. Trends in Endocrinology & Metabolism 29, 795-807 (2018).

47. K. Kawamura, Y. Cheng, N. Suzuki, M. Deguchi, Y. Sato, S. Takae, C. H. Ho, N. Kawamura, M. Tamura, S. Hashimoto, Y. Sugishita, Y.Morimoto, Y. Hosoi, N. Yoshioka, B. Ishizuka, A. J. Hsueh, Hippo signaling disruption and Akt stimulation of ovarian follicles for infertility treatment. Proc Natl Acad Sci U S A 110, 17474-17479 (2013).

48. E. G. Pamer, Cellular immunity to intracellular bacteria. Current Opinion In Immunology 5, 492-496 (1993).

49. D. M. Duffy, C. Ko, M. Jo, M. Brannstrom, T. E. Curry, Ovulation: Parallels With Inflammatory Processes. Endocrine reviews 40, 369-416(2019).

50. R. G. Khalifah, J. W. Baynes, B. G. Hudson, Amadorins: novel post-Amadori inhibitors of advanced glycation reactions. Biochem Biophys Res Commun 257, 251-258 (1999).

51. C. Y. Ewald, The Matrisome during Aging and Longevity: A Systems-Level Approach toward Defining Matreotypes Promoting Healthy Aging. Gerontology 66, 266-274 (2020).

52. E. Ouni, A. Peaucelle, K. T. Haas, O. Van Kerk, M.-M. Dolmans, T. Tuuri, M. Otala, D. Vertommen, C. A. Amorim, A multi-scale readout of the microarchitecture, topography and mechanics of human ovary from prepuberty to menopause for the next generation of tissue engineered ovary and clinical diagnosis. Nature Communications (under review), (2021).

53. J.-l. Zhu, Y.-q. Cai, S.-l. Long, Z. Chen, Z.-c. Mo, The role of advanced glycation end products in human infertility. Life Sciences 255, 117830 (2020).

54. C. N. Cordeiro, M. S. Christianson, J. H. Selter, J. H. Segars, Jr., In Vitro Activation: A Possible New Frontier for Treatment of Primary Ovarian Insufficiency. Reproductive sciences (Thousand Oaks, Calif.) 23, 429-438 (2016).

55. Y. Cheng, Y. Feng, L. Jansson, Y. Sato, M. Deguchi, K. Kawamura, A. J. Hsueh, Actin polymerization-enhancing drugs promote ovarian follicle growth mediated by the Hippo signaling effector YAP. FASEB J 29, 423- 2430 (2015).

56. Y. Cheng, J. Kim, X. X. Li, A. J. Hsueh, Promotion of ovarian follicle growth following mTOR activation: synergistic effects of AKT stimulators. PloS one 10, e0117769 (2015).

57. Y. Tong, F. Li, Y. Lu, Y. Cao, J. Gao, J. Liu, Rapamycin-sensitive mTORC1 signaling is involved in physiological primordial follicle activation in mouse ovary. Mol Reprod Dev 80, 1018-1034 (2013).

58. L. Li, S. Y. Ji, J. L. Yang, X. X. Li, J. Zhang, Y. Zhang, Z. Y. Hu, Y. X. Liu, Wnt/β-catenin signaling regulates follicular development by modulating the expression of Foxo3a signaling components. Mol Cell Endocrinol 382, 915-925 (2014).

59. L. Li, S. Y. Ji, J. L. Yang, X. X. Li, J. Zhang, Y. Zhang, Z. Y. Hu, Y. X. Liu, Wnt/β-catenin signaling regulates follicular development by modulating the expression of Foxo3a signaling components. Mol Cell Endocrinol 382, 915-925 (2014).

60. A. D. Stapp, B. I. Gomez, C. A. Gifford, D. M. Hallford, J. A. Hernandez Gifford, Canonical WNT signaling inhibits follicle stimulating hormone mediated steroidogenesis in primary cultures of rat granulosa cells.PloS one 9, e86432 (2014).

61. D. Herr, I. Bekes, C. Wulff, Local Renin-Angiotensin system in the reproductive system. Front Endocrinol (Lausanne) 4, 150 (2013).

62. H. Yan, J. Wen, T. Zhang, W. Zheng, M. He, K. Huang, Q. Guo, Q. Chen, Y. Yang, G. Deng, J. Xu, Z. Wei, H. Zhang, G. Xia, C. Wang, Oocyte-derived E-cadherin acts as a multiple functional factor maintaining the primordial follicle pool in mice. Cell Death & Disease 10, 160 (2019).

63. C. Sonigo, I. Beau, N. Binart, M. Grynberg, The Impact ofChemotherapy on the Ovaries: Molecular Aspects and the Prevention of Ovarian Damage. Int J Mol Sci 20, (2019).

64. Y. Wang, K. G. Pringle, E. R. Lumbers, The effects of cyclic AMP, sex steroids and global hypomethylation on the expression of genes controlling the activity of the renin-angiotensin system in placental cell lines. Placenta 34, 275-280 (2013).

65. T. Takenaka, T. Inoue, T. Miyazaki, H. Kobori, A. Nishiyama, N. Ishii, M. Hayashi, H. Suzuki, Klotho suppresses the renin-angiotensin system in adriamycin nephropathy. Nephrol Dial Transplant 32, 791-800 (2017).

66. A. Abdul-Hafez, R. Shu, B. D. Uhal, JunD and HIF-1alpha mediate transcriptional activation of angiotensinogen by TGF-beta1 in human lung fibroblasts. FASEB J 23, 1655-1662 (2009).

67. B. Li, G. Wen, Y. Zhao, J. Tong, T. K. Hei, The role of TGFBI in mesothelioma and breast cancer: association with tumor suppression. BMC Cancer 12, 239 (2012).

68. Y. Liu, F. Li, F. Gao, L. Xing, P. Qin, X. Liang, J. Zhang, X. Qiao, L. Lin, Q. Zhao, L. Du, Periostin promotes the chemotherapy resistance to gemcitabine in pancreatic cancer. Tumour Biol 37, 15283-15291 (2016).

69. J. Tang, Z. Qin, P. Han, W. Wang, C. Yang, Z. Xu, R. Li, B. Liu, C. Qin, Z. Wang, M. Tang, W. Zhang, High Annexin A5 expression promotes tumor progression and poor prognosis in renal cell carcinoma. Int J Oncol 50, 1839-1847 (2017).

70. E. Ouni, D. Vertommen, M. C. Chiti, M. M. Dolmans, C. A. Amorim, A Draft Map of the Human Ovarian Proteome for Tissue Engineering and Clinical Applications. Mol Cell Proteomics 18, S159-S173 (2019).

71. T. K. Woodruff, L. D. Shea, The role of the extracellular matrix in ovarian follicle development. Reproductive sciences (Thousand Oaks, Calif.)14, 6-10 (2007).

72. C. B. Berkholtz, B. E. Lai, T. K. Woodruff, L. D. Shea, Distribution of extracellular matrix proteins type I collagen, type IV collagen, fibronectin, and laminin in mouse folliculogenesis. Histochemistry and Cell Biology 126, 583-592 (2006).

73. R. Abir, P. Roizman, B. Fisch, S. Nitke, E. Okon, R. Orvieto, Z. Ben Rafael, Pilot study of isolated early human follicles cultured in collagen gels for 24 hours. Human Reproduction 14, 1299-1301 (1999).

74. R. Abir, B. Fisch, S. Nitke, E. Okon, A. Raz, Z. Ben Rafael, Morphological study of fully and partially isolated early human follicles. FertilSteril 75, 141-146 (2001).

75. E. Telfer, C. Torrance, R. G. Gosden, Morphological study of cultured preantral ovarian follicles of mice after transplantation under the kidney capsule. J Reprod Fertil 89, 565-571 (1990).

76. J. Carroll, D. G. Whittingham, M. J. Wood, Effect of gonadotrophin environment on growth and development of isolated mouse primary ovarianfollicles. Journal of reproduction and fertility 93, 71-79 (1991).

77. S. Itami, K. Yasuda, Y. Yoshida, C. Matsui, S. Hashiura, A. Sakai, S. Tamotsu, Co-culturing of follicles with interstitial cells in collagen gel reproduce follicular development accompanied with theca cell layer formation. Reprod Biol Endocrinol 9, 159-159 (2011).

78. M. Cescon, F. Gattazzo, P. Chen, P. Bonaldo, Collagen VI at aglance. Journal of cell science 128, 3525-3531 (2015).

79. S. R. Lamandé, J. F. Bateman, Collagen VI disorders: Insights on form and function in the extracellular matrix and beyond. Matrix biology journal of the International Society for Matrix Biology 71-72, 348-367 (2018).

80. T. Neill, A. Kapoor, C. Xie, S. Buraschi, R. V. Iozzo, A functional outside-in signaling network of proteoglycans and matrix molecules regulating autophagy. Matrix biology : journal of the International Society for Matrix Biology, (2021).

81. P. Mermillod, R. Dalbiès-Tran, S. Uzbekova, A. Thélie, J. M. Traverso, C. Perreau, P. Papillier, P. Monget, Factors affecting oocyte quality: who is driving the follicle? Reproduction in domestic animals = Zuchthygiene 43 Suppl 2, 393-400 (2008).

82. E. Ouni, C. Bouzin, M. M. Dolmans, E. Marbaix, S. Pyr Dit Ruys, D. Vertommen, C. A. Amorim, Spatiotemporal changes in mechanical matrisome components of the human ovary from prepuberty to menopause. Hum Reprod 35, 1391-1410 (2020).

83. E. R. Lumbers, K. G. Pringle, Roles of the circulating renin- angiotensin-aldosterone system in human pregnancy. American journal of physiology. Regulatory, integrative and comparative physiology 306, R91- 101(2014).

84. C. B. Tempfer, R. M. Moreno, A. R. Gregg, Genetic Control of Fertility and Embryonic Waste in the Mouse: A Role for Angiotensinogen 1. Biology of Reproduction 62, 457-462 (2000).

85. S. A. Ye, S. Everman, E. D. Torres Fernandez, D. G. Romero, L. L. Yanes Cardozo, Renal Androgen and Renin Angiotensin System mRNA Expression in Polycystic Ovary Syndrome. FASEB J 34, 1-1 (2020).

86. J. Filmus, M. Capurro, J. Rast, Glypicans. Genome Biol 9, 224 (2008).

87. R. S. Robinson, K. J. Woad, A. J. Hammond, M. Laird, M. G. Hunter, G. E. Mann, Angiogenesis and vascular function in the ovary. Reproduction 138, 869-881 (2009).

88. D. A. Redmer, L. P. Reynolds, Angiogenesis in the ovary. Reviews of reproduction 1, 182-192 (1996).

89. C. H. Lin, J. Chen, Z. Zhang, G. V. Johnson, A. J. Cooper, J. Feola,A. Bank, J. Shein, H. J. Ruotsalainen, T. A. Pihlajaniemi, M. S. Goligorsky, Endostatin and transglutaminase 2 are involved in fibrosis of the aging kidney. Kidney international 89, 1281-1292 (2016).

90. L. Montecinos, J. D. Eskew, A. Smith, What Is Next in This "Age" of

Heme-Driven Pathology and Protection by Hemopexin? An Update and Links with Iron. Pharmaceuticals (Basel) 12, (2019).

91. D. Harman, Aging: a theory based on free radical and radiation chemistry. Journal of gerontology 11, 298-300 (1956).

92. S. Wang, Y. Zheng, J. Li, Y. Yu, W. Zhang, M. Song, Z. Liu, Z. Min, H. Hu, Y. Jing, X. He, L. Sun, L. Ma, C. R. Esteban, P. Chan, J. Qiao, Q. Zhou, J. C. Izpisua Belmonte, J. Qu, F. Tang, G.-H. Liu, Single-Cell Transcriptomic Atlas of Primate Ovarian Aging. Cell 180, 585-600.e519 (2020).

93. Y. Huang, C. Hu, H. Ye, R. Luo, X. Fu, X. Li, J. Huang, W. Chen, Y. Zheng, Inflamm-Aging: A New Mechanism Affecting Premature Ovarian Insufficiency. J Immunol Res 2019, 8069898-8069898 (2019).

94. F. Prattichizzo, L. Micolucci, M. Cricca, S. De Carolis, E. Mensà, A. Ceriello, A. D. Procopio, M. Bonafè, F. Olivieri, Exosome-based immunomodulation during aging: A nano-perspective on inflamm-aging.

Mechanisms of ageing and development 168, 44-53 (2017).

95. N. Thevaranjan, A. Puchta, C. Schulz, A. Naidoo, J. C. Szamosi, C.P. Verschoor, D. Loukov, L. P. Schenck, J. Jury, K. P. Foley, J. D. Schertzer, M. J. Larché, D. J. Davidson, E. F. Verdú, M. G. Surette, D. M. E. Bowdish, Age-Associated Microbial Dysbiosis Promotes Intestinal Permeability, Systemic Inflammation, and Macrophage Dysfunction. Cell host & microbe 21, 455-466.e454 (2017).

96. A. Salminen, J. Huuskonen, J. Ojala, A. Kauppinen, K. Kaarniranta,T. Suuronen, Activation of innate immunity system during aging: NF- kB signaling is the molecular culprit of inflamm-aging. Ageing research reviews7, 83-105 (2008).

97. D. Geroldi, C. Falcone, E. Emanuele, Soluble receptor for advanced glycation end products: from disease marker to potential therapeutic target. Curr Med Chem 13, 1971-1978 (2006).

98. M. Laszczyńska, A. Brodowska, A. Starczewski, M. Masiuk, J. Brodowski, Human postmenopausal ovary--hormonally inactive fibrous connective tissue or more? Histology and histopathology 23, 219-226 (2008).

99. C. WB, The Wisdom of the Body. Rev. and Enl. (Peter Smith Pub Inc,ed. Ed edition, 1963).

100. N. Ogrinc, P. Saudemont, J. Balog, Y.-M. Robin, J.-P. Gimeno, Q. Pascal, D. Tierny, Z. Takats, M. Salzet, I. Fournier, Water-assisted laser desorption/ionization mass spectrometry for minimally invasive in vivo and real-time surface analysis using SpiderMass. Nature Protocols 14, 3162- 3182 (2019).

101. World Health Organization, "World report on disability," (2011).

102. V. Pampanini, J. Hassan, E. Oliver, J. B. Stukenborg, P. Damdimopoulou, K. Jahnukainen, Fertility Preservation for Prepubertal Patients at Risk of Infertility: Present Status and Future Perspectives. Hormone research in paediatrics, 1-10 (2021).

103. T. K. Woodruff, A win-win for women's reproductive health: A nonsteroidal contraceptive and fertoprotective neoadjuvant. Proc Natl Acad Sci U S A 114, 2101-2102 (2017).

Acknowledgement

We thank the SMCS platform (Louvain Institute of Data Analysis and Modeling in Economics and Statistics, Université Catholique de Louvain) for their guidance and advice on the used statistical tests. We highly appreciate the help of Valentina Alabani and Elsa Seijnhaeve from the pathology department of Saint-Luc Clinique in collecting the fixed ovarian samples used in immunofluorescence. We are also thankful to Paolo Chiappa for his technical assistance with JMP Genomics software and Samy Memmi and Sergei Snovida from Thermo Fischer for their help with the experimental design using 16-plex TMT pro. We thank Proteintech for generously providing free antibody samples that have been used in immunofluorescence. We are grateful to Mira Hryniuk for reviewing the English language of the manuscript.

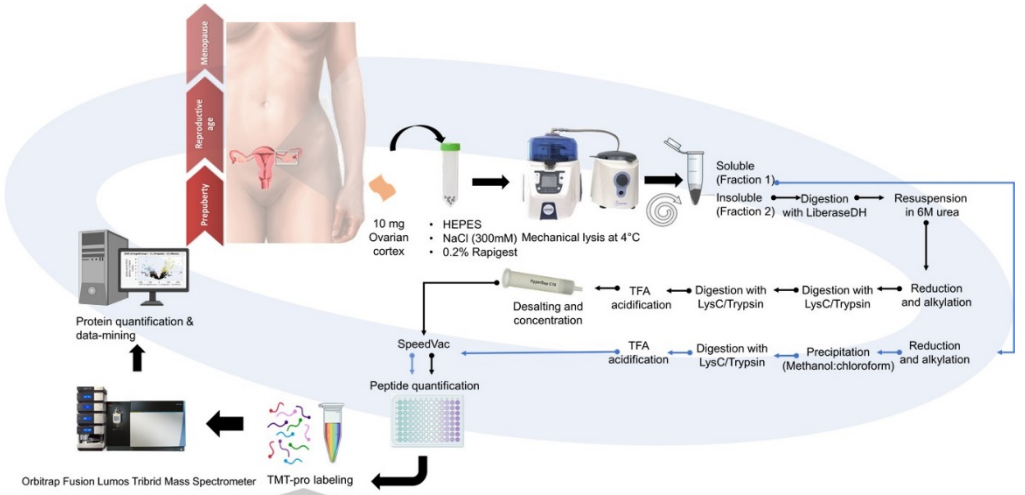
Funding

This study was supported by grants from the Fonds National de la Recherche Scientifique de Belgique (FNRS) (grant MIS #F4535 16 awarded to C. A.

Amorim), Université Catholique de Louvain (PhD grant ‘Coopération au développement’ awarded and ‘Mandats fin de thèse COVID’ to E. Ouni) and CooperSurgical and Planer for sponsoring part of the experimental expenses.

Competing interests

All authors have no competing interests to declare.



16-plex sample sets	Reporter 1	2	3	4	5	6	7	8	9	10	11	12	13	14	15	16
Set 1	A2	A1	A3	C2	B1	C3	B4	C5	A5	C1	B3	C4	A4	B5	B2	bridge
Set 2	C5	A4	B4	A3	B1	A2	C2	B5	B3	B2	C1	C4	A1	C3	A5	bridge

A1 : fraction 1 (soluble)
A1: fraction 2 (insoluble)

- 3 age groups (A, B, C)
- 5 patients per group = 15 samples (1-15)

Figure 1. Experimental workflow of quantitative analysis using the DC-MaP fractionation and TMT pro 16-plex isobaric labelling strategy.

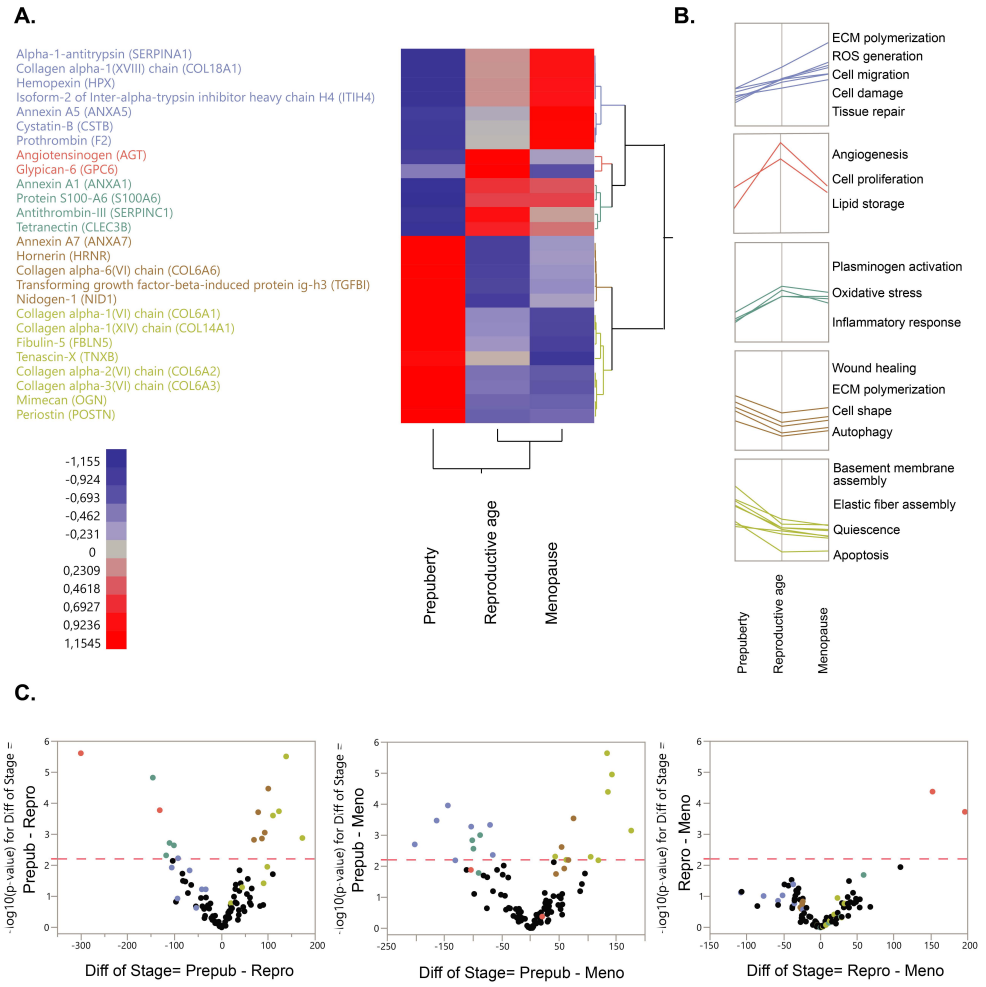


Figure 2. Ovarian matrisome remodeling throughout life. A. Hierarchical clustering of 26 matrisome proteins, with significantly different expression levels between prepubertal, reproductive-age and menopausal ovaries (one-way ANOVA, FDR<0.05). Five clusters of these proteins are depicted based on different intensity profiles. **B.** To decipher main cellular processes where each cluster is implicated, we used GSEA with a $p \leq 0.05$. Parallel plots highlight the protein expression tendency throughout age in each cluster.

C. Volcano plots showing pairwise comparisons of protein expression levels between various stages. Points above horizontal dashed lines represent significantly altered proteins (two-sided t test, p value < 0.05, p values were adjusted by Benjamini–Hochberg correction for multiple comparisons).

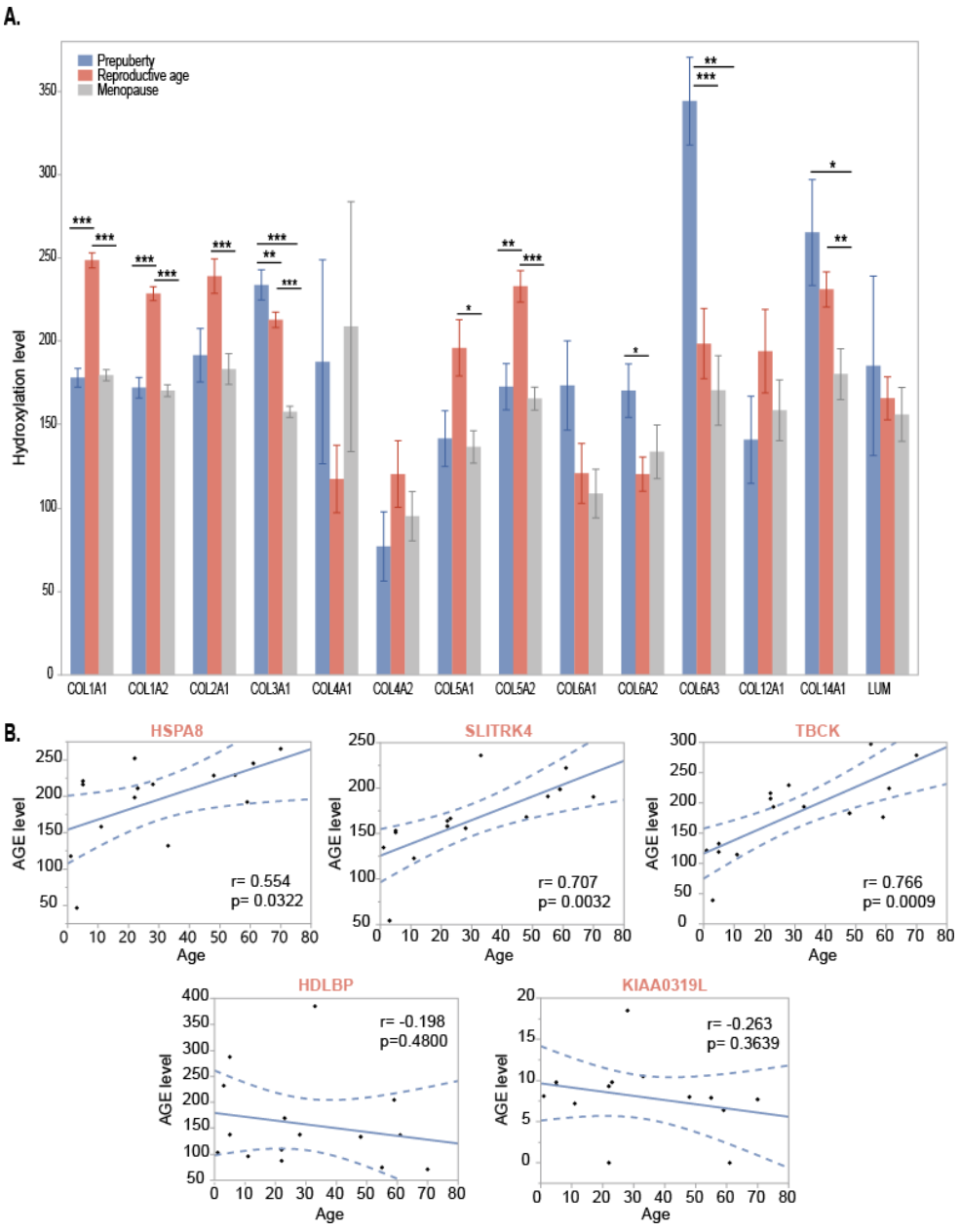


Figure 3. Postranscriptional modification at the extra-and intracellular compartments. A. Hydroxylation intensities. Histogram represents means and standard errors. **B.** Advanced glycation end products (AGEs) intensities

according to age. Pearson's correlation was used to study age- AGEs relationship. Kruskal- wallis test (post hoc: Tukey) was used to compare intensities between groups (*p<0.05, **p<0.01, ***p<0.001). Full statistical interactive reports with details on each modification position atevery data point can be found on (.html format): https://data.mendeley.com/datasets/nvjsyyg43h/draft?a=2565d0c7-4e1b-46a1-9de2- 2a96546c5f5d

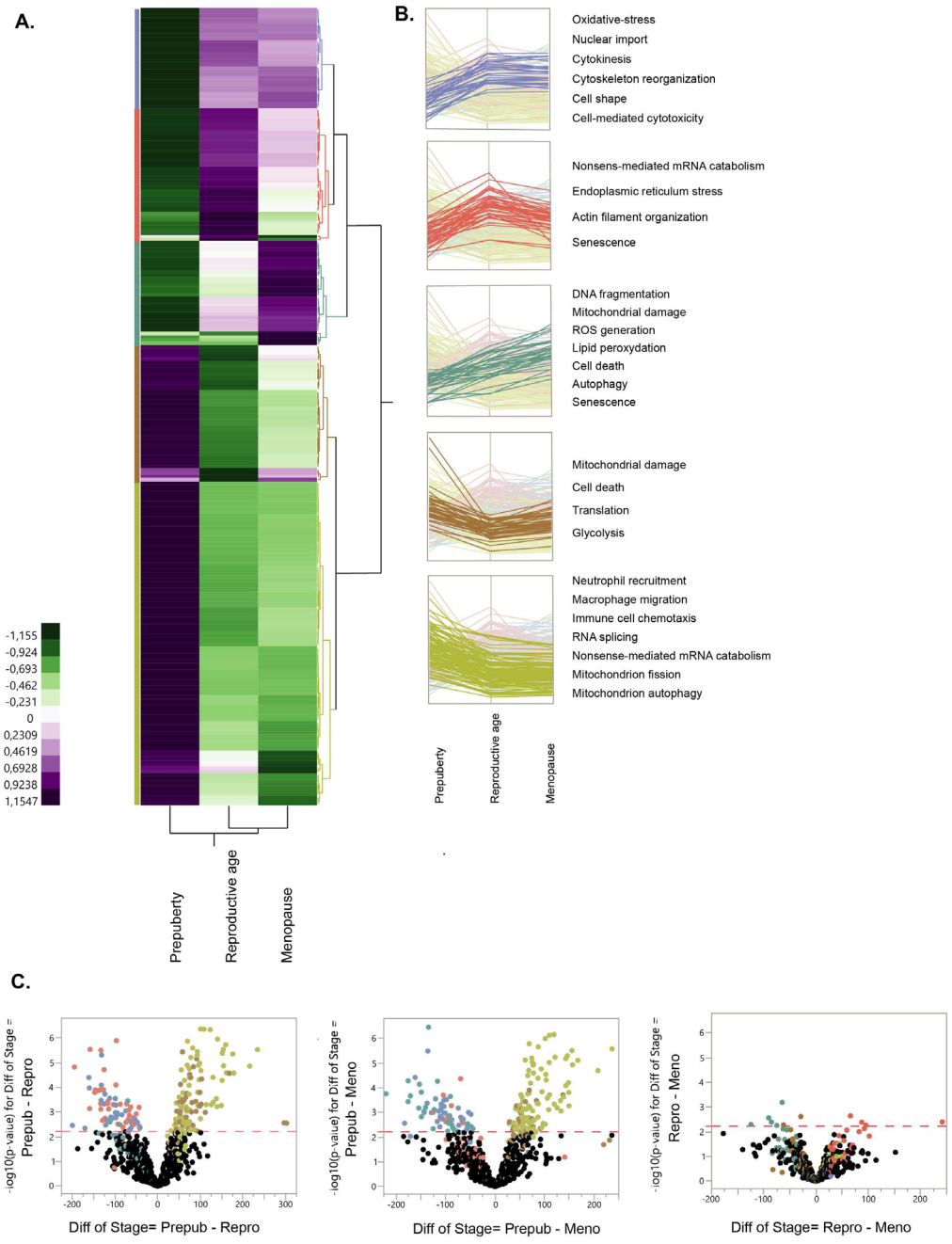


Figure 4. Cellular protein shift with age. A. Hierarchical clustering of 246 cellular proteins, with significantly different expression levels between

prepubertal, reproductive-age and menopausal ovaries (one-way ANOVA, FDR 0.05). Five clusters of these proteins are depicted based on different intensity profiles. **B.** To decipher main cellular processes where each cluster is implicated, we used GSEA with a p≤0.05. Parallel plots highlight the protein expression tendency throughout age in each cluster. **C.** Volcano plots showing pairwise comparisons of protein expression levels between various stages. Points above horizontal dashed lines represent significantly altered proteins (two-sided t test, p value < 0.05, p values were adjusted by Benjamini– Hochberg correction for multiple comparisons).

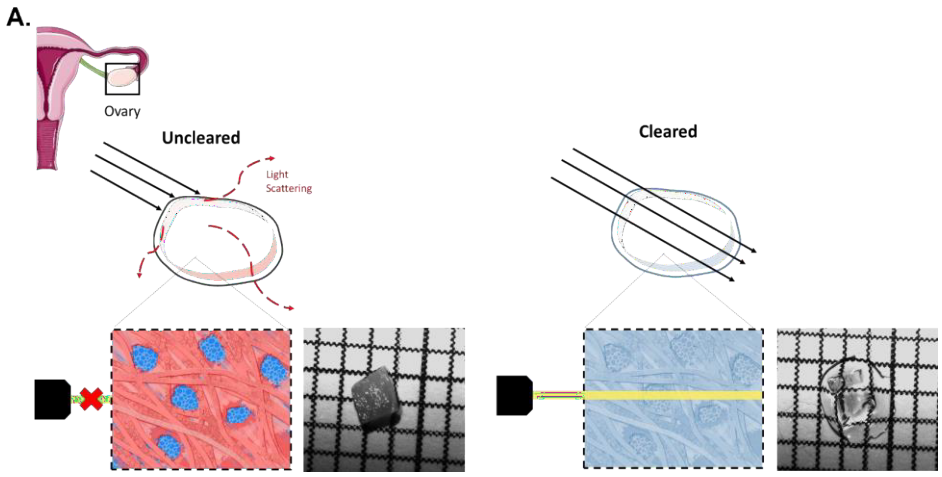
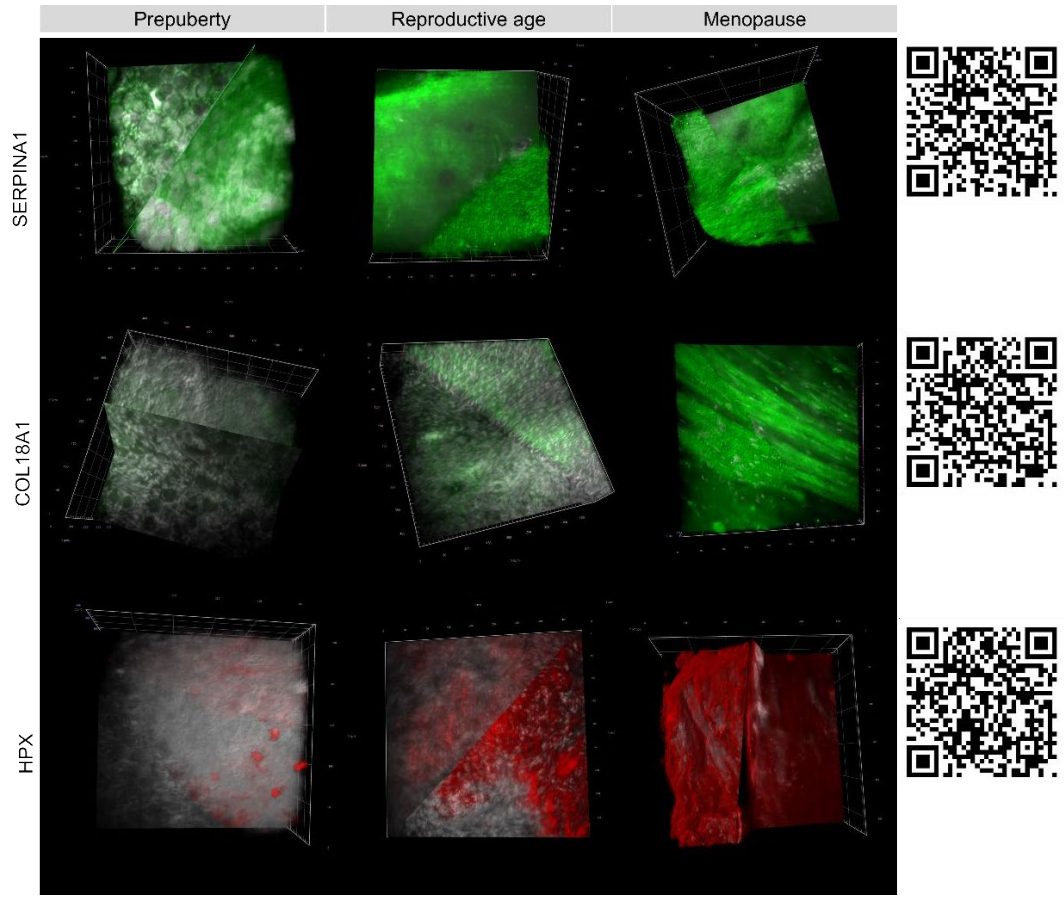
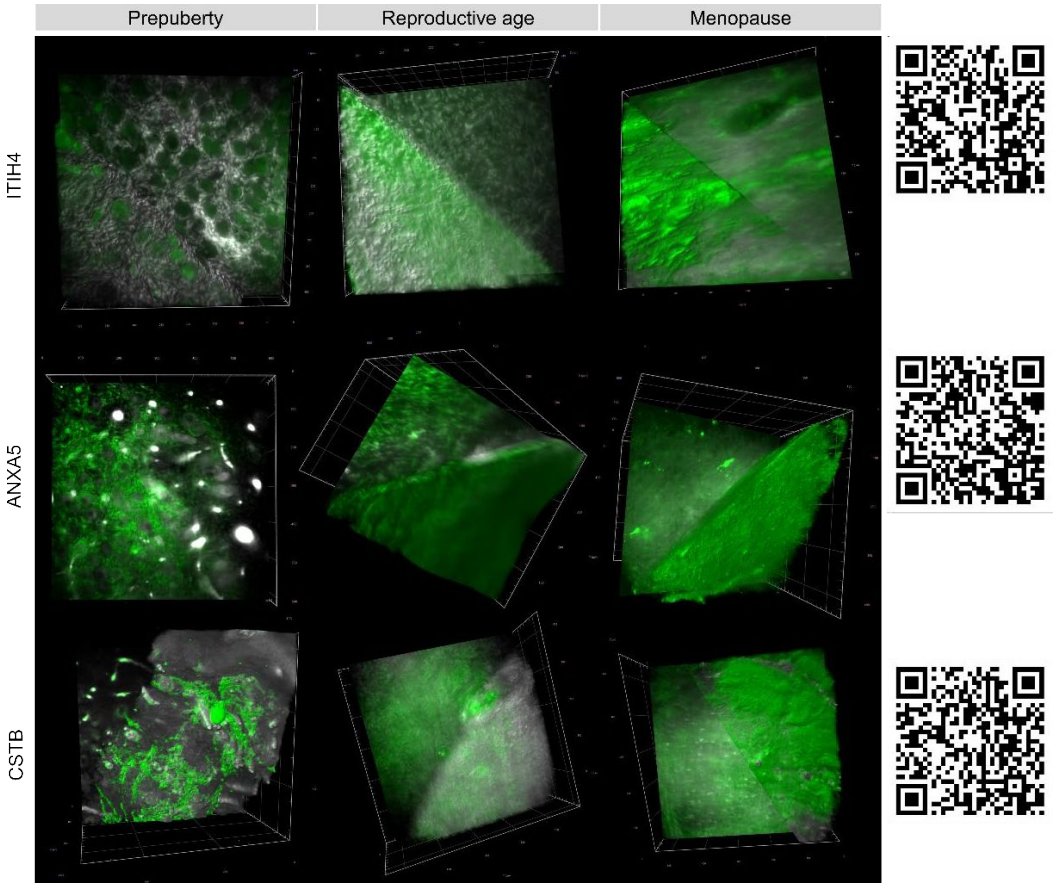


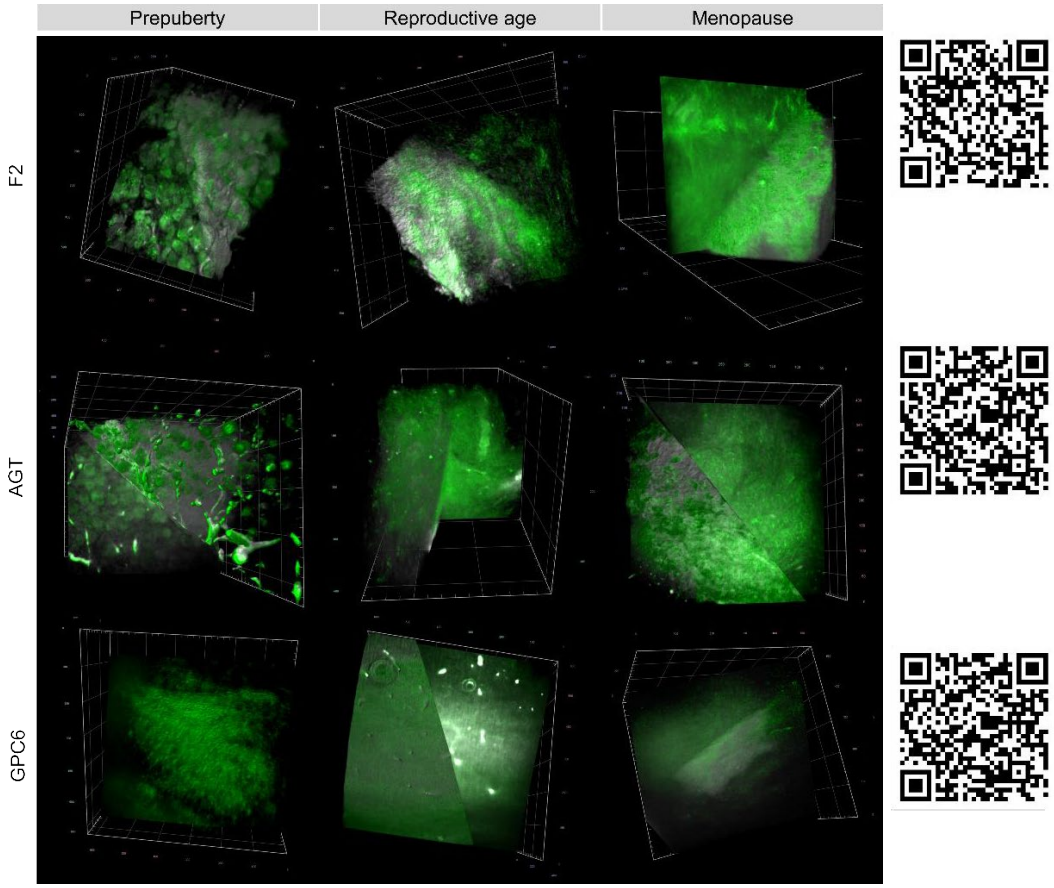
Figure 5. 3D visualization of ECM biomarkers through cleared ovarian tissues. A. The need for volumetric imaging of ovarian tissue is related to the inherent three-dimensional structure of its cells and ECM. But even with the advent of optical sectioning, this has remained a challenge when it comes to imaging thick tissues. Tissue opacity undermines sharp images and represents an impediment for volumetric observations. This inherent opacity is caused by light scattering. Light rays that should travel in straight lines are deviated many times as light is reflected off of molecules, membranes, organelles, and cells in the tissue. Therefore, we used our tissue clearing method to assure that there is a high uniform density of scatterers so that

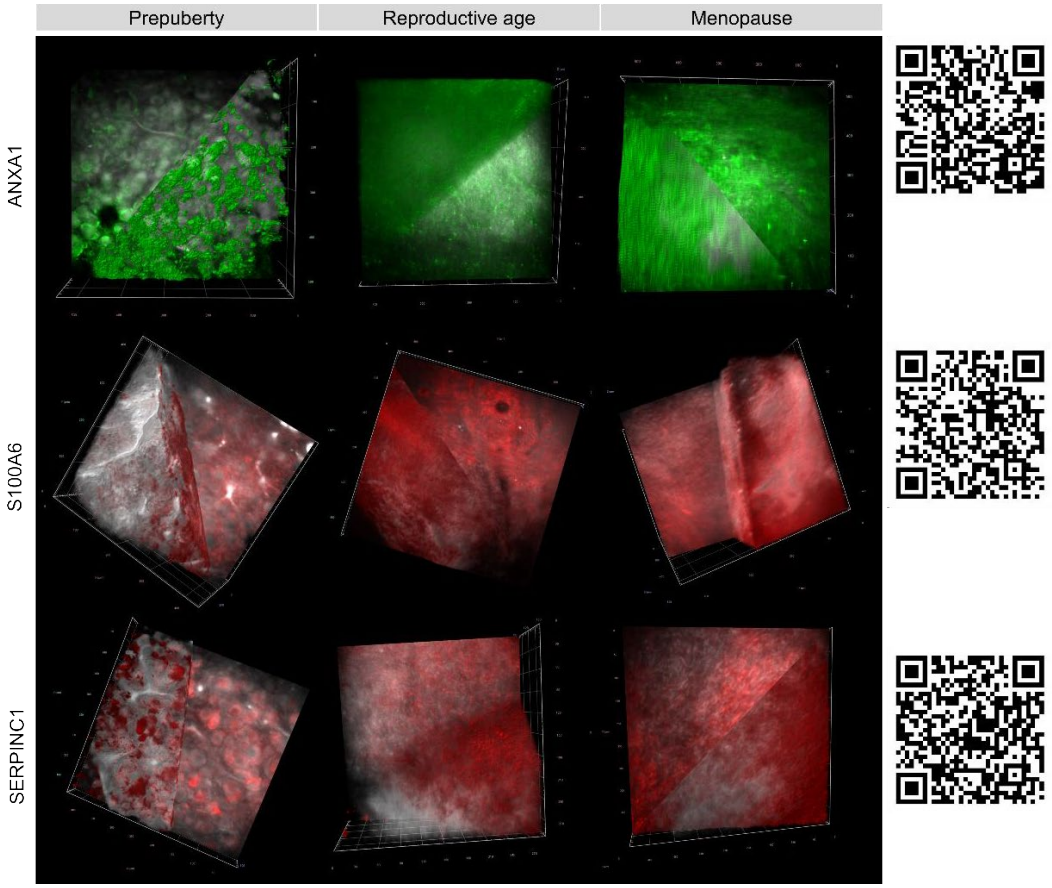
lateral scattering is minimal and that all wavelengths of light pass ‘‘through’’ the tissue and enable the observation of fluorescent targets in their 3D native structure. **B.** Captures of the 26 matrisomal biomarkers that have been validated by immunofluorescence and 3D imaging of cleared labeled tissues under lightsheet microscopy at 20X magnification with a digital zoom between 0.7 and 1.5. 3D visualization can be accessed by scanning the corresponding QR code. Qualitative trends in protein levels corroborate MS data. All used antibodies have been validated priorly with 3, 3'-diaminobenzidine immunohistochemical staining (Supp Figure 4). Proteins of interest were revealed with anti-mouse Ig (red) and anti-rabbit Ig secondary antibodies (green). Hoechst (blue) was used for nuclear staining (Table 1).

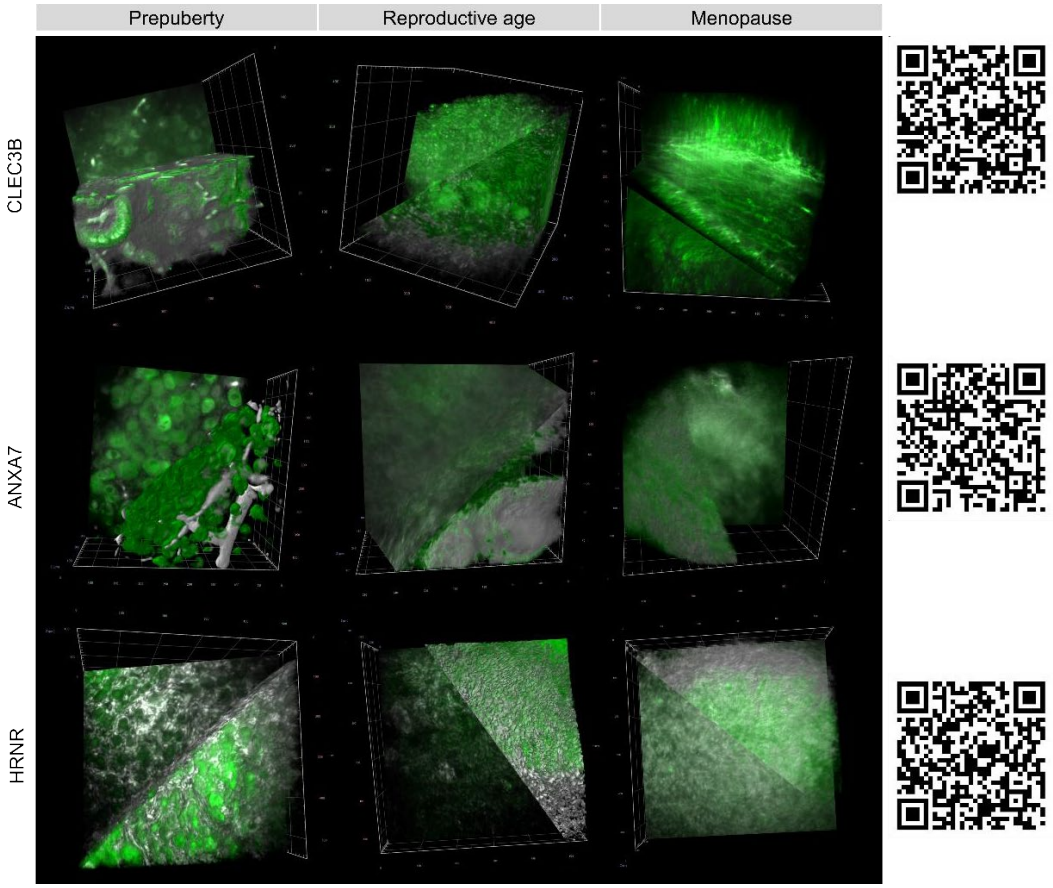
B.

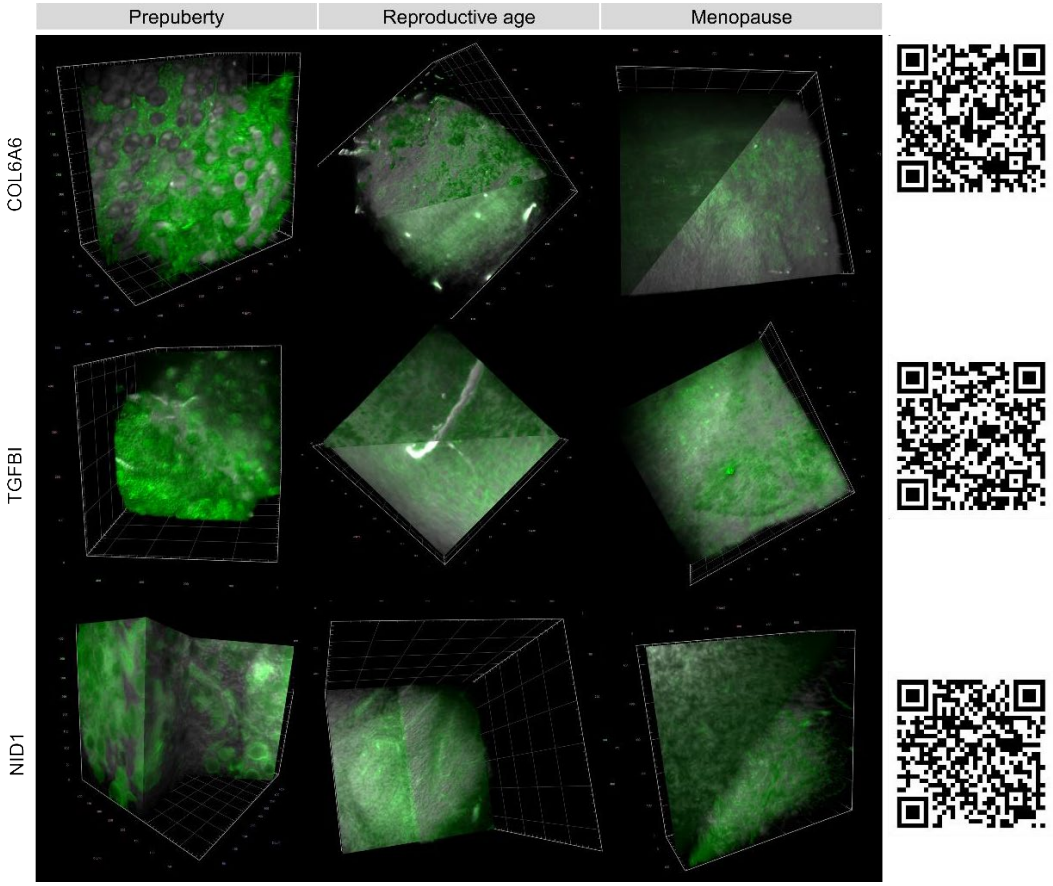

Prepuberty
Reproductive age
Menopause
SERPINA1
COL18A1
HPX

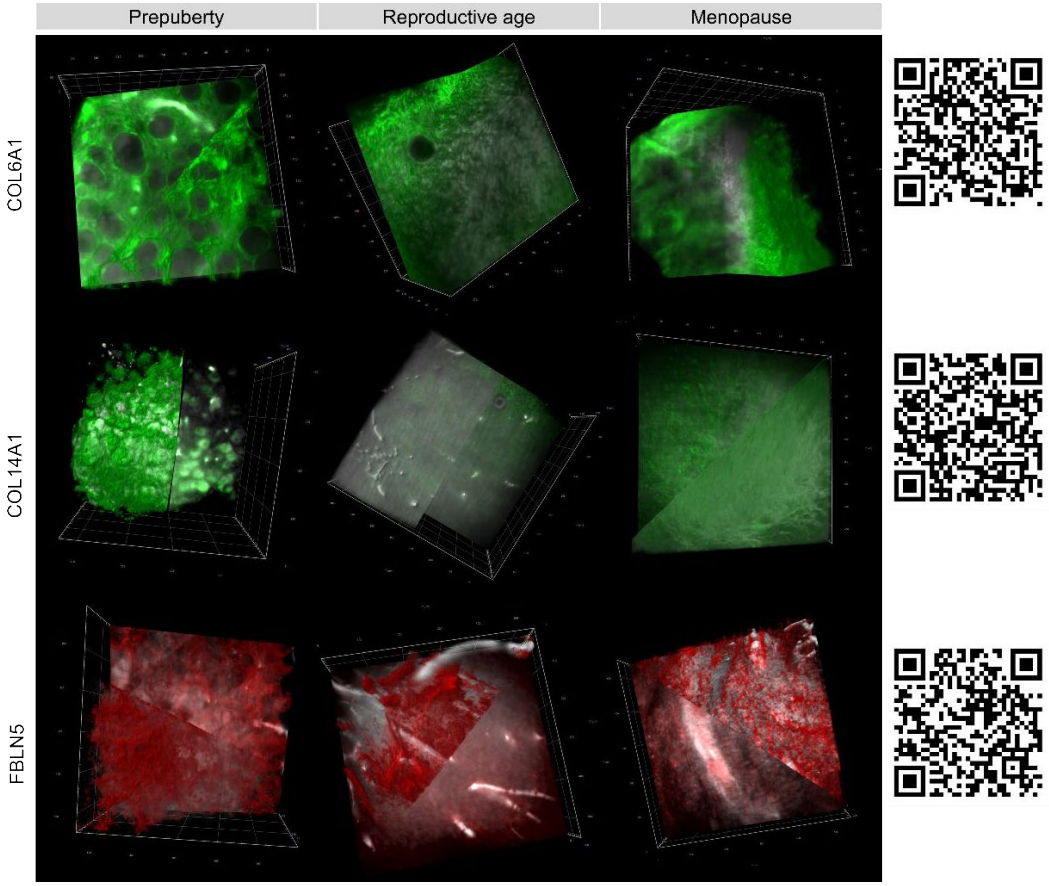

Prepuberty
Reproductive age
Menopause
ITIH4
ANXA5
CSTB

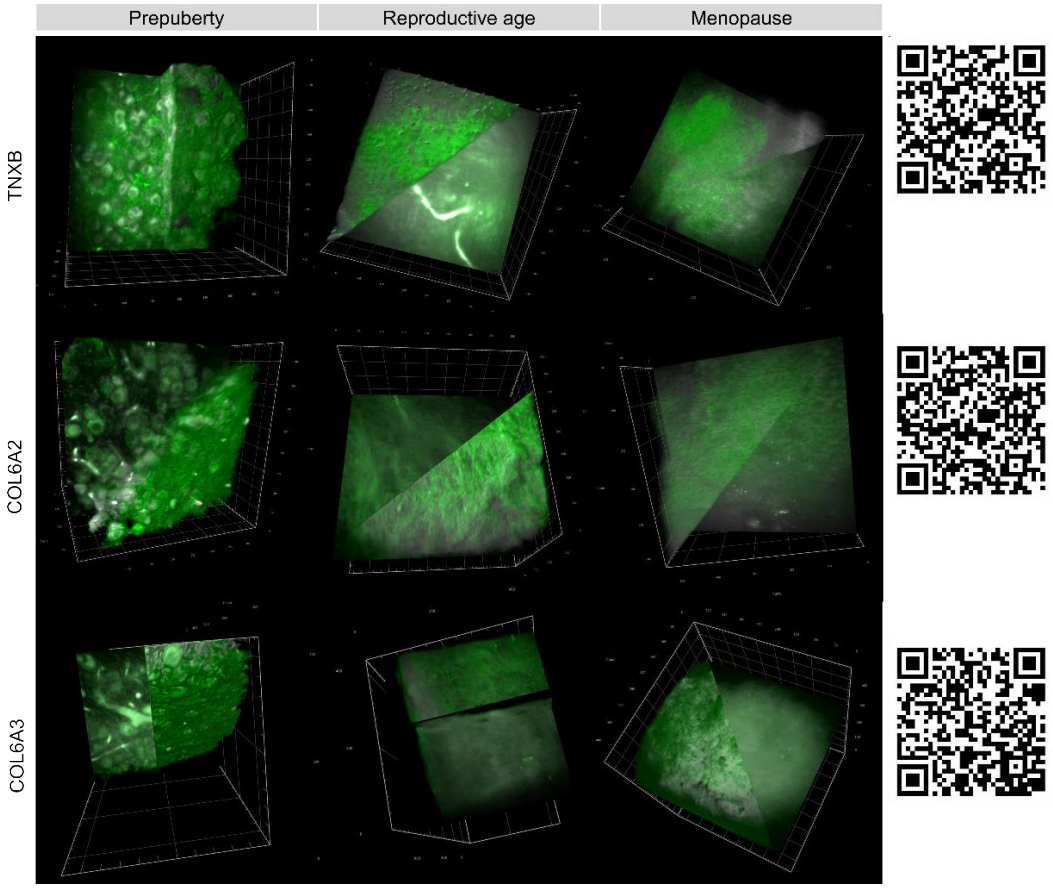

Prepuberty
Reproductive age
Menopause
F2
AGT
GPC6

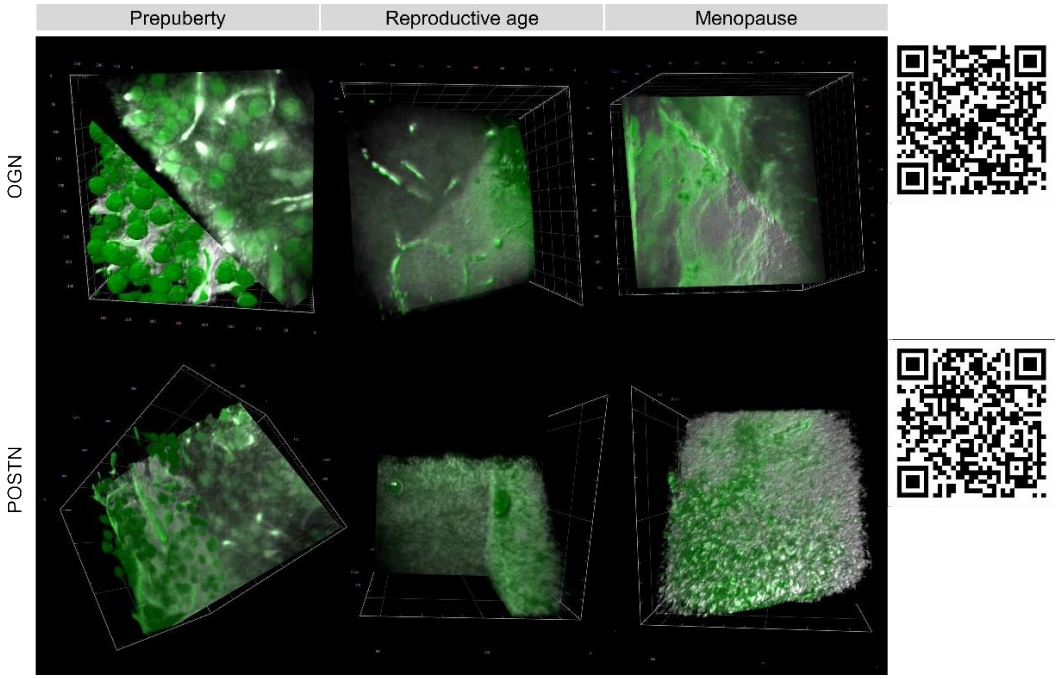

Prepuberty
Reproductive age
Menopause
ANXA1
S100A6
SERPINC1


Prepuberty
Reproductive age
Menopause
CLEC3B
ANXA7
HRNR


Prepuberty
Reproductive age
Menopause
COL6A6
TGFBI
NID1


Prepuberty
Reproductive age
Menopause
COL6A1
COL14A1
FBLN5


Prepuberty
Reproductive age
Menopause
TNXB
COL6A2
COL6A3


Prepuberty
Reproductive age
Menopause
OGN
POSTN

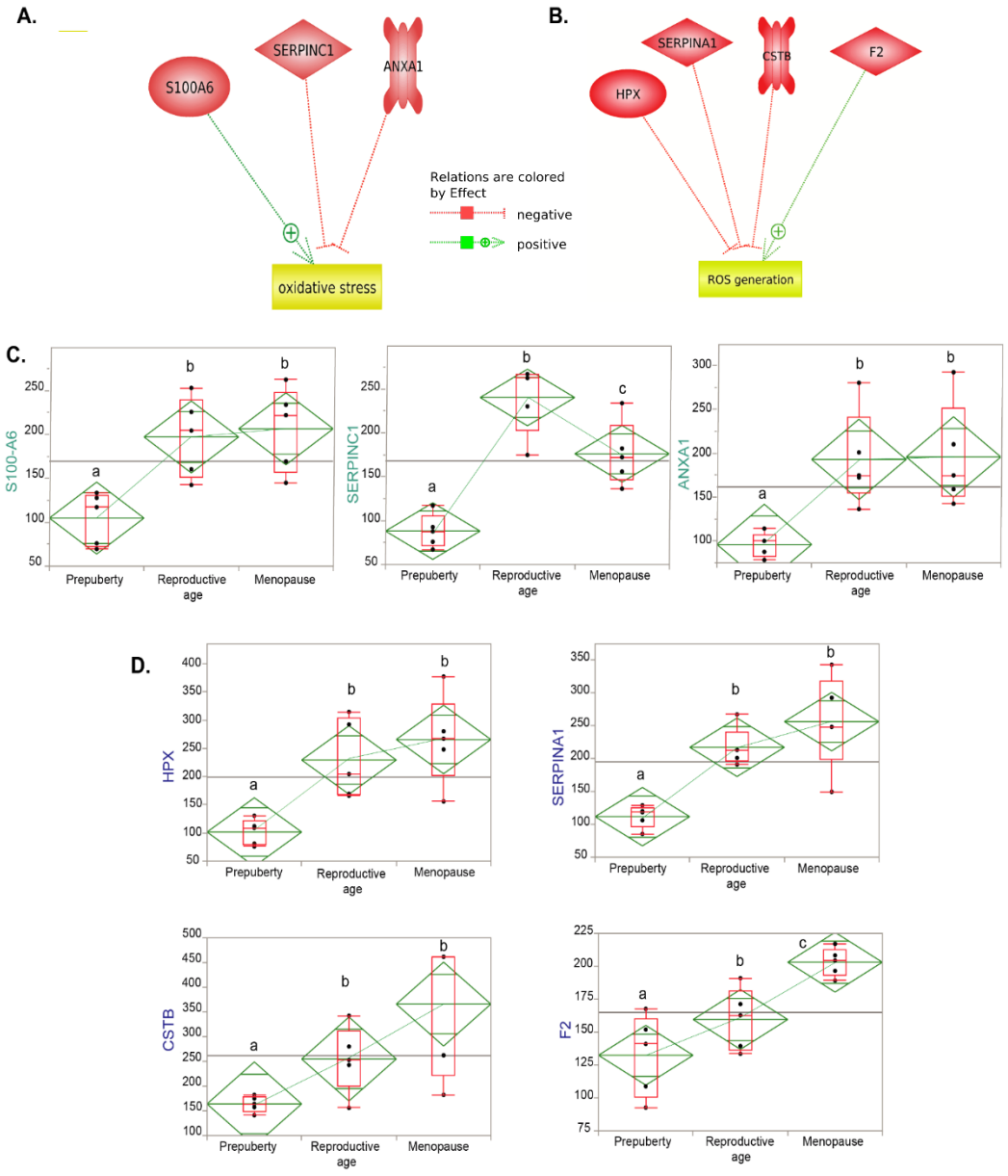


Figure 6. ROS and oxidative-stress regulation under the control of matrisome proteins during ovarian life span. A. Pro and anti-oxidative stress/ ROS regulators upregulated during adulthood (at reproductive- and menopausal age). **B.** An overall increase in the expression of matrisome

proteins responsible of anti-ROS generation with age. References used by Pathway Studio to create relationships in A and B are reported in Supp Table 5. **C-D.** Box plots showing expression levels of selected proteins from prepuberty til menopause. Protein names are labeled according to their cluster highlighted in Figure 2 (green is the cluster shared between reproductive-age and menopausal patients, the blue cluster refers to the proteins upregulated during menopause). Black dots indicate data points per patient. All box plots indicate median (center line), 25th and 75th percentiles (bounds of box), and minimum and maximum (whiskers). Means diamonds (95% confidence intervals for each mean) are also displayed. All paired comparisons were conducted with one way-ANOVA (post hoc: Tukey), different letters stand for statistical significance ($p<0.05$).

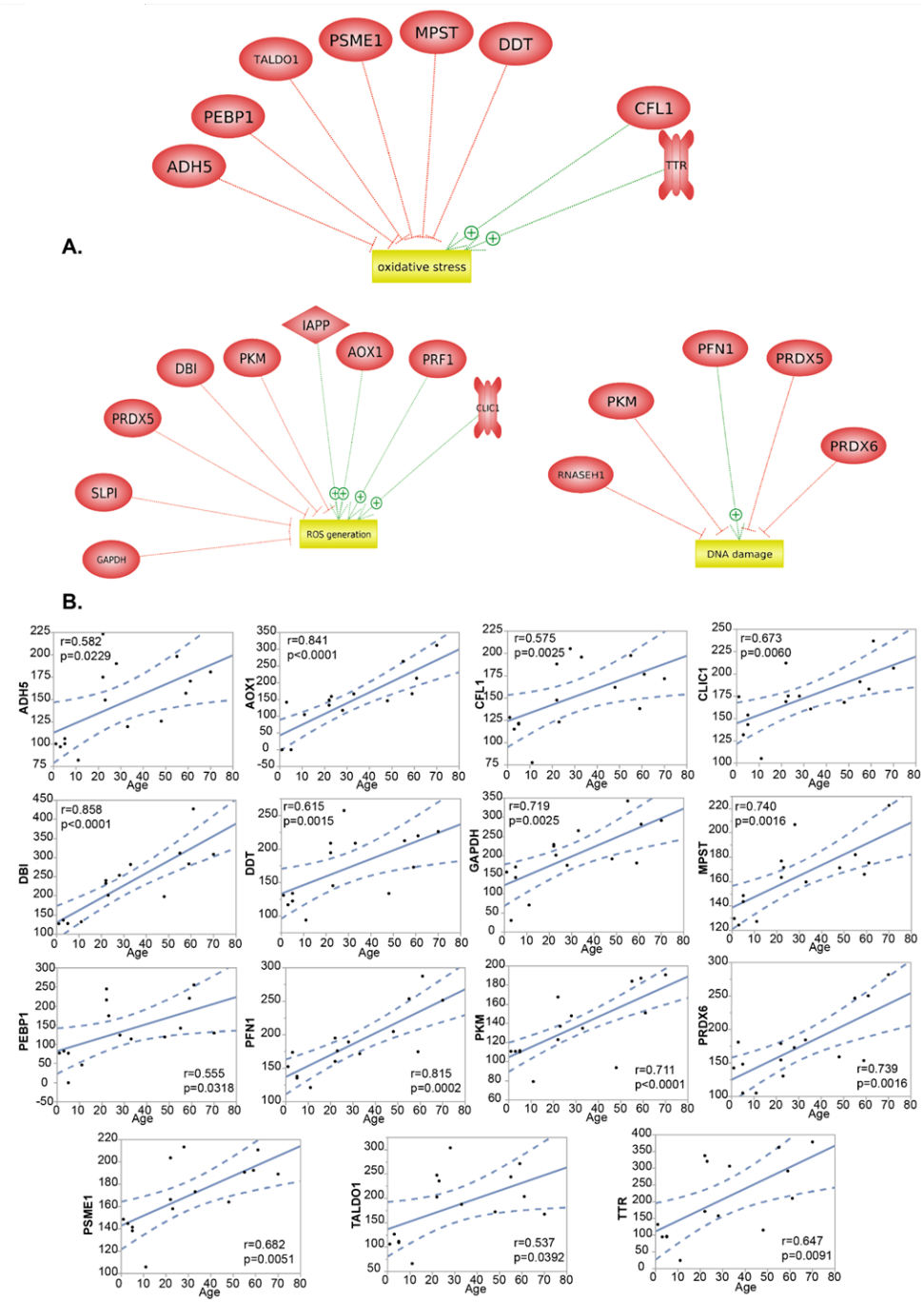


Figure 7. Upregulated intracellular proteins during menopause regulating oxidative stress, DNA damage and ROS generation.

A. Graphical representation generated with pathway studio highlighting positive (green) and negative (red) regulation of oxidative stress, DNA damage and ROS generation under the control of intracellular proteins upregulated during menopause and highlighting the superiority in number of cytoprotective proteins**.** References used by Pathway Studio to create relationships in A are reported in Supp Table 5. **B.** Positive significant correlation (Pearson) between age and highlighted proteins in A.

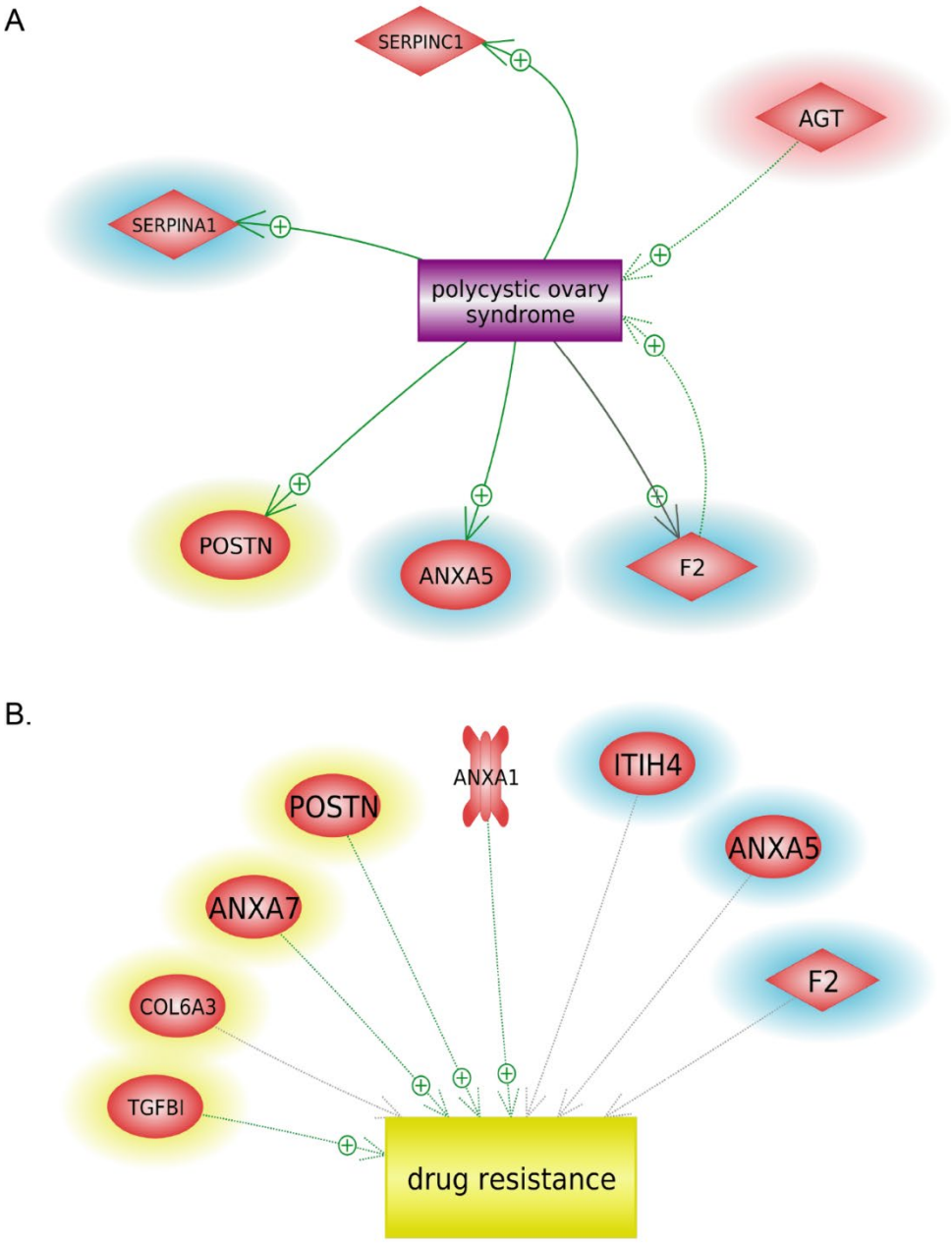


Figure 8. Matrisome proteins related to PCOS and responsible of chemo-drug resistance. NLP technology of pathway studio was used to detect matrisome proteins described in the literature as **A.** upregulated in

COS patients or **B.** responsible of chemo-drug resistance. Proteins highlighted in yellow, pink and blue belong respectively to the prepubertal, reproductive- age and menopausal matrisome clusters. Unhighlighted proteins are equally expressed in reproductive-age and menopausal tissues. References used by Pathway Studio to create relationships in Aand B are reported in Supp Table 5.

Table 1. Used primary antibodies and respective parameters. Secondary antibodies recognizing mouse IgG (Invitrogen, #A21236) and rabbit IgG (Invitrogen, #A11034) were used at a 1/250 dilution.

Antigen	Dilution	Company	Reference	Host
S100A6	1/50	Invitrogen	MA5-29537	Mouse
SERPINC1	1/50	Proteintech	66052-1-Ig	Mouse
HPX	1/100	Proteintech	66479-1-Ig	Mouse
ITIH4	1/50	Proteintech	24069-1-AP	Rabbit
SERPINA1	1/100	Proteintech	16382-1-AP	Rabbit
COL6A6	1/50	Invitrogen	PA5-60958	Rabbit
COL6A1	1/100	Proteintech	17023-1-AP	Rabbit
AGT	1/50	Proteintech	11992-1-AP	Rabbit
CLEC3B	1/50	Invitrogen	MA5-34760	Rabbit
COL14A1	1/100	Invitrogen	PA5-104514	Rabbit
CSTB	1/50	Proteintech	10823-1-AP	Rabbit
COL18A1	1/50	Proteintech	18301-1-AP	Rabbit
TGFBI	1/100	Proteintech	10188-1-AP	Rabbit
ANXA7	1/200	Proteintech	10154-2-AP	Rabbit
COL6A2	1/100	Proteintech	14853-1-AP	Rabbit

ANXA1	1/100	Proteintech	66344-1-Ig	Mouse
FBLN5	1/200	Proteintech	60081-1-Ig	Mouse
HRNR	1/50	Invitrogen	PA5-56756	Rabbit
OGN	1/50	Invitrogen	PA5-48255	Rabbit
TNXB	1/50	Proteintech	13595-1-AP	Rabbit
POSTN	1/50	Proteintech	19899-1-AP	Rabbit
F2	1/50	Proteintech	24295-1-AP	Rabbit
ANXA5	1/100	Proteintech	11060-1-AP	Rabbit
NID1	1/50	Proteintech	13766-1-AP	Rabbit
COL6A3	1/50	Invitrogen	PA5-49914	Rabbit
GPC6	1/50	Invitrogen	PA5-53622	Rabbit

Table 2. Matrisome biomarkers interaction with mTOR and Hippo pathways. To understand the possible interaction of ovarian matrisome biomarkers with key signalling pathways related to fertility and mainly follicle activation and development, we relied on pathway studio and its NLP technology (described in materials and methods) to study all thepossible bidirectional regulation happening between each of the 26 matrisome biomarkers and members of Hippo or mTOR signaling pathways. All connections were manually supervised and curated to select the most relevant relationships between the matrisome and cellular proteins. Illustrations of all the described connections can be seen in supp Figure 1 and supp Figure 2 (----> Regulation; --+> Positif effect; ---| Negatif effect; binding).

Accessible on:
https://data.mendeley.com/datasets/nvjsyyg43h/draft?a=2565d0c7-4e1b-46a1-9de2-2a96546c5f5d

Multi-scale study of the architecture, topography and mechanics of the human ovary from prepuberty to menopause: a blueprint for next-generation bioengineering and diagnosis

Elucidating the composition of the ovarian matrisome is not enough to be able to develop a biomimetic matrix. The lack of knowledge regarding the ovarian architecture and multiscale organization as well as biomechanical trademarks of the healthy human ovary are hampering our attempts to achieve ovarian biomimicry, a practice also defined as “innovation inspired by nature,” or “the conscious emulation of nature’s genius.”

The study reveals, for the first time, numerous human ovarian ECM properties, such as fiber morphology, interstitial and perifollicular fiber orientation, pore geometry, topography and surface roughness, and elastic and viscoelastic properties. The human ovary is considered as one of the most dynamic organs in the human body during a woman’s life. Therefore, we characterized its ECM from prepuberty to menopause to extract structural and mechanical phenotypes of these different periods. This study led to the description of features unique to each group (Figure 24).

We applied automated bioinformatic analyses based on Fourier transformation of multi-scale images obtained with SEM. The SEM micrographs revealed that ovarian ECM is constituted of few free fibrils and mostly of assembled fibrils (fibers), and fiber bundles. With age, fibers increase in size and density. The porosity analysis at the micrometers (5,000X) and hundreds of nanometers scale (20,000X) reveals that at the prepubertal stage, the bundles assemble into a tight network with a high number of small pores of the average diameter D_{av} ~70 nm. The mature pubertal tissue network presents bigger pores, D_{av} ~200 nm at 20000X, and a few micrometer-sized pores, D_{av} ~5 µm at 5000X.

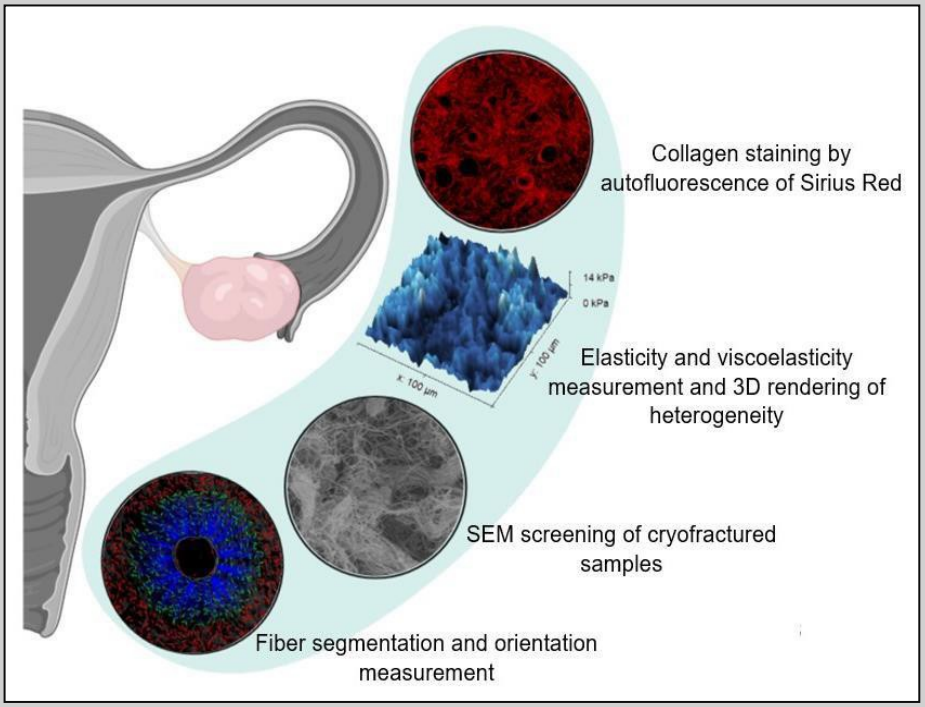


Figure 24 | Graphical illustration of essential procedures used for the characterization of ECM topology and biomechanics.

In contrast, the menopause tissue presents lesser and bigger micrometers scaled pores, D_{av} ~3 µm at 5,000X, whereas the nanometer scaled ones are fewer and larger, D_{av} ~300 nm at 20,000X. This network organization could affect the elastic and viscoelastic properties of the tissue, as well as limit the diffusion of water, nutrients, and cells. Pore geometry is also dependent on the fiber orientation. We applied Curvelet transformation on Sirius Red (histological staining of collagen) scans of the ovarian tissue to extract fiber orientation. Our results revealed the anisotropy of human ovarian tissue described by directional variations in the tissue organization along the female life with a specific arrangement at each age.

Analysis of the collagen fiber orientation around the borders of preantral

ovarian follicles at both prepubertal and reproductive age delineates a dramatic reorganization of their fibrous microenvironment (perifollicular ECM) with follicle stage. Indeed, fiber orientation frequency between 0° to 90° changes significantly at the secondary stage compared to primordial and primary follicles, before and after puberty. Secondary follicles have a 2 to 3 fold larger diameter than earlier stages, explaining the fiber rearrangement below 50° in compliance with the follicle enlargement. This suggests that human follicles at this stage require higher fiber contact and adhesion signaling to fulfill their development and maturation toward ovulation, as previously indicated in the murine model. Moreover, we report significant differences between prepubertal and reproductive tissue at the preantral stage of follicle development. Thus, perifollicular remodeling of follicle surroundings depends on follicle stage and ovarian tissue age.

ECM fibrous proteins also possess micro- and nano-scale features that provide topographic stimuli to cells and act as instructive cues to influence gene expression, cell behavior, and morphology, as evidenced by emergent publications on this topic. Therefore, we investigated the topography of ovarian tissue and its changes from prepuberty to menopauseand measured its microrugosity. To achieve this goal, we used a novel technique based on 3D reconstruction of stereo pairs of SEM images taken at the same tissue region at 12,000X magnification, created by tilting the sample by + 5° along the X axis. We found that soft ovarian tissue at reproductive age is characterized by a smoother tissue surface (99 nm ±33) compared to the rougher prepubertal (228 nm ± 87) and menopausal (238 nm ± 28) tissues, which are more rigid, which points to a possible synergy between tissue rigidity and surface roughness. Indeed, we conducted ovarian tissue elasticity and viscoelasticity measurements from prepubertal to menopausal age using AFM. This tool allowed us to adequately assess the

microenvironment felt by cells due to its high microscale sensitivity and effectiveness in distinguishing small mechanical changes between tissues and within tissues at microscale resolution. Elasticity measurement revealed a relatively rigid ovarian tissue at prepubertal age, softening significantly at reproductive age and stiffening remarkably upon menopause.

Contrary to most studies evaluating biological tissue mechanics and assimilating them to perfect elastic materials, we further used AFM to investigate the viscoelasticity of the human ovarian tissue. ECM viscoelasticity depends on fluid retention and flow through the porous matrix, as well as rearrangement of individual ECM fibers to absorb stress. Although elasticity significantly changes upon puberty, the viscoelasticity of prepubertal and reproductive age tissues is comparable, highlighting the relevance of recording both measurements. Conversely, menopausal tissue has a faster viscoelastic response, which can be described by a higher sequestration of fluid compared to other groups related to its high GAG content, fiber network architecture and pore geometry promoting water retention and stronger collagen bonds, limiting the collagen rearrangement time.

Our analyses demonstrated that ovarian ECM at reproductive age represents an ideal microenvironment for ovarian cell- and follicle- function and development due to its unique topological and mechanical features. Thus, our study provides the ECM cues necessary to replicate ovarian tissue properties in a functional engineered ovary and represents a reliable reference to compare physiological and pathological ovarian conditions based on ECM status.

Multi-scale study of the architecture, topography and mechanics of the human ovary from prepuberty to menopause: a blueprint for next-generation bioengineering and diagnosis

Emna Ouni[1], Alexis Peaucelle[2,¥], Kalina T. Haas[2,¥], Olivier VanKerk[1], Marie-Madeleine Dolmans[1,3], Timo Tuuri[4], Marjut Otala[4],Christiani A. Amorim[1,*]

[1]Pôle de Recherche en Gynécologie, Institut de Recherche Expérimentale et Clinique, Université Catholique de Louvain, 1200 Brussels, Belgium

[2]Institut Jean-Pierre Bourgin, INRAE, AgroParisTech, Université Paris-Saclay, 78000 Versailles, France

[3]Gynecology and Andrology Department, Cliniques Universitaires Saint-Luc, 1200 Brussels, Belgium

[4]Department of Obstetrics and Gynecology, Helsinki University Hospital, University of Helsinki, 00029 Helsinki, Finland

*Corresponding author

¥ These authors have equally contributed to the current study

Abstract

Although the first dissection of the human ovary dates back to the 17th century, the biophysical characteristics of the ovarian cell microenvironment are still poorly understood. However, this information is vital to deciphering cellular processes such as proliferation, morphology and differentiation, as well as pathologies like tumor progression, as demonstrated in other biological tissues. Here, we provide the first readout of human ovarian fiber morphology, interstitial and perifollicular fiber orientation, pore geometry, topography and surface roughness, and elastic and viscoelastic properties. By determining differences between healthy prepubertal, reproductive-age, and menopausal ovarian tissue, we unravel and elucidate a unique biophysical phenotype of reproductive-age tissue, bridging biophysics and female fertility. Our ultimate goal is to apply these data to design biomimetic scaffolds for the tissue-engineered ovary. We also hope that our analysis pipeline can serve as a standard for other tissues and organs, in physiological or pathological states to reveal their biophysical properties, which could be very useful for future clinical applications and prognoses.

Introduction

Since 1976, more than 7 million babies have been born around the world using assisted reproductive technology [1], making medical intervention to aid men and women with infertility routine practice and an increasingly requested technology. Novel fertility restoration strategies, such as ovarian tissue engineering, have emerged in the last decade to respond to patient needs, manage their clinical condition, and offer reliable models for reproductive biology research. Ovarian engineering has relied on synthetic [2] and natural [3, 4, 5] hydrogels, decellularized scaffolds [6, 7, 8] and microfluidics [9]. However, these techniques were designed based on knowledge acquired from two-dimensional cell culture and animal models. Finding a relevant model for the human ovary is almost impossible as only a few mammals, including several whale species and elephants, have long pre- and post-reproductive stages.

Indeed, our lack of information on the human ovary hampers our ability to mimic the main features of this organ, either in an in vitro model or functional transplantable engineered ovary. The complex composition and hierarchical structure of the extracellular matrix (ECM) complicates the design of truly biomimetic constructs, notably multi-scale ECM organization and architecture, as well as its biomechanical features controlling follicle activation and mechanotransduction [10, 11, 12]. Moreover, the ovarian ECM is very dynamic, owing to ovarian tissue changes from prepubertal through reproductive to menopausal age.

In the past, da Vinci drew human corpses in the famed Codex Leicester [13] and depicted the analogy between Earth and the human body in an attempt to understand the human organism. Centuries after his death, modern anatomists were still learning through Leonardo's sketches. This historical fact further highlights the importance of having a reference base upon which we can advance future therapies and technologies.

Today, manufacture of hydrogels with tailored biochemical, architectural and mechanical features is feasible and constantly developing. Nevertheless, the absence of reliable characterization of the human ovarian ECM is still lacking. Even da Vinci was not able to reproduce the female reproductive tract realistically in his drawings [14].

Here, we directly investigate the changes to human ovarian tissue during its lifespan to confirm our hypothesis that the human ovary has unique physical and topological ECM features at reproductive age. Such properties are tailored to ECM biological function and play an active role in fertility and ovarian activity compared to prepubertal and menopausal tissue, which are known for their quiescent follicles and ovarian inactivity. Our work reveals new facets of the ovarian ECM on multiple scales, and their evolution from prepuberty to menopause, aspects that have so far been missing from the engineered ovary. More specifically, all analyses were performed using samples from the ovarian cortical layer, where the ovarian follicle reserve resides. ECM fiber thickness, assembly, orientation and directionality around follicle borders, pore number and size, topography, and elastic and viscoelastic properties of the human ovarian cortex are all depicted. Our study highlights the impact of local and global fibril orientation, and nanoscale and mesoscale ECM porosity on the mechanical properties of ovarian tissue. By affecting chemical and mechanical signaling, these features, are critical determinants of ovarian function and should become a blueprint for designing functional artificial ovaries in the near future.

Results

Multi-scale fiber thickness and pore properties demonstrate microstructural remodeling with age

In this study, we define fibrils as individual entities with discrete diameters in the order of several nanometers, whereas fibers are defined as a pack of multiple fibrils that can be assembled into bundles (Fig. 1A). While it is rare to observe isolated fibrils in ovarian cortex (Fig. 1B), we were able to capture the main features of its fibers at 20,000X magnification and their arrangement into bundles at 5,000X magnification (Fig. 1, B and C). After identifying fiber bundles at 5,000X, we zoomed in to pinpoint the features of their elementary fibers at 20,000X (Fig. 2).

The results revealed specific organization of the ovarian ECM at prepuberty, characterized by thin fibers (vs reproductive age $p<0.01$; vs menopause $p<0.0001$) assembled into thin bundles (vs reproductive age $p<0.0001$; vs menopause $p<0.01$) (Fig. 1, D and E). These fibers became increasingly thicker with age (vs reproductive age $p<0.01$; vs menopause $p<0.001$). However, their assembly change upon puberty, as we observe at low magnification the densification of fibers into thickest bundles at reproductive age (vs prepubertal age $p<0.0001$; vs menopause $p<0.0001$; Fig. 1D).

Pore area and number analyses were used to investigate the spacing between fibers and establish the network tightness (Fig. 1, F and I). This approach demonstrated that at prepuberty, thin bundles are assembled into a tight network represented here by high numbers of pores (vs reproductive age $p<0.0001$; vs menopause $p<0.0001$) occupying the smallest area (vs reproductive age $p<0.0001$; vs menopause $p<0.001$). By comparing prepubertal and menopausal ovarian tissues, we were able to observe different pore characteristics at 5,000X and 20,000X. Indeed, while at high magnification we found that menopausal tissue is composed of a smaller

pore number ($p<0.001$) occupying a larger area than at reproductive age ($p<0.01$); a similar observation at lower magnification revealed tighter network organization at menopause (Fig. 1, F and I). This evidences a particular ECM deposition and overlapping with age, which can be translated into limited flow diffusion in menopausal tissue (Fig. 2). Such network organization could affect the elastic and viscoelastic properties of tissue, as well as limit the diffusion of water, nutrients and cells (Fig. 2).

Interstitial fiber orientation and straightness change with age and hormonal state

All age groups showed directional collagen alignment, as demonstrated by fiber orientation analysis (Supplementary Fig. S1; Table.1). They all displayed preferred average fiber orientation centered around 90°: 89.53° ± 0.3 at prepuberty; 91.63° ± 0.9 at reproductive age; and 89.14° ± 0.3 at menopause (Fig. 3B). Although the difference in average fiber direction was discreet, it was statistically significant between reproductive-age and prepubertal ($p<0.0001$) as well as menopausal ($p<0.0001$) tissue, while no difference was detected between prepubertal and menopausal fiber orientation ($p=0.0681$).

Angular dispersion of collagen fibers was, however, unique to each age group ($p<0.001$, all paired comparisons). During its reproductive life, the ovary operates under cyclic tension and release synchronously with follicle development [15], which may lead to fiber straightness [16].

Our follow-up of collagen fiber waviness from prepuberty to menopause reveals increasing fiber straightness with age ($p<0.001$, all paired comparisons), probably related to greater stretching force applied to fibers (Fig. 3C). Earlier during prepuberty, in the presence of high numbers of preantral follicles, we observed fiber rearrangement around follicles with a curvier aspect (Fig. 3). Curvy fibrils were found mainly around follicles and

were analyzed separately, as discussed in the next section (Fig. 4).

Perifollicular fiber orientation reveals directional fiber remodeling during folliculogenesis

Analysis of collagen fiber orientation around the borders of preantral ovarian follicles at both prepuberty and reproductive age showed a dramatic reorganization of their fibrous microenvironment (perifollicular ECM [17]) with follicle stage. Indeed, the frequency of fibers oriented between 0° and 90° changed significantly at the secondary stage, compared to primordial ($p \leq 0.001$) and primary ($p < 0.01$) follicles before and after puberty (Fig. 4, A-D; Table.1). Secondary follicles are characterized by a 2- to 3-fold larger diameter than earlier stages, which explains fiber rearrangement below 50° consistent with follicle enlargement. When comparing prepubertal and reproductive-age perifollicular fiber directionality between follicles at the same developmental stage, we found significant differences at all stages: primordial ($p < 0.01$), primary ($p < 0.05$) and secondary ($p < 0.01$) (Fig. 4, E-G). All these differences reveal local perifollicular remodeling of the follicle environment that depends on follicle stage and ovarian tissue age.

Elastic and viscoelastic characteristics of human ovarian cortex

Given that mechanical ECM properties are one of the main epigenetic environmental factors in all biological tissues, including the human ovary, respecting native ovarian mechanical features is key to engineering a functional bioinspired ovary. We therefore conducted elastic and viscoelastic measurements of human ovarian tissue and followed its evolution with age. Both of these physical characteristics coexist and could be measured by choosing appropriate measurement parameters (Fig. 5).

We explored how the change in ECM organization is reflected in the mechanical properties of ovarian tissue (Fig. 5). Using the indentation

technique, we assessed its micrometer-scale mechanical characteristics, which reflect the mechanical properties sensed by a cell in the tissue. We used atomic force microscopy (AFM) tips mounted with a round bead 5 µm in diameter. Despite complex ECM organization, the observed tissue response was similar to that of continuous media with Young's Modulus (elastic constant) of around 3178 Pa (± 245) for reproductive-age ovaries, and significantly more rigid for prepubertal (6538 Pa ± 351; $p<0.01$) and menopausal (7117 Pa ± 714; $p<0.01$) ovaries (Fig. 5, A-D). These changes in the mechanical properties may relate to the increased micro-porosity encountered in fertile tissues (Fig. 1G), as it was comparable in prepubertal and menopausal tissues. Other factors could also explain these mechanical changes, such as the local mechanical anisotropy as well as chemical ECM change.

We also observed a viscoelastic behaviour, namely a time-delayed response following mechanical stimulation.

The viscoelastic constant was evaluated by performing stepwise deformation of the tissue. The measured viscoelastic response can be described by two relaxation time constants, T1 ~0.2 s, and T2 ~2 s (Fig. 5E). At short testing period, no differences were observed between all age groups. However, at longer time range, prepubertal tissue appears to have a significantly different viscoelastic phenotype from other age groups ($p<0.05$), characterized by the longest relaxation time ~2.34 s against 1.95 s and 1.86 s recorded respectively in reproductive-age and menopausal tissues (Fig. 5E).

When combining elastic and viscoelastic results, we noticed that despite significant changes in elasticity between reproductive-age and menopausal tissue, both ovaries show similar viscoelastic behaviors characterized by a short relaxation time. By contrast, prepubertal ECM is rigid, with a higher pore number, a tighter fibrous network (Fig. 2) and responds slower to deformation

by regaining in a longer time its initial state (Fig. 5D-E). These two time-dependent viscoelastic responses can be explained by initial local fluid outflow from small pores separating ECM fibers, followed by their rearrangement under stress with further fluid outflow from larger pores at the indentation site within a longer time range [16] (Fig. 2).

Topography

Our results reveal the roughness footprint of healthy ovary at each age using stereoscopic reconstruction of scanning electron microscopy (SEM) images (Fig. 6). We note that soft ovarian tissue at reproductive age is characterized by a smoother surface (99 nm ± 33) than rougher prepubertal (228 nm ± 87; $p<0.0001$) and menopausal (238 nm ± 28; $p<0.0001$) tissues, which are also more rigid (Fig. 6).

Discussion

In this study, we explore the role of the ECM in the functioning of human ovaries. Combining different imaging modalities, we analyze the fibrillary organization, topology, and mechanical properties of ovarian tissue before, during and after reproductive age. Along with the cell niche, the ECM has been shown to orchestrate cell behavior and fate [18]. For instance, the multiscale architecture of ECM collagen fibers influences cell polarity and promotes migration by providing contact guidance cues [19]. While a normal ECM can restore transformed cells to quiescence [18], a damaged ECM can trigger malignancy [20] or differentiation[21]. ECM architecture plays a role in the specialized function of the tissue of which it is a part [22]. Indeed, collagen forms thick fibers in load-bearing tendons that are aligned along the tendon to optimize force transmission and tendon strength [23]. By contrast, collagen in the cornea forms woven sheets of thin fibers that provide strength combined with optical transparency [23]. In interstitial tissue, collagen forms mostly

isotropic networks, which provide mechanical strength combined with porosity to facilitate nutrient transport and cell migration.

While secretory patterns of hormones and paracrine and autocrine functions in the human ovary have been investigated for several decades, little is known about the role of ECM biomechanics and topology in ovarian function. Since its first description more than a century ago, the human ovary has been known to have a dynamic architecture, with a stiffer collagen-rich cortex and a softer medullary layer. Follicles are distributed along this collagen gradient: early preantral follicles are located in the firm cortex and late secondary and antral follicles are found in the less rigid medullary layer. Only recently, studies highlighted the fact that the mechanical properties of the ovarian ECM, including this rigidity gradient, play a crucial role in supporting follicle survival and folliculogenesis [24]. Studies are finally revealing that the ovary is a dynamic mechano-responsive organ and that crosstalk between the ECM and follicles and the ECM and ovarian cells is essential for folliculogenesis and oogenesis. Indeed, ovulation would never occur without remodeling of the dense and rigid ECM of the ovarian cortex. The 'weakening' of the ECM by enzymes synthesized by cells from preovulatory follicles is vital for oocyte expulsion [25]. Another example of the influence of ECM composition and architecture on follicle development has been seen insubjects with polycystic ovary syndrome (PCOS). Ovaries from PCOS patients have a densely collagenized and thickened cortex that probably creates a biomechanically non-permissive environment, possibly altering mechanical signaling. This environment is likely to play a role in boosting numbers of growing follicles through a cascade of events, culminating in increased secretion of growth factors, which leads to primordial follicle activation and development [26]. PCOS ovaries are also characterized by anovulation, probably a result of the lack of degradation of the fibrous ECM [11] or an undiagnosed abnormal ECM architecture. Kawamura et al. [27] reported an increase in primordial

follicle activation in PCOS patients after cutting ovarian tissue into small cubes. This procedure was found to modify ovarian mechanical forces by releasing tension on ovarian cells and disrupting the Hippo signaling pathway, characterized by polymerization of globular actin to filamentous actin. Actin polymerization may connect biophysical changes with suppression of Hippo signaling, increasing nuclear YAP concentrations and stimulating follicle growth [28]. Moreover, Telfer and McLaughlin (patent WO2014043835A1) proved that stretching small strips of cortical ovarian tissue in one direction by more than 10% of the initial length prior to in vitro culture enhances primordial follicle activation to the secondary stage. These initial observations highlight the role of ECM architecture as a regulator of cellular/follicle behavior in the ovary, demonstrating the importance of microenvironmental cues to female fertility. Although mechanical stimulation is mediated by specific architecture in different tissues [29], there is still a lack of understanding of ovarian ECM topology that needs to be addressed. We therefore believe that identifying differences in the ECM architecture of ovaries before and after puberty and during menopause will help us elucidate how biochemical regulation can be correlated to ECM morphology. Our spatiotemporal follow-up of fibrous ECM morphology provides novel phenotyping of ovarian tissue at different ages, shedding light on the possible effect of the fibrillar structure on the signaling of growth factors binding to the fiber surface. Here, the ECM brings active molecules into close proximity with the cell surface and facilitates interactions between growth factors and integrins, or sequesters them within the fibrous network and tight pores [30].

Our results revealed a unique ECM architecture at reproductive age, where fibers of intermediate diameter are assembled into thickest bundles compared to prepubertal and menopausal tissues. This is probably due to the estrogen surge at reproductive age that stimulates the activity of LOX [31], the crosslinker of collagen. These data are consistent with previous collagen

crosslinking analyses under polarized light [17]. Fiber and bundle spacing deduced from pore number and area show a looser fiber network at reproductive age compared to other age groups. While fiber thickness reflects fibril crosslinking and participates in the physical properties of tissue, multi-scale pore size and distribution contribute to diffusion and access of key molecules (nutrients, waste, hormones and oxygen) to/from cells. Hence, changes in tissue pore spacing from prepuberty to menopause can be translated into changes in permeability and molecule selectivity from one age to another. This information may be useful for the pharmacokinetics of new ovarian treatments that might require age-personalization.

Pore geometry is also dependent on fiber orientation. Our results demonstrated the anisotropy of human ovarian tissue characterized by directional variations in tissue organization throughout female life, with a specific arrangement at each age. The interwoven anisotropic fiber structure of the human ovary provides the tissue with great adaptability to multidirectional loads [32]. Interestingly, reproductive-age tissue fibers follow a common average orientation, which is significantly different from prepubertal and menopausal age groups that share comparable average fiber orientation. Taking into account the implication of pulling forces by cells in fiber orientation [33, 34], this diversity in directional fiber distribution reveals a different multidirectional mechanical load in each group. This further delineates the peculiar organization of the ECM related to ovarian activity at reproductive age and hormonal homeostasis, and highlights possible differences in force transmission between age groups [29]. Considering the uniqueness of fiber orientation in ovarian cortex at reproductive age, fiber directionality may become a hallmark of female fertility, as is the case for breast cancer prognosis [35, 36]. Although detected differences in average fiber

angles are in the order of 2°, no available data in the literature rule out the relevance of this discrete difference in the physiological function of ovarian tissue. Future studies need to elucidate the involvement of fiber orientation and stability range in functional tissue.

By comparing local fiber directionality around follicle borders at primordial, primary and secondary stages, we noted that before and after puberty, secondary follicles appear to modify their microenvironment arrangement locally compared to follicles at earlier stages of development, by reorienting the majority of collagen fibers below 50°. Our results complement and corroborate in vitro studies demonstrating that regulation of ovarian follicle development depends on the architecture of the perifollicular ECM, in addition to endocrine- and paracrine-acting hormones [37]. Beyond providing structural support for follicle formation and growth, the fibrous ECM network acts as a reservoir for paracrine and endocrine signals inside the ovary and permits or restricts their access to cells within follicles. Similarly to other organs, the ovarian ECM is prone to mechanical and enzymatic remodeling in different physiological and pathological conditions [37]. Hence, our observation of differences between perifollicular ECM architecture in prepubertal and reproductive-age follicles at similar stages could be a cause of differences in molecular signaling and interfollicular communication, responsible for the life cycle of preantral follicles. Throughout folliculogenesis, ECM architecture ensures appropriate hormone secretion, somatic cell differentiation, and oocyte maturation [11]. In conjunction with this activity, the ovary accommodates a large reserve of inactive primordial follicles that contain nongrowing oocytes and nondividing, flattened (squamous) pregranulosa cells surrounded by a basal lamina. Following entry into the growing follicle pool upon activation, squamous pregranulosa cells surrounding the oocyte become cuboidal granulosa cells (primary

follicles). They proliferate to form multiple layers, a morphological hallmark of secondary follicles. At this stage, the theca cell layer is recruited from the stroma to surround the basal lamina, which involves intricate polarity changes and cell migration processes. Fortunately, advances in in vitro follicle culture have allowed us to decipher the role of ECM architecture in follicle and ovarian development. It was found that cell adhesion, supported by the ECM, induces changes in cell shape and motility necessary for various cellular functions during folliculogenesis. A number of studies have also shown that in vitro culture of granulosa cells plated on matrices of ECM proteins of various densities also leads to alterations in cell adhesion and shape [38], highlighting the importance of using biomimetic scaffolds to achieve completion of folliculogenesis in vitro. This can only be accomplished by following our blueprint of fiber orientation and angular density of the perifollicular ECM, and our previous description of elastic matrisome spatiotemporal changes [17]. Our results also revealed that at all stages of folliculogenesis, prepubertal follicles are surrounded by a higher density of fibers. This can predict a non-permissive environment at a very early stage of preantral development, as already suggested [39], or peculiar architectural regulation of molecular signaling and transmission activity, as described above, which both play key roles in follicle quiescence and ovarian reserve preservation during prepuberty. Moreover, follicle survival has been described in vitro as dependent on scaffold geometry, where greater adhesion of follicles to ECM fibers oriented below 90° resulted in the highest survival rates [40]. By comparing local fiber directionality around follicle borders at primordial, primary and secondary stages, we noted that before and after puberty, secondary follicles appear to modify their microenvironment arrangement locally compared to follicles at earlier stages of development by reorienting the majority of collagen fibers below 50°. This could indicate that follicles at this stage require a higher degree of fiber contact and adhesion

signaling [36] to thrive and complete their development and maturation towards ovulation [41]. Indeed, this was previously suggested by Laronda et al. when designing a three-dimensional (3D) bioprosthetic ovary made of 3D-printed gelatin fibers encapsulating preantral mouse follicles, where fibers oriented at 30° and 60° offered higher follicle-scaffold contact than 90° and resulted in offspring [40]. Comparably, our results offer an opportunity to fine-tune 3D fiber printing and architectural design in accordance with native fiber and pore geometry of human ovarian tissue.

ECM fibers possess micro- and nano-scale features that provide cells with topographic stimuli and act as instructive cues to influence gene expression, cell behavior and morphology [42]. Topographical deregulations have been described in several pathological conditions, which underlines the importance of topographical ECM homeostasis, as evidenced by emerging publications on this topic [43, 44, 45]. The mechanism of topographical cell sensing on a nanoscale level is believed to be due to the clustering of integrins and other cell adhesion molecules, because surface roughness ensures particular spacing of adhesive sites [16]. Growing evidence points to the involvement of topography in cell morphology and Hippo pathway signaling [46].

Mechanical approaches are now clinically used to disrupt ovarian Hippo signaling and promote follicle growth as infertility treatments, by releasing mechanical tension applied to quiescent follicles [47]. Indeed, maintenance of follicle quiescence in infertile, prepubertal and menopausal subjects was thought to be due to mechanical retention by the ovarian ECM [10]. Although this theory has been supported by many researchers over the last decade, our knowledge of healthy ovarian tissue biophysics remains limited. The only rheological study conducted to date used multi-modal magnetic resonance elastography on ovaries of women diagnosed with PCOS versus age-

matched controls [48]. The results revealed an overall higher degree of stiffness in PCOS tissues. Despite the non-invasivenessof this technique and clinical transferability, it provides only bulk rheology. Depth penetration of acoustic waves was patient-specific in some cases, yielding low mathematical confidence, as reported by the authors [48]. Nevertheless, this work shed light on ovarian rigidity as a clinical sign of spreading ovarian pathology.

In this study, we chose to use AFM for its high sensitivity and effectiveness in distinguishing small mechanical changes between and within tissues at micro-scale resolution, and hence adequately assessing the mechanical stimuli felt by cells [49]. Elasticity measurement evidenced a relatively rigid ovarian tissue at prepuberty, softening significantly at reproductive age, then stiffening considerably upon menopause. Again, ovarian tissue was found to display its own unique mechanical phenotype during reproductive age.These differences are not only structure-dependent, but also related to biochemical differences in ECM composition, as previously demonstrated inour follow-up of variations in elastic matrisome components from prepubertyto menopause [17], and further corroborated by our samples (Fig.5, F-G; Fig.S3). While collagen levels that are associated with tensile strength [50] rose by less than 5% after puberty, we observed a very significant difference in glycosaminoglycans (GAGs) in reproductive-age tissues. The increase was around 30% higher than prepubertal tissue, which explains the elasticity differences between groups [17] (Fig.5, F-G). Thanks to their water sequestration properties, through their highly negative charges, GAGs generate a water-rich network with unique elastic properties, as seen in reproductive-age tissue [51]. Conversely, the levels of collagen and GAGs are maintained from reproductive age to menopause. Thus, a plausible explanation for the elasticity change accompanying aging is the significant drop in elastin upon menopause [17] (Fig.5, F-G).

Elastin fibers provide tissues with recoil to allow repeated stretching and contraction, and their aging-associated degradation appears to have profound effects on ovarian tissue elasticity. Moreover, ovarian rigidity seems to act in synergy with surface roughness. Our results disclose surface characteristics unique to reproductive-age ovaries characterized by a smoother surface compared to other age groups.

Despite widespread application of AFM for mechanical measurement of biological tissues, the majority of existing studies are limited to the framework of standard Hertzian contact mechanics, measuring only the apparent elastic modulus of materials and disregarding their viscoelastic properties. Here, in addition to the apparent elastic modulus measurement, we also investigated the viscoelasticity of human ovarian tissue. ECM viscoelasticity depends on fluid retention and flow through the porous matrix, as well as rearrangement of individual ECM fibers to absorb stress [52]. During short deformation period, the similar viscoelastic behavior observed between age groups can be explained by fast rearrangement of the flexible chains of ECM macromolecules [16]. At longer time range, disentanglement of the chains takes place, and relaxation time associated with this process shows a stronger dependence on the ECM architecture rather than ECM biochemistry [53]. At this time point, the viscoelasticity of reproductive-age and menopausal tissues is comparable, although elasticity changes significantly upon menopause. This finding further underscores the relevance of recording both measurements. Conversely, prepubertal tissue has a slower viscoelastic response, that we can explain by its higher fluid sequestration compared to the other groups. This is related to its unique tight fiber network and small pore size, promoting long term water retention and extending relaxation time.

The described age-dependent characteristics of ovarian ECM impact differently the follicle ovarian reserve and consequently affect the ovarian

activity. While reproductive activity ceases upon menopause, the follicle reserve is not always completely consumed and some preantral follicles remain quiescent for the rest of a woman's life. We speculate that menopausal ovarian tissue can be subject to formation of advanced glycation end-products (AGEs), which are characteristic of aging ECM [54]. These AGEs are able to crosslink and thereby stiffen collagen structures, consequently hindering their movement, as observed in the menopausal group. Certainly, such a stiff matrix incompliant to deformation cannot accommodate the developing ovarian follicles with their evolving size.

In order to avoid any heterogeneity within the same group, we decided to focus only on fertile patients taking hormone contraceptive treatment. Since most adult women in the consultation practice declared to use such a type of contraceptive strategy, it was faster to collect tissue samples from them. Indeed, considering that in today's society the majority of women use hormone-based contraceptives, as described by the World Health Organization (ST/ESA/SER.A/349), our study shows the ovarian ECM architecture of the most significant subgroup of the modern female population. Moreover, to the best of our knowledge, a direct effect of estroprogestatives on the ovarian ECM has never been reported, especially from a biomechanical perspective. On the other hand, it would be interesting to investigate if the cycle phase could influence the ECM architecture. However, such a study would be much more challenging as collecting the required number of ovarian samples from healthy women (not using hormone-based contraceptives) undergoing a laparoscopic procedure during the luteal or follicular phase would demand years. Moreover, since it is rarely necessary to assess and record the cycle stage of patients, this information is hardly ever found in their medical files.

Our study might therefore be the first step to unlocking the mysteries of follicle

quiescence and envisaging an extended reproductive lifetime, and even ovarian rejuvenation, by paving the way for possible therapeutic targetsat the ECM level to treat infertility. The shared information herein will serve to develop new strategies for infertility prognoses based on ECM biophysics,as was done for early breast cancer, based on tissue rigidity, fiber orientationand straightness [35, 55, 56].

In conclusion, our study provides the first conclusive proof of a link between ECM rigidity and fertility by comparing different stages of ovarian transformation related to a woman's reproductive life. A clearer understanding of the mechanisms by which ovarian cells respond to ECM cues should also bolster efforts to judiciously prioritize material properties for therapeutic benefit. Fortunately, new techniques are increasingly being developed to create scaffolds with precise fiber morphology [30, 57], network architecture [58], topography [59], elasticity and even viscoelasticity [60]. Our work emphasizes the importance of nano-meter scale fibril orientation and ECM porosity. Indeed, development of artificial ovarian tissue will require technology capable of highly precise scaffold printing, such as nano 3D printers and FluidFM. We are confident that our work represents the missing piece of the puzzle to leap to the next generation of bio-inspired tissue-engineered ovaries.

Materials and methods

Ovarian biopsies included in the study

Use of human ovarian cortex was approved by the Institutional Review Board of the Université Catholique de Louvain on May 13, 2019 (IRB reference 2012/23MAR/125, registration number B403201213872). Ovarian biopsies were taken from prepubertal (mean age [±SD]=7±3 years), reproductive age (mean age [±SD]=27±5) and menopausal (mean age [±SD]=61±6 years)

patients after obtaining their informed consent. All participating adult subjects were undergoing laparoscopic surgery for benign gynecological diseases not affecting the ovaries. Prepubertal tissue was derived from young cancer patients scheduled for ovarian cortex cryopreservation as a fertility preservation strategy, before being subjected to acute gonadotoxic cancer treatments.

All samples were cryopreserved by slow freezing [61] and kept frozen until the day of their analysis. Tissues provided from the same patients (n=5 per age group) were investigated by SEM (fiber, pore and topography analyses) and AFM. A larger number of paraffin-fixed biopsies (prepubertal, n=16, reproductive-age, n=21, and menopausal, n=24) obtained from the biobank of St-Luc's Hospital were used to complete our fiber orientation evaluation, as described below.

Patients enrolled in this study were carefully selected to avoid any possible bias or heterogeneity related to non-synchronous cycle phases between reproductive-age patients or use of hormone replacement therapy after menopause. Therefore, only fertile patients under ovarian contraceptive treatment and menopausal patients not taking hormonal replacement therapy were included in this study.

Fiber and pore characterization

SEM images were analyzed using the Diameter J plugin [62] of ImageJ software (Wayne Rasband, NIH, USA) to measure fiber thickness as well as pore space and number at 5,000X and 20,000X magnification. Briefly, all images were converted to binary images (black and white pixels only) and segmented into background and foreground, according to one of the 24 segmentation methods generated by DiameterJ [62]. Segmented pictures contain only black and white pixels, with black pixels representing the background and white

pixels representing fibers. After visual inspection of all generated binary pictures, only those that closely resembled to the original SEM image were manually selected for further analyses in batch mode.

Fiber thickness (diameter) was calculated using super pixel determination [62], and mean fiber diameter was calculated by fitting a Gaussian Curve to the radius data and finding the curve's mean value. Pores were considered as black pixel clusters. The algorithm counts the number of pixels in each cluster not touching the picture frame edges, and then reports their area, which equates to pore area. Mean pore area was calculated by averaging all cluster areas.

Scanning electron microscopy

Ovarian samples were fixed in Karnovsky solution immediately upon thawing [61] overnight at 4°C. After fixation, the ovarian fragments were washed five times for 5 min each, before being immersed overnight in a solution of 30% glycerol in 0.1 M phosphate-buffered saline (PBS) at 4°C, then plunged into liquid nitrogen and cryofractured to examine the cortex beyond the epithelial surface. The samples were again washed in fresh 0.1 M PBS three times for 5 min each, before post-fixation in a solution of 2% osmium tetroxide (OsO4) in 0.1 M PBS in the dark to preserve their structure and increase conductivity. After one hour, the washing step was repeated three times, as previously described. The fragments were then dehydrated using a graded series of ethanol (30-100%), dried to the critical point, coated with gold film (Quorum Q150T ES, Quorum Technologies, East Sussex, UK) and scanned by SEM (JSM-7500F, JEOL, Tokyo, Japan) with electron beam energy set at 15-keV. At least three regions were acquired from each sample under SEM at 3 different magnifications: 5,000X, 12,000X and 20,000X.

Sirius Red staining

Five-µm-thick paraffin sections were deparaffinized, rehydrated and treated with a saturated picric acid solution containing 1.3% Sirius Red for one hour at room temperature for collagen staining. Mounted slides were digitized at 20X magnification by automated whole-slide image capture using a Mirax digital slide scanner (3DHISTECH Ltd, Budapest, Hungary). Images were acquired at the following settings: excitation length, 450 nm; emission length, 550 nm; and exposure time, 100 ms.

Orientation analysis

Three to five regions per slide were selected from Sirius Red scans for fiber orientation analysis, using CaseViewer (3DHISTECH Ltd, Budapest, Hungary). CT-FIRE V2.0 Beta 56 Matlab- based open source software was used for fiber tracking, segmentation and orientation analysis. The software combines curvelet transform (CT), a fast discrete preprocessing mechanism that de-noises the image and enhances fiber edges, and fiber tracking (FIRE), an algorithm to extract single fibers from fiber networks and measure individual fiber metrics. The fiber angle in CT-FIRE is defined as the angle between the line linking two endpoints of a fiber and the positive horizontal direction or positive X axis (Supplementary Fig.S1; Table.1). To calculate average fiber orientation and its confidence interval, and visualize data on semi-polar plots, we used the Matlab toolbox CircHist [63].

To investigate fiber organization and remodeling around primordial, primary and secondary follicles at prepuberty and reproductive age, follicles were selected from 40X-magnified images and their borders were delineated manually and selected as regions of interest (ROI). CurvAlign V4.0 Beta [56] was applied to study fiber orientation relative to ROI borders (Table.1).

To visualize data on fiber orientation against follicle borders, we used the Polarplot function on Matlab 2019a (MathWork, Eindhoven, the Netherlands).

Fiber straightness analysis

Fiber straightness is defined as the ratio of fiber Feret length divided by its geodesic length, and its value ranges from 0 to 1 (Table.1). A perfectly straight fiber would have a straightness value of one and increasing complexity ('non-straightness') as the value approaches zero. This parameter was quantified using CT-FIRE software on Sirius Red-stained slides.

Sample preparation for AFM

After thawing, cryopreserved ovarian biopsies were immediately embedded in optimal cutting temperature compound (OCT Tissue-Tek, VWR International, Edmonton, Canada) and snap-frozen in liquid nitrogen, without prior labeling, fixation or dehydration. Fifty-µm-thick ovarian cortex cryosections were obtained using a cryostat (Microm HM 560, Walldorf, Germany) and mounted on Superfrost Plus glass slides (Menzel-Glaser, Germany). The first 200 µm from the surface was cut away to go beyond the mesothelial layer, and tissue slides 300- 500 µm in depth within the ovarian cortex were selected for AFM analyses. On the day of AFM analyses, tissue sections were incubated at room temperature for 5 min to thaw the OCT compound and reinforce tissue adhesion to slides. The slides were then rinsed in pure water several times to remove excess OCT and incubated in PBS at room temperature for 20 min to equilibrate ion charges, while conducting AFM calibration steps, as detailed below. Finally, the samples were mounted for AFM and covered with fresh PBS to conduct biomechanical characterization.

AFM measurements

The 50-µm-thick cryosections of ovarian tissue were kept at -80°C until the start of the experiment and prepared as described in the section 'sample preparation for AFM'. Rheological properties were measured with the NanoWizard 1 BioScience (JPK Instruments) AFM operating in force

spectroscopy mapping mode, as previously described [64, 65, 66]. Force-indentation curves were collected using a rectangular silicon nitride cantilever with a 0.07 N/m nominal spring constant, and 5-µm-diameter borosilicate glass spherical particle attached to the tip. A spherical probe was selected because it produces considerable force with minimal damage to the surface, so is ideal for compliant materials like ovarian tissue [67]. The measured spring constant was very close to the nominal value of 0.07 ± 0.05 N/m using the thermal tune method. This step is designed to transform the laser position signal on the AFM receptor into deformation of the cantilever by evaluating its spring constant in order to translate it into a force. The same cantilever was used for all experiments (Novascan, Ames, IA, USA). The indentation force was set to limit maximum indentation to ~0.5-1 µm, so the bead −tissue contact area during all tests never exceeded 7.068 μm^2. The experiments were performed at room temperature using 1X PBS buffer. To prevent mechanical modifications arising from tissue damage, the tests were limited to 40 minutes per sample. This included at least three 100 x 100 μm^2 force maps and nine positions each with six repetitions of viscoelasticity measurements. No significant difference was observed between measured areas within the same tissue sample, indicating that the ovarian tissue was homogeneously mechanically averaged over the spatial window of 100 x 100 μm^2. Further mapping would have led to experimentally induced variability. For a 100 x 100 μm^2 area, we performed 50 x 50 measurements, resulting in 2,500 force-indentation experiments. The tissue sections were immobilized on Superfrost Plus glass slides Adhesion slides (Menzel-Glaser, Germany). Tight interaction between the samples and the glass did not induce local ECM modifications (artificial solvents, tapes and glues could dissolve or otherwise disturb the physiological state of the ECM, leading to local softening affecting AFM measurements).

Prior to tissue measurements, AFM sensitivity and alignment were ensured with an undeformable (compared to the biological sample) empty glass slide in PBS. The difference between cantilever deflection on a rigid surface and the compliant tissue sample illustrates the deformation of the tissue under the bead load. The force-indentation (F-δ) curves can be fitted with a single exponential following the Hertzian contact model. The Hertzian contact model generates the relationship between the applied force, F, and the resulting indentation, δ, allowing the extraction of an apparent Young's modulus, Ea (a for apparent); namely the correlation constant between the force and area of indentation. Ea is a standard measure for soft tissue elastic properties. We considered the tissue to be incompressible (assumed Poisson ratio: 0.5). The Ea of the probed samples was calculated by fitting the contact part of the measured approach force curves to a standard Hertzian model for a spherical indenter (tip) of radius, R [68:]

$$F = (4E\sqrt{R})*(\delta 3/2)/(3(1 - v2))E = 3(1-v2)\ F/(4\sqrt{R})*(\delta 3/2)$$

where v=0.5 is the Poisson ratio and δ is the indentation depth, calculated by subtracting cantilever deflection from tip displacement. The Hertzian model is typically used to determine contact between two linear elastic bodies. As such, several assumptions had to be checked concerning our biological tissues: i) that they displayed linear elasticity at the scale examined; and ii) that the nonhomogeneity of ovarian tissue (as a composite material) was negligible at the scale examined. Our data are well fitted by the Hertzian model, which is the best approximation for Young's modulus of biological tissues [69].

Young's modulus is presented using a violin distribution plot overlaid with mean and median values calculated over F-δ curves (i.e., pixelwise). For topographical reconstructions, the height of each point was determined by the point of contact from the F-δ curve, with each contact point issuing from

the same curve used to determine Ea. Stiffness data were projected onto topographical maps using Matlab.

To measure the viscoelasticity of ovarian tissue, we conducted repeated and successive long indentation cycles, followed by partial force release. For indentation portion, force was kept constant, while for the release portion, deformation was constant, allowing us to monitor the evolution of both deformation and force. The viscoelastic measurement (force spectroscopy) immediately followed elastic measurement (force mapping scan) and was performed in two points of the same tested region according to a force ramp design loop of ~240 s duration: cantilever extension with force increase (4-µm indention, 100 ms); constant height maintenance at the contact point (20 s); cantilever retraction and force decrease (0.8 µm, 20 ms); and finally constant force maintenance (20 s). Data sampling frequency was set to 4 000 Hz.

Viscoelastic materials retain their shape after deformation, but with a time delay, as shown by the relaxation constant. In slow deformations, we can assume that the ECM is incompressible (Young modulus measurements). However, fast viscoelasticity measurements demonstrate that the tissue may be (reversibly) compressible in short time scales. In this context, viscoelasticity was described by the generalized Kelvin-Voigt model composed of spring constants (elasticity) and dashpots (relaxation time).

Relaxation time was obtained by fitting the modified Kelvin-Voigt model (spring and dashpot connected in parallel), assuming exponentially decaying force at a constant deformation [64]. Thus, it permits establishing bulk elastic constant and relaxation time. The modified Kelvin-Voigt model can be described by the following:

$F(t) = a\Delta x(1 - e^{-bt})$, where $b = \frac{K_1 + k_2}{n}$, and $a = \frac{K_1 k_2}{K_1 + k_2}$

We focused on the part of a curve where the deformation (Δx) was kept constant and the force evolved as a negative exponential (Supplementary Fig.S2). We observed that our experimental data are best fitted by two different relaxation times, which could be described by the generalized Kelvin-Voigt model. The double exponential fit modeled our data better than a single exponential [64], suggesting the presence of at least two processes behind the viscoelastic response. For more details on the model fitting, please consult the Matlab scripts at: https://github.com/inatamara/AFManalysisMatlab.

Topography measurement

Stereo pairs of SEM images of the same tissue region at 12,000X magnification were created by tilting samples by +5° along the X axis (Fig.6D). By rotating the stage between two image takes, we ensured that a significant feature of the sample was always positioned at the same point and that contrast and intensity between images were similar in order to facilitate point matching and guarantee eucentricity. Mountains SEM software 8 (Digital Surf, Besançon, France) was used to enable 3D stereoscopic reconstruction and characterize surface roughness by

calculating the arithmetic average of 3D roughness (Sa) according to calculation conditions defined in ISO25178. In case of a highly uneven surface, Mountains SEM filters were used to level and normalize surface data prior to analysis.

Statistical analysis

Statistical analysis was conducted using the GraphPad Prism software package, version 8.0 (San Diego, USA). Descriptive analyses of values (D'agostino-Pearson or Shapiro-Wilk normality tests) were performed before each evaluation to select the appropriate statistical test. The kruskal-Wallis test followed by Dunn's multiple comparison correction were used to compare

ovarian tissue differences between age groups, including fiber thickness, pore number and viscoelasticity. One-way ANOVA followed by Tukey's post hoc multiple comparisons were applied to compare fiber straightness, pore area, surface roughness (Sa), and elasticity and angle frequency of fiber orientation around different follicle stages within the same age group. Differences in fiber remodeling around follicles at the same follicle stage between prepubertal and reproductive-age tissue were determined by comparing their angle frequencies using the paired t-test. Circular statistics[70] were used to compare global collagen fiber orientation at prepuberty, reproductive age and menopause. The Rayleigh test was applied using the Matlab CircHist toolbox [63] to assess whether fibers were uniformly oriented from 0° to 180° within each age group, or had a commonmean direction [71]. Watson's parametric multiple sample test and Kuiper's test were carried out using the circular statistics toolbox from Matlab [72] to successively compare mean directions and directional distributions between study groups. Differences were considered significant at values of $p<0.05$.

Data and material availability

All analytical data associated with this study are available in the main text or supplementary materials. The Matlab code used in this study, unless otherwise stated in the text, can be found at: https://github.com/inatamara/AFManalysisMatlab.

References

1. Crawford GE, Ledger WL. In vitro fertilisation/intracytoplasmic sperm injection beyond 2020. BJOG 126, 237-243 (2019).
2. Shikanov A, Smith RM, Xu M, Woodruff TK, Shea LD. Hydrogel network design using multifunctional macromers to coordinate tissue maturationin ovarian follicle culture. *Biomaterials* **32**, 2524-2531 (2011).
3. Vanacker J, Amorim CA. Alginate: A Versatile Biomaterial to Encapsulate Isolated Ovarian Follicles. *Ann Biomed Eng* **45**, 1633-1649 (2017).
4. Joo S*, et al.* The effect of collagen hydrogel on 3D culture of ovarian follicles. *Biomed Mater* **11**, 065009 (2016).
5. Chiti MC, Dolmans MM, Donnez J, Amorim CA. Fibrin in Reproductive Tissue Engineering: A Review on Its Application as a Biomaterial for FertilityPreservation. *Ann Biomed Eng* **45**, 1650-1663 (2017).
6. Laronda MM, Jakus AE, Whelan KA, Wertheim JA, Shah RN, Woodruff TK. Initiation of puberty in mice following decellularized ovary transplant. *Biomaterials* **50**, 20-29 (2015).
7. Pors SE*, et al.* Initial steps in reconstruction of the human ovary: survival of pre-antral stage follicles in a decellularized human ovarian scaffold. *Hum Reprod* **34**, 1523-1535 (2019).
8. Hassanpour A, Talaei-Khozani T, Kargar-Abarghouei E, Razban V, Vojdani Z. Decellularized human ovarian scaffold based on a sodium lauryl ester sulfate (SLES)-treated protocol, as a natural three- dimensional scaffold for construction of bioengineered ovaries. *Stem CellRes Ther* **9**, 252 (2018).
9. Aziz AUR*, et al.* A Microfluidic Device for Culturing an Encapsulated Ovarian Follicle. *Micromachines (Basel)* **8**, (2017).
10. Woodruff TK, Shea LD. A new hypothesis regarding ovarian follicle development: ovarian rigidity as a regulator of selection and health. *J Assist Reprod Genet* **28**, 3-6 (2011).
11. Shah JS, Sabouni R, Cayton Vaught KC, Owen CM, Albertini DF, Segars JH. Biomechanics and mechanical signaling in the ovary: a systematic review. *J Assist Reprod Genet* **35**, 1135-1148 (2018).
12. Jorge S, Chang S, Barzilai JJ, Leppert P, Segars JH. Mechanical signaling in reproductive tissues: mechanisms and importance. *Reprod Sci* **21**, 1093-1107 (2014).
13. Leonardo dV. *Codex Leicester* (1909).
14. Schultheiss D, Laurenza D, Gotte B, Jonas U. The Weimar anatomical sheet of Leonardo da Vinci (1452-1519): an illustration of the genitourinary tract. *BJU Int* **84**, 595-600 (1999).
15. Thorne JT, Segal TR, Chang S, Jorge S, Segars JH, Leppert PC. Dynamic reciprocity between cells and their microenvironment in reproduction. *Biol Reprod* **92**, 25 (2015).
16. Akhmanova M, Osidak E, Domogatsky S, Rodin S, Domogatskaya A. Physical, Spatial, and Molecular Aspects of Extracellular Matrix of In VivoNiches and Artificial Scaffolds Relevant to Stem Cells Research. *Stem CellsInt* **2015**, 167025 (2015).
17. Ouni E, et al. Spatiotemporal changes in mechanical matrisome components of the human ovary from prepuberty to menopause. Hum Reprod 35, 1391-1410 (2020).

18. Aitken KJ, Bagli DJ. The bladder extracellular matrix. Part I: architecture, development and disease. *Nat Rev Urol* **6**, 596-611 (2009).
19. Kim DH, Provenzano PP, Smith CL, Levchenko A. Matrix nanotopography as a regulator of cell function. *J Cell Biol* **197**, 351-360 (2012).
20. Xu R, Boudreau A, Bissell MJ. Tissue architecture and function: dynamic reciprocity via extra- and intra-cellular matrices. *Cancer Metastasis Rev* **28**,167-176 (2009).
21. Padhi A, Nain AS. ECM in Differentiation: A Review of Matrix Structure, Composition and Mechanical Properties. *Ann Biomed Eng* **48**, 1071- 1089 (2020).
22. Muiznieks LD, Keeley FW. Molecular assembly and mechanical properties of the extracellular matrix: A fibrous protein perspective. *Biochim Biophys Acta* **1832**, 875 (2013).
23. Jansen KA, Licup AJ, Sharma A, Rens R, MacKintosh FC, Koenderink GH. The Role of Network Architecture in Collagen Mechanics. *Biophys J* **114**, 2665-2678 (2018).
24. Hornick JE, Duncan FE, Shea LD, Woodruff TK. Isolated primate primordial follicles require a rigid physical environment to survive and grow in vitro. *Hum Reprod* **27**, 1801-1810 (2012).
25. Ko C*, et al.* Endothelin-2 in ovarian follicle rupture. *Endocrinology* **147**, 1770- 1779 (2006).
26. Hsueh AJ, Kawamura K, Cheng Y, Fauser BC. Intraovarian control of early folliculogenesis. *Endocr Rev* **36**, 1-24 (2015).
27. Kawamura K*, et al.* Hippo signaling disruption and Akt stimulation of ovarian follicles for infertility treatment. *Proc Natl Acad Sci U S A* **110**, 17474-17479 (2013).
28. Cheng Y*, et al.* Actin polymerization-enhancing drugs promote ovarian follicle growth mediated by the Hippo signaling effector YAP. *FASEB J* **29**, 2423-2430 (2015).
29. Ronceray P, Broedersz CP, Lenz M. Fiber networks amplify active stress. *Proc Natl Acad Sci U S A* **113**, 2827-2832 (2016).
30. Prince E*, et al.* Patterning of Structurally Anisotropic Composite Hydrogel Sheets. *Biomacromolecules* **19**, 1276-1284 (2018).
31. Hiroyuki Sanada JS, Hajime Hamamoto, Yasuo Ueba, Takao Yamamuro, ToshioTakeda. Changes in collagen cross-linking and lysyl oxidase by estrogen. *Biochimica et Biophysica Acta (BBA) - General Subjects* **541**, 408-413 (1978).
32. Lin J, Shi Y, Men Y, Wang X, Ye J, Zhang C. Mechanical Roles in Formationof Oriented Collagen Fibers. *Tissue Eng Part B Rev* **26**, 116-128 (2020).
33. Steinwachs J*, et al.* Three-dimensional force microscopy of cells in biopolymer networks. *Nat Methods* **13**, 171-176 (2016).
34. Friedl P, Maaser K, Klein CE, Niggemann B, Krohne G, Zanker KS. Migration of highly aggressive MV3 melanoma cells in 3-dimensional collagen lattices results in local matrix reorganization and shedding of alpha2 and beta1 integrins and CD44. Cancer Res 57, 2061-2070 (1997)

35. Bredfeldt JS, Liu Y, Conklin MW, Keely PJ, Mackie TR, Eliceiri KW. Automated quantification of aligned collagen for human breast carcinoma prognosis. *J Pathol Inform* **5**, 28 (2014).
36. Majeed H, Okoro C, Kajdacsy-Balla A, Toussaint KC, Jr., Popescu G.Quantifying collagen fiber orientation in breast cancer using quantitative phase imaging. *J Biomed Opt* **22**, 46004 (2017).
37. Woodruff TK, Shea LD. The role of the extracellular matrix in ovarian follicle development. *Reprod Sci* **14**, 6-10 (2007).
38. Kreeger PK, Woodruff TK, Shea LD. Murine granulosa cell morphology and function are regulated by a synthetic Arg-Gly-Asp matrix. *Mol Cell Endocrinol* **205**, 1-10 (2003).
39. West-Farrell ER, Xu M, Gomberg MA, Chow YH, Woodruff TK, Shea LD. The mouse follicle microenvironment regulates antrum formation and steroid production: alterations in gene expression profiles. *Biol Reprod* **80**, 432-439(2009).
40. Laronda MM*, et al.* A bioprosthetic ovary created using 3D printed microporous scaffolds restores ovarian function in sterilized mice. *Nat Commun* **8**, 15261 (2017).
41. Frantz C, Stewart KM, Weaver VM. The extracellular matrix at a glance. *J Cell Sci* **123**, 4195-4200 (2010).
42. Janson IA, Putnam AJ. Extracellular matrix elasticity and topography: material-based cues that affect cell function via conserved mechanisms. *J Biomed Mater Res A* **103**, 1246-1258 (2015).
43. Lu P, Weaver VM, Werb Z. The extracellular matrix: a dynamic niche in cancer progression. *J Cell Biol* **196**, 395-406 (2012).
44. Abagnale G*, et al.* Surface Topography Guides Morphology and Spatial Patterning of Induced Pluripotent Stem Cell Colonies. *Stem Cell Reports* **9**, 654-666 (2017).
45. Paul CD*, et al.* Probing cellular response to topography in three dimensions. *Biomaterials* **197**, 101-118 (2019).
46. Liangliang Yang LG, Qihui Zhou, Taraneh Mokabber, Yutao Pei, Reinier Bron, Patrick van Rijn. Biomimetic Multiscale Hierarchical Topography Enhances Osteogenic Differentiation of Human Mesenchymal Stem Cells. *Advanced Material Interfaces* **7**, (2020).
47. Hsueh AJW, Kawamura K. Hippo signaling disruption and ovarian follicle activation in infertile patients. *Fertil Steril*, (2020).
48. Wood CD*, et al.* Multi-modal magnetic resonance elastography for noninvasive assessment of ovarian tissue rigidity in vivo. *Acta Biomater* **13**, 295-300 (2015).
49. Kao AP, Connelly JT, Barber AH. 3D nanomechanical evaluations of dermal structures in skin. *J Mech Behav Biomed Mater* **57**, 14-23 (2016).
50. Bonnans C, Chou J, Werb Z. Remodelling the extracellular matrix in development and disease. *Nat Rev Mol Cell Biol* **15**, 786-801 (2014).
51. Kurylo MP, Grandfield K, Marshall GW, Altoe V, Aloni S, Ho SP. Effect of proteoglycans at interfaces as related to location, architecture, and mechanical cues. *Arch Oral Biol* **63**, 82-92 (2016).
52. van Helvert S, Friedl P. Strain Stiffening of Fibrillar Collagen during Individual

and Collective Cell Migration Identified by AFM Nanoindentation. *ACS Appl Mater Interfaces* **8**, 21946-21955 (2016).
56. Cerrada ML. Introduction to the Viscoelastic Response in Polymers.) (2012).
57. Ewald CY. The Matrisome during Aging and Longevity: A Systems-Level Approach toward Defining Matreotypes Promoting Healthy Aging. *Gerontology* **66**, 266-274 (2020).
58. Kaushik S, Pickup MW, Weaver VM. From transformation to metastasis: deconstructing the extracellular matrix in breast cancer. *Cancer Metastasis Rev* **35**, 655-667 (2016).
59. Bredfeldt JS*, et al.* Computational segmentation of collagen fibers from second-harmonic generation images of breast cancer. *J Biomed Opt* **19**, 16007 (2014).
60. De France KJ, Yager KG, Chan KJW, Corbett B, Cranston ED, Hoare T. Injectable Anisotropic Nanocomposite Hydrogels Direct in Situ Growth and Alignment of Myotubes. *Nano Lett* **17**, 6487-6495 (2017).
61. Gladman AS, Matsumoto EA, Nuzzo RG, Mahadevan L, Lewis JA. Biomimetic 4D printing. *Nat Mater* **15**, 413-418 (2016).
62. Norman JJ, Desai TA. Methods for fabrication of nanoscale topography for tissue engineering scaffolds. *Ann Biomed Eng* **34**, 89-101 (2006).
63. Charrier EE, Pogoda K, Wells RG, Janmey PA. Control of cell morphology and differentiation by substrates with independently tunable elasticity and viscous dissipation. *Nat Commun* **9**, 449 (2018).
64. Amorim CA, Van Langendonckt A, David A, Dolmans MM, Donnez J.Survival of human pre-antral follicles after cryopreservation of ovarian tissue, follicular isolation and in vitro culture in a calcium alginate matrix. *Hum Reprod* **24**, 92-99 (2009).
65. Hotaling NA, Bharti K, Kriel H, Simon CG, Jr. DiameterJ: A validated open source nanofiber diameter measurement tool. *Biomaterials* **61**, 327-338 (2015).
66. Zittrell F. CircHist - circular / polar / angle histogram) (2020).
67. Peaucelle A, Braybrook SA, Le Guillou L, Bron E, Kuhlemeier C, Hofte H. Pectin-induced changes in cell wall mechanics underlie organ initiation in Arabidopsis. *Curr Biol* **21**, 1720-1726 (2011).
68. Peaucelle A, Wightman R, Hofte H. The Control of Growth Symmetry Breaking in the Arabidopsis Hypocotyl. *Curr Biol* **25**, 1746-1752 (2015).
69. Peaucelle A. AFM-based mapping of the elastic properties of cell walls: at tissue, cellular, and subcellular resolutions. *J Vis Exp*, (2014).
70. Miri AK, Heris HK, Mongeau L, Javid F. Nanoscale viscoelasticity of extracellular matrix proteins in soft tissues: A multiscale approach. *J Mech Behav Biomed Mater* **30**, 196-204 (2014).
71. Frey MT, Engler A, Discher DE, Lee J, Wang YL. Microscopic methods for measuring the elasticity of gel substrates for cell culture: microspheres, microindenters, and atomic force microscopy. *Methods Cell Biol* **83**, 47-65 (2007).
72. Dimitriadis EK, Horkay F, Maresca J, Kachar B, Chadwick RS. Determination of elastic moduli of thin layers of soft material using the atomic force microscope. *Biophys J* **82**, 2798-2810 (2002).

73. Landler L, Ruxton GD, Malkemper EP. Circular data in biology: advice for effectively implementing statistical procedures. Behav Ecol Sociobiol 72, 128 (2018).
74. N. I. Fisher DoAP, CSIRO, Canberra. *Statistical Analysis of Circular Data*. the Press Syndicate of the University of Cambridge (1993).
75. Berens P. CircStat: A MATLAB Toolbox for Circular Statistics. *Journal of* Statistical Software 31, (2009).

Acknowledgment

The authors thank Corry Charlier (Electron Microscopy Department, University of Namur) for his technical assistance during SEM image acquisition and François Petiteau (Digital Surf) for his help with Mountains SEM software. We also thank Vincent Fleury for moderating the established collaboration to conduct AFM analyses and Didier Vertommen for his critical review of the manuscript from a biochemical perspective. We greatly thank Yuming Liu for sharing his expertise on using CT-FIRE. We are also very grateful to Mira Hryniuk, BA, for reviewing the English language of the manuscript.

Funding. This study was supported by grants from the Fonds National de la Recherche Scientifique de Belgique (FNRS) (C. A. Amorim is an FRS-FNRS Research Associate; grant MIS #F4535 16 awarded to C. A. Amorim) and the Université Catholique de Louvain (PhD grant 'Coopération au développement' awarded to E. Ouni).

Author contributions. Conceptualization, E.O., and C.A.A. Methodology, validation, data analysis, and investigation, E.O., O.V., A.P., and K.H. Software, E.O., A.P. and K.H. Resources, T.T., M.O.,CA.A and M.M.D. Writing—original draft, E.O. Writing—review and editing, E.O., A.P., K.H., O.V., M.M.D., and C.A.A. Data visualization, E.O. Supervision, C.A.A. Funding acquisition, C.A.A. and E.O.

Competing interests. None of the authors have any competing interests to declare.

Materials and correspondence. Correspondence and material requests should be addressed to Christiani Andrade Amorim (christiani.amorim@uclouvain.be) and Emna Ouni (emna.ouni@uclouvain.be).

Figures

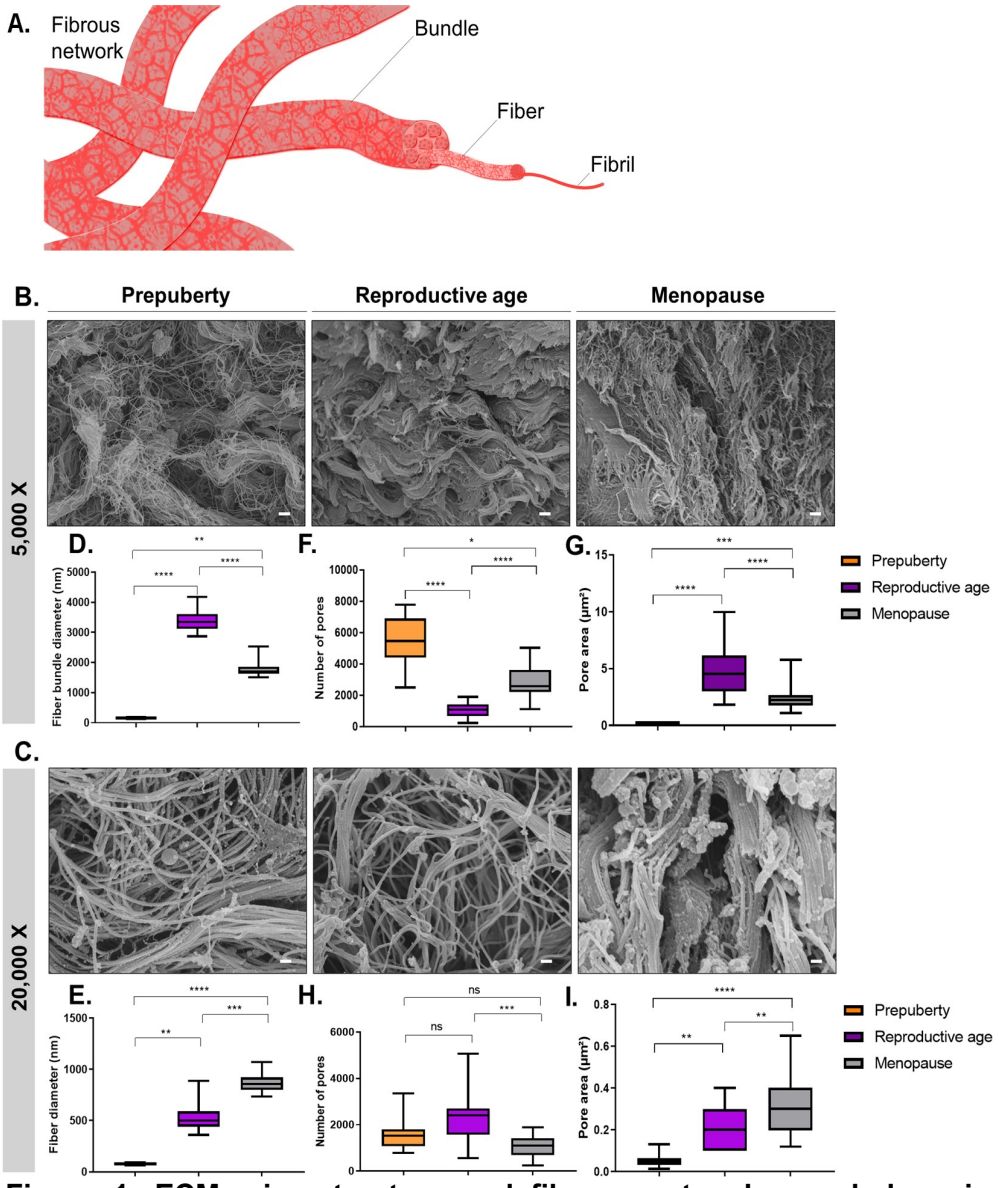


Figure 1. ECM microstructure and fibrous network morphology in human ovarian tissue from prepuberty to menopause. A) Schematic illustration of the fibrous network anatomy composed of fibrils, fibers and fiber bundles, as defined in this study. SEM micrographs revealed: B) the ECM

network structure at fiber bundle scale (5,000X magnification) and C) fiber scale (20,000X magnification). D, E) At prepuberty (number of biological replicates [n]=5), ovarian tissue is composed of the thinnest fibers (mean ± SD: 76 nm ± 10) assembled into the thinnest bundles (160 nm ± 21), densifying upon puberty (fiber scale: 529 nm ± 128; fiber bundle scale: 3379 nm ± 368). F-I) Fiber and bundle spacing deduced from pore number and area revealed a tight ECM network at prepuberty, illustrated here by large numbers of pores (5,430 ± 1,688) occupying the smallest area (0.19 μm^2 ± 0.05). At reproductive age (n=5), human ovarian tissue is characterized by fibers of intermediate diameter (528 nm ± 13) assembled into the thickest bundles compared to prepubertal (n=5) and menopausal (n=5) tissues, forming a looser fibrous network with greater pore spaces (4.9 μm^2 ± 2.4). While at high magnification we found menopausal tissue to be composed of smaller pore numbers occupying greater areas than at reproductive age (1,054 ± 470), a similar observation at lower magnification revealed tighter network organization at menopause (0.32 μm^2 ± 0.15). These pore spacing differences between age groups may play a role in permeability change with age. Fiber and pore analyses were conducted using DiameterJ. One-way ANOVA (post hoc: Tukey) was used to compare pore area. Differences in fiber morphology and pore number were analyzed by the Kruskal-Wallis test (post hoc: Dunn) (*p<0.05; **p<0.01; ***p<0.001; ****p<0.0001). Scale: 1 µm.

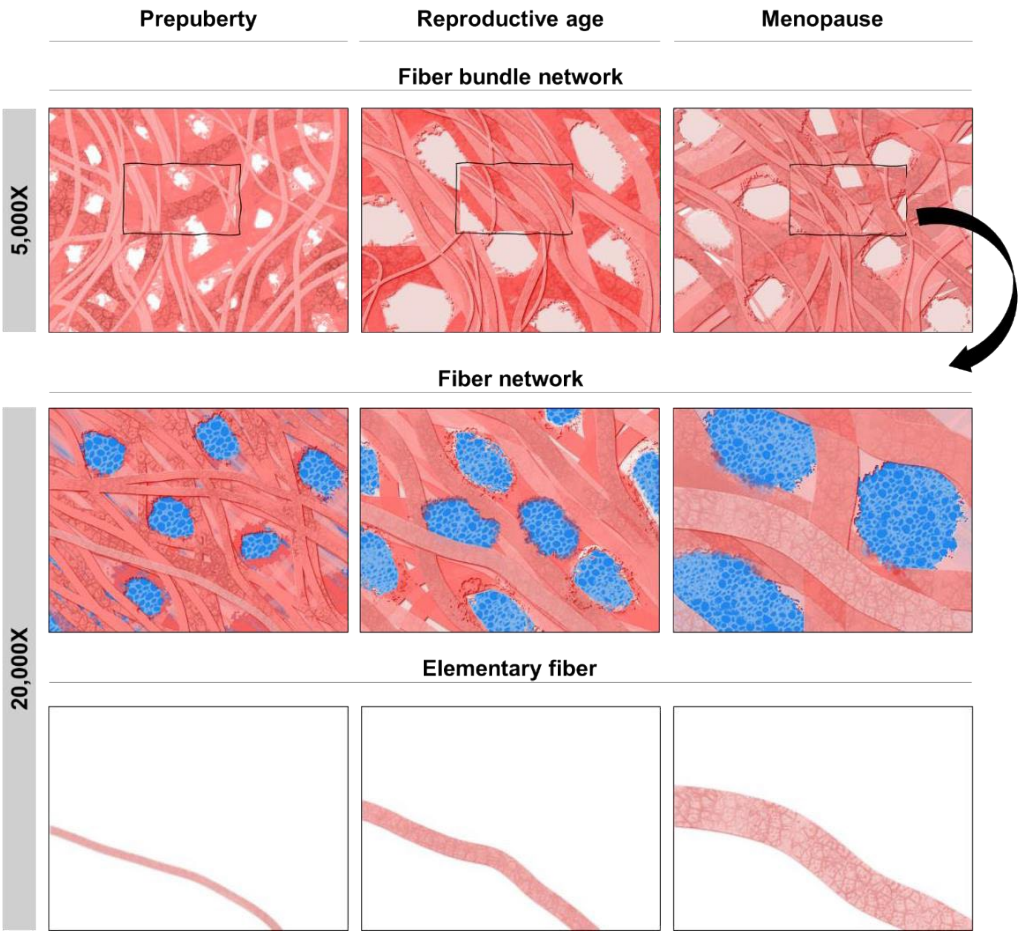


Figure 2. Schematic illustration of fibrous ECM structure deduced from SEM image analyses. Simplified illustration of ECM structural remodeling with age at fiber (20,000X) and fiber bundle (5,000X) scale, showing changes in fibrous network morphology (thickness, spacing).

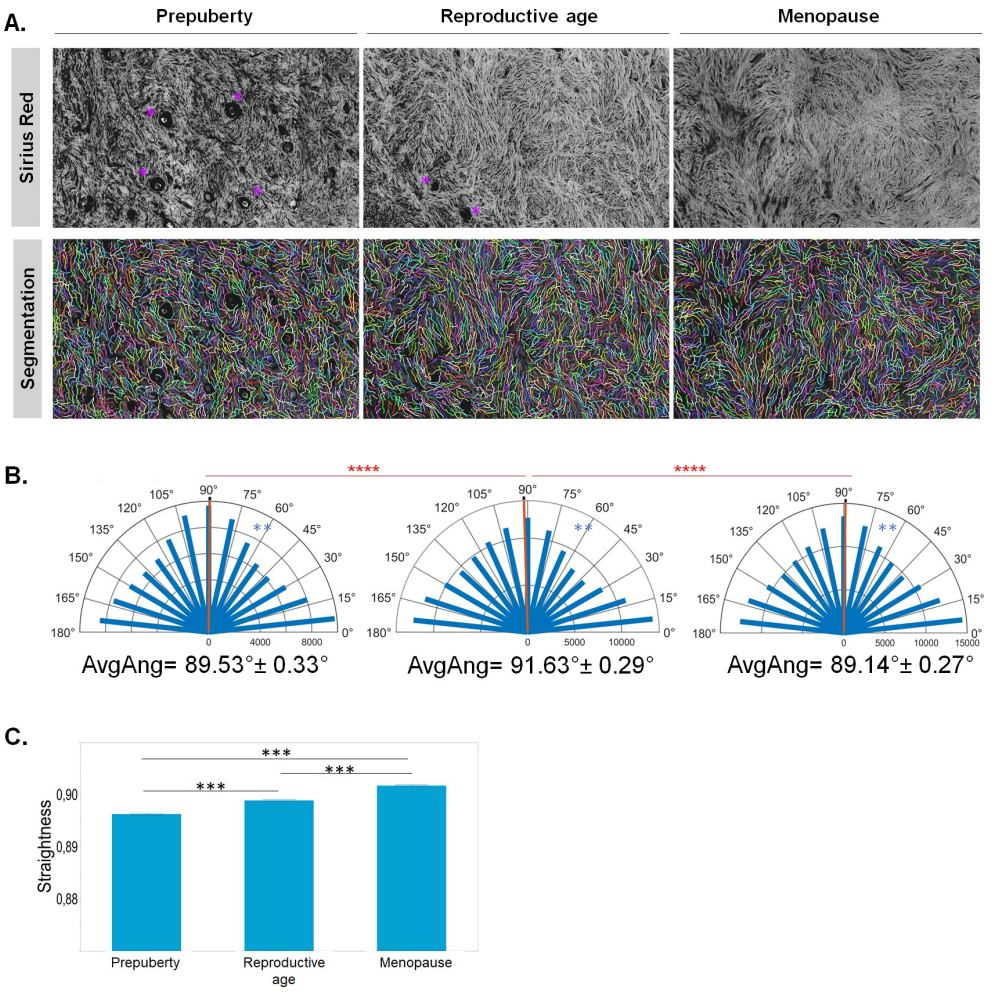


Figure 3. Fiber orientation and straightness in the interstitial ECM. A) Sirius Red-stained paraffin sections show collagen autofluorescence, which was used for collagen fiber segmentation by curvelet transform that enabled measurement of directional fiber distribution and fiber straightness. Asterisks point to preantral follicles. B) Angular fiber distribution changes with age (blue) demonstrate the anisotropic nature of human ovarian tissue, but average angles change only at reproductive age (red), and no significant differences were noted between prepubertal and menopausal tissues. C) Fiber straightness increases significantly with age. Straightness results are

expressed as mean ± SD. Rayleigh test was applied to assess whether fibers are uniformly oriented from 0° to 180° within each age group or display a common mean direction. Watson's parametric multiple sample test and Kuiper's test were applied to successively compare mean directions and directional distribution between study groups (***p<0.001; ****p<0.0001). Scale: 100 µm.

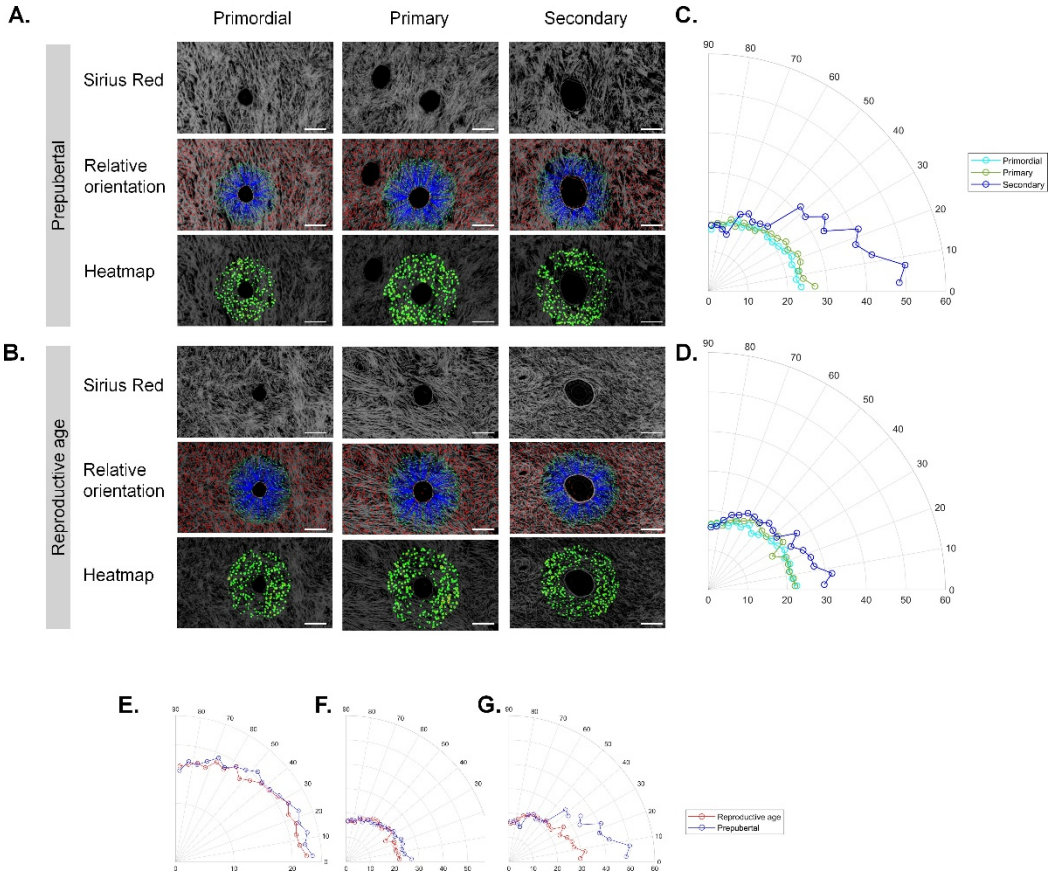
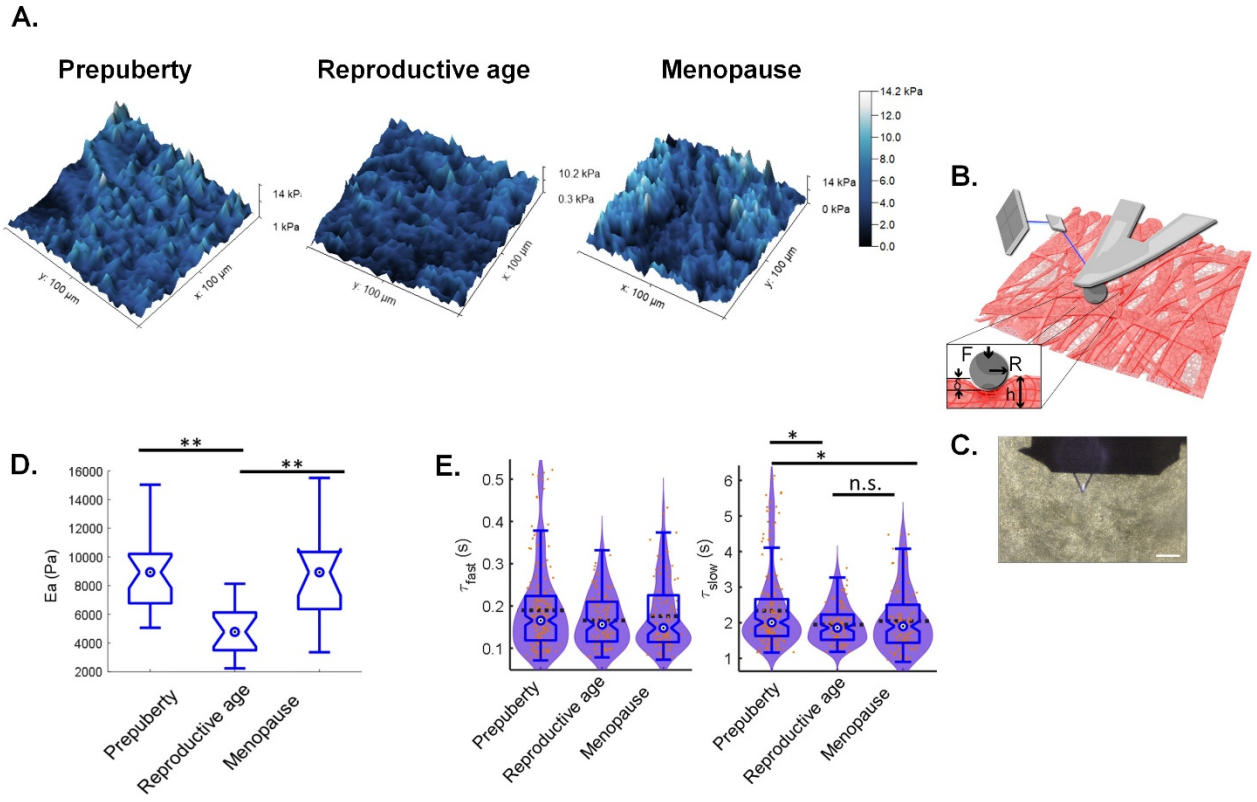
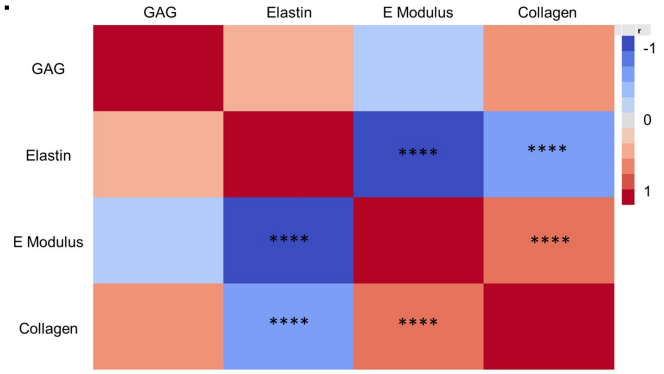


Figure 4. Fiber orientation in the perifollicular ECM around preantral follicles at prepuberty and reproductive age. A, B) Analysis of fiber orientation around the borders of primordial, primary and secondary follicles at prepubertal and reproductive age using Sirius Red-stained sections. The blue line associates the center of fibers extracted by CT-FIRE with corresponding boundary locations, while the red line shows fibers located either beyond the distance range or within the boundary; boundaries are highlighted in yellow; the heatmap uses red or warm colors to indicate larger relative angles. **C, D)** Circular plots of fiber orientation frequency during folliculogenesis in prepubertal and reproductive age tissues revealed significant fiber reorientation at the secondary stage compared to primordial

and primary stages, and at both ovarian ages. E-G) When comparing the difference in fiber orientation around follicles from prepubertal and reproductive- age tissues at each follicular stage, we found significant differences between age groups at all stages. One-way ANOVA (post hoc: Tukey) was used to compare fiber directionality between follicle stages and age groups (*p<0.05;**p<0.01; ***p<0.001; ****p<0.0001). Scale: 200 μm.


A.
Prepuberty
Reproductive age
Menopause
14.2 kPa
12.0
10.0
8.0
6.0
4.0
2.0
0.0
14 kPa
1 kPa
10.2 kPa
0.3 kPa
14 kPa
0 kPa
y: 100 µm
x: 100 µm
B.
F
R
h
C.
D.
Ea (Pa)
16000
14000
12000
10000
8000
6000
4000
2000
**
**
Prepuberty
Reproductive age
Menopause
E.
τ_{fast} (s)
0.5
0.4
0.3
0.2
0.1
τ_{slow} (s)
6
5
4
3
2
1
*
*
n.s.
Prepuberty
Reproductive age
Menopause

F.


GAG
Elastin
E Modulus
Collagen
GAG
Elastin
E Modulus
Collagen
****
****
****
****
****
****
-1
0
1

G.

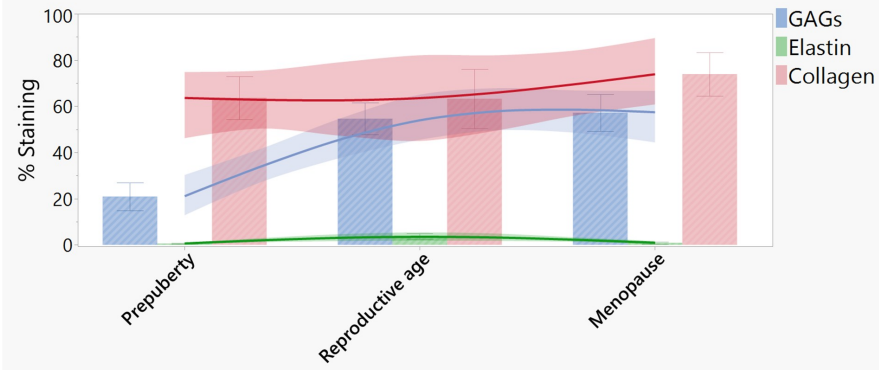
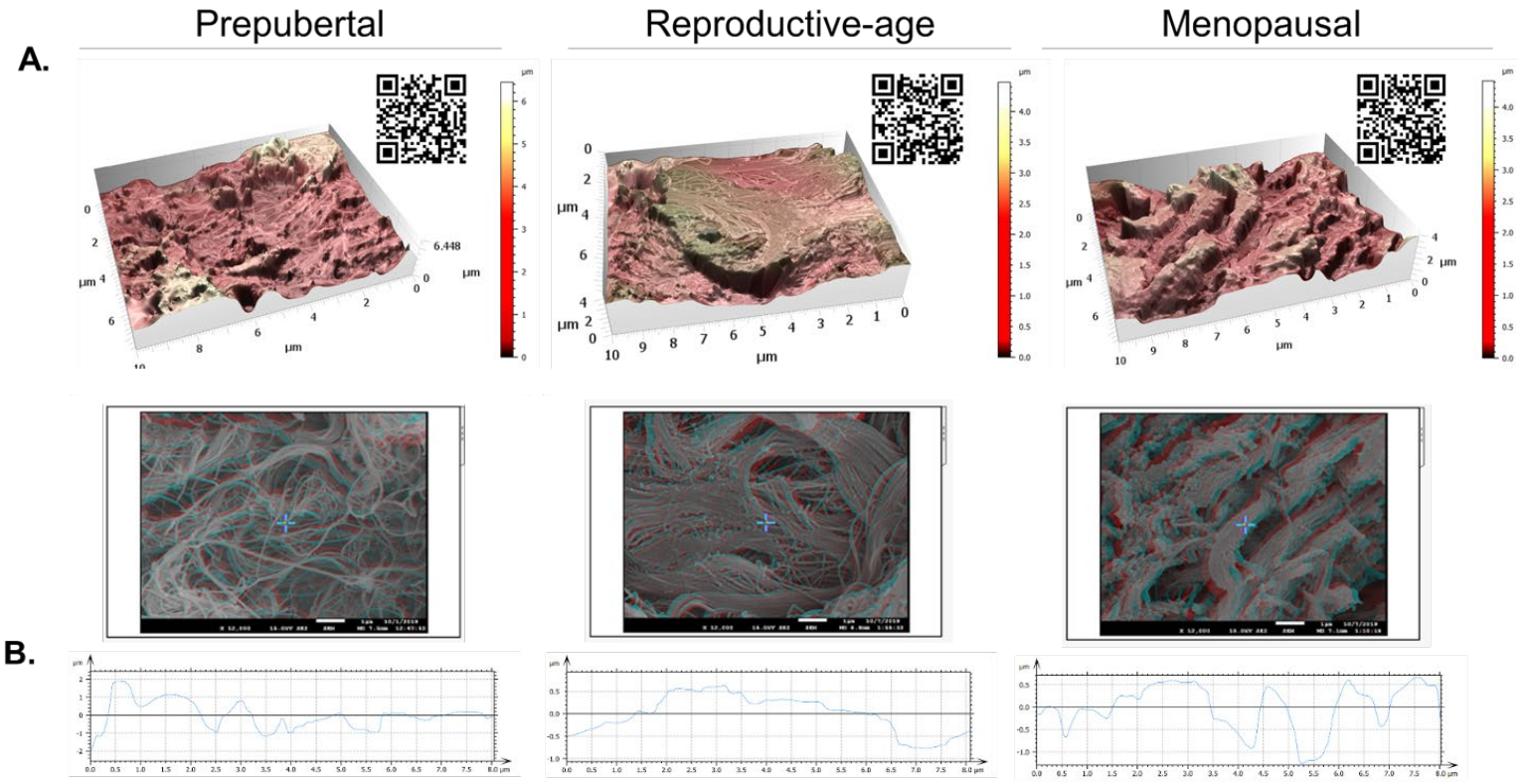

% Staining
100
80
60
40
20
0
Prepuberty
Reproductive age
Menopause
GAGs
Elastin
Collagen

Figure 5. Elasticity and viscoelasticity of human ovarian tissue. A) 3D rendering of AFM maps such as surface height and color, reflects Young's modulus amplitude measured using a Hertzian model. **B)** Graphic representation of a Hertzian model and AFM measurement of ovarian tissue deformation under AFM spherical probe indentation: R is the probe radius (2.5 µm); F is the applied force; δ is the indentation; and h is tissue thickness (50 µm). Deformation induces cantilever deflection. An optical system using a laser to detect the tip's deflection helped to measure Young's modulus using the Hertzian model. **C)** Transmission microscopy image of the AFM cantilever positioned on top of ovarian tissue in PBS. scale: 100 µm. **D)** Elasticity measurements revealed that ovarian tissue is equally rigid at prepubertal and menopausal age, while it is significantly softer at reproductive age. Boxplots display 25th and 75th percentile, median (blue circle), and the whiskers extending to the last data point not considered outlier. **E)** At prepuberty, ovarian tissue is characterized by a slower relaxation time compared to reproductive-age and menopausal tissue ($p<0.05$). Although ovarian tissue shows significant elasticity change upon menopause, no significant difference was recorded in terms of viscoelasticity (**λ**: relaxation time) between reproductive-age and menopausal tissues. The graphic shows the overlay of violin plots with boxplots displaying 25th and 75th percentile, median (blue circle), and the whiskers extending to the last data point not considered outlier (ns: non-significant; *$p<0.05$; **$p<0.01$). F) Correlation matrix of elastic matrisome components and apparent elastic modulus measured in study subjects.

Histological staining was used to characterize glycosaminoglycans (GAGs) and collagen abundance, and immunofluorescent staining of elastin was achieved using monoclonal anti-elastin (Abcam, EPR 20603). GAGs were labeled with Alcian blue (pH=2.5) and collagen was stained with Sirius Red, as described elsewhere[17]. Slides were digitized by automated whole- slide image capture with a Pannoramic 250 Flash III scanner (3DHISTECH Ltd, Budapest, Hungary). Computer- assisted quantification of immunofluorescent labeling and histological staining was carried out with Oncotopix, version 2017.2 (Visiopharm, Hoersholm, Denmark). Tailored software applications were developed by our team to detect tissue regions of interest (ROIs), quantify ROI area, and measure stained areas within a given ROI. Vessels, oocytes and artifacts were manually discarded from ROIs. Computer-assisted quantification of staining was based on the following equation: % stained area = (stained area /ROI area)*100 expressed as a percentage. A correlation matrix was constructed using JMP Pro 14.3.0 (SAS, France, Grégy-sur- Yerres). Spearman's correlation was used to measure the strength (****p≤0.0001) and direction of association (r) between each pair of variables. G) Changes in collagen, elastin and GAG levels with age are summarized in bar charts, presented as mean ± SD. The data plot fits a smoothing spline with a lambda value of 0.05. The curves also include the bootstrap confidence region for each fit generated by JMP Pro 14.3.0. Drawn circles highlight the presence of preantral follicles.


Prepubertal
Reproductive-age
Menopausal
A.
B.
6.448
µm

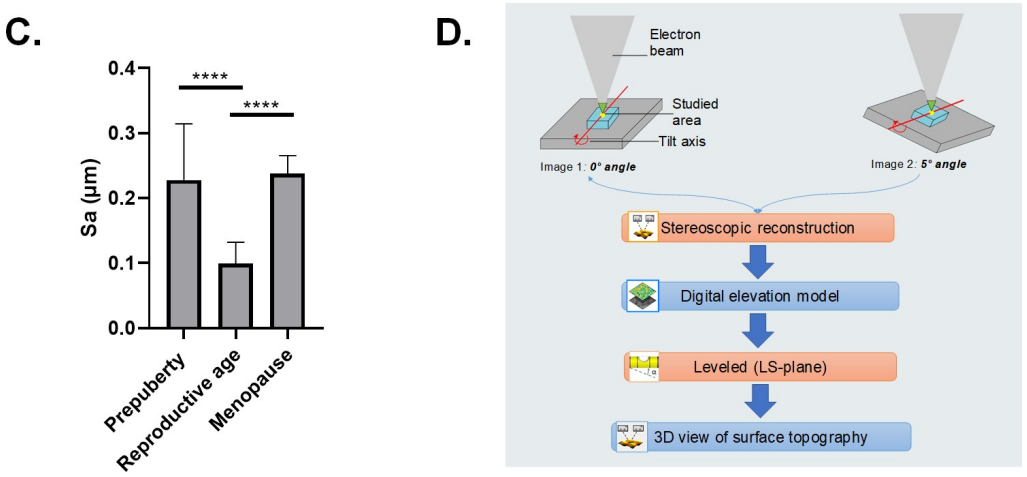


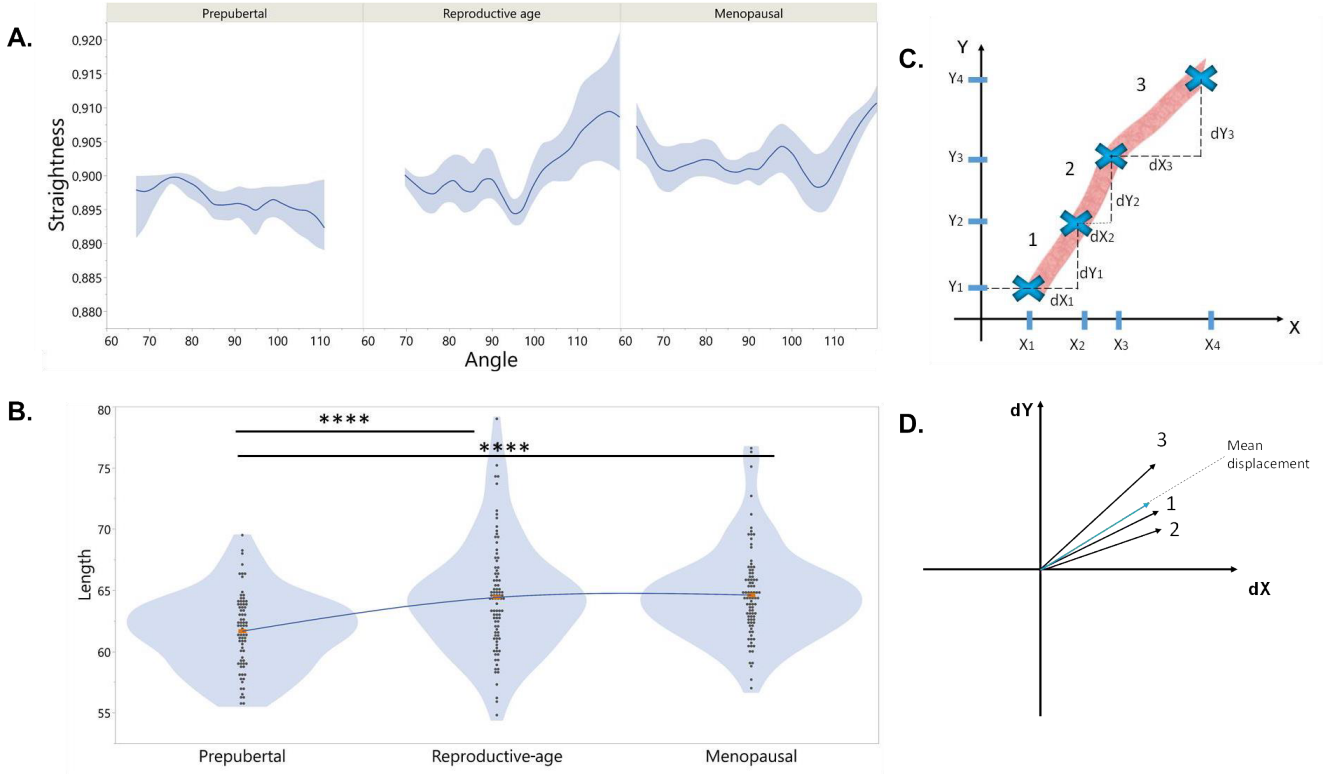
Figure 6. Topography and surface analyses. A) 3D rendering of surface topography from stereoscopic reconstruction of two SEM images acquired using eucentric rotation around the y axis with a 5° tilt at 12,000X magnification. Color scales indicate the height range on each surface. QR codes open video animation of 3D topography representations. B) Extracted rugosity profiles from 3D reconstructions. C) Surface roughness was measured by calculating the arithmetic average of 3D roughness (Sa) according to calculation conditions defined in ISO25178. One-way ANOVA (post hoc: Tukey) was used to compare surface roughness (****p<0.0001).

Table1. Number of segmented and tracked fibers in perifollicular and interstitial ECM.

	Interstitial ECM	*Perifollicular ECM*		
		Primordial	*Primary*	*Secondary*
Prepubertal	▪ *117,005 fibers* ▪ *74 images*	▪ *17,025 fibers* ▪ *48 follicles**	▪ *10,224 fibers* ▪ *28 follicles*	▪ *3,659 fibers* ▪ *8 follicles*
Reproductive-age	▪ *157,445 fibers* ▪ *104 images*	▪ *19,246 fibers* ▪ *56 follicles*	▪ *10,781 fibers* ▪ *31 follicles*	▪ *2,069 fibers* ▪ *6 follicles*
Menopausal	▪ *173,325 fibers* ▪ *102 images*			

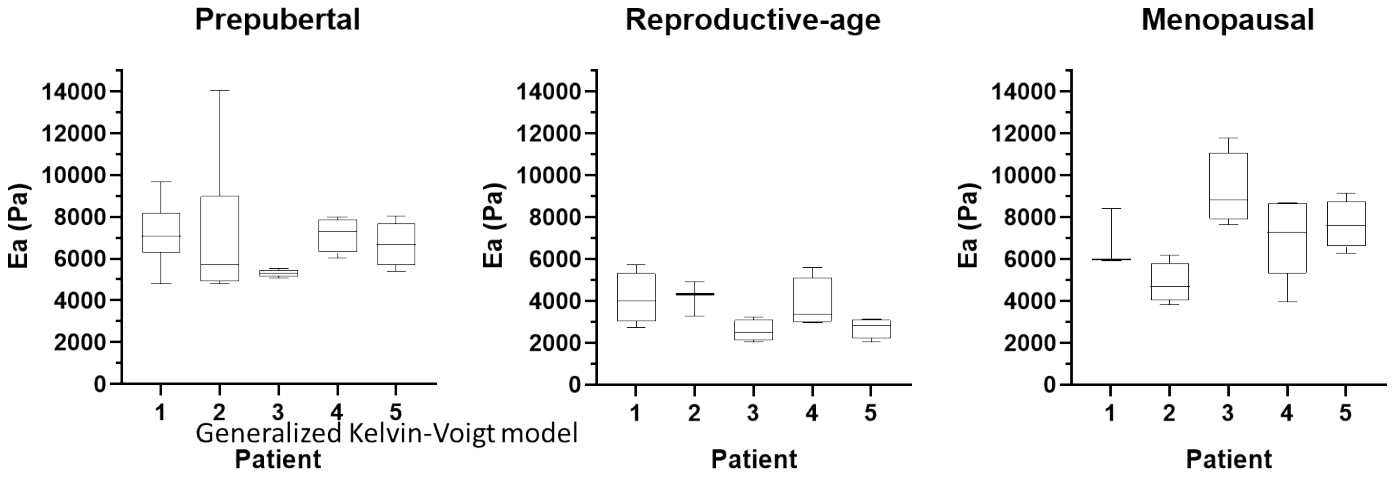
**One follicle per image was analyzed.*

Supplementary data



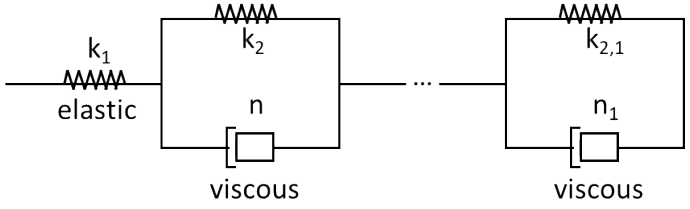
Supplementary Fig S1. Fiber straightness, length and angle measurement. Fiber straightness and length are two factors that might influence fiber tracking and orientation measurement on CT-FIRE, since long curvy fibers can lead to biased mean displacement. Based on fiber length and straightness measurement in all groups, we demonstrate that angle measurement is not influenced by these factors. A) To check whether fiber straightness impacts angle measurement, summarized statistics of straightness data were plotted against corresponding fiber orientation in each sample. No direct interdependence was noted between the two variables, which demonstrates that fiber straightness did not affect measured angles. The data plot fits a smoothing spline with a lambda value of 0.05. The curves also include the bootstrap confidence region for each fit generated by JMP Pro 14.3.0. B) Fiber length variation with age expressed in pixels. Fiber length was measured using CT-FIRE on Sirius Red-stained slides. The Tukey-Kramer HSD test was used to compare mean fiber lengths (orange), ****$p<0.0001$. C-D). Examples of mean displacement of a fiber trajectory and angle measurement are shown. C) Trajectory consisting of four XY coordinates; displacement from one coordinate to the next is denoted as dXY1, dXY2 and dXY3. D) The displacements (blue: dXY1, dXY2 and dXY3) are averaged to calculate the mean displacement of the trajectory (black arrow).

A.

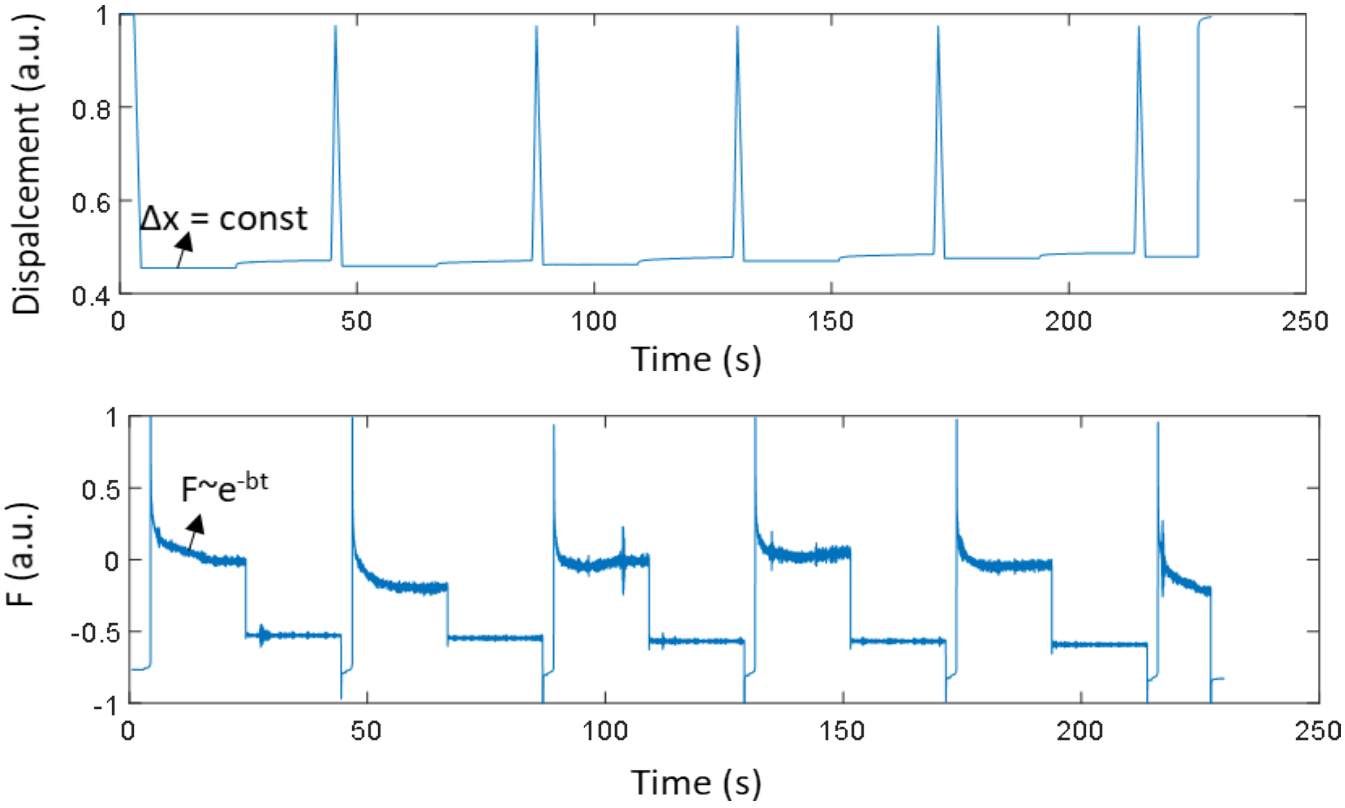


Generalized Kelvin-Voigt model

B.

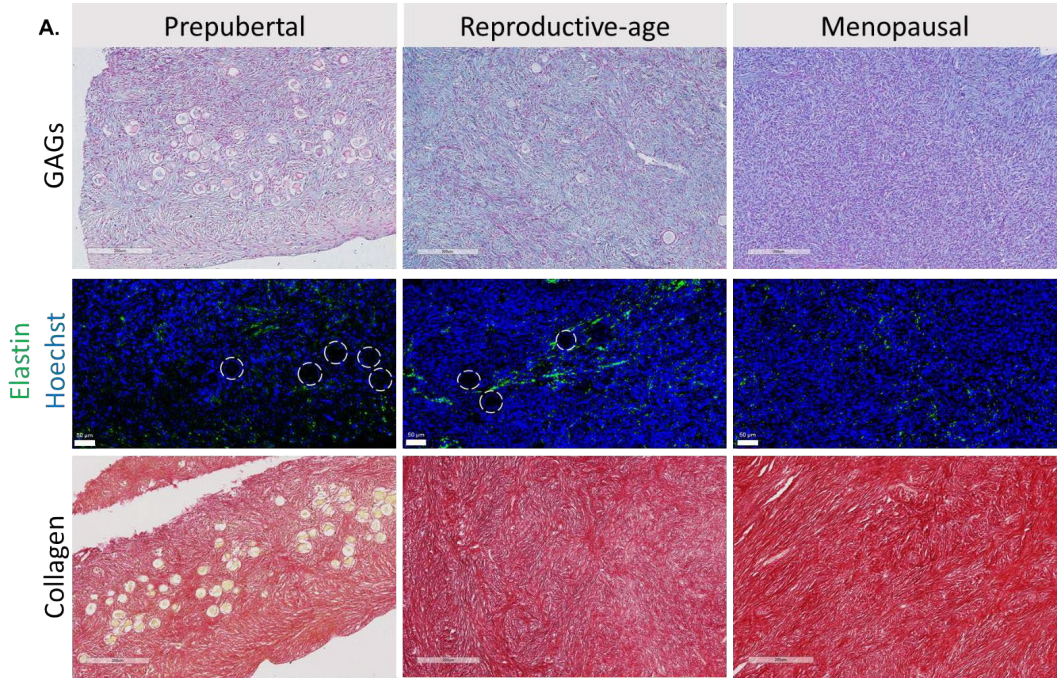


C.


Dispalcement (a.u.)
1
0.8
0.6
0.4
Δx = const
0
50
100
150
200
250
Time (s)
F (a.u.)
1
0.5
0
-0.5
-1
F~e-bt
0
50
100
150
200
250
Time (s)

Supplementary Fig S2. Elasticity and viscoelasticity measurement details. A) Apparent elasticity (Ea) measurement in all replicates used in this study. Ea was calculated over different regions in the same sample for different patients within each group. At least three maps of 100x100 μm2 area were measured per sample. Boxplots display 25th and 75th percentile, median, and the whiskers extending to the last data point not considered outlier. B-C) Viscoelasticity measurement. Viscoelastic materials retain their shape after deformation, but with a time delay, as shown by the relaxation constant. In slow deformations, we can assume that the ECM is incompressible (Young's modulus measurements). However, fast viscoelasticity measurements demonstrate that the tissue may be (reversibly) compressible in short time scales. In this context, viscoelasticity was described by the generalized Kelvin- Voigt model model composed of spring constants (elasticity) and dashpots (relaxation time). Relaxation time was obtained by fitting the modified Kelvin-Voigt model (spring and dashpot connected in parallel), assuming exponentially decaying force at a constant deformation [63]. Thus it permits establishing bulk elastic constant and relaxation time. The modified Kelvin-Voigt model can be described by the following: $F(t) = a\Delta x(1 - e^{-bt})$, where $b = \frac{K_1+k_2}{n}$, and $a = \frac{K_1 k_2}{K_1+k_2}$

We focused on the part of a curve where the deformation (Δx) was kept constant and the force evolved as a negative exponential. We observed that our experimental data are best fitted by two different relaxation times, which could be described by the generalized Kelvin-Voigt model. The double exponential fit modeled our data better than a single exponential [63], suggesting the presence of at least two processes behind the viscoelastic response. For more details on data processing and the model fitting, please consult the Matlab scripts athttps://github.com/inatamara/AFManalysisMatlab.



Supplementary Fig S3. Collagen, elastin and GAGs evolution with age in study subjects. Histological and elastin immunofluorescent staining of human ovarian tissue at prepubertal, reproductive and menopausal age.

CHAPTER 4

Discussion, perspectives and emerging opportunities

I. Discussion

When it comes to the human ovary, Flaubert's prescient comment, "Le bon Dieu est dans le detail" hits the mark. Although "Diable" is often substituted, this poignant statement of the human condition also applies to the study of ovarian cells microenvironment. At all levels of human effort, the devil is indeed in the details, and nowhere are the "details" as convoluted, diversified, and obscure as found in the study of the ovarian ECM.

Indeed, the ECM, this complex meshwork of proteins has been shown to orchestrate cell behavior and fate through its multiple facets, namely proteomics, biomechanics and architecture (Aitken and Bagli 2009). While a normal ECM protein can restore transformed cells to quiescence (Aitken and Bagli 2009), a damaged ECM can trigger malignancy (Xu et al. 2009) or differentiation (Padhi and Nain 2020). For instance, the multiscale architecture of ECM collagen fibers influences cell polarity and promotes migration by providing contact guidance cues (Kim et al. 2012).

Although the first dissection of the human ovary dates back to the 17th century, many aspects of its interstitial and perifollicular ECM has remained undercovered til our study. Paradoxically, ovarian engineering has emerged in recent years to provide novel fertility solutions and in vitro models that relied on synthetic (Shikanov et al. 2011) and natural (Chiti et al. 2017a;Joo et al. 2016; Vanacker and Amorim 2017) hydrogels, decellularized scaffolds (Hassanpour et al. 2018; Laronda et al. 2015; Pors et al. 2019) and microfluidics (Aziz et al. 2017). All of which, claimed biomimicry with various results but none has faithfully mimic specific ovarian ECM characteristics because they have never been covered and quantified in detail before. Whereas ovarian engineering has become a mature scientific discipline (a recent PubMed search for keyword "ovarian engineering" returned 3,409

citations), the addition of the keyword “ECM” returned only 47 citations.

Given the World Health Organization’s ranking of female infertility as the fifth highest global disability, a deeper understanding of basic human ovarian ECM and physiology served as motivation for our studies.

Our work represents the missing piece of the puzzle at the interface between proteomics, biomechanics and architecture of the human ovarian ECM from prepuberty to menopause, to leap to the next generation of bio- inspired tissue- engineered ovaries and unfold the power of biomimetism, also known as ‘innovation inspired by nature’, or alternatively ‘conscious emulation of nature’s genius’, with a goal of eventually putting a small “d” in Diable.

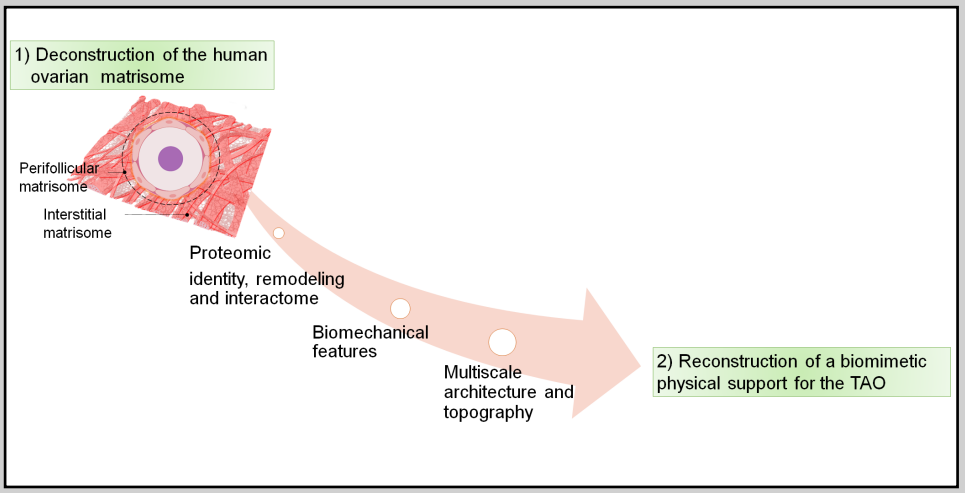


Figure 25 | Preliminary steps for reverse engineering the human ovarian matrisome. *(Ouni. Unpublished).*

I.1. Proteomic characteristics of the human ovary and reproductive-age biomarkers at the ECM level

I.1.1. Discovery proteomics

Although genomics is the most used procedure in clinical research and provides valuable information on certain biological functions, the proteome is the complete representation of proteins expressed by a genome at a certain time and developmental stage. It is therefore more representative of the phenotype and able to provide complementary information that is yielded by gene expression studies. Indeed, gene expression studies of RNA transcripts often cannot predict the abundance or function of proteins or their post-translational modifications (Vogel and Marcotte 2012). For several years now, ovarian proteomic studies have focused on characterizing follicular fluid composition in human preovulatory follicles (Ambekar et al. 2015; Jarkovska et al. 2010), emphasizing the functional selectivity of the basement membrane toward plasma proteins (Angelucci et al. 2006). Efforts have also been made to identify ovary-related transcription in different species to explore the complex functions of the ovary in an integrated manner. This is necessary because of obvious difficulties in obtaining human ovaries, as well as the feasibility of conducting experimental research in humans because of ethical and logistical constraints. Indeed, the only aspect of the ovarian ECM to have been investigated so far is the basement follicular membrane, and this was done through immunohistochemical tests, which only offer a limited characterization restricted by the type and number of antibodies used (Angelucci et al. 2006; Rodgers et al. 2003).

Therefore, the first step we conducted on the pursuit of ovarian tissue characterization consisted of a proteomic pilot study of the human ovarian cortex by turning ovarian ECM dissolution during mechanoenzymatic follicle isolation into our favor. To scrutinize its composition, we conducted a non-

targeted proteomic characterization of premenopausal ovarian tissue by MS. And this is how we ran our study: we collected fresh cortex samples from the Saint Luc clinic, which we divided into two groups fresh and frozen from the same patient where the frozen samples were cryopreserved by slow freezing. We used a modified version of our follicle isolation routine to digest the tissue. But after centrifugation instead of taking the pellet containing isolated follicle, we collected the supernatant containing solubilized proteins. The suspensions were then analyzed with 2D-LC-MS; a mass spectrometry technique developed to characterize proteomic samples with broad diversity and large dynamic ranges. The results confidently identified more than 1500 proteins in fresh and frozen human ovarian cortex. This study demonstrated an important correlation between frozen and fresh ovarian tissues with an approximate 70% overlap between the two proteomes raising the possibility for additional extended studies using cryopreserved samples. The used one step procedure, with no ECM specific enrichment enabled a deep coverage of intra and extracellular proteins and unravelled for the first time the composition of the ovarian ‘matrisome’, a term that was not ever used in the gynecology field before.

Using bioinformatic tools and data mining analysis, we gained a deeper understanding of the function, cellular distribution and signaling role of the detected proteins.

Our used enzymatic digestion led to rupture of some cellular membranes, which yielded further information on intracellular proteins. Fundamental cellular biological processes at the intracellular compartment, and several oocyte-related events were detected, namely cell communication pathways involving ECM-receptor interaction, focal adhesion and gap junctions, emphasizing the primordial functional importance of ovarian cell interaction and communication.

Focal adhesion proteins made up one of the top largest groups of detected proteins. Proteins included in this category were considered necessary for ovarian function, because focal adhesion is a key means by which cells sense and respond to the extracellular environment. Gap junction channels, another detected protein category, allow direct cell-cell communication and diffusion of fundamental nutrients and chemical cues essential for follicular development (McGinnis and Kinsey 2015). Their assembly is promoted by the WNT/β- catenin pathway of gap junction proteins. Other pathways of interest were also detected, such as cGMP/PKG implicated in oocyte meiotic arrest (Bodis et al. 2014), and RAS which is presumed to regulate oocyte maturation and quality. Up today, RAS involvement in hormonal regulation remains unclear because of significant differences between species (Herr et al. 2013). Hence, through our data set acquired by MS, we hope to contribute to the elucidation of unexplored proteins in the RAS pathway in the human ovary. Numerous coagulation- and angiogenesis- related proteins were identified and further elucidated by KEGG pathway analysis, such as coagulation factors (e.g. fibrinogen, prothrombin and plasminogen), as well as those linked to the coagulation and platelet- associated regulatory system (e.g. antithrombin, von Willebrand factor, platelet-activating factor acetyl hydrolase IB and serpins), revealing their potential function in reproduction. In the light of recent discoveries, coagulation proteins in the ovary appear to occupy new roles beyond plugging blood leakage that go as far as stem cell awakening in the ovary and ovarian rejuvenation (Bukovsky 2015; Hirota et al. 2003), clearly requiring further investigation.

Other rarely explored proteins in human ovaries were documented in our data set, namely 14-3-3 protein isoforms delta and epsilon, which are among the top 50 most abundant proteins. The 14-3-3 proteins central mediators modifying cell-signaling processes, including cell cycle regulation and

apoptosis (Aitken 2006; Morrison 2009; Pozuelo Rubio et al. 2004). It has been suggested that these proteins are involved, at least in the Xenopus genus, in maintaining prophase I arrest in germinal vesicle-intact oocytes by sequestering the essential phosphatase, in meiosis resumption M-phase inducer phosphatase 2 (CDC25B), in an inactive state (Duckworth et al. 2002).

At the extracellular compartment, we discovered the dominant collagen type in the human ovary collagen VI, which we showed to be ubiquitously expressed throughout the ECM by immunohistochemistry. It is a basement membrane-anchoring molecule that interacts with collagen IV and may have additional cytoprotective and regulatory functions (Cescon et al. 2015). In addition, it has been suggested that type VI collagen microfibrils are resistant to MMPs but are susceptible to degradation by serine proteases, which are enzymes secreted by granulocytes and neutrophils and known to be present in the ovary during the inflammatory phase preceding ovulation (Iwahashi et al. 2000).

Within the category of glycoproteins, we identified laminin, fibrillin and thrombospondin, fundamental proteins of the basement membrane, of crucial importance for cellular attachment, cell proliferation and ECM organization. Most importantly, however, they share EGF-like intrinsic domains, which might bind to EGF receptors and modulate its signaling following their release by ECM proteolysis.

Within the category of proteoglycans, HSPG2 was of interest. Like many proteoglycans, HSPG2 can bind growth factors and cytokines and sequester them in the ECM and may be crucially important in the action of bFGF, a key growth factor with pro-angiogenic and anti-apoptotic effects in the ovary. Localized in the basement membrane, HSPG2 provides a barrier, which is

both size- and charge-selective, and promotes cell adhesion, endothelial cell growth and regeneration. In the ovary, it has been identified as a major estrogen-binding protein in follicular fluid (Bentov et al. 2016).

Another proteoglycan that was unexpectedly detected is OGN, also known as osteoglycin. Its down-regulation in vascular smooth muscle cells results in an increased cell proliferation (Deckx et al. 2018), which can provide insights into possible vascular stimulation of the ovarian tissue grafting site by controlling OGN expression. In osteoblasts, bone morphogenetic protein 2 (BMP2) increases OGN expression. In contrast, in the ovary, the same protein is implicated in primordial follicle assembly during fetal life (Chakraborty and Roy2015), suggesting the possible involvement of OGN in fetal ovarian remodeling and follicular assembly under the action of BMP-2. Further research is nevertheless needed to elucidate its function in the ovary, especially in adult life. Enzymatic ECM degradation is required to allow activated follicle expansion. However, to protect surrounding cells from proteolysis, different protease inhibitors appear to be secreted in the ovary, such as protein AMBP, alpha-2- macroglobulin and serpins. The latter is the most widely detected ECM regulator protein family and its expression is closely related to ovarian function (Ny et al. 2002).

Most of ECM-affiliated proteins have seldom been studied, especially in the human ovary, where we detected galectin-1 and galectin-3. Galectins are a family of β-galactoside-binding proteins implicated in modulating cell-cell and cell-matrix interactions. In 2004, Walzel et al. demonstrated the inhibitory effect of galectin-1 on the steroidogenic activity of granulosa cells,interfering with hormone-receptor interaction and resulting in decreased responses to FSH stimulation in pigs (Walzel et al. 2004). Although galectin-3 has similar functions to galectin-1, it has been associated with loss of progesterone synthesis in the mouse ovary, showing increased presence in atretic

preantral follicles and the later stages of luteolysis (Nio and Iwanaga 2007). This protein has been described in various tissues, but not explicitly in the healthy human ovarian cortex.

The technique described can be broadly applied to different tissues of unknown composition to provide a basic understanding of their most abundant proteins and ECM characteristics in one fraction analysis without ECM enrichment. This first exploratory step did not only inspire our subsequent studies (see section 'Elasticity and viscoelasticity of the ovarian ECM') but also motivated other groups to explore ovarian ECM for animal models (Henning et al. 2019). All our data set is accessible via the PRIDE partner repository with the data set identifier PXD008183 (https://www.ebi.ac.uk/pride/archive/projects/PXD008183).

I.1.2. An ECM-tailored proteomic method

Our first discovery proteomics based on non-enriched samples is informative, however if we intend to dive into the details of the matrisome and discover its low abundant and discrete components (eg. matrisome- associated proteins) or biomarkers, an enrichment step is mandatory, since only the most abundant proteins are identified in non-targeted proteomics. However, unbiased proteomic identification of ECM still encounters some limitations mainly due to partial ECM enrichment by precipitation, sequential fractionation using unfriendly-MS detergents, and resuspension with harsh reagents that need to be entirely removed prior to analysis to prevent high level of background noise and consequent biases in protein identification (Loo et al. 1996). Therefore, we set out to overcome the major challenges hampering our ability to characterize the matrisome accurately: MS-unfriendly detergents, irreproducibility, labor-intensive processing and consequent loss of low-abundance proteins and incomplete core matrisome

solubilization. To this end, we used the non-ionic saccharide surfactant DDM and acid-labile detergents 3273, RP, and PM, which are MS-friendly reagents that have similar properties to conventional detergents (Norris et al.2005) and have been described as trypsin enhancers (Chen et al. 2007). These molecules contain an acid-labile functional group, which quickly degrades into innocuous and insoluble non-surfactant byproducts upon addition of acid, eliminating the need to remove the detergent prior to MS analysis (effectively rendering it MS-compatible). These surfactants have been applied for many years for insoluble membranous protein characterization (Chen et al. 2007), but they have never been used for matrisome characterization. Therefore, we sought the first application of MS- compatible detergents in matrisome proteomics by comparing their outcomes at 0.1%, 0.2% and 0.5% concentration to choose the optimal option. With scarce samples such as healthy ovarian biopsies, it can be difficult to obtain sufficient amounts of proteins to generate high-quality MS data. We therefore optimized all steps starting from tissue sampling standardization where we screened different mechanical disruption lysis matrices to select the one that yielded the highest amounts of protein. This turned out to be the stainless-steel beads measuring 0.3 mm in diameter. This approach overcame ill-adapted, time-consuming, partial mechanical lysis and possible cross-contamination encountered when using other methods (e.g., pestle and grinder).

Matrisome-associated protein detection is quite challenging due to the high solubility of this category of proteins, which are embedded within the highly abundant core matrisome components (like collagen) that hamper their detection. To tackle this problem, our technique, after optimal mechanical lyses in MS-compatible detergents, relies on high speed centrifugation (16,000g for 30min) to separate core matrisome proteins, which are highly insoluble from cellular and matrisome-associated proteins, which are highly

soluble. This fractionation enhanced the detection of low-abundance soluble proteins in fraction 1 (supernatant) by sending glycoproteins and collagens to fraction 2 (insoluble pellet). Similarly to our discovery proteomic step, we here used Liberase DH to decrease insoluble protein agglomeration and cleave collagen as the most abundant substrate without any interference with non-collagenous protein detection. Moreover, Kuljanin et al. (2017) already demonstrated that collagenase preferentially cleaves collagen, with minor off target effects, and described the advantages of its use in proteomics.

Following LiberaseDH and upon double trypsin/Lys-C digestion, we did not observe any residual undigested material in our samples, which could easily be left behind and discarded in widely accepted proteomic methods.
Subsequently, by combining at post-processing the MS results obtained from both fractions we captured the full picture of the ovarian matrisome.

Our approach, combining centrifugation and MS-compatible detergent along with LC-MS/MS successfully identified 131 matrisome proteins with high reproducibility (Intraclass correlation: 0.887), which is the highest number of ECM proteins to have ever been described in the human ovary thanks to the use of Rapigest at 0.2%, which yielded an optimal ECM enrichment and detection with a simple 2-step fractionation compared to its counterparts. Moreover, RP has a major advantage over its commercialized competitors, as its cleavage does not result in amine products following degradation. Thus enabling quantitative MS applications with isobaric amine-reactive tandem mass tag labelling reagents, such as TMT (Chang et al. 2015; Y. Q. Yu et al. 2003), which we used later on to detect fertility biomarkers in ovarian ECM (see next section).

Interestingly, our study also revealed that a high percentage of ECM proteins could be lost, even in detergent-free buffers in intermediate fractions, which

are not considered for analysis in most published ECM proteomic studies (Naba et al. 2015). This observation is another key element behind our matrisome-tailored proteomic pipeline based on the principle of divide-and-conquer matrisome proteins (DC-MaP).

Our DC-MaP technique using 2-step fractionation with 0.2% Rapigest complemented by insoluble pellet digestion with Liberase DH is the first validated application of an MS-compatible detergent in matrisome proteomics, representing a robust, affordable and straightforward proteomic procedure tailored to matrisome protein discovery.

We believe the most accurate characterization of ECM proteins from different tissue types and even those with limited availability can be achieved with our DC-MaP method.

I.1.3. Potential fertility biomarkers at the ECM level

By applying our DC-MaP approach and adopting a tailored experimental design of TMT labelling to compare the matrisome of prepubertal, reproductive-age and menopausal ovarian tissue, we unravelled for the first time 26 potential biomarkers phenotyping ovarian ECM at each age phase of female reproductive life. These biomarkers were validated by a clearing method tailored for human ovarian tissue developed in this project to unravel their 3D-spatial distribution and localization. Beyond descriptive analyses, this study relied on advanced text-mining to relate ECM proteins of interest to known biological processes regulating ovarian activity and follicle quiescence, activation and development to complement our knowledge of the human ovary and create new interconnections between intra and extracellular regulators. We also used machine learning and statistics to build a neural network that can predict all ovarian matrisome quantities of any ovarian tissue starting from one quantification of a specific matrisome

component. Moreover, our model could be used to predict the probability of a specific ovarian tissue matrisome to resemble prepubertal, reproductive-age or menopausal tissue. This could be in the future a predictor of fertility potential, premature aging or even an evaluation tool of the efficiency of ovarian rejuvenation or fertility restoration solutions acting at the level of the ECM.

Beyond data mining and visualization, this project presents a unique approach to understanding the data and depicting the ECM remodeling with age through listening to the data, a recently growing discipline known as data sonification. We believe that this technique could help scientists identify ovarian anomalies in proteins more easily by listening to them. Indeed, the ears might detect more than the eyes, and if the ears are doing some of the work, then the eyes will be free to look at other things.

I.2. Multi-scale architecture and topography ofthe human ovary

The complex composition and hierarchical structure of ECM complicate the design of genuinely biomimetic constructs, notably: fiber morphology, interstitial and perifollicular fiber orientation and porosity, especially when these features are non-characterized, which is the case for the human ovarian ECM.

Multiple techniques have been deployed in this project to characterize the ovarian ECM architecture and develop a readout of its topology from prepuberty to menopause: immunofluorescence, polarized light microscopy, Sirius Red staining-autofluorescence and SEM screening. Corresponding data image analyses have been employed such as pixel and fiber segmentation as well as Fourier and Curvelet transformations.

At mesoscale level under polarized microscopy, collagen birefringence

informed us on collagen fiber crosslinking and overlapping. Using this technique, we found that collagen fiber content in ECM surrounding primordial follicles differs between prepubertal and reproductive-age ovaries. Indeed, the microenvironment of primordial follicles at different ages revealed a significantly higher proportion of thick fibers and lower levels of intermediate and thin fibers at prepuberty. High levels of thick collagen fibers seen in perifollicular areas of prepubertal ovaries do not appear to significantly change during early folliculogenesis. On the other hand, a significant decrease in thick collagen fibers was observed in the perifollicular ECM of reproductive-age ovaries, from primary to secondary follicles. Thicker collagen fibers are less elastic and offer great resistance to tension forces, which could account for preserving primordial follicles in a resting state (Jorge et al. 2014). After puberty, on the other hand, concomitant with the decrease in thicker fibers following follicle activation, there is a significant increase in thinner collagen fibers, probably due to enzymatic degradation. These findings highlight a profound difference in collagen deposition between young and adult perifollicular ECM, which is most pronounced in primordial follicles, and demonstrate that perifollicular ECM remodeling is vital for follicle growth (Hornick et al. 2012).

Similarly, with polarized light microscopy we inspected interstitial ECM, where we revealed that thick collagen fibers are the least abundant in the human ovarian cortex at any age and represent <7% of total collagen. Interestingly, the reproductive-age group retained the highest proportion of thick collagen fibers of all groups. Thin fibers and average-size fibers were found at equivalent rates (~48%) in all groups except prepubertal, where we detected the highest percentage of thin fibers (61 Ñ 3.1%) and the lowest percentage ofaverage fibers (35 Ñ 2.8%).

Although this preliminary study is descriptive in its nature, it provided the first

proof of an architectural difference in ovarian cell and follicular environment and how these differences could dictate their development and are not independent of endocrine functions. This prompted us to conduct more advanced studies on the complex architecture of ovarian tissue throughout the ovary life span and understand the anatomy of fibrous ovarian network.

To conduct micro and nanoscale quantitative data, we used SEM to screen ovarian fibrils, which are defined as individual entities with discrete diameters in the order of several nanometers, whereas fibers are defined as a pack of multiple fibrils that can be assembled into bundles. We adopted a multiscale observation and managed to capture the main features of ovarian fibers at 20,000X magnification and their arrangement into bundles at 5,000X magnification. After recognizing fiber bundles at 5,000X, we zoomed in to identify the features of their elementary fibers at 20,000X.

Using this approach, our results revealed a unique ECM architecture at reproductive age, where fibers of intermediate diameter (528 nm ± 128) are assembled into thickest bundles (3 379 nm ± 369) compared to prepubertal (Fiber scale: mean ± SD: 76 nm ± 10; fiber bundle scale: 160 nm ± 21) and menopausal (Fiber scale: 864 nm ± 94; fiber bundle scale: 1 768 nm ± 214) tissues.

This is probably due to the estrogen surge at reproductive age that stimulates the activity of LOX (Sanada et al. 1978), the crosslinker of collagen. These data are consistent with previous collagen crosslinking analyses under polarized (Ouni et al. 2020). Fiber and bundle spacing deduced from pore number and area show a looser fiber network at reproductive age compared to other age groups. During prepuberty the bundles assemble into a tight network with a high number of small poreswhile reproductive-age ovaries gain more porosity. However, at menopause tissue pore number and area change significantly. While fiber thickness reflects fibril crosslinking and participates in the physical properties of tissue, multi-

scale pore size and distribution contribute todiffusion and access of key molecules (nutrients, waste, hormones andoxygen) to/from cells. Hence, changes in tissue pore spacing from prepuberty to menopause can be translated into changes in permeabilityand molecule selectivity from one age to another. This information maybe helpful in the pharmacokinetics of new ovarian treatments that mightrequire age-personalization.

Pore geometry is also dependent on fiber orientation. Our results demonstrated the anisotropy of human ovarian tissue characterized by directional variations in interstitial space organization throughout female life, with a specific arrangement at each age. The interwoven anisotropic fiber structure of the human ovary provides the tissue with great adaptability to multidirectional loads (Kim et al. 2012). Interestingly, reproductive-age tissue fibers follow a common average orientation centered around 90°, with significantly different distribution from prepubertal and menopausal age groups that share comparable average fiber orientation. Considering the implication of pulling forces by cells in fiber orientation (Padhi and Nain 2020; Xu et al. 2009), this diversity in directional fiber distribution reveals a different multidirectional mechanical load in each group. This further delineates the peculiar organization of the ECM related to ovarian activity at reproductive age and hormonal homeostasis, and highlights possible differences in force transmission between age groups (Muiznieks and Keeley 2013). Thus, considering the uniqueness of fiber orientation in the ovarian cortex at reproductive age, fiber directionality may become a hallmark of female fertility, as is the case for breast cancer prognosis (Hornick et al. 2012; Jansen et al. 2018). Future studies need to elucidate the involvement of fiber orientation and stability range in functional tissue.

Fiber directionality around follicle borders at preantral stages revealed that before and after puberty, secondary follicles appear to modify their

microenvironment arrangement locally compared to follicles at earlier development stages, by reorienting the majority of collagen fibers below 50°. This could indicate that follicles at this stage require higher fiber contact and adhesion signaling to complete their development and maturation towards ovulation. This was previously suggested by Laronda et al when designing a 3D-bioprosthetic ovary made of 3D-printed gelatin fibers encapsulating preantral mouse follicles, where fibers oriented at 30° and 60° offered higher follicle-scaffold contact than 90° and resulted in offspring (Laronda et al. 2017). Comparably, our results provide an opportunity to fine-tune 3D fiber printing and architectural design in accordance with native fiber and pore geometry of human ovarian tissue.

ECM fibrous proteins also possess micro- and nano-scale features that provide topographic stimuli to cells and act as instructive cues to influence gene expression, cell behavior and morphology as evidenced by emergent publications on this topic. Therefore, we investigated the topography of ovarian tissue and its changes from prepuberty to menopause and measured its microrugosity. Roughness measurements are directly extracted from SEM images, which allows to explore the surface properties that can be sensed by ovarian cells at the cell scale and directly reflects the topography of the ECM fibrous network observed and analyzed by SEM. Contrary to profilometry analyses, our technique directly links architecture to roughness and revealed that ovarian tissue at reproductive age is characterized by a significantly smoother surface (99 nm ± 33) than prepubertal (227 nm ± 87) and menopausal (238 nm ± 28) tissues.

We hope that our data on multi-scale architecture and topography of the human ovary and their remodeling with age would alert researchers on the importance of these factors that should be present in ovarian biomimetic models and prompt novel discoveries in this direction as is the case for

skeletal muscle engineering (Fallahi et al. 2020), cardiac tissue engineering (D'Amore et al. 2018), stem cell research (Yang et al. 2020) or biomimetic oral mucosa development (Andablo-Reyes et al. 2020).

I.3. Elasticity and viscoelasticity of the ovarianECM

In recent years, we have witnessed a new dawn in mechanobiology dictating that mechanical forces generated within tissues can provide regulatory signals that are just as important as those conveyed by chemicals and genes (Mammoto et al. 2013). This fact is reflected in the field of fertility preservation by numerous theories (Choi et al. 2014; Thorne et al. 2015; Woodruff and Shea 2011), and lately by the work of Kawamura et al. (Kawamura et al. 2013; Kawashima and Kawamura 2018), which associates ovarian follicle activation to mechanical stress release. However, a lack of knowledge of the biomechanical behaviour of cortical ovarian tissue in vivo and poor quantitative characterization of the mechanical challenges do not allow us to correctly estimate the extent of mechanical stimulation and the possible remodeling of ECM with age. This ultimately hampers reproducible and elective treatments.

In our study, AFM evidenced a relatively rigid ovarian tissue at prepuberty (6538 Pa ± 351), softening significantly at reproductive age (3178 Pa ± 245), then stiffening (7117 Pa ± 714) considerably upon menopause. These differences are not only architecture-dependent, but also related to biochemical differences in ECM composition, as previously demonstrated in our follow-up of variations in elastic matrisome components from prepuberty to menopause (Figure 26). While collagen levels associated with tensile strength (Friedl et al. 1997) rose by less than 5% after puberty, we observed a very significant difference in GAGs in reproductive-age tissues. The increase was around 20% higher than prepubertal tissue, which explains the

elasticity differences between groups (Ouni et al. 2020). Thanks to their water sequestration properties, through their highly negative charges, GAGs generate a water-rich network with unique elastic properties, as seen in reproductive-age tissue (Bredfeldt et al. 2014b).

Conversely, the levels of collagen and GAGs are maintained from reproductive age to menopause. Thus, a plausible explanation for the elasticity change accompanying aging is the significant drop in elastin upon menopause (Ouni et al. 2020). Elastin fibers provide tissues with recoil to allow repeated stretching and contraction, and their aging-associated degradation appears to have profound effects on ovarian tissue elasticity. Moreover, ovarian rigidity seems to act in synergy with surface roughness as we noted that soft ovarian tissue at reproductive age is characterized by a smoother surface than rougher prepubertal and menopausal tissues, which are also more rigid.

In addition to the apparent elastic modulus measurement, we also investigated viscoelasticity. Like most biological soft tissues, the ovarian cortex can be assimilated to a polymer impregnated with fluid that has mechanical properties that cannot be completely described in the context of elastic (or ‘‘Hertzian’’) contact. Its behavior combines both solid- and liquid-like aspects, attributes of its viscoelasticity, defined by a time-dependent relationship between stress, strain and strain rate over time. Ovarian ECM viscoelasticity depends on fluid retention and flow through the porous matrix, as well as rearrangement of individual ECM fibers to absorb stress (Majeed et al. 2017). During a short deformation period, similar viscoelastic behavior was observed between age groups and can be explained by fast rearrangement of the flexible chains of ECM macromolecules (Akhmanova et al. 2015). At a longer time range, disentanglement of the chains takes place, and relaxation time associated with this process shows a stronger

dependence on the ECM architecture rather than ECM biochemistry (Woodruff and Shea 2007).

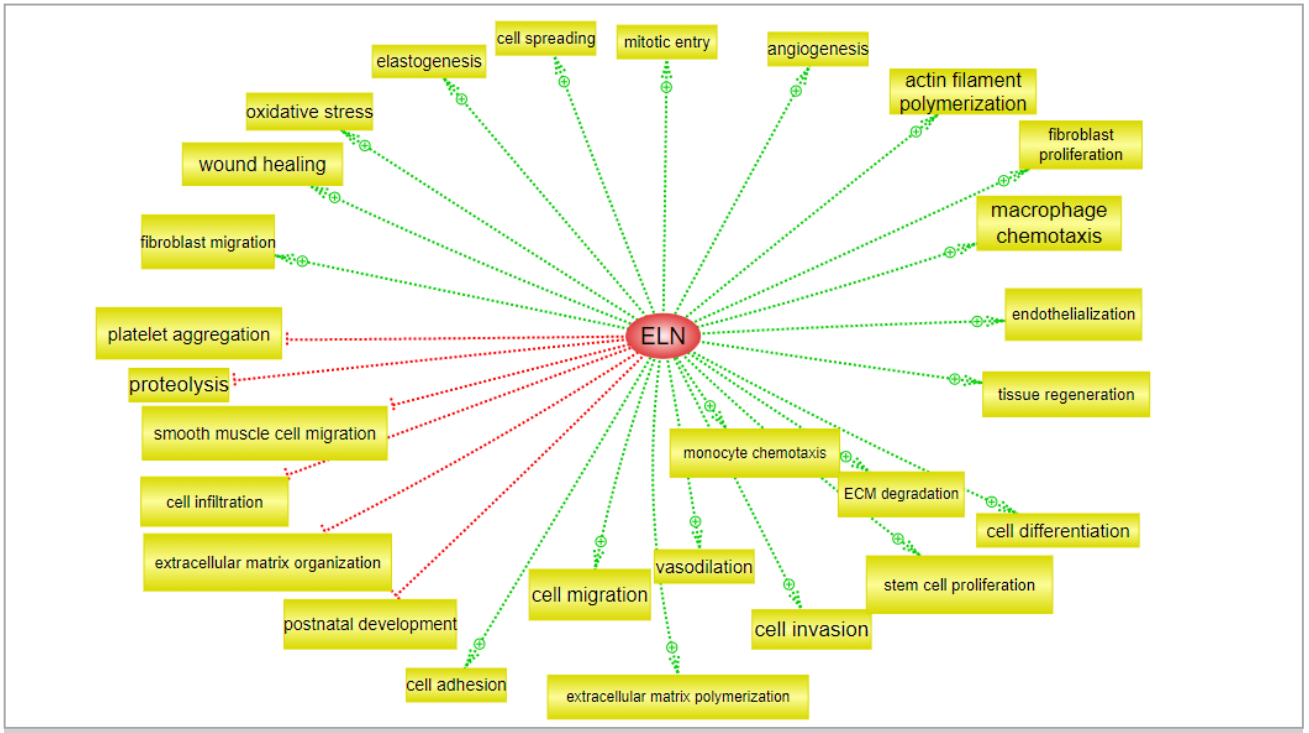


Figure 26 | Bioprocesses where elastin (ELN) has been implicated. Text-mining of literature using PathwayStudio software. (*Ouni, Unpublished)*

At this time point, the viscoelasticity of reproductive-age and menopausal tissues is comparable, although elasticity changes significantly upon menopause. This finding further underscores the relevance of recording both measurements. Conversely, prepubertal tissue has a slower viscoelastic response, which we can explain by its higher fluid sequestration compared to the other groups. This is related to its unique tight f iber network and small pore size, promoting long term water retention and extending relaxation time.

The described age-dependent mechanocharacteristics of ovarian ECM impact differently the follicle reserve and consequently affect the ovarian activity as has been demonstrated in vitro and in vivo in other species (Choi et al. 2014; Hornick et al. 2012; Xu et al. 2006). The human ovary is considered to be one of the most dynamic organs in the human body throughout a woman's lifetime, we therefore characterized its ECM from prepuberty to menopause to elicit structural and mechanical phenotypes at each age, and determine unique reproductive-age features,t hat may play a role in its reproductive capacity compared to other age groups. Indeed, the ovarian ECM at reproductive age is an ideal microenvironment for ovarian cell and follicle function and development. Our study thus elucidates the ECM cues required to replicate ovarian tissue properties in a functional bioengineered ovary and represents a reliable reference for comparing physiological and pathological ovarian conditions based on ECM status. Our study provides the first conclusive proof of a link between ECM biophysics (topology and mechanics) and fertility by comparing different stages of ovarian transformation related to a woman's reproductive life. By affecting chemical and mechanical signaling, these features, are critical determinants of ovarian function and should become a blueprint for designing functional artificial ovaries in the near future. The shared information herein will serve to develop new strategies for infertility prognoses based on ECM biophysics.

The data collected in this project represent the first attempt of óreverse engineeringô human ovarian ECM to break through all the discussed limits of engineering a TAO (Figure 25). Reverse engineer biology means applying the engineering concept of taking apart a process or mechanism in order to understand it and re-engineer it (perhaps in a new way)ð and using it to the biological world. In our project, we deconstructed ovarian ECM to better understand its proteomic, architectural and mechanical cues and their role in ovarian activity in order to reintegrate them into an in lab-build up construct in a functional manner.

II. Perspectives and emerging opportunities

II.1. How to build a TAO

The more we knew about ECM, the more we acknowledged the complexity of reproducing its features faithfully from scratch. Nevertheless, the following options might be a starting point to recreate key features distinguishing ovarian ECM at reproductive-age, which is our gold standard of fertility compared to its age counterparts (Figure 27).

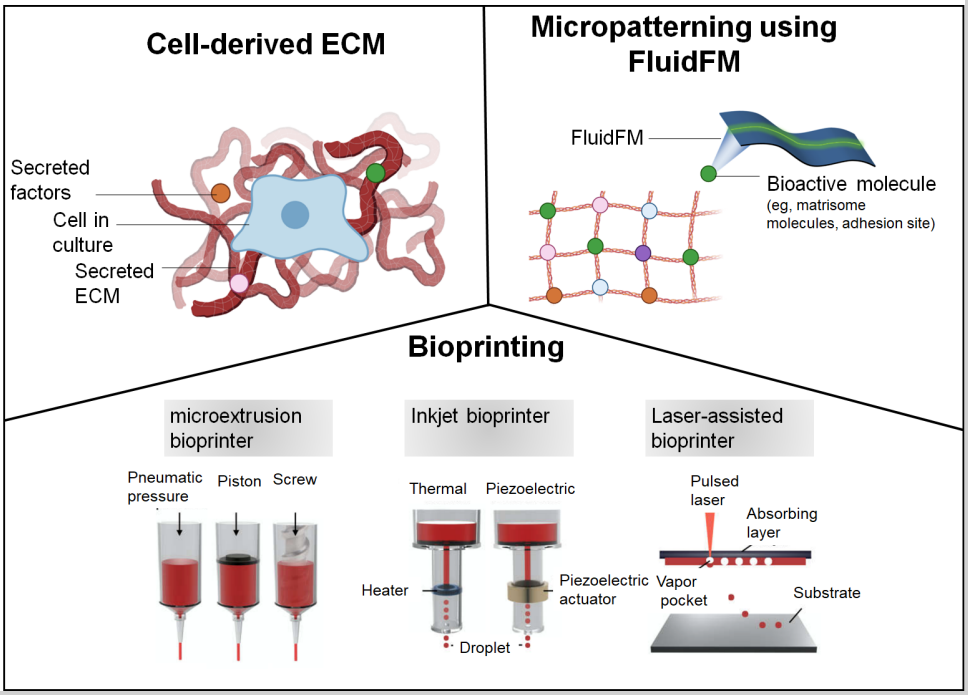


Figure 27 | Possible strategies to build a TAO. *(Ouni. Unpublished).*

II.1.1. Cell derived ECM

Recently, ECM scaffolds derived from cultured cells have received interest from biomedical scientists and became a hotspot for many tissue engineering applications (Blache et al. 2020). The ability to create cell-derived matrices in a dish gives researchers the opportunity to possess a bioactive, biocompatible material made up of fibrillar proteins and other factors that recapitulate key features of the native structure and composition of in vivo cell microenvironment.

Cultured cells offer several advantages compared to animal tissues (Cheng et al. 2009; Narayanan et al. 2009). First, cultured cells can be screened for pathogens and then maintained in a pathogen-free condition for ECM harvesting thus overcoming zoonose risks related to animal derived-

decellularized organs. Second, cell-derived ECM scaffolds may provide tunable architecture and porosity without the limitation of poor cell penetration during the repopulating of decellularized native tissues (Lu et al. 2011a). Third, the use of in vitro cultured cells provides the flexibility of mixing ECM samples that have been harvested from different cell types. Furthermore, another important advantage of cell-derived ECM scaffolds is that they can be synthesized by autologous cells isolated from patients and then expanded in the laboratory. The use of autologous ECM scaffolds avoids the undesired host responses that may be induced by allogenic or xenogenic materials and circumvents the limited supply of autologous tissues. In this context, we have conducted a preliminary study where ECM was in vitro synthesized by human ovarian stromal cells (Maruhashi et al. 2020) in two different medias: FBS-based medium and the other with platelet lysate-based medium. We have found in both groups, that cell layers appear to emulate tissue extracellular matrix, with a clear presence of collagen VI, the most predominant type of collagen detected in the ovary and collagen IV (Maruhashi et al. 2020). Alcian blue stain analysis showed GAGs in both cultured cell layers and native tissue. Immunofluorescent staining further revealed the presence of elastic matrisome proteins EMILIN-1 and elastin in the cell layers. This preliminary characterization, particularly in culture conditions lacking animal derivatives, unveiled encouraging similarities between 2D cell-derived and native ovarian matrices, which the team continues to explore for the transplantable engineered ovary assembly.

It is important to highlight that the selection of cell types to secrete ECM is crucial to define the composition of the desired scaffold and its use for the TAO. Indeed, our in-depth characterization of ovarian matrisome has highlighted a perifollicular ECM specific to each follicle stage and distinct from interstitial ECM. This further prompts the development of more intricatein vitro

models to recapitulate this complexity, control ECM topology and add mechanical stimuli to prompt the secretion of in vivo like ECM scaffold. Another possible option to reach biomimicry in vitro is to conduct a single cell multi-omics characterization to identify the different ovarian cell populations and their role in ECM synthesis. This will enable a better selection of cell types to include in vitro in order to obtain the desired scaffold. A scale up of this method will require the immortalization of the selected cell populations to create out of the bench scaffolds, commercially available.

Nevertheless, even cell-derived ECMs require a decellulaization step that carries on all the disadvantages of this process and might lead to the loss of secreted factors and proteins of interest. Our DC-MaP protocol might be useful for this application to recuperate the decellularized ECM while removing the risk of inflammation and toxicity related to the use of standard non cleavable detergents (White et al. 2017). However, further toxicity and viability studies must be conducted to check the compatibility of our method for in vitro and in vivo applications. It is also important to bear in mind that cell-derived ECMs are usually softer than their in vivo counterparts. To recapitulate in vivo rigidity, it is possible to enrich the obtained hydrogel with genipin, a natural crosslinker with low toxicity and high stability, usually usedin vitro to reinforce hydrogel's stiffness (Vyborny et al. 2019).

II.1.2. Bioprinting

Bioprinting is a variant of 3D printing and refers to the 3D-manufacturing of biological constructs through the layer-by-layer deposition of inks with living cells. This technology has been gathering enormous attention from the scientific community of regenerative medicine due to its ability tomanufacture organs from native cells. Although the bio-additive production of an entire transplantable organ has not been achieved yet, this technology is advancing,

and it could be used in the future to build the TAO. The successful application of this technology will depend on: the type of bioprinter, used bioink and cell viability with the used laters.

To date, three bioprinting technologies have been established: inkjet-, laser- and micro extrusion assisted bioprinting and have been concisely compared and their advantages and disadvantages have been detailed (Gu et al. 2016; Mandrycky et al. 2016; Murphy and Atala 2014; Shafiee and Atala 2016). Among these, the laser-assisted bioprinting (LAB) represents a promising technology for creating artificially designed tissues at higher resolution. This technology is based on the laser-induced forward-transfer (LIFT) effect. LIFT-based bioprinters, or laser-assisted bioprinters, are composed of three main components: (i) a pulsed laser source, (ii) a target or ribbon from which a biological material is printed, and (iii) a receiving substrate that collects the printed material (Figure 27). The LAB setup, previously described in several studies (Guillemot et al. 2010), is based on a near infrared pulsed laser beam coupled to a scanning mirror and a focusing system. This setup allows the precise focusing of a laser beam, usually in the infrared spectrum, on the ribbon (a transparent quartz glass slide coated with a gold absorbing layer), onto which a thin layer of cellular ink is spread. The energy generated by the laser beam creates a cavitation that propels a microdroplet, containing cells, at a kHz range speed, towards the receiving substrate (Figure 27). As LAB is based on a nozzle-free hardware, it can prevent cell clogging, a problem recurrent in other bioprinting approaches, while permitting an excellent control over the cell density, their microscale distribution, and their viability, and also providing high deposition speed (Guillotin et al. 2010). Due to its unprecedented printing precision, LAB offers an ultimate control over cell deposition and, ultimately, cell organization. As such, LAB is an emerging and promising technology to fabricate 3D cellular models that mimick the physiological functionality of their native counterparts such as the TAO, thanks to its

inherent automation, reproducibility, and high throughput capability.

For the fabrication of an ideal 3D biomimetic structure using such a printing module, bio-inks should be carefully selected. To be used as a source of a bio-ink, biomaterials should meet the following requirements: (i) biocompatibility, (ii) biodegradability, (ii) bioprintability, and (iv) structural integrity after printing (Yu et al. 2020). To satisfy such requirements, cell derived ECM hydrogels could be a promising option. Nevertheless, no such material has been used as a bioink since its slow polymerization and lack of control over its geometry might represent some limitations. Nevertheless, a hybrid scaffold composed of the cell-derived ECM hydrogel and a synthetic polymer with tunable printing could overcome these limitations.

A 3D printed bioprosthetic ovary has been already manufactured using gelatin as bioink to embed preantral mouse follicles, where fibres oriented at 30° and 60° offered higher follicle-scaffold contact compared to 90° and resulted in offspring (Laronda et al. 2017). Comparably, our study on the perifollicular and interstitial ECM architecture offer an opportunity to fine tune 3D-fibre printing and architectural design in compliance with the native fibre and pore geometry of human ovarian tissue.

II.1.3. FluidFM

The above-mentioned techniques might not fully recapitulate the biochemical or topographical ECM characteristics we report on the ovarian tissue. Therefore, we can refer to FluidFM as a technique for micropatterning the TAO scaffold. FluidFM (fluidic force microscope) is a unique micromechanical and microfluidic device that combines the force-controlled high spatial precision of AFM with the capability of direct liquid delivery by microfluidics (Meister et al. 2009). The device enables the printing of micro-

scale patterns on large, several millimeter–centimeter- sized areas directly from the aqueous solution of biomolecules intended to be printed. This way, the TAO scaffold can topographically be modified and could be enriched with growth factors, adhesion molecules such as RGD motifs or matrisome components carried within the aqueous solution to control their spatial deposition. This feature, supplemented with the possibility of measuring adhesion forces or injecting other biomolecules or drugs into cells with FluidFM can open new application of the TAO in vivo and in vitro.

II.1.4. Shape morphing polymers

Smart polymers capable of controlled shape transformations under external stimuli have attracted significant attention in recent years due to the resemblance of this behavior to the biological intelligence observed in nature. Shape-morphing polymer-based materials are great candidates for TAO design due to their adaptive properties, controlled shape transformations, and enriched dynamic functionality which may recapitulate the ever evolving plasticity and architecture of ovarian ECM from prepuberty to menopause. Since the control of these polymers depend on external stimuli their imminent application can be currently restricted to the development of a TAO as an in vitro model to recapitulate ECM physical and architectural turnover during folliculogenesis to better study mechanotransduction signalling pathways and their impact on oocytes.

Intelligent shape transformations in polymers require a great mastery of chemistry and covalent and non-covalent bonds composing the polymer, and can be incorporated upon external stimulation: direct or indirect heating, radiation and laser heating, microwaves, pressure, moisture, solvent or solvent vapors, and change in the pH values (Pilate et al. 2016). There are two types of intelligent polymer groups that have the ability to actively change

their shape: shape-memory polymers (SMP) and shape-changing polymers (SCP) (Lendlein et al. 2010). These concepts are based on specific functional groups or stimuli-responsive domains in the polymer structure that act as switches. The shape transformation starts upon triggering these switches by exposing them to a suitable external stimulus. The key differences defining shape changes in SMPs and SCPs arise from the different degree of freedom that influences the final geometry of the shape, the reversibility of the shape changes, and the effect of the stimulus (Lendlein et al. 2010).

A shape-memory polymer (SMP) can be deformed by the application of external stress and fixed in a second temporary shape (Behl et al. 2010). This temporary shape is maintained until an appropriate stimulus is implemented on the material. Exposure to this stimulus induces the recovery of the original form. The movement occurring during shape recovery is predefined: it reverses the mechanical deformation, which lead to the temporary shape.

In contrast to SMPs, SCPs change their shape gradually (e.g. shrink or bend), as long as they are exposed to a particular stimulus. They recover their original shape as soon as the stimulus is terminated. Such shape transformations are reversible and can be repeated multiple times. The main difference between an SCP and an SMP is in the geometry of the movement of the structure: in SCPs, it is determined by the material's original 3D shape (Lendlein et al. 2010).The key factors required for shape transformations in SMPs and SCPs are: (1) a polymer network structure that possesses elasticity to enable shape deformation and transformation of the material; (2) netpoints implemented in the polymer network structure that define the material's permanent shape (can be of chemical or physical nature); (3) stimuli-responsive molecular switches that provide additional temporary crosslinks to reversibly fix the network in a temporary shape; (4) a tailored shape-change programming process for the deformation of the material,

including the selection of appropriate stimuli (Kirillova and Ionov 2019).

One of the recent advances in this field is the creation of 'kinomorphs' (Viola et al. 2020), which are ECM sheets that change their shape, size, and density depending on patterns of cell contractility within them. It is shown that these changes can manipulate structure-forming behaviors of epithelial cells in many spatial locations at once. Kinomorphs currently have a distinct advantage over most bioprinting approaches in the spatial resolution at which multiple cell populations can be printed. Specifically, kinomorphs achieve printing resolutions of ≈10 μm and do not require multiple nozzles or cell/polymer blends to accommodate multiple cell types such as 3D printing since it relies on a new photolithography technology (Lin et al. 2019). Kinomorphs also directly account for changes in the spatial structure of cell-ECM composites that occur due to mechanical remodeling by cells. This phenomenon otherwise contributes to uncontrolled losses in spatial integrity of bioprinted objects (Morley et al. 2019).

II.2. The virtual ovary

Our comprehensive proteomic data and 3D imagery of ovarian tissue can be soon publicly available within the first online interactive database devoted to ovarian science, called the virtual ovary platform. Open research will provide a solid ground for further developing the TAO by other groups and sharing mutual findings. The platform will represent a reliable reference to compare healthy and pathological tissues and can be enriched with other information gathered by our team and other collaborators on the human ovary such as interactomic and structuromic data which will help to develop dynamic models that can be used to rationally analyze the morphology and physiology of the ovary across different scales, from the molecular to the organ scale. This will require close collaboration of biologists and gynaecologists with

proteomic experts, mathematicians, data scientists and programmers.

II.3. In vivo mass-spectrometry for personalized therapy

Rapid, sensitive, precise and accurate analysis of samples in their native environment (in vivo conditions) has become a critical part of routine analysis. By preserving samples in their original state, without the need for sample preparation, we can better decipher the underlying biological mechanisms. A ground-breaking new technology that might provide the impetus to propel MS from the laboratory to the operating room is at an advanced development stage by Fournier's team (Ogrinc et al. 2019; Saudemont et al. 2018). Their new device, the SpiderMass, consists of a pulsed laser excitation device tuned to heat water in order to create vapor to carry ionized molecules from in vivo tissue to the MS analyzer for measurement and protein identification. The device is already in use in animals (cows, dogs, etc.), but needs final optimization of protein detection rates before clinical implementation.

This technology may finally open the door to noninvasive, real-time in vivo proteomics. Such an advance might enable us to one day build more extensive ovarian proteomic databases, with references to compare pathological and healthy tissues, and accelerate the identification of biomarkers that could potentially change the approach to early diagnosis and tailored infertility treatments. Moreover, it may obviate the need to collect biopsies from volunteer patients in order to run proteomic studies, which will help overcome the difficulties of conducting proteomic analyses on scarce human samples such as ovarian tissue. Beyond the potential applications of the SpiderMass device in gynecology, it may someday allow surgeons to pinpoint markers of cancer in a living patient's tissue during surgery, without having to wait for the pathology report that can take up to

45 risky minutes under anesthesia. With the sonification of proteomic data, interpretation of results can become easily achieved, fastening considerably the clinical application of proteomics.

II.4. Ovarian rejuvenation

Since modern women postpone childbirth until later in life, they are more likely to face the problem of ovarian aging by the time they are ready to have children. So, the ability to restore ovarian function safely is crucially important. Ovarian aging has been so far defined by a diminished ovarian reserve (Ata et al. 2019), a decline in the quality and quantity of oocytes as a result of telomere shortening (Polonio et al. 2020), senescence (Yang et al. 2020), inflammation and oxidative stress (Foley et al. 2021). Among the clinical consequences of ovarian-aging, an increased risk for diabetes, heart disease, cancer, and other age-related conditions have been described (Zhang et al. 2019). Therefore, ovarian aging is considered as the pacemaker of female body aging, which drives the aging of multiple organs of the body. Hence, anti- ovarian aging has become a research topic of compelling interest.

Several pharmacological agents have been used as an attempt to reverse ovarian aging mainly in animal models whether through the use of: anti-oxydants (e.g. curcumin, COQ10), telomerase activators (e.g. N-acetyl-L-cysteine, resveratrol), caloric restriction mimetics (e.g. rapamycin, metformin),immunomodulators (e.g. diethyleneethanol, freund's adjuvant) or hormones (e.g. melatonin, leptin) (Zhang et al. 2019). Nevertheless, the implication of ECM in ovarian aging has not yet come to light although our data and the results of other groups highlight the eventual implication of ECM in aging and present it as a promising target for future rejuvenation strategies (Mavrogonatou et al. 2019). For instance, we found that ovaries of menopausal patients undertaking hormonal replacement therapy (HRT) have

seen a significant rise in their elastin production contrary to menopausal patients without HRT. It is widely acknowledged that elastin synthesis in human starts from late fetal stages to the early postnatal period, gradually decreasing and ceasing in adults (Swee et al. 1995). However, our study indicates that when estrogen is present, elastin continues to be synthesized and can even be produced de novo under the influence of HRT in menopausal ovaries (Ouni et al. 2020). Moreover, other groups have reported that interaction of senescent cells with ECM secreted by young cells is sufficient to restore their youthful phenotype. These senescent cells on top of a "young" ECM displayed lower crosslinking activity, improved mitochondrial function and reduced intracellular reactive oxygen species, as well as elongated telomeres (Choi et al. 2011).

Another key feature of human aged ovarian tissue is its characteristic rigidity and uncompliant viscoelasticity that we successfully measured (Ouni et al. 2021). These features could be also considered as potential targets for mechanomedicine which is an emerging field focused on therapeutically targeting tissue mechanics, either by directly altering the mechanical cues presented to cells or by disrupting the cellular response to mechanics (Lampi and Reinhart-King. 2018). Currently, ECM cues are fueling preclinical drug development efforts and ongoing clinical trials but they have not reached yet the fertility field (Lampi and Reinhart-King. 2018).

Although it is not time to turn back the clock for human ovaries, our investigation on aging-related matrisome transformations might prompt the discovery of novel therapeutic targets to achieve ovarian rejuvenation or at least prevent premature aging. Our proteomic data have revealed several shifts in ECM protein expression between reproductive-age and menopausal ovarian tissues that prompt further investigation in ovarian tissue rejuvenation. In the future, by combining SpiderMass technology as a

diagnostic tool of ovarian ECM proteomic shortage, a personalized ovarian rejuvenation solution can be formulated to enrich in situ the patient ovaries with the lacking matrisome components or with targeting drugs that can stimulate them.

CHAPTER 5

Other contributions to the field

Review

Ouni E, Vertommen D., Amorim CA. (2019). The Human Ovary and Future of Fertility Assessment in the Post-Genome Era. International Journal of Molecular Science. 20(17), 4209.

Articles

Chiti MC, Dolmans MM, Mortiaux L, Zhuge F, **Ouni E**, Shahri P, Van Ruymbeke E, Champagne SD, Donnez J, Amorim C A. (2018). A novel fibrin-based artificial ovary prototype resembling human ovarian tissue in terms of architecture and rigidity. Journal of assisted reproduction and genetics, 35(1), 41–48.

Chiti MC, Vanacker J, **Ouni E**, Tatic N, Viswanath A, des Rieux A, Dolmans MM, White LJ, Amorim CA. (2021). Ovarian extracellular matrix-based hydrogel for human ovarian follicle survival in vivo: a pilot work. Journal of Biomedical Materials Research Part B: Applied Biomaterials. (Under review).

Book chapter

Amorim CA, Asiabi P, **Ouni E**, Vilela J, Camboni A, Chiti MC. Chapter 30: Transplantation of isolated follicles and the engineered ovary. Female and Male Fertility Preservation.Springer.2021.


International Journal of
Molecular Sciences

MDPI

Review

The Human Ovary and Future of Fertility Assessment in the Post-Genome Era

Emna Ouni [1], Didier Vertommen [2] and Christiani A. Amorim [1,*]

[1] Pôle de Recherche en Gynécologie, Institut de Recherche Expérimentale et Clinique, Université Catholique de Louvain, 1200 Brussels, Belgium
[2] PHOS Unit, Institut de Duve, Université Catholique de Louvain, 1200 Brussels, Belgium
* Correspondence: christiani.amorim@uclouvain.be; Tel.: +322-764-5287

Received: 30 July 2019; Accepted: 27 August 2019; Published: 28 August 2019



Abstract: Proteomics has opened up new avenues in the field of gynecology in the post-genome era, making it possible to meet patient needs more effectively and improve their care. This mini-review aims to reveal the scope of proteomic applications through an overview of the technique and its applications in assisted procreation. Some of the latest technologies in this field are described in order to better understand the perspectives of its clinical applications. Proteomics seems destined for a promising future in gynecology, more particularly in relation to the ovary. Nevertheless, we know that reproductive biology proteomics is still in its infancy and major technical and ethical challenges must first be overcome.

Keywords: mass spectrometry; ovary; fertility; biomarkers; oocyte competence

1. Introduction

Proteomics is an emerging discipline that involves studying the proteome, namely the gene expression of a cell, tissue or organism, through analyzing proteins and their subsequent translational modifications by mass spectrometry (MS). The proteomic bottom-up strategy (proteolytic peptide mixture analysis) is the most commonly used method for analysis of biological samples. Strategies applied to prepare proteins or more complex proteomic samples for MS analysis involve many steps, and in bottom-up proteomics, the protein constituent is first scaled down into peptides, either by chemical or enzymatic digestion, prior to MS analysis. Peptides are then separated by liquid mono- or two-dimensional chromatography to fractionate samples and thereby reduce their complexity and dynamic range. One of the parameters that comes into play in the quality of obtained results relates to the wide range of protein concentrations in studied samples. Indeed, proteins present in low copy numbers in samples would be hard to identify without a prior step of enrichment [1].

MS analysis is then performed on individual peptides, and data are merged and consolidated to reveal the protein identity and/or its characteristics [1]. This automated process is greatly facilitated by the use of well-annotated proteome databases and bioinformatics (Figure 1).

In the post-genome era, while analysis of mRNA expression remains as the technique of choice to elucidate mechanisms of function and regulation in ovarian tissue, the use of proteomics is still relatively limited. Although genomics provides valuable information on certain biological functions, the proteome is the complete representation of proteins expressed by a genome. It is therefore more representative of the phenotype and able to provide complementary information that is yielded by gene expression studies. Indeed, gene expression studies of RNA transcripts often cannot predict the abundance or function of proteins or their post-translational modifications [3].

Int. J. Mol. Sci. **2019**, *20*, 4209

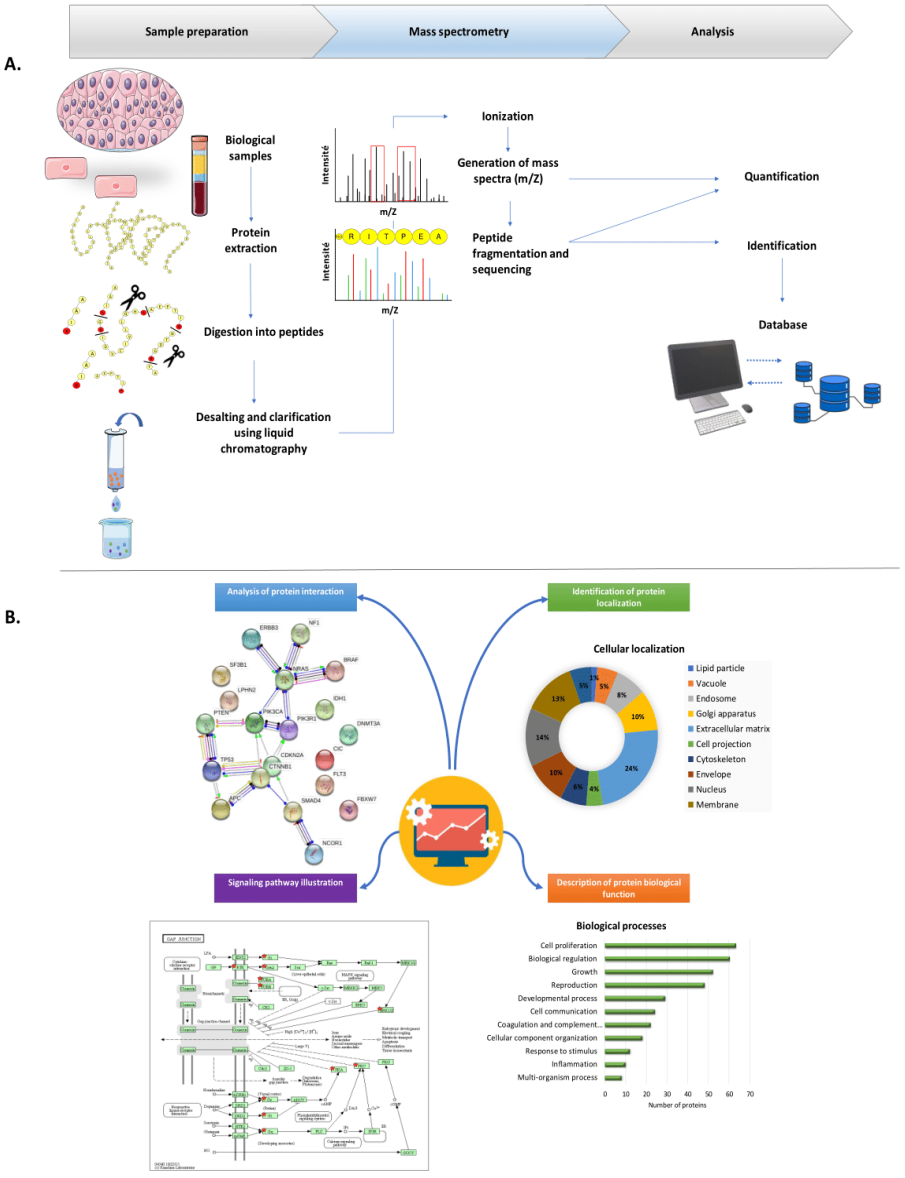


Figure 1. Sample preparation and proteomic data analysis at a glance. (**A**) Standard protocol for proteomic analysis. Proteins extracted from biological samples (tissue, cells, serum, etc.) are first digested by a proteolytic enzyme (generally trypsin). The peptides generated are clarified and separated by liquid chromatography according to their hydrophobicity and/or hydrophilicity. The eluted peptides are then ionized as soon as they enter the analysis unit of the mass spectrometer. This step will further fractionate the peptides and give them mobility that will depend on their charge (z) and molecular weight (m). These two parameters are detected and acquired by mass spectrometry (MS). The peptides are subsequently fragmented and sequenced to obtain information on their amino acid chain. The resulting spectral data allow identification of the starting proteins through use of databases. (**B**) Proteomic data processing through bioinformatic analysis. Bioinformatic tools available today make it possible to handle hundreds or even thousands of proteins detected by MS. Applications may include determining the localization of identified proteins and characterizing biological processes, signaling pathways in which they are involved and possible interactions that bind the different proteins, as well as streamlining potential new physiological mechanisms. More information on open source bioinformatics tools can be found in [2].

Unlike other techniques, proteomics can identify hundreds or even thousands of proteins in the same experiment from the same sample, giving access to a whole range of potentially interesting proteins and allowing them to be quantified relatively [4]. Thus, it allows investigation without a priori knowledge, in contrast to targeted studies using specific antibodies.

In the last decade, growing interest in proteomic approaches in gynecology [5] has aimed to (i) define biomarker profiles for appraisal of oocyte quality to improve success rates in in vitro fertilization (IVF), (ii) limit the complications of high-risk pregnancies, (iii) create proteomic maps for biomarker identification and (iv) fine-tune ovarian tissue-engineered models.

2. Proteomics for Selection of Competent Embryos and Oocytes in IVF

Since the birth of the first IVF baby, assisted procreation techniques have come a long way. Despite these advances, it has been reported that 70–80% of in vitro-produced embryos fail to implant, and 66% of IVF cycles do not result in pregnancy [6].

2.1. Follicular Fluid: An Inexhaustible Biosource for Investigation of Competence Biomarkers

Oocyte and embryo selection are principally based on morphological criteria, despite the contentiousness of morphological evaluation and its limitations [7]. Since human ovarian follicular fluid constitutes the in vivo microenvironment for oocytes during folliculogenesis and is also one of the most abundant 'waste products' in assisted reproduction, it is a readily available source of biomolecules for competence evaluation of collected oocytes and embryos. This noninvasive technique could be used to predict IVF success rates [7]. Indeed, understanding the protein expression profile of follicular fluid and the functional correlations between its components and corresponding IVF results could play a key role in the development of new methodologies, which would not only target oocyte and embryo viability, but also predict the chances of success in assisted reproduction programs.

Many research teams have focused their efforts on the proteomic profiling of follicular fluid and, through proteomic and bioinformatic analysis, have found that the main signaling pathways involving identified proteins are chiefly related to inflammation, coagulation, tissue remodeling and lipid metabolism [8,9]. One of the advantages of using proteomics is being able to correlate the detected proteins with their corresponding signaling pathways to better understand their role (Figure 1).

2.1.1. Role of Inflammation and Coagulation Cascades in IVF

Ovulation is an inflammation-like process during which the ovarian balance is achieved through pro-inflammatory action mediated by cytokines (such as interleukins IL-1, IL-6 and IL-8, and tumor

necrosis factor alpha (TNF-α)) and negative feedback from anti-inflammatory cytokines, accompanied by leukocyte recruitment by monocyte chemotactic protein-1 (MCP-1) [9].

Balanced and chronologically regulated cytokine activity is an absolute requisite for physiological maturation and follicle rupture. By contrast, aberrant cytokine activity could significantly affect follicle dynamics, as is the case with TNF-α. High intrafollicular levels of TNF-α have been linked to insufficient development of oocytes and inhibition of their maturation, which has led to a decline in their quality [10]. Inappropriate complement activation has been correlated with an increased risk of miscarriage. Nevertheless, the functions of the complement and coagulation cascade during IVF are still being debated. While some studies show that inhibition of complement activation improves angiogenesis and saves pregnancies [8], others, by comparing human follicular fluid from fertilized and unfertilized oocytes, reveal higher concentrations of C3 in fertilized oocytes [11]. This contradiction may be partially explained by the involvement of C3, C4 and C9, as well as complement factor H and clusterin, in complement inhibition in women following controlled ovarian stimulation for IVF [11]. However, the role of coagulation and inflammation cascades during IVF requires further investigation.

Proteins of the complement system promote coagulation through inhibition of fibrinolysis; in return, coagulation enhances complement activation. Key players in this synergy are plasmin and thrombin. During follicular development, proteins involved in coagulation in follicular fluid contribute to its liquefaction, fibrinolysis and rupture of the follicle wall. Deregulation of fibrinolysis has been correlated with implantation failure and recurrent abortions [9].

2.1.2. Impact of Extracellular Matrix Turnover on Oocyte Quality

Numerous studies have demonstrated the involvement of coagulation proteins in tissue remodeling and repair, namely the effect of thrombin and plasmin on the activity of other serine proteases and matrix metalloproteinases (MMPs) responsible for extracellular matrix (ECM) turnover [7,9]. Proteomic analysis of follicular fluid coupled with bioinformatics has successfully revealed potential major players in the evaluation of oocyte quality. These proteins of interest interact indirectly with thrombin and plasmin and are implicated in modifications to the pre- and postovulatory ECM. For example, plasmatic carboxypeptidase B2 (CPB2) and hyaluronan-binding protein 2 (HABP2) are involved in tissue repair and coagulation in response to ovulation [7,8]. While CPB2 controls lysis of blood clots, HABP2 activates extrinsic coagulation pathways and the fibrinolysis-inducing urokinase enzyme [8].

Among the serine proteases potentially of interest for predicting oocyte quality is kallikrein kininogenase (KKS) [12]. This family of proteins possibly plays a role in the formation of the thecal vascular network, the contraction of the follicle walls during ovulation and the vascularization of avascular follicles after release of the oocyte [7]. Moreover, some serine protease inhibitors detected in the latest proteomic studies have emerged as indicators of oocyte quality, such as alpha-1-antitrypsin (A1AT) in mature follicles. Indeed, the inflammatory process that accompanies ovulation and is associated with release of reactive oxygen species (ROS) induces polymerization of A1AT and deactivates it accordingly, which is essential for oocyte release. We may then conclude that A1AT plays a primary role in the follicle maturation and temporal control of mature oocyte release [7].

Other effector proteins implicated in ECM degradation and remodeling and involved in follicle growth, angiogenesis, apoptosis and embryo implantation are MMPs, namely MMP-9, MMP-12, MMP-13 and MMP-25 [9]. The link between regulation of MMP activity and ovarian activity emphasizes the importance of ECM homeostasis to fertility, follicle growth and ovulation control. Indeed, MMPs control the bioavailability of hormones, growth factors and osmotically active molecules, as well as cellular response [7,9]. Experiments have shown that unregulated MMPs may have adverse effects on oocyte development and maturation, causing excessive degradation not only of the follicular ECM and resident growth factors and co-factors, but also of surface receptors in follicular somatic cells, and potentially the maturing oocyte itself [13].

Aberrant MMP activity could also have a significant impact on the cumulus–oocyte complex and the integrity of the zona pellucida. Because of the metabolic dependence of the growing oocyte on

cumulus cells and the firm control exerted by the oocyte on the physiology of these cells, the functional integrity of tight junctions (gap junctions) is fundamental to the development and maturation of oocytes. In this case, uncontrollable MMP activity could degrade intra-cumulus and cumulus–oocyte junctions, damaging the maturation of oocytes and hence their required fertilization competence. MMP access to the zona pellucida may also lead to partial degradation, affecting interaction and fertilization of spermatozoa [7,9,13]. Finally, disruptions to the MMP/TIMP (tissue inhibitors of MMPs) ratio have been reported to be negative predictors of oocyte release, fertility and IVF success [9,14,15].

2.1.3. Involvement of Lipid Metabolism in the Success of IVF

Another major class of proteins identified by follicular fluid proteomic strategies are those active in lipid metabolism, including the vitamin D receptor (VDR) and the retinoid X receptor alpha (RXR-α) heterodimer. These receptors belong to the family of steroid/thyroid hormone nuclear receptors, and their heterodimerization regulates expression of genes encoding proteins involved in various cellular functions: proliferation, differentiation, apoptosis or even angiogenesis. Curiously, VDR/RXR-α controls the MMP/TIMP balance, plasminolysis, fibrinolysis and other proteolytic activities by different mechanisms [9].

Clearly, qualitative and/or quantitative variations in these proteins between follicular fluid samples could affect follicle and oocyte development and maturation during IVF. Their use as biomarkers to assess the quality of oocytes is therefore justified. In addition, some follicular fluid proteins may change quantitatively because of different patient responses to hyperstimulation protocols and different causes of infertility. Use of proteomics in this context could therefore have a significant impact, not only on determining the quality of oocytes, but also on the development of personalized fertilization treatment programs.

2.2. A New Way of Predicting IVF Success: The Cumulus–Oocyte Complex

In addition to follicular fluid analysis by MS, the team of Braga et al. (2016) was interested in investigating the cumulus-oocyte complex [6]. Among proteins exclusively identified both in blastocysts and oocyte cumulus cells that have generated successful pregnancies, they found glutathione S-transferase A4 (GSTA4), heavy chain Ig V-III region TUR, protein disulfide-isomerase (PDI) and proto-oncogene serine/threonine-protein kinase mos. This study also demonstrated that overexpression of GSTA4 is implicated in protecting cells against apoptosis, while overexpression of glutathione S-transferase P (GSTP) may be associated with the c-Jun N-terminal kinase signaling pathway (JNK), shielding cells from death signals or oxidative stress [6]. Expression of certain proteins from the glutathione S-transferase (GST) family is promoted through mitogen-activated protein kinase (MAPK) signaling pathways as a self-defense response against toxins and growth factors. It is essential to stress the involvement of p38 MAPK at the level of reproductive cells in oocyte maturation and steroidogenesis. The results of this study suggest that proteins identified in cumulus cells may play a role not only in folliculogenesis, but also in the immune response. The importance of the immune system to embryonic development and reproduction remains unproven, but it appears to serve a function in the implantation of embryos.

Another protein whose key role was highlighted in this study is the proto-oncogene serine/threonine-protein kinase mos. In addition to being vital for the initiation of oocyte maturation, progression of meiosis I and II and arrest of meiosis in metaphase, it is also potentially important for assessing oocyte quality, embryonic development and implantation.

Since communication between the oocyte and cumulus cells is essential for acquisition of oocyte competence, proteins identified in the course of proteomic characterization of these cells could have therapeutic targets and may be used for enrichment of culture media. This characterization also provides a clearer picture of the physiology of in vivo maturation during controlled stimulation cycles. Furthermore, a proteomic study of cumulus cells might well be useful for predicting successful

pregnancies and identifying patients who should be included in extended embryo culture programs or those who could benefit from cleavage-stage embryo transfer [6].

Despite progress in IVF at the clinical level, embryo selection is still based on unsatisfactory morphological criteria. A more appropriate selection of proteomic-based oocytes and competent embryos could enhance IVF success rates. However, while a number of biomarkers have been identified in basic research, these data are not used clinically. It is therefore essential to translate these new findings into clinical settings that could offer patients a significantly better chance of conceiving through IVF.

3. Ensuring Normal Pregnancy in Patients with Polycystic Ovary Syndrome through Proteomics

Polycystic ovary syndrome (PCOS) is often a source of pregnancy complications in patients with ovarian hyperstimulation syndrome (OHSS), pre-eclampsia and/or premature delivery, which is why proteomic studies have been conducted on PCOS patients. They were able to identify early biomarkers of these complications in an attempt to better diagnose and treat affected women, and thus ensure normal pregnancy.

PCOS patients who wish to have a child often require controlled ovarian stimulation to restore the hormone balance needed to resume ovulation. However, PCOS increases the risk of developing OHSS [16], a potentially life-threatening iatrogenic complication that occurs during assisted human reproduction. For this reason, a more efficient early prediction technique for OHSS is vital. With this in mind, the team of Wu et al. (2017) identified overexpression of haptoglobin, fibrinogen and lipoprotein lipase as early serum biomarkers for predicting OHSS in PCOS patients [16].

A systematic review showed that pregnant women with PCOS were actually four times more likely to develop pre-eclampsia than controls [17]. Therefore, finding the molecular mechanisms underpinning the link between PCOS and pre-eclampsia could serve to minimize the occurrence of maternal and fetal morbidity/mortality associated with this complication. Detecting the relevant biomarkers by proteomic approaches would address this need. Indeed, five biomarkers were found to be differently expressed in women with pre-eclampsia and PCOS compared to controls; transferrin, fibrinogen chain variants α, β and Υ, and kininogen-1 were overexpressed, while annexin 2 and peroxiroxin 2 were underexpressed. These biomarkers were found in serum, follicular fluid and ovarian biopsies [17].

Premature births are also a major cause of neonatal mortality and morbidity, and women with PCOS are at a high risk of giving birth prematurely [18]. Research studies are needed to investigate the mechanisms linking PCOS and preterm delivery in order to facilitate detection and develop new preventive strategies. In this context, six biomarkers were found to be similarly overexpressed in women affected by the threat of preterm birth and PCOS compared to controls, including M1/M2 pyruvate kinase (PKM1/M2), vimentin, fructose bisphosphonate aldolase A, HSP27, peroxiredoxin-1 and transferrin [18].

Proteomics offers great potential for acquiring new knowledge to help manage high-risk pregnancies, such as in women with PCOS, but it is not without limits. The relative delay in translating research results to clinical applications is still a cause for concern.

4. The Future of Human Ovary Proteomics

4.1. In Vivo Mass Spectrometry

Groundbreaking new technology that might provide the impetus to propel MS from the laboratory to the operating room is at an advanced stage of development by Fournier's team [19]. Their new device, the SpiderMass, consists of a pulsed laser excitation device tuned to heat water in order to create vapor to carry ionized molecules from in vivo tissue to the MS analyzer for measurement and protein identification. The device is already in use in animals (cows, dogs, etc.), but needs final optimization with respect to protein detection rates before clinical implementation.

This technology may finally open the door to noninvasive, real-time in vivo proteomics. Such an advance might enable us to one day build larger ovarian proteomic databases, with references to compare pathological and healthy tissues, and accelerate identification of biomarkers that could potentially change the approach to early diagnosis and tailored infertility treatments. Moreover, it may obviate the need to collect biopsies from volunteer patients in order to run proteomic studies, which will help overcome the difficulties of conducting proteomic analyses on scarce human tissues such as ovarian tissue.

Beyond the potential applications of the SpiderMass device in gynecology, it may someday allow surgeons to pinpoint markers of cancer in a living patient's tissue during surgery, without having to wait for the pathology report that can take up to 45 risky minutes under anesthesia.

4.2. Proteomics to Help Engineer a Transplantable Artificial Ovary

In addition to detecting biomarkers, proteomics is used to monitor the development of cells in contact with synthetic or natural biopolymers both in vivo and in vitro, and to check the suitability of used scaffolds and their safety. In case of bioartificial organs, proteomics can be applied to verify the biomimicry of created organs by comparing their biochemical composition with the real thing. This serves to improve development protocols and ensure their reproducibility before applying them in a clinical context [20]. Indeed, a number of decellularized matrices that have been commercialized and clinically applied have undergone proteomic characterization [21]. A similar approach has been adopted with respect to the ovary. The team of Amorim is currently working on the development of a transplantable artificial ovary, whose main purpose is to safeguard the fertility of leukemia patients who cannot undergo assisted reproduction techniques or grafting of frozen-thawed ovarian tissue due to the risk of reintroducing cancer cells.

The artificial ovary is composed of follicles isolated from cryopreserved tissue and confined inside a physical support, mimicking the natural microenvironment of follicles in the ovary. However, in order to evaluate the quality of this bioengineered environment, a reliable reference is needed. On this basis, any synthetic process used can be monitored and improved, which also allows for the tracking of the composition of the neoformed ECM after transplantation. The team has already succeeded in establishing the most complete proteomic description of the human ovary to date, while at the same time revealing the composition of its ECM [22].

4.3. Challenges of Proteomic Studies of the Human Ovary

Available proteomic studies of the ovary rely primarily on the analysis of body fluids such as serum and follicular fluid, or evaluation of ovarian tissue and cells. However, the heterogeneity of biological samples, their collection, storage conditions and preparation make comparison and interpretation of results somewhat problematic.

Although serum is relatively easy to collect given the availability and accessibility of blood samples, the dynamic range of proteins involved—namely the differences in amounts of proteins present and the extreme complexity of the blood proteome—hampers analysis by MS, preventing detection of valuable but scarce proteins in samples [23]. Moreover, a high concentration of albumin and other circulating proteins such as immunoglobulins in serum make separation of proteins difficult. While there are techniques to isolate them by affinity, this approach risks eliminating proteins of interest because of their low specificity to albumin and immunoglobulins [23]. There are also significant variations between serum sample studies, since the composition of blood is likely to alter under the influence of different conditions, such as smoking, age, metabolic diseases, medications and body mass index.

Follicular fluid is likewise easy to collect in a noninvasive way, especially in assisted reproduction centers. However, its limits of application in proteomics do not differ from those of serum, also due to its complexity. The same albumin depletion techniques can be performed, and several studies have actually shown that concentrations of isoforms/albumin fragments in follicular fluid may be able to predict the quality of oocytes and even embryos [7,24,25].

On the other hand, since follicular fluid is usually collected from patients undergoing hormone hyperstimulation, levels of some inflammatory factors could well be affected, which would introduce bias into the interpretation of results. The same is true of signaling pathways with which detected proteins are correlated, such as in tissue repair, in how they complement activation and coagulation [7].

Although analysis of ovarian tissue presents its own challenges (Table 1) mainly related to the invasiveness of the sampling technique and the restriction caused by a small biopsy size, it is more likely to reflect the pathogenesis of ovarian disorders [17] that manifest particularly through periodic changes to the ECM. ECM proteomics can not only reveal novel diagnostic tumor markers and offer new therapeutic leads, it can also enable detection of cellular development effectors in the extracellular space. Improved understanding of the ECM will promote application of reproductive tissue engineering in vivo and in vitro, namely the development of an artificial ovary and creation of biomimetic matrices for maturation of ovarian follicles by 3D culture [26].

Table 1. Challenges of biological sample proteomics in gynecology.

- Difficulty detecting scarce proteins in complex biological samples.
- Introduction of bias into the interpretation of results due to inappropriate sample preparation protocols.
- Heterogeneity of proteins detected because of different experimental protocols and proteomic platforms used.
- Need for corroboration of proteomic results by other techniques before validating a hypothesis.
- Available protocols not suitable for analysis of small quantities of biological material, especially needed when analyzing scarce samples such as ovarian tissue biopsies.

However, the question is how can we overcome the complexity of ovarian tissue and manage to extract ECM proteins? Indeed, extracellular proteins present an analytical challenge because of the biochemical properties of their highly crosslinked and therefore insoluble molecules, even in the strongest organic detergents and denaturants. Nevertheless, the high insolubility of the ECM could be exploited to reduce the complexity of tissue samples and detect scarce proteins in the ECM [27]. To this end, it is first necessary to eliminate its intracellular proteins, which are much more soluble, without losing the rest of the proteins in the ECM. This can be achieved by varying salt concentrations and the pH of the tissue homogenate solution.

Once the intracellular proteins have been extracted and removed, we must ensure that total solubilization has been obtained, since only soluble proteins can be analyzed by MS. Incomplete solubilization results in incomplete characterization. Although a number of teams use very strong solvents and detergents to solubilize the matrix, the most common of which is sodium dodecyl sulfate (SDS), these reagents are difficult to remove from samples and are responsible for serious artifacts in the mass spectrometer, even at very low concentrations (<0.01% SDS) [28]. There is therefore a real need to develop appropriate techniques with reproducible and reliable MS-compatible reagents for proteomic characterization of the ECM and biomarker investigation, in order to allow extrapolation of this technology to a clinical setting.

There is an array of potential biomarkers reported in the literature and lists of proteins distinguishing different compartments of healthy and pathological ovaries generated by MS. However, the sheer heterogeneity of analyzed samples and techniques serves to impede validation of these data and their clinical application. Indeed, pre-analytical variables, such as sample processing and specimen storage conditions, should be addressed when comparing different studies, as these factors may have a notable impact on the results [23].

Meticulous selection of pre-analytical sample processing, application of validated techniques (Figure 2) and statistical evaluation of data are essential to generate reliable results. Every effort should be made to ensure that study and control samples are subjected to the same techniques throughout the

Int. J. Mol. Sci. **2019**, *20*, 4209

proteomic process, from sample collection to data analysis [29]. In this regard, clear guidelines are needed to design clinically applicable proteomic analyses.

Appropriate bioinformatic analysis is key to accurate interpretation of results, since management, evaluation and interpretation of large volume of raw and processed data require a combination of different bioinformatic techniques, from data mining to comparison of data sequences and predictive models. Data acquisition, filtering and normalization are also important, and each of these steps can have a profound effect on the results. Complementary validation techniques, such as immunoassays or western blots, need to be employed before formulating physiopathological hypotheses based on quantitative (Figure 2) or qualitative differences in proteins [30].

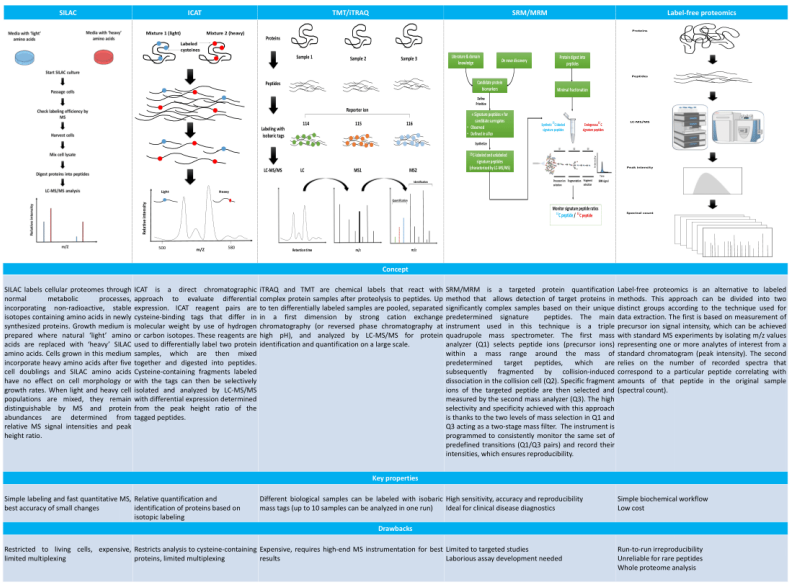


Figure 2. Key features of the main quantitative MS methods. Full names of abbreviated techniques: stable isotope labeling of amino acids (SILAC); isotope-coded affinity tags (ICAT); tandem mass tag (TMT); multiplexed isobaric tags for relative and absolute quantification (iTRAQ); selected reaction monitoring (SRM); multiple reaction monitoring (MRM) and label-free quantification (LFQ).

4.4. Proteomics Is Not an Island: The Added Value of Proteogenomics

Proteins serve as a critical link between genotypes and phenotypes. Proteomic profiles reflect cellular responses to genomic, epigenomic and environmental alterations, and in turn shape these responses. Thus, proteomics is not an island entirely of itself. Proteogenomics has now emerged as a rapidly evolving field at the intersection of genomics, transcriptomics, and proteomics. Its essential goal is integration of multiomic data for accurate annotation and reciprocal refinement of genomic and proteomic models [31]. This integrative approach has the potential to provide solid evidence for translation of previously unknown transcripts. Indeed, newly reported peptides can represent single amino acid variants, splice variants, gene fusions, RNA editing events, novel open reading frames, translated noncoding RNAs and pseudogenes, among many other things. Proteogenomic platforms can be used to investigate which of these novel events gets translated at the protein level, making them potential candidates for new druggable targets or new diagnostic or prognostic biomarkers for a wide spectrum of diseases, including ovarian cancer [32]. Indeed, this

approach is increasingly used in oncology, since many patients do not respond as predicted to therapies recommended based on genomic profiles of their tumors [31]. Recent studies pairing genomic and proteomic analyses in the same tumors have shown that the proteome encodes novel information that cannot be discerned by genomic analysis alone. Moreover, from a clinical perspective, the majority of molecular therapies do not target the patient genome, but rather cellular and extracellular proteins (kinase inhibitors, PARP, immunomodulatory proteins, etc). The National Cancer Institute (NCI) has funded a major initiative in cancer proteogenomics through its Clinical Proteomic Tumor Analysis Consortium (CPTAC). The CPTAC flagship reports on ovarian cancer have provided a resource for the cancer research community, both by indicating which of the genomic and transcriptomic features associated with this cancer was recapitulated at the protein level, and by providing new insights into the substantial impact of post-translational modifications, specifically phosphorylation and acetylation, on the functional activities associated with DNA repair, proliferation and survival. Furthermore, proteogenomics can complement proteomic databases used for protein sequencing and identification (such as rEFsEQ or Ensembl), which are unable to identify any novel cancer-specific sequence [33]. This can be achieved by incorporating candidate protein sequences derived from exome sequencing or RNA-Seq data into a customized database for MS/MS spectra interpretation, allowing identification of sample-specific peptides that are missing from the reference database, or even protein isoforms. Using this approach, the CPTAC studies into ovarian cancer have provided proteomic validation for 14 somatic mutations [34]. In a few cases, it has been shown that protein profiling is more closely aligned with function than mRNA profiling data, suggesting that protein translation and degradation are tightly regulated and play a critical role in determining gene function [35].

On the other hand, for many genes, mRNA measurements are considered poor predictors and very few mRNA biomarkers have been translated into clinical practice, however, new approaches are emerging. The use of somatic copy-number alteration, DNA methylation, mRNA, microRNA and reverse phase protein array (RPPA) may well fulfill the promise of protein measurement in a clinical setting by providing novel insights into multilevel gene expression regulation, signaling networks, disease subtypes and clinical predictions [36]. However, to bridge the gap between proteogenomic biomarker candidate detection and clinical validation, greater precision and highly sensitive techniques are required, especially on a one-cell scale. Until recently, traditional sequencing methods were only able to determine the average of large number of cells, but were incapable of analyzing small numbers or acquiring cellular heterogeneity information.

Single-cell sequencing technologies can sequence and quantify the whole genome of germ cells and embryonic cells at the single-cell level. This will help elucidate the emergence of germ cells and facilitate screening, diagnosis and treatment of reproductive and genetic diseases [37]. Detection of female egg cells, polar cells or embryonic cells by single-cell sequencing to select healthy embryos for transfer can reduce the number of newborns with congenital genetic diseases and help prevent genetic diseases. Li et al. applied genome-wide mapping of human embryos prior to implantation by single-cell multi-sequence sequencing [38]. This study has implications for the analysis of complex and highly-coordinated epigenetic processes involved in the pre-implantation development of human embryos. Vento-Tormo et al. performed a transcriptome analysis of placental cells in early pregnancy by single-cell sequencing technology and mapped placental cell maps. Through the cell map, three subpopulations of perivascular and stromal cells located in different decidual layers and dNK (decidual natural killer) were found [39]. It also identified regulatory factors that may minimize harmful immune responses to the placenta, and interactions contributing to placental competence and reproductive success. These findings are important for understanding early pregnancy processes and improving the diagnosis and treatment of pregnancy-related disorders. The first step towards clinical translation of these genomic discoveries is validation of their expression at the protein level. Although single-cell genome sequencing preceded single-cell proteomics, the latter has so far achieved significant milestones, highlighted in the review by Couvillion et al. [40].

Clearly, with the help of multi-omics, we can shed further light on physiological processes and pathological mechanisms by deciphering how information flows from gene to protein. However, the field of female fertility is not yet taking full advantage of these applications. Moreover, multi-omics approaches still have issues, such as cumbersome utilization and high detection costs, which limit the promotion of this technology. The hope is that techniques will become increasingly simplified and effective and detection costs will fall, and thus these tools can be applied to basic research and play a key role in clinical diagnosis and fertility assessment (Figure 3).

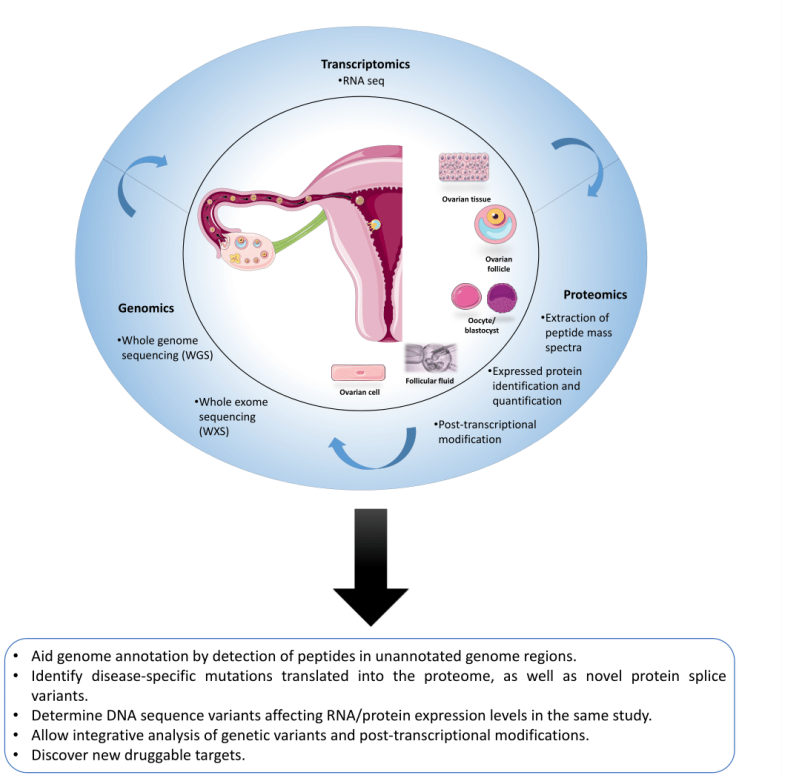


Figure 3. Multi-omics perspectives. When combined, the coding proteome and noncoding transcriptome represent products of the sequence-to-phenotype continuum (DNA to RNA to protein). By combining genomic, transcriptomic and proteomic technologies in the same workflow, these technologies can inform each other and complement our knowledge of the human ovary and procreation.

5. Conclusions

Proteomics has emerged as a powerful tool, with applications ranging from biomarker identification for effective embryo and oocyte selection and high-risk pregnancy management, to tissue engineering guidance. However, while a number of data sets have been generated in basic research, such data cannot be used clinically. It is therefore essential to translate these new findings into clinical applications, whose impact could significantly enhance patient health and care.

Author Contributions: Conceptualization: E.O. and D.V.; Writing: E.O.; Writing-review & editing: D.V. and C.A.A.

Funding: This study was supported by grants from the Fonds National de la Recherche Scientifique de Belgique (FNRS) (C. A. Amorim is FRS-FNRS research associate; grant M 4/1/2/5 MCF/SD awarded to C. A. Amorim) and Université Catholique de Louvain (PhD grant "Coopération au développement" awarded to E. Ouni).

Acknowledgments: The authors thank Mira Hryniuk for reviewing the English language of the manuscript.

Conflicts of Interest: The authors declare no conflict of interest.

References

1. Wisniewski, J.R.; Zougman, A.; Nagaraj, N.; Mann, M. Universal sample preparation method for proteome analysis. *Nat. Methods* **2009**, *6*, 359–362. [CrossRef] [PubMed]
2. Calderón-González, K.G.; Hernández-Monge, J.; Herrera-Aguirre, M.E.; Luna-Arias, J.P. Bioinformatics Tools for Proteomics Data Interpretation. In *Modern Proteomics–Sample Preparation, Analysis and Practical Applications*; Mirzaei, H., Carrasco, M., Eds.; Springer International Publishing: Cham, Switzerland, 2016; pp. 281–341.
3. Vogel, C.; Marcotte, E.M. Insights into the regulation of protein abundance from proteomic and transcriptomic analyses. *Nat. Rev. Genet.* **2012**, *13*, 227–232. [CrossRef] [PubMed]
4. Rauniyar, N.; Yates, J.R., 3rd. Isobaric labeling-based relative quantification in shotgun proteomics. *J. Proteome Res.* **2014**, *13*, 5293–5309. [CrossRef] [PubMed]
5. Upadhyay, R.D.; Balasinor, N.H.; Kumar, A.V.; Sachdeva, G.; Parte, P.; Dumasia, K. Proteomics in reproductive biology: Beacon for unraveling the molecular complexities. *Biochim. Biophys. Acta Proteins Proteom.* **2013**, *1834*, 8–15. [CrossRef]
6. Braga, D.P.; Setti, A.S.; Lo Turco, E.G.; Cordeiro, F.B.; Cabral, E.C.; Cortezzi, S.S.; Ono, E.; Figueira, R.C.; Eberlin, M.N.; Borges, E., Jr. Protein expression in human cumulus cells as an indicator of blastocyst formation and pregnancy success. *J. Assist. Reprod. Genet.* **2016**, *33*, 1571–1583. [CrossRef]
7. Bianchi, L.; Gagliardi, A.; Campanella, G.; Landi, C.; Capaldo, A.; Carleo, A.; Armini, A.; De Leo, V.; Piomboni, P.; Focarelli, R.; et al. A methodological and functional proteomic approach of human follicular fluid en route for oocyte quality evaluation. *J. Proteom.* **2013**, *90*, 61–76. [CrossRef] [PubMed]
8. Shen, X.; Liu, X.; Zhu, P.; Zhang, Y.; Wang, J.; Wang, Y.; Wang, W.; Liu, J.; Li, N.; Liu, F. Proteomic analysis of human follicular fluid associated with successful in vitro fertilization. *Reprod. Biol. Endocrinol.* **2017**, *15*, 58. [CrossRef]
9. Bianchi, L.; Gagliardi, A.; Landi, C.; Focarelli, R.; De Leo, V.; Luddi, A.; Bini, L.; Piomboni, P. Protein pathways working in human follicular fluid: The future for tailored IVF? *Expert Rev. Mol. Med.* **2016**, *18*, e9. [CrossRef]
10. O'Brien, M. The reciprocal relationship between inflammation and coagulation. *Top. Companion Anim. Med.* **2012**, *27*, 46–52. [CrossRef]
11. Jarkovska, K.; Martinkova, J.; Liskova, L.; Halada, P.; Moos, J.; Rezabek, K.; Gadher, S.J.; Kovarova, H. Proteome mining of human follicular fluid reveals a crucial role of complement cascade and key biological pathways in women undergoing in vitro fertilization. *J. Proteome Res.* **2010**, *9*, 1289–1301. [CrossRef]
12. Hillmeister, P.; Persson, P.B. The Kallikrein-Kinin system. *Acta Physiol. (Oxf.)* **2012**, *206*, 215–219. [CrossRef] [PubMed]
13. Goldman, S.; Shalev, E. MMPS and TIMPS in ovarian physiology and pathophysiology. *Front. Biosci.* **2004**, *9*, 2474–2483. [CrossRef] [PubMed]
14. Horka, P.; Malickova, K.; Jarosova, R.; Janatkova, I.; Zima, T.; Kalousova, M. Matrix metalloproteinases in serum and the follicular fluid of women treated by in vitro fertilization. *J. Assist. Reprod. Genet.* **2012**, *29*, 1207–1212. [CrossRef] [PubMed]
15. Schlage, P.; auf dem Keller, U. Proteomic approaches to uncover MMP function. *Matrix Biol.* **2015**, *44–46*, 232–238. [CrossRef] [PubMed]
16. Wu, L.; Sun, Y.; Wan, J.; Luan, T.; Cheng, Q.; Tan, Y. A proteomic analysis identifies candidate early biomarkers to predict ovarian hyperstimulation syndrome in polycystic ovarian syndrome patients. *Mol. Med. Rep.* **2017**, *16*, 272–280. [CrossRef] [PubMed]

Journal of Assisted Reproduction and Genetics (2018) 35:41–48
https://doi.org/10.1007/s10815-017-1091-3

FERTILITY PRESERVATION

A novel fibrin-based artificial ovary prototype resembling human ovarian tissue in terms of architecture and rigidity

Maria Costanza Chiti[1] · Marie-Madeleine Dolmans[1,2] · Lucie Mortiaux[3] · Flanco Zhuge[3] · Emna Ouni[1] · Parinaz Asiabi Kohneh Shahri[1] · Evelyne Van Ruymbeke[3] · Sophie-Demoustier Champagne[3] · Jacques Donnez[4] · Christiani Andrade Amorim[1]

Received: 20 July 2017 / Accepted: 14 November 2017 / Published online: 13 December 2017
© Springer Science+Business Media, LLC, part of Springer Nature 2017

Abstract

Purpose The aim of this study is to optimize fibrin matrix composition in order to mimic human ovarian tissue architecture for human ovarian follicle encapsulation and grafting.

Methods Ultrastructure of fresh human ovarian cortex in age-related women ($n = 3$) and different fibrin formulations (F12.5/T1, F30/T50, F50/T50, F75/T75), rheology of fibrin matrices and histology of isolated and encapsulated human ovarian follicles in these matrices.

Results Fresh human ovarian cortex showed a highly fibrous and structurally inhomogeneous architecture in three age-related patients, but the mean ± SD of fiber thickness (61.3 to 72.4 nm) was comparable between patients. When the fiber thickness of four different fibrin formulations was compared with human ovarian cortex, F50/T50 and F75/T75 showed similar fiber diameters to native tissue, while F12.5/T1 was significantly different (p value < 0.01). In addition, increased concentrations of fibrin exhibited enhanced storage modulus with F50/T50, resembling physiological ovarian rigidity. Excluding F12.5/T1 from further analysis, only three remaining fibrin matrices (F30/T50, F50/T50, F75/T75) were histologically investigated. For this, frozen-thawed fragments of human ovarian tissue collected from 22 patients were used to isolate ovarian follicles and encapsulate them in the three fibrin formulations. All three yielded similar follicle recovery and loss rates soon after encapsulation. Therefore, based on fiber thickness, porosity, and rigidity, we selected F50/T50 as the fibrin formulation that best mimics native tissue.

Conclusions Of all the different fibrin matrix concentrations tested, F50/T50 emerged as the combination of choice in terms of ultrastructure and rigidity, most closely resembling human ovarian cortex.

Keywords Human ovarian tissue microstructure · Scanning electron microscopy · Fibrin matrix · Porosity · Isolated follicles · Artificial ovary

✉ Marie-Madeleine Dolmans
marie-madaleine.dolmans@uclouvain.be

Maria Costanza Chiti
maria.chiti@clouvain.be

Lucie Mortiaux
luciemortiaux@gmail.com

Flanco Zhuge
flanco.zhuge@uclouvain.be

Emna Ouni
emna.ouni@uclouvain.be

Parinaz Asiabi Kohneh Shahri
parinaz.asiabi@uclouvain.be

Evelyne Van Ruymbeke
evelyne.vanruymeke@uclouvain.be

Sophie-Demoustier Champagne
sophie.demoustier@uclouvain.be

Jacques Donnez
jacque.donnez@gmail.com

Christiani Andrade Amorim
christiani.amorim@uclouvain.be

[1] Pôle de Recherche en Gynécologie, Institut de Recherche Expérimentale et Clinique, Université Catholique de Louvain, Avenue Mounier 52, bte. B1.52.02, 1200 Brussels, Belgium

[2] Gynecology Department, Cliniques Universitaires Saint-Luc, 1200 Brussels, Belgium

[3] Institute of Condensed Matter and Nanosciences, Bio and Soft Matter, Université Catholique de Louvain, Croix du Sud 1, 1348 Louvain-la-Neuve, Belgium

[4] Society for Research into Infertility, Brussels, Belgium

Introduction

Ovarian tissue cryopreservation and transplantation after cancer remission is a promising fertility restoration strategy that has already led to more than 100 live births worldwide [1–3]. Nevertheless, cancer patients at high risk of ovarian involvement cannot undergo ovarian tissue transplantation after being cured because of reasonable concerns about disease recurrence [4–7]. With a view to offering these women future alternatives allowing them to conceive, in recent years, we have been developing a transplantable artificial ovary. Conceptually, the artificial ovary requires cryopreservation of ovarian tissue before initiation of cancer treatment, followed by follicle isolation and encapsulation inside an artificial matrix, before grafting to the patient with the goal of restoring her endocrine and reproductive functions [8]. Despite encouraging results showing that a safe and efficient follicle isolation procedure is now feasible for human application [9–12], creating the appropriate scaffold to encapsulate and temporarily support human follicles after grafting remains a challenge [13].

Many different matrices have already been tested [14–21], with a fibrin-based scaffold emerging as the elective choice for construction of an artificial ovary prototype [22]. Since the majority of studies in this field have been conducted with mouse follicles, it is vital to investigate the right combination of fibrinogen and thrombin (F/T) to use in humans. These two components are the principal constituents of fibrin and key players in controlling the porosity and rigidity of the scaffold, and hence the ability to encapsulate and graft human follicles. Previous studies [23, 24] have suggested that while a fibrin matrix with low concentrations of fibrinogen and thrombin (F12.5/T1) is suitable for encapsulation and grafting of mouse secondary follicles, it may lack adequate stiffness to support primordial-primary follicles. This hypothesis was subsequently confirmed by Paulini et al. [21] using a scaffold with higher concentrations of fibrinogen and thrombin (F50/T10) to encapsulate and graft human primordial-primary follicles [21]. However, in order to design an artificial matrix that mimics the physiological ovarian environment, it is first necessary to gather more knowledge on the physical structure of the native human ovary.

Our study therefore aims to investigate human ovarian tissue microstructure in order to identify the fibrin formulation that best resembles the natural milieu of the human ovary in terms of architecture, porosity, and rigidity.

Materials and methods

Experimental design

Fresh human ovarian cortex samples ($n = 3$) were obtained from three age-related women (28–34 years of age) after laparoscopic surgery for benign gynecological disease after gaining informed consent. These biopsies and four different fibrin clot formulations (F12.5/T1, F30/T50, F50/T50, F75/T75) were analyzed by scanning electron microscopy (SEM) to assess and compare their ultrastructure. Fibrin matrices were also investigated for storage or elastic modulus (G') in order to evaluate their stiffness. Based on the significant difference in fiber thickness and porosity between F12.5/T1 and human ovarian cortex, as well as our previous unpublished findings on human follicles [25], we excluded F12.5/T1 from subsequent histological analysis. Frozen cryovials of ovarian cortex from different patients ($n = 22$) were then collected from the ovarian tissue bank, thawed and processed for follicle isolation, as previously described in one of our recently submitted papers [26]. Once isolated, preantral follicles (between 14 and 50) were embedded in the three remaining fibrin clot formulations (F30/T50, F50/T50, F75/T75) in order to compare follicle recovery and loss rates after fibrin encapsulation.

Ethics

Use of human ovarian tissue was approved by the Institutional Review Board of the Université Catholique de Louvain on 2 June, 2014 (IRB reference 2012/23MAR/125, registration number B403201213872). After obtaining informed consent, fragments of ovarian tissue were collected from patients affected by mesothelial cysts, rectovaginal nodules without associated ovarian endometriomas, and pelvic inflammatory disease.

Fibrin clot reconstitution

Reconstitution and dilution of the two components (fibrinogen and thrombin) of the fibrin sealant kit (Tissucol, Baxter, Lessines, Belgium) and fibrin clot formation were previously described by Paulini et al. [21]. Fibrinogen (100 mg/mL) was diluted in saline solution (0.9% NaCl) to obtain four concentrations, 12.5, 30, 50, and 75 mg/mL, and thrombin (500 IU/mL) in 40 mmol/L $CaCl_2$ to achieve concentrations of 1, 50, and 75 IU/mL. For fibrin polymerization, 100 μL of the appropriate fibrinogen concentration was mixed once with 100 μL of the corresponding thrombin concentration and incubated at 37 °C for 15 or 45 min depending on the F/T combination. The samples were then fixed in Karnovsky solution (2.5% glutaraldehyde [Agar Scientific, Brussels, Belgium] and 4% paraformaldehyde in 0.1 M phosphate-buffered saline [PBS]) for 24 h or immediately processed for rheological investigations.

Morphological analysis of human ovarian cortex and different fibrin matrices

Ovarian biopsies were immediately transported on ice to the laboratory in minimal essential medium plus Glutamax™

(MEM; Gibco, Invitrogen, Merelbeeke, Belgium). The medulla was removed with surgical scissors and the cortex fixed in Karnovsky solution for 24 h. After fixation, the ovarian fragments and four different fibrin matrices were immersed overnight in a solution of 30% glycerol in 0.1 M PBS (4 °C), plunged into liquid nitrogen, and cryofractured. The samples were washed in fresh 0.1 M PBS three times for 5 min each, before post-fixation with a solution of 2% osmium tetroxide (OsO_4) in 0.1 M PBS in the dark. After 1 h, the washing step was repeated three times, as previously described. The samples were then dehydrated with a graded series of ethanol (30–100%), dried to the critical point, coated with gold film (Cressington sputter coater 208HR), and analyzed by SEM (JSM-7600F, JEOL) set at 15-keV electron beam energy.

Rheological analysis of the mechanical properties of different fibrin formulations

In order to measure the rigidity of the four different fibrin matrices, their linear viscoelastic properties were investigated by small-amplitude oscillatory shear rheology using an MCR 301 (Anton Paar, Germany) rheometer. Temperature was controlled by a convection oven operating under air. Measurements were obtained at 37 °C using 8-mm parallel-plate geometry. Sandpaper was fixed to the lower plate to avoid slipping and ensure good adhesion of the samples to the steel surface. Each fibrin formulation was analyzed and compared for G'.

Thawing of frozen ovarian cortex and follicle isolation

Cryovials of frozen ovarian cortex from different patients (n = 22) were thawed and processed for follicle isolation, as recently described [26]. Briefly, after mechanical tissue dissociation, the ovarian tissue was incubated in 10 mL of PBS with Ca^{2+} and Mg^{2+} (Gibco, Thermo Fisher Scientific, Ghent, Belgium) in the presence of 0.28 Wünsch units/mL Liberase DH (Roche Diagnostics) and 8 Kunitz units/mL DNase I (Roche Diagnostics, Brussels, Belgium) in a water bath (37 °C) for up to 90 min with gentle agitation and pipetted every 15 min. The enzymatic digestion step was halted by adding a similar volume of PBS + 10% heat-inactivated fetal bovine serum. Fully isolated follicles were retrieved with the help of a stereomicroscope and 130-μm micropipette by two operators.

Follicle encapsulation and histological analysis

Because of the considerable difference in fiber thickness and porosity between human ovarian cortex and the F12.5/T1 combination encountered after SEM analysis, this fibrin formulation was not further investigated for follicle encapsulation. Only the three remaining F/T combinations were used to embed human follicles for histological analysis. For follicle encapsulation, a droplet of 12 μL fibrinogen (30, 50, and 75 mg/mL) was deposited on a glass petri dish, to which between 14 and 50 isolated preantral follicles were added (3 μL). The droplet was then mixed with 15 μL thrombin (50 and 75 IU/mL) and incubated at 37 °C for 15 min. After polymerization, the fibrin clot was gently detached, covered with 2% melted agarose (UltraPure, Thermo Fisher Scientific, Ghent, Belgium) and immediately fixed in 4% formalin [27]. After 24 h of fixation, the clots were embedded in paraffin for histology. Each fibrin clot was cut into 5-μm serial sections and every second section was stained with hematoxylin and eosin to count and compare the encapsulated follicles and follicular structures. Follicles were identified by a surrounding basal lamina and GCs with a central oocyte. Follicular structures were defined as groups of cells organized in round formations with no visible oocyte.

Statistical analysis

The Kruskal-Wallis test was applied to compare fiber thickness between ovarian tissue samples and fibrin matrices, and follicle recovery and loss rates after fibrin encapsulation. A p value < 0.05 was considered statistically significant. All statistical analyses were performed with GraphPad Prism 7 software (GraphPad, La Jolla, USA). Dunn's multiple comparison test was also conducted post hoc.

Results

Microstructure of human ovarian cortex and fibrin matrices

The overall architecture of ovarian tissue showed no significant difference in fiber density or fiber organization between patients (Fig. 1). Indeed, all ovarian cortex fragments were found to be highly fibrous and structurally inhomogeneous. A visible cluster of primordial-primary follicles is shown in Fig. 1c. There was also no significant difference in mean ± SD fiber thickness (61.3 to 72.4 nm) between patients.

As illustrated in Fig. 2, all fibrin formulations exhibited a fibrillary structure and more homogeneous organization of their filaments than did human ovarian tissue. Moreover, when F/T concentrations were raised, we observed an increase in the number of fibers, and hence fibrin consistency. On the other hand, the porosity of fibrin networks as well as fiber diameter decreased at higher F/T concentrations (Table 1). When mean ± SD fiber thickness was compared with human ovarian tissue, a significant difference was observed only with F12.5/T1 (p < 0.01), while F50/T50 and F75/T75 showed very similar fiber thickness values to ovarian cortex (Fig. 2).

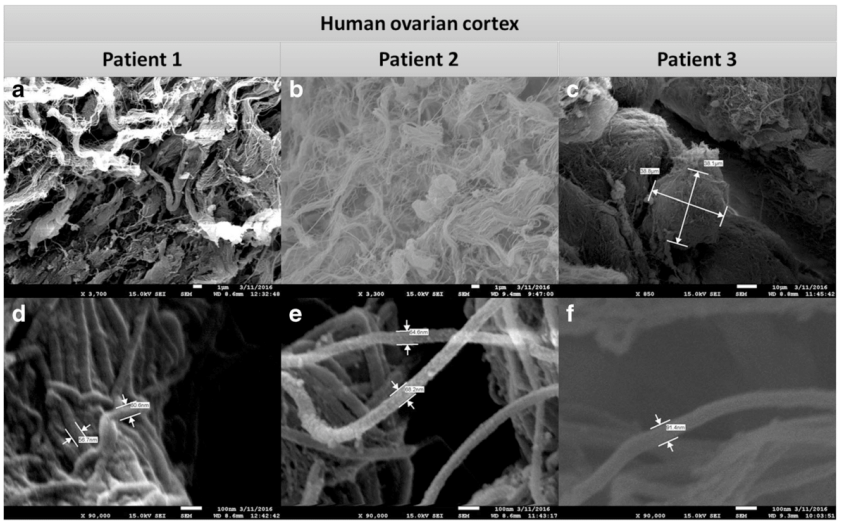


Fig. 1 SEM analysis of fresh human ovarian cortex. No significant difference was found between ovarian tissue fragments from the three patients. Patients 1 (**a**) and 2 (**b**) show heterogeneous distribution of collagen fibers. In patient 3, we can observe a cluster of primordial-primary follicles (one of them marked with crossed white arrows) of 38 μm (**c**). Fiber thickness (white arrows and bars) was measured in ovarian samples from all patients (**d**–**f**)

Viscoelastic properties of different fibrin formulations

As previously mentioned, four different fibrin matrices (F12.5/T1, F30/T50, F50/T50, F75/T75) were investigated for G'. Dynamic oscillatory shear measurements were taken at 37 °C in order to characterize the viscoelastic response of the samples. First, strain sweep tests were conducted at a frequency of 1 rad/s to determine the limits of the linear regime of deformation. Based on these results, the amplitude of deformation used in frequency sweep tests was fixed at 0.4% for all samples to ensure measurements within the linear regime. In all samples, experimental storage moduli showed fully elastic behavior (namely with G' almost independent of the frequency of oscillatory shear flow). Corresponding values of the storage moduli (140, 1100, 3800, and 9300 Pa) are presented in Fig. 3 for all four concentrations. Higher F/T concentrations gave rise to increased G', resulting from more cross-linking points within the systems, yielding a more rigid fibrin matrix.

Follicle encapsulation and histological analysis

After follicle isolation, a total of 696 follicles were retrieved and encapsulated in the three selected fibrin formulations: 216, 228, and 252 follicles were placed in F30/T50 ($n = 7$ clots), F50/T50 ($n = 7$ clots), and F75/T75 ($n = 7$ clots) fibrin clots, respectively, and processed for hematoxylin and eosin staining. Then, to evaluate whether fibrin matrix concentrations would influence follicle recovery and loss, we counted and compared the number of follicles detected in the three different fibrin formulations. As shown in Table 2, mean follicle recovery and loss rates ranged between 44 and 47% and 29 and 39%, respectively. However, when mean ± SD values of follicles found and lost were compared, no statistical difference was noted between the three fibrin formulations shortly after encapsulation (Table 2). Figure 4 shows isolated follicles encapsulated in the different fibrin scaffold concentrations.

Discussion

With a view to creating a transplantable artificial ovary, our aim was to optimize fibrin scaffold composition [16, 21, 23, 24] for human follicle encapsulation and grafting.

Human ovarian cortex and fibrin matrix microstructure

One of the key aspects in the design of the artificial ovary is a supporting matrix [8]. Among all different matrices used in in vivo studies [14–21, 28], a fibrin-based scaffold appears to be the best choice [22]. However, our previous studies have demonstrated that while a fibrin matrix with low concentrations of fibrinogen and thrombin (F12.5/T1) may well be

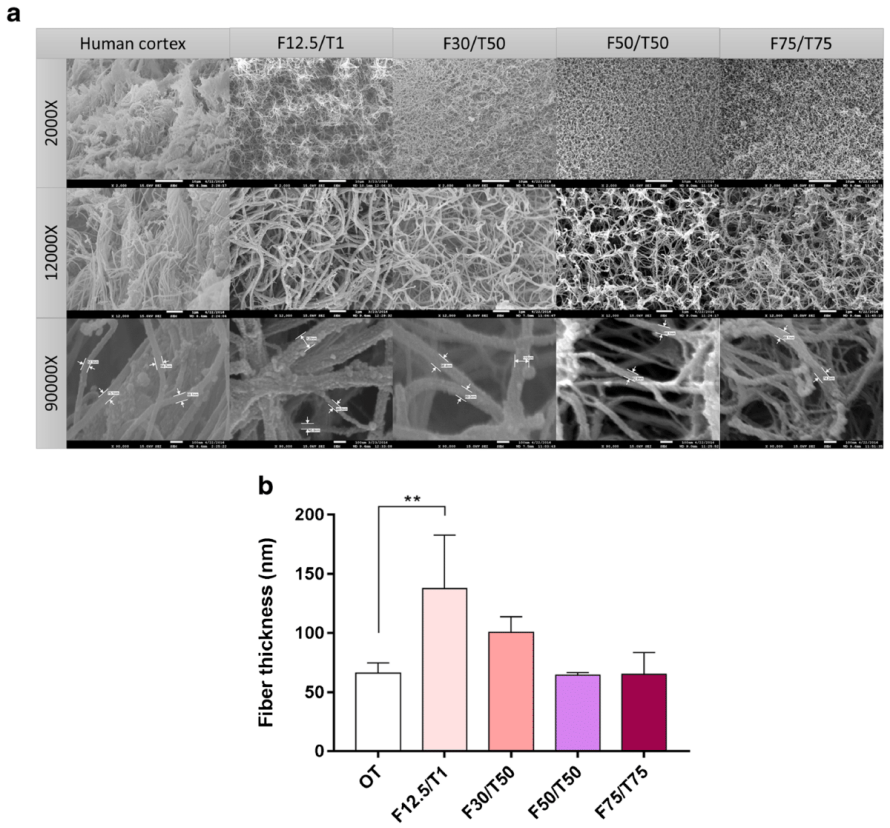


Fig. 2 Ultrastructure of human ovarian cortex and different fibrin formulations. SEM image of human ovarian cortex and fibrin matrix formulations at different magnifications (× 2000; × 12,000; × 90,000) (**a**). Graphic representation of fiber thickness in human ovarian tissue (OT) and four fibrin formulations (**b**)

suitable for encapsulation and grafting of mouse secondary follicles, it could lack the required stiffness to support human primordial-primary follicles [16, 23, 24]. This hypothesis was reinforced when we observed that human preantral follicles showed better survival rates with higher F/T concentrations (F50/T10) [21]. We therefore decided to conduct a more in-depth analysis of the ultrastructure of human ovarian cortex and compare our findings with different fibrin formulations based on in vivo studies from the existing literature [22].

Table 1 Fibrin fiber thickness according to different fibrin formulations. Increased F/T concentrations exhibited decreased fiber thickness

	Fiber thickness (mean ± SD)
F12.5/T1	137.5 ± 45.5 nm
F30/T50	100.8 ± 13.2 nm
F50/T50	64.5 ± 2.3 nm
F75/T75	65.4 ± 18.4 nm

Indeed, our goal was to identify the fibrin formulation that most closely mimics physiological ovarian cortex architecture.

In the present study, we demonstrated that fragments of ovarian cortex collected from women of similar age have a generally similar architecture, with a very dense, fibrous, and inhomogeneous structure characterized by interlaced collagen fibers of comparable thickness. It has been proved that collagen fibrils, which constitute one of the most abundant components of the ovarian extracellular matrix [29, 30], tend to increase in number [31] and diameter with age [32]. We showed that conducting a comparative analysis between human ovarian cortex microstructure and fibrin formulations is an efficient way of identifying a supporting scaffold that best resembles the architecture of the human ovary, achieving optimal porosity to encapsulate and transplant follicles. Considering the vast physiological differences that exist between rodent

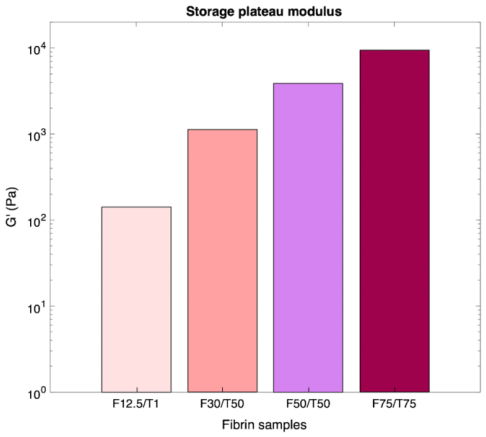


Fig. 3 Graphic representation of fibrin rigidity (storage modulus G') according to different fibrin formulations. The stiffness (G') of fibrin matrices was positively correlated with increased concentrations of fibrinogen and thrombin

and primate ovaries [33], use of mouse follicles for the design of an artificial ovary prototype, as suggested by Laronda et al. [19], may not necessarily be translatable to humans, so caution should be exercised. Hence, in our study, we considered human ovarian tissue architecture as the reference standard for creation of the artificial ovary prototype. Importantly, the great difference found between F12.5/T1 and ovarian tissue ultrastructure may also explain the low human follicle recovery rates encountered in our previous study, when preantral follicles were encapsulated in F12.5/T1 and grafted to mice [25]. Indeed, some fibrin matrix combinations exhibited a less dense and compact structure, with more homogeneous and organized distribution of fibrin fibers than human ovarian cortex. In addition, an inverse correlation was found between F/T concentrations, fiber thickness, and pore size, as documented in other reports [34–36]. Interestingly, when F/T concentrations were increased to F50/T50 and F75/T75, the formulations exhibited fiber thickness comparable to human ovarian cortex. This led us to hypothesize that these combinations may mimic the physiological environment of human follicles more closely, making them good candidates for the artificial ovary prototype. However, another important feature to consider in the development of a transplantable artificial ovary is the rigidity of the matrix. It has been previously demonstrated that ovary stiffness [37], hence also that of the artificial ovary prototype [21, 38], may influence follicle behavior. We therefore decided to investigate the storage modulus of the four selected fibrin matrices and compare it with that of human ovarian tissue [39]. As expected, increased concentrations of fibrinogen and thrombin yielded higher G' levels, and consequently greater rigidity, in line with earlier reports from the literature [36, 40]. Nevertheless, only F50/T50 showed similar rigidity to human ovarian tissue [39].

Table 2 Follicle recovery rates, follicular structures, and follicle loss after fibrin matrix encapsulation. Follicle recovery rates, follicular structures, and follicle loss with different fibrin formulations were compared shortly after encapsulation

Fibrin formulation	Follicle recovery	Follicular structures	Follicle loss
F30/T50 ($n = 7$)	46 ± 21%a	26 ± 17%b	38 ± 21%c
F50/T50 ($n = 7$)	44 ± 24% a	18 ± 11%b	39 ± 20%c
F75/T75 ($n = 7$)	47 ± 22%a	23 ± 14%b	29 ± 30%c

Different letters in each column (a, b, c) indicate significant differences ($p < 0.05$)

Follicle encapsulation

Based on the great difference encountered between human ovarian cortex and F12.5/T1 ultrastructure, as well as previously discouraging findings with human follicles encapsulated in F12.5/T1 and subsequently grafted [25], we excluded this fibrin formulation from further histological investigations. From the other three fibrin combinations, around 50% of follicles were recovered soon after fibrin polymerization, which is consistent with earlier studies using human follicles [21]. However, a non-negligible percentage of follicle loss was found with all fibrin formulations, as previously stated for mouse follicles [24]. Taking into account that most follicles are normally located at the border of the fibrin clot, this loss may be partially explained by retraction of the fibrin matrices after fixation and dehydration, which typically occurs during histological processing. In the context of future clinical application, it should be borne in mind that the fibrin clot needs to be grafted to the patient as soon as it is created.

General conclusion

In conclusion, among all the different fibrin matrix concentrations tested, F50/T50 appears to be the combination of choice in terms of ultrastructure and rigidity, most closely resembling human ovarian cortex. Such findings are essential to help us standardize fibrin matrix architecture.

Acknowledgments The authors thank Patricia Meijers for her collaboration and scientific advice on fibrin in the project. They also thank Mira Hryniuk, BA, for reviewing the English language of the manuscript and Delphine Magnin, Dolores Gonzalez, and Olivier Van Kerk for their technical assistance. This study was supported by grants from the Fonds National de la Recherche Scientifique de Belgique (FNRS) awarded to C. A. Amorim as a research associate for the FRS-FNRS and M.M. Dolmans (grant 5/4/150/5), Fonds Spéciaux de Recherche, Fondation St Luc,

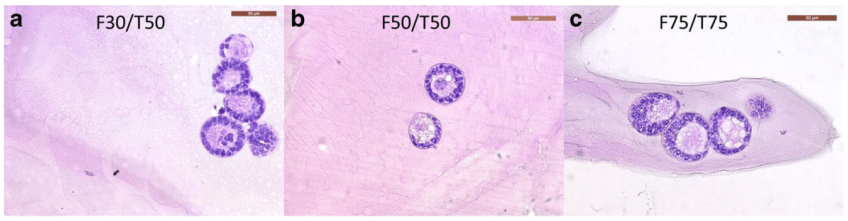


Fig. 4 Histology of isolated human follicles in different fibrin formulations. Follicles encapsulated in F30/T50 (**a**), F50/T50 (**b**), and F75/T75 (**c**). Scale bar 50 μm

Foundation Against Cancer, and Wallonie-Bruxelles International, and donations from the Ferrero family.

Compliance with ethical standards

Conflict of interest The authors declare that they have no conflict of interest.

References

1. Donnez J, Dolmans MM. Ovarian cortex transplantation: 60 reported live births brings the success and worldwide expansion of the technique towards routine clinical practice. J Assist Reprod Genet. 2015;32(8):1167–70.
2. Anderson RA, Wallace WHB, Telfer EE. Ovarian tissue cryopreservation for fertility preservation: clinical and research perspectives. Human Reproduction Open. 2017;2017(1):hox001-hox.
3. Jensen AK, Macklon KT, Fedder J, Ernst E, Humaidan P, Andersen CY. 86 successful births and 9 ongoing pregnancies worldwide in women transplanted with frozen-thawed ovarian tissue: focus on birth and perinatal outcome in 40 of these children. J Assist Reprod Genet. 2017;34(3):325–36.
4. Smitz J, Dolmans MM, Donnez J, Fortune JE, Hovatta O, Jewgenow K, et al. Current achievements and future research directions in ovarian tissue culture, in vitro follicle development and transplantation: implications for fertility preservation. Hum Reprod Update. 2010;16(4):395–414.
5. Dolmans MM, Luyckx V, Donnez J, Andersen CY, Greve T. Risk of transferring malignant cells with transplanted frozen-thawed ovarian tissue. Fertil Steril. 2013;99(6):1514–22.
6. Donnez J, Dolmans MM. Fertility preservation in women. Nat Rev Endocrinol. 2013;9(12):735–49.
7. Soares M, Saussoy P, Maskens M, Reul H, Amorim CA, Donnez J, et al. Eliminating malignant cells from cryopreserved ovarian tissue is possible in leukaemia patients. Br J Haematol. 2017;178(2):231–239.
8. Amorim CA. Artificial ovary. In: Suzuki N, Donnez J. Gonadal tissue cryopreservation in fertility preservation. Tokyo: Springer; 2016. p. 175–192.
9. Kristensen SG, Rasmussen A, Byskov AG, Andersen CY. Isolation of pre-antral follicles from human ovarian medulla tissue. Human reproduction (Oxford, England). 2011;26(1):157–66.
10. Vanacker J, Camboni A, Dath C, Van Langendonckt A, Dolmans MM, Donnez J, et al. Enzymatic isolation of human primordial and primary ovarian follicles with Liberase DH: protocol for application in a clinical setting. Fertil Steril. 2011;96(2):379–83.e3.
11. Lierman S, Tilleman K, Cornelissen M, De Vos WH, Weyers S, T'Sjoen G, et al. Follicles of various maturation stages react differently to enzymatic isolation: a comparison of different isolation protocols. Reprod BioMed Online. 2015;30(2):181–90.
12. Soares M, Sahrari K, Amorim CA, Saussoy P, Donnez J, Dolmans MM. Evaluation of a human ovarian follicle isolation technique to obtain disease-free follicle suspensions before safely grafting to cancer patients. Fertil Steril. 2015;104(3):672–80.e2.
13. Amorim CA, Shikanov A. The artificial ovary: current status and future perspectives. Future oncology (London, England). 2016;12(20):2323–32.
14. Dolmans MM, Martinez-Madrid B, Gadisseux E, Guiot Y, Yuan WY, Torre A, et al. Short-term transplantation of isolated human ovarian follicles and cortical tissue into nude mice. Reproduction (Cambridge, England). 2007;134(2):253–62.
15. Vanacker J, Dolmans MM, Luyckx V, Donnez J, Amorim CA. First transplantation of isolated murine follicles in alginate. Regen Med. 2014;9(5):609–19.
16. Luyckx V, Dolmans MM, Vanacker J, Legat C, Fortuno Moya C, Donnez J, et al. A new step toward the artificial ovary: survival and proliferation of isolated murine follicles after autologous transplantation in a fibrin scaffold. Fertil Steril. 2014;101(4):1149–56.
17. Kniazeva E, Hardy AN, Boukaidi SA, Woodruff TK, Jeruss JS, Shea LD. Primordial follicle transplantation within designer biomaterial grafts produce live births in a mouse infertility model. Sci Rep. 2015;5:17709.
18. Laronda MM, Jakus AE, Whelan KA, Wertheim JA, Shah RN, Woodruff TK. Initiation of puberty in mice following decellularized ovary transplant. Biomaterials. 2015;50:20–9.
19. Laronda MM, Rutz AL, Xiao S, Whelan KA, Duncan FE, Roth EW, et al. A bioprosthetic ovary created using 3D printed microporous scaffolds restores ovarian function in sterilized mice. Nat Commun. 2017;8:15261.
20. Kim J, Perez AS, Claflin J, David A, Zhou H, Shikanov A. Synthetic hydrogel supports the function and regeneration of artificial ovarian tissue in mice. Npj Regenerative Medicine. 2016;1:16010.
21. Paulini F, Vilela JM, Chiti MC, Donnez J, Jadoul P, Dolmans MM, et al. Survival and growth of human preantral follicles after cryopreservation of ovarian tissue, follicle isolation and short-term xenografting. Reprod BioMed Online. 2016;33(3):425–32.
22. Chiti MC, Dolmans MM, Donnez J, Amorim CA. Fibrin in reproductive tissue engineering: a review on its application as a biomaterial for fertility preservation. Ann Biomed Eng. 2017;45(7):1650–1663.
23. Chiti MC, Dolmans MM, Orellana R, Soares M, Paulini F, Donnez J, et al. Influence of follicle stage on artificial ovary outcome using fibrin as a matrix. Human reproduction (Oxford, England). 2016;31(2):427–35.
24. Chiti MC, Dolmans MM, Lucci CM, Paulini F, Donnez J, Amorim CA. Further insights into the impact of mouse follicle stage on graft outcome in an artificial ovary environment. Mol Hum Reprod. 2017;23(6):381–392.
25. Amorim CA. The ovarian follicle microenviroment and the artificial ovary. Shanghai: 4th World Congress of International Society for Fertility Preservation; 2015.

26. Chiti MC. A modified and tailored human follicle isolation procedure improve follicle survival in an artificial ovary prototype after short term xenografting. J Ovarian Res. 2017;10(1):71.
27. Fox CH, Johnson FB, Whiting J, Roller PP. Formaldehyde fixation. The journal of histochemistry and cytochemistry : official journal of the Histochemistry Society. 1985;33(8):845–53.
28. Smith RM, Shikanov A, Kniazeva E, Ramadurai D, Woodruff TK, Shea LD. Fibrin-mediated delivery of an ovarian follicle pool in a mouse model of infertility. Tissue Eng A. 2014;20(21–22):3021–30.
29. Rodgers RJ, Irving-Rodgers HF, Russell DL. Extracellular matrix of the developing ovarian follicle. Reproduction (Cambridge, England). 2003;126(4):415–24.
30. Cho A, Howell VM, Colvin EK. The extracellular matrix in epithelial ovarian cancer—a piece of a puzzle. Front Oncol. 2015;5:245.
31. Herraiz S, Diaz-Garcia C, Pellicer A. Ovarian tissue cryopreservation: slow freezing. In: Suzuki N, Donnez J, editors. Gonadal tissue cryopreservation in fertility preservation. Tokyo: Springer Japan; 2016. p. 53–77.
32. Armstrong CG, Mow VC. Variations in the intrinsic mechanical properties of human articular cartilage with age, degeneration, and water content. J Bone Joint Surg Am. 1982;64(1):88–94.
33. Chaffin CL, Vandevoort CA. Follicle growth, ovulation, and luteal formation in primates and rodents: a comparative perspective. Experimental biology and medicine (Maywood, NJ). 2013;238(5):539–48.
34. Wolberg AS. Thrombin generation and fibrin clot structure. Blood Rev. 2007;21(3):131–42.
35. Kim BS, Sung HM, You HK, Lee J. Effects of fibrinogen concentration on fibrin glue and bone powder scaffolds in bone regeneration. J Biosci Bioeng. 2014;118(4):469–75.
36. Germain L, De Berdt P, Vanacker J, Leprince J, Diogenes A, Jacobs D, et al. Fibrin hydrogels to deliver dental stem cells of the apical papilla for regenerative medicine. Regen Med. 2015;10(2):153–67.
37. Woodruff TK, Shea LD. A new hypothesis regarding ovarian follicle development: ovarian rigidity as a regulator of selection and health. J Assist Reprod Genet. 2011;28(1):3–6.
38. Choi JK, Agarwal P, Huang H, Zhao S, He X. The crucial role of mechanical heterogeneity in regulating follicle development and ovulation with engineered ovarian microtissue. Biomaterials. 2014;35(19):5122–8.
39. Wood CD, Vijayvergia M, Miller FH, Carroll T, Fasanati C, Shea LD, et al. Multi-modal magnetic resonance elastography for noninvasive assessment of ovarian tissue rigidity in vivo. Acta Biomater. 2015;13:295–300.
40. Duong H, Wu B, Tawil B. Modulation of 3D fibrin matrix stiffness by intrinsic fibrinogen-thrombin compositions and by extrinsic cellular activity. Tissue Eng A. 2009;15(7):1865–76.

Ovarian extracellular matrix-based hydrogel for human ovarian follicle survival in vivo: a pilot work

Chiti Maria-Costanza[1], Vanacker Julie[2], Ouni Emna1, Tatic Natalija[3], Viswanath Aiswarya[2], des Rieux Anne[2], Dolmans Marie-Madeleine[1,4], White Lisa Jane[3,*], Amorim Christiani Andrade[1,*,**]

[1] Pôle de Recherche en Gynécologie, Institut de Recherche Expérimentale et Clinique

[2] Louvain Drug Research Institute, Advanced Drug Delivery and Biomaterials Unit, Université Catholique de Louvain, 1200, Brussels, Belgium

[3] School of Pharmacy, Biodiscovery Institute, University of Nottingham, Nottingham NG7 2RD, UK

**Prof. Amorim Christiani Andrade (corresponding author)

Université Catholique de Louvain

Avenue Mounier 52, bte B1.52.02, 1200 Brussels, Belgium

e-mail: christiani.amorim@uclouvain.be

telephone: +32(0)7645287

*Dr Lisa White and Professor Christiani Andrade Amorim contributed equally to this manuscript and should be considered joint senior authors

Running title

Ovarian ECM hydrogel for a bio-engineered ovary

Keywords: Ovarian decellularized extracellular matrix, ECM hydrogels, ovarian follicles, bio-engineered ovary

Abstract

To successfully assemble a bio-engineered ovary, we need to create a three-dimensional matrix able to accommodate isolated follicles and cells. The goal of this study was to develop an extracellular matrix hydrogel (oECM) derived from decellularized bovine ovaries able to support, in combination with alginate, human ovarian follicle survival and growth in vitro. Two different hydrogels (oECM1, oECM2) were produced and compared in terms of decellularization efficiency (dsDNA), ECM preservation (collagen and glycosaminoglycan levels), ultrastructure, rigidity and cytotoxicity. oECM2 showed significantly less dsDNA, greater retention of glycosaminoglycans and better rigidity than oECM1. Isolated human ovarian follicles were then encapsulated in 4 selected hydrogel combinations: (1) 100% oECM2, (2) 90% oECM2 + 10% alginate, (3) 75% oECM2 + 25% alginate and (4) 100% alginate. After one week of in vitro culture, follicle recovery rate, viability and growth were analyzed. On day 7 of in vitro culture, follicle recovery rates were 0%, 23%, 65%, 82% in groups 1 to 4 respectively, rising proportionally with increased alginate content. However, there was no difference in follicle viability or growth between groups 2 and 3 and controls (group 4). In conclusion, since pure alginate cannot be used to graft preantral follicles due to its poor revascularization and degradation after grafting, oECM2 hydrogel combined with alginate may provide a new and promising alternative to graft isolated human follicles in a bio-engineered ovary.

Introduction

In some cancers grafting of frozen/thawed ovarian tissue cannot be performed due to the risk of reintroducing malignant cells [1, 2]. An alternative to restore fertility in these patients is development of a transplantable engineered ovary (TEO) [3-5]. It consists of isolated ovarian follicles, the morpho-functional units of the ovary, which are co- encapsulated with isolated ovarian cells in a three-dimensional (3D) scaffold, essential to providing a bio-engineered environment where follicles can be supported, grow and interact with ovarian cells [6]

Encouraging results with mouse follicles have been obtained in vitro and in vivo with alginate scaffolds [7, 8]. While alginate has several advantages for follicle encapsulation, one of the main limitations is its biological inertness, which has hampered its use in in vivo applications due to poor cell adhesion, limited degradation and revascularization after transplantation [8]. To circumvent this problem, previous studies with mouse follicles aimed to combine alginate with other natural polymers [9-12]. Despite their promising results, alginate-based hydrogels still lack many bioactive factors present in the ovarian extracellular matrix (ECM) [13].To develop a 3D scaffold as similar as possible to the native organ, hydrogels from decellularized ECM have been proposed. Decellularization of mammalian tissues aims to remove antigenic components, while maintaining the biochemical composition of native ECM. Decellularized tissues can be comminuted to form ECM powders that, once digested and solubilized into constituent protein monomers, can be further pH- and temperature-neutralized to induce spontaneous reformation into a hydrogel. ECM hydrogels are collagen-based and enriched with native sulfated glycosaminoglycans (GAGs), proteoglycans, and ECM proteins [14]. When processed appropriately, ECM hydrogels retain the inherent bioactive features of native ECM, including peptide domains, which play a major role in integrin-cell attachment, cell survival, proliferation, and deposition of de novo ECM components. Moreover, they can be easily administered in a minimally invasive manner. The thermoresponsive nature of ECM hydrogels allows injection of liquid-like, solubilized ECM that will form a scaffold at physiological body temperatures [14]. However, one of the limitations of pure ECM-derived hydrogels is their low mechanical properties and rigidity which has led to combinations with other polymers[15]. Tissue-derived ECM hydrogels have already demonstrated their potential in a variety of different tissues and organs, including heart [16, 17], brain [18, 19], bone[20-22], skin [23], intestine [24], liver [25], kidney [26], meniscus [27] and spinal cord [21].

Since each ECM is unique in its topological, mechanical and biochemical profile, one of the major challenges in developing ECM-derived hydrogels is tailoring tissue-specific decellularization protocols able to preserve the biochemical and physical characteristics of native ECM. Xenogeneic ECM-derived scaffolds are already being tested in increasing numbers of preclinical trials [28], and no cases of zoonosis have been reported to date [14]. Moreover, better outcomes were achieved in terms of efficacy and reproducibility when animal-derived ECMs were compared with human-derived ECM [29]. Importantly, the feasibility and safety of animal-derived ECM hydrogels have recently been documented in human clinical trials [30]. These important studies open up the possibility of using animal-derived ECM hydrogels in many other applications.

The goal of this pilot study was to develop and characterize a hydrogel derived from decellularized bovine ovarian extracellular matrix (oECM) to support survival and development of isolated human follicles when it was combined with alginate. Bovine ovaries were chosen due to their similarity to human ovaries in terms of ultrastructure, follicle dynamics, rigidity, ECM organization and composition [31-36] and unlimited supply, since they are normally discarded. Furthermore, some bovine-ECM products have already been commercialized [28] and reportedly used without any safety issues which is promising for extending possible clinical applications.

In this work, two different decellularization protocols were tested in order to assess their impact on the hydrogel properties and ECM preservation: the first protocol had a prolonged enzymatic treatment, and the second had a short enzymatic treatment in combination with detergents. As bovine ECM-derived hydrogels (oECM) have not previously been used to encapsulate isolated ovarian preantral follicles, we first evaluated hydrogel impact on mouse and human follicle viability. Then to obtain mechanical properties closer to the human ovary, the selected oECM hydrogel was combined with alginate to increase its stiffness.

Materials and methods

Ethics

The Institutional Review Board of the Université Catholique de Louvain approved use of human ovarian tissue to isolate preantral ovarian follicles for this study (reference 2012/23 mar/125). Guidelines for animal welfare were approved by the Committee on Animal Research of the Université Catholique de Louvain on June 29, 2016 (reference 2014/UCL/MD/007).

Chemicals and reagents

All reagents were purchased from Sigma-Aldrich (Bornem, Belgium), unless otherwise stated.

Bovine ovary-based ECM hydrogel (oECM)

Bovine ovaries (n=2) were obtained from young animals (aged 8-10 years old) from a local slaughterhouse (Abattoir d'Anderlecht, Brussels, Belgium), transported in Dulbecco's phosphate-buffered saline (DPBS) at 4°C, and processed within 1 hour. A longitudinal incision was made to remove the medulla, all the antral follicles were aspirated, and corpora lutea were removed. The tissue was cut into 1 cm^2 fragments, plunged into liquid nitrogen for immediate freezing, and stored at -80°C until further use. The choice of decellularization protocol depends on tissue specific factors including cellularity and density, with most protocols utilizing chemical, physical or enzymatic agents [37]. In this study, ovaries were decellularised using enzymatic agents alone (protocol 1) or with detergents (protocol 2) (Fig.1).

Decellularization of ovarian tissue: protocol 1 (enzymatic)

Thawed ovarian fragments were washed thoroughly in deionized water and incubated in a 0.05% trypsin-0.02% EDTA solution for 24 hours at 37°C and shaken at 300 rpm. The following day, the fragments were washed in DPBS (1X) and then incubated in DPBS for 24 hours at room temperature (RT), under agitation. After a final wash in deionized water, decellularized ovarian fragments were freeze-dried.

Decellularization of ovarian tissue: protocol 2 (enzymatic+detergents)

Thawed ovarian fragments were washed thoroughly in deionized water and incubated in a 0.05% trypsin-0.02% EDTA solution for 1 hour at 37°C and shaken at 300 rpm. The material was then washed in deionized water, incubated in 3% Triton X-100 for 1 hour at RT agitated, washed again in deionized water, and incubated in 4% sodium deoxycholate under agitation for 1 hour at RT. After a final wash with deionized water, the tissue was stored in water overnight at 4°C and then incubated in 4% ethanol and 0.2% peracetic acid for 2 hours at RT under agitation, before being washed thoroughly in DPBS and then deionized water before freeze-drying.

ECM digestion and solubilization

Pepsin digestion and solubilization were carried out to obtain pre-gel solutions [14]. Briefly, lyophilized ECM was added to 1 mg/mL of pepsin in 0.01 N hydrochloric acid (HCl) for a final concentration of 10 mg ECM/ml. The suspension was stirred at RT for 72 hours. The resulting pepsin digests were aliquoted and stored at -20°C. Gelation of pepsin digests was induced by neutralization of salt concentrations and pH at 4°C, followed by warming to 37°C. Pre-gel solutions of 8 mg/ml were prepared and incubated for 1 hour at 37°C to obtain solid hydrogels according to each protocol, designated as oECM1 and oECM2.

oECM characterization

DNA, collagen, and sulphated glycosaminoglycan quantification

More detailed protocols are described in the supplementary file.

Determination of decellularization efficiency was based on quantification of dry weight double stranded DNA (dsDNA) [21, 38]. Concentrations of dsDNA were measured using a Quant-iT™ Picogreen® assay kit (Invitrogen, Merelbeeke, Belgium) following the supplier's instructions.

Since collagen and sulfated GAGs are structural ECM proteins, their content was investigated to determine the rate of ECM preservation.

Collagen content was measured by quantification of hydroxyproline [21, 39]. Briefly, bovine ovarian tissue, oECMs and a blank pepsin solution were treated in the same way. The hydrolyzed blank pepsin solution served as a negative control as well as diluent for the assay. A standard curve was prepared using known concentrations of hydroxyproline, ranging from 0 to 100 µg/ml, and absorbance was measured at 540 nm with a Tecan Infinite M200 plate reader. Sulfated GAGs were determined using the 1,9 dimethyl-methylene blue (DMMB) assay [21, 40], while a blank pepsin solution served as negative control as well as diluent for the assay. 50 µl of samples were mixed with 200 µl of DMMB solution (0.03 M sodium formate, 046 M DMMB, ethanol [0.5% v/v] and formic acid [0.2% v/v] in a 96-well plate. Thestandard curve ranged from 0 to 75 µg/ml chondroitin-4-sulphate. Absorbance was measured immediately at 525 nm.

Mechanical properties of oECM hydrogel

Rheological and gelation characteristics of oECM1 and oECM2 were determined as previously described [20] using a Malvern Kinexus ultra+ rheometer (Malvern Kinexus Pro rotational rheometer and rSpace software, Malvern Instruments, Worcestershire, UK). Data were recorded every 30 seconds (n=3).

Microstructure of oECM hydrogel

Both oECM1 and oECM2 (300 µL per well) were fixed in 5% glutaraldehyde at RT. Samples were dehydrated in a graded series of ethanol (25-100%), dried using a critical point dryer (Balzers Union, Balzers, Finland) andsputter-coated with gold using a Cressington 208HR metalizer (Eloise s.a.r.l., Tremblay, France). Images were acquired using a JSM-7600F (JEOL, Zaventem, Belgium) scanning electron microscope at a voltage of 15 kV. Bovine ovarian tissue was used as a control.

Isolation and viability of preantral follicles
Isolation and viability of mouse preantral follicles

All procedures were carried out under a laminar flow hood using sterilized materials. The ovaries of four severe combined immunodeficient (SCID) mice (5 weeks of age) were removed, as already reported [5] and follicles were

isolated according to our routine procedure [41]. To assess the impact of the follicle isolation procedure, follicle viability was evaluated soon after isolation using live/dead assays (Life Technologies, Ghent, Belgium), as previously described [42]. Follicles were classified into four categories [43] based on oocyte and granulosa cell viability: V1 and V2 represented follicles with high viability (0% and <10% dead granulosa cells respectively) and V3 and V4, follicles with poor viability (≥10% and >50% dead granulosa cells or a dead oocyte).

Isolation and viability of human preantral follicles

Frozen ovarian tissue samples from 3 patients of reproductive age with non-ovarian pathologies were taken from the ovarian tissue bank, after obtaining written informed consent. Tissues were thawed [44] and follicles isolated [45]. Follicle viability was calculated as described above (see 1.5.1).

Ovarian follicle encapsulation
Mouse ovarian follicle encapsulation

Mouse ovarian follicles were encapsulated only in oECM1 and oECM2 to evaluate the cytotoxicity of the ovarian ECM hydrogels and avoid any waste of precious human follicles.

Firstly 339 follicles were divided into 2 groups (oECM1 and oECM2), and their diameter was recorded before being encapsulated separately in each group. Between 10 and 15 follicles were embedded in 50 µl oECM1 (8 mg/ml) or oECM2 (8 mg/ml), placed in a 4-well plate and incubated at 37°C for 1 hour to allow gelation (oECM1 n=20 beads, oECM2 n=3 beads). Thereafter, 500 µl pre-equilibrated in vitro culture medium (MEM, GlutaMAX) supplemented with 10% fetal bovine serum, 2 mM pyruvic acid, 50 µg/ml ascorbic acid, 0.1 IU/ml follicle stimulating hormone (FSH) (Gonal F), 1% Anti-anti were added. The hydrogels were cultured at 37°C and 5% CO2 for one week. Every 2 days, half of the culture medium was removed and replaced with fresh medium.

Human ovarian follicle encapsulation

A more detailed protocol is described in the supplementary file. Isolated primordial and primary follicles (n=114) were divided into 4 groups and their diameter was recorded before being encapsulated in: (1) 100% oECM2 (8 mg/ml); (2) 90% oECM2 + 10% of 1% alginate (SLM100, Pronova,Nova

Matrix); (3) 75% oECM2 + 25% of 1% alginate; or (4) 100% of 1% alginate[42]. Incubation at 37°C for 1 hour was performed to allow oECM2 to gel, which was then followed by addition of 100 µl CaCl2 100 mM for a few seconds to induce alginate cross-linking. One hundred µl of culture medium was then added to each well and the samples were stored at 37°C and 5% CO2 for one week. Every 2 days, half of the culture medium was removed and replaced with fresh medium.

Follicle recovery rate, viability and in vitro growth

Follicle recovery rates, viability and growth were evaluated after 7 days of in vitro culture. On day 7, the follicle recovery rate was calculated for each bead and then compared (mean ± SD) for each group as follow:

Number of recovered follicles = (FE/FF)*100 Where,

FE = encapsulated follicles on day 0

FF = follicles found on day 7

In order to measure follicle viability, live/dead assays were conducted as previously documented (see 1.5.1).

Follicle growth was evaluated by measuring follicle diameters under an inverted microscope, using a scale incorporated in the objective lens at 10X magnification. On days 0 and 7 of in vitro culture, each follicle was measured and the mean ± SD was compared between these time points for each group.

Statistical analysis

Statistical analyses were performed with Prism 8.1.2.

Detailed methods are described in the supplementary file. This research has benefited greatly from statistical consultation with the Statistical Methodology and Computing Service technological platform at the UCL – SMCS/IMMAQ, UCL.

Results

Decellularization impacted residual DNA and GAGs content, but not collagen proportions in oECM hydrogels

oECM1 and oECM2 dsDNA, collagen and GAGs content was quantified and compared to native bovine ovarian tissue. The concentration of nucleic acid (mean ± SD) was significantly higher ($p<0.0001$) in native tissue (1750-fold) than in oECM1 or in oECM2 (Fig. 2a). When comparing oECM1 and oECM2, a significantly($p<0.0001$) higher concentration of dsDNA was found in the oECM1 hydrogel.

No difference in collagen content was observed between native tissue (n=2, 0.67 ± 0.3 mg/mg of dry weight), oECM1 (n=3, 0.89 ± 0.06 mg/mg of dry weight) or oECM2 (n=3, 0.67 ± 0.2mg/mg of dry weight) (Fig. 2b). sGAG content was significantly higher ($p<0.01$) in oECM2 (2.7-fold) compared to oECM1 and equivalent to native tissue (Fig. 2c).

Decellularization influenced oECM hydrogel mechanical properties

Storage modulus (G') and the loss modulus (G'') represent the mechanical strength and the viscous portion of hydrogel respectively. G' and G'' of pre-gel solutions increased after 5 minutes after pH neutralization and temperature elevation (Fig. 2d), indicating the beginning of the gelation process that plateaued after 8 minutes. G' was always higher than G" in both hydrogels. Irrespective of the decellularization protocol, gelation kinetics were similar, even though the final moduli were statistically different (Table 1). Indeed, oECM2 showed a G' value superior ($p<0.05$) to the oECM1 hydrogel modulus, while oECM1 hydrogel G'' was significantly higher ($p<0.0001$) than the oECM2 hydrogel.

Influence of decellularization on oECM hydrogel microstructure

Bovine ovarian tissue was structurally heterogeneous. Dense and compact regions alternated with fibrous regions showing fibers of variable thickness. The porosity of the bovine ovarian ECM appeared to correlate inversely with the degree of crosslinking of tissue fibers. Regions with thicker tissue fibers and apparently inferior porosity alternated with regions of thinner fibers and greater porosity (Fig. 3a). Decellularization of oECM hydrogels strongly influenced their morphology (Fig. 3). While the oECM1 hydrogel had a highly porous and fibrillary structure with small and homogeneous fibers (Fig. 3b), oECM2 hydrogel displayed a sponge-like structure with thicker walls and

heterogeneous pores (Fig. 3c).

Impact of decellularization on follicle recovery, viability and growth

Mouse follicle recovery rate, viability and growth

A total of 339 mouse follicles were isolated under the stereomicroscope. Before follicle encapsulation and in vitro culture, 50 follicles were investigated for follicle viability. Percentages (n=50 follicles) of fully viable (V1) and minimally damaged (V2) follicles were 22% and 52% respectively, while highly damaged (V3) or dead (V4) follicles represented 10% and 16% respectively. Hence, 74% of follicles were viable soon after isolation from mouse ovaries.

After encapsulation in oECM hydrogels and one week of culture, the follicle morphology was similar between oECM1 and oECM2 (Fig.4). Follicle recovery rates (54 ± 27% oECM1 [n=20 beads], 47.5 ± 39% oECM2 [n=3 beads]) and viability (V1+V2, 69.5 and 50%) were not statistically different. Regarding follicle diameter, no statistical difference was observed regardless of oECM hydrogels used between day 0 and day 7 (Table 2).

Human follicle recovery rate, viability and growth

For experiments with human follicles, only oECM2 was selected, based on its lower dsDNA content, higher GAG content and higher storage modulus. A total of 127 human follicles were identified under the stereomicroscope. Percentages of fully viable (V1) and minimally damaged (V2) follicles were 61% and 31% respectively, which means that 92% of isolated follicles were viable before follicle encapsulation. No highly damaged (V3) and very few dead (V4) follicles (8%) were counted before follicle encapsulation.

On day 7 follicle morphology was similar between all groups but one (group 1, no follicle found). Follicle recovery rates increased proportionally with the percentage of alginate added to oECM2: 0%, 23%, 65% and 85% from group 1 to group 4 respectively. No follicles were recovered in group 1, but granulosa cells were attached and spread all over the hydrogel beads. After 1 week of culture in the different hydrogels, no difference was observed in follicle viability (Table 3) in any but one (group 1). (Table 4).

Discussion

In this study, two different ECM-derived hydrogels were produced from bovine ovaries. When decellularization efficiency was investigated, both hydrogels showed a drastic reduction in dsDNA compared to native tissue. According to Crapo et al., (2011) decellularized hydrogels should possess less than 50 ng dsDNA per mg of initial dry weight of decellularized ECM to limit the presence of residual antigenic material, which may induce an immune response in vivo. Although both hydrogels contained less than 50 ng/mg dsDNA, a significantly greater reduction in dsDNA (>99%) was obtained with the second protocol (oECM2) compared to native tissue. One of the main reasons for this difference is likely the addition of ionic (Triton X-100) and non-ionic (sodium deoxycholate) detergents to the second decellularization protocol. Indeed, Triton X-100 is known to disrupt DNA-protein interactions, and sodium deoxycholate to efficiently disrupt cell nuclei and membranes [46]. Compared to other protocols for decellularization of mouse, bovine, porcine and even human ovaries [4, 34, 47-50], we achieved a greater reduction in initial dsDNA without using DNase, which has been shown to induce cytotoxicity of reseeded cells [51].

Quantification of collagen and GAGs, major structural components of the ECM, provided assessment of ECM preservation in our oECM hydrogels. Similarly to other studies [4, 48], we did not observe any difference in collagen content between native tissue and either of the two hydrogels. However, only protocol oECM2 allowed preservation of similar levels of GAGs to native tissue. GAGs are heteropolysaccharides, not only involved in ECM structure, but also in water retention and growth factor sequestering. GAGs can thereby promote cell adhesion, growth, differentiation and migration [52]. A recent proteomic study on human ovarian tissue demonstrated that GAGs are widely distributed throughout human ovarian cortex, making them key components of the native ovarian ECM [53]. Several authors have also shown that GAGs are directly or indirectly involved in follicle development, granulosa cell differentiation, and cumulus-oocyte expansion [54, 55]. Hence an enriched GAG hydrogel, such as oECM2 maybetter support human follicle survival in vitro than oECM1.

Physical scaffold properties, such as hydrogel rigidity and nanostructure, are other essential parameter for the creation of a TEO [35, 56]. As expected, both oECM1 and oECM2 exhibited a lower storage modulus than native ovarian tissue (~3.5 KPa) [33, 57], but more interestingly, they differed significantly from each other, with oECM2 being more rigid than oECM1.

Because both hydrogels were derived from the same tissue source, with equal concentration and similar collagen content, the difference in stiffness is likely due to either the higher numbers of sulfated GAG retained in oECM2 and/or different ultrastructure observed by scanning electron microscopy. Structurally, oECM2 exhibited a less fibrous architecture with thicker and more compact walls than oECM1, which may reflect a distinct collagen fiber reorganization during gelation and hence a different degree of rigidity [58]. It could also be the result of the shorter enzymatic decellularization process in the second protocol, which in turn better preserves GAG concentration and generated larger fibers [14].

To assess hydrogel cytocompatibility, isolated mouse preantral follicles were initially used in order to safeguard precious human follicles. No statistical differences were found in follicle recovery rates or viability between oECM1 and oECM2 after one week of in vitro culture, so both hydrogels were equally able to support mouse follicle survival in vitro. However, since the aim of this study was to create a supportive scaffold for human ovarian follicles, it is important to bear in mind that the follicle requirements of a TEO are species-specific and differ substantially between rodents and humans [59, 60]. Therefore, based on the lower dsDNA content, greater GAG retention and superior stiffness, which are all favorable conditions to better support human follicle survival [35, 61], we selected oECM2 as a promising new scaffold material for the TEO, using it to encapsulate and culture human follicles. In contrast to what we observed with mouse follicles, no human follicles were found in the oECM2 after one week of in vitro culture, although fully viable and elongated granulosa cells (as evidenced by live/dead assays) were present throughout this hydrogel. Importantly, this confirmed also that mouse and human follicles require different environments, and that decellularized ovarian ECM hydrogels may not be able to uniformly support species-independent follicle survival and growth.

Considering the impact of matrix rigidity on human follicle survival [35, 61], and because the oECM2 modulus was lower than in native ovary [33, 57], we decided to increase the mechanical properties of the ECM hydrogel by adding alginate. As expected, when alginate was combined with oECM2, the follicle recovery rates increased proportionally, up to a maximum achieved with alginate alone. In 7-day cultures of oECM2, human follicles lost their spherical shape and granulosa cells consequently spread throughout the hydrogel and proliferated. It is therefore likely that oECM2 alone was not rigid enough to maintain the 3D structure of isolated human follicles, but it was not toxic and so was able to support cell attachment and proliferation. While

alginate alone was superior in terms of follicle recovery rate to other hydrogels combinations, it is unfortunately unsuitable alone for possible future clinical application in the TEO due to its low degradability and poor revascularization after transplantation [41, 62]. However, given that no differences were observed between human ovarian follicle viability and growth in alginate and oECM2-alginate combinations, addition of alginate to oECM2 may well improve scaffold rigidity. The hypothesis that scaffold rigidity may influence follicle survival has already been posited [35, 61, 63-65]. Hornick et al. (2012) showed that when isolated non-human primate preantral follicles were cultured in 0.5% (soft) and 2% (stiff) alginate, follicles maintained their spherical structure and survived only in the stiffer alginate (2%). Additionally, Lambricht et al., 2014 [66] characterized the chemical and physical properties of different hydrogels and demonstrated that SLM 100 alginate (1%) exhibited rigidity (~4 KPa) similar to bovine and human ovarian tissue.

Although no other studies to date have reported on ovarian ECM derived hydrogels, Pors et al. (2019) recently obtained encouraging findings with isolated human ovarian follicles cultured in a decellularized human ovarian ECM scaffold. Unlike our study, human ovarian follicles were first wrapped between two sheets of previously cultured ovarian cells and only then placed together inside the decellularized ovarian scaffold [4]. Hence, the presence of ovarian stromal cells, essential for appropriate bidirectional communication with follicles, as well as secreted autologous ovarian cell-derived ECM, may have contributed to follicle survival. Therefore, in order to support longer human follicle survival in vitro, addition of ovarian cells shouldbe considered in future studies.

We are aware that this is a pilot study and it requires further longer in vivo investigations (e.g. xenografting model) to confirm its potential for supporting human folliculogenesis and to assess its degradation, vascularization and host immunogenic response.

Conclusions:

Both hydrogels were able to support mouse follicle survival in vitro. However, taking into account that requirements to support follicle survival in TEO are species-specific, we selected oECM2 as it proved better than oECM1 to culture human ovarian follicles. Nevertheless, pure oECM2 was not able to sustain human follicle survival in vitro, probably due to its relative softness compared to human ovarian tissue. On the other hand, when alginate was

combined with oECM2, up to 65% of fully viable and growing follicles were detected on day 7 of culture. Since alginate alone is not suitable for TEO clinical translation, combined oECM2-alginate hydrogels may offer an innovative strategy. We hope that this derived oECM hydrogel may function as a biomimetic environment, with retention of ovarian ECM proteins essential for proper follicle development, greater degradability and enhanced revascularization after grafting.

Acknowledgments

The authors thank Mira Hryniuk, BA, for reviewing the English language of the manuscript, and Dolores Gonzales and Olivier Van Kerk for their technical assistance.

This study was supported by grants from the EOS (grant 30443682) and Fonds National de la Recherche Scientifique de Belgique (FNRS) (C.A. Amorim is an FRS-FNRS Research Associate, grant 5/4/150/5 awarded to M.M. Dolmans). Anne des Rieux is a Senior Research Associate at the FRS-FNRS. A. Viswanath and N. Tatic were funded by the Erasmus Mundus program, NanoFar doctorate.

Author contributions

MCC, JV, LJW, CAA were responsible for the study design and manuscript preparation. MCC, JV, EO, NT, AV performed the experimental procedures and acquired the data. AdR, LJW, CAA and MMD assisted in revising the manuscript and added critical feedback. All the authors are aware of this submission. LJW and CAA contributed equally to this manuscript and should be considered joint senior authors.

Disclosures

None of the authors have any competing interests to declare in relation to the topic.

References

1. Dolmans, M.M. and C.A. Amorim, FERTILITY PRESERVATION: Construction and use of artificial ovaries. Reproduction, 2019. 158(5): p. F15-f25.
2. Donnez, J. and M.M. Dolmans, Fertility Preservation in Women. N Engl J

Med, 2017. 377(17): p. 1657-1665.

3. Kniazeva, E., et al., Primordial Follicle Transplantation within Designer Biomaterial Grafts Produce Live Births in a Mouse Infertility Model.Sci Rep, 2015. 5: p. 17709.
4. Pors, S.E., et al., Initial steps in reconstruction of the human ovary: survival of pre-antral stage follicles in a decellularized human ovarian scaffold. Hum Reprod, 2019. 34(8): p. 1523-1535.
5. Chiti, M.C., et al., Influence of follicle stage on artificial ovary outcome using fibrin as a matrix. Hum Reprod, 2016. 31(2): p. 427-35.
6. Amorim, C.A. and A. Shikanov, The artificial ovary: current status and future perspectives. Future Oncol, 2016. 12(20): p. 2323-32.
7. Filatov, M.A., Y.V. Khramova, and M.L. Semenova, In Vitro Mouse Ovarian Follicle Growth and Maturation in Alginate Hydrogel: Current State of the Art. Acta Naturae, 2015. 7(2): p. 48-56.
8. Vanacker, J. and C.A. Amorim, Alginate: A Versatile Biomaterial to Encapsulate Isolated Ovarian Follicles. Ann Biomed Eng, 2017. 45(7): p. 1633-1649.
9. Shikanov, A., et al., Interpenetrating fibrin-alginate matrices for in vitro ovarian follicle development. Biomaterials, 2009. 30(29): p. 5476-85.
10. Zhou, H., et al., Hydrogel Based 3-Dimensional (3D) System for Toxicity and High-Throughput (HTP) Analysis for Cultured Murine Ovarian Follicles. PLoS One, 2015. 10(10): p. e0140205.
11. Zhou, H. and A. Shikanov, Three-Dimensional Hydrogel-Based Culture to Study the Effects of Toxicants on Ovarian Follicles. Methods Mol Biol, 2018. 1758: p. 55-72.
12. Jamalzaei, P., et al., Applicability of Hyaluronic Acid-Alginate Hydrogel and Ovarian Cells for In Vitro Development of Mouse Preantral Follicles. Cell J, 2020. 22(Suppl 1): p. 49-60.
13. Sun, J. and H. Tan, Alginate-Based Biomaterials for Regenerative Medicine Applications. Materials (Basel), 2013. 6(4): p. 1285-1309.
14. Saldin, L.T., et al., Extracellular matrix hydrogels from decellularized tissues: Structure and function. Acta Biomater, 2017. 49: p. 1-15.
15. Bracaglia, L.G. and J.P. Fisher, Extracellular Matrix-Based Biohybrid

Materials for Engineering Compliant, Matrix-Dense Tissues. Adv Health Mater, 2015. 4(16): p. 2475-87.

16. Singelyn, J.M., et al., Naturally derived myocardial matrix as an injectable scaffold for cardiac tissue engineering. Biomaterials, 2009. 30(29): p. 5409-16.

17. Seif-Naraghi, S.B., et al., Design and characterization of an injectable pericardial matrix gel: a potentially autologous scaffold for cardiac tissue engineering. Tissue Eng Part A, 2010. 16(6): p. 2017-27.

18. Zhang, L., et al., Effect of an inductive hydrogel composed of urinary bladder matrix upon functional recovery following traumatic brain injury. Tissue Eng Part A, 2013. 19(17-18): p. 1909-18.

19. Ghuman, H., et al., ECM hydrogel for the treatment of stroke: Characterization of the host cell infiltrate. Biomaterials, 2016. 91: p. 166-181.Sawkins, M.J., et al., Hydrogels derived from demineralized and decellularized bone extracellular matrix. Acta Biomater, 2013. 9(8): p. 7865-73.

20. Viswanath, A., et al., Extracellular matrix-derived hydrogels for dental stem cell delivery. J Biomed Mater Res A, 2017. 105(1): p. 319-328.

21. Alom, N., et al., Bone extracellular matrix hydrogel enhances osteogenic differentiation of C2C12 myoblasts and mouse primary calvarial cells. J Biomed Mater Res B Appl Biomater, 2018. 106(2): p. 900-908.

22. Kim, E.J., et al., Injectable and Thermosensitive Soluble Extracellular Matrix and Methylcellulose Hydrogels for Stem Cell Delivery in Skin Wounds.Biomacromolecules, 2016. 17(1): p. 4-11.

23. Keane, T.J., et al., Restoring Mucosal Barrier Function and Modifying Macrophage Phenotype with an Extracellular Matrix Hydrogel: Potential Therapy for Ulcerative Colitis. J Crohns Colitis, 2017. 11(3): p. 360-368.

24. Lee, J.S., et al., Liver extracellular matrix providing dual functions of two-dimensional substrate coating and three-dimensional injectable hydrogel platform for liver tissue engineering. Biomacromolecules, 2014. 15(1): p. 206-18.

25. Nagao, R.J., et al., Decellularized Human Kidney Cortex Hydrogels Enhance Kidney Microvascular Endothelial Cell Maturation and Quiescence.Tissue Eng Part A, 2016. 22(19-20): p. 1140-1150.

26. Wu, J., et al., An injectable extracellular matrix derived hydrogel for meniscus repair and regeneration. Acta Biomater, 2015. 16: p. 49-59.

27. Parmaksiz, M., et al., Clinical applications of decellularized extracellular matrices for tissue engineering and regenerative medicine. Biomed Mater, 2016. 11(2): p. 022003.

28. Johnson, T.D., et al., Human versus porcine tissue sourcing for an injectable myocardial matrix hydrogel. Biomater Sci, 2014. 2014: p. 60283d.

29. Traverse, J.H., et al., First-in-Man Study of a Cardiac Extracellular Matrix Hydrogel in Early and Late Myocardial Infarction Patients. JACC Basic Transl Sci, 2019. 4(6): p. 659-669.

30. Irving-Rodgers, H.F., et al., Phenotypes of the ovarian follicular basal lamina predict developmental competence of oocytes. Hum Reprod, 2009. 24(4): p. 936-44.

31. Baerwald, A.R., R.A. Walker, and R.A. Pierson, Growth rates of ovarian follicles during natural menstrual cycles, oral contraception cycles, and ovarian stimulation cycles. Fertil Steril, 2009. 91(2): p. 440-9.

32. Wood, C.D., et al., Multi-modal magnetic resonance elastography for noninvasive assessment of ovarian tissue rigidity in vivo. Acta Biomater, 2015. 13: p. 295-300.

33. Laronda, M.M., et al., Initiation of puberty in mice followingdecellularized ovary transplant. Biomaterials, 2015. 50: p. 20-9.

34. Chiti, M.C., et al., A novel fibrin-based artificial ovary prototype resembling human ovarian tissue in terms of architecture and rigidity. J Assist Reprod Genet, 2018. 35(1): p. 41-48.

35. Tahir, M.S., et al., Proteomics Recapitulates Ovarian Proteins Relevant to Puberty and Fertility in Brahman Heifers (Bos indicus L.). Genes (Basel), 2019. 10(11).

36. Crapo, P.M., T.W. Gilbert, and S.F. Badylak, An overview of tissue and whole organ decellularization processes. Biomaterials, 2011. 32(12): p. 3233-43.

37. Gilbert, T.W., J.M. Freund, and S.F. Badylak, Quantification of DNA in biologic scaffold materials. J Surg Res, 2009. 152(1): p. 135-9.

38. Woessner, J.F., Jr., The determination of hydroxyproline in tissue and

protein samples containing small proportions of this imino acid. Arch Biochem Biophys, 1961. 93: p. 440-7.

39. Farndale, R.W., C.A. Sayers, and A.J. Barrett, A direct spectrophotometric microassay for sulfated glycosaminoglycans in cartilagecultures. Connect Tissue Res, 1982. 9(4): p. 247-8.
40. Vanacker, J., et al., First transplantation of isolated murine follicles in alginate. Regen Med, 2014. 9(5): p. 609-19.
41. Amorim, C.A., et al., Survival of human pre-antral follicles after cryopreservation of ovarian tissue, follicular isolation and in vitro culture in acalcium alginate matrix. Hum Reprod, 2009. 24(1): p. 92-9.
42. Martinez-Madrid, B., et al., Ficoll density gradient method for recovery of isolated human ovarian primordial follicles. Fertil Steril, 2004. 82(6): p. 1648-53.
43. Manavella, D.D., et al., Two-step transplantation with adipose tissue-derived stem cells increase follicle survival by enhancing vascularization in xenografted frozen-thawed human ovarian tissue. Human reproduction, 2018.
44. Chiti, M.C., et al., A modified and tailored human follicle isolation procedure improves follicle recovery and survival. J Ovarian Res, 2017. 10(1): p. 71.
45. White, L.J., et al., The impact of detergents on the tissue decellularization process: A ToF-SIMS study. Acta Biomater, 2017. 50: p. 207-219.
46. Jakus, A.E., et al., “Tissue Papers” from Organ-Specific Decellularized Extracellular Matrices. Adv. Funct. Mater. , 2017.
47. Liu, W.Y., et al., Xenogeneic Decellularized Scaffold: A Novel Platform for Ovary Regeneration. Tissue Eng Part C Methods, 2017. 23(2): p. 61-71.
48. Hassanpour, A., et al., Decellularized human ovarian scaffold based on a sodium lauryl ester sulfate (SLES)-treated protocol, as a natural three-dimensional scaffold for construction of bioengineered ovaries. Stem Cell Res Ther, 2018. 9(1): p. 252.
49. Alshaikh, A.B., et al., Decellularization of the mouse ovary: comparison of different scaffold generation protocols for future ovarian bioengineering. J Ovarian Res, 2019. 12(1): p. 58.

50. Gilpin, A. and Y. Yang, Decellularization Strategies for Regenerative Medicine: From Processing Techniques to Applications. Biomed Res Int, 2017. 2017: p. 9831534.

51. Oliveira, G.B.d., et al., Composition and significance of glycosaminoglycans in the uterus and placenta of mammals. Brazilian Archives of Biology and Technology, 2015. 58: p. 512-520.

52. Ouni, E., et al., A draft map of human ovarin proteome for tissue engineering and clinical applications. Submitted., 2017.

53. Berkholtz, C.B., et al., Distribution of extracellular matrix proteins type I collagen, type IV collagen, fibronectin, and laminin in mouse folliculogenesis. Histochem Cell Biol, 2006. 126(5): p. 583-92.

54. Irving-Rodgers, H.F., et al., Dynamics of extracellular matrix in ovarian follicles and corpora lutea of mice. Cell Tissue Res, 2010. 339(3): p. 613-24.

55. Shea, L.D., T.K. Woodruff, and A. Shikanov, Bioengineering the ovarian follicle microenvironment. Annu Rev Biomed Eng, 2014. 16: p. 29- 52.

56. Mortiaux, L., Physical aspect of the artificial ovary: characterization of human ovarin tissue and fibrin scaffolds, in Ecole politechnique de Louvain. 2016, Université Catholique de Louvain.

57. Frantz, C., K.M. Stewart, and V.M. Weaver, The extracellular matrix at a glance. J Cell Sci, 2010. 123(Pt 24): p. 4195-200.

58. Telfer, E.E. and M.B. Zelinski, Ovarian follicle culture: advances and challenges for human and nonhuman primates. Fertil Steril, 2013. 99(6): p. 1523-33.

59. Chiti, M.C., C.A. Amorim, and D. MM, Fibrin-based artificial ovary prototype: from animal models to human clinical application. Current Trends in Clinical Embryology, 2018. 5(3): p. 122-129.

60. Paulini, F., et al., Survival and growth of human preantral follicles after cryopreservation of ovarian tissue, follicle isolation and short-term xenografting. Reprod Biomed Online, 2016. 33(3): p. 425-32.

61. Rios, P.D., et al., Retrievable hydrogels for ovarian follicle transplantation and oocyte collection. Biotechnol Bioeng, 2018. 115(8): p. 2075-2086.

62. Hornick, J.E., et al., Isolated primate primordial follicles require a rigid

physical environment to survive and grow in vitro. Hum Reprod, 2012. 27(6):p. 1801-10.

63. Luyckx, V., et al., A new step toward the artificial ovary: survival and proliferation of isolated murine follicles after autologous transplantation in a fibrin scaffold. Fertil Steril, 2014. 101(4): p. 1149-56.

64. Chiti, M.C., et al., Further insights into the impact of mouse follicle stage on graft outcome in an artificial ovary environment. Mol Hum Reprod, 2017. 23(6): p. 381-392.

65. Lambricht, L., et al., The type and composition of alginate and hyaluronic-based hydrogels influence the viability of stem cells of the apical papilla. Dent Mater, 2014. 30(12): p. e349-61.

Tables

Table 1. Storage and loss modulus (mean ± SD) in oECM1 and oECM2 hydrogels

	oECM1 (n=3)	oECM2 (n=3)
Storage modulus (G')	65 ±18 Pa[a]	107 ± 27 Pa[b]
Loss modulus (G'')	9.5 ± 2 Pa[a]	7 ± 1.7Pa[b]

Different superscript letters indicate statistical differences (a, b $p<0.05$)

oECM1: ovarian-derived extracellular matrix hydrogel 1

oECM2: ovarian-derived extracellular matrix hydrogel 2

Table 2. Mouse ovarian follicle diameter (mean ± SD) in oECM1 and oECM2 on day 0 and day 7 of in vitro culture

	Mouse follicle diameter (mean ± SD)	
	oECM1	oECM2
Day 0	45 ± 22 μm[a] (n=235)	51 ± 27.5 μm[a] (n=54)
Day 7	43 ± 21 μm[a] (n=174)	65 ± 34 μm[a] (n=12)

Different superscript letters indicate statistical differences (a,b $p<0.05$).

oECM1: ovarian-derived extracellular matrix hydrogel 1

oECM2: ovarian-derived extracellular matrix hydrogel 2

Table 3. Human ovarian follicle viability (mean ± SD) in oECM2-based hydrogels on day 7 of in vitro culture

Human ovarian follicle viability (V1+V2)			
Group 1	Group 2	Group 3	Group 4
*ND	87.5%[a]	97.2%[a]	87.5%[a]

Different superscript letters indicate statistical differences (a,b $p<0.05$).

*ND: no follicles were found in oECM2 onday 7.Group 1: 100% oECM2 hydrogel

Group 2: 90% oECM2 hydrogel +10% alginate

Group 3: 75% oECM2 hydrogel +25% alginate

Group 4: 100% alginate

Table 4. Human ovarian follicle diameter (mean±SD) in boECM2-based hydrogels on day 0 and day 7 in vitro culture

Human follicle diameter (mean ± SD)				
	Group 1	Group 2	Group 3	Group 4
Day0	33 ± 20 μm[a] (n= 2)	38 ± 12 μm[a](n=15)	43 ± 12 μm[a](n=22)	38 ± 12 μm[a](n=20)
Day7	*ND (n=0)	59 ± 24 μm[b](n=8)	58 ± 24 μm[b](n=12)	58 ± 19 μm[b](n=17)

Different superscript letters indicate statistical differences (a,b $p<0.05$).

*ND: no follicles were found in oECM2 on day 7.

Group 1: 100% oECM2 hydrogel
Group 2: 90% oECM2 hydrogel +10% alginate
Group 3: 75% oECM2 hydrogel +25% alginate
Group 4: 100% alginate

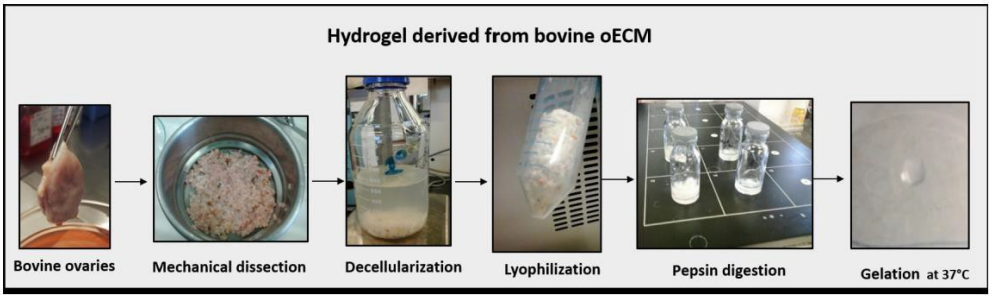


Figure 1. Development of a decellularized ovarian extracellular matrix hydrogel. Bovine ovaries were mechanically dissociated with scalpel and forceps to obtain a homogeneous mixture of small ovarian fragmentswhich were then treated with enzyme and/or detergents, lyophilized and pepsin digested to obtain a hydrogel for follicle encapsulation and in vitro culture.

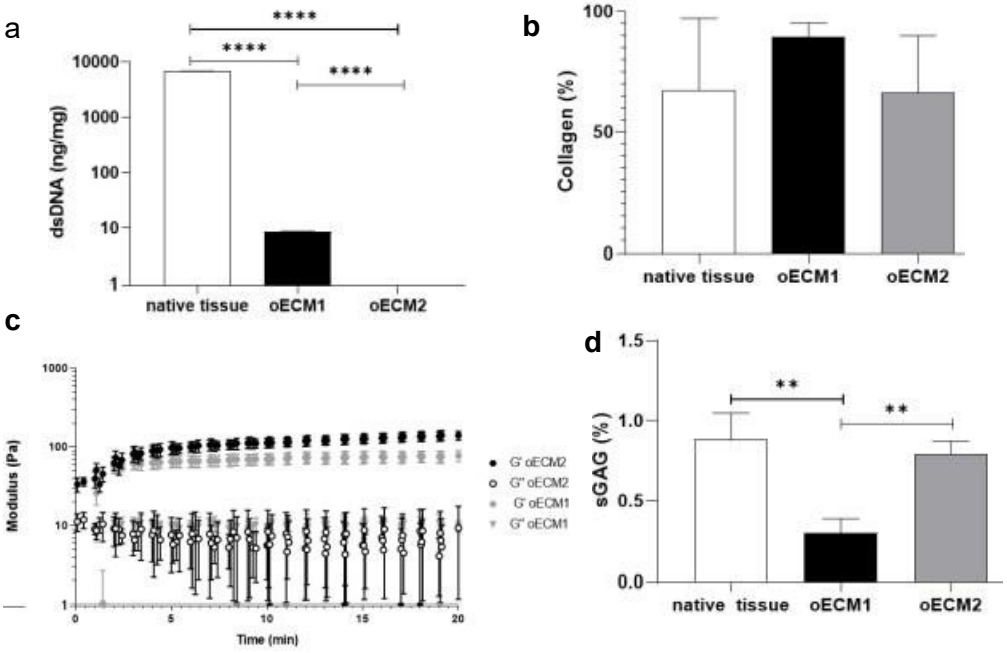


Figure 2. Influence of the ovarian decellularization protocol on dsDNA, collagen and GAG content. Efficiency of decellularization was assessed by quantifying level of dry weight dsDNA/mg (a). Preservation of the ECM after decellularization was assessed by quantifying collagen (b) sulfated GAG (c) and rheological properties (d) through investigation of storage (G') and loss moduli (G'') Data are presented as mean ± SD. Significant differences are represented by asterisks. (** p<0.01; **** p-<0.0001). Each group was analysed in triplicate.

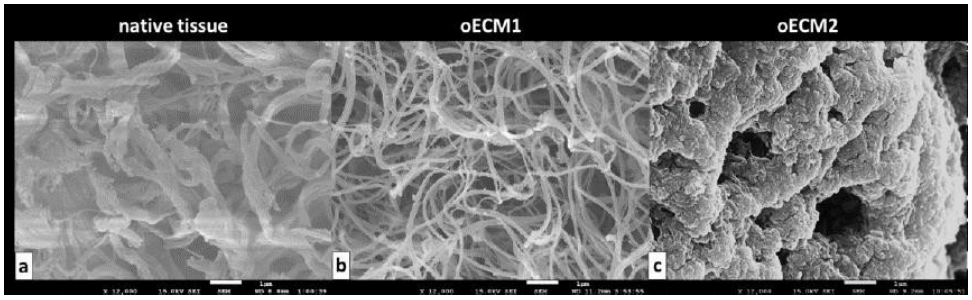


Figure 3. Influence of decellularization on oECM hydrogel microstructure. Native bovine ovarian tissue (a), oECM1 (b) and oECM 2 (c) hydrogels were processed for scanning electron microscopy. Magnification: 12,000X; scale bar: 1 μm.

SUPPLEMENTARY MATERIAL

Materials and methods

oECM characterization

DNA, collagen, and sulfated glycosaminoglycan quantification

Determination of decellularization efficiency was based upon quantification of double stranded DNA (dsDNA) (Gilbert et al., 2009, Viswanath et al., 2017), which was extracted by addition of an equal volume (25:24:1) of phenol/chloroform/isoamyl to 1 ml of sample (10 mg/ml). Phenol was removed using an equal volume (24:1) of chloroform/isoamyl alcohol, and dsDNA was precipitated by addition of two volumes of ice-cold ethanol and 0.1 volume of 3 M sodium acetate (pH 5.2), before being frozen at −80°C for 30 minutes. The samples were then centrifuged at 13,000 rpm for 10 minutes and washed in ethanol, dried at RT and resuspended in 0.1 ml TE buffer. Concentrations of dsDNA were measured using a Quant- iT™ Picogreen® assay kit (Invitrogen, Merelbeeke, Belgium) following the supplier's instructions. A standard curve was prepared with known DNA concentrations from 0 to 100 ng/ml and samples were read using a Tecan Infinite M200 plate reader (Tecan UK, Reading, UK).

Since collagen and sulfated GAGs are structural ECM components, their content was investigated to determine the rate of ECM preservation.

Collagen content was measured by quantification of hydroxyproline (Viswanath et al., 2017, Woessner, 1961). Briefly, bovine ovarian tissue, oECMs and a blank pepsin solution were hydrolyzed with 1 volume of concentrated HCl (12 N) overnight at 120°C. The samples were dried by incubation at 90°C for 2 hours followed by addition of 4 volumes of 0.25 M sodium phosphate buffer (pH 6.5). The hydrolyzed blank pepsin solution served as a negative control as well as diluent for the assay. The samples were oxidized by incubation with 1 volume of 3-chloramine T solution (0.07 M) at RT for 20 minutes, followed by the addition of 4-p-dimethylaminobenzaldehyde (p-DAB) solution (1.16 M p-DAB in 60% perchloric acid [6.5 ml] and isopropanol [15 ml]) and incubation at 60°C for 30 minutes. A standard curve was prepared using known concentrations of hydroxyproline, ranging from 0 to 100 µg/ml, and absorbance was measured at 540 nm with a Tecan Infinite M200 plate reader. Collagen content was determined using the relationship that hydroxyproline forms 14.3% of total amount of collagen.

Sulfated GAGs were determined using the 1,9 dimethyl-methylene blue (DMMB) assay (Farndale et al., 1982, Viswanath et al., 2017). The applied protocol is a spectrophotometric assay where the digested solution is mixed with the dye 1,9-dimethylmethylene blue to detect the amount of sulfated glycosaminoglycans. The assay is based on the metachromatic shift in absorption maximum which occurs when the dye is complexed with sulfated glycosaminoglycans. It is a protocol with a sensitivity of 4 micrograms/ml of chondroitin sulfate.

Specifically 1 ml of pre-gel solutions were incubated with 0.1 mg/ml of Proteinase K with 1 volume of concentrated HCl (12N) overnight at 37°C while a blank pepsin solution served as negative control as well as diluent for the assay. Fifty µl of samples were mixed with 200 µl of DMMB solution (0.03 M sodium formate, 0.046 M DMMB, ethanol [0.5% v/v] and formic acid [0.2% v/v] in a 96-well plate. The standard curve ranged from 0 to 75 µg/ml chondroitin-4-sulphate. Absorbance was measured immediately at 525 nm.

Ovarian follicle encapsulation

Mouse ovarian follicle encapsulation

To assess the possible cytotoxic effect of the two different hydrogels, isolated mouse preantral follicles were encapsulated in oECM1 and oECM2 and then cultured for 7 days. The follicles (n=339) were divided into 2 groups (oECM1 and oECM2), and their diameter was recorded before being encapsulated separately in each group.

Firstly isolated mouse ovarian follicles (n=339) were divided into 2 groups (oECM1 and oECM2) and their diameter was recorded before being encapsulated separately in each group. Between 10 and 15 follicles were embedded in 50 µl oECM1 (8 mg/ml) or oECM2 (8 mg/ml), placed in a 4-well plate and incubated at 37°C for 1 hour to allow hydrogel gelation to occur (oECM1 n=20 beads, oECM2 n=3 beads). Thereafter, 500 µl pre-equilibrated in vitro culture medium (MEM, GlutaMAX) supplemented with 10% fetal bovine serum, 2 mM pyruvic acid, 50 µg/ml ascorbic acid, 0.1 IU/ml follicle stimulating hormone (FSH) (Gonal F), 1% Anti-anti was added.

The hydrogels were cultured at 37°C and 5% CO2 for one week. Every 2 days, half of the culture medium was removed and replaced with fresh medium.

Human ovarian follicle encapsulation

Considering the softness of both oECM1 and oECM2 hydrogels, we

hypothesized that it would not be suitable to support human follicular structure by itself. To test our theory, in the second in vitro culture experiment with human follicles, the previously selected oECM2 was combined with different alginate proportions in order to assess the influence of difference stiffness on follicle survival and growth.

In order to assess the gelation of ovarian ECM-based hydrogels, a series of preliminary tests were conducted (data not shown), which led us to select two combinations of oECM with alginate: 90% oECM2+10% alginate and 75% oECM2+25% alginate. Alginate and pre-gel solutions of oECM were mixed in a mini eppendorf tube and distributed into 4-well plate. Then, isolated follicles were injected, and the plate was incubated at 37% for 1 hour to allow oECM gelation. Following for alginate cross-linking, a solution of 100mM CaCl2 was added in each well. Thereafter, 500 µl pre-equilibrated in vitro culture medium (MEM, GlutaMAX) supplemented with 10% fetal bovine serum, 2 mM pyruvic acid, 50 µg/ml ascorbic acid, 0.1 IU/ml follicle stimulating hormone (FSH) (Gonal F), 1% Anti-anti was added. The hydrogels were cultured at 37°C and 5% CO2 for one week. Every 2 days, half of the culture medium was removed and replaced with fresh medium.

Isolated follicles (n=114) were divided into 4 groups and their diameter was recorded before being encapsulated in: (1) 100% oECM2 (8 mg/ml); (2) 90% oECM2 + 10% of 1% alginate (SLM100, Pronova, Nova Matrix); (3) 75% oECM2 + 25% of 1% alginate; or (4) 100% of 1% alginate.

Statistical analysis

Statistical analyses were performed with Prism 8.1.2. Normality tests were done prior to conducting any further evaluation. One Way ANOVA was applied for comparison between native tissue, oECM1 and oECM2 hydrogels for dsDNA, collagen and GAGs. Bonferroni or Tukey's post-hoc tests were adopted for multiple comparison when appropriate. The unpaired t-test with Welch's correction was used to compare maximum storage moduli, mouse follicle diameters, recovery rates and viability between oECM1 and oECM2 hydrogels. One-way ANOVA was utilized to compare human follicle diameter between groups at each time point. Fisher's exact test was conducted for human follicle viability. Furthermore, the Mann-Whitney test was performed to study follicle growth over time. A p-value of less than 0.05 was considered statistically significant. This research has benefited greatly from statistical consultation with the Statistical Methodology and Computing Service technological platform at the UCL – SMCS/ IMMAQ, UCL.

CHAPTER 30

TRANSPLANTATION OF ISOLATED FOLLICLES AND THE ENGINEERED OVARY

Christiani A. Amorim, Parinaz Asiabi, Emna Ouni, Janice Vilela, Alessandra Camboni, Maria C. Chiti

Université Catholique de Louvain, Institut de Recherche Expérimentale et Clinique, Pôle de Recherche en Gynécologie, Avenue Mounier 52, bte. B1.52.02, 1200 Brussels, Belgium

Abstract

For over a decade, increasing numbers of research groups all over the world have focused their efforts on development of a transplantable engineered ovary. With the growing incidence of curable cancer among young girls and women and greater awareness of the need to safeguard fertility, the number of patients who can benefit from this strategy has also been rising, as having the possibilities of other applications. However, this scenario is still quite far from a clinical setting. Indeed, development of an engineered ovary has proved to be very challenging and our lack of knowledge of human ovaries makes this task even more difficult. While studies in mice have proved the feasibility of the concept, demonstrating the ability of engineered ovary prototypes to restore both endocrine and reproductive functions, new discoveries about human ovaries and their follicle populations show discrepancies between mammalian species. These relate to ovarian extracellular matrix composition and stiffness, and follicle development. Therefore, in this chapter, we will highlight progress that has already been made in constructing a transplantable engineered ovary and discuss possible future directions.

Key-words: Preantral follicles, ovary, leukemia, fertility preservation, transplantable engineered ovary, cancer

Introduction

Cancer is one of the major health issues worldwide, and the first or second leading cause of death depending on the world area investigated. Indeed, the International Agency for Research on Cancer estimated that in 2018, more than 276,000 people under 44 years were diagnosed with cancer in Europe (1). Incidence rates are significantly higher in females (65%) than males (35%) in these younger age groups (Fig. 1). However, thanks to vast improvements in cancer treatments, 5-year survival rates are now 65% in adults, and as high as 83% in children (2). Taking into account the known gonadotoxicity of some cancer treatments and increasing numbers of cancer survivors, fertility preservation is becoming a clinical and moral duty in oncological practice.

While most cancer patients can choose among different fertility preservation strategies, prepubertal patients and women who cannot delay the start of their chemo- or radiotherapy have had to rely on ovarian tissue cryopreservation followed by orthotopic reimplantation once cured (3). Despite successful outcomes reported with this approach, including more than 130 live births to date (3), it cannot be universally applied. Indeed, in certain types of cancer, malignant cells may be present in the ovaries, so transplantation of frozen-thawed ovarian tissue fragments is not advised(4). Although most malignant tumors in reproductive-age subjects do not metastasize to the ovaries, hematological malignancies like leukemia and Burkitt's lymphoma, as well as neuroblastoma, carry a high risk of ovarian metastasis (5). Leukemia is the most common cancer in Europe among young girls up to 19 years of age, and the seventh most prevalent in women of reproductive age (20-44 years old), representing 5% of all cancer cases in women. Thanks to early diagnosis and improved treatments, almost 50% of patients survive (1). Burkitt's lymphoma accounts for around half of all malignant non-Hodgkin's lymphomas in children (6), with an estimated annual incidence of 3,000 girls aged between 0 and 14 years (1).Fortunately, around 85% of patients survive after treatment (6). Neuroblastoma represents around 10% of solid tumors in children under 15years of age, affecting one in every 70,000 (7). In patients aged over one year, 5-year survival rates can reach 95% for some localized tumors (7).

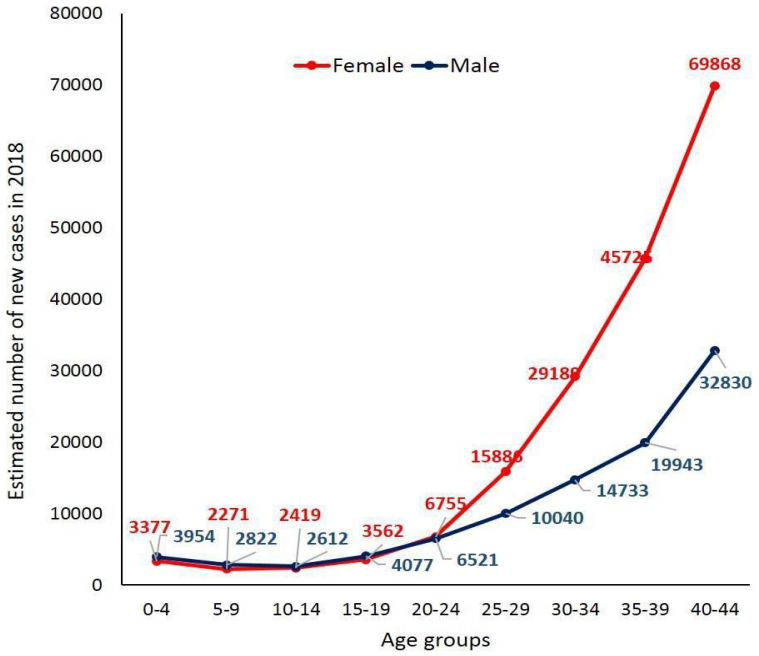


Figure 1. Estimated number of new cancer cases and age-specific incidence rates (1).

Since studies have shown that cancer cells are able to resist the freeze-thawing procedure and spread in the host after xenotransplantation (8), autografting of cryopreserved tissue can potentially lead to recurrence of the disease in affected patients. Sadly, there are no currently available options for fertility restoration in these women. However, there are two main approaches under development: in vitro growth of preantral follicles followed by in vitro maturation of their oocytes (see Chapter 29), or transplantation of isolated preantral follicles, also known as the engineered ovary. In the last decade, the idea of engineering an ovary has been gaining ground and increasing numbers of research teams worldwide have been concentrating their efforts on developing this strategy. The aim of this chapter is therefore to discuss the latest advances in the field and future directions of this emerging fertility restoration approach.

Transplantable engineered ovary concept

By definition, the transplantable engineered ovary has the essential role of replacing the natural organ, thereby allowing complete folliculogenesis, with production of fertilizable mature oocytes and secretion of sex hormones. In order to construct a tissue-engineered ovary, we need to consider three essential points: (i) safe isolation of a large number of preantral follicles; (ii) presence of different populations of ovarian cells; and (iii) creation of a three-dimensional (3D), biodegradable matrix to encapsulate isolated follicles and cells, and protect them during and after grafting.

In practice, after patient remission, fragments of her frozen ovarian tissue would be thawed for further follicle isolation. In the meantime, a second ovarian biopsy would be taken from the patient after her cancer treatment for cell isolation. In this way, we could ensure that only ovarian cells would be added to the transplantable engineered ovary, as all malignant cells would have been destroyed by chemo- or radiotherapy. Isolated preantral follicles and ovarian cells would then be encapsulated inside the matrix and transplanted back to the patient.

Are isolated follicles able to survive and resume folliculogenesis after transplantation?

The follicle is the functional unit of the ovary and has two main functions: it is responsible for hormone production and providing the ideal environment for oocyte growth and development. Follicles are present in the ovary at different stages: primordial, primary, secondary andantral. Preantral follicles (primordial, primary and secondary) represent 90-95% of all follicles but, of this number, only 0.1% will go on to develop to the antral stage, while the rest will undergo atresia. Why so few follicles are destined to ovulate remains a mystery. However, it is known that not only follicle themselves, but also surrounding ovarian cells and extracellular matrix (ECM) play a role in the process.

Isolation of preantral follicles potentially allows us to safely use these structures in the transplantable engineered ovary, as they are enclosed inside a basement membrane that prevents their granulosa cells and oocyte coming into contact with capillaries, white blood cells and nerve processes (9). However, they cannot survive alone, as demonstrated in some in vitro culture studies. Indeed, while isolated mouse follicles enclosed in a collagen

gel matrix were able to survive in vitro for at least two weeks, when they grew to multilayer stages, they showed signs of degeneration and no antrum or theca cell formation (10, 11). On the other hand, when isolated mouse follicles were transplanted together with ovarian cells, they successfully reached the antral stage in three days, with blood vessels appearing after five days and theca cells six days post-grafting (11). After 10 days, 16 oocytes were recovered for in vitro fertilization and 12 developed up to the 2-cell embryo stage (11).

After incorporating mouse ovarian tissue digests (isolated follicles and ovarian cells) in plasma clots, Gosden (12) transplanted them to the ovarian bursa of sterile mice. These constructs were able to restore fertility in their hosts, as pregnancies and offspring were obtained after mating. Following graft removal, this author found ovary-like structures, with follicles at different stages of development. Carroll and Gosden (13) subsequently repeated the experiment using frozen-thawed ovaries and obtained similar results.

After isolation of follicles from human tissue, encapsulation of preantral follicles in plasma clots and xenotransplantation to immunodeficient mice, Dolmans et al. (14, 15) also reported follicle survival and growth. Moreover, stroma-like tissue of human origin was formed, suggesting the presence of isolated human stromal cells in the constructs. Indeed, when retrieving isolated follicles, we may inadvertently pick up isolated cells too (16). The constructs were found to be well vascularized already one week after xenografting (14) and, like in mice (12, 13), ovary-like tissue was observed (14, 15).

Based on these pioneering studies, we can confirm that preantral follicles are able to survive and resume growth after isolation and transplantation, but they need to be transplanted along with their accompanying ovarian cells and encapsulated in a 3D matrix.

How can we improve survival and growth of isolated follicles after transplantation?

The pioneering studies mentioned above revealed the basic requirements for survival of isolated follicles after transplantation. In recent years, numerous experiments have investigated matrix materials and cell populations for development of the transplantable engineered ovary.

Matrix materials: from polymers to decellularized ovarian tissue

One of the key steps in the development of the transplantable engineered ovary is finding the right matrix material to encapsulate isolated ovarian preantral follicles. Different hydrogels have been used for transplantation of isolated follicles in an attempt to enhance efficacy (11, 12, 17-22). Despite great advances, we still not identified the best matrix material to support complete human folliculogenesis. Indeed, our knowledge of human ovarian tissue remains incomplete, and great differences emerged when murine and human follicles were transplanted inside an engineered ovary prototype (23). Therefore, in this section, we will first briefly mention the general features of a 3D matrix for isolated preantral follicles, and then discuss the main findings obtained from murine and human ovarian follicles in various in vivo studies. Irrespective of the nature of the matrix (biological, synthetic or hybrid), there are other crucial points to consider before selecting one material over another. First of all, we must look at biocompatibility and biodegradability, features that are normally closely interconnected. Greater biocompatibility and biodegradability have been demonstrated with natural polymers (collagen, gelatin, alginate, fibrin, decellularized ECM) than synthetic ones (poly(ethylene glycol) [PEG]) because cell metalloproteinases cleave them without producing toxic compounds that may affect cell survival (24, 25). Indeed, broader application of biological matrices rather than synthetic scaffolds is documented in the literature (26). In addition, natural hydrogels like collagen or fibrin provide better cell adhesion than their synthetic counterparts thanks to the presence of peptides containing arginine- glycine-aspartate (RGD) sequences involved in integrin binding on cell surfaces. The architecture of the hydrogel's structure, as well as its viscoelastic properties and biochemical constitution, are also key elements.

The composition and porosity of the network will determine not only the rate at which nutrients, gas and metabolic waste move through the hydrogel, but also how follicle survival and development are affected. A recent study (27) showed how the controlled microporous geometry of the applied scaffold impacted mouse follicle survival, growth and maturation in vitro. The ovarian environment is indeed highly dynamic. Unlike any other cellular complex in the body, human ovarian follicles, once activated, increase in size up to 600X during growth and release various proteases essential to modifying their surrounding ovarian ECM and generating a more acquiescent milieu for their complete development. A hydrogel's viscoelastic properties are therefore key parameters to consider in the choice of matrix material. In this context, the

ideal matrix should be rigid enough to mimic the stiffness of the collagen-rich ovarian cortex in the first few days post-transplantation, but then provide enough elasticity to allow complete follicle growth and protease degradation. A more challenging goal is mimicking the native biochemical ovarian environment. A recent study (23) was able to distinguish 1,508 different proteins in the human ovary,with more than 80 of them derived from the ovarian ECM. Although our knowledge of the biochemical composition of ovarian tissue is still in its infancy, complete characterization of the ovarian follicle microenvironmentis vital to design a bioengineered ovary ressembling native tissue.

Animal studies

After groundbreaking studies on transplantation of isolated mouse follicles by Gosden's group (11-13), several decades passed before new attempts were made to graft these structures. Laronda et al. (27) developed a gelatin-based matrix using a 3D bioprinter, selecting specific architecture to maximize follicle-matrix interaction. When mouse ovarian follicles were grafted inside this matrix, restoration of fertility was achieved, demonstrating the importance of the architecture of the supporting scaffold for complete follicle development in mice.

Alginate-based matrices showed encouraging results with murine and non-human primate follicles after in vitro culture (28), but efficiency was diminished in in vivo studies. Vanacker et al. (18, 29) were the first to encapsulate and transplant isolated mouse preantral follicles in alginate. Although these follicles were able to grow to the antral stage, poor matrix degradation and revascularization were noted one week after autotransplantation. Both softer and more rigid alginate remain a good choice for culture of isolated murine (30) and human (31-33) follicles respectively, but new hydrogels are needed for follicle transplantation. Int his context, fibrin matrices have found broader application. Unlike the previously mentioned natural matrix materials, this protein has shown numerous advantages. First of all, it was already being applied in diverse surgical settings. Moreover, thanks to the combination of its two mainconstituents, namely thrombin and fibrinogen, fibrin formulations and architecture could be adjusted according to the desired application (34). Indeed, softer fibrin formulations (made from lower fibrinogen and thrombin concentrations) were

found to be optimal for mouse ovarian follicle transplantation (17, 35, 36), also leading to restoration of endocrine and reproductive functions when vascular endothelial growth factor (VEGF) was crosslinked to the matrix and gradually released after transplantation (19).

To date, only one synthetic hydrogel has been tested as a material for the engineered ovary. A combined PEG-vinyl sulfone (PEG-VS) matrix, with integrin-binding peptides like RGD crosslinking PEG-VS with protease-sensitive peptides, was used to encapsulate partially isolated mouse preantral follicles before transplantation to mice (37). After 30 days, multiple antral follicles, corpora lutea and reduced follicle-stimulating hormone levels were observed, demonstrating that PEG-VS was able to support folliculogenesis and steroidogenesis. Furthermore, on day 60, around 60% of primordial and primary follicles were still detected in the graft, proving selective follicle recruitment over time (37).

An emerging new generation of matrices is now being derived from decellularized ovarian ECM. Ideally, allogeneic (22, 38) or even xenogeneic cell-free matrices retain the natural architecture of native tissue and, to a variable extent, most of the physiological components inside the native ECM. A few studies have reported decellularization of murine (39), porcine (40), bovine (38) and human (22, 38, 41) ovarian tissue. It is important to stress that decellularization protocols have been shown to affect matrix composition differently, changing concentrations of collagen, glycosaminoglycans (GAGs) and elastic fibers (39). When rodent ovarian cells were seeded in such a matrix, they were able to survive, proliferate, synthesize estradiol (38, 40) and even induce puberty in mice after grafting (38). This matrix was also successfully tested in the context of isolated mouse follicle transplantation (22).

Human studies

While fertility restoration using an engineered ovary prototype has already been proved in mice (12, 13, 19, 27), studies in humans have been rather more challenging (14, 20-22, 31). One of the main reasons is the physiological difference in folliculogenesis and the ovaries between rodents and humans. Extrapolating data from murine models to humans is therefore unreliable and disappointing.

To transplant isolated human preantral follicles, plasma clots (14, 15) were

replaced by a fibrin matrix, as it was shown to have highly variable composition and fast degradation rates, but it led to follicle loss and irregular results after transplantation. Moreover, due to its very delicate structure, it could potentially be damaged during laparoscopic surgery.

Although softer fibrin formulations have been successfully used to transplant isolated mouse follicles (17, 35), our experience has shown that isolated human follicles require a stiffer fibrin matrix. After xenografting them inside a fibrin matrix containing increased fibrinogen and thrombin concentrations, follicle recovery rates were 20-35% (20, 21), comparable to results of xenografting of human ovarian tissue (42).

As in rodents, decellularized ovarian ECM has also been tested as an alternative to transplant isolated human preantral follicles. However, when a whole ovary or fragments of ovarian tissue are decellularized (38, 41), we obtained a heterogeneous tissue architecture with small and very large pores that were once occupied by different-sized follicles (Fig. 2). For this reason, routine cell seeding protocols to repopulate the matrix (43) cannot be applied. Instead, it is necessary to resort to different strategies that may actually defeat the purpose of one of the best features of decellularized matrices, namely structure. Indeed, when Pors et al. (22) created scalpel- made pockets in decellularized human ovarian ECM to insert isolated human follicles, they did not find any follicles after transplantation to mice. Positive results were achieved only when isolated follicles were embedded in Matrigel before being poured onto the constructs (22), which demonstrates the need for another material to be used alongside decellularized ovarian ECM. It is, however, important to bear in mind that use of Matrigel, which is not approved in clinical practice, may also have positively influenced these findings.



Figure 2. Decellularized human ovary (41).

Another strategy to take advantage of the biochemical cues of ovarian ECM is its application in the form of decellularized hydrogels. Studies have revealed that these hydrogels can promote de novo formation of functional tissue (44), as they retain their biological characteristics and encourage tissue regeneration (45). After the decellularization process, numerous ECM proteins from native tissue can be found in the hydrogel (45), as well as cytokines stored in tissues or cells (46), which may promote tissue growth as they are released into regenerating tissue during hydrogel remodeling (45). We recently developed a decellularized bovine ovarian ECM hydrogel (47), in which ovarian follicles and cells could easily be seeded. Our preliminary results showedthat after 10 days of in vitro culture, preantral follicles remained viable in the hydrogels (47).

Ovarian cells and their role in the transplantable engineered ovary

While the main players in the creation of a transplantable engineered ovary are isolated preantral follicles, the co-presence of cells may be fundamental to achieving complete folliculogenesis and improving ovarian regeneration. Indeed, several studies have pointed out that the number and spatial distribution of ovarian cells in an engineered ovary appear to play a key role in follicle development (48-50).

Ovarian stromal cells

Initial studies by Gosden's group (11-13) provided the first evidence of the role of ovarian stromal cells in the transplantable engineered ovary. These cells were needed for ovarian tissue reconstitution and possibly had an impact on follicle development. Indeed, stromal cells can synthesize numerous factors that regulate primordial follicle activation (51). In turn, granulosa cells and oocytes from growing primary follicles will secrete growth factors to recruit and differentiate cells from the ovarian stromal compartment into theca cells (52, 53) essential for further follicle development.

Autologous stromal cells can be easily isolated from fresh or frozen- thawed ovarian tissue biopsies (54). The safest option is to harvest them from ovarian samples collected after patient disease remission, namely after cancer treatment, so there is no risk of malignant cell contamination of the engineered ovary. However, it is possible that some patients may not have any remaining ovarian tissue to collect these cells. In such cases, stromal cells can be retrieved from tissue samples cryopreserved before chemo- or radiotherapy. Cells can be isolated after follicle pick-up (20, 21), but a purging step is required to avoid any possible malignant cell contamination (55, 56). Soares (57) compared stromal cells collected from fresh ovarian tissue procured from patients after cancer treatment to frozen- thawed ovarian samples. This author did not observe any difference in the cells from the two groups in terms of survival (57). Moreover, isolated ovarian stromal cells can successfully proliferate after transplantation inside different matrices (17, 18, 20, 21, 29, 35, 57-59), and have been shown to contribute to matrix degradation and ECM synthesis (Fig. 3).

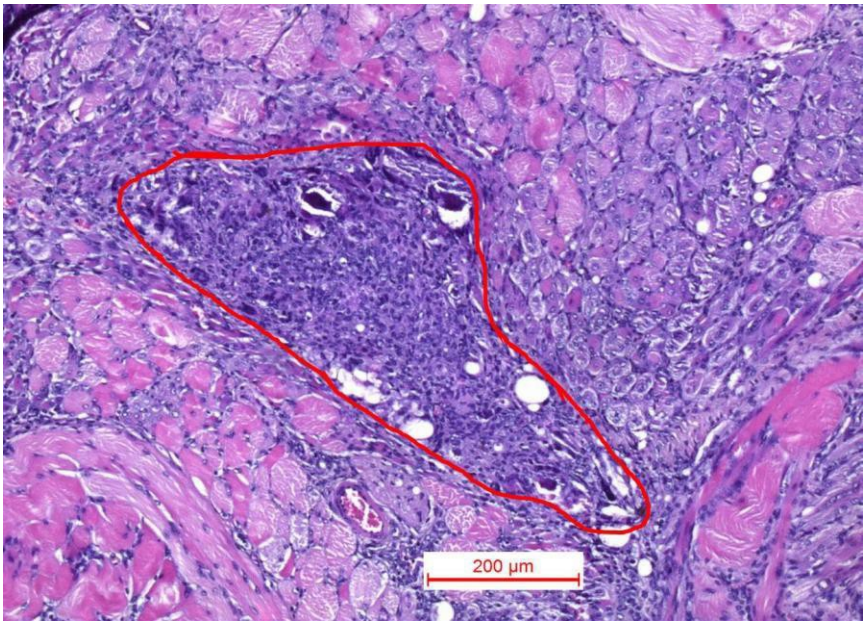


Figure 3. Isolated human ovarian stromal cells after encapsulation in a fibrin matrix (outlined in red) and 7 days of xenotransplantation to immunodeficient mouse.

Ovarian endothelial cells

Our first evidence that endothelial cells isolated from ovarian tissue play a significant role in the engineered ovary came from the study by Dath et al. (59). After comparing grafts containing isolated stromal cells with or without endothelial cells, they observed a large grafted area showing an impressive number of vessels as early as one week after transplantation (Fig. 4). Soares et al. (54) subsequently assessed the influence of endothelial cell concentrations on vessel area and demonstrated a positive correlation between the number of grafted isolated cells and vascularization after 7 days of xenografting to immunodeficient mice (54). As endothelial cell concentrations are quite low in ovarian cortex, we could consider isolating these cells from the medullary layer, as suggested by Soares et al.(54). While vascularization in the transplantable engineered ovary can initially be induced by the presence of isolated endothelial cells encapsulated in the matrix, it is important to stress that the number of vessels may also be influenced by growing follicles (60). Indeed, when isolated mouse secondary

follicles were transplanted separately from small primordial and primary follicles, the grafts exhibited a greater vessel surfacearea and more vessels (60), possibly due to expression of angiogenic factors like VEGF by these growing follicles (61).

Deconstructing the native human ovary to construct an engineered ovary

Ovarian matrisome

Ovarian follicles and cells are inherently surrounded by a complex meshwork of proteins forming the ECM, which is destroyed by isolation procedures. Therefore, in order to develop a transplantable bioengineered ovary that offers an environment in which isolated human follicles can survive and grow, it is necessary to provide them with a biomimetic ECM. While numerous attempts by various research teams have demonstrated the feasibility of this concept (17, 18, 29, 34), they also revealed that developing an engineered ovary requires more than simple use of biomaterials and application of tissue engineering strategies. Indeed, an essential requirement for replicating the complexity of a functional ovary is a comprehensive understanding of the composition, architecture and plasticity of the human ovarian ECM, something we do not yet have. Thus, deconstructing the microenvironment of ovarian cells and follicles is a prerequisite to constructing a bioinspired engineered ovary.

Proteomics is a powerful tool that can be used to scrutinize the composition of the ovarian ECM without a priori knowledge, in contrast to targeted studies using specific antibodies (62). Very recently, proteomics was used to characterize the composition of human ovarian tissue in reproductive- age subjects and develop the first draft map of the human ovarian matrisome (23). The matrisome is essentially an extended description of the ECM (63), including not only all structural ECM components, but also proteins able to regulate and remodel the ECM. It can be categorized as follows:

- Core matrisome proteins:
    - ECM glycoproteins
    - Collagens
    - Proteoglycans

- ECM-associated proteins:
    - ECM-affiliated proteins, namely proteins showing biochemical and architectural analogy with ECM proteins or known to be associated
    - ECM regulators, namely proteins responsible for ECM turnover
    - Secreted factors, namely secreted proteins interacting with core ECM proteins.

Ouni et al.'s study shows the human ovarian matrisome to be composed of: 49% collagen, 7% proteoglycans, 15% glycoproteins, 18% ECM- affiliated proteins, 10% ECM regulators and 1% secreted factors (23). Indeed, around 100 proteins make up the ovarian matrisome, so the task of developing a bioinspired engineered matrix is quite challenging. Selection criteria need to focus on key proteins whose presence is absolutely required in the engineered ovary. Only comparative studies between different age groups can elucidate specific features of the reproductive-age ovary that make it more inclined to follicle survival and development than its younger and older counterparts.

Understanding the composition of the ovarian matrisome is not enough to be able to construct a biomimetic ovary. It is also crucial to bear in mind that ovarian follicles are exceptional in that they can grow toaround 600X their size during folliculogenesis (for instance, human follicles grow from 30 μm at the primordial stage to 18–24 mm when they are ready to ovulate). It is therefore important to explore the intrinsic elasticity of the human ovary. In contrast to proteomics, very few studies have investigated the elasticity of human ovarian tissue (64,65). However, only recently, Ouni et al. (unpublished results) revealed the true elastic system components that confer intrinsic mechanical features to biological tissues, including collagen, known as the provider of tensile strength to tissue. On the other hand, elastin, elastin microfibril interface-located protein 1 (EMILIN-1), fibrillin-1 and GAGs are known to temper the rigidity of collagen by providing recoil and elasticity. This study revealed some interesting spatiotemporal changes to elastic ECM deposition and turnover, dictating the mechanical features of the human ovary in the course of a woman's lifetime. This is consistent with the emerging hypothesis related to the mechanobiology of the human ovary and dynamic reciprocity that exists between ovarian cells and theirmicroenvironment (66-68).

Ouni et al.'s study also shed light on follicle-specific ECM composition, dependent on follicle stage and age. These data will prove very useful in developing the bioengineered ovary. Indeed, they emphasize the importance of encapsulating each type of isolated follicle in an appropriate biomaterial that must replicate the corresponding functional perifollicular ECM and respect ovarian tissue heterogeneity (69) to guarantee its biomimicry.

Another facet of the ovarian matrisome that needs to be investigated is its microarchitecture and ultrastructure. Indeed, it is essential to respect native tissue porosity and fiber organization because they are involved in nutrient and oxygen transport (70). Moreover, fibrous matrisome proteins provide cells with external stimuli and instructive cues to influence gene expression, cell behavior and morphology, as evidenced by emerging publications on this subject (71-73). Proof of the involvement of matrisome ultrastructure in dictating cell phenotype is how collagen alignment has been used as a prognostic signature for survival in human breast carcinoma (74). However, in the context of the ovary, these data are still lacking. Novel analytical techniques must therefore be applied to conduct in-depth studies of the ovarian microarchitecture and produce a map of the ultrastructural features of reproductive-age tissue and follicle stage niche.

Increasing evidence today points to different roles of the matrisome, particularly the ovarian matrisome, beyond its apparent primary function of physical support. Knowing that biodegradable matrices cannot replicate the complexity of a given microenvironment, decellularization has emerged as the ultimate means of creating more efficient biomimetic scaffolds (75). However, it is worth mentioning that decellularization methods rely on use of harsh physical, enzymatic and chemical procedures (for example, sodium dodecyl sulfate) (22, 76) that can deplete the decellularized scaffold and erase key matrisome elements. Therefore, without comparing the properties of such matrices against a reference of the native human ovarian matrisome, it is impossible to monitor their reliability to reproduce the ovarian cell microenvironment.

In contrast to most tissue engineering strategies relying on the presence of generic ECM components (collagen, fibrin, laminin, etc.) as indicators of the success of their biomimetic constructs, deconstructing the natural human ovary seeks to map the ovarian matrisome with its multiple facets. The aim

is to build a reliable reference of its unique features, which will serve as a roadmap for developing a more closely biomimetic matrix tailored to human ovarian cells and follicles, and applicable in the field of fertility preservation.

Subpopulations of ovarian cells

While it is known that human ovaries contain a vast majority of stromal cells, followed by endothelial cells (77), it was only recently that in-depth characterization of cell populations was undertaken in human ovarian tissue (78, 79). In their study analyzing the ovarian cortical layer, Wagner etal. (78) not only identified other subpopulations of cells, but also reported their proportions; stromal, endothelial and perivascular cells correspond to around 83%, 5% and 10% of cells in the ovarian cortex respectively, while macrophages and T-cells account for around 0.5%. These findings are extremely important for development of an engineered ovary. For instance, macrophages play a role in matrix remodeling and synthesize growth factors and cytokines (80). Moreover, M1 macrophages appear to be implicated in folliculogenesis in mouse ovaries (81), while M2 macrophages are involved in tissue repair through synthesis of anti-inflammatory cytokines, such as VEGF and transforming growth factor beta (82). Interestingly, these authors did not find a population of germline stem cells, which was a rather contentious finding by Tilly's group (83, 84). Analysis of the inner cortical layer of human ovaries revealed clusters of stromal, endothelial, theca, immune, smooth muscle and granulosa cells (79). Most importantly, Fan et al. (79) reported several types of these cells.

As these cell populations are essential to folliculogenesis, ECM synthesis, tissue remodeling, vascularization and other such processes, it is vital to ensure that they are present in the transplantable engineered ovary. Information generated by such studies is also crucial to evaluating the constructs after transplantation and understanding our findings.

Theca cells

Theca cells have been poorly investigated compared to granulosa cells and oocytes, but their role in folliculogenesis is undeniable. Indeed, if they were not included in engineered ovaries, follicles could not develop beyond the secondary stage and, consequently, ovarian function and fertility would never be restored.

Theca cells start to appear at the later stage of secondary follicles and form a layer around granulosa-oocyte structures (85). They play an indispensable role in folliculogenesis by providing structural support for follicles, and androstenedione as a substrate for granulosa cells to convert to estradiol (86-88). Besides such key tasks for theca cells, we have limited knowledge about their recruitment, growth and differentiation due to a lack of information concerning their origin (53, 89). A few studies using murine models have shown the presence of a subpopulation of ovarian cells, called theca progenitor stem cells, that are recruited to differentiate into theca cells under the influence of factors secreted by oocytes and granulosa cells (53, 89). Honda et al. (53) studied neonatal mouse ovaries and reported thattheca progenitor stem cells express GLI family zinc finger 3 (GLI3) and protein patched homolog 1 (Ptch1) as markers, and can differentiate into theca cells in the presence of factors issuing from oocytes and granulosa cells. After differentiation, these cells express luteinizing hormone receptor (LHR), GLI2 and Ptch2. Liu et al. (89) found that there are two origins of theca progenitor cells in embryonic mouse gonads: (i) Wilm's tumor 1- positive mesenchymal cells intrinsic to the ovary, which differentiate into theca cells after birth, giving rise to theca fibroblasts, perivascular smooth muscle cells and interstitial ovarian cells; and (ii) GLI1-positive cells, which migrate from the mesonephros to the ovary and become steroidogenic androgen-producing cells inside the ovary. In large animal models, like cows (52) and goats (90), ovarian cortical stromal cells can differentiate into theca cells in the presence of granulosa cells by expressing cytochrome P450 17A1 (CYP17A1) and LHR as markers, as well as and androstenedione (52, 91), but there are no studies confirming the presence of a subpopulation of theca precursor cells in human ovaries. However, Fanet al. (79) detected a theca cell populationin human ovaries that they termed common progenitor theca cells, which progress to theca interna or externa cells, but these findings still need to be confirmed. Moreover, these cells were found surrounding small antral follicles, in the inner cortical layer, while recruitment and differentiation of theca cells take place during the early primary/secondary stage of follicle development. One may therefore wonder if these cells surround follicles right from the start or are spread throughout the ovarian cortex.

In a study using isolated bovine cortical stromal cells, Orisaka et al. (52) reported that cells can differentiate into theca cells under stimuli provided by granulosa cells in vitro, as evidenced by the steroidogenic markers they

assessed.

Subsequent to these intriguing results, Asiabi et al. (unpublished data) isolated stromal cells from the cortical layer of postmenopausal ovaries and in vitro-cultured them using a medium supplemented with growth factors presumed to be involved in theca cell differentiation. After 8 days of in vitro culture, up to 43% of cells differentiated into theca interna cells. Moreover, a modest proportion of small luteal cells was also identified. These findings indicate the presence of theca precursor cells spread throughout the cortical layer, which remain in the human ovary throughout its lifetime. In vivo, factors used by Asiabi et al. (unpublished data) are synthesized by granulosa cells and oocytes from growing follicles. We can therefore hypothesize that once isolated follicles and ovarian cells are transplanted along with the 3D matrix, these follicles can induce recruitment and differentiation of theca cells.

Conclusions

Pioneering studies into murine and human follicles (11-15) have demonstrated the feasibility of grafting isolated follicles, but recent findings indicate that this approach can be improved through utilization of a transplantable engineered ovary. Over the last years, we have shown that human preantral follicles can be safely isolated in large numbers by adapting the isolation protocol according to ovarian tissue type (16, 21, 92,93). We have also learned that in order to restore ovarian function and fertility, ovarian cells need to be incorporated into the engineered ovary. Indeed, we witnessed their impact on the formation of ovary-like tissue, with vascularization and synthesis of the ECM (21, 35, 54, 59, 60). Under the influence of growing follicles, a subpopulation of these cells can be recruited to differentiate into theca cells (Asiabi et al., unpublished data). Taking advantage of insights acquired from single- cell analysis of human ovarian cortex (78, 79), we know it is possible to enrich the engineered ovary with specific subpopulations of ovarian cells to enhance tissue remodeling, or release growth factors that can positively affect folliculogenesis or synthesis of elastic proteins, for instance. Regardingthe 3D matrix to be used to encapsulate and transplant isolated follicles and cells, numerous biomaterials have been tested (11, 14, 27, 28, 34, 36,37). While they offer good mechanical support for follicles, they do not possess the biomechanical and biochemical cues normally present in the ovarian ECM. In recent years, investigations have shed new light on the composition and structure of

human ovaries (23, 65), showing that the complexity of the ovarian ECM is impossible to replicate with a polymer. On the other hand, we may get closer to our goal with the use of decellularized ovarian matrices (22, 38- 41, 43, 47). However, studies are still in their infancy and it is not yet possible to determine if this type of structure will be the matrix of choicefor the engineered ovary.

Definitions

- Decellularization: a procedure first developed by Prof Stephen F. Badylak, where cells from a given tissue or organ are destroyed and removed, leaving only the extracellular matrix scaffold. The purpose of this procedure is to create matrices to be used in tissue engineering and regenerative medicine approaches.
- Folliculogenesis: a process describing the activation and growth of ovarian primordial follicles up to preovulatory stage.
- Tissue engineering: an interdisciplinary field that uses the combination of cells, materials, biochemical and physicochemical factors and engineering with the goal of replacing, repairing, or improve tissues and organs in the body.

Take home messages

- Human preantral follicles can be safely isolated in large numbers.
- Survival and development of isolated ovarian preantral follicles is feasible.
- Ovarian cells have an important role in transplantable engineered ovary, as they aid in the scaffold degradation, synthesis of extracellular matrix and vascularization.
- A subpopulation of ovarian cells is able to differentiate into theca cells, which are essential for follicle development.
- Current biomaterials used to transplant isolated follicles and cells do not possess the biomechanical and biochemical cues normally present in the ovarian ECM.
- New studies have start revealing the complexity of the ovarian ECM in terms of composition and microarchitecture, which are crucial for the development of a 3D matrix for the transplantableengineered ovary.

Key readings

Papers underlined in the reference list are key readings in this topic.

References

1. Observatory GC. Cancer Today: International Agency for Research on Cancer 2019 [updated March, 2019; cited 2020 February 3]. Available from: http://gco.iarc.fr/today/online-analysis-table?v=2018&mode=cancer&mode_population=continents&population=900&populations=900&key=asr&sex=0&cancer=39&type=0&statistic=5&prevalence=0&population_group=0&ages_group%5B%5D=0&ages_group%5B%5D=8&nb_items=5&group_cancer=1&include_nmsc=1&include_nmsc_other=1.

2. Siegel RL, Miller KD, Jemal A. Cancer statistics, 2018. CA Cancer J Clin. 2018;68(1):7-30.

3. Donnez J, Dolmans MM. Fertility Preservation in Women. N Engl J Med. 2017;377(17):1657-65.

4. Dolmans MM, Masciangelo R. Risk of transplanting malignant cells in cryopreserved ovarian tissue. Minerva Ginecol. 2018;70(4):436-43.

5. Sonmezer M, Oktay K. Fertility preservation in female patients.Hum Reprod Update. 2004;10(3):251-66.

6. Orphanet. Burkitt lymphoma 2010 [updated February 2010; cited 2020 February 3]. Available from:

https://www.orpha.net/consor/cgi-bin/Disease_Search.php?lng=EN&data_id=3747&Disease_Disease_Search_diseaseGroup=Burkitt-lymphoma&Disease_Disease_Search_diseaseType=Pat&Disease(s)/group%20of%20diseases=Burkitt-lymphoma&title=Burkitt%20lymphoma&search=Disease_Search_Simple.

7. Orphanet. Neuroblastoma 2009 [updated March 2009; cited 2020 February 3]. Available from: https://www.orpha.net/consor/cgi-bin/Disease_Search.php?lng=EN&data_id=548&Disease_Disease_Search_diseaseGroup=Neuroblastoma&Disease_Disease_Search_diseaseType=Pat&Disease(s)/group%20of%20diseases=Neuroblastoma&title=Neur

oblastoma&search=Disease_Search_Simple.

8. Dolmans MM, Marinescu C, Saussoy P, Van Langendonckt A, Amorim C, Donnez J. Reimplantation of cryopreserved ovarian tissue from patients with acute lymphoblastic leukemia is potentially unsafe. Blood. 2010;116(16):2908-14.

9. Rodgers RJ, Irving-Rodgers HF, Russell DL. Extracellular matrix of the developing ovarian follicle. Reproduction. 2003;126(4):415-24.

10. Torrance C, Telfer E, Gosden RG. Quantitative study of the development of isolated mouse pre-antral follicles in collagen gel culture. J Reprod Fertil. 1989;87(1):367-74.

11. Telfer E, Torrance C, Gosden RG. Morphological study of cultured preantral ovarian follicles of mice after transplantation under the kidney capsule. J Reprod Fertil. 1990;89(2):565-71.

12. Gosden RG. Restitution of fertility in sterilized mice by transferring primordial ovarian follicles. Hum Reprod. 1990;5(5):499- 504.

13. Carroll J, Gosden RG. Transplantation of frozen-thawed mouse primordial follicles. Hum Reprod. 1993;8(8):1163-7.

14. Dolmans MM, Martinez-Madrid B, Gadisseux E, Guiot Y, Yuan WY, Torre A, et al. Short-term transplantation of isolated human ovarian follicles and cortical tissue into nude mice. Reproduction. 2007;134(2):253-62.

15. Dolmans MM, Yuan WY, Camboni A, Torre A, Van Langendonckt A, Martinez-Madrid B, et al. Development of antral follicles after xenografting of isolated small human preantral follicles. Reprod Biomed Online. 2008;16(5):705-11.

16. Soares M, Saussoy P, Sahrari K, Amorim CA, Donnez J, Dolmans MM. Is transplantation of a few leukemic cells inside an artificial ovary able to induce leukemia in an experimental model? J Assist Reprod Genet. 2015;32(4):597-606.

17. Luyckx V, Dolmans MM, Vanacker J, Legat C, Fortuno Moya C, Donnez J, et al. A new step toward the artificial ovary: survival and proliferation of isolated murine follicles after autologous transplantation in a fibrin scaffold. Fertil Steril. 2014;101(4):1149-56.

18. Vanacker J, Dolmans MM, Luyckx V, Donnez J, Amorim CA. First

transplantation of isolated murine follicles in alginate. Regen Med. 2014;9(5):609-19.

19. Kniazeva E, Hardy AN, Boukaidi SA, Woodruff TK, Jeruss JS, SheaLD. Primordial Follicle Transplantation within Designer Biomaterial Grafts Produce Live Births in a Mouse Infertility Model. Sci Rep. 2015;5:17709.

20. Paulini F, Vilela JM, Chiti MC, Donnez J, Jadoul P, Dolmans MM, etal. Survival and growth of human preantral follicles after cryopreservation of ovarian tissue, follicle isolation and short-term xenografting. Reprod Biomed Online. 2016;33(3):425-32.

21. Chiti MC, Dolmans MM, Hobeika M, Cernogoraz A, Donnez J,Amorim CA. A modified and tailored human follicle isolation procedure improves follicle recovery and survival. J Ovarian Res. 2017;10(1):71.

22. Pors SE, Ramlose M, Nikiforov D, Lundsgaard K, Cheng J, AndersenCY, et al. Initial steps in reconstruction of the human ovary: survival of pre- antral stage follicles in a decellularized human ovarian scaffold. HumReprod. 2019;34(8):1523-35.

23. Ouni E, Vertommen D, Chiti MC, Dolmans MM, Amorim CA. A Draft Map of the Human Ovarian Proteome for Tissue Engineering and Clinical Applications. Mol Cell Proteomics. 2019;18(Suppl 1):S159-S73.

24. Yoon DM, Fisher JP. Natural and synthetic polymeric scaffolds. In: Narayan R, editor. Biomedical Materials. Berlin, Germany: Springer; 2009. p. 415-42.

25. Caliari SR, Burdick JA. A practical guide to hydrogels for cell culture. Nat Methods. 2016;13(5):405-14.

26. Amorim CA, Shikanov A. The artificial ovary: current status and future perspectives. Future Oncol. 2016;12(20):2323-32.

27. Laronda MM, Rutz AL, Xiao S, Whelan KA, Duncan FE, Roth EW, et al. A bioprosthetic ovary created using 3D printed microporous scaffolds restores ovarian function in sterilized mice. Nat Commun. 2017;8:15261.

28. Vanacker J, Amorim CA. Alginate: A Versatile Biomaterial to Encapsulate Isolated Ovarian Follicles. Ann Biomed Eng. 2017;45(7):1633-49.

29. Vanacker J, Luyckx V, Dolmans MM, Des Rieux A, Jaeger J, Van

Langendonckt A, et al. Transplantation of an alginate-matrigel matrix containing isolated ovarian cells: first step in developing a biodegradable scaffold to transplant isolated preantral follicles and ovarian cells. Biomaterials. 2012;33(26):6079-85.

30. Filatov MA, Khramova YV, Semenova ML. In Vitro Mouse Ovarian Follicle Growth and Maturation in Alginate Hydrogel: Current State of theArt. Acta Naturae. 2015;7(2):48-56.

31. Amorim CA, Van Langendonckt A, David A, Dolmans MM, Donnez J. Survival of human pre-antral follicles after cryopreservation of ovarian tissue, follicular isolation and in vitro culture in a calcium alginate matrix.Hum Reprod. 2009;24(1):92-9.

32. Camboni A, Van Langendonckt A, Donnez J, Vanacker J, Dolmans MM, Amorim CA. Alginate beads as a tool to handle, cryopreserve and culture isolated human primordial/primary follicles. Cryobiology. 2013;67(1):64-9.

33. Vanacker J, Luyckx V, Amorim C, Dolmans MM, Van Langendonckt A, Donnez J, et al. Should we isolate human preantral follicles before or after cryopreservation of ovarian tissue? Fertil Steril. 2013;99(5):1363- 8 e2.

34. Chiti MC, Dolmans MM, Donnez J, Amorim CA. Fibrin in Reproductive Tissue Engineering: A Review on Its Application as a Biomaterial for Fertility Preservation. Ann Biomed Eng. 2017;45(7):1650- 63.

35. Chiti MC, Dolmans MM, Orellana R, Soares M, Paulini F, Donnez J, et al. Influence of follicle stage on artificial ovary outcome using fibrin as a matrix. Hum Reprod. 2016;31(2):427-35.

36. Smith RM, Shikanov A, Kniazeva E, Ramadurai D, Woodruff TK, Shea LD. Fibrin-mediated delivery of an ovarian follicle pool in a mouse model of infertility. Tissue Eng Part A. 2014;20(21-22):3021-30.

37. Kim J, Perez AS, Claflin J, David A, Zhou H, Shikanov A. Synthetic hydrogel supports the function and regeneration of artificial ovarian tissue in mice. NPJ Regen Med. 2016;1.

38. Laronda MM, Jakus AE, Whelan KA, Wertheim JA, Shah RN, Woodruff TK. Initiation of puberty in mice following decellularized ovary transplant. Biomaterials. 2015;50:20-9.

39. Alshaikh AB, Padma AM, Dehlin M, Akouri R, Song MJ, Brannstrom M, et al. Decellularization of the mouse ovary: comparison of different scaffold generation protocols for future ovarian bioengineering. J Ovarian Res. 2019;12(1):58.

40. Liu WY, Lin SG, Zhuo RY, Xie YY, Pan W, Lin XF, et al. Xenogeneic Decellularized Scaffold: A Novel Platform for Ovary Regeneration. Tissue Eng Part C Methods. 2017;23(2):61-71.

41. Hassanpour A, Talaei-Khozani T, Kargar-Abarghouei E, Razban V, Vojdani Z. Decellularized human ovarian scaffold based on a sodium lauryl ester sulfate (SLES)-treated protocol, as a natural three- dimensional scaffold for construction of bioengineered ovaries. Stem Cell Res Ther. 2018;9(1):252.

42. Nisolle M, Casanas-Roux F, Marbaix E, Jadoul P, Donnez J. Transplantation of cultured explants of human endometrium into nude mice. Hum Reprod. 2000;15(3):572-7.

43. Mirzaeian L, Eivazkhani F, Hezavehei M, Moini A, Esfandiari F, Valojerdi MR, et al. Optimizing The Cell Seeding Protocol to Human Decellularized Ovarian Scaffold: Application of Dynamic System for Bio-Engineering. Cell J. 2020;22(2):227-35.

44. Badylak SF, Brown BN, Gilbert TW, Daly KA, Huber A, Turner NJ. Biologic scaffolds for constructive tissue remodeling. Biomaterials. 2011;32(1):316-9.

45. Hoganson DM, Owens GE, O'Doherty EM, Bowley CM, Goldman SM, Harilal DO, et al. Preserved extracellular matrix components and retained biological activity in decellularized porcine mesothelium. Biomaterials. 2010;31(27):6934-40.

46. Voytik-Harbin SL, Brightman AO, Kraine MR, Waisner B, Badylak SF. Identification of extractable growth factors from small intestinal submucosa. J Cell Biochem. 1997;67(4):478-91.

47. Chiti MC, Viswanath A, Vanacker J, Germain L, White LJ, Dolmans MM, et al., editors. Hydrogel from bovine decellularized ovarianextracellularmatrix supports mouse follicle survival in vitro. 10th World Biomaterials Congress; 2016 17-22 May 2016; Montréal, Canada: Frontiers.

48. Da Silva-Buttkus P, Marcelli G, Franks S, Stark J, Hardy K. Inferring

biological mechanisms from spatial analysis: prediction of a local inhibitor in the ovary. Proc Natl Acad Sci U S A. 2009;106(2):456-61.

49. Hornick JE, Duncan FE, Shea LD, Woodruff TK. Multiple follicle culture supports primary follicle growth through paracrine-acting signals. Reproduction. 2013;145(1):19-32.

50. Gaytan F, Morales C, Leon S, Garcia-Galiano D, Roa J, Tena-Sempere M. Crowding and Follicular Fate: Spatial Determinants of Follicular Reserve and Activation of Follicular Growth in the Mammalian Ovary. PLoS One. 2015;10(12):e0144099.

51. Knight PG, Glister C. TGF-beta superfamily members and ovarian follicle development. Reproduction. 2006;132(2):191-206.

52. Orisaka M, Tajima K, Mizutani T, Miyamoto K, Tsang BK, Fukuda S, et al. Granulosa cells promote differentiation of cortical stromal cells into theca cells in the bovine ovary. Biol Reprod. 2006;75(5):734-40.

53. Honda A, Hirose M, Hara K, Matoba S, Inoue K, Miki H, et al. Isolation, characterization, and in vitro and in vivo differentiation of putative thecal stem cells. Proc Natl Acad Sci U S A. 2007;104(30):12389-94.

54. Soares M, Sahrari K, Chiti MC, Amorim CA, Ambroise J, DonnezJ, et al. The best source of isolated stromal cells for the artificial ovary: medulla or cortex, cryopreserved or fresh? Hum Reprod. 2015;30(7):1589- 98.

55. Schroder CP, Timmer-Bosscha H, Wijchman JG, de Leij LF, Hollema H, Heineman MJ, et al. An in vitro model for purging of tumour cells from ovarian tissue. Hum Reprod. 2004;19(5):1069-75.

56. Mouloungui E, Zver T, Roux C, Amiot C. A protocol to isolate and qualify purified human preantral follicles in cases of acute leukemia, for future clinical applications. J Ovarian Res. 2018;11(1):4.

57. Soares M. Fertility preservation and leukemia: cellular components of the artificial ovary and disease retransmission through the graft. Brussels: Université Catholique de Louvain; 2015.

58. Luyckx V, Dolmans MM, Vanacker J, Scalercio SR, Donnez J, Amorim CA. First step in developing a 3D biodegradable fibrin scaffold for an artificial ovary. J Ovarian Res. 2013;6(1):83.

59. Dath C, Dethy A, Van Langendonckt A, Van Eyck AS, Amorim CA, Luyckx V, et al. Endothelial cells are essential for ovarian stromal tissue restructuring after xenotransplantation of isolated ovarian stromal cells. Hum Reprod. 2011;26(6):1431-9.

60. Chiti MC, Dolmans MM, Lucci CM, Paulini F, Donnez J, Amorim CA. Further insights into the impact of mouse follicle stage on graft outcome in an artificial ovary environment. Mol Hum Reprod. 2017;23(6):381-92.

61. Kaczmarek MM, Schams D, Ziecik AJ. Role of vascular endothelial growth factor in ovarian physiology - an overview. Reprod Biol. 2005;5(2):111-36.

62. Ouni E, Vertommen D, Amorim CA. The Human Ovary and Future of Fertility Assessment in the Post-Genome Era. Int J Mol Sci. 2019;20(17).

63. Naba A, Clauser KR, Ding H, Whittaker CA, Carr SA, Hynes RO. The extracellular matrix: Tools and insights for the "omics" era. Matrix Biol. 2016;49:10-24.

64. Wood CD, Vijayvergia M, Miller FH, Carroll T, Fasanati C, Shea LD, et al. Multi-modal magnetic resonance elastography for noninvasive assessment of ovarian tissue rigidity in vivo. Acta Biomater. 2015;13:295-300.

65. Chiti MC, Dolmans MM, Mortiaux L, Zhuge F, Ouni E, Shahri PAK, et al. A novel fibrin-based artificial ovary prototype resembling human ovarian tissue in terms of architecture and rigidity. J Assist Reprod Genet. 2018;35(1):41-8.

66. Woodruff TK, Shea LD. A new hypothesis regarding ovarian follicle development: ovarian rigidity as a regulator of selection and health. J Assist Reprod Genet. 2011;28(1):3-6.

67. Kawamura K, Cheng Y, Suzuki N, Deguchi M, Sato Y, Takae S, et al. Hippo signaling disruption and Akt stimulation of ovarian follicles for infertility treatment. Proc Natl Acad Sci U S A. 2013;110(43):17474-9.

68. Thorne JT, Segal TR, Chang S, Jorge S, Segars JH, Leppert PC. Dynamic reciprocity between cells and their microenvironment in reproduction. Biol Reprod. 2015;92(1):25.

69. Choi JK, Agarwal P, Huang H, Zhao S, He X. The crucial role of

mechanical heterogeneity in regulating follicle development and ovulation with engineered ovarian microtissue. Biomaterials. 2014;35(19):5122-8.

70. Kelleher CM, Vacanti JP. Engineering extracellular matrix through nanotechnology. J R Soc Interface. 2010;7 Suppl 6:S717-29.

71. Janson IA, Putnam AJ. Extracellular matrix elasticity and topography: material-based cues that affect cell function via conserved mechanisms. J Biomed Mater Res A. 2015;103(3):1246-58.

72. Alkmin S, Brodziski R, Simon H, Hinton D, Goldsmith RH, Patankar M, et al. Migration dynamics of ovarian epithelial cells on micro- fabricated image-based models of normal and malignant stroma. Acta Biomater. 2019;100:92-104.

73. Li Y, Xiao Z, Zhou Y, Zheng S, An Y, Huang W, et al. Controlling the Multiscale Network Structure of Fibers To Stimulate Wound Matrix Rebuilding by Fibroblast Differentiation. ACS Appl Mater Interfaces. 2019;11(31):28377-86.

74. Conklin MW, Eickhoff JC, Riching KM, Pehlke CA, Eliceiri KW, Provenzano PP, et al. Aligned collagen is a prognostic signature for survival in human breast carcinoma. Am J Pathol. 2011;178(3):1221-32.

75. Crapo PM, Gilbert TW, Badylak SF. An overview of tissue and whole organ decellularization processes. Biomaterials. 2011;32(12):3233-43.

76. White LJ, Taylor AJ, Faulk DM, Keane TJ, Saldin LT, Reing JE, et al. The impact of detergents on the tissue decellularization process: A ToF-SIMS study. Acta Biomater. 2017;50:207-19.

77. Asiabi P, Chiti MC, Amorim CA. Isolation and characterization of the human ovarian cell population for transplantation into an artificial ovary. Anim Reprod. 2019;16(1):39-44.

78. Wagner M, Yoshihara M, Douagi I, Damdimopoulos A, Panula S, Petropoulos S, et al. Single cell map of the human ovarian cortex. 2019:791343.

79. Fan X, Bialecka M, Moustakas I, Lam E, Torrens-Juaneda V, Borggreven NV, et al. Single-cell reconstruction of follicular remodeling in the human adult ovary. Nat Commun. 2019;10(1):3164.

80. Wu R, Van der Hoek KH, Ryan NK, Norman RJ, Robker RL. Macrophage contributions to ovarian function. Hum Reprod Update. 2004;10(2):119-33.

81. Ono Y, Nagai M, Yoshino O, Koga K, Nawaz A, Hatta H, et al. CD11c+ M1-like macrophages (MPhis) but not CD206+ M2-like MPhi are involved in folliculogenesis in mice ovary. Sci Rep. 2018;8(1):8171.

82. Sica A, Erreni M, Allavena P, Porta C. Macrophage polarization in pathology. Cell Mol Life Sci. 2015;72(21):4111-26.

83. Martin JJ, Woods DC, Tilly JL. Implications and Current Limitations of Oogenesis from Female Germline or Oogonial Stem Cells in Adult Mammalian Ovaries. Cells. 2019;8(2).

84. Woods DC, Tilly JL. Isolation, characterization and propagation of mitotically active germ cells from adult mouse and human ovaries. Nat Protoc. 2013;8(5):966-88.

85. Young JM, McNeilly AS. Theca: the forgotten cell of the ovarianfollicle. Reproduction. 2010;140(4):489-504.

86. Edson MA, Nagaraja AK, Matzuk MM. The mammalian ovary from genesis to revelation. Endocr Rev. 2009;30(6):624-712.

87. Hirshfield AN. Development of follicles in the mammalian ovary. Int Rev Cytol. 1991;124:43-101.

88. Nilsson E, Skinner MK. Cellular interactions that control primordial follicle development and folliculogenesis. J Soc Gynecol Investig. 2001;8(1 Suppl Proceedings):S17-20.

89. Liu C, Peng J, Matzuk MM, Yao HH. Lineage specification of ovarian theca cells requires multicellular interactions via oocyte and granulosa cells. Nat Commun. 2015;6:6934.

90. Qiu M, Quan F, Han C, Wu B, Liu J, Yang Z, et al. Effects of granulosa cells on steroidogenesis, proliferation and apoptosis of stromal cells and theca cells derived from the goat ovary. J Steroid Biochem Mol Biol. 2013;138:325-33.

91. Vitt UA, McGee EA, Hayashi M, Hsueh AJ. In vivo treatment with GDF-9 stimulates primordial and primary follicle progression and theca cell marker CYP17 in ovaries of immature rats. Endocrinology. 2000;141(10):3814-20.

92. Soares M, Sahrari K, Amorim CA, Saussoy P, Donnez J, Dolmans MM. Evaluation of a human ovarian follicle isolation technique to obtain disease-free follicle suspensions before safely grafting to cancer patients. Fertil Steril. 2015;104(3):672-80 e2.

93. Soares M, Saussoy P, Maskens M, Reul H, Amorim CA, Donnez J, et al. Eliminating malignant cells from cryopreserved ovarian tissue is possible in leukaemia patients. Br J Haematol. 2017;178(2):231-9.

CHAPTER 6

References

Abagnale G, Sechi A, Steger M, Zhou Q, Kuo CC, Aydin G, Schalla C, Muller-Newen G, Zenke M, Costa IG *et al.* Surface Topography Guides Morphology and Spatial Patterning of Induced Pluripotent Stem Cell Colonies. *Stem Cell Reports* 2017;9: 654-666.

Abbassi L, Malki S, Cockburn K, Macaulay A, Robert C, Rossant J, Clarke HJ. Multiple Mechanisms Cooperate to Constitutively Exclude the Transcriptional Co-Activator YAP from the Nucleus During Murine Oogenesis. *Biol Reprod* 2016;94: 102.

Abir R, Fisch B, Nitke S, Okon E, Raz A, Ben Rafael Z. Morphological study of fully and partially isolated early human follicles. *Fertil Steril* 2001;75: 141-146.

Abir R, Roizman P, Fisch B, Nitke S, Okon E, Orvieto R, Ben Rafael Z. Pilot study of isolated early human follicles cultured in collagen gels for 24 hours. *Human Reproduction* 1999;14: 1299-1301.

Adam M, Saller S, Strobl S, Hennebold JD, Dissen GA, Ojeda SR, Stouffer RL, Berg D, Berg U, Mayerhofer A. Decorin is a part of the ovarian extracellular matrix in primates and may act as a signaling molecule. *Hum Reprod* 2012;27: 3249-3258.

Adhikari AS, Chai J, Dunn AR. Mechanical load induces a 100-fold increase in the rate of collagen proteolysis by MMP-1. *J Am Chem Soc* 2011;133: 1686-1689.

Adhikari D, Liu K. Molecular mechanisms underlying the activation of mammalian primordial follicles. *Endocr Rev* 2009;30: 438-464.

Adhikari D, Zheng W, Shen Y, Gorre N, Hamalainen T, Cooney AJ, Huhtaniemi I, Lan ZJ, Liu K. Tsc/mTORC1 signaling in oocytes governs the quiescence and activation of primordial follicles. *Hum Mol Genet* 2010;19: 397-410.

Adriaens I, Cortvrindt R, Smitz J. Differential FSH exposure in preantral follicle culture has marked effects on folliculogenesis and oocyte developmental competence. *Hum Reprod* 2004;19: 398-408.

Aebersold R, Mann M. Mass-spectrometric exploration of proteome structure and function. *Nature* 2016;537: 347-355.

Aitken A. 14-3-3 proteins: a historic overview. *Semin Cancer Biol* 2006;16: 162-172.

Aitken KJ, Bagli DJ. The bladder extracellular matrix. Part I: architecture, development and disease. *Nat Rev Urol* 2009;6: 596-611.

Akhmanova M, Osidak E, Domogatsky S, Rodin S, Domogatskaya A. Physical, Spatial, and Molecular Aspects of Extracellular Matrix of In Vivo Niches and Artificial Scaffolds Relevant to Stem Cells Research. *Stem Cells Int* 2015;2015: 167025.

Al-Alem L, Bridges PJ, Su W, Gong MC, Iglarz M, Ko C. Endothelin-2 induces oviductal contraction via endothelin receptor subtype A in rats. *J Endocrinol* 2007;193: 383-391.

Alshaikh AB, Padma AM, Dehlin M, Akouri R, Song MJ, Brannstrom M, Hellstrom M. Decellularization of the mouse ovary: comparison of different scaffold generation protocols for future ovarian bioengineering. *J Ovarian Res* 2019;12: 58.

Ambekar AS, Kelkar DS, Pinto SM, Sharma R, Hinduja I, Zaveri K, Pandey A, Prasad TS, Gowda H, Mukherjee S. Proteomics of follicular fluid from women with polycystic ovary syndrome suggests molecular defects in follicular development. *J Clin Endocrinol Metab* 2015;100: 744-753.

Amorim CA. Artificial Ovary. In Suzuki N and Donnez J (eds) *Gonadal Tissue Cryopreservation in Fertility Preservation*. 2016. Springer Japan, Tokyo, pp. 175-192.

Amorim CA, Dolmans MM, David A, Jaeger J, Vanacker J, Camboni A, Donnez J, Van Langendonckt A. Vitrification and xenografting of human ovarian tissue. *Fertil Steril* 2012;98: 1291-1298 e1291-1292.

Amorim CA, Shikanov A. The artificial ovary: current status and future perspectives. *Future Oncol* 2016;12: 2323-2332.

Amorim CA, Van Langendonckt A, David A, Dolmans MM, Donnez J. Survival of human pre-antral follicles after cryopreservation of ovarian tissue, follicular isolation and in vitro culture in a calcium alginate matrix. *Hum Reprod* 2009;24: 92-99.

Andablo-Reyes E, Bryant M, Neville A, Hyde P, Sarkar R, Francis M,Sarkar A. 3D Biomimetic Tongue-Emulating Surfaces for Tribological Applications. *ACS Appl Mater Interfaces* 2020;12: 49371-49385.

Anderson RA, McLaughlin M, Wallace WH, Albertini DF, Telfer EE. The immature human ovary shows loss of abnormal follicles and increasing follicle developmental competence through childhood andadolescence. *Hum Reprod* 2014;29: 97-106.

Angelucci S, Ciavardelli D, Di Giuseppe F, Eleuterio E, Sulpizio M, Tiboni GM, Giampietro F, Palumbo P, Di Ilio C. Proteome analysis of human follicular fluid. *Biochim Biophys Acta* 2006;1764: 1775-1785.

Apte SS. A disintegrin-like and metalloprotease (reprolysin-type) with thrombospondin type 1 motif (ADAMTS) superfamily: functions and mechanisms. *J Biol Chem* 2009;284: 31493-31497.

Aszodi A, Legate KR, Nakchbandi I, Fassler R. What mouse mutants teach us about extracellular matrix function. *Annu Rev Cell Dev Biol* 2006;22: 591-621.

Ata B, Seyhan A, Seli E. Diminished ovarian reserve versus ovarian aging: overlaps and differences. *Curr Opin Obstet Gynecol* 2019;31: 139- 147.

Aziz AUR, Fu M, Deng J, Geng C, Luo Y, Lin B, Yu X, Liu B. A Microfluidic Device for Culturing an Encapsulated Ovarian Follicle. *Micromachines (Basel)* 2017;8.

Badylak S. Perspective: Work with, not against, biology. *Nature* 2016;540: S55.

Badylak SF, Brown BN, Gilbert TW, Daly KA, Huber A, Turner NJ. Biologic scaffolds for constructive tissue remodeling. *Biomaterials* 2011;32: 316-319.

Baird DT, Webb R, Campbell BK, Harkness LM, Gosden RG. Long-term ovarian function in sheep after ovariectomy and transplantation of autografts stored at -196 C. *Endocrinology* 1999;140: 462-471.

Banyai L, Sonderegger P, Patthy L. Agrin binds BMP2, BMP4 and TGFbeta1. *PLoS One* 2010;5: e10758.

Bateman JF, Boot-Handford RP, Lamande SR. Genetic diseases of connective tissues: cellular and extracellular effects of ECM mutations. *Nat Rev Genet* 2009;10: 173-183.

Behl M, Razzaq MY, Lendlein A. Multifunctional shape-memory polymers. *Adv Mater* 2010;22: 3388-3410.

Bentov Y, Jurisicova A, Kenigsberg S, Casper RF. What maintains the high intra-follicular estradiol concentration in pre-ovulatory follicles? *J Assist Reprod Genet* 2016;33: 85-94.

Berg JM, Tymoczko JL, Stryer L. Carbohydrates Can Be Attached to Proteins to Form Glycoproteins
In Freeman WH (ed) *Biochemistry 5th edition* 2002, New York.

Berkholtz CB, Lai BE, Woodruff TK, Shea LD. Distribution of extracellular matrix proteins type I collagen, type IV collagen, fibronectin, and laminin in mouse folliculogenesis. *Histochem Cell Biol* 2006;126: 583-592.

Biela SA, Su Y, Spatz JP, Kemkemer R. Different sensitivity of human endothelial cells, smooth muscle cells and fibroblasts to topography in the nano-micro range. *Acta Biomater* 2009;5: 2460-2466.

Bilodeau C, Goltsis O, Rogers IM, Post M. Limitations of recellularized biological scaffolds for human transplantation. *J Tissue Eng Regen Med* 2020;14: 521-538.

Birch HL. Extracellular Matrix and Ageing. *Subcell Biochem* 2018;90: 169-190.

Bix G, Iozzo RV. Matrix revolutions: "tails" of basement-membrane components with angiostatic functions. *Trends Cell Biol* 2005;15: 52-60.

Bodis J, Papp S, Vermes I, Sulyok E, Tamas P, Farkas B, Zambo K, Hatzipetros I, Kovacs GL. "Platelet-associated regulatory system (PARS)" with particular reference to female reproduction. *J Ovarian Res* 2014;7: 55.

Bonnans C, Chou J, Werb Z. Remodelling the extracellular matrix in development and disease. *Nat Rev Mol Cell Biol* 2014;15: 786-801.

Bredfeldt JS, Liu Y, Conklin MW, Keely PJ, Mackie TR, Eliceiri KW. Automated quantification of aligned collagen for human breast carcinoma prognosis. *J Pathol Inform* 2014;5: 28.

Bredfeldt JS, Liu Y, Pehlke CA, Conklin MW, Szulczewski JM, Inman DR, Keely PJ, Nowak RD, Mackie TR, Eliceiri KW. Computational

segmentation of collagen fibers from second-harmonic generation images of breast cancer. *J Biomed Opt* 2014;19: 16007.

Bridges PJ, Jo M, Al Alem L, Na G, Su W, Gong MC, Jeoung M, Ko C. Production and binding of endothelin-2 (EDN2) in the rat ovary:endothelin receptor subtype A (EDNRA)-mediated contraction. *Reprod Fertil Dev* 2010;22: 780-787.

Brigstock DR. The connective tissue growth factor/cysteine-rich 61/nephroblastoma overexpressed (CCN) family. *Endocr Rev* 1999;20: 189-206.

Briley SM, Jasti S, McCracken JM, Hornick JE, Fegley B, Pritchard MT, Duncan FE. Reproductive age-associated fibrosis in the stroma of the mammalian ovary. *Reproduction* 2016;152: 245-260.

Bukovsky A. Novel methods of treating ovarian infertility in older and POF women, testicular infertility, and other human functional diseases. *Reprod Biol Endocrinol* 2015;13: 10.

Byron A, Humphries JD, Humphries MJ. Defining the extracellular matrix using proteomics. *Int J Exp Pathol* 2013;94: 75-92.

Cacciottola L, Nguyen TYT, Chiti MC, Camboni A, Amorim CA, Donnez J, Dolmans MM. Long-Term Advantages of Ovarian Reserve Maintenance and Follicle Development Using Adipose Tissue- Derived Stem Cells in Ovarian Tissue Transplantation. *Journal of clinical medicine* 2020;9.

Cai K, Bossert J, Jandt KD. Does the nanometre scale topography of titanium influence protein adsorption and cell proliferation? *Colloids Surf B Biointerfaces* 2006;49: 136-144.

Caliari SR, Burdick JA. A practical guide to hydrogels for cell culture. *Nat Methods* 2016;13: 405-414.

Campbell BK, Hernandez-Medrano J, Onions V, Pincott-Allen C, Aljaser F, Fisher J, McNeilly AS, Webb R, Picton HM. Restoration of ovarian function and natural fertility following the cryopreservation and autotransplantation of whole adult sheep ovaries. *Hum Reprod* 2014;29: 1749-1763.

Campbell KR, Campagnola PJ. Assessing local stromal alterations in human ovarian cancer subtypes via second harmonic generation microscopyand analysis. *J Biomed Opt* 2017;22: 1-7.

Cantley LC. The phosphoinositide 3-kinase pathway. *Science* 2002;296: 1655-1657.

Carey SP, Kraning-Rush CM, Williams RM, Reinhart-King CA. Biophysical control of invasive tumor cell behavior by extracellular matrix microarchitecture. *Biomaterials* 2012;33: 4157-4165.

Carlsson IB, Scott JE, Visser JA, Ritvos O, Themmen AP, Hovatta O. Anti-Mullerian hormone inhibits initiation of growth of human primordial ovarian follicles in vitro. *Hum Reprod* 2006;21: 2223-2227.

Castrillon DH, Miao L, Kollipara R, Horner JW, DePinho RA. Suppression of

ovarian follicle activation in mice by the transcription factor Foxo3a. *Science* 2003;301: 215-218.
Cawston TE, Young DA. Proteinases involved in matrix turnover during cartilage and bone breakdown. *Cell Tissue Res* 2010;339: 221-235.
Cecconi S, Mauro A, Cellini V, Patacchiola F. The role of Akt signalling in the mammalian ovary. *Int J Dev Biol* 2012;56: 809-817.
Cescon M, Gattazzo F, Chen P, Bonaldo P. Collagen VI at a glance. *J Cell Sci* 2015;128: 3525-3531.
Chakraborty P, Roy SK. Bone morphogenetic protein 2 promotes primordial follicle formation in the ovary. *Sci Rep* 2015;5: 12664.
Chang YH, Gregorich ZR, Chen AJ, Hwang L, Guner H, Yu D,Zhang J, Ge Y. New mass-spectrometry-compatible degradable surfactant for tissue proteomics. *J Proteome Res* 2015;14: 1587-1599.
Chaudhuri PK, Pan CQ, Low BC, Lim CT. Topography induces differential sensitivity on cancer cell proliferation via Rho-ROCK-Myosin contractility. *Sci Rep* 2016;6: 19672.
Chen EI, Cociorva D, Norris JL, Yates JR, 3rd. Optimization of mass spectrometry-compatible surfactants for shotgun proteomics. *JProteome Res* 2007;6: 2529-2538.
Cheng HW, Tsui YK, Cheung KM, Chan D, Chan BP. Decellularization of chondrocyte-encapsulated collagen microspheres: a three- dimensional model to study the effects of acellular matrix on stem cellfate. *Tissue Eng Part C Methods* 2009;15: 697-706.
Cheng Y, Feng Y, Jansson L, Sato Y, Deguchi M, Kawamura K, Hsueh AJ. Actin polymerization-enhancing drugs promote ovarian follicle growth mediated by the Hippo signaling effector YAP. *FASEB J* 2015;29: 2423-2430.
Cheng Y, Kim J, Li XX, Hsueh AJ. Promotion of ovarian follicle growth following mTOR activation: synergistic effects of AKT stimulators. *PLoS One* 2015;10: e0117769.
Chiti MC, Dolmans MM, Donnez J, Amorim CA. Fibrin in Reproductive Tissue Engineering: A Review on Its Application as a Biomaterial for Fertility Preservation. *Ann Biomed Eng* 2017;45: 1650-1663.
Chiti MC, Dolmans MM, Hobeika M, Cernogoraz A, Donnez J, Amorim CA. A modified and tailored human follicle isolation procedure improves follicle recovery and survival. *J Ovarian Res* 2017;10: 71.
Chiti MC, Dolmans MM, Lucci CM, Paulini F, Donnez J, Amorim CA. Further insights into the impact of mouse follicle stage on graft outcome in an artificial ovary environment. *Mol Hum Reprod* 2017;23: 381-392.
Chiti MC, Dolmans MM, Orellana R, Soares M, Paulini F, Donnez J, Amorim CA. Influence of follicle stage on artificial ovary outcome using fibrin as a matrix. *Hum Reprod* 2016;31: 427-435.
Chiti MC, White LJ, Vanacker J, Ouni E, Des Rieux A, Dolmans MD, Amorim

CA. Hydrogel derived from decellularized bovine ovarian extracellular matrix supports human follicle survival in vitro. In Press OU (ed) *ESHRE*. 2020.

Cho E, Kim YY, Noh K, Ku SY. A new possibility in fertility preservation: The artificial ovary. *J Tissue Eng Regen Med* 2019;13: 1294-1315.

Choi HR, Cho KA, Kang HT, Lee JB, Kaeberlein M, Suh Y, Chung IK, Park SC. Restoration of senescent human diploid fibroblasts by modulation of the extracellular matrix. *Aging Cell* 2011;10: 148-157.

Choi JK, Agarwal P, Huang H, Zhao S, He X. The crucial role of mechanical heterogeneity in regulating follicle development and ovulation with engineered ovarian microtissue. *Biomaterials* 2014;35: 5122-5128.

Choi MG, Hynes RO. Biosynthesis and processing of fibronectin in NIL.8 hamster cells. *J Biol Chem* 1979;254: 12050-12055.

Colombatti A, Spessotto P, Doliana R, Mongiat M, Bressan GM, Esposito G. The EMILIN/Multimerin family. *Front Immunol* 2011;2: 93.

Cordeiro CN, Christianson MS, Selter JH, Segars JH, Jr. In Vitro Activation: A Possible New Frontier for Treatment of Primary Ovarian Insufficiency. *Reprod Sci* 2016;23: 429-438.

Cordeiro MH, Kim S-Y, Woodruff TK. Chapter 1 - Ovarian Follicle Biology and the Basis for Gonadotoxicity. In Anderson RA and Spears N (eds)*Cancer Treatment and the Ovary*. 2015. Academic Press, Boston, pp.3-20.

Cox SL, Shaw J, Jenkin G. Transplantation of cryopreserved fetal ovarian tissue to adult recipients in mice. *J Reprod Fertil* 1996;107: 315-322.

Curry TE, Jr., Osteen KG. Cyclic changes in the matrix metalloproteinase system in the ovary and uterus. *Biol Reprod* 2001;64: 1285-1296.

D'Amore A, Nasello G, Luketich SK, Denisenko D, Jacobs DL, Hoff R, Gibson G, Bruno A, M TR, Wagner WR. Meso-scale topological cues influence extracellular matrix production in a large deformation, elastomeric scaffold model. *Soft Matter* 2018;14: 8483-8495.

Da Silva-Buttkus P, Marcelli G, Franks S, Stark J, Hardy K. Inferring biological mechanisms from spatial analysis: prediction of a local inhibitor in the ovary. *Proc Natl Acad Sci U S A* 2009;106: 456-461.

Dalby MJ, Gadegaard N, Tare R, Andar A, Riehle MO, Herzyk P, Wilkinson CD, Oreffo RO. The control of human mesenchymal cell differentiation using nanoscale symmetry and disorder. *Nat Mater* 2007;6: 997-1003.

Dalby MJ, Riehle MO, Johnstone HJ, Affrossman S, Curtis AS. Polymer-demixed nanotopography: control of fibroblast spreading and proliferation. *Tissue Eng* 2002;8: 1099-1108.

Daley WP, Peters SB, Larsen M. Extracellular matrix dynamics in development and regenerative medicine. *J Cell Sci* 2008;121: 255- 264.

Dath C, Dethy A, Van Langendonckt A, Van Eyck AS, Amorim CA, Luyckx V, Donnez J, Dolmans MM. Endothelial cells are essential for ovarian stromal tissue restructuring after xenotransplantation of isolated ovarian

stromal cells. *Hum Reprod* 2011;26: 1431-1439.
Davis SR, Lambrinoudaki I, Lumsden M, Mishra GD, Pal L, Rees M, Santoro N, Simoncini T. Menopause. *Nat Rev Dis Primers* 2015;1: 15004.
Deckx S, Heggermont W, Carai P, Rienks M, Dresselaers T, Himmelreich U, van Leeuwen R, Lommen W, van der Velden J, Gonzalez A *et al.* Osteoglycin prevents the development of age-related diastolic dysfunction during pressure overload by reducing cardiac fibrosis and inflammation. *Matrix Biol* 2018;66: 110-124.
Desai N, Abdelhafez F, Calabro A, Falcone T. Three dimensional culture of fresh and vitrified mouse pre-antral follicles in a hyaluronan-based hydrogel: a preliminary investigation of a novel biomaterial for in vitro follicle maturation. *Reprod Biol Endocrinol* 2012;10: 29.
Dietrich F, Lelkes PI. Fine-tuning of a three-dimensional microcarrier-based angiogenesis assay for the analysis of endothelial-mesenchymal cellco-cultures in fibrin and collagen gels. *Angiogenesis* 2006;9: 111- 125.
Dolmans M-M, Amorim CA. FERTILITY PRESERVATION: Construction and use of artificial ovaries. *Reproduction* 2019;158: F15-F25.
Dolmans MM, Amorim CA. FERTILITY PRESERVATION: Construction and use of artificial ovaries. *Reproduction* 2019;158: F15-F25.
Dolmans MM, Cacciottola L, Amorim CA, Manavella D. Translational research aiming to improve survival of ovarian tissue transplants using adipose tissue-derived stem cells. *Acta obstetricia et gynecologica Scandinavica* 2019;98: 665-671.
Dolmans MM, Cordier F, Amorim CA, Donnez J, Vander Linden C. In vitro Activation Prior to Transplantation of Human Ovarian Tissue: Is It Truly Effective? *Front Endocrinol (Lausanne)* 2019;10: 520.
Dolmans MM, Donnez J. Fertility preservation in women for medical and social reasons: Oocytes vs ovarian tissue. *Best Pract Res Clin Obstet Gynaecol* 2021;70: 63-80.
Dolmans MM, Falcone T, Patrizio P. Importance of patient selection to analyze in vitro fertilization outcome with transplanted cryopreserved ovarian tissue. *Fertil Steril* 2020;114: 279-280.
Dolmans MM, Martinez-Madrid B, Gadisseux E, Guiot Y, Yuan WY, Torre A, Camboni A, Van Langendonckt A, Donnez J. Short-term transplantation of isolated human ovarian follicles and cortical tissue into nude mice. *Reproduction* 2007;134: 253-262.
Dolmans MM, Yuan WY, Camboni A, Torre A, Van Langendonckt A, Martinez-Madrid B, Donnez J. Development of antral follicles after xenografting of isolated small human preantral follicles. *Reprod Biomed Online* 2008;16: 705-711.
Donnez J, Dolmans MM, Demylle D, Jadoul P, Pirard C, Squifflet J, Martinez-Madrid B, van Langendonckt A. Livebirth after orthotopic transplantation

of cryopreserved ovarian tissue. *Lancet (London, England)* 2004;364: 1405-1410.

Donnez J, Martinez-Madrid B, Jadoul P, Van Langendonckt A, Demylle D, Dolmans MM. Ovarian tissue cryopreservation and transplantation: a review. *Hum Reprod Update* 2006;12: 519-535.

Duckworth BC, Weaver JS, Ruderman JV. G2 arrest in Xenopus oocytes depends on phosphorylation of cdc25 by protein kinase A. *Proc Natl Acad Sci U S A* 2002;99: 16794-16799.

DuFort CC, Paszek MJ, Weaver VM. Balancing forces: architectural control of mechanotransduction. *Nat Rev Mol Cell Biol* 2011;12: 308-319.

Duncan FE, Jasti S, Paulson A, Kelsh JM, Fegley B, Gerton JL. Age-associated dysregulation of protein metabolism in the mammalian oocyte. *Aging Cell* 2017;16: 1381-1393.

Durlinger AL, Gruijters MJ, Kramer P, Karels B, Ingraham HA, Nachtigal MW, Uilenbroek JT, Grootegoed JA, Themmen AP. Anti-Mullerian hormone inhibits initiation of primordial follicle growth in the mouse ovary. *Endocrinology* 2002;143: 1076-1084.

Ebner T, Moser M, Sommergruber M, Puchner M, Wiesinger R, Tews G. Developmental competence of oocytes showing increased cytoplasmic viscosity. *Hum Reprod* 2003;18: 1294-1298.

Edson MA, Nagaraja AK, Matzuk MM. The mammalian ovary from genesis to revelation. *Endocr Rev* 2009;30: 624-712.

Edwards RG, Fowler RE, Gore-Langton RE, Gosden RG, Jones EC, Readhead C, Steptoe PC. Normal and abnormal follicular growth in mouse, rat and human ovaries. *J Reprod Fertil* 1977;51: 237-263.

El-Hayek S, Yang Q, Abbassi L, FitzHarris G, Clarke HJ. Mammalian Oocytes Locally Remodel Follicular Architecture to Provide the Foundation for Germline-Soma Communication. *Curr Biol* 2018;28: 1124-1131 e1123.

Eppig JJ. Oocyte control of ovarian follicular development and function in mammals. *Reproduction* 2001;122: 829-838.

Ernst EH, Grondahl ML, Grund S, Hardy K, Heuck A, Sunde L, Franks S, Andersen CY, Villesen P, Lykke-Hartmann K. Dormancy and activation of human oocytes from primordial and primary follicles: molecular clues to oocyte regulation. *Hum Reprod* 2017;32: 1684- 1700.

Ewald CY. The Matrisome during Aging and Longevity: A Systems-Level Approach toward Defining Matreotypes Promoting Healthy Aging. *Gerontology* 2020;66: 266-274.

Eyre DR, Weis MA, Wu JJ. Advances in collagen cross-link analysis. *Methods* 2008;45: 65-74.

Ezzati MM, Baker MD, Saatcioglu HD, Aloisio GM, Pena CG, Nakada Y, Cuevas I, Carr BR, Castrillon DH. Regulation of FOXO3 subcellular

localization by Kit ligand in the neonatal mouse ovary. *J AssistReprod Genet* 2015;32: 1741-1747.

Faddy MJ, Gosden RG. A mathematical model of follicle dynamics in the human ovary. *Hum Reprod* 1995;10: 770-775.

Faire M, Skillern A, Arora R, Nguyen DH, Wang J, Chamberlain C, German MS, Fung JC, Laird DJ. Follicle dynamics and global organization in the intact mouse ovary. *Dev Biol* 2015;403: 69-79.

Fallahi A, Yazdi IK, Serex L, Lesha E, Faramarzi N, Tarlan F, Avci H, Costa-Almeida R, Sharifi F, Rinoldi C *et al.* Customizable Composite Fibersfor Engineering Skeletal Muscle Models. *ACS Biomater Sci Eng* 2020;6: 1112-1123.

Fan X, Bialecka M, Moustakas I, Lam E, Torrens-Juaneda V, Borggreven NV, Trouw L, Louwe LA, Pilgram GSK, Mei H *et al.* Single-cellreconstruction of follicular remodeling in the human adult ovary. *Nat Commun* 2019;10: 3164.

Fisher GJ, Quan T, Purohit T, Shao Y, Cho MK, He T, Varani J, Kang S, Voorhees JJ. Collagen fragmentation promotes oxidative stress and elevates matrix metalloproteinase-1 in fibroblasts in aged human skin. *Am J Pathol* 2009;174: 101-114.

Foley KG, Pritchard MT, Duncan FE. Macrophage-derived multinucleated giant cells: hallmarks of the aging ovary. *Reproduction* 2021;161: V5-V9.

Forabosco A, Sforza C. Establishment of ovarian reserve: a quantitative morphometric study of the developing human ovary. *Fertil Steril*2007;88: 675-683.

Ford EA, Beckett EL, Roman SD, McLaughlin EA, Sutherland JM. Advances in human primordial follicle activation and premature ovarian insufficiency. *Reproduction* 2020;159: R15-R29.

Fratzl P. Collagen: Structure and Mechanics, an Introduction. In Fratzl P (ed) *Collagen: Structure and Mechanics*. 2008. Springer US, Boston, MA,pp. 1-13.

Friedl P, Maaser K, Klein CE, Niggemann B, Krohne G, Zanker KS. Migration of highly aggressive MV3 melanoma cells in 3-dimensional collagen lattices results in local matrix reorganization and shedding of alpha2 and beta1 integrins and CD44. *Cancer Res* 1997;57: 2061-2070.

Ganeva I, Kukulski W. Membrane Architecture in the Spotlight of Correlative Microscopy. *Trends Cell Biol* 2020;30: 577-587.

Gaytan F, Morales C, Leon S, Garcia-Galiano D, Roa J, Tena-Sempere M. Crowding and Follicular Fate: Spatial Determinants of Follicular Reserve and Activation of Follicular Growth in the Mammalian Ovary.*PLoS One* 2015;10: e0144099.

Gershon E, Dekel N. Newly Identified Regulators of Ovarian Folliculogenesis and Ovulation. 2020;21: 4565.

Gjaltema RA, Bank RA. Molecular insights into prolyl and lysyl hydroxylation of fibrillar collagens in health and disease. *Crit Rev Biochem Mol Biol* 2017;52: 74-95.

Gosden RG. Restitution of fertility in sterilized mice by transferring primordial ovarian follicles. *Hum Reprod* 1990;5: 499-504.

Gosden RG, Baird DT, Wade JC, Webb R. Restoration of fertility to oophorectomized sheep by ovarian autografts stored at -196 degreesC. *Hum Reprod* 1994;9: 597-603.

Goto M, Iwase A, Ando H, Kurotsuchi S, Harata T, Kikkawa F. PTEN and Akt expression during growth of human ovarian follicles. *J Assist Reprod Genet* 2007;24: 541-546.

Gougeon A. Regulation of ovarian follicular development in primates: facts and hypotheses. *Endocr Rev* 1996;17: 121-155.

Gougeon A. Human ovarian follicular development: from activation of resting follicles to preovulatory maturation. *Ann Endocrinol (Paris)* 2010;71: 132-143.

Grive KJ, Freiman RN. The developmental origins of the mammalian ovarian reserve. *Development* 2015;142: 2554-2563.

Gu BK, Choi DJ, Park SJ, Kim MS, Kang CM, Kim CH. 3-dimensional bioprinting for tissue engineering applications. *Biomater Res* 2016;20: 12.

Guillemot F, Mironov V, Nakamura M. Bioprinting is coming of age: Report from the International Conference on Bioprinting and Biofabrication in Bordeaux (3B'09). *Biofabrication* 2010;2: 010201.

Guillotin B, Souquet A, Catros S, Duocastella M, Pippenger B, Bellance S, Bareille R, Remy M, Bordenave L, Amedee J *et al.* Laser assisted bioprinting of engineered tissue with high cell density and microscale organization. *Biomaterials* 2010;31: 7250-7256.

Hagen CP, Aksglaede L, Sorensen K, Mouritsen A, Andersson AM, Petersen JH, Main KM, Juul A. Individual serum levels of anti-Mullerian hormone in healthy girls persist through childhood and adolescence: a longitudinal cohort study. *Hum Reprod* 2012;27: 861-866.

Hansen KR, Knowlton NS, Thyer AC, Charleston JS, Soules MR, Klein NA. A new model of reproductive aging: the decline in ovarian non-growing follicle number from birth to menopause. *Hum Reprod* 2008;23: 699-708.

Harjanto D, Maffei JS, Zaman MH. Quantitative analysis of the effect of cancer invasiveness and collagen concentration on 3D matrix remodeling. *PLoS One* 2011;6: e24891.

Harp R, Leibach J, Black J, Keldahl C, Karow A. Cryopreservation of murine ovarian tissue. *Cryobiology* 1994;31: 336-343.

Hartshorne GM, Lyrakou S, Hamoda H, Oloto E, Ghafari F. Oogenesis and cell death in human prenatal ovaries: what are the criteria for oocyte selection? *Mol Hum Reprod* 2009;15: 805-819.

Hassanpour A, Talaei-Khozani T, Kargar-Abarghouei E, Razban V, Vojdani Z. Decellularized human ovarian scaffold based on a sodium lauryl ester sulfate (SLES)-treated protocol, as a natural three-dimensional scaffold for construction of bioengineered ovaries. *Stem Cell Res Ther* 2018;9: 252.

Henning NF, LeDuc RD, Even KA, Laronda MM. Proteomic analyses of decellularized porcine ovaries identified new matrisome proteins and spatial differences across and within ovarian compartments. *Scientific Reports* 2019;9: 20001.

Herr D, Bekes I, Wulff C. Local Renin-Angiotensin system in the reproductive system. *Front Endocrinol (Lausanne)* 2013;4: 150.

Hertig AT. The Aging Ovary—A Preliminary Note. *The Journal of Clinical Endocrinology & Metabolism* 1944;4: 581-582.

Hirota Y, Osuga Y, Yoshino O, Koga K, Yano T, Hirata T, Nose E, Ayabe T, Namba A, Tsutsumi O *et al.* Possible roles of thrombin-inducedactivation of protease-activated receptor 1 in human luteinized granulosa cells. *J Clin Endocrinol Metab* 2003;88: 3952-3957.

Hoganson DM, Owens GE, O'Doherty EM, Bowley CM, Goldman SM, Harilal DO, Neville CM, Kronengold RT, Vacanti JP. Preserved extracellular matrix components and retained biological activity in decellularized porcine mesothelium. *Biomaterials* 2010;31: 6934-6940.

Honda A, Hirose M, Hara K, Matoba S, Inoue K, Miki H, Hiura H, Kanatsu-Shinohara M, Kanai Y, Kono T *et al.* Isolation, characterization, and in vitro and in vivo differentiation of putative thecal stem cells. *Proc Natl Acad Sci U S A* 2007;104: 12389-12394.

Hornick JE, Duncan FE, Shea LD, Woodruff TK. Isolated primate primordial follicles require a rigid physical environment to survive and grow in vitro. *Hum Reprod* 2012;27: 1801-1810.

Hornick JE, Duncan FE, Shea LD, Woodruff TK. Multiple follicle culture supports primary follicle growth through paracrine-acting signals. *Reproduction* 2013;145: 19-32.

Hovatta O, Silye R, Krausz T, Abir R, Margara R, Trew G, Lass A, Winston RM. Cryopreservation of human ovarian tissue using dimethylsulphoxide and propanediol-sucrose as cryoprotectants. *Hum Reprod* 1996;11: 1268-1272.

Howarth S, Dourmashkin R. A technique for the study of myogenesis in vitro.*Exp Cell Res* 1958.

Howlett AR, Bailey N, Damsky C, Petersen OW, Bissell MJ. Cellular growth and survival are mediated by beta 1 integrins in normal human breast epithelium but not in breast carcinoma. *J Cell Sci* 1995;108 (Pt 5): 1945-1957.

Hsieh M, Lee D, Panigone S, Horner K, Chen R, Theologis A, Lee DC,

Threadgill DW, Conti M. Luteinizing hormone-dependent activation ofthe epidermal growth factor network is essential for ovulation. *Mol Cell Biol* 2007;27: 1914-1924.

Hsueh AJ, Kawamura K, Cheng Y, Fauser BC. Intraovarian control of early folliculogenesis. *Endocr Rev* 2015;36: 1-24.

Hsueh AJW, Kawamura K. Hippo signaling disruption and ovarian follicle activation in infertile patients. *Fertil Steril* 2020;114: 458-464.

Huang J, Chen Y, Tang C, Fei Y, Wu H, Ruan D, Paul ME, Chen X, Yin Z, Heng BC *et al.* The relationship between substrate topography and stem cell differentiation in the musculoskeletal system. *Cell Mol Life Sci* 2019;76: 505-521.

Huebsch N, Arany PR, Mao AS, Shvartsman D, Ali OA, Bencherif SA, Rivera-Feliciano J, Mooney DJ. Harnessing traction-mediated manipulation of the cell/matrix interface to control stem-cell fate. *Nat Mater* 2010;9: 518-526.

Huet C, Pisselet C, Mandon-Pepin B, Monget P, Monniaux D. Extracellular matrix regulates ovine granulosa cell survival, proliferation and steroidogenesis: relationships between cell shape and function. *J Endocrinol* 2001;169: 347-360.

Hummitzsch K, Irving-Rodgers HF, Schwartz J, Rodgers RJ. Chapter 4 - Development of the Mammalian Ovary and Follicles. In Leung PCK and Adashi EY (eds) *The Ovary (Third Edition)*. 2019. Academic Press, pp. 71-82.

Humphrey JD, Dufresne ER, Schwartz MA. Mechanotransduction and extracellular matrix homeostasis. *Nat Rev Mol Cell Biol* 2014;15: 802-812.

Hynes RO. Cell-matrix adhesion in vascular development. *J Thromb Haemost* 2007;5 Suppl 1: 32-40.

Hynes RO. The extracellular matrix: not just pretty fibrils. *Science* 2009;326: 1216-1219.

Hynes RO, Naba A. Overview of the matrisome--an inventory of extracellular matrix constituents and functions. *Cold Spring Harb Perspect Biol* 2012;4: a004903.

Iismaa SE, Mearns BM, Lorand L, Graham RM. Transglutaminases and disease: lessons from genetically engineered mouse models and inherited disorders. *Physiol Rev* 2009;89: 991-1023.

Iozzo RV, Murdoch AD. Proteoglycans of the extracellular environment: clues from the gene and protein side offer novel perspectives in molecular diversity and function. *FASEB J* 1996;10: 598-614.

Iozzo RV, Zoeller JJ, Nyström A. Basement membrane proteoglycans: modulators Par Excellence of cancer growth and angiogenesis. *Mol Cells* 2009;27: 503-513.

Irving-Rodgers HF, Harland ML, Rodgers RJ. A novel basal lamina matrix of

the stratified epithelium of the ovarian follicle. *Matrix Biol* 2004;23: 207-217.

Irving-Rodgers HF, Mussard ML, Kinder JE, Rodgers RJ. Composition and morphology of the follicular basal lamina during atresia of bovine antral follicles. *Reproduction* 2002;123: 97-106.

Iwahashi M, Muragaki Y, Ooshima A, Nakano R. Type VI collagen expression during growth of human ovarian follicles. *Fertil Steril*2000;74: 343-347.

Jansen KA, Licup AJ, Sharma A, Rens R, MacKintosh FC, Koenderink GH. The Role of Network Architecture in Collagen Mechanics. *Biophys J* 2018;114: 2665-2678.

Janson IA, Putnam AJ. Extracellular matrix elasticity and topography: material-based cues that affect cell function via conserved mechanisms. *J Biomed Mater Res A* 2015;103: 1246-1258.

Jarkovska K, Martinkova J, Liskova L, Halada P, Moos J, Rezabek K, Gadher SJ, Kovarova H. Proteome mining of human follicular fluid reveals a crucial role of complement cascade and key biological pathways in women undergoing in vitro fertilization. *J Proteome Res* 2010;9:1289-1301.

Jarvelainen H, Sainio A, Koulu M, Wight TN, Penttinen R. Extracellular matrix molecules: potential targets in pharmacotherapy. *Pharmacol Rev* 2009;61: 198-223.

Jeppesen JV, Anderson RA, Kelsey TW, Christiansen SL, Kristensen SG, Jayaprakasan K, Raine-Fenning N, Campbell BK, Yding Andersen C. Which follicles make the most anti-Mullerian hormone in humans?

Evidence for an abrupt decline in AMH production at the time of follicle selection. *Mol Hum Reprod* 2013;19: 519-527.

Jiang ZZ, Hu MW, Ma XS, Schatten H, Fan HY, Wang ZB, Sun QY. LKB1 acts as a critical gatekeeper of ovarian primordial follicle pool. *Oncotarget* 2016;7: 5738-5753.

John GB, Gallardo TD, Shirley LJ, Castrillon DH. Foxo3 is a PI3K-dependent molecular switch controlling the initiation of oocyte growth. *Dev Biol* 2008;321: 197-204.

Joo S, Oh SH, Sittadjody S, Opara EC, Jackson JD, Lee SJ, Yoo JJ, Atala A. The effect of collagen hydrogel on 3D culture of ovarian follicles. *Biomed Mater* 2016;11: 065009.

Jorge S, Chang S, Barzilai JJ, Leppert P, Segars JH. Mechanical signaling in reproductive tissues: mechanisms and importance. *Reprod Sci* 2014;21: 1093-1107.

Judd HL. Hormonal dynamics associated with the menopause. *Clin Obstet Gynecol* 1976;19: 775-788.

Kao AP, Connelly JT, Barber AH. 3D nanomechanical evaluations of dermal structures in skin. *J Mech Behav Biomed Mater* 2016;57: 14-23.

Karsdal MA, Daniels SJ, Holm Nielsen S, Bager C, Rasmussen DGK,

Loomba R, Surabattula R, Villesen IF, Luo Y, Shevell D *et al.* Collagen biology and non-invasive biomarkers of liver fibrosis. *Liver Int* 2020;40: 736-750.

Karsdal MA, Nielsen SH, Leeming DJ, Langholm LL, Nielsen MJ, Manon-Jensen T, Siebuhr A, Gudmann NS, Ronnow S, Sand JM *et al.* The good and the bad collagens of fibrosis - Their role in signaling and organ function. *Adv Drug Deliv Rev* 2017;121: 43-56.

Karuri NW, Liliensiek S, Teixeira AI, Abrams G, Campbell S, Nealey PF, Murphy CJ. Biological length scale topography enhances cell-substratum adhesion of human corneal epithelial cells. *J Cell Sci* 2004;117: 3153-3164.

Kawamura K, Cheng Y, Suzuki N, Deguchi M, Sato Y, Takae S, Ho CH, Kawamura N, Tamura M, Hashimoto S *et al.* Hippo signaling disruption and Akt stimulation of ovarian follicles for infertility treatment. *Proc Natl Acad Sci U S A* 2013;110: 17474-17479.

Kawashima I, Kawamura K. Regulation of follicle growth through hormonal factors and mechanical cues mediated by Hippo signaling pathway. *Syst Biol Reprod Med* 2018;64: 3-11.

Keith Moore TVNP, Mark Torchia. *Before We Are Born 9thEdition*, 2015. Saunders.

Kelsey TW, Anderson RA, Wright P, Nelson SM, Wallace WH. Data-driven assessment of the human ovarian reserve. *Mol Hum Reprod* 2012;18:79-87.

Kelsey TW, Wright P, Nelson SM, Anderson RA, Wallace WH. A validated model of serum anti-mullerian hormone from conception to menopause. *PLoS One* 2011;6: e22024.

Kerr JB, Myers M, Anderson RA. The dynamics of the primordial follicle reserve. *Reproduction* 2013;146: R205-215.

Kessenbrock K, Plaks V, Werb Z. Matrix metalloproteinases: regulators of the tumor microenvironment. *Cell* 2010;141: 52-67.

Khalilian M, Navidbakhsh M, Valojerdi MR, Chizari M, Yazdi PE. Estimating Young's modulus of zona pellucida by micropipette aspiration in combination with theoretical models of ovum. *J R Soc Interface*2010;7: 687-694.

Khang D, Choi J, Im YM, Kim YJ, Jang JH, Kang SS, Nam TH, Song J, Park JW. Role of subnano-, nano- and submicron-surface features on osteoblast differentiation of bone marrow mesenchymal stem cells. *Biomaterials* 2012;33: 5997-6007.

Khatiwala CB, Kim PD, Peyton SR, Putnam AJ. ECM compliance regulates osteogenesis by influencing MAPK signaling downstream of RhoA and ROCK. *J Bone Miner Res* 2009;24: 886-898.

Kilian KA, Bugarija B, Lahn BT, Mrksich M. Geometric cues for directing the differentiation of mesenchymal stem cells. *Proc Natl Acad Sci U S A*

2010;107: 4872-4877.
Kim DH, Provenzano PP, Smith CL, Levchenko A. Matrix nanotopography as a regulator of cell function. *J Cell Biol* 2012;197: 351-360.

Kim J, Perez AS, Claflin J, David A, Zhou H, Shikanov A. Synthetic hydrogel supports the function and regeneration of artificial ovarian tissue in mice. *NPJ Regen Med* 2016;1.
Kim SS. Fertility preservation in female cancer patients: current developments and future directions. *Fertil Steril* 2006;85: 1-11.
Kim SY, Ebbert K, Cordeiro MH, Romero M, Zhu J, Serna VA, Whelan KA, Woodruff TK, Kurita T. Cell autonomous phosphoinositide 3-kinase activation in oocytes disrupts normal ovarian function through promoting survival and overgrowth of ovarian follicles. *Endocrinology* 2015;156: 1464-1476.
Kinnear HM, Tomaszewski CE, Chang FL, Moravek MB, Xu M, Padmanabhan V, Shikanov A. The ovarian stroma as a new frontier. *Reproduction* 2020;160: R25-R39.
Kino T, Segars JH, Chrousos GP. The Guanine Nucleotide Exchange Factor Brx: A Link between Osmotic Stress, Inflammation and Organ Physiology and Pathophysiology. *Expert Rev Endocrinol Metab* 2010;5: 603-614.
Kirillova A, Ionov L. Shape-changing polymers for biomedical applications. *J Mater Chem B* 2019;7: 1597-1624.

Kirshner J, Chen CJ, Liu P, Huang J, Shively JE. CEACAM1-4S, a cell-cell adhesion molecule, mediates apoptosis and reverts mammary carcinoma cells to a normal morphogenic phenotype in a 3D culture. *Proc Natl Acad Sci U S A* 2003;100: 521-526.
Kleinman HK, McGarvey ML, Hassell JR, Star VL, Cannon FB, Laurie GW, Martin GR. Basement membrane complexes with biological activity. *Biochemistry* 1986;25: 312-318.
Kniazeva E, Hardy AN, Boukaidi SA, Woodruff TK, Jeruss JS, Shea LD. Primordial Follicle Transplantation within Designer Biomaterial Grafts Produce Live Births in a Mouse Infertility Model. *Sci Rep* 2015;5: 17709.
Knight PG, Satchell L, Glister C. Intra-ovarian roles of activins and inhibins. *Mol Cell Endocrinol* 2012;359: 53-65.
Ko C, Gieske MC, Al-Alem L, Hahn Y, Su W, Gong MC, Iglarz M, Koo Y. Endothelin-2 in ovarian follicle rupture. *Endocrinology* 2006;147: 1770-1779.
Kong YP, Tu CH, Donovan PJ, Yee AF. Expression of Oct4 in human embryonic stem cells is dependent on nanotopographical configuration. *Acta Biomater* 2013;9: 6369-6380.
Konishi I, Fujii S, Okamura H, Parmley T, Mori T. Development of interstitial cells and ovigerous cords in the human fetal ovary: an ultrastructural study. *J Anat* 1986;148: 121-135.

Koubova J, Menke DB, Zhou Q, Capel B, Griswold MD, Page DC. Retinoic acid regulates sex-specific timing of meiotic initiation in mice. *Proc Natl Acad Sci U S A* 2006;103: 2474-2479.

Kurylo MP, Grandfield K, Marshall GW, Altoe V, Aloni S, Ho SP. Effect of proteoglycans at interfaces as related to location, architecture, and mechanical cues. *Arch Oral Biol* 2016;63: 82-92.

Lampi MC, Reinhart-King CA. Targeting extracellular matrix stiffness to attenuate disease: From molecular mechanisms to clinical trials. *Sci Transl Med* 2018;10.

Laronda MM, Duncan FE, Hornick JE, Xu M, Pahnke JE, Whelan KA, Shea LD, Woodruff TK. Alginate encapsulation supports the growth and differentiation of human primordial follicles within ovarian cortical tissue. *J Assist Reprod Genet* 2014;31: 1013-1028.

Laronda MM, Jakus AE, Whelan KA, Wertheim JA, Shah RN, Woodruff TK. Initiation of puberty in mice following decellularized ovary transplant. *Biomaterials* 2015;50: 20-29.

Laronda MM, Rutz AL, Xiao S, Whelan KA, Duncan FE, Roth EW, Woodruff TK, Shah RN. A bioprosthetic ovary created using 3D printed microporous scaffolds restores ovarian function in sterilized mice. *Nat Commun* 2017;8: 15261.

Laronda MM, Woodruff TK. Opportunities for Enabling Puberty. In Woodruff TK and Gosiengfiao YC (eds) *Pediatric and Adolescent Oncofertility: Best Practices and Emerging Technologies*. 2017. Springer International Publishing, Cham, pp. 99-118.

Le Bellego F, Pisselet C, Huet C, Monget P, Monniaux D. Laminin-alpha6beta1 integrin interaction enhances survival and proliferation and modulates steroidogenesis of ovine granulosa cells. *J Endocrinol* 2002;172: 45-59.

Lee KY, Mooney DJ. Hydrogels for Tissue Engineering. *Chemical Reviews* 2001;101: 1869-1880.

LeMaire WJ. Mechanism of mammalian ovulation. *Steroids* 1989;54: 455-469.

Lendlein A, Behl M, Hiebl B, Wischke C. Shape-memory polymers as a technology platform for biomedical applications. *Expert review of medical devices* 2010;7: 357-379.

Levillain A, Orhant M, Turquier F, Hoc T. Contribution of collagen and elastin fibers to the mechanical behavior of an abdominal connective tissue.*J Mech Behav Biomed Mater* 2016;61: 308-317.

Li HW, Wong CY, Yeung WS, Ho PC, Ng EH. Serum anti-mullerian hormone level is not altered in women using hormonal contraceptives. *Contraception* 2011;83: 582-585.

Li J, Kawamura K, Cheng Y, Liu S, Klein C, Liu S, Duan EK, Hsueh AJ. Activation of dormant ovarian follicles to generate mature eggs. *Proc Natl*

Acad Sci U S A 2010;107: 10280-10284.
Li Y, Meng H, Liu Y, Lee BP. Fibrin gel as an injectable biodegradable scaffold and cell carrier for tissue engineering. *ScientificWorldJournal* 2015;2015: 685690.
Lim JY, Dreiss AD, Zhou Z, Hansen JC, Siedlecki CA, Hengstebeck RW, Cheng J, Winograd N, Donahue HJ. The regulation of integrin- mediated osteoblast focal adhesion and focal adhesion kinase expression by nanoscale topography. *Biomaterials* 2007;28: 1787- 1797.
Lin NYC, Homan KA, Robinson SS, Kolesky DB, Duarte N, Moisan A, Lewis JA. Renal reabsorption in 3D vascularized proximal tubule models. *Proc Natl Acad Sci U S A* 2019;116: 5399-5404.
Lin S, Sandig M, Mequanint K. Three-dimensional topography of synthetic scaffolds induces elastin synthesis by human coronary artery smooth muscle cells. *Tissue Eng Part A* 2011;17: 1561-1571.
Lindsey ML, Jung M, Hall ME, DeLeon-Pennell KY. Proteomic analysis of the cardiac extracellular matrix: clinical research applications. *Expert Rev Proteomics* 2018;15: 105-112.
Lintern-Moore S, Peters H, Moore GP, Faber M. Follicular development in the infant human ovary. *J Reprod Fertil* 1974;39: 53-64.
Liu WY, Lin SG, Zhuo RY, Xie YY, Pan W, Lin XF, Shen FX. Xenogeneic Decellularized Scaffold: A Novel Platform for Ovary Regeneration. *Tissue Eng Part C Methods* 2017;23: 61-71.
Liu X, Fernandes R, Jurisicova A, Casper RF, Sun Y. In situ mechanical characterization of mouse oocytes using a cell holding device. *Lab Chip* 2010;10: 2154-2161.
Loo RR, Dales N, Andrews PC. The effect of detergents on proteins analyzed by electrospray ionization. *Methods Mol Biol* 1996;61: 141-160.
Lorand L, Graham RM. Transglutaminases: crosslinking enzymes with pleiotropic functions. *Nat Rev Mol Cell Biol* 2003;4: 140-156.
Lu D, Luo C, Zhang C, Li Z, Long M. Differential regulation of morphology and stemness of mouse embryonic stem cells by substrate stiffness and topography. *Biomaterials* 2014;35: 3945-3955.
Lu H, Hoshiba T, Kawazoe N, Koda I, Song M, Chen G. Cultured cell-derived extracellular matrix scaffolds for tissue engineering. *Biomaterials* 2011;32: 9658-9666.
Lu P, Takai K, Weaver VM, Werb Z. Extracellular matrix degradation and remodeling in development and disease. *Cold Spring Harb Perspect Biol* 2011;3.
Lu X, Guo S, Cheng Y, Kim JH, Feng Y, Feng Y. Stimulation of ovarian follicle growth after AMPK inhibition. *Reproduction* 2017;153: 683-694.
Luck MR, Zhao Y, Silvester LM. Identification and localization of collagen types I and IV in the ruminant follicle and corpus luteum. *J Reprod Fertil Suppl* 1995;49: 517-521.

Lunding SA, Andersen AN, Hardardottir L, Olesen HO, Kristensen SG, Andersen CY, Pors SE. Hippo signaling, actin polymerization, and follicle activation in fragmented human ovarian cortex. *Mol Reprod Dev* 2020;87: 711-719.

Luyckx V, Dolmans MM, Vanacker J, Legat C, Fortuno Moya C, Donnez J, Amorim CA. A new step toward the artificial ovary: survival and proliferation of isolated murine follicles after autologous transplantation in a fibrin scaffold. *Fertil Steril* 2014;101: 1149-1156.

Luyckx V, Dolmans MM, Vanacker J, Scalercio SR, Donnez J, Amorim CA. First step in developing a 3D biodegradable fibrin scaffold for an artificial ovary. *J Ovarian Res* 2013;6: 83.

Majeed H, Okoro C, Kajdacsy-Balla A, Toussaint KC, Jr., Popescu G. Quantifying collagen fiber orientation in breast cancer using quantitative phase imaging. *J Biomed Opt* 2017;22: 46004.

Malmsten M, Emoto K, Van Alstine JM. Effect of Chain Density on Inhibition of Protein Adsorption by Poly(ethylene glycol) Based Coatings. *Journal of Colloid and Interface Science* 1998;202: 507-517.

Mammoto T, Mammoto A, Ingber DE. Mechanobiology and developmental control. *Annu Rev Cell Dev Biol* 2013;29: 27-61.

Mandrycky C, Wang Z, Kim K, Kim DH. 3D bioprinting for engineering complex tissues. *Biotechnol Adv* 2016;34: 422-434.

Marin L, Bedoschi G, Kawahara T, Oktay KH. History, Evolution and Current State of Ovarian Tissue Auto-Transplantation with Cryopreserved Tissue: a Successful Translational Research Journey from 1999 to 2020. *Reproductive Sciences* 2020;27: 955-962.

Martin JJ, Woods DC, Tilly JL. Implications and Current Limitations of Oogenesis from Female Germline or Oogonial Stem Cells in Adult Mammalian Ovaries. *Cells* 2019;8.

Maruhashi E, Ouni E, Vilela JMV, Amorim CA. Xeno-free human ovarian cell-derived extracellular matrix: prospects for a transplantable engineered ovary and beyond. *11th World Biomaterials Congress*. 2020, Virtual.

Masse V, Ferrari P, Boucoiran I, Delotte J, Isnard V, Bongain A. Normal serum concentrations of anti-Mullerian hormone in a population of fertile women in their first trimester of pregnancy. *Hum Reprod* 2011;26: 3431-3436.

Matousek M, Carati C, Gannon B, Brannstrom M. Novel method for intrafollicular pressure measurements in the rat ovary: increased intrafollicular pressure after hCG stimulation. *Reproduction* 2001;121: 307-314.

Matti N, Irving-Rodgers HF, Hatzirodos N, Sullivan TR, Rodgers RJ. Differential expression of focimatrix and steroidogenic enzymes before size deviation during waves of follicular development in bovineovarian follicles. *Mol Cell Endocrinol* 2010;321: 207-214.

Matzuk MM, Li Q. How the Oocyte Influences Follicular Cell Function and Why. In Coticchio G, Albertini DF and De Santis L (eds) *Oogenesis*. 2013. Springer London, London, pp. 75-92.

Mavrogonatou E, Pratsinis H, Papadopoulou A, Karamanos NK, Kletsas D. Extracellular matrix alterations in senescent cells and their significance in tissue homeostasis. *Matrix Biol* 2019;75-76: 27-42.

Mayorca-Guiliani AE, Madsen CD, Cox TR, Horton ER, Venning FA, Erler JT. ISDoT: in situ decellularization of tissues for high-resolution imaging and proteomic analysis of native extracellular matrix. *Nat Med* 2017;23: 890-898.

McArthur ME, Irving-Rodgers HF, Byers S, Rodgers RJ. Identification and immunolocalization of decorin, versican, perlecan, nidogen, and chondroitin sulfate proteoglycans in bovine small-antral ovarian follicles. *Biol Reprod* 2000;63: 913-924.

McGinnis LK, Kinsey WH. Role of focal adhesion kinase in oocyte-follicle communication. *Mol Reprod Dev* 2015;82: 90-102.

McLaughlin M, Patrizio P, Kayisli U, Luk J, Thomson TC, Anderson RA, Telfer EE, Johnson J. mTOR kinase inhibition results in oocyte loss characterized by empty follicles in human ovarian cortical strips cultured in vitro. *Fertil Steril* 2011;96: 1154-1159 e1151.

McMurray RJ, Gadegaard N, Tsimbouri PM, Burgess KV, McNamara LE, Tare R, Murawski K, Kingham E, Oreffo RO, Dalby MJ. Nanoscale surfaces for the long-term maintenance of mesenchymal stem cell phenotype and multipotency. *Nat Mater* 2011;10: 637-644.

Meister A, Gabi M, Behr P, Studer P, Voros J, Niedermann P, Bitterli J, Polesel-Maris J, Liley M, Heinzelmann H *et al.* FluidFM: combining atomic force microscopy and nanofluidics in a universal liquid deliverysystem for single cell applications and beyond. *Nano Lett* 2009;9: 2501-2507.

Meyer U. The History of Tissue Engineering and Regenerative Medicine in Perspective. In Meyer U, Handschel J, Wiesmann HP and Meyer T (eds) *Fundamentals of Tissue Engineering and RegenerativeMedicine*. 2009. Springer Berlin Heidelberg, Berlin, Heidelberg, pp. 5-12.

Mintz B, Illmensee K. Normal genetically mosaic mice produced from malignant teratocarcinoma cells. *Proc Natl Acad Sci U S A* 1975;72: 3585-3589.

Morley CD, Ellison ST, Bhattacharjee T, O'Bryan CS, Zhang Y, Smith KF, Kabb CP, Sebastian M, Moore GL, Schulze KD *et al.* Quantitative characterization of 3D bioprinted structural elements under cell generated forces. *Nat Commun* 2019;10: 3029.

Morrison DK. The 14-3-3 proteins: integrators of diverse signaling cues that impact cell fate and cancer development. *Trends Cell Biol* 2009;19: 16-23.

Mott JD, Werb Z. Regulation of matrix biology by matrix metalloproteinases.

Curr Opin Cell Biol 2004;16: 558-564.
Mouloungui E, Zver T, Roux C, Amiot C. A protocol to isolate and qualify purified human preantral follicles in cases of acute leukemia, for future clinical applications. *J Ovarian Res* 2018;11: 4.
Muiznieks LD, Keeley FW. Molecular assembly and mechanical properties of the extracellular matrix: A fibrous protein perspective. *Biochim Biophys Acta* 2013;1832: 866-875.
Munger JS, Sheppard D. Cross talk among TGF-beta signaling pathways, integrins, and the extracellular matrix. *Cold Spring Harb Perspect Biol* 2011;3: a005017.
Murayama Y, Mizuno J, Kamakura H, Fueta Y, Nakamura H, Akaishi K, Anzai K, Watanabe A, Inui H, Omata S. Mouse zona pellucida dynamically changes its elasticity during oocyte maturation, fertilization and early embryo development. *Hum Cell* 2006;19: 119- 125.
Murayama Y, Yoshida M, Mizuno J, Nakamura H, Inoue S, Watanabe Y, Akaishi K, Inui H, Constantinou CE, Omata S. Elasticity Measurementof Zona Pellucida Using a Micro Tactile Sensor to Evaluate Embryo Quality. 2008;25 %J Journal of Mammalian Ova Research: 8-16, 19.
Murdoch WJ. Proteolytic and cellular death mechanisms in ovulatory ovarian rupture. *Biol Signals Recept* 2000;9: 102-114.
Murdoch WJ, Gottsch ML. Proteolytic Mechanisms in the Ovulatory Folliculo-Luteal Transformation. *Connective Tissue Research* 2003;44: 50-57. Murphy G. The ADAMs: signalling scissors in the tumour microenvironment. *Nat Rev Cancer* 2008;8: 929-941.
Murphy SV, Atala A. 3D bioprinting of tissues and organs. *Nat Biotechnol* 2014;32: 773-785.
Naba A, Clauser KR, Ding H, Whittaker CA, Carr SA, Hynes RO. The extracellular matrix: Tools and insights for the "omics" era. *Matrix Biol* 2016;49: 10-24.
Naba A, Clauser KR, Hoersch S, Liu H, Carr SA, Hynes RO. The matrisome: in silico definition and in vivo characterization by proteomics of normaland tumor extracellular matrices. *Mol Cell Proteomics* 2012;11: M111014647.
Naba A, Clauser KR, Hynes RO. Enrichment of Extracellular Matrix Proteins from Tissues and Digestion into Peptides for Mass Spectrometry Analysis. *J Vis Exp* 2015: e53057.
Naba A, Hoersch S, Hynes RO. Towards definition of an ECM parts list: an advance on GO categories. *Matrix Biol* 2012;31: 371-372.
Nagyova E. Organization of the expanded cumulus-extracellular matrix in preovulatory follicles: a role for inter-alpha-trypsin inhibitor. *Endocr Regul* 2015;49: 37-45.
Nahata L, Woodruff TK, Quinn GP, Meacham LR, Chen D, Appiah LC, Finlayson C, Orwig KE, Laronda MM, Rowell EE *et al.* Ovarian tissue

cryopreservation as standard of care: what does this mean for pediatric populations? *Journal of Assisted Reproduction and Genetics* 2020;37: 1323-1326.

Narayanan K, Leck KJ, Gao S, Wan AC. Three-dimensional reconstituted extracellular matrix scaffolds for tissue engineering. *Biomaterials* 2009;30: 4309-4317.

Nauroy P, Hughes S, Naba A, Ruggiero F. The in-silico zebrafish matrisome: A new tool to study extracellular matrix gene and protein functions. *Matrix Biol* 2018;65: 5-13.

Nejat EJ, Chervenak JL. The continuum of ovarian aging and clinicopathologies associated with the menopausal transition. *Maturitas* 2010;66: 187-190.

Nelson CM, Bissell MJ. Of extracellular matrix, scaffolds, and signaling: tissue architecture regulates development, homeostasis, and cancer. *Annu Rev Cell Dev Biol* 2006;22: 287-309.

Newton H, Aubard Y, Rutherford A, Sharma V, Gosden R. Ovary and ovulation: Low temperature storage and grafting of human ovarian tissue. *Human Reproduction* 1996;11: 1487-1491.

Nguyen T, Lee S, Hatzirodos N, Hummitzsch K, Sullivan TR, Rodgers RJ, Irving-Rodgers HF. Spatial differences within the membrana granulosa in the expression of focimatrix and steroidogenic capacity. *Mol Cell Endocrinol* 2012;363: 62-73.

Nio J, Iwanaga T. Galectins in the mouse ovary: concomitant expression of galectin-3 and progesterone degradation enzyme (20alpha-HSD) in the corpus luteum. *J Histochem Cytochem* 2007;55: 423-432.

Noori A, Ashrafi SJ, Vaez-Ghaemi R, Hatamian-Zaremi A, Webster TJ. A review of fibrin and fibrin composites for bone tissue engineering. *Int J Nanomedicine* 2017;12: 4937-4961.

Norris JL, Porter NA, Caprioli RM. Combination detergent/MALDI matrix: functional cleavable detergents for mass spectrometry. *Analytical chemistry* 2005;77: 5036-5040.

Ny T, Wahlberg P, Brändström IJM. Matrix remodeling in the ovary: regulation and functional role of the plasminogen activator and matrix metalloproteinase systems. *Molecular and Cellular Endocrinology* 2002;187: 29-38.

Nyberg P, Xie L, Kalluri R. Endogenous inhibitors of angiogenesis. *Cancer Res* 2005;65: 3967-3979.

Ogrinc N, Saudemont P, Balog J, Robin YM, Gimeno JP, Pascal Q, Tierny D, Takats Z, Salzet M, Fournier I. Water-assisted laser desorption/ionization mass spectrometry for minimally invasive invivo and real-time surface analysis using SpiderMass. *Nat Protoc* 2019;14: 3162-3182.

Oktay K. Ovarian tissue cryopreservation and transplantation: preliminary

findings and implications for cancer patients. *Hum Reprod Update* 2001;7: 526-534.

Ono Y, Nagai M, Yoshino O, Koga K, Nawaz A, Hatta H, Nishizono H, Izumi G, Nakashima A, Imura J *et al.* CD11c+ M1-like macrophages (MPhis) but not CD206+ M2-like MPhi are involved in folliculogenesis in mice ovary. *Sci Rep* 2018;8: 8171.

Orisaka M, Tajima K, Mizutani T, Miyamoto K, Tsang BK, Fukuda S, Yoshida Y, Kotsuji F. Granulosa cells promote differentiation of cortical stromalcells into theca cells in the bovine ovary. *Biol Reprod* 2006;75: 734- 740.

Ouni E, Bouzin C, Dolmans MM, Marbaix E, Pyr Dit Ruys S, Vertommen D, Amorim CA. Spatiotemporal changes in mechanical matrisome components of the human ovary from prepuberty to menopause. *Hum Reprod* 2020;35: 1391-1410.

Ouni E, Peaucelle A, T. Haas K, Van Kerk O, Dolmans M-M, Tuuri T, Otala M, Vertommen D, A. Amorim C. A multi-scale readout of the microarchitecture, topography and mechanics of human ovary from prepuberty to menopause for the next generation of tissue engineered ovary and clinical diagnosis. *Nature Communications (under review)* 2021.

Ouni E, Vertommen D, Amorim CA. The Human Ovary and Future of Fertility Assessment in the Post-Genome Era. *Int J Mol Sci* 2019;20.

Ozsvar, J., Yang, C., Cain, S.A., Baldock, C., Tarakanova, A., and Weiss,
A.S. (2021). Tropoelastin and Elastin Assembly. *9*.

Padhi A, Nain AS. ECM in Differentiation: A Review of Matrix Structure, Composition and Mechanical Properties. *Ann Biomed Eng* 2020;48: 1071-1089.

Padiolleau L, Chanseau C, Durrieu S, Ayela C, Laroche G, Durrieu MC. Directing hMSCs fate through geometrical cues and mimetics peptides. *J Biomed Mater Res A* 2020;108: 201-211.

Page-McCaw A, Ewald AJ, Werb Z. Matrix metalloproteinases and the regulation of tissue remodelling. *Nat Rev Mol Cell Biol* 2007;8: 221- 233.

Palermo GD, Alikani M, Bertoli M, Colombero LT, Moy F, Cohen J, Rosenwaks Z. Oolemma characteristics in relation to survival and fertilization patterns of oocytes treated by intracytoplasmic sperm injection. *Hum Reprod* 1996;11: 172-176.

Parenteau-Bareil R, Gauvin R, Berthod F. Collagen-Based Biomaterials for Tissue Engineering Applications. *Materials* 2010;3.

Parrott DMV. The fertility of mice with orthotopic ovarian grafts derived from frozen tissue. *Journal of Reproduction and Fertility* 1960;1: 230-241.

Paulini F, Vilela JM, Chiti MC, Donnez J, Jadoul P, Dolmans MM, Amorim CA. Survival and growth of human preantral follicles after cryopreservation of ovarian tissue, follicle isolation and short-term xenografting. *Reprod Biomed Online* 2016;33: 425-432.

Pepling ME, Spradling AC. Mouse ovarian germ cell cysts undergo programmed breakdown to form primordial follicles. *Dev Biol* 2001;234: 339-351.

Peters H, Byskov AG, Grinsted J. Follicular growth in fetal and prepubertal ovaries of humans and other primates. *Clinics in Endocrinology and Metabolism* 1978;7: 469-485.

Piez KA. History of extracellular matrix: a personal view. *Matrix Biol* 1997;16: 85-92.

Pilate F, Toncheva A, Dubois P, Raquez J-M. Shape-memory polymers for multiple applications in the materials world. *European Polymer Journal* 2016;80: 268-294.

Pina S, Ribeiro VP, Marques CF, Maia FR, Silva TH, Reis RL, Oliveira JM. Scaffolding Strategies for Tissue Engineering and Regenerative Medicine Applications. *Materials (Basel)* 2019;12.

Polonio AM, Chico-Sordo L, Cordova-Oriz I, Medrano M, Garcia-Velasco JA, Varela E. Impact of Ovarian Aging in Reproduction: From Telomeresand Mice Models to Ovarian Rejuvenation. *Yale J Biol Med* 2020;93: 561-569.

Pors SE, Ramlose M, Nikiforov D, Lundsgaard K, Cheng J, Andersen CY, Kristensen SG. Initial steps in reconstruction of the human ovary: survival of pre-antral stage follicles in a decellularized human ovarianscaffold. *Hum Reprod* 2019;34: 1523-1535.

Porter S, Clark IM, Kevorkian L, Edwards DR. The ADAMTS metalloproteinases. *Biochem J* 2005;386: 15-27.

Pozuelo Rubio M, Geraghty KM, Wong BH, Wood NT, Campbell DG, Morrice N, Mackintosh C. 14-3-3-affinity purification of over 200 human phosphoproteins reveals new links to regulation of cellular metabolism, proliferation and trafficking. *Biochem J* 2004;379: 395- 408.

Quan N, Mara JN, Grover AR, Pavone ME, Duncan FE. Spatial Analysis of Growing Follicles in the Human Ovary to Inform Tissue Engineering Strategies. *Tissue Eng Part A* 2020;26: 733-746.

Racowsky C, Gelety TJ. Chapter 4 The Biology of the ovary. In Edward Bittar E and Edward Bittar N (eds) *Principles of Medical Biology*. 1998. Elsevier, pp. 77-102.

Rahman S, Patel Y, Murray J, Patel KV, Sumathipala R, Sobel M, Wijelath ES. Novel hepatocyte growth factor (HGF) binding domains on fibronectin and vitronectin coordinate a distinct and amplified Met-integrin induced signalling pathway in endothelial cells. *BMC Cell Biol* 2005;6: 8.

Rajabzadeh AR, Eimani H, Mohseni Koochesfahani H, Shahvardi AH, Fathi R. Morphological study of isolated ovarian preantral follicles using fibrin gel plus platelet lysate after subcutaneous transplantation. *Cell J* 2015;17: 145-152.

zamanujan S, Pluen A, McKee TD, Brown EB, Boucher Y, Jain RK. Diffusion

and Convection in Collagen Gels: Implications for Transport in the Tumor Interstitium. *Biophysical Journal* 2002;83: 1650-1660.
Ramirez F, Dietz HC. Extracellular microfibrils in vertebrate development and disease processes. *J Biol Chem* 2009;284: 14677-14681.
Ramirez F, Rifkin DB. Extracellular microfibrils: contextual platforms for TGFbeta and BMP signaling. *Curr Opin Cell Biol* 2009;21: 616-622.
Reddy P, Adhikari D, Zheng W, Liang S, Hamalainen T, Tohonen V, Ogawa W, Noda T, Volarevic S, Huhtaniemi I *et al.* PDK1 signaling in oocytes controls reproductive aging and lifespan by manipulating the survivalof primordial follicles. *Hum Mol Genet* 2009;18: 2813-2824.
Reddy P, Liu L, Adhikari D, Jagarlamudi K, Rajareddy S, Shen Y, Du C, Tang W, Hamalainen T, Peng SL *et al.* Oocyte-specific deletion of Pten causes premature activation of the primordial follicle pool. *Science* 2008;319: 611-613.
Reddy P, Zheng W, Liu K. Mechanisms maintaining the dormancy and survival of mammalian primordial follicles. *Trends Endocrinol Metab* 2010;21: 96-103.
Ren Y, Suzuki H, Jagarlamudi K, Golnoski K, McGuire M, Lopes R, Pachnis V, Rajkovic A. Lhx8 regulates primordial follicle activation and postnatal folliculogenesis. *BMC Biol* 2015;13: 39.
Ricard-Blum S. The collagen family. *Cold Spring Harb Perspect Biol* 2011;3: a004978.
Richard S, Tartia AP, Boison D, Baltz JM. Mouse Oocytes Acquire Mechanisms That Permit Independent Cell Volume Regulation at theEnd of Oogenesis. *J Cell Physiol* 2017;232: 2436-2446.
Robins SP. Biochemistry and functional significance of collagen cross-linking. *Biochem Soc Trans* 2007;35: 849-852.
Rodgers RJ, Irving-Rodgers HF, Russell DL. Extracellular matrix of the developing ovarian follicle. *Reproduction* 2003;126: 415-424.
Rodgers RJ, Irving-Rodgers HF, van Wezel IL. Extracellular matrix in ovarian follicles. *Molecular and Cellular Endocrinology* 2000;163: 73-79.
Rodgers RJ, van Wezel IL, Irving-Rodgers HF, Lavranos TC, Irvine CM, Krupa M. Roles of extracellular matrix in follicular development. *J Reprod Fertil Suppl* 1999;54: 343-352.
Saatcioglu HD, Cuevas I, Castrillon DH. Control of Oocyte Reawakening by Kit. *PLoS Genet* 2016;12: e1006215.
Samuel BH, Young SK. *Glycoproteins and Glycosylation Changes inCancer*. Second Edition edn, 2002.
Sanada H, Shikata J, Hamamoto H, Ueba Y, Yamamuro T, Takeda T. Changes in collagen cross-linking and lysyl oxidase by estrogen. *Biochimica et Biophysica Acta (BBA) - General Subjects* 1978;541: 408-413.
Sarraj MA, Drummond AE. Mammalian foetal ovarian development:

consequences for health and disease. *Reproduction* 2012;143: 151- 163.
Saudemont P, Quanico J, Robin YM, Baud A, Balog J, Fatou B, Tierny D, Pascal Q, Minier K, Pottier M *et al.* Real-Time Molecular Diagnosis of Tumors Using Water-Assisted Laser Desorption/Ionization Mass Spectrometry Technology. *Cancer Cell* 2018;34: 840-851 e844.
Schaefer L, Iozzo RV. Biological functions of the small leucine-rich proteoglycans: from genetics to signal transduction. *J Biol Chem* 2008;283: 21305-21309.
Schaefer L, Schaefer RM. Proteoglycans: from structural compounds to signaling molecules. *Cell Tissue Res* 2010;339: 237-246.
Schenck A, Vera-Rodriguez M, Greggains G, Davidson B, Fedorcsak P. Spatial and temporal changes in follicle distribution in the human ovarian cortex. *Reprod Biomed Online* 2021;42: 375-383.
Schroder CP, Timmer-Bosscha H, Wijchman JG, de Leij LF, Hollema H, Heineman MJ, de Vries EG. An in vitro model for purging of tumour cells from ovarian tissue. *Hum Reprod* 2004;19: 1069-1075.
Schwarzbauer JE, DeSimone DW. Fibronectins, their fibrillogenesis, and in vivo functions. *Cold Spring Harb Perspect Biol* 2011;3.
Seybold D, Schildhauer TA, Gessmann J, Muhr G, Koller M, Roetman B. Osteogenic differentiation of human mesenchymal stromal cells is promoted by a leukocytes containing fibrin matrix. *Langenbecks Arch Surg* 2010;395: 719-726.
Shafiee A, Atala A. Printing Technologies for Medical Applications. *Trends Mol Med* 2016;22: 254-265.
Shalgi R, Kraicer P, Rimon A, Pinto M, Soferman N. Proteins of Human Follicular Fluid: The Blood-Follicle Barrier**Presented at the Annual Conference of the Society for the Study of Fertility, Reading, England,July 18–22, 1972. *Fertility and Sterility* 1973;24: 429-434.
Shaw JM, Oranratnachai A, Trounson AO. Fundamental cryobiology of mammalian oocytes and ovarian tissue. *Theriogenology* 2000;53: 59-72.
Shikanov A, Smith RM, Xu M, Woodruff TK, Shea LD. Hydrogel network design using multifunctional macromers to coordinate tissue maturation in ovarian follicle culture. *Biomaterials* 2011;32: 2524- 2531.
Sica A, Erreni M, Allavena P, Porta C. Macrophage polarization in pathology. *Cell Mol Life Sci* 2015;72: 4111-4126.
Skalak R. Tissue engineering *Proceedings of the 15th Annual International Conference of the IEEE Engineering in Medicine and Biology Societ*. 1993, pp. 1112-1113.
Skinner MK. Regulation of primordial follicle assembly and development. *Hum Reprod Update* 2005;11: 461-471.
Smith RM, Shikanov A, Kniazeva E, Ramadurai D, Woodruff TK, Shea LD. Fibrin-mediated delivery of an ovarian follicle pool in a mouse model of infertility. *Tissue Eng Part A* 2014;20: 3021-3030.

Soares M, Sahrari K, Chiti MC, Amorim CA, Ambroise J, Donnez J, Dolmans MM. The best source of isolated stromal cells for the artificial ovary: medulla or cortex, cryopreserved or fresh? *Hum Reprod* 2015;30: 1589-1598.

Soares M, Saussoy P, Maskens M, Reul H, Amorim CA, Donnez J, Dolmans MM. Eliminating malignant cells from cryopreserved ovarian tissue is possible in leukaemia patients. *Br J Haematol* 2017;178: 231-239.

Socovich AM, Naba A. The cancer matrisome: From comprehensive characterization to biomarker discovery. *Semin Cell Dev Biol* 2019;89: 157-166.

Stefanelli VL, Barker TH. The evolution of fibrin-specific targeting strategies. *J Mater Chem B* 2015;3: 1177-1186.

Suzuki N, Yoshioka N, Takae S, Sugishita Y, Tamura M, Hashimoto S, Morimoto Y, Kawamura K. Successful fertility preservation following ovarian tissue vitrification in patients with primary ovarian insufficiency. *Hum Reprod* 2015;30: 608-615.

Swee MH, Parks WC, Pierce RA. Developmental regulation of elastin production. Expression of tropoelastin pre-mRNA persists after down-regulation of steady-state mRNA levels. *J Biol Chem* 1995;270: 14899-14906.

Sztein J, Sweet H, Farley J, Mobraaten L. Cryopreservation and orthotopic transplantation of mouse ovaries: new approach in gamete banking. *Biol Reprod* 1998;58: 1071-1074.

Tagler DJ, Shea LD, Woodruff TK. Contributions of ovarian stromal cells to follicle culture. In Donnez J and Kim SS (eds) *Principles and Practiceof Fertility Preservation*. 2011. Cambridge University Press, Cambridge, pp. 409-420.

Taufalele PV, VanderBurgh JA, Munoz A, Zanotelli MR, Reinhart-King CA. Fiber alignment drives changes in architectural and mechanical features in collagen matrices. *PLoS One* 2019;14: e0216537.

Telfer E, Torrance C, Gosden RG. Morphological study of cultured preantral ovarian follicles of mice after transplantation under the kidney capsule. *J Reprod Fertil* 1990;89: 565-571.

Telfer EE, McLaughlin M, Ding C, Thong KJ. A two-step serum-free culture system supports development of human oocytes from primordialfollicles in the presence of activin. *Hum Reprod* 2008;23: 1151-1158.

Telfer EE, Zelinski MB. Ovarian follicle culture: advances and challenges for human and nonhuman primates. *Fertil Steril* 2013;99: 1523-1533.

Thomson J, Singh M, Eckersley A, Cain SA, Sherratt MJ, Baldock C. Fibrillin microfibrils and elastic fibre proteins: Functional interactions and extracellular regulation of growth factors. *Semin Cell Dev Biol* 2019;89: 109-117.

Thorne JT, Segal TR, Chang S, Jorge S, Segars JH, Leppert PC. Dynamic

reciprocity between cells and their microenvironment in reproduction.*Biol Reprod* 2015;92: 25.

Tong Y, Li F, Lu Y, Cao Y, Gao J, Liu J. Rapamycin-sensitive mTORC1 signaling is involved in physiological primordial follicle activation in mouse ovary. *Mol Reprod Dev* 2013;80: 1018-1034.

Umehara T, Richards JS, Shimada M. The stromal fibrosis in aging ovary. *Aging (Albany NY)* 2018;10: 9-10.

Van Eyck AS, Bouzin C, Feron O, Romeu L, Van Langendonckt A, Donnez J, Dolmans MM. Both host and graft vessels contribute to revascularization of xenografted human ovarian tissue in a murine model. *Fertil Steril* 2010;93: 1676-1685.

Van Eyck AS, Jordan BF, Gallez B, Heilier JF, Van Langendonckt A, DonnezJ. Electron paramagnetic resonance as a tool to evaluate human ovarian tissue reoxygenation after xenografting. *Fertil Steril* 2009;92:374-381.

Vanacker J, Amorim CA. Alginate: A Versatile Biomaterial to Encapsulate Isolated Ovarian Follicles. *Ann Biomed Eng* 2017;45: 1633-1649.

Vanacker J, Dolmans MM, Luyckx V, Donnez J, Amorim CA. First transplantation of isolated murine follicles in alginate. *Regen Med* 2014;9: 609-619.

Vanacker J, Luyckx V, Dolmans MM, Des Rieux A, Jaeger J, Van Langendonckt A, Donnez J, Amorim CA. Transplantation of an alginate-matrigel matrix containing isolated ovarian cells: first step in developing a biodegradable scaffold to transplant isolated preantral follicles and ovarian cells. *Biomaterials* 2012;33: 6079-6085.

Viji Babu PK, Rianna C, Mirastschijski U, Radmacher M. Nano-mechanical mapping of interdependent cell and ECM mechanics by AFM force spectroscopy. *Scientific Reports* 2019;9: 12317.

Viola JM, Porter CM, Gupta A, Alibekova M, Prahl LS, Hughes AJ. Guiding Cell Network Assembly using Shape-Morphing Hydrogels. *Adv Mater* 2020;32: e2002195.

Vogel C, Marcotte EM. Insights into the regulation of protein abundance from proteomic and transcriptomic analyses. *Nat Rev Genet* 2012;13: 227-232.

Vyborny K, Vallova J, Koci Z, Kekulova K, Jirakova K, Jendelova P, Hodan J, Kubinova S. Genipin and EDC crosslinking of extracellular matrix hydrogel derived from human umbilical cord for neural tissue repair. *Sci Rep* 2019;9: 10674.

Wada K, Itoga K, Okano T, Yonemura S, Sasaki H. Hippo pathway regulation by cell morphology and stress fibers. *Development* 2011;138: 3907-3914.

Wagner M, Yoshihara M, Douagi I, Damdimopoulos A, Panula S,Petropoulos S, Lu H, Pettersson K, Palm K, Katayama S *et al.* Single-cell analysis of human ovarian cortex identifies distinct cell populations but no oogonial

stem cells. *Nat Commun* 2020;11: 1147.

Wallace WH, Anderson RA, Irvine DS. Fertility preservation for young patients with cancer: who is at risk and what can be offered? *Lancet Oncol* 2005;6: 209-218.

Wallace WH, Kelsey TW. Human ovarian reserve from conception to the menopause. *PLoS One* 2010;5: e8772.

Walzel H, Brock J, Pohland R, Vanselow J, Tomek W, Schneider F, Tiemann U. Effects of galectin-1 on regulation of progesterone production in granulosa cells from pig ovaries in vitro. *Glycobiology* 2004;14: 871- 881.

Wang F, Hansen RK, Radisky D, Yoneda T, Barcellos-Hoff MH, Petersen OW, Turley EA, Bissell MJ. Phenotypic reversion or death of cancer cells by altering signaling pathways in three-dimensional contexts. *J Natl Cancer Inst* 2002;94: 1494-1503.

Wang S, Zheng Y, Li J, Yu Y, Zhang W, Song M, Liu Z, Min Z, Hu H, Jing Y *et al.* Single-Cell Transcriptomic Atlas of Primate Ovarian Aging. *Cell* 2020;180: 585-600 e519.

Wang X, Harris RE, Bayston LJ, Ashe HL. Type IV collagens regulate BMP signalling in Drosophila. *Nature* 2008;455: 72-77.

West ER, Xu M, Woodruff TK, Shea LD. Physical properties of alginate hydrogels and their effects on in vitro follicle development. *Biomaterials* 2007;28: 4439-4448.

White LJ, Taylor AJ, Faulk DM, Keane TJ, Saldin LT, Reing JE, Swinehart IT, Turner NJ, Ratner BD, Badylak SF. The impact of detergents on the tissue decellularization process: A ToF-SIMS study. *Acta Biomater* 2017;50: 207-219.

Wijayarathna R, de Kretser DM. Activins in reproductive biology and beyond. *Hum Reprod Update* 2016;22: 342-357.

Winter JS, Faiman C. The development of cyclic pituitary-gonadal function in adolescent females. *J Clin Endocrinol Metab* 1973;37: 714-718.

Winter JS, Hughes IA, Reyes FI, Faiman C. Pituitary-gonadal relations in infancy: 2. Patterns of serum gonadal steroid concentrations in man from birth to two years of age. *J Clin Endocrinol Metab* 1976;42: 679-686.

Wolf K, Te Lindert M, Krause M, Alexander S, Te Riet J, Willis AL, Hoffman RM, Figdor CG, Weiss SJ, Friedl P. Physical limits of cell migration: control by ECM space and nuclear deformation and tuning by proteolysis and traction force. *J Cell Biol* 2013;201: 1069-1084.

Woodruff TK, Shea LD. The role of the extracellular matrix in ovarian follicle development. *Reproductive sciences (Thousand Oaks, Calif)* 2007;14: 6-10.

Woodruff TK, Shea LD. A new hypothesis regarding ovarian follicle development: ovarian rigidity as a regulator of selection and health. *J Assist Reprod Genet* 2011;28: 3-6.

Woods DC, Tilly JL. Isolation, characterization and propagation of mitotically

active germ cells from adult mouse and human ovaries. *Nat Protoc* 2013;8: 966-988.
Wu CC, Yates JR, 3rd. The application of mass spectrometry to membrane proteomics. *Nat Biotechnol* 2003;21: 262-267.
Wu J, Lee KC, Dickinson RB, Lele TP. How dynein and microtubules rotate the nucleus. *J Cell Physiol* 2011;226: 2666-2674.
Wu J, Zhao C, Lin W, Hu R, Wang Q, Chen H, Li L, Chen S, Zheng J. Binding characteristics between polyethylene glycol (PEG) and proteins in aqueous solution. *J Mater Chem B* 2014;2: 2983-2992.
Wu R, Van der Hoek KH, Ryan NK, Norman RJ, Robker RL. Macrophage contributions to ovarian function. *Hum Reprod Update* 2004;10: 119-133.
Xiang C, Li J, Hu L, Huang J, Luo T, Zhong Z, Zheng Y, Zheng L. Hippo signaling pathway reveals a spatio-temporal correlation with the size of primordial follicle pool in mice. *Cell Physiol Biochem* 2015;35: 957-968.
Xie J, Bao M, Bruekers SMC, Huck WTS. Collagen Gels with Different Fibrillar Microarchitectures Elicit Different Cellular Responses. *ACS Appl Mater Interfaces* 2017;9: 19630-19637.
Xu J, Bishop CV, Lawson MS, Park BS, Xu F. Anti-Mullerian hormone promotes pre-antral follicle growth, but inhibits antral follicle maturation and dominant follicle selection in primates. *Hum Reprod* 2016;31: 1522-1530.
Xu M, West E, Shea LD, Woodruff TK. Identification of a stage-specific permissive in vitro culture environment for follicle growth and oocyte development. *Biol Reprod* 2006;75: 916-923.
Xu R, Boudreau A, Bissell MJ. Tissue architecture and function: dynamic reciprocity via extra- and intra-cellular matrices. *Cancer Metastasis Rev* 2009;28: 167-176.
Xu S, Xu H, Wang W, Li S, Li H, Li T, Zhang W, Yu X, Liu L. The role of collagen in cancer: from bench to bedside. *J Transl Med* 2019;17: 309.
Yanez LZ, Han J, Behr BB, Pera RAR, Camarillo DB. Human oocyte developmental potential is predicted by mechanical properties within hours after fertilization. *Nat Commun* 2016;7: 10809.
Yang DZ, Yang W, Li Y, He Z. Progress in understanding human ovarian folliculogenesis and its implications in assisted reproduction. *J Assist Reprod Genet* 2013;30: 213-219.
Yang L, Chen Y, Liu Y, Xing Y, Miao C, Zhao Y, Chang X, Zhang Q. The Role of Oxidative Stress and Natural Antioxidants in Ovarian Aging. *Front Pharmacol* 2020;11: 617843.
Yang L, Ge L, Zhou Q, Mokabber T, Pei Y, Bron R, van Rijn P. Biomimetic Multiscale Hierarchical Topography Enhances Osteogenic Differentiation of Human Mesenchymal Stem Cells. 2020;7: 2000385.
Yang MY, Cushman RA, Fortune JE. Anti-Mullerian hormone inhibits activation and growth of bovine ovarian follicles in vitro and is localized

to growing follicles. *Mol Hum Reprod* 2017;23: 282-291.

Yim EK, Reano RM, Pang SW, Yee AF, Chen CS, Leong KW. Nanopattern-induced changes in morphology and motility of smooth muscle cells. *Biomaterials* 2005;26: 5405-5413.

Yin H, Kristensen SG, Jiang H, Rasmussen A, Andersen CY. Survival and growth of isolated pre-antral follicles from human ovarian medulla tissue during long-term 3D culture. *Hum Reprod* 2016;31: 1531-1539.

Yoon DM, Fisher JP. Natural and Synthetic Polymeric Scaffolds. In Narayan R (ed) *Biomedical Materials*. 2009. Springer US, Boston, MA, pp. 415-442.

Young S, Wong M, Tabata Y, Mikos AG. Gelatin as a delivery vehicle for the controlled release of bioactive molecules. *J Control Release*2005;109: 256-274.

Yu J, Park SA, Kim WD, Ha T, Xin YZ, Lee J, Lee D. Current Advances in 3D Bioprinting Technology and Its Applications for Tissue Engineering. *Polymers (Basel)* 2020;12.

Yu YQ, Gilar M, Lee PJ, Bouvier ES, Gebler JC. Enzyme-friendly, mass spectrometry-compatible surfactant for in-solution enzymatic digestion of proteins. *Analytical chemistry* 2003;75: 6023-6028.

Yue B. Biology of the extracellular matrix: an overview. *J Glaucoma* 2014;23: S20-23.

Zhai J, Yao G, Dong F, Bu Z, Cheng Y, Sato Y, Hu L, Zhang Y, Wang J, Dai S *et al.* In Vitro Activation of Follicles and Fresh Tissue Auto-transplantation in Primary Ovarian Insufficiency Patients. *J Clin Endocrinol Metab* 2016;101: 4405-4412.

Zhang H, Liu K. Cellular and molecular regulation of the activation of mammalian primordial follicles: somatic cells initiate follicle activationin adulthood. *Human Reproduction Update* 2015;21: 779-786.

Zhang J, Chen Q, Du D, Wu T, Wen J, Wu M, Zhang Y, Yan W, Zhou S, Li Y *et al.* Can ovarian aging be delayed by pharmacological strategies? *Aging (Albany NY)* 2019;11: 817-832.

Zhang L, Elias JE. Relative Protein Quantification Using Tandem Mass Tag Mass Spectrometry. *Methods Mol Biol* 2017;1550: 185-198.

Zhang XM, Li L, Xu JJ, Wang N, Liu WJ, Lin XH, Fu YC, Luo LL. Rapamycin preserves the follicle pool reserve and prolongs the ovarian lifespan of female rats via modulating mTOR activation and sirtuin expression.*Gene* 2013;523: 82-87.

Zhao Y, Luck MR. Gene expression and protein distribution of collagen, fibronectin and laminin in bovine follicles and corpora lutea. *J Reprod Fertil* 1995;104: 115-123.

Zhao Y, Zhang Y, Li J, Zheng N, Xu X, Yang J, Xia G, Zhang M. MAPK3/1 participates in the activation of primordial follicles through mTORC1-KITL signaling. *J Cell Physiol* 2018;233: 226-237.

Zhou SF, Gopalakrishnan S, Xu YH, To SKY, Wong AST, Pang SW, Lam YW. Substrates with patterned topography reveal metastasis of human cancer cells. *Biomed Mater* 2017;12: 055001.

Zhu Y, Liu Y, Jin K, Pang Z. 13 - Polysaccharide nanoparticles for cancer drug targeting. In Maiti S and Jana S (eds) *Polysaccharide Carriers for Drug Delivery*. 2019. Woodhead Publishing, pp. 365-396